MYLODONTID GROUND SLOTHS FROM SOUTH AMERICA: NEW ADVANCES IN ANATOMY, TAXONOMY, INTRASPECIFIC VARIATION, PHYLOGENY, AND PALEONEUROLOGY

LOS PEREZOSOS MILODONTES DE AMÉRICA DEL SUR: NUEVOS AVANCES EN ANATOMÍA, TAXONOMÍA, VARIACIÓN INTRAESPECÍFICA, FILOGENIA Y PALEONEUROLOGÍA

ALBERTO BOSCAINI MSC

SUPERVISOR:
DR. FRANÇOIS PUJOS

CO-SUPERVISOR:
PROF. TIMOTHY J. GAUDIN

Thesis submitted for the degree of Doctor of Philosophy (PhD)

Tesis para optar al título de Doctor en Ciencias Biológicas
Universidad Nacional de Cuyo, Mendoza, Argentina
Programa de posgrado en Biología

2019

"Und was verschwand, wird mir zu Wirklichkeiten"

"And what disappeared becomes reality to me"

Johann Wolfgang von Goethe, Faust: Part I (Dedication)

ACKOWLEDGMENTS / *AGRADECIMIENTOS / RINGRAZIAMENTI*

Through the past four years, there were several people who influenced my work, delighted my days in Argentina, and thus helped this thesis to be realized.

My greatest debt is to my supervisors, François Pujos and Tim Gaudin, for their constant help, availability for questions, and careful supervision throughout my entire PhD. I would also like to thank Dawid Iurino, Cástor Cartelle, Gerry De Iuliis, Néstor Toledo, German Tirao, André Strauss, Guillaume Billet, Lionel Hautier, Philippe Münch, Pierre-Olivier Antoine, and Raffaele Sardella, who, in these latest years, supported my research and decided to collaborate with me in some projects.

Unas gracias especiales van a Bernardino Mamani Quispe quien, además de colaborar conmigo, me permitió acceder a la colección de vertebrados del Museo Nacional de Historia Natural de La Paz, y me incluyó en varias campañas en el Altiplano boliviano. A Rubén Andrade, por los buenos momentos y los mates compartidos, en el campo y en el museo de La Paz. A todos los compañeros de aventuras en Bolivia, especialmente a Laurent "don't expect too much" *Marivaux y a Mercedes Prámparo por su apoyo constante.*

Quiero también agradecer a Sergio Vizcaíno y Analía Forasiepi por el inmejorable seguimiento durante estos años de doctorado, así como los consejos adicionales que siempre se necesitan.

Durante estos años tuve la oportunidad de girar por el mundo y conocer gente enriquecedora en todo momento. Muchos me abrieron las puertas a museos y colecciones, y con su buena disposición hicieron muy amenas mis estadías. Entre ellos quiero agradecer a Alejandro Kramarz, Laura Chornogubsky, Stella M. Álvarez, Matías Taglioretti, Fernando Scaglia, Pablo Teta, Sergio Lucero, Marcelo Reguero, Alejo Scarano, Martín de los Reyes, Federico Anaya, José Luis Aguilar, Ascanio Rincón, Rodolfo Sánchez, Bertilde Rossi, Guillermo Campos, Freddy Paredes.

I need to thank also many people from the northern hemisphere, who significantly facilitated the data collection of this thesis. I am indebted to Bruce MacFadden, Richard C. Hulbert Jr, John Bloch, Bill Simpson, Adrienne Stroup, Kenneth Angielczyk, Ross D. MacPhee, J. J. Flynn, Maria Dickon Ríos, Judy Galkin, Gerry de Iuliis, Guillaume Billet, and Christian de Muizon.

También agradezco a quienes compartieron algunas fotos de perezosos fósiles, bibliografía, o contribuyeron con útiles consejos y enseñanzas a mis tareas de investigación, como Julia Tejada-Lara, Martín Ubilla, Esperanza Cerdeño, Alfredo Carlini, Marcelo R. Sánchez-Villagra, David Flores, Valentina Segura, Diego Brandoni, Raúl Vezzosi, Diego Pol, Pablo Goloboff, Guillermo Rougier, Santiago Catalano, Kevin Jiménez-Lara, Santiago Hernández del Pino.

A Elisa, María Cecilia y Mariana del Probiol, siempre atentas y disponibles.

He de agradecer también a Francisco J. Prevosti y otra vez a Analía Forasiepi por haberme incluido en el proyecto Huayquerías, y por la oportunidad de excavar en un yacimiento tan especial a lo largo de estos últimos años. A Junior Bonini, Cristo Omar Romano, Cristian Sancho, Marcelo Bourguet, Sebastián Echarri, Federico Seoane, Sergio Tarquini, Alberto Garrido y Guillermo Ré por compartir esos lindos momentos en el campo. A Cristian y Marcelo, especialmente, por enseñarme técnicas de preparación en el laboratorio de paleo: ¡unos grosos!

Por si no se hubiese entendido, en mi lugar de trabajo, como en la ciudad de Mendoza, encontré el ambiente ideal para crecer a nivel científico y personal. Por esto he de agradecer a todas las personas que compartieron su tiempo conmigo, en estos ultimo años. Gracias especiales a Sebas, Tucu, Mati, Vale, Manuela, Pao, Nacho, Cari, Osvaldo, Diego, Cristian, Robin, Ana, Andrea, Lidia, Pierre, Rafa, Leandro, Marco y Fer. A Sergio Mosconi va mi especial reconocimiento por su fundamental ayuda.

En particular he de agradecer a mi familia mendocina, Marcos y Eva, por las charlas, las risas, los vinos y la buena onda. En fin, por haber hecho del "Rancho Jofré" un lugar que se pueda llamar "casa". A Kata y Rasputín por defenderla.

También en Buenos Aires encontré un hogar, buenos amigos y, además, una mujer hermosa. Quiero agradecer a Marina, por acompañarme en todo momento, estando cerca o lejos. Por los viajes a través de Pangea, por los abrazos tardígrados y por enseñarme a querer los fósiles. A Dani y Lilia, por los buenos momentos juntos. A mis amigos porteños: Spada, Kinki, Guille, Yani, Manu, Franco, y toda "la Blue". A los del MACN: a Sebastián Echarri, Guillermo Cassini, Martín Ezcurra, Agustín, el Tano, la Mechis, Pablo, Sergio, las dos Lauras, Augusto, y a los técnicos Marce y Sebas.

A aquellos paleontólogos lejanos, pero a la vez cercanos, que siempre han mantenido conmigo un contacto que supera las barreras del tiempo y del espacio, como Joan Madurell-Malapeira, David Alba, Raef Minwer-Barakat, Miriam Pérez de los Ríos (e a Stefano, ovvio!), Marc Furió, Soledad de Esteban Trivigno, Damián Ruiz Ramoni, Pedro Piñero. Un legame particolare l'ho avuto, non solo per ragioni linguistiche, con Lorenzo Rook, Dawid Iurino, Alessandro Minelli, Raffaele Sardella, Laura Longo, e Mattia Baiano.

Gracias a Jorge A. González por su reconstrucción del perezoso Simomylodon uccasamamensis.

Grazie a D. Bonadonna per la ricostruzione del bradipo Glossotherium robustum.

Vorrei infine ringraziare la moltitudine di amici, familiari, conoscenti, e tutti coloro che hanno incrociato il mio cammino fino ad ora. Un grazie ai nonni, ai cugini, agli zii e a tutti i parenti che in qualche momento hanno voluto sapere di "quel là che l'è andà".

A mio padre, che mi ha insegnato a lavorare con passione.

A mio fratello Andrea, che più grande non può essere.

A Sandra, mia madre, sempre al mio fianco.

Other thanks are for AC/DC, Bob Dylan, Pink Floyd, Gustavo Cerati, Juan D'Arienzo and Antonio Vivaldi, who significantly helped the ideas flowing.

Quiero agradecer especialmente al CONICET (Consejo Nacional de Investigaciones Científicas y Técnicas) por la oportunidad concedida de desarrollar mis estudios doctorales en Argentina. Agradezco también a toda la República Argentina, por haberme abierto las puertas y haberme hecho sentir como un argentino más. Ojalá pasara lo mismo en mi país de origen que, al contrario, en estos tiempos oscuros, se jacta de cerrar sus fronteras a quienes más lo necesitan.

This research was made possible thanks to the cooperation agreement between the *Museo Nacional de Historia Natural de Bolivia* (MNHN-Bol), the *Instituto Argentino de Nivología, Glaciología y Ciencias Ambientales* (IANIGLA) and the *Institut des Sciences de l'Evolution de Montpellier* (ISEM) (CONICET Cooperation Agreement N°864/2014) and was partially funded by the ECOS-FonCyT cooperative program (A14U01) and the National Geographic Society (NGS 9971-16). I am particularly indebted to the Field Museum of Natural History of Chicago, USA (FMNH), the American Museum of Natural History, New York, USA (AMNH), the Florida Museum of Natural History, Gainesville, USA (FLMNH) and the University of Tennessee at Chattanooga, USA (UTC) for funding that greatly facilitated data collection for the present study.

Finally, I want to especially thank the National Geographic Society, which put faith in the present project by actively funding the paleontological campaigns at Ayo Ayo-Viscachani through an Early Career Grant (EC-44712R-18).

ABSTRACT

Terrestrial sloths are some of the most emblematic mammals of the Cenozoic South American fossil faunas. Among them, Mylodontidae constitutes a major clade of extinct sloths. Their remains, which are relatively abundant in the Neogene and Quaternary fossil record, have also been discovered in Central and North American localities. Despite their abundance, many aspects of their evolutionary history remain obscure.

Recent paleontological expeditions in Late Miocene–Pliocene deposits of the Bolivian Altiplano provided several new and well-preserved remains referable to the mylodontid species *Simomylodon uccasamamensis*. These fossils were recovered in various localities of the Bolivian Altiplano, including Ayo Ayo-Viscachani, Casira, Choquecota, Inchasi, and Pomata-Ayte. These new remains of *S. uccasamamensis* comprise several previously unknown bony elements, allowing an almost complete characterization of the skeletal anatomy of the latter species, including cranium, dentition, ear region, and postcranial elements. The analysis of this material, and comparisons with other mylodontines, allowed the differentiation of this species on both morphological and morphometric grounds, and permitted a revision of the systematics of Mylodontinae previously recognized for the Neogene of the continent.

The large available sample of *Simomylodon uccasamamensis* from the Bolivian Altiplano also allowed for recognition of significant intraspecific variation in the latter species, suggesting the presence of sexual dimorphism, detectable on the basis of both shape and size, in cranial and postcranial remains. Sexual dimorphism was previously proposed for other extinct sloth species, and particularly in Mylodontinae, as a possible explanation for the observed intraspecific variation. Accordingly, also the variation *S. uccasamamensis* clusters into two well-defined, gracile and robust, morphs. The presence of two distinct morphs in *Simomylodon uccasamamensis* represents the earliest well-documented occurrence of sexual dimorphism in an extinct sloth. Dimorphic traits are mainly recognized in the shape of the muzzle region and the size of some long bones, such as femur and tibia. Therefore, dimorphism in *S. uccasamamensis* was related with general size, and probably associated with different diets between males and females. This, in turn, could have been related with ecological niche separation, that allowed for a non-competitive habit use of the two sexes.

In light of the new information, a reappraisal of the phylogeny of Mylodontidae was conducted based on 286 craniodental characters and, for the first time, 97 postcranial features, detected across the entire skeletal anatomy of 40 taxa. In this way, it was possible to perform a new species-level parsimony-based analysis of Mylodontinae, including some taxa previously unexplored from a phylogenetic perspective. The results strongly corroborate the monophyly of both Mylodontini and Lestodontini, which experienced independent adaptive radiations from Late Miocene to Pleistocene. The mylodontid from the Bolivian Altiplano, *Simomylodon uccasamamensis*, is recovered among the basal members of Mylodontini, currently constituting the most complete early member of the clade.

In the attempt of further clarifying the evolutionary history of mylodontid sloths, some previously unknown anatomical regions were explored. Advances in knowledge of mylodontid anatomy were achieved through the study of digital cranial endocasts obtained from CT-scans, using the Pleistocene species *Glossotherium robustum* from Argentina as a reference taxon. Therefore, it was possible to reconstruct and describe in detail the first 3D digital models of the brain cavity, cranial sinuses, inner ear, and the trajectories of nerves and blood vessels of an endocranial cast of a mylodontid sloth.

In morphometric geometric analyses, the shape of the bony labyrinth of extant xenarthrans shows a strong phylogenetic signal but, after the inclusion of fossil specimens, the distribution of the labyrinthine shapes in the morphospace shows significant departure from the previous distribution. Given the low effect of allometry in the dataset, it appears that functional aspects may concur in shaping the morphology of the inner ear in the xenarthran clade.

Other endocranial structures, such as the brain cavity, cranial nerves, cranial sinuses, and blood vessels have been digitally reconstructed for *Glossotherium* and compared with those of the extant tree-sloths *Bradypus* and *Choloepus*. The obtained results represent the first exhaustive characterization of the endocranial anatomy of an extinct sloth. A qualitative analysis of the aspect of the 3D models of these endocranial structures, suggests the influence of mixed phylogenetic, functional, and allometric signals that concur in shaping their morphology.

RESUMEN

Los perezosos terrestres son unos de los mamíferos más representativos de las faunas sudamericanas del Cenozoico. Entre ellos, los Mylodontidae constituyen uno de los principales grupos de perezosos extintos. Restos de perezosos milodontes son relativamente abundantes en el registro fósil Neógeno y Cuaternario de Suramérica, hallándose también el centro y norte del continente americano. Sin embargo, a pesar de su representatividad, muchos aspectos de su historia evolutiva permanecen oscuros.

Recientes excavaciones paleontológicas en depósitos del Mioceno tardío–Plioceno del Altiplano boliviano han permitido el hallazgo de abundantes restos asignables a la especie *Simomylodon uccasamamensi*s. Estos fósiles fueron encontrados en varias localidades del Altiplano, como Ayo Ayo-Viscachani, Casira, Choquecota, Inchasi y Pomata-Ayte. Los nuevos restos de *Simomylodon uccasamamensis* incluyen elementos óseos previamente desconocidos, permitiendo una mejor comprensión de su anatomía craneana, dental, poscraneal y de la región auditiva. A través del estudio de este material y su comparación con otros milodontinos, se pudo caracterizar esta especie tanto morfológicamente como morfométricamente y realizar una revisión de los taxones de perezosos milodontinos previamente reconocidos para el Neógeno del continente.

El amplio muestreo disponible de *Simomylodon uccasamamensis* del Altiplano boliviano ha permitido también reconocer una importante variación intraespecífica, sugiriendo la existencia de dimorfismo sexual, reconocible tanto en forma como en tamaño, en restos craneales y poscraneales. La presencia de dimorfismo sexual fue previamente propuesta para varias especies de perezosos extintos, y particularmente para los Mylodontinae, como una posible explicación de la variación intraespecífica observada. Análogamente, la presencia de dos distintos morfotipos, grácil y robusto, se observa en *Simomylodon uccasamamensis*, representando el registro más antiguo de dimorfismo sexual en perezosos fósiles. Los rasgos dimórficos están mayormente relacionados con la forma del hocico y el tamaño de los huesos largos, como el fémur y la tibia. Esto sugiere que el dimorfismo en *Simomylodon uccasamamensis* está relacionado con el tamaño general de los individuos, y probablemente esté asociado con dietas diferentes entre machos y hembras. Esto, a la vez, puede indicar una divergencia de nichos ecológicos, que permitiría un uso no competitivo de los recursos entre los dos sexos.

A la luz de la nueva información, un nuevo estudio filogenético de los Mylodontidae se ha realizado basándose en 286 caracteres cráneo-dentales y, por primera vez, 97 caracteres poscraneales, detectados en el esqueleto de 40 taxones. De esta manera, se pudo conducir un nuevo estudio basado en parsimonia de los Mylodontinae a nivel de especie, incluyendo taxones previamente no estudiados desde un punto de vista filogenético. Los resultados confirman la monofilia tanto de los Mylodontini como de los Lestodontini. Ambos grupos experimentaron independientes radiaciones adaptativas entre el Mioceno tardío y el Pleistoceno. El milodonte del Altiplano boliviano, *Simomylodon uccasamamensis*, se recupera entre los miembros más basales de los Mylodontini, representando actualmente el taxón más basal mejor representado de este grupo.

Con el objetivo de clarificar ulteriormente la historia evolutiva de los perezosos milodontes, fueron exploradas otras regiones anatómicas previamente desconocidas. Se han sumado avances en la comprensión de la anatomía de los milodontes con estudios de las cavidades endocraneanas, a través de tomografías computadas y reconstrucciones 3D, usando *Glossotherium robustum* del Pleistoceno de Argentina como taxón de referencia. De esta manera ha sido posible reconstruir y describir los primeros modelos digitales de la cavidad encefálica, los senos craneanos, el oído interno, los nervios craneanos y los principales vasos sanguíneos de un perezoso milodonte.

La forma del laberinto óseo del oído interno de los xenartros actuales muestra una fuerte señal filogenética, pero tras la inclusión de especímenes fósiles, la distribución de los individuos en el morfoespacio se aleja del patrón filogenético. Dado el escaso efecto de la alometría en el set de datos, se sugiere que aspectos funcionales puedan afectar sustancialmente la forma del oído interno de los xenartros.

Otras estructuras endocraneanas, como la cavidad encefálica, los nervios, los senos craneanos y los vasos sanguíneos, han sido reconstruidos digitalmente para *Glossotherium*, y comparados con los de los perezosos actuales *Bradypus* y *Choloepus*. Este estudio representa la primera caracterización exhaustiva de la anatomía endocraneana de un perezoso extinto. Un análisis cualitativo del aspecto de los modelos 3D reconstruidos a partir de tomografías computadas, sugiere la influencia de distintas señales filogenéticas, funcionales y alométricas que han contribuido a dar forma a estas estructuras.

TABLE OF CONTENTS

LIST OF FIGURES

Chapter 1
INTRODUCTION

1.1 HISTORICAL BACKGROUND

Among Folivora (Mammalia: Xenarthra), the mylodontids constitute a group of extinct "ground" sloths that appeared at the end of the Paleogene and progressively came to be distributed across the entire American continent over the course of the Cenozoic. These iconic mammals owe part of their fame to their eminent discoverer, Charles Robert Darwin (1809–1882), who found the first fossils of mylodontids during his famous travels on the HMS Beagle, between 1831 and 1836. These remains were recovered on the Atlantic coasts of Argentina and Uruguay, during the first two years of this travels, and subsequently were studied by the English naturalist Richard Owen (1804–1892). The first mylodontid species to be elevated was dedicated to his discoverer, and consequently named *Mylodon darwinii* Owen, 1839. In this same work, Owen also created the mylodontid genera *Glossotherium* and *Scelidotherium*. A larger non-mylodontid sloth, *Megatherium americanum* Cuvier, 1796 was previously studied by the French naturalist, George Cuvier (1769–1832).

Since these first steps of these renown naturalists, our understanding of the evolutionary history of extinct sloths has made impressive improvements. Among the most important scientists, including both foreigners and native South Americans, who made great advances during the XIX and XX centuries, I must mention Peter W. Lund (1801–1880), Richard Lydekker (1849–1915), Florentino Ameghino (1854–1911), Lucas Kraglievich (1886–1932), William B. Scott (1859–1947), Carlos de Paula Couto (1910–1982), Robert Hoffstetter (1908–1999), and George Gaylord Simpson (1902–1984). Their enormous production, together with the effort of many other scientists, allowed the depiction of a clearer scenario for the evolution of extinct South American endemic mammals.

Among these extinct animals, sloths exhibited a great amount taxonomic diversity and morphological variation, reaching at least 90 recognized genera (e.g., Mones 1986a; McKenna & Bell 1997) that displayed a great variety of dietary habits and locomotory modes (e.g., Bargo *et al.* 2006a, b; Bargo & Vizcaíno 2008; Pujos *et al.* 2012; Toledo 2016). They were extremely abundant, especially in Argentina, southern Brazil, and the USA, rather than in the tropics. However, this has long been attributed to biases, due to both the greater accessibility of fossil-bearing deposits (i.e., more open habitats) and the longer paleontological tradition in the countries that lie outside the tropical latitudes of the American continent (Pujos *et al.* 2012, 2017; Rincón *et al.* 2016). For this reason, central and northern areas of South America are considered by many authors as extremely promising for intensive investigations, with the aim of elucidating major aspects of the evolutionary history of extinct sloths (e.g., Carlini *et al.* 2006;

Pujos *et al.* 2012, 2017; Rincón *et al.* 2016). One of these promising areas is the central Andes, and more precisely most of the Plurinational State of Bolivia, which constitutes the heart of the South American continent.

Since the beginning of the 20th century, many paleontologists have worked in Bolivia, mainly in the Pleistocene deposits of the Tarija Valley in Southern Bolivia (e.g., Ameghino 1902, Boule & Thévenin 1920; Hoffstetter 1963; Takai 1982; MacFadden *et al.* 1983, 2013; Takai *et al.* 1984; Coltorti *et al.* 2007). Great efforts have also been made to investigate the early Paleocene deposits of Tiupampa (e.g., Muizon 1991; Gelfo *et al.* 2009), the late Oligocene site of Salla (e.g., Hoffstetter 1968; Shockey & Anaya 2008), and the middle Miocene deposits of Quebrada Honda (e.g., Hoffstetter 1977; Croft 2007; Pujos *et al.* 2011). The area of the Altiplano, however, occupies a large portion of eastern Bolivia, and its fossil richness is still poorly known. Paleontological exploration of this vast region benefited from pioneering work by Robert Hoffstetter (e.g., Hoffstetter 1968, 1977, 1986), Hoffstetter *et al.* (e.g., 1971a, 1971b, 1972), and colleagues (e.g., MacFadden *et al.* 1993; Saint-André 1994; Anaya & MacFadden 1995; Muizon 1999; Pujos *et al.* 2016). Pierre-Antoine Saint-André (IFEA, Institut Français d'Études Andines), together with Federico Anaya (MNHN-Bol, Museo Nacional de Historia Natural, La Paz, Bolivia) and other colleagues, conducted several campaigns in the Bolivian Altiplano in the 1990s, collecting numerous well-preserved fossils of vertebrates (almost exclusively mammals), part of them figured in Saint-André's PhD dissertation (Saint-André 1994) and subsequently formally published (e.g., Saint-André 1993, 1996; Saint-André & De Iuliis 2001; Saint-André *et al.* 2010). During the same period, the MNHN-Bol collaborated in excavations with several other foreign scientific institutions like the University of Florida and the Duke University (USA) and the Primate Institute of Kyoto (Japan). Since 2005, more than a dozen paleontological campaigns have been conducted in collaboration with CONICET (Consejo Nacional de Investigaciones Científicas y Tecnicas, Argentina) and later with the ISE-M of Montpellier (Institut des Sciences de l'Évolution, France). Some mylodontid remains discovered during the last three decades were described in published works (e.g., Saint-André 1994; Anaya & MacFadden 1995; Saint-André *et al.* 2010), yet many others have long remained undescribed and will be the subject of extensive study in the present work.

However, the realm of the latest discoveries on extinct sloths not only pertains to new and previously unexplored geographical regions of the American continent. Virtually unexplored morphologies also exist, such as the internal cavities of the fossilized skulls, whose digital reconstructions allow observation of anatomical features that had previously remained obscure. Novel techniques of CT scanning and digital reconstructions, in fact, enable non-destructive

access to the internal cranial features, thereby improving our knowledge of aspects of the evolutionary history of both extinct and extant vertebrates. The applications of these new techniques to xenarthrans (i.e., sloths, anteaters, armadillos and their extinct kin) started less than one decade ago, and are now undergoing a rapid increase (e.g., Billet *et al.* 2012, 2013, 2015a, 2017; Coutier *et al.* 2017; Amson *et al.* 2018). At the time that this thesis was started, *Megatherium* was the only extinct sloth whose endocranial anatomy had been analyzed using this methodology (Billet *et al.* 2013). CT-scanning techniques are here applied for the first time to the mylodontid *Glossotherium*, revealing the importance of the application of these techniques for elucidating the evolutionary history of this peculiar mammalian clade.

During the pleasing years that I lived in Mendoza, I had the opportunity to present some of the results of my studies, in collaboration with several co-authors, at both national and international conferences and in published scientific papers (e.g., Boscaini *et al.* 2018a, b; 2019a, b, c). For this reason, the reader will probably be already familiar with some of these results, yet many other are original to this comprehensive work.

1.2 THE STATE OF THE ART

1.2.1 Extant and extinct xenarthrans

Xenarthrans are among the most peculiar mammals of the endemic South American Cenozoic fauna (Simpson 1980). South America's period of isolation began in the late Paleocene, when its land connection with Antarctica was lost (Reguero *et al.* 2014), and ended with the formation of the Panamanian isthmus and connection with North America, around 2.8 Ma (Woodburne 2010, but see Montes *et al.* 2015). During the Paleogene and the Neogene, only some "sweepstakes" or "island hopping" interchanges took place, such as the middle Eocene and early Oligocene immigration of rodents and primates, respectively, from Africa (Antoine *et al.* 2012; Bond *et al.* 2015). Other migrations before the G.A.B.I. (Great American Biotic Interchange) were observed in the early Miocene (about 18 Ma, through the West Indies; MacPhee & Iturralde-Vinent 1994, 1995) and in the late Miocene (about 7 Ma, probably through Central America; Pascual 2006; McDonald & De Iuliis 2008).

The fossil record of xenarthrans begins in the early Eocene, with armadillos from the Itaboraí fauna (Itaboraian SALMA [South American Land Mammal Ages], southeastern Brazil; Bergqvist *et al.* 2004; Gelfo *et al.* 2009b) and continues throughout the Cenozoic, with

representatives of all three major groups of Xenarthra persisting to the present: Cingulata (armadillos; also including extinct glyptodonts and pampatheres), Vermilingua (anteaters), and Folivora (sloths) (e.g., Engelmann 1985; Gaudin 2004). The oldest representatives of these clades date back to the early Eocene, the early Miocene, and the late Eocene, respectively (Gaudin & Croft 2015). Following the latest calibrations of molecular (DNA) data, Cingulata, Vermilingua and Folivora respectively diverged in the early Eocene, the middle Eocene and the late Oligocene (Delsuc *et al.* 2018).

1.2.2 Extant and extinct sloths

Extant sloths (Folivora = Tardigrada = Phyllophaga; Delsuc *et al.* 2001; Fariña & Vizcaíno 2003) are represented by the genera *Bradypus* and *Choloepus*, ecologically and geographically restricted to tropical rain forests of South and Central America (Fig. 1.1; Hayssen 2010, 2011). However, the fossil record of sloths extends geographically throughout the Americas, and ranges chronologically from the late Eocene to the late Pleistocene/Holocene (e.g., Gaudin & Croft 2015; Pujos *et al.* 2017). Over their long history, extinct sloths have occupied a great number of ecological niches, as demonstrated by their marked variability in locomotory modes (with facultative bipeds, obligate quadrupeds, arboreal and semi-arboreal taxa, and even some swimming taxa; Pujos *et al.* 2012; Toledo 2016) and in dietary habits (with browsers, grazers, and mixed feeders; Bargo *et al.* 2006a, b; Bargo & Vizcaíno 2008). By contrast, extant sloths are only represented by the two genera *Bradypus* and *Choloepus*, and are almost exclusively arboreal and folivorous animals. Their peculiar upside-down posture and suspensory behavior were independently acquired in both lineages, and considered one of the most striking examples of convergence among mammals (Gaudin 1995, 2004; Nyakatura 2012; Pujos *et al.* 2012, 2017).

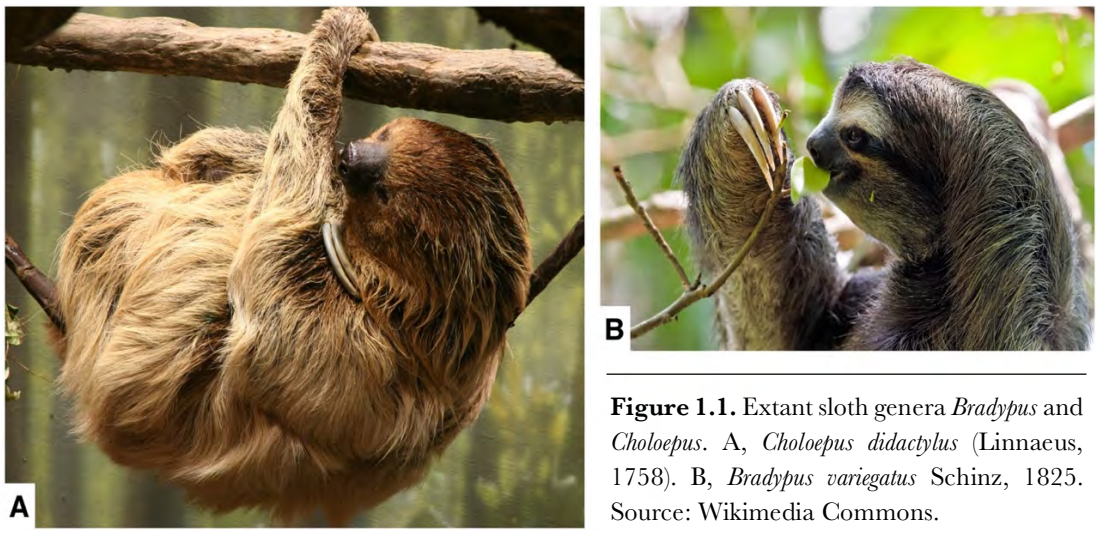

Figure 1.1. Extant sloth genera *Bradypus* and *Choloepus*. A, *Choloepus didactylus* (Linnaeus, 1758). B, *Bradypus variegatus* Schinz, 1825. Source: Wikimedia Commons.

The diphyletic origin of the two extant sloth genera is henceforth accepted (e.g., Engelmann 1985; Delsuc *et al.* 2001; Gaudin 2004; Pujos *et al.* 2017; Delsuc *et al.* 2019; Presslee *et al.* 2019), and recent phylogenetic analyses based on osteological characters (i.e., Gaudin 1995, 2004) consider *Bradypus* the sole representative of Bradypodidae and the sister taxon of the other sloths, and *Choloepus* as the only living member of Megalonychidae (Fig. 1.2).

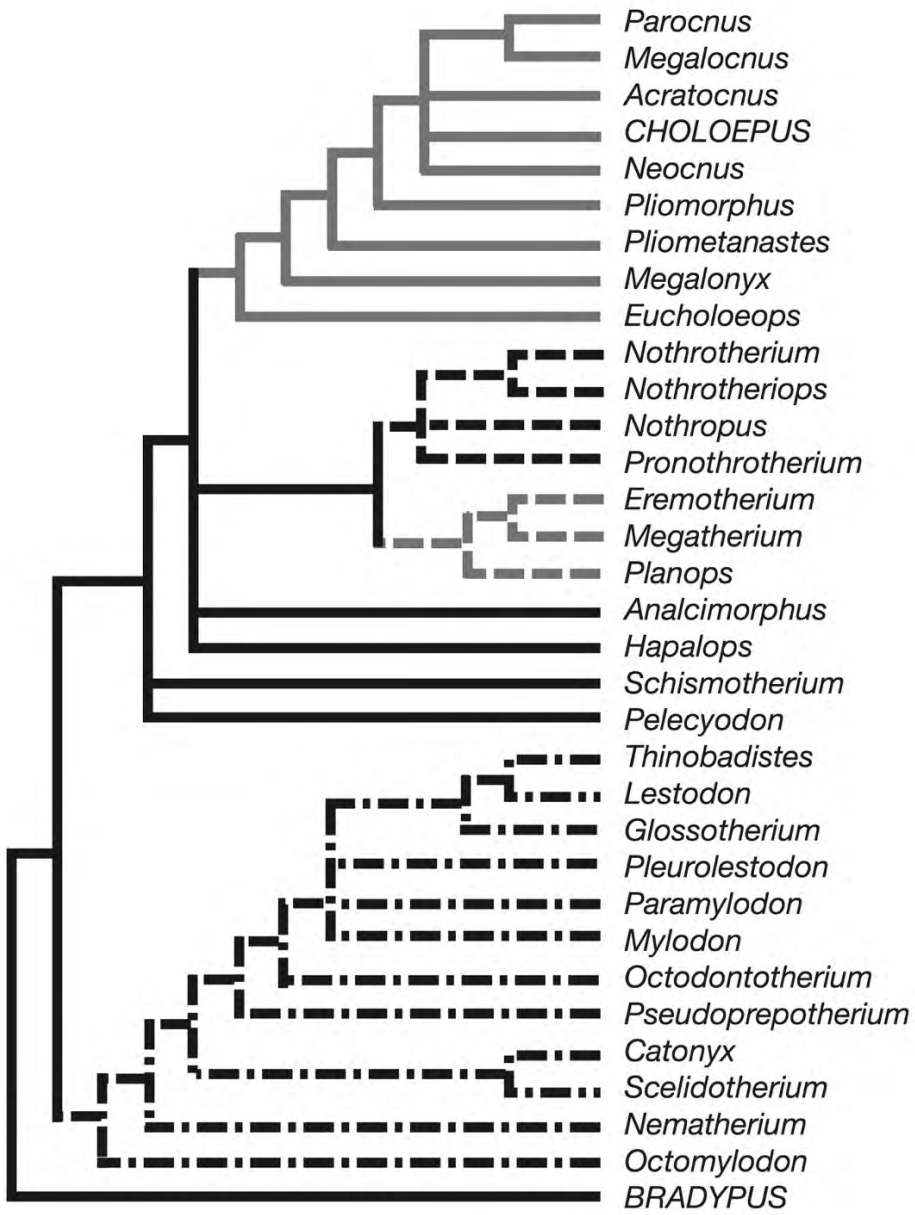

Figure 1.2. Phylogeny of Folivora following Gaudin (2004). This tree represents a strict consensus of all MPT obtained in Gaudin (2004) under various weighting and outgroup schemes, and is based on PAUP analysis of 286 craniodental characters, including the 85 auditory region characters from Gaudin (1995), in 33 extinct and extant sloth genera. Extant taxa are written in all-capital letters. The clade illustrated with dark grey lines represents the family Megalonychidae. The clade illustrated with single-dashed black lines represents the family Nothrotheriidae; that with single-dashed dark grey lines the family Megatheriidae; that with double-dashed black lines the family Mylodontidae. Modified from Gaudin (2004).

Even if the exact phylogenetic position of the extant sloths is still highly debated, the diphyly of the two genera is confirmed by several studies, based on both morphological and molecular evidence (e.g., Gaudin 1995, 2004; Greenwood *et al.* 2001; Clack *et al.* 2012; Slater *et al.* 2016; but see Buckley *et al.* 2015; Delsuc *et al*. 2019; Presslee *et al*. 2019). The other three major extinct sloth clades, traditionally considered as families (Fig. 1.2), are the Nothrotheriidae, the Megatheriidae, and the Mylodontidae (e.g., Engelmann 1985; Gaudin 2004; McDonald & De Iuliis 2008), but their relationships are still debated (e.g., Gaudin 2004; Slater *et al.* 2016; Delsuc *et al*. 2019; Presslee *et al*. 2019). The peculiar "glypto-sloth" *Pseudoglyptodon* (Oligocene and probably also late Eocene; McKenna *et al*. 2006) is the oldest and perhaps most primitive sloth, but it has not been assigned to any of the families mentioned above (Varela *et al.* 2018).

1.2.3 Fossil record of Mylodontinae

The mylodontids and megalonychids are the first groups of sloths to radiate in South America during the late Oligocene, and both are represented by isolated remains (e.g., Pujos & De Iuliis, 2007; McDonald & De Iuliis, 2008; Shockey & Anaya, 2011; Gaudin & Croft, 2015). These fossils, considered to be the earliest unquestionable representatives of South American folivorans (McDonald & De Iuliis 2008) are included in the genera *Deseadognathus* (the only megalonychid; La Flecha, Patagonia Argentina; Carlini & Scillato-Yané 1994), *Orophodon*, *Octodontotherium* (La Flecha, Patagonia Argentina; Hoffstetter 1956) and *Paroctodontotherium* (Salla Beds, Bolivia; Shockey & Anaya 2011). Originally, Ameghino (1894) placed *Octodontotherium* among Mylodontidae, but subsequently regarded *Octodontotherium* and *Orophodon* as members of an "orophodontid" group, considered to be an early independent offshoot in the evolutionary history of Folivora (Ameghino 1897). This approach was followed by several authors (e.g., Hoffstetter 1956; Pujos & De Iuliis 2007) but the latest findings and phylogenetic analyses suggest that *Octodontotherium* and *Paroctodontotherium* should be considered as members of Mylodontinae (e.g., Gaudin 2004; Shockey & Anaya 2011). According to Gaudin (2004), *Octomylodon* from the late Miocene of Buenos Aires Province (Argentina; Scillato-Yané 1977) is the most basal mylodontid sloth, and *Nematherium* from the early Miocene of Santa Cruz Province (Argentina; Scott 1903-1904) has more derived features. The latter taxon is recovered outside the Scelidotheriinae, a major mylodontid clade considered as the sister group of Mylodontinae (McDonald 1987; Gaudin 2004). Following Gaudin (2004), *Pseudoprepotherium* from the middle Miocene Colombian locality of La Venta (Laventan SALMA; Hirschfeld 1985; Flynn & Swisher 1995) is the most basal mylodontine, and *Octodontotherium* is one node more

derived. The other Mylodontinae included in the comprehensive phylogenetic analysis performed by Gaudin (2004) are *Pleurolestodon*, from the late Miocene of Argentina, and the more widespread Pleistocene genera *Mylodon* and *Glossotherium* from South America, and *Paramylodon* from North America (Fig. 1.2). According to Gaudin (2004), *Lestodon* (Pliocene and Pleistocene of South America; Deschamps *et al.* 2001; Czerwonogora & Fariña 2013) and *Thinobadistes* (late Miocene of North America; Webb 1989) form a derived subgroup of Mylodontinae, comprising the tribe Lestodontini (Fig. 1.2).

It is in the Miocene that mylodontines spread all over South America, also reaching North America, in the case of *Thinobadistes*, well prior to the stable formation of the Panamanian Isthmus (Webb 1989; Woodburne 2010).

Even though mylodontines range from South to North America, their Neogene fossil record is quite scarce and the poor quality of the craniodental remains has often discouraged their inclusion in updated phylogenetic analyses. The Miocene mylodontines that preserve a significant number of craniodental features are *Glossotheriopsis pascuali* Scillato-Yané, 1976, from the Friasian, Colloncuran and Laventan SALMAs of Argentina and Colombia (middle Miocene; Scillato-Yané 1976; McDonald 1997) and *Pleurolestodon acutidens* Rovereto, 1914, from the Huayquerian SALMA of Argentina (late Miocene; Rovereto 1914). In his pioneering work, Rovereto (1914) described three *Pleurolestodon* species that were later synonymized by Kraglievich (1921a) and Saint-André *et al.* (2010) under the single species *P. acutidens*. The latter authors also established the new species *Pleurolestodon dalenzae* Saint-André *et al.*, 2010, on the basis of a single well-preserved skull discovered in the latest Miocene or earliest Pliocene deposits of the Choquecota locality (Oruro Department, Bolivia; Saint-André *et al.* 2010). In this work, the authors also defined the new genus and species *Simomylodon uccasamamensis* Saint-André *et al.*, 2010 from the Pliocene deposits of Ayo Ayo-Viscachani and Pomata-Ayte localities (La Paz and Oruro Departments, respectively, Bolivia; Saint-André *et al.* 2010). In the Pliocene, *Glossotheridium chapadmalense* (Kraglievich 1925) is well represented in the Chapadmalalan SALMA of Argentina (Kraglievich 1925; Cattoi 1966). Remains tentatively assigned to the latter taxon were also identified in North America (Robertson 1976) and Bolivia (Anaya & MacFadden 1995). However, the specimens from North America (including some scanty remains from Mexico) are now assigned to *Paramylodon garbanii* (Montellano-Ballesteros & Carranza-Castañeda 1986; Morgan 2008; McDonald & Morgan 2011). During the Pliocene, mylodontid terrestrial sloths were widely spread in the Americas and diversified into a large number of mainly quadrupedal and grazing/browsing genera that persisted until the late Pleistocene/earliest Holocene periods (Pujos *et al.* 2012, 2017; Gaudin & Croft 2015; Slater *et*

al. 2016). As recent discoveries testify, early members of the clade occupied the central and northern areas of South America in the late Oligocene–early Miocene period (Shockey & Anaya 2011; Rincón *et al.* 2016). This suggests that attention should be paid to these poorly known areas of South America, in order to better elucidate the evolutionary history of mylodontid sloths (Pujos *et al.* 2012, 2017).

The aim of Chapter 6 is to present descriptions of many previously unpublished remains assignable to the extinct sloth *Simomylodon uccasamamensis*, providing new data on its morphological variability and new insights into the anatomy and paleobiogeography of this Andean mylodontid species.

1.2.4 Intraspecific variation of mylodontines

In a recent compendium on the current methodology employed in sloth taxonomy, De Iuliis (2018) argued that special attention should be paid to the study of intraspecific variation in extinct sloth species. In fact, even today there is still a strong typological practice that tends to emphasize minor differences in detail or size to justify the erection of new species (De Iuliis 2018), often neglecting the dramatic intraspecific variability that is known to have characterized many extinct sloth lineages (e.g., Lydekker 1894; McDonald 2006; Prothero & Raymond 2008). Nowadays, one of the most commonly advocated explanations for the high level of intraspecific variation in many extinct sloth species is sexual dimorphism, here abbreviated as "SD."

For extinct sloths, the presence of SD was first proposed more than a century ago by Lydekker (1894). The latter author suggested the presence of a gracile (female) and a robust (male) morph in the late Pleistocene South American species "*Mylodon*" (= *Glossotherium*) *robustum* (Owen, 1842) on the basis of differences in cranial morphology, and particularly in the shape of the rostrum. However, with the exception of brief mentions of the possible presence of SD in the small megalonychids *Eucholoeops* (early Miocene; Argentine Patagonia) and *Acratocnus* (late Pleistocene; Greater Antilles) (Scott 1903-1904; Anthony 1919; Paula Couto 1967), this topic was ignored in extinct sloths for most of the twentieth century. Moreover, in a subsequent revision of the aforementioned gracile and robust morphotypes of Lydekker (1894), these remains were assigned to distinct species, i.e., *Glossotherium lettsomi* (Gervais & Ameghino, 1880) and *G. robustum*, respectively (Cabrera 1936).

Beginning in the 1980s, dimorphism in "ground" sloths began to be actively investigated once more. Multiple specimens of the giant Pleistocene megatheriid *Eremotherium laurillardi* (Lund, 1842) from a single Brazilian locality were the first extinct sloths to be analysed

for dimorphic traits, revealing differences in postcranial elements and in the skull, mainly related to relative robustness and the morphology exhibited by the sagittal crest and temporal lines (Cartelle & Bohórquez 1982; Cartelle & De Iuliis 1995, 2006; De Iuliis & Cartelle 1999). In a later revision of the genus *Eucholoeops*, SD appeared to be doubtful in this Santacrucian megalonychid, but could not be adequately tested with the available sample (De Iuliis *et al.* 2014). For megatherioid sloths, the possible presence of sexual dimorphism was also mentioned for *Thalassocnus* (late Miocene–Pliocene; coasts of Peru and Northern Chile), and was recently proposed for *Proeremotherium* (late Pliocene; Northwestern Venezuela) (Muizon *et al*. 2003, 2004; Amson *et al*. 2015a, b; Carlini *et al*. 2018). Claims for sexual dimorphism in Pleistocene scelidotherine sloths were made on the basis of the morphology of the dorsal skull crests (Miño-Boilini & Zurita 2015). However, the most exhaustive study of sexual dimorphism in an extinct sloth was McDonald's (2006) analysis of the North-American mylodontine species *Paramylodon harlani* (Owen, 1839), based on the large sample from the Rancho La Brea tar pits (late Pleistocene, Los Angeles, USA). In the latter taxon, sexual dimorphism was established based on features previously interpreted as indicating the presence of two different subspecies: *P. harlani harlani* and *P. harlani tenuiceps* (Stock 1917, 1925; McDonald 2006). In *P. harlani*, no consistent bimodal size differences have been detected (McDonald 2006; Prothero & Raymond 2008). The main differences observed between the two morphs of *P. harlani* pertain to the general robustness of the skull, with the robust form having greater transverse cranial dimensions (especially for the muzzle) compared to skull length, relative to the gracile form (McDonald 2006). In lateral view, the robust morph also has a more vertically orientated occiput than the gracile morph, so that occipital condyles project less far posteriorly than in gracile specimens (McDonald 2006). Other differences are indicated in the shape of the upper caniniforms, which vary in robustness and in the inclination of their wear surfaces (McDonald 2006). Robust and gracile morphotypes have been also observed in a recently described species of the genus *Glossotherium* from the Pleistocene of Brazil (i.e., *G. phoenesis* Cartelle *et al.,* 2019).

The intraspecific variation of the latest Miocene–late Pliocene sloth species *Simomylodon uccasamamensis* is stressed in Chapter 6, and specifically investigated in the light of the possible presence of sexual dimorphism in Chapter 7. Moreover, intraspecific variation is taken into account for character coding in Chapter 8, but also in Chapters 9 and 10, in the study of the bony labyrinth and the endocranial cavities of the Pleistocene mylodontine *Glossotherium*, representing a sort of *leitmotiv* for this entire work.

1.2.5 Phylogenetic studies of Mylodontinae

As previously stated, among Folivora five monophyletic clades are commonly recognized and traditionally considered as families: Mylodontidae, Megalonychidae, Nothrotheriidae, Megatheriidae, and Bradypodidae (e.g., Gaudin 2004; McDonald & De Iuliis 2008; Slater *et al.* 2016). Three Mylodontidae subfamilies are recognized by most authors: Mylodontinae, Lestodontinae and Scelidotheriinae (see Pitana *et al.* 2013 and references therein). Additionally, the subfamilies Octomylodontinae, Nematheriinae, and Urumacotheriinae are considered valid by some authors (e.g., Scillato-Yané 1977; Rinderknecht *et al.* 2010; Pitana *et al.* 2013), but their monophyly has never been demonstrated.

A preliminary but pioneering study of the relationships among mylodontid sloths was conducted by Saint-André (1994), based on 16 taxa and 25 characters (18 craniodental and 7 of postcranial). However, the first comprehensive parsimony-based phylogenetic analysis of sloth relationships, including the extant representatives and the main extinct folivoran groups, is that of Gaudin (1995), which analyzed 85 features in 21 taxa. In this study, based on characters of the basicranium and the ear region, Mylodontidae appears to be a monophyletic clade, with a major dichotomy separating the Scelidotheriinae from Mylodontinae (mylodontines plus lestodontines), a result that is maintained in all the other subsequent studies of mylodontid phylogeny. Esteban (1996) analyzed a matrix composed by 13 mylodontid taxa and 50 features: of them, 45 are craniodental and only 5 are postcranial. Subsequently, Gaudin (2004) included 201 characters from the skull, mandible and dentition, reaching a total of 286 features observed in 33 sloth taxa. The latter author incorporated previous observations (e.g., Engelmann 1985; Webb 1985, 1989; Patterson *et al.* 1992; Gaudin 1995) into a single matrix, but did not include postcranial characters.

Some postcranial remains of mylodontid sloths were codified in other works, such as Pujos *et al.* (2007), who included 17 postcranial features observed in all the major folivoran clades. McDonald & Perea (2002) and Miño-Boilini (2012) codified 4 and 8 postcranial features for 10 and 12 scelidotherine taxa, respectively. Mylodontid femora and tibiae were codified for 24 characters observed in several sloth lineages by Rincón *et al.* (2015). Recently, Haro *et al.* (2016, 2107) made observations on the forelimb of *Mylodon darwinii*, extending them to other taxa, using information taken from the literature. Some of these studies using postcranial features were recently included in an enlarged matrix built by Varela *et al.* (2018) with the aim of exploring sloth relationships using Bayesian methods. Finally, Boscaini *et al.* (2019a) and Cartelle *et al.* (2019) analyzed the phylogenetic positions of *Simomylodon uccasamamensis* and

Glossotherium phoenesis, respectively, performing phylogenetic analyses largely based on the craniodental dataset of Gaudin (2004).

As noted above, all the aforementioned studies that explore the evolutionary relationships among mylodontid sloths agree on the presence of an early split between Scelidotheriinae and Mylodontinae. However, these studies show general disagreement in the relationships inside Mylodontinae, with different scenarios depicted for the relationships among mylodontine and lestodontine sloths. Early phylogenetic hypotheses, such as those of Engelmann (1985) and Webb (1989), ally the lestodontines (*Lestodon* and *Thinobadistes*) to a clade including *Mylodon* and *Glossotherium*. However, the hypothesis of Engelmann (1985) considers *Lestodon* and *Thinobadistes* to be paraphyletic, whereas Webb (1989) considers the latter genera to represent a monophyletic group. The hypothesis of Webb (1989) was later corroborated by Saint-André (1994).

This idea is not confirmed in subsequent phylogenetic studies based mainly on craniodental features, such as those of Gaudin (1995, 2004), Esteban (1996) and Boscaini *et al.* (2019a). In these studies, lestodontines are considered the most derived subgroup of Mylodontinae, thus constituting the tribe Lestodontini (*sensu* Gaudin 2004). However, this result is not reflected in other recent studies (Haro *et al.* 2016, 2017; Varela *et al.* 2018; Cartelle *et al.* 2019). In Haro *et al.* (2016, 2017) Lestodontini is not even retrieved as a monophyletic group, a probable consequence of the lack of phylogenetic signal of their matrix, the analysis of which provides an extremely high number of most parsimonious trees (MPTs). In Varela *et al.* (2018) and Cartelle *et al.* (2019), Lestodontini constitutes a monophyletic group, but does not represent the most derived mylodontid clade as in Gaudin (1995, 2004), Esteban (1996), and Boscaini *et al.* (2019a). Varela *et al.* (2018) position the lestodontine sloths as the sister group of a clade that includes *Pleurolestodon*, *Simomylodon*, *Glossotherium*, and *Paramylodon*, with *Mylodon* as an external taxon to this clade and the lestodontines. A similar result is obtained by Cartelle *et al.* (2019), suggesting that the lestodontines could occupy a different position than that observed in previous phylogenetic studies (Gaudin 1995, 2004; Esteban 1996; Boscaini *et al.* 2019a).

A comprehensive study of postcranial remains in the family Mylodontidae, with the aim of elucidating the relationships among the mylodontine and lestodontine sloths at the species level, is treated in Chapter 8.

1.2.6 Ear region anatomy in mylodontid sloths

In order to reconstruct the phylogeny of extinct xenarthrans, it is necessary to explore in detail the cranial anatomy, and in particular their auditory region. From a morphological point of view, the ear region of extinct sloths has proved to be an important source of information, providing diagnostic features which have been useful in clarifying phylogenetic relationships (e.g., Patterson *et al.* 1992; Gaudin 1995, 2004). Indeed, De Iuliis (2018) has recently drawn attention to both the importance of the ear region in this regard, and the need for increased rigor in treating this region in descriptions of new xenarthran taxa. Detailed anatomical analyses of this skull region date back to the first descriptions of sloth fossil specimens in the 19th century (e.g., Owen 1842), but have become more prevalent during the last few decades (e.g., Patterson *et al.* 1992; Gaudin 1995, 2011; De Iuliis *et al.* 2011; Gaudin *et al.* 2015). For this reason, this anatomical area is treated extensively in Chapter 6 for *Simomylodon uccasamamensis*, and coded in the extended matrix for the phylogenetic analyses (Chapter 8).

Besides phylogeny, the bony anatomy of the ear region has also been useful in revealing some aspects of the palaeobiology of Pleistocene ground sloths, such as their hearing capabilities. For example, based on the area of the ectotympanic and the form of the middle ear ossicles, Blanco & Rinderknecht (2008, 2012) suggested that giant mylodontid sloths such as *Glossotherium* and *Lestodon* were particularly sensitive to low-frequency sounds.

Studies on the inner ear of extinct xenarthrans are limited, but important advances have been made in the last few years. The only bony labyrinth of an extinct sloth described before the present thesis project is that of *Megatherium,* which shows a peculiar morphology, very different from those of extant sloths and more similar to that of the extant armadillos and anteaters (Billet *et al.* 2013). Billet *et al.* (2015a), in an extended database, studied the effect of allometry and the phylogenetic information contained in the morphology of the xenarthran inner ear (mostly extant taxa), using morphometric analyses based on 3D landmarks data. Finally, Coutier *et al.* (2017) analyzed and discussed a possible relationship between the orientation of the lateral semicircular canal and the usual position of the head in their sample of xenarthrans, which included the extinct sloths *Megatherium* and *Pelecyodon*.

In fact, the morphology of this particular anatomical region is strongly influenced by both phylogeny and function (Ekdale 2013, 2016). The cochlea is strictly related to the sense of hearing, whereas the vestibule and the semicircular canals are associated with the sense of balance and equilibrium (Ekdale 2016). In recent years, several aspects of the shape, size, and orientation of the bony labyrinth in mammals have been linked to physiological features. For

instance, the size of the semicircular canals correlates with body mass and agility categories (Spoor *et al.* 2007; Silcox *et al.* 2009). In addition, the angles among the semicircular canals have been associated with vestibular sensitivity (Malinzak *et al.* 2012; Berlin *et al.* 2013), and the shape of the cochlea with lower frequency hearing limits (Manoussaki *et al.* 2008).

These analyses have also been tentatively applied to extinct animals, with the aim of inferring functional aspects from inner ear morphology (e.g., Orliac *et al.* 2012; Macrini *et al.* 2013; Ekdale & Racicot 2015). However, these methodologies have also been criticized by several authors, who found the proposed methods partly unreliable or difficult to replicate (e.g., David *et al.* 2010, 2016; Billet *et al.* 2013; Danilo *et al.* 2015; Orliac & O'Leary 2016; Perier *et al.* 2016; Ruf *et al.* 2016).

The first digital reconstructions of a mylodontid bony labyrinth are treated for *Glossotherium robustum* (Fig. 1.3) in Chapter 9. The shape of the bony labyrinth of this species is compared with the available xenarthran dataset, in order to discuss phylogenetic and allometric aspects of this peculiar anatomical region in sloths, and is complemented by a discussion of its possible functional attributes.

1.2.7 Digital endocasts of extinct sloths

Another potential source of information that could be extremely informative for morphology-based phylogenetic analyses can be recovered from the anatomy of internal cranial structures, such as the brain cavity, paranasal sinuses and the trajectory of canals and grooves for nerves and blood vessels.

Nevertheless, to date, digital endocranial reconstructions are unknown in any extinct or extant sloth. Traditional studies of the encephalic cavity of extinct sloths, and the neuroanatomy of the brains of living sloths, date back to the nineteenth century (e.g., Gervais 1869; Elliot-Smith 1898). Additional descriptive works on the anatomy of the internal encephalic cavity of extinct sloths were conducted by Colette Dechaseaux in the mid-twentieth century (i.e., Dechaseaux 1958, 1962a, b, 1971). This author described and figured many genera, such as *Glossotherium*, *Hapalops, Lestodon, Megatherium*, and *Oreomylodon*, based on plaster casts of the brain cavity, the most commonly employed technique at that time. Following the same methodology, Dozo (1987, 1994) studied the early Miocene forms *Eucholoeops* and *Hapalops* from Santacrucian SALMA deposits.

At present, only limited information is available on the paranasal pneumaticity in xenarthrans, and exhaustive studies are restricted to two cingulates: the extant genus *Dasypus*

(Billet *et al.* 2017) and the peculiar extinct glyptodont *Neosclerocalyptus* (Fernicola *et al.* 2012). The most detailed study on sinuses in anteaters is that of Storch & Habersetzer (1991). The morphology of the frontal sinuses in extant sloths was briefly mentioned by Moore (1981), Langworthy (1935), and Goffart (1971) for *Choloepus,* and illustrated for *Bradypus* and *Choloepus* by Naples (1982) using radiographs. In extinct sloths, some annotations on the development of frontal and sphenoidal sinuses are made in Dechaseaux (1971) and McDonald *et al.* (2013), concerning the mylodontid *Oreomylodon* and the megalonychid *Megistonyx*, respectively. Pterygoid and epitympanic sinuses in the squamosal are described by Patterson *et al.* (1992) for several extinct sloths. These authors noted the remarkable pneumatization of the skull in the large Pleistocene Antillean sloth *Megalocnus*. Inflation of the pterygoid and frontal bones was codified as characters 137 and 174 by Gaudin (2004), also coinciding with the matrix employed in this thesis.

The aim of Chapter 10 is to provide the first digital reconstruction of a mylodontine sloth's endocranial spaces, with preliminary discussions on their possible phylogenetic, allometric, and functional value. Particular emphasis is placed on the brain cavity, along with the cranial nerves, the intracranial vasculature, and the pneumatized structures of the cranium, to provide an anatomical characterization of the main features, alongside comprehensive comparisons with the available literature (Gervais 1869; Dechaseaux 1958, 1962a, b, 1971; Dozo 1987, 1994). However, due to a paucity of data on these features in extinct sloths, the structures in *Glossotherium* will primarily be compared with their homologues in the extant forms *Bradypus* and *Choloepus*.

Figure 1.3. Reconstruction of the extinct sloth *Glossotherium robustum* from the Pleistocene of Argentina. Credits: D. Bonadonna.

Chapter 2
RESEARCH OBJECTIVES AND HYPOTHESES

2.1 GENERAL OBJECTIVE

There are several aspects of the evolutionary history of Mylodontidae that remain currently unresolved. These are in part related to the limited fossil specimens available in the tropical latitudes in comparison with the austral ones, the lack of attention paid to the intraspecific variation of folivoran extinct species. Moreover, novel digital imaging techniques allow to observe anatomical regions previously inaccessible and have the potential of shedding new light on the evolutionary history of Mylodontidae.

The general objective of this thesis is therefore the resolution of several open problems regarding the evolutionary history of Mylodontidae, and especially related to Neogene and Pleistocene forms from both South and North America. The main objective is to provide further insights into the anatomy, taxonomy, phylogeny, intraspecific variation, and paleoneurology of mylodontid sloths, and increasing our comprehension of folivorans' evolution from a multidisciplinary standpoint.

2.2 SPECIFIC OBJECTIVES

2.2.1 Geography and geology

A first goal is to produce an overview and update of the available data on both the geography and the geology of Bolivian localities from which mylodontid remains have been recovered during the last decades (i.e., the late Miocene–Pliocene localities of Choquecota, Casira, Pomata-Ayte, Inchasi, and Ayo Ayo-Viscachani, belonging to the Rosa Pata and Umala Formations). This section is conducted mainly through a review of the related literature, but also introducing some *in situ* observations and novel data achieved by colleagues, especially on absolute dates obtained from volcanic ashes.

2.2.2 Systematic revision of Mylodontinae

A second objective is to realize a detailed study of the fossil material of mylodontines from Bolivia, and compare them with coeval late Miocene–Pliocene taxa from both South and North America. However, older and younger Mylodontidae are also taken into account for the purpose of comparison. Consequently, several museum collections have been visited, to obtain

photos and measurements of all these taxa, and a detailed bibliographic review is conducted with the main objective of confirming the validity and the taxonomic assignment of mylodontid species previously described in the literature.

2.2.3 Anatomical studies of mylodontids from the Bolivian Altiplano

The new and unpublished fossil skeletal material of mylodontids from the Bolivian Altiplano allow to conduct detailed descriptions of the most diagnostic anatomical areas, including craniodental features, with special emphasis on the ear region, and postcranial elements. Descriptions and comparisons are mainly centered on *Simomylodon uccasamamensis*, which constitutes the most abundant mylodontid taxon from the Neogene of the Bolivian Altiplano. Also, the presence of several homologous skeletal elements from multiple individuals offers the unique opportunity to consider and critically discuss the intraspecific variation of the latter taxon. This allows to evaluate the presence of well-defined morphs, and ultimately consider whether they are the product of different ontogenetic stages, geographically- and/or chronologically-related morphotypes or sexual dimorphism.

2.2.4 Reappraisal of the phylogeny of Mylodontidae

Another goal of the present thesis is to conduct a new and more complete phylogenetic study of Mylodontidae, with special emphasis on the relationships among Mylodontinae. This analysis is conducted after coding features on the entire skeleton and, for Mylodontinae, considering taxa at the specific level, again taking into account the presence of intraspecific variation. To date, the latter three approaches have not been incorporated in phylogenetic studies of mylodontid sloths. The main objectives of this portion of the study are: testing the phylogenetic affinities of several poorly known Mylodontinae, and shedding new light on the strongly debated relationships among the members of Mylodontini and Lestodontini.

2.2.5 Digital endocasts of Mylodontinae

The last objective of the present thesis is the acquisition of the first 3D models of the endocranial cavities of a mylodontid sloth, such as the bony labyrinth of the inner ear, the brain cavity, the paranasal sinuses, and the canals and grooves for the nerves and blood vessels. These structures, in fact, have the potential of being highly phylogenetically-informative, but also of

carrying other kinds of paleobiological information. Given that these anatomical regions are still unexplored for mylodontid sloths, the reference taxon (i.e., *Glossotherium robustum*), is compared with the extant sloth representatives, with the aim of revealing the possible phylogenetic, allometric and functional effects that converge in shaping these structures.

2.3 HYPOTHESES

2.3.1 Geography and geology

New paleontological excavations in the late Miocene–Pliocene localities of the Bolivian Altiplano can provide further materials of extinct sloths, with the capacity to increase the number and diversity of fossil remains to be studied. Moreover, observations in the field and new analyses of the volcanic ashes, can allow for refinements of our estimated ages for the deposits considered in this study.

2.3.2 Systematic revision of Mylodontinae

The diversity of the poorly known mylodontids from the Bolivian Altiplano may currently be overestimated. In fact, once the mylodontid remains from the Bolivian Altiplano have been studied both qualitatively and quantitatively, and compared with those of other coeval localities from both South and North America, it is possible that some species will be synonymized. The enriched fossil record of *Simomylodon uccasamamensis* will help in defining other poorly known Neogene mylodontids, and clarifying some dubious taxonomic attributions at a larger geographical scale. For example, it is highly improbable that the South American species *Glossotheridium chapadmalense* (Kraglievich, 1925) had a Pan-American distribution during the Pliocene epoch, as suggested by Robertson (1976) and Anaya & MacFadden (1995).

2.3.3 Anatomical studies of mylodontids from the Bolivian Altiplano

Abundant new and undescribed fossil skeletal remains of *S. uccasamamensis* from the Bolivian Altiplano will extend our knowledge on the anatomy of the Neogene Mylodontinae, especially in relation to the skull, dentition, ear region, and postcranial elements. Also, the study of the intraspecific variation of several homologous elements from multiple individuals of the same

species will shed light on of the intraspecific variation of this Andean mylodontid species. It will be possible to evaluate the existence of two morphotypes of *S. uccasamamensis* (i.e., gracile and robust), as observed in other Pleistocene mylodontid species (e.g., *Paramylodon*; see McDonald, 2006), suggesting the presence of sexual dimorphism. If this is the case, *S. uccasamamensis* would represent the oldest sexually dimorphic sloths, and as such, would provide the opportunity to infer the possible evolutionary implications of the emergence of sexual dimorphism in the clade.

2.3.4 Reappraisal of the phylogeny of Mylodontidae

The addition of a substantial number of postcranial characters to the matrix built by Gaudin (2004), will permit a codification of the entire skeleton of extinct mylodontids and may thus help to clarify previously unresolved phylogenetic relationships. This will also allow to more reliably test the phylogenetic position of some taxa, with special attention paid to species from tropical latitudes of South America, but may also call into question some commonly accepted phylogenetic hypotheses. The inclusion of postcranial characters will help to resolve the controversies regarding the phylogenetic relationships among Mylodontidae, such as the validity and the problematic placement of both Lestodontini and Mylodontini.

2.3.5 Digital endocasts of Mylodontinae

The production of the first digital, three-dimensional models of the endocranial cavities of the mylodontid sloth *Glossotherium robustum*, and their comparison with the extant sloth taxa *Bradypus* and *Choloepus*, represents the first effort to study these anatomical regions among folivorans. It will be possible, for example, to characterize the anatomy of several internal regions of the skull, such as the brain cavity, the inner ear, the paranasal sinuses, and the main cranial nerves, arteries, and veins.

Phylogeny, allometry, and functional factors probably act in different ways to shape these structures. For example, the inner ear is directly related to locomotion and hearing abilities, and its shape and size is probably strongly affected by functional constraints. In contrast, because the function of paranasal sinuses (if present) is still poorly known in mammals, explanations for variation in these structures will need to rely more heavily on phylogeny and general body size.

Chapter 3
MATERIALS AND METHODS

3.1 *SIMOMYLODON UCCASAMAMENSIS*: DESCRIPTIONS AND COMPARISONS OF THE NEW REMAINS (Chapter 6)

3.1.1 Remains examined and comparative sample

The remains of *Simomylodon uccasamamensis* presented here are housed in the MNHN-Bol of La Paz (Museo Nacional de Historia Natural, Plurinational State of Bolivia) and in the MNHN (Muséum national d'Histoire naturelle, Paris, France). The unpublished fossils consist of several well-preserved craniodental and postcranial remains that, in addition to the remains previously presented by Saint-André (1994) and Saint-André *et al.* (2010), considerably extend our knowledge of the morphology and the intraspecific variation of this poorly known extinct mylodontid sloth (a complete list of the new and other previously studied remains is available in Appendix I, Table S1). The materials attributed to *S. uccasamamensis* come from different late Miocene–late Pliocene localities in the Bolivian Altiplano, namely Ayo Ayo-Viscachani, Casira, Choquecota, Inchasi, and Pomata-Ayte (see Chapter 4).

The observed features are compared with the other well-known mylodontids, especially the Neogene taxa from both South and North America housed in the following institutions: AMNH, American Museum of Natural History, New York, USA; FMNH, Field Museum of Natural History, Chicago, USA; MACN, Museo Argentino de Ciencias Naturales "Bernardino Rivadavia", Buenos Aires, Argentina; MLP, Museo de La Plata, La Plata, Argentina; MMP, Museo Municipal de Ciencias Naturales "Lorenzo Scaglia", Mar del Plata, Argentina; UF, University of Florida, Florida Museum of Natural History (FLMNH), Gainesville, USA (for a complete list of the comparison material observed for this thesis, see Appendix II).

Neogene mylodontines are in need of urgent revision. These taxa (i.e., the genera *Glossotheridium*, *Glossotheriopsis*, *Pleurolestodon* and *Simomylodon*) were erected on the basis of characteristics mainly derived from fragmentary skulls and teeth (e.g., Rovereto 1914; Robertson 1976; Scillato-Yané 1976; Anaya & MacFadden 1995; McAfee 2009). For this reason, and to properly conduct a revision of the taxonomic attribution of some previously described remains (see Chapter 6), I preferred to separate descriptions and comparisons for skulls, mandibles and dentition. Moreover, these remains were also analyzed morphometrically, using statistical multivariate methods (see also section 3.1.2). In contrast, I preferred to incorporate comparisons to related taxa into the descriptions for the ear region and the postcranial anatomy. In fact, the latter areas have still not been treated in detail for Neogene mylodontines due to a substantial lack of data. For postcranial remains, this lack of

data also impedes the collection of a reliable number of specimens for interspecific comparisons, and consequently postcranial bones were not used in statistical analyses (see also section 3.1.2).

Descriptions, comparisons and measurements were conducted by first-hand examination of the specimens, with the exception of the holotype of *Pleurolestodon acutidens* MACN Pv 2952-2953. This specimen is missing from the vertebrate paleontological collection of MACN (Curator A. Kramarz, pers. comm. 2017). However, the morphological and morphometric comparisons have been conducted on the basis of the photographs and measurements available in Rovereto (1914). The set of measurements performed on the skulls, mandibles, and both upper and lower dentitions of mylodontid taxa is based, with some modifications, on the unpublished PhD dissertation of Esteban (1996), whereas the postcranial measurements were largely taken from Toledo *et al.* (2014) (Appendix III). All the measurements here presented (Chapters 6-7-8) were taken with a digital caliper to the nearest 0.1 mm (Appendix IV).

3.1.2 Statistical analyses for interspecific comparisons

The remains of *S. uccasamamensis* were also compared morphometrically to the other Miocene and Pliocene mylodontines from both South and North America. However, given the near complete absence of postcranial remains for some taxa (e.g., *Pleurolestodon acutidens, Glossotheridium chapadmalense* and *Glossotheriopsis pascuali*), the interspecific morphometric comparisons are limited to craniodental remains.

Multivariate analyses were conducted using Principal Component Analyses (PCA) on the set of craniodental measurements (Appendix IV, Datasets S1) using the program PAST v. 3.20 (Hammer *et al*. 2001). Due to the paucity of crania associated with mandibles, these two anatomical regions (i.e., crania and mandibles, with their respective dentitions) were considered separately in the multivariate analyses. The PCAs were conducted on the raw measurements of a reduced subset of specimens and variables, in order to minimize the missing data due to preservation (see Appendix IV, Datasets S1, for further details). In this way, the missing data imputation, conducted using the "Mean Value Imputation" algorithm (the default option of PAST v. 3.20), was reduced to a minimum. Percentages of explained variance and the main loadings of the single variables are reported in Appendix V, Tables S1.

3.2 SEXUAL DIMORPHISM IN *SIMOMYLODON UCCASAMAMENSIS* (Chapter 7)

To investigate the presence of SD in *Simomylodon uccasamamensis*, the remains ascribed to this species in Chapter 6 have been analyzed in more detail.

First, the sample has been analyzed qualitatively, to detect the presence of robust and gracile individuals, as previously observed in other extinct sloth species (Lydekker 1894; Cartelle & Bohórquez 1982; Anaya & MacFadden 1995; McDonald 2006; Cartelle *et al.* 2019). Robustness was determined for cranial remains on the general mediolateral width of the skull, in particular the rostral region, whereas for the mandibles robustness was reflected in the height and divergence of the horizontal mandibular rami. Postcranial remains were grouped on the basis of general size. Every specimen was then assigned to one of these categories (robust or gracile; see Appendix I, Table S2), in order to analyze quantitatively the differences between the two morphs in both shape and size. Using homologous well-preserved elements that were available in reasonable numbers for comparisons, different datasets were generated, including a dataset based on the cranium and upper dentition (n = 7), on the mandibles and lower dentition (n = 13), on femora (n = 8), and on tibiae (n = 10) (Appendix IV, Datasets S2). When paired homologous elements of the same specimen were present (e.g., mandibles, femora, or tibiae), dimensions were averaged *a priori* in order to avoid repetition for the same individual. These three types of remains were considered as independent datasets, in order to maximize the number of specimens available for inclusion in the analyses. Cumulatively, 26 variables for the cranium and upper dentition, and 25 variables for the mandibles and lower dentition, were considered, the same used in Chapter 6. However, to increase the accuracy for intraspecific comparisons, when dentition was lacking, alveolar measurements were not used as a substitute. Also, this dataset was restricted to adult specimens, in order to minimize the effects of ontogenetic variation. For the postcranial elements, 12 variables for the femora and 11 for the tibiae, largely taken from Toledo *et al.* (2014), were used. A complete list of the variables and their descriptions is available in Appendix III.

The different datasets were again analyzed using the multivariate statistical tools available in the software PAST (versions 2.17 and 3.20; Hammer *et al.* 2001). For each dataset, Principal Component Analyses (PCA) were employed to observe the distribution of the robust (blue) and gracile (red) specimens in the morphospace. When separate groups were recognised in the PCA, the significance of their differences was tested both graphically (using hierarchical clustering analyses based on squared Euclidean distances) and numerically, through NPMANOVA tests (Non-Parametric MANOVA; Anderson 2001) on raw

measurements, at a conventional α level of 0.05. For shape variation between the two morphs, the influence of latent size in the dataset was tested using the "multivariate allometry" function implemented in PAST 2.17 (see also Jolicoeur 1963, and Klingenberg 2016). The percentages of variance explained and the main loadings for all PCAs are detailed in Appendix V, Tables S2.

3.3 THE PHYLOGENY OF MYLODONTIDAE (Chapter 8)

In order to test the phylogenetic relationships of Mylodontidae, with special emphasis on mylodontines, a new data matrix was built. The data matrix for the phylogenetic analysis was based on that of Gaudin (2004), including 46 taxa and 286 osteological characters. New taxa and characters were added to this matrix using the program Mesquite (Maddison & Maddison 2011), and the phylogenetic analyses were performed using the parsimony software TNT v. 1.5 (Goloboff *et al.* 2008). Pholidotans and four extant representatives of Cingulata and Vermilingua from Gaudin's (2004) study were used as outgroups (i.e., the armadillo *Euphractus* and the anteaters *Cyclopes*, *Myrmecophaga*, and *Tamandua*). All the other outgroup taxa present in Gaudin (2004) were inactivated using the "inactive taxa" TNT function. Moreover, all the non-mylodontid sloths were inactivated *a priori*, with the exception of the modern tree-toed sloth *Bradypus* and the Santacrucian megatherioid *Hapalops*, which were also used as outgroups.

The analysis was conducted following the procedure of Gaudin (2004), using equally weighted characters and maintaining the same ordination of the craniodental features (1-286). Only 5 of the 286 features were modified from the original codification, in part following Cartelle *et al.* (2019). Characters 6 (ordered) and 25 (unordered) were modified as follows: "char. 6 diastema between Cf1 and Mf1: (0) absent, (1) moderate (<1/2 of the mesiodistal length of the Cf1), and (2) elongated (>1/2 of the mesiodistal length of the Cf1); and char. 25 diastema between Mf1 and Mf2: (0) absent and (1) moderate (<1/2 of the mesiodistal length of the Mf1)" (Cartelle *et al.* 2019). To properly define the cross-section shape of the dentition of the peculiar genus *Pseudoglyptodon*, another state (i.e., "trilobate") was added to the features 31, 32 and 34 of Gaudin (2004). A complete list of the features 1-286 of Gaudin (2004), that includes the present changes, is available in Appendix VI, Data S1.

A new set of 97 postcranial characters was then added to the matrix of Gaudin (2004). These new postcranial features are numbered 287–383 in order to maintain a continuity with the work of Gaudin (2004). Among the postcranial characters described and figured in the

"Results" section of Chapter 8, 30 are multistate and ordered. Raw data used to calculate ratios are available in Appendix VI, Data S2. The final matrix consists of 383 features, 110 of which are multistate and ordered. Almost all these features were directly observed by first-hand examination of the specimens (see Appendices I and II for a total list of the materials observed and their collection codes), with a smaller number coded based on high quality photographs generously shared by colleagues (Appendix II) and bibliographic sources (Appendix VI, Data S3). All the species of Mylodontinae revised in the literature and considered valid as of the date of this analysis have been added to the matrix, available in Appendix VI, Data S4. The taxonomic review of Mylodontinae, together with the explanation on how the taxonomic units have been utilized in the phylogenetic analyses, are detailed in Chapter 5. Moreover, other Mylodontidae of uncertain classification have been considered, in order to test their phylogenetic affinities.

The analyses were performed using the "traditional search" function implemented in TNT, with 200 replications, and applying the tree bisection reconnection [TBR] swapping algorithm, saving 10 trees for each replication, always collapsing zero length branches. This protocol was applied to the total dataset, but the craniodental block of characters was also analyzed independently, in order to determine the amount information provided by the added postcranial features. Support values were calculated using Total Bremer Support (Bremer 1994), Bootstrap (Felsenstein 1985), and Jackknife (Farris *et al.* 1996) resampling methods, always using 300 replications. TNT v. 1.5 (Goloboff *et al.* 2008) also allows to automatically detect taxa which occupy different positions into the recovered most parsimonious trees (MPTs). Through this option (*Trees*: *Comparisons*: *Pruned Trees*), the software shows a reduced consensus tree which ignores the alternative positions of the unstable taxa. For this reason, the analysis was also repeated after pruning the most unstable (and incomplete) taxa, and the common synapomorphies were listed in both cases (Appendix VI, Data S5 and S6).

One of the two single MPTs that resulted from the analysis of the pruned matrix was then imported into the software environment R (R Development Core Team 2013) for temporal calibration. The calibration of the MPT was obtained using the temporal ranges of extinct taxa taken from the literature (Appendix VI, Table S7), using the timePaleoPhy function of the package "paleotree" (Bapst 2012), setting a minimum branch length of 0.5 Ma. Finally, the time-scaled phylogeny was plotted against the international geological time scale using the function geoscalePhylo of the package "strap" (Bell & Lloyd 2015). The script was modified by introducing the absolute chronology of the SALMAs, according to the latest calibrations provided in Slater *et al.* (2016) (Appendix VI, Table S8).

3.4 THE INNER EAR OF *GLOSSOTHERIUM ROBUSTUM* (Chapter 9)

3.4.1 Specimen studied and data processing

The inner ear of a mylodontid sloth was reconstructed based on a specimen of *Glossotherium robustum* (i.e., MACN Pv 13553; Fig. 3.1). The larger size of this taxon and its younger age compared with *S. uccasamamensis*, as well as the availability of Argentinian medical centers, offered the ideal conditions to use this taxon as a model for the study of the first digitally reconstructed endocranial cavities for a mylodontid sloth. The analyzed remains consisted of an undescribed neurocranium found in 1933 in the vicinity of Tandil (Buenos Aires Province, Argentina). This incomplete skull was chosen because of the excellent preservation of its internal cavities, but also for logistical reasons. It could be easily transported to the city of Mendoza, where it was scanned using the General Electric Lightspeed CT scanner in the FUESMEN Institute. The scanning resulted in 839 slices with a thickness of 0.62 mm. The image segmentation process was performed using OsiriX v.5.6 and Materialise Mimics v.17 software. Both the left and right bony labyrinths were digitally reconstructed, both of them being slightly damaged at the level of the lateral semicircular canal. However, the trajectory of the latter canal was still strongly marked on the petrosal and a reliable reconstruction was obtained.

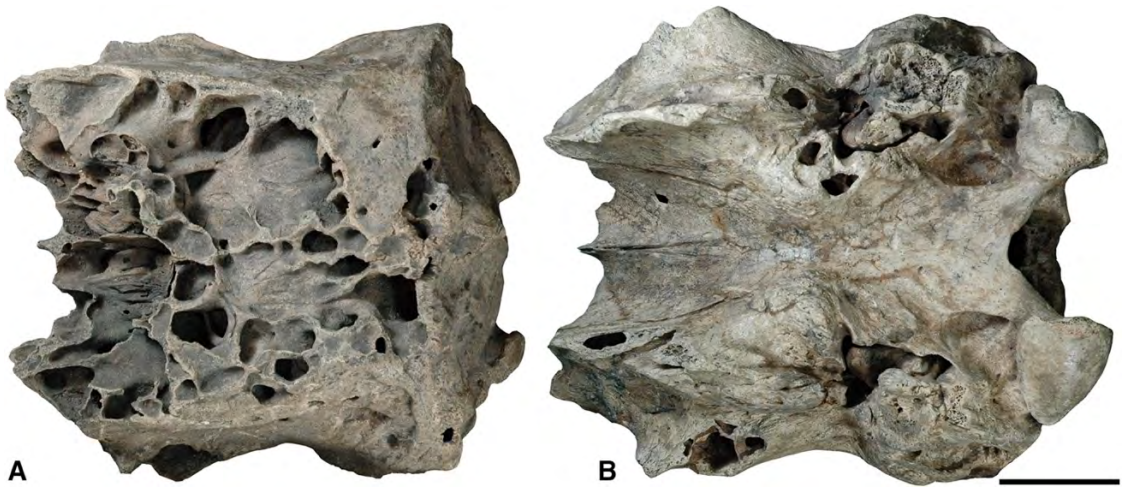

Figure 3.1. Posterior portion of the cranium of *Glossotherium robustum* (MACN Pv 13553) in dorsal (A) and ventral (B) views. Scale bar equals 5 cm.

The description and comparison is based on the right labyrinth, but, given the similarity between the two sides, it is valid for both sides. Linear and angular measurements of the bony

labyrinths were taken using the 3D measurement tools of Mimics v.17 and AVIZO (Appendix VII, Table S1).

3.4.2 Morphometric comparisons of the bony labyrinth

The 3D reconstruction of the bony labyrinth of *Glossotherium robustum* MACN Pv 13553 was compared to the database of Billet *et al.* (2015a), composed of 40 adult xenarthran specimens, and representing 13 extant genera (including living sloths, armadillos and anteaters) and the extinct ground sloth *Megatherium*. Following Billet *et al.* (2015a), 80 semilandmarks were digitized on the bony labyrinth of *G. robustum* with the interactive software ISE-MeshTools (Lebrun 2014). The semilandmarks were equally distributed on the three semicircular canals and the cochlea, and the digitization was conducted by Guillaume Billet, in order to minimize interobserver errors. Analysis and visualization of shape variation patterns were conducted using the interactive software package Morphotools (Specht 2007; Specht *et al.* 2007; Lebrun 2008; Lebrun *et al.* 2010).

The Principal Component Analyses (PCA) were conducted alternatively with and without correction of the shape data for allometry, using either body mass values or centroid size of the inner ears as estimators of size. The estimated body mass for *G. robustum* (1216 kg) was taken from Fariña *et al.* (1998), the same source used by Billet *et al.* (2013, 2015a) for the body mass estimation of *Megatherium*. Both the estimators, body mass and centroid size of the inner ear, were also used as external variables so as to obtain the respective allometric shape vectors (ASV). An allometric shape vector represents a direction in shape space, which characterizes the main transformations related to size changes. A Partial Least Squares (PLS) analysis was also performed using the landmark configurations of the semicircular canals and the cochlea as distinct blocks, in order to assess the morphological features that covary among them (for more information on the applied methods, see Billet *et al.* 2015a).

3.4.3 Functional aspects/attributes of the bony labyrinth

In an attempt to explain the peculiar morphology of the bony labyrinth in *Glosstherium robustum* that emerged from the morphometric geometric analyses (see Chapter 9), some studies that have been proposed in recent years, relating the shape of labyrinthine features to functional aspects of the ear (e.g., Spoor *et al.* 2007; Manoussaki *et al.* 2008; Silcox *et al.* 2009; Malinzak *et al.* 2012; Berlin *et al.* 2013) have been replicated. However, in doing so, the criticisms that other

authors have offered on the accuracy and reliability of these methods (e.g., David *et al.* 2010, 2016; Malinzak *et al.* 2012; Billet *et al.* 2013; Danilo *et al.* 2015; Orliac & O'Leary 2016; Perier *et al.* 2016; Ruf *et al.* 2016) have been taken into account. For example, the *a priori* agility categories established by Spoor *et al.* (2007) correspond to subjective impressions according to Malinzak *et al.* (2012), whereas Billet *et al.* (2013) and Ruf *et al.* (2016) demonstrated the difficulty of using the equations of Silcox *et al.* (2009) for extremely large and small-sized taxa. For this reason, the semicircular canal ratio (SCR) values are plotted over the body mass estimation of the *G. robustum* specimen MACN Pv 13553, in order to visualize it in the mammalian graphs published by Spoor *et al.* (2007: fig. 1b). However, the predictive agility equations of Silcox *et al.* (2009) have not been used.

The studies of Malinzak *et al.* (2012) and Berlin *et al.* (2013) related the average deviation from orthogonality of the ipsilateral semicircular canals with the pattern of locomotor head movements and the average sensitivity of the semicircular canals. Both studies, however, failed to consider intraspecific variation and have quite low regression correlation coefficients (Ruf *et al.* 2016). The deviation from orthogonality of the ipsilateral semicircular canals in *Glossotherium* (90_{var} *sensu* Berlin *et al.* 2013) is nevertheless calculated here, but is discussed in the context of Ruf *et al.*'s (2016) critiques.

In both marine and terrestrial mammals, the radii ratio of the cochlea (calculated as the ratio between the radius of the basal turn and the radius of the apical turn of the cochlea) is linearly correlated with the lower limit of low-frequency hearing abilities (Manoussaki *et al.* 2008). Following the procedure of the latter authors, the radii of curvature for the basal and apical cochlear turns were calculated. Their ratio was used in the equation:

$$f = 1.507 \exp [0.578 (p - 1)]$$

where f = low-frequency hearing limit and p = radii ratio (R_{base}/R_{apex}), in order to predict the low-frequency hearing limit for *G. robustum*. This approach was criticized by Danilo *et al.* (2015), Ekdale & Racicot (2015), and Orliac & O'Leary (2016), who experienced problems in repeating the protocol. Similar difficulties were observed during the calculation of this index for *G. robustum* MACN Pv 13553, and for this reason a range of minimum and maximum values is provided. The results have been coupled with observations of cochlear morphological features that have been previously linked with hearing abilities in mammals (for a summary see Ekdale 2016).

3.5 DIGITAL ENDOCASTS OF *GLOSSOTHERIUM ROBUSTUM* (Chapter 10)

The neurocranium of *Glossotherium robustum* MACN Pv 13553 was also used to obtain the digital reconstructions of the brain cavity, the trajectory of nerves and blood vessels, and the cranial sinuses. In this case, the comparative sample is based on two complete skulls of the extant sloths *Choloepus hoffmanni* (AMNH 30765) and *Bradypus variegatus* (AMNH 95105). Their CT images were downloaded from the Digital Morphology library (www.digimorph.org). *Choloepus hoffmanni* (AMNH 30765) was scanned with a slice thickness of 0.241 mm, producing a total of 441 slices, whereas the slice thickness for *B. variegatus* (AMNH 95105) was 0.197 mm, yielding a total of 369 slices. The image segmentation process for the three specimens was performed using the digital tools from OsiriX v.5.6 32-bit and Materialise Mimics v.17. The 3D models of skulls were obtained following the same procedure previously described, and finally imported into ZBrush 4R6 for the rendering process. Because of the presence of infilled sediment in different cranial cavities of MACN Pv 13553, the segmentation process was carried out manually, slice-by-slice.

All the specimens considered in Chapter 10 are adults, as shown by the complete fusion of cranial sutures. Analyzing taxa of comparable developmental stages helps to avoid variability due to ontogenetic development.

Identification of endocranial structures was based on previous descriptions of sloth endocasts (e.g., Dechaseaux 1958, 1962a, b, 1971; Dozo 1987, 1994), as well as classic manuals on the anatomy of domestic mammals (Evans 1993; Barone & Bortolami 2004; Constantinescu & Schaller 2012), and previously published works on the anatomy of extant xenarthrans (Hyrtl 1854; Tandler 1901; Bugge 1979).

3.6 ABBREVIATIONS

Anatomical abbreviations: Cf, upper caniniform tooth; cf, lower caniniform tooth; Mf, upper molariform tooth; mf, lower molariform tooth, mtc, metacarpal, mtt, metatarsal.

Other abbreviations: CI, Consistency Index; Fm., Formation; MPT(s), Most Parsimonious Tree(s); NALMA, North American Land Mammal Age; SALMA, South American Land Mammal Age; RI, Retention Index; TL, Tree Length.

Complete list of institutional abbreviations: A, Gervais Collection, Laboratoire d'Anatomie Comparée du Muséum national d'Historie naturelle, Paris, France; AMNH, American Museum of Natural History, New York, USA; AMU-CURS, Colección de Paleontología de Vertebrados de la Alcaldía de Urumaco, Estado Falcón, Venezuela; CIAAP, Centro de Investigaciones Antropológicas, Arqueológicas y Paleontológicas, Coro, Venezuela; EPN, Escuela Politécnica Nacional, Quito, Ecuador; F:AM, Frick collection, American Museum of Natural History, New York, USA; FCDPV, Colección de Paleontología de Vertebrados de la Facultad de Ciencias de Montevideo, Montevideo, Uruguay; FMNH, Field Museum of Natural History, Chicago, USA; FUESMEN, Fundación Escuela de Medicina Nuclear, Mendoza, Argentina; IGCU, Instituto de Geología de la Ciudad Universitaria, Guanajuato, Mexico; IVIC, Instituto Venezolano de Investigaciones Científicas, Caracas, Venezuela; GB, GEOBOL, (former) Servicio Geológico de Bolivia, La Paz, Bolivia; LACM, Los Angeles County Museum, California, USA; LV, Colecciones Paleontológicas del Departamento de Geociencias, Universidad Nacional de Colombia, Bogotá, Colombia; MACN, Museo Argentino de Ciencias Naturales "Bernardino Rivadavia", Buenos Aires, Argentina; MBLUZ, Museo de Biología de la Universidad del Zulia, Maracaibo, Venezuela; MCL, Museo de Ciências Naturais da Pontifícia Universidade Católica de Minas Gerais, Belo Horizonte, Brazil; MCN, Museo de Ciencias Naturales, Caracas, Venezuela; MEPN, Museo de Historia Natural "Gustavo Orces", Escuela Politécnica Nacional, Quito, Ecuador; MLP, Museo de La Plata, La Plata, Argentina; MMP, Museo Municipal de Ciencias Naturales "Lorenzo Scaglia", Mar del Plata, Argentina; MNHN, Muséum national d'Histoire naturelle, Paris, France; MNHN-Bol, Museo Nacional de Historia Natural de Bolivia, La Paz, Bolivia; NHMUK, Natural History Museum, London, UK; ROM, Royal Ontario Museum, Toronto, Canada; SGO, Museo Nacional de Historia Natural, Santiago, Chile; UATF, Museo de la Universidad Autónoma Tomas Frias, Potosí, Bolivia; UCMP, Museum of Paleontology, University of California, Berkeley, USA; UF, University of Florida, Florida Museum of Natural History (FLMNH), Gainesville, USA; UFAC, Universidade Federal do Acre, Rio Branco, Acre, Brasil; USNM, National Museum of Natural History, Smithsonian Institution, Washington, D.C., USA; YPM-PU, Princeton University collection housed at Peabody Museum, Yale University, New Haven, USA; ZMUC, Zoological Museum, University of Copenhagen, Copenhagen, Denmark.

Chapter 4
GEOGRAPHICAL AND GEOLOGICAL SETTINGS

4.1 THE TUFFACEOUS LEVEL "TOBA 76"

The fossil remains assigned to *Simomylodon uccasamamensis* and considered in this work (see Appendix I for further details) come from five distinct localities in three departments of the Bolivian Altiplano (Fig. 4.1). The stratigraphy of deposits has been constrained by geochronological data obtained from various volcanic tuffs interbedded within the sedimentary series (Evernden *et al.* 1966, 1977; Lavenu *et al.* 1989; Marshall *et al.* 1992; MacFadden *et al.* 1993; Anaya & MacFadden 1995). The age of the "Toba 76" (Saint-André 1994; Saint-André *et al.* 2010), an index-bed tuff occurring throughout the Neogene series of the central Altiplano and near the Miocene–Pliocene transition (Marshall *et al.* 1992), has been recently refined by Boscaini *et al.* (2019a). This tuff was previously dated by K/Ar method (Evernden *et al.* 1966, 1977; Marshall *et al.* 1992) and by $^{40}Ar/^{39}Ar$ (Marshall *et al.* 1992). K/Ar ages are very imprecise and cannot be retained. The best estimate is a $^{40}Ar/^{39}Ar$ mean age on four sanidine single crystals at 5.348 ± 0.005 Ma obtained by Marshall *et al.* (1992). These authors retained an age of 5.4 Ma for the "Toba 76" thus pointing to a latest Miocene age. It must be highlighted that the age of the monitor used for age calculation has been recalibrated many times since the work of Marshall *et al.* (1992) (e.g., Renne *et al.* 2010) and that their error calculation did not consider

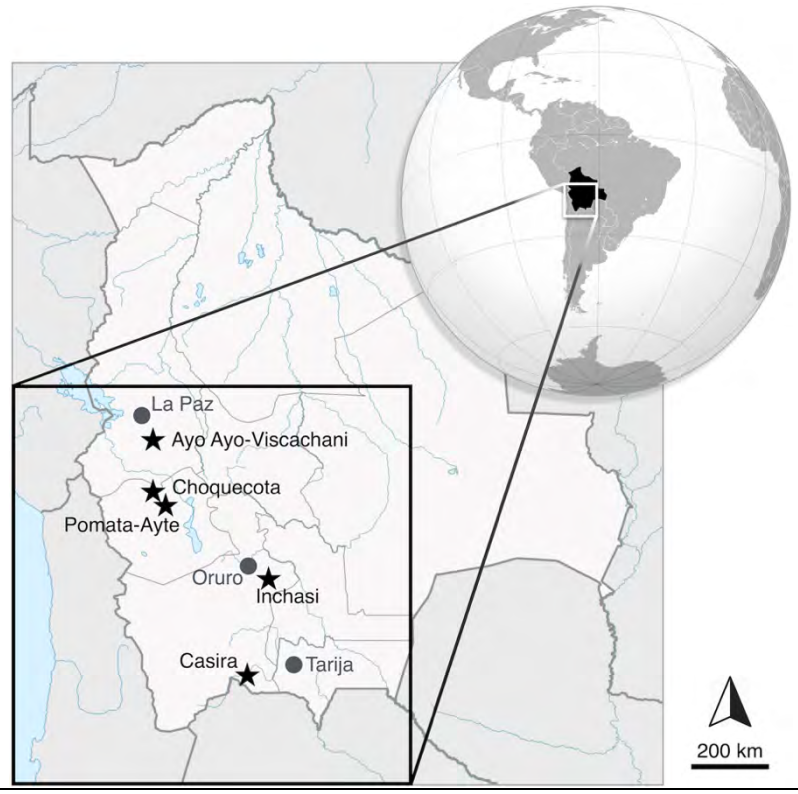

Figure 4.1. Map of the late Neogene fossil-bearing localities of Bolivia in which the remains of the mylodontid sloth *Simomylodon uccasamamensis* have been recovered.

the error on the irradiation factor J. New $^{40}Ar/^{39}Ar$ dating on four single crystals of sanidine were performed from the "Toba 76" samples from the classic paleontological site of Pomata (Saint-André 1994; Boscaini *et al.* 2019a). The four obtained ages are 5.26 ± 0.02 Ma, 5.25 ± 0.02 Ma, 5.27 ± 0.03 Ma, 5.27 ± 0.02 Ma, corresponding to 99.67, 100, 90.43 and 100% of ^{39}Ar released, respectively. The retained weighted mean age is 5.26 ± 0.02 Ma for the "Toba 76", that points to earlymost Pliocene age (see Boscaini *et al.* 2019a for further details).

4.2 CHOQUECOTA

The most important fossil locality lies near the village of Choquecota (Choquecota-Hakallinca; Saint-André 1994; Fig. 4.2). The classic site is middle Miocene in age (Colloncuran SALMA; Saint-André 1994) and located 3 km north of the homonym village (Carangas Province, Oruro Department). However, the only specimen of *S. uccasamamensis* from this area was recovered approximately 3.5 km southwest of Choquecota village, at the top of a Miocene sedimentary sequence capped by the tuff commonly called "Toba 76" (Saint-André 1994; Saint-André *et al.* 2010; see above). The material of *S. uccasamamensis* was found 15 meters below the "Toba 76," in a reddish sandstone layer from the Rosa Pata Formation (late Miocene)

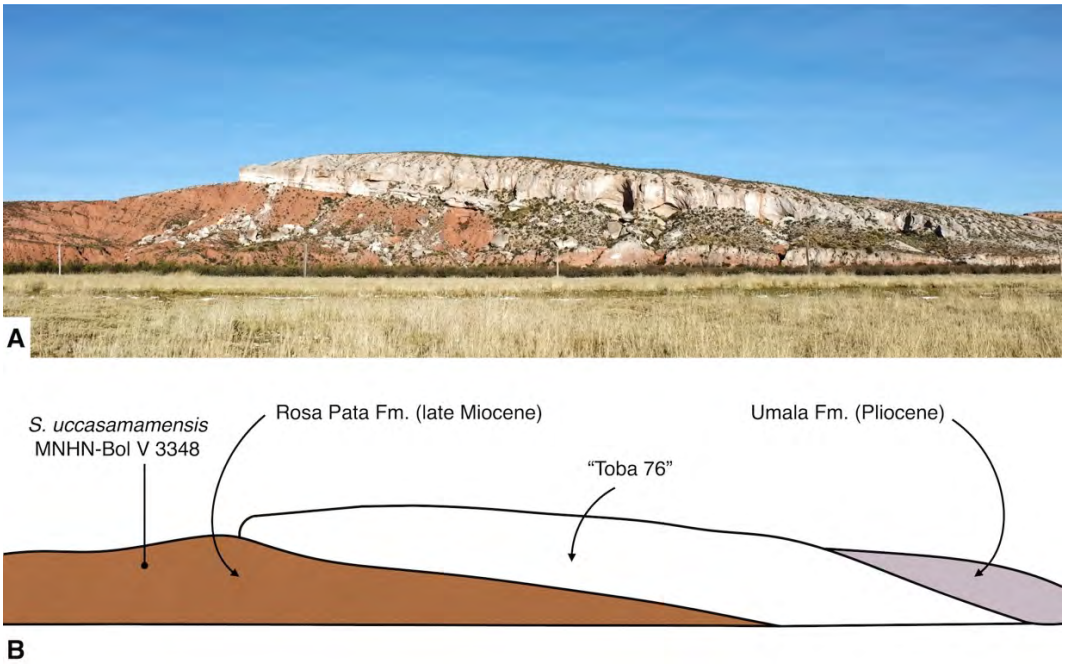

Figure 4.2. A. Panoramic view of the late Miocene and Pliocene outcrops of the locality of Choquecota. B. Schematic representation of the different formations and the position of the earliest remain of *S. uccasamamensis* (MNHN-Bol V 3348).

unconformably overlain by the Umala Formation (Pliocene; Saint-André *et al.* 2010). This single specimen (MNHN-Bol V 3348) consists of a partial skull lacking its posterior region (Saint-André 1994; Saint-André *et al.* 2010).

Originally assigned by Saint-André (1994) to *Glossotheriscum dalenzae* and later published under the genus *Pleurolestodon* in Saint-André *et al.* (2010), this skull is here assigned to *S. uccasamamensis* on the basis of morphological and morphometric data (see Chapters 5 and 6). This specimen is considered to represent the oldest known remains of *S. uccasamamensis*, just prior to the Huayquerian–Montehermosan transition, and most likely predating the Miocene–Pliocene transition.

4.3 POMATA-AYTE

This locality, early Pliocene in age, is located 2.5 km east-northeast of the homonym village (Carangas Province, Oruro Department; Saint-André 1994). Lithostratigraphically it belongs to the Umala Formation, which lies above the Totora and Pomata Formations. Five meters above the base of the section, the "Toba 76" is recovered. The fossil remains from the Pomata-Ayte locality were found above this tuff, in the basal ~60 m deposits of the Pliocene Umala Formation (Saint-André *et al.* 2010).

Figure 4.3. Panoramic view of the early Pliocene outcrops of the locality of Pomata-Ayte.

The vertebrate fauna includes the sloths *Simomylodon uccasamamensi*s, *Aymaratherium jeani* and *Megatherium (Megatherium) altiplanicum*, the litoptern *Macrauchenia* sp., the toxodontid *Posnanskytherium* cf. *viscachanense*, the pampatheriid *Plaina* sp. and two other armored cingulates of uncertain affinities, a rodent, and a giant carnivorous phorusrhacoid bird (Pujos *et al.* 2016). The faunal composition is consistent with an earliest Pliocene age (Montehermosan; Hoffstetter *et al.* 1972; Marshall *et al.* 1983; Hoffstetter 1986; Marshall & Sempéré 1991; Saint-André 1994; Pujos *et al.* 2016).

4.4 CASIRA

The locality of Casira (= Kasira; Suárez-Soruco & Díaz-Martínez 1996) is situated south-west of the Khellu Khakha Loma Mountain (Modesto Omiste Province, Potosí Department) and close to the Bolivian-Argentinian frontier (Anaya *et al.* 1989). The age of these deposits is not well established (Anaya *et al.* 1989; Zurita *et al.* 2017). Shockey *et al.* (2007) proposed a Pliocene age for these sediments, whereas Cerdeño *et al.* (2012) considered them late Miocene. However, the presence of *Megatherium (Megatherium) altiplanicum* and the low diversity of the mesotheriid taxa (M. Fernández Monescillo, pers. comm.) suggest an early Pliocene age (i.e., Montehermosan-Chapadmalalan SALMAs) would be more consistent for the Casira fauna.

4.5 INCHASI

The Inchasi locality (Fig. 4.4) is situated 50 km southeast of the city of Potosí (Province of Linares, Department of Potosí; MacFadden *et al.* 1993; Anaya & MacFadden 1995). Its fossiliferous beds have been dated to between 4.0 and 3.3 Ma (early Pliocene; MacFadden *et al.* 1993; Anaya & MacFadden 1995). The Inchasi locality is Chapadmalalan in age (Cione & Tonni 1996), and presents the most diversified Pliocene mammalian assemblage of the Bolivian Altiplano (MacFadden *et al.* 1993; Anaya & MacFadden 1995).

The mammalian fauna of Inchasi includes the notoungulates *Posnanskytherium* and *Hypsitherium*, two endemic genera of the Bolivian Altiplano, as well as many other mammals typical of the Pliocene of Argentina, such as *Promacrauchenia*, *Caviodon*, *Phugatherium*, *Paraglyptodon*, *Plohophorus* and *Plaina* (MacFadden *et al.* 1993; Anaya & MacFadden 1995). In Inchasi, sloths are represented by some unidentified remains of Mylodontidae and Megatheriidae, as well as

Proscelidodon patrius and *Glossotheridium chapadmalense* (Anaya & MacFadden 1995). The latter species is represented by three mandibles that are here reassigned to *Simomylodon uccasamamensis* on the basis of morphological and morphometric data (see Chapters 5 and 6).

Figure 4.4. Panoramic view of the early Pliocene outcrops of the locality of Inchasi.

4.6 AYO AYO-VISCACHANI

The Ayo Ayo-Viscachani locality (Fig. 4.5) is situated between the two homonym villages in the Aroma Province (La Paz Department), about 70 km south of the city of La Paz (e.g., Hoffstetter *et al.* 1971b; Marshall & Sempéré 1991; Saint-André 1994). The fossils come from the upper part of the Umala Formation, which ranges the late Pliocene and is further coeval with the Remedios Formation found at more southern latitudes (Lavenu 1984). The sandy and clayish deposits at Ayo Ayo-Viscachani provide both late Pliocene and Pleistocene vertebrate assemblages (i.e., Hoffstetter *et al.* 1971b). Pliocene and Pleistocene layers were seemingly deposited conformably (Saint-André 1994). However, the two successive faunas present distinct faunal associations and are separated by volcanic ashes (the Ayo Ayo tuff) which yield a mean age of approximately 2.8 Ma (Lavenu *et al.* 1989; Marshall *et al.* 1992; Saint-André 1994).

The Pliocene fauna includes the marsupials *Sparassocynus heterotopicus* and *Microtragulus bolivianus*, the litoptern *Macrauchenia minor* and the notoungulate *Posnanskytherium* cf. *P. viscachanense*, the rodents *Praectenomys*, cf. *Lagostomopsis* and *Phugatherium*, and the armored xenarthrans *Pampatherium* sp. and *Macroeuphractus* cf. *moreni* (Saint-André 1994 and references therein). Sloths are assigned to the giant megatheriid *Megatherium* (*M.*) *altiplanicum* and the mylodontid *Simomylodon uccasamamensis* (Saint-André 1994; Saint-André *et al.* 2010).

According to the latest proposed adjustments of the bio- and geo-chronologic scales (Reguero *et al.* 2007; Tomassini *et al.* 2013), the late Pliocene period roughly coincides with the early Marplatan SALMA (Barrancolabian and Vorohuean subages).

Figure 4.5. Panoramic view of the late Pliocene outcrops of the locality of Ayo Ayo-Viscachani.

Overall, the remains of *S. uccasamamensis* are from deposits that are virtually bracketed below by the "Toba 76", now considered 5.26 ± 0.02 Ma in age, and above by the 2.8 Ma Ayo Ayo tuff, which correspond to the base and the top of the Umala Formation, and roughly coincide with the Pliocene (Marshall & Sempéré 1991).

Chapter 5
SYSTEMATIC PALEONTOLOGY

This chapter includes an annotated review of the taxa that have been traditionally attributed to Mylodontinae in the latest works on the subject (i.e., Gaudin 2004; Saint-André *et al.* 2010; Pujos *et al.* 2017) and those that have been recovered among this clade in the phylogenetic analysis presented in this thesis (see Chapter 8). Special emphasis is given for Mylodontinae taxa from the Bolivian Altiplano (see also Chapters 6 and 7).

All the putative valid mylodontine species are listed in this chapter, with exception of the taxa that are exclusive of the late Miocene of the Entre Ríos Province (Argentina). Following Brandoni (2013), the supposedly valid species from this locality are *Megabradys darwini* Scillato-Yané, 1981, *Promylodon paranensis* (Ameghino, 1883), *Prolestodon antiquus* (Ameghino, 1885), *Pr. paranensis* (Ameghino, 1889), *Ranculcus scalabrinianus* Ameghino, 1891a, *Strabosodon acuticavus* Ameghino, 1891a, and *St. obtusicavus* Ameghino, 1891a. However, these taxa were not revised since their original description, more than a century ago, an endeavor that is still impeded by the fragmentary nature of these remains (Brandoni 2013). In fact, many of these taxa have been erected on the basis of scanty material (i.e., isolated teeth or mandibular fragments) that doesn't exhibit reliable diagnostic features (Brandoni 2013). Moreover, the confounding effect of including some of these taxa in a phylogenetic analysis was stressed by Esteban (1996). Additionally, three intertropical Mylodontinae species have been treated in this chapter but not included in the phylogenetic analyses of Chapter 8. These are *Oreomylodon wegneri* (Spillmann, 1931), *Mylodonopsis ibseni* Cartelle, 1991, and *Ocnotherium giganteum* (Lund, 1839), that are currently under study by C. Cartelle and collaborators. The same applies to *Archaeomylodon sampedrinensis* (Brambilla & Ibarra 2019) which was published after the completion of the present study. In any case, the phylogenetic relationships of the latter clade were tested by Brambilla & Ibarra (2019).

The taxonomic units of the "ingroup" Mylodontinae, are defined herewith, and analyzed phylogenetically in Chapter 8, together with several other Mylodontidae members. Among the mylodontids outgroup taxa, the genera *Orophodon* (late Oligocene; Argentina; Ameghino 1894; Pujos & De Iuliis 2007), *Urumacotherium* (middle Miocene to early Pliocene; Brazil, Peru, and Venezuela; Santos & De Iuliis 1993; Santos *et al.* 1993a), and *Octodontobradys* (late Miocene to early Pliocene; Brazil; Santos *et al.* 1993b) are included. These taxa have been respectively attributed to the clades Orophodontinae, Octodontobradyinae, or Urumacotheriinae, whose validity is still not tested or is only weakly supported (Ameghino 1894; Santos *et al.* 1993b; Negri & Ferigolo 2004; Varela *et al.* 2018). For this reason, their phylogenetic relationships are tested in Chapter 8. Phylogenetic nomenclature (i.e., using rank-free suprageneric taxonomy) is applied herewith.

The classification of Mylodontinae is as follows:

MAMMALIA LINNAEUS, 1758

XENARTHRA COPE, 1889

PILOSA FLOWER, 1883

FOLIVORA DELSUC *ET AL.*, 2001

[= TARDIGRADA LATHAM & DAVIES, 1795; = PHYLLOPHAGA OWEN, 1842]

MYLODONTIDAE GILL, 1872

MYLODONTINAE GILL, 1872

PSEUDOPREPOTHERIUM HOFFSTETTER, 1961

Notes: This genus was erected by Hoffstetter (1961) based on a complete femur previously described, and erroneously ascribed, to the megatherioid genus *Prepotherium* (i.e., *Pr. venezuelanum*) by Collins (1934).

Type species: Pseudoprepotherium venezuelanum (Collins, 1934)

Other species: Pseudoprepotherium confusum Hirschfeld, 1985

PSEUDOPREPOTHERIUM VENEZUELANUM (COLLINS, 1934)

Holotype: right femur figured by Collins (1934: pl. XV), without data on storage locality.

Type locality and age: Along Río Tucupido (Portuguesa State, Venezuela; see Collins 1934; Hirschfeld 1985). However, according to Hirschfeld (1985), there is strong uncertainty of the provenance and age of the type material.

Known distribution: *P. venezuelanum* is also recognized in the late Miocene Solimões Fm. (Acre, Brazil: Bocquentín & Guilherme 1999; Negri *et al.* 2010), considerably extending considerably southward the range of this species. Given the uncertainty of the chronological data associated to the type material, the age estimated for the Solimões Fm. is taken as reference for the taxon (Bocquentín & Guilherme 1999; Negri *et al.* 2010).

Observed material: see Collins (1934), Bocquentín & Guilherme (1999), and Negri *et al.* (2010).

Diagnosis: see Collins (1934); Bocquentín & Guilherme (1999).

PSEUDOPREPOTHERIUM CONFUSUM HIRSCHFELD, 1985

Holotype: UCMP 39957, skull strongly mediolaterally compressed with alveoli of Cf1s and left and right molariform series.

Type locality and age: La Venta localities close to Hacienda Argentina (Huila, Colombia); middle Miocene (Hirschfeld 1985).

Known distribution: same as for the type material.

Observed material: see Appendix II and Hirschfeld (1985).

Diagnosis: see Hirschfeld (1985).

URUMACOTHERIUM BOCQUENTIN-VILLANUEVA, 1984

Notes: The genus *Urumacotherium* was originally erected by Bocquentin-Villanueva (1984) for a new genus of a megatherioid sloth from the Urumaco Fm. (Estado Falcón, Venezuela). Santos & De Iuliis (1993) and Santos *et al.* (1993a) ascribed more material recovered in the Solimões Fm. (Acre, Brazil) to the same genus, further suggesting its inclusion in Mylodontidae, a classification later followed in the large compilation conducted by McKenna & Bell (1997). In the latest revisions of the sloths from Acre, the material from the Solimões Fm. is referred as *Urumacotherium campbelli* (for a resume see Negri & Ferigolo 2004 and Negri *et al.* 2010) and included in the independent mylodontid subfamily Urumacotheriinae (Negri & Ferigolo 2004). Given the scanty material ascribed to the genus *Urumacotherium*, the two species (*U. garciai* and *U. campbelli*) were treated as *Urumacotherium* sp. and consequently their monophyly (and the possible validity of Urumacotheriinae) was not tested. Saint-André *et al.* (2010) included *Urumacotherium* sp. in Mylodontinae but without testing this hypothesis. The inclusion of *Urumacotherium* in Mylodontinae is reinforced in this analysis (see Chapter 8). The earliest appearance of the genus *Urumacotherium* is settled in the middle Miocene Fitzcarrald fauna (Peruvian Amazonia; Tejada-Lara *et al.* 2015).

Type species: Urumacotherium garciai Bocquentin-Villanueva, 1984

Other species: Urumacotherium campbelli (Frailey, 1986)

URUMACOTHERIUM GARCIAI BOCQUENTIN-VILLANUEVA, 1984

Holotype: CIAAP 443, strongly diagenetic skull fragment and associated mandible (Bocquentin-Villanueva 1984).

Type locality and age: Urumaco, Estado Falcón, Venezuela; Urumaco Fm., late Miocene (Bocquentin-Villanueva 1984).

Known distribution: same as for the type material (Bocquentin-Villanueva 1984).

Observed material: see Appendix II and Bocquentin-Villanueva (1984). The material included for the codification are the holotypes CIAAP 443 and CIAAP 443–1, which consists of several postcranial remains of a single individual. The other remain of *U. garciai* is CIAAP 431, an incomplete left femur of unknown provenance from the Urumaco area. This remain, given the strikingly smaller size if compared with CIAAP 443–1, is not considered here as belonging to *U. garciai*.

Diagnosis: see Bocquentin-Villanueva (1984)

URUMACOTHERIUM CAMPBELLI (FRAILEY, 1986)

Holotype: LACM 117502, skull without dentition (Frailey 1986).

Type locality and age: Alto Rio Acre (Brazil); late Miocene (see Negri *et al.* 2010 for the latest absolute age estimations of the Solimões Fm.).

Known distribution: same as for the type material (Negri & Ferigolo 2004; Negri *et al.* 2010).

Observed material: see Appendix II, Negri & Ferigolo (2004), and Negri *et al.* (2010).

Diagnosis: see Frailey (1986); Negri & Ferigolo (2004).

PAROCTODONTOTHERIUM SHOCKEY & ANAYA, 2011

Type (and only) species: Paroctodontotherium calleorum Shockey & Anaya, 2011

PAROCTODONTOTHERIUM CALLEORUM SHOCKEY & ANAYA, 2011

Holotype: UATF-V-127, partial skull with right and left Mf1–3, much of the cranial vault, isolated Mf4, and a small portion of the basicranium with both condyles and a portion of the right otic region (Shockey & Anaya 2011).

Type locality and age: Calaboza Pata locality (Salla, Bolivia); late Oligocene (Shockey & Anaya 2011).

Known distribution: same as for the type material.

Observed material: see Shockey & Anaya (2011) and Appendix II.

Diagnosis: see Shockey & Anaya (2011).

OCTODONTOTHERIUM AMEGHINO, 1894

Notes: This genus was erected by Ameghino (1894) for the species *Octodontotherium grande* and placed it in Mylodontidae [*O. grande* is the correct spelling for this species, and not *O. grandae* as originally spelled by Ameghino (1894) and reported by many authors (see ICZN 1999, arts 31–34 and Slater *et al.* 2016)]. In the same work, Ameghino (1894) also created the family Orophodontidae, to include the taxon *Orophodon hapaloides*, also erected in the same work. In a subsequent study, Ameghino (1897) included both these genera in Orophodontidae, and this scheme has been largely followed by many authors. In the latest analyses, both *Octodontotherium* and *Paroctodontotherium* are placed among Mylodontinae (Gaudin 2004; Shockey & Anaya 2011). All these three genera have been included in the analyses of Chapter 8 in order to test their phylogenetic affinities.

Type (and only) species: Octodontotherium grande Ameghino, 1894

OCTODONTOTHERIUM GRANDE AMEGHINO, 1894

Previously proposed synonymies: see Pujos & De Iuliis (2007)

Type material: MACN A 343 (lectotype), left mf3; MACN A 343a (syntype), four isolated teeth.

Type locality and age: La Flecha locality (Santa Cruz Province, Argentina); late Oligocene (Hoffstetter 1956; Pujos & De Iuliis 2007; Shockey & Anaya 2011).

Known distribution: same as for the type material.

Observed material: see Ameghino (1894), Hoffstetter (1956), Pujos & De Iuliis (2007), and Appendix II.

Diagnosis: see Hoffstetter (1956).

GLOSSOTHERIOPSIS SCILLATO-YANÉ, 1976

Type (and only) species: Glossotheriopsis pascuali Scillato-Yané, 1976

GLOSSOTHERIOPSIS PASCUALI SCILLATO-YANÉ, 1976

Type material: MLP 76-VIII-30-I, anterior part of cranium with right and left Cf1s and Mf1–2s, mandibular fragment, and two isolated teeth (Scillato-Yané 1976).

Type locality and age: Estancia "Los Sauces" (Rio Negro Province, Argentina); middle or late Miocene (Scillato-Yané 1976). The age of this deposits is quite dubious and the geological formation of provenance is not reported (see Scillato-Yané 1976).

Known distribution: Outside the type locality, scanty remains of *G. pascuali* have been recognized also in the Argentinian Provinces of Tucumán (unknown age; Esteban & Abdala 1993) and Catamarca (late Miocene; Esteban *et al.* 2014) but also in the deposits of the Colombian locality of La Venta (middle Miocene; McDonald 1997).

Observed material: only the holotype (Scillato-Yané 1976) has been observed for the purposes of present work (see Appendix II and comments below).

Diagnosis: see Scillato-Yané (1976).

Comments: Villarroel (2000) erected a new mylodontine genus and species from La Venta (middle Miocene; Colombia), *Brievabradys laventensis*. The latter author also ascribes to *B. laventensis* all the remains of *G. pascuali* from the same locality and previously described by McDonald (1997). The latter author does not agree with Villarroel's opinion and maintains that the holotype of *B. laventensis* is conspecific with *G. pascuali* or, at best, could represent a new species of *Glossotheriopsis* (McDonald, pers. comm. 2017). However, the direct observation of the holotype of *G. pascuali* and the high-quality photographs of the holotype of *B. laventensis* (kindly provided by J. Tejada-Lara), together with the available information in McDonald (1997) and Villarroel (2000), allow to observe striking differences between the holotypes, in both shape and size. This suggests that both genera are valid and monospecific and so they are treated for the purposes of this thesis. Therefore, for the Colombian locality of La Venta, the two mylodontines *G. pascuali* and *B. laventensis* are recognized.

BRIEVABRADYS VILLARROEL, 2000

Type (and only) species: Brievabradys laventensis Villarroel, 2000

BRIEVABRADYS LAVENTENSIS VILLARROEL, 2000

Type material: LV-4-12, cranium and mandibles with complete dentition but lacking the posterior portion (Villarroel 2000).

Type locality and age: Quebrada La Venta, Colombia; Victoria Fm., middle Miocene (Villarroel 2000).

Known distribution: same as for the type material.

Observed material: only the holotype (Villarroel 2000) has been observed for the purposes of present work (see Appendix II).

Comments: see comments above of *G. pascuali.*

Diagnosis: see Villarroel (2000).

MYLODONTINI SAINT-ANDRE, 1994

MYLODON OWEN, 1839

Notes: Both Mylodontidae and Mylodontinae are typified by the genus *Mylodon*, established by Owen (1839) on the basis of an almost complete right and left dentaries with complete dentition. The latter author created the species *Mylodon darwinii* in honor of Charles Darwin, who discovered these remains in Punta Alta (Buenos Aires Province, Argentina) in 1832 (Fernicola *et al.* 2009). The taxonomic history of *Mylodon* is among the more complex for the taxa erected by Owen (Fernicola *et al.* 2009), mainly due to the confusion with the genus *Glossotherium* (for reviews on the subject see Fernicola *et al.* 2009, McAfee 2009, and De Iuliis *et al.* 2017). Moreover, several species have been attributed to the genus *Mylodon* (see Mones 1986a) but only some of them have been maintained until recently (e.g., *M. listai* (Ameghino, 1898) and *M. insigne* Kraglievich, 1928, as considered by Carlini & Scillato-Yané 1999). However, in the revision of Pleistocene giant mylodontids from southern South America of Esteban (1996) all of them have been considered junior synonyms of *M. darwinii*. The latter author considered that *M. listai* and *M. insigne* lack of reliable diagnostic features and their variability falls within the range of *M. darwinii*. Brandoni *et al.* (2010: 1553) also considered that "*M. darwini* is the only well determined, diagnosed, and valid species of the genus", an approach that is followed here.

Type (and only) species: Mylodon darwinii Owen, 1839

MYLODON DARWINII OWEN, 1839

Previously proposed synonymies: see Esteban (1996), Brandoni *et al.* (2010), and McAfee (2016).

Holotype: NHMUK PV M 16563a (ex RCS 3490), left and right dentaries with complete dentition but lacking the anteriormost portion of the mandibular symphysis and the ascending processes. Information obtained in the Natural History Museum Data Portal

(http://data.nhm.ac.uk/dataset/collection-specimens/resource/05ff2255-c38a-40c9-b657-4ccb55ab2feb/record/442048; retrieved 04 Nov 2018).

Type locality and age: Punta Alta (Bahía Blanca, Buenos Aires Province, Argentina); late Pleistocene.

Observed material: see Appendix II.

Diagnosis: see Esteban (1996), and McAfee (2016).

Comments: *M. darwinii* is the correct usage, and not *M. darwini* as reported by many authors (see ICZN 1999, art. 31.1 and De Iuliis *et al*. 2017).

GLOSSOTHERIUM OWEN, 1839

Notes: The genus *Glossotherium* was established by Owen (1839) based on the left posterior half of a skull recovered from Arroyo Sarandí (Soriano Department, Uruguay), discovered by Charles Darwin during his travels on the HMS Beagle (Fernicola *et al*. 2009). As for the genus *Mylodon*, also the genus *Glossotherium* experienced several taxonomic ambiguities, and numerous authors speculated on whether these latter taxa were congeneric or conspecific (see De Iuliis *et al*. 2017 and references therein). In the most recent revisions, both genera are considered valid and respectively typified by the species *M. darwinii* and *G. robustum* (Esteban 1996; McAfee 2009; Brandoni *et al*. 2010). Another problem that affected the taxonomy of *Glossotherium* is the extreme proliferation of specific names ascribed to the latter genus (e.g., Mones 1986a, listed 32 specific and sub-specific names). The recent systematic revision performed by Esteban (1996) on the basis of abundant material mainly from Argentina, recognized only two *Glossotherium* species: *G. robustum* and *G. chapadmalensis*. McAfee (2009) shared the same opinion, even though he allowed for the possibility that *G. chapadmalensis* belonged to another genus (i.e., *Eumylodon*), following the original description of Kraglievich (1925) [for this latter genus an independent generic attribution is adopted here, on the basis of its smaller size and several morphological peculiarities; see the genus *Glossotheridium* at page 58]. Recently, Pitana *et al.* (2013) also considered valid *G. lettsomi* from the Pleistocene of Argentina, Chile, and Uruguay (Ameghino 1889; Pitana *et al.* 2013 and references therein), *G. wegneri* from the Pleistocene of Brazil and Ecuador (Hoffstetter 1952; Simpson & Paula-Couto 1981; but see the genus *Oreomylodon* at page 55), *G. tropicorum* from the late Pleistocene of Ecuador and Venezuela

(Hoffstetter 1952; Bocquentin 1979), and an indeterminate *Glossotherium* species, widely distributed into the intertropical latitudes of the South American continent. In the most recently updated listing of extant and extinct intertropical sloths, Pujos *et al.* (2017) ascribed five species under the genus *Glossotherium*: *G. robustum*, *G. tarijense*, *G. wegneri*, *G. tropicorum*, and the intertropical *Glossotherium* species (i.e., *Glossotherium phoenesis*; Cartelle *et al.* 2019). Except for *G. wegneri*, this latter arrangement of the genus *Glossotherium* is followed here.

Type species: *Glossotherium robustum* (Owen, 1842)

Other species: Glossotherium tarijense (Ameghino, 1902); *Glossotherium tropicorum* (Hoffstetter, 1952); *Glossotherium phoenesis* (Cartelle *et al.*, 2019)

GLOSSOTHERIUM ROBUSTUM (OWEN, 1842)

Previously proposed synonymies: see Esteban (1996) and McAfee (2009).

Holotype: lost. Almost complete skeleton described by Owen (1842) but destroyed by the bombing of London during World War II (see McAfee 2009; De Iuliis *et al.* 2017). A neotype is still not designated (Dr. Pip Brewer, NHMUK curator, pers. comm. 2018).

Type locality and age: "seven leagues north of the city of Buenos Aires" (Buenos Aires Province, Argentina); Pleistocene (Owen 1842: 3).

Known distribution: late Pleistocene of many localities throughout southern cone, between latitudes of 20°S and 40°S (Carlini & Scillato-Yané 1999; McAfee 2009; Pitana *et al.* 2013).

Observed material: see Appendix II.

Diagnosis: see Esteban (1996) and McAfee (2009).

GLOSSOTHERIUM TARIJENSE (AMEGHINO, 1902)

Holotype: MACN Pv 1002, cranium with almost complete dentition, lacking right Cf1 and left Mf4 (Ameghino 1902).

Type locality and age: Tarija Valley (Tarija Department, Southern Bolivia); middle and/or late Pleistocene (see Coltorti *et al.* 2007 and MacFadden *et al.* 2013).

Known distribution: same as for the type material.

Observed material: see Appendix II.

Diagnosis: see Ameghino (1902).

GLOSSOTHERIUM TROPICORUM HOFFSTETTER, 1952

Holotype: MNHN.F.LAR 237 (ex EPN V. 1230), left maxillary fragment with Cf1-Mf3 (see Hoffstetter 1948, 1952; Montellano-Ballesteros & Román-Carrión 2011; De Iuliis *et al.* 2017).

Paratype: see De Iuliis *et al.* (2017).

Type locality and age: La Carolina (Santa Elena Peninsula, Ecuador); late Pleistocene (Hoffstetter 1952).

Known distribution: late Pleistocene of coastal lowland areas of Ecuador and Peru.

Observed material: see De Iuliis *et al.* (2017) and Appendix II.

Diagnosis: see De Iuliis *et al.* (2017).

GLOSSOTHERIUM PHOENESIS CARTELLE *ET AL.*, 2019

Holotype: MCL 4303, almost complete skeleton.

Paratype: MCL 4027, complete skull lacking the processes of the jugals and part of the dentition.

Type locality and age: Toca dos Ossos, Ouro Branco, Bahia, Brazil; late Pleistocene (Cartelle *et al.* 2019).

Known distribution: intertropical region of Brazil (Minas Gerais and Bahia States).

Observed material: see Cartelle *et al.* (2019).

Diagnosis: see Cartelle *et al.* (2019).

OREOMYLODON (HOFFSTETTER, 1949)

Type (and only) species: Oreomylodon wegneri (Spillmann, 1931)

OREOMYLODON WEGNERI (SPILLMANN, 1931)

Notes: This species was originally erected as *Mylodon wegneri* by Spillmann (1931). This attribution later changed in *Glossotherium wegneri* (Hoffstetter 1948), *Glossotherium* (*Oreomylodon*) *wegneri* (Hoffstetter 1949, 1952) and *Oreomylodon wegneri* (Dechaseaux 1971). Still today, its taxonomic status is uncertain, as some authors consider it a valid species of the genus *Glossotherium* (*G. wegneri*; e.g., Pitana *et al.* 2013; Pujos *et al.* 2017), a junior synonym of *G. robustum* (McAfee 2009) or belonging to *Oreomylodon wegneri* (Esteban 1996). This latter species is currently under study by C. Cartelle and colleagues, with the aim of clarifying these obscure nomenclatural aspects. For the aims of the present study, the work of Dechaseaux (1971) and the revisions of Esteban (1996), Saint-André *et al.* (2010), and Antoine *et al.* (2017) are followed here, in recognizing *Oreomylodon* as a separate genus, with the only valid species being *Oreomylodon wegneri*.

Previously proposed synonymies: see Esteban (1996).

Holotype: lost (see Hoffstetter 1948; Montellano-Ballesteros & Román-Carrión 2011).

Neotype: EPN V. 120, cranium without mandibles, atlas, right scapula, elements of the third digit of the left hand (mtc3, proximal and distal phalanges, lateral sesamoid), fragment of pelvis, left navicular, and dermal ossicles. This neotype was designated by Hoffstetter (1948) based on remains that himself previously found in 1946 (Montellano-Ballesteros & Román-Carrión 2011).

(Neo)type locality and age: La Cocha locality (close to Alangasí, Pichincha Province, Ecuador); late Pleistocene (Hoffstetter 1948; Montellano-Ballesteros & Román-Carrión 2011).

Known distribution: inland and highland areas of the Andes of Ecuador (Hoffstetter 1949; De Iuliis *et al.* 2017).

Observed material: see Appendix II.

Diagnosis: see Hoffstetter (1948, 1949, 1952)

PARAMYLODON BROWN, 1903

Notes: After long debates on how to refer to the large-sized mylodontine sloth from the Pleistocene of North America (for a synopsis see McDonald 1995), the latest agreement is to consider it as part of the genus *Paramylodon*, differentiable in craniodental traits from the South American *Glossotherium* (e.g., McDonald 1995; Gaudin 2004; McDonald *et al.* 2004; McAfee 2009). The focus of this debate successively moved to the smaller-sized mylodontine sloth from the Blancan of Florida, unfortunately lacking several anatomical parts, and initially referred to *Glossotherium* (*Glossotherium*) *chapadmalense* by Robertson (1976). McDonald demonstrated reluctance in the usage of this nomenclature and addressed the Blancan species as "*Glossotherium*" *chapadmalense*. In the latest years, many authors consider also this species as belonging to the genus *Paramylodon*, using the name *Paramylodon garbanii* (Montellano-Ballesteros & Carranza-Castañeda, 1986), as proposed by Morgan (2008). Consequently, the genera *Paramylodon* and *Glossotherium* are considered as having different distributions: the former being strictly North American, the latter exclusively South American.

Type species: *Paramylodon harlani* (Owen, 1839)

Other species: Paramylodon garbanii (Montellano-Ballesteros & Carranza-Castañeda, 1986)

PARAMYLODON HARLANI (OWEN, 1839)

Previously proposed synonymies: see McDonald (1995).

Holotype: lost (partially right mandible formerly housed in the New York Lyceum; see McDonald 1995)

Known distribution: Pleistocene localities of North America, from Central America to a latitude of ~50ºN (major localities are Rancho La Brea, California; Haile, Florida and American Falls, Idaho; see McAfee 2009).

Observed material: see Appendix II.

Diagnosis: see McAfee (2009).

PARAMYLODON GARBANII (MONTELLANO-BALLESTEROS & CARRANZA-CASTAÑEDA, 1986)

Notes: Morgan (2008) proposed the new combination for *P. garbanii*, based on previous observations of McDonald (1995), for the small-sized Blancan mylodontid remains of Mexico and Southern USA. This approach has been followed to establish a taxonomic unit for the material described by Robertson (1976), in order to test the phylogenetic affinities of this small-sized mylodontine sloth with the other members of the group from both South and North America.

Previously proposed synonymies: see Morgan (2008).

Holotype: IGCU, 3882 fragment of left mandible with alveoli of mf2, several carpals and tarsals, dermal ossicles (see Montellano-Ballesteros & Carranza-Castañeda 1986).

Type locality and age: Arroyo El Tanque (San Miguel de Allende, Municipality, Guanajuato, Mexico); early Pliocene (see Montellano-Ballesteros & Carranza-Castañeda 1986; Morgan 2008 and references therein).

Known distribution: Pliocene of Mexico and Southern USA (see Morgan 2008 and references therein).

Observed material: see Appendix II.

Diagnosis: see Montellano-Ballesteros & Carranza-Castañeda (1986).

GLOSSOTHERIDIUM KRAGLIEVICH, 1934

Type (and only) species: Glossotheridium chapadmalense (Kraglievich, 1925)

GLOSSOTHERIDIUM CHAPADMALENSE (KRAGLIEVICH, 1925)

Notes: Kraglievich (1925) erected *Eumylodon chapadmalensis* on the basis of a damaged skull, associated with mandibles, recovered from the Chapadmalal Fm. (Pliocene; Miramar, Buenos Aires Province, Argentina). The genus *Eumylodon* was previously erected by Ameghino (1904) for the Pleistocene species *Eumylodon robustus* (= *Mylodon robustus* Owen, 1842), now considered

Glossotherium robustum (Owen, 1842) (see Esteban 1996 and previous notes on the genus *Glossotherium*, at page 53). In a subsequent revision of Mylodontinae, Kraglievich identifies only three valid genera: *Glossotherium*, *Mylodon* and *Paramylodon* (Kraglievich, 1928). Consequently, on the basis of similarities on the dental formula, the latter author ascribed the Pliocene mylodontine to the former genus (i.e., *Glossotherium chapadmalense*). However, some years later, detecting differences in the shape of the muzzle region, between *G. robustum* and *G. chapadmalense*, Kraglievich (1934) erected a new subgenus (*Glossotheridium*) for allocating the latter species. Cattoi (1966) elevated *Glossotheridium* at the generic level, stressing the differences between the Pleistocene and Pliocene forms. However, this approach was not followed by Esteban (1996), who considered this species as belonging to *Glossotherium*. McAfee (2009) was on the same opinion, but he stressed the fact that knowledge of the Pliocene form is still too limited and that an independent generic classification is also plausible. In the present thesis, this taxon has been intensively used for comparisons with *Simomylodon uccasamamensis*, and considered, for the moment, as belonging to the genus *Glossotheridium*, following Cattoi (1966). In this way, its phylogenetic affinities are tested, for the first time, in Chapter 8, with the aim of shedding new light on this long scientific debate.

Holotype: MACN Pv 8675, cranium lacking the posterior portion, right Mf1 and left Mf1–2. Mandibles lacking both ascending processes and right mf2 (Kraglievich 1925).

Type locality and age: Baliza Chica locality (Miramar, Buenos Aries Province, Argentina); Chapadmalal Fm., early Pliocene (Kraglievich 1925).

Known distribution: same as for the type material (Kraglievich 1925).

Observed material: see Appendix II.

Diagnosis: see Kraglievich (1925).

PLEUROLESTODON ROVERETO, 1914

Notes: The genus *Pleurolestodon* was erected by Rovereto (1914) who established three species, coming from the Catamarca Province (Argentina) without precise geographic and stratigraphic data. These species were synonymized by Kraglievich (1921a), and later by Saint-André *et al.* (2010) under the type species *P. acutidens*. The latter authors also established a new species of

Pleurolestodon (i.e., *Pleurolestodon* [= *Glossotheriuscum*] *dalenzae*) from the Bolivian locality of Choquecota (Saint-André *et al.* 2010). However, this species is here considered a junior synonym of *Simomylodon uccasamamensis* (see below and Chapter 6). Consequently, the genus *Pleurolestodon* is henceforth considered monospecific.

Type (and only) species: *Pleurolestodon acutidens* Rovereto, 1914

PLEUROLESTODON ACUTIDENS ROVERETO, 1914

Previously proposed synonymies: see Kraglievich (1921a) and Saint-André *et al.* (2010).

Holotype: lost (MACN Pv 2952–2953 cranium and mandible with complete dentition; A. Kramarz, MACN curator pers. comm. 2017). However, photos and measurements of the holotype are available in the original publication of Rovereto (1914).

Type locality and age: precise geographic and stratigraphic data of the material described by Rovereto (1914) is lacking.

Known distribution: Río Corral Quemado (Catamarca Province, Argentina); late Miocene (Marshall & Patterson 1981).

Observed material: see Appendix II.

Diagnosis: see Rovereto (1914), and Kraglievich (1921a).

SIMOMYLODON SAINT-ANDRÉ *ET AL.*, 2010

Type (and only) species: *Simomylodon uccasamamensis* Saint-André *et al.*, 2010

SIMOMYLODON UCCASAMAMENSIS SAINT-ANDRÉ *ET AL.*, 2010

Synonymy:

Glossotheriscum dalenzae Saint-André, 1994: 174–183, fig. 18, pl. 13.

Simotherium uccasamamense Saint-André, 1994: 184–228, figs 19–20, pls 14–20.

Glossotheridium chapadmalense: Anaya & MacFadden, 1995: 94–98, figs 3–5, table 1, nec Kraglievich 1925

Mylodontinae indet. Anaya & MacFadden, 1995: 98–99, figs 6–7.

Pleurolestodon dalenzae Saint-André *et al.*, 2010: 261–269, figs 2–4, table 1.

Holotype: MNHN-Bol V 11731 (ex GB 078), anterior part of cranium without dentition (Saint-André *et al.* 2010).

Paratype: MNHN-Bol V 3321, maxillary and premaxillary fragments with left Mf1-Mf3 and right Mf2--Mf4 (Saint-André *et al.* 2010).

Observed material: see Appendix I.

Type locality and age: Ayo Ayo-Viscachani (La Paz Department, Bolivia); Umala Fm., late Pliocene (Saint-André *et al.* 2010).

Known distribution: latest Miocene–earliest Pliocene of Choquecota, early Pliocene of Pomata-Ayte, Casira and Inchasi (Oruro and Potosí Departments, Bolivia), and late Pliocene of Ayo Ayo-Viscachani (La Paz Department, Bolivia).

Revised diagnosis: Extinct sloth smaller in size than *Glossotheridium chapadmalense*, *Paramylodon garbanii* and *Pleurolestodon acutidens*, and roughly biometrically similar to *Glossotheriopsis pascuali*; long zygomatic processes of squamosal; wide braincase in relation to the total cranial length and wide V-shaped palate; in ventral view, the medial palatal process of the maxilla is more extended mediolaterally than anteroposteriorly and the occipital condyles are well-separated from the condyloid foramina, as in the Miocene species *Pleurolestodon acutidens*; the foramen magnum shows a detached notch located on its dorsal border, similar to that observed in *Pleurolestodon* and *Mylodon*; long and slender ascending process of the jugal which strongly resembles that of *Glossotheridium chapadmalense*; the diastema between Cf1 and Mf1 is absent or extremely reduced and, in lateral view, Cf1 presents an almost vertical wear facet similar to the condition in *Pleurolestodon acutidens*; Mf2 and Mf3 possess a marked lingual sulcus, comparable to *Pleurolestodon acutidens* and *Paramylodon garbanii*; cf1 is beveled with well-developed mesial and distal wear surfaces; mf3 is marked by a deep apicobasal sulcus on its lingual side, absent in the labial side and not covered by the ascending ramus of the mandible in lateral view (like *G. chapadmalense* and unlike *P. acutidens* and *P. garbanii*); the symphyseal spout is anteriorly flat as in *G. chapadmalense* and not rounded as in *P. acutidens* and *P. garbanii*.

KIYUMYLODON RINDERKNECHT, PEREA & MCDONALD, 2007

Type (and only) species: Kiyumylodon lecuonai Rinderknecht, Perea & McDonald, 2007

KIYUMYLODON LECUONAI RINDERKNECHT, PEREA & MCDONALD, 2007

Holotype: FCDPV 1829, almost complete right mandible with dentition (Rinderknecht *et al.* 2007).

Type locality and age: Kiyú beach coastal platform, Department of San José, Uruguay; Camacho Fm., late Miocene (Rinderknecht *et al.* 2007).

Known distribution: same as for the type material (Rinderknecht *et al.* 2007).

Observed material: see Appendix II and Rinderknecht *et al.* (2007).

Diagnosis: see Rinderknecht *et al.* (2007).

MYLODONOPSIS CARTELLE, 1991

Type (and only) species: Mylodonopsis ibseni Cartelle, 1991

MYLODONOPSIS IBSENI CARTELLE, 1991

Holotype: MCL 450, several elements belonging to the same individual (Cartelle 1991), now under revision.

Type locality and age: Brejões Cave (Morro do Chapéu, Bahia, Brazil), late Pleistocene – Holocene (Cartelle 1991).

Known distribution: late Pleistocene (and probably also early Holocene) of the intertropical Brazilian region (Bahia and Minas Gerias States; Cartelle 1991).

Observed material: see Cartelle (1991).

Diagnosis: see Cartelle (1991).

ARCHAEOMYLODON Brambilla & Ibarra, 2019

Type (and only) species: Archaeomylodon sampedrinensis Brambilla & Ibarra, 2019

ARCHAEOMYLODON SAMPEDRINENSIS Brambilla & Ibarra, 2019

Holotype: MPS 119, cranium without premaxilla and jugals, and with fragmented zygomatic processes of the squamosal.

Type locality and age: Cantera Iglesias (San Pedro, Buenos Aires Province, Argentina), early-middle Pleistocene (Brambilla & Ibarra 2019).

Known distribution: same as for the type material.

Observed material: see Brambilla & Ibarra (2019).

Diagnosis: see Brambilla & Ibarra (2019).

OCNOTHERIUM LUND, 1842

Type (and only) species: Ocnotherium giganteum (Lund, 1839)

OCNOTHERIUM GIGANTEUM (LUND, 1839)

Holotype: ZMUC 1/1845:2399, isolated cf1.

Type locality and age: late Pleistocene and/or early Holocene, under study by C. Cartelle and colleagues.

Known distribution: same as for the type material.

Observed material: only the holotype is currently known.

Diagnosis: see Lund (1839, 1842).

LESTODONTINI AMEGHINO, 1889 *SENSU* GAUDIN (2004)

Notes: The first suprageneric aggrupation of lestodontines sloths was created by Ameghino (1889) and included several species of the genus *Lestodon*, but also the genera *Laniodon* and *Diodomus* (Ameghino 1889). *Laniodon* was later synonymized under *Glossotherium* (McKenna & Bell 1997) and *Diodomus* was declared *nomen dubium* (Mones 1986b).

Lestodontidae was later considered Lestodontinae (included into Mylodontidae) by Ameghino (1895), an approach followed by Kraglievich (1921b, 1934), but not by Cattoi (1966). Engelmann (1985) did not consider *Lestodon* and *Thinobadistes* to form a monophyletic group. Webb (1989) used Lestodontinae for the group including *Lestodon* and *Thinobadistes*. A similar result was obtained in the preliminary phylogenetic study of Saint-André (1994) who recovered independent clades for lestodontines and mylodontines. However, Esteban (1996), who reviewed the Quaternary mylodontines from the southern cone, considered *Lestodon* as a member of Mylodontinae. Finally, Gaudin (2004) recovered a strongly supported clade for the group including *Lestodon* and *Thinobadistes*, inside the traditionally recognized Mylodontinae, and attributed the latter genera to Lestodontini. For this reason, this latter usage is followed here, and tested in the phylogenetic analyses of this work (see Chapter 8).

LESTODON GERVAIS, 1855

Notes: The genus *Lestodon* was erected by P. Gervais who created the species *L. armatus* and *L. myloides* (Gervais 1855). Many other species of the genus *Lestodon* were established in the following years (e.g., Gervais & Ameghino 1880; Ameghino 1889; Kraglievich 1934). The majority of these names were later synonymized by Esteban (1996) who considered the genus *Lestodon* represented by only two species: *L. armatus* Gervais, 1855 and *L. australis* Kraglievich, 1934. In the latest revisions of the genus (Czerwonogora & Fariña 2013) only the former species is considered valid, an approach that is followed here.

Type (and only) species: *Lestodon armatus* Gervais, 1855

LESTODON ARMATUS GERVAIS, 1855

Previously proposed synonymies: see Esteban (1996) and Czerwonogora & Fariña (2013).

Holotype: MNHN.F.PAM90, left and right mandibular fragments with alveoli of cf1 and mf1-3; MNHN.F.PAM91, left maxillary fragment with cf1, mf1, and part of the mf2 alveolus.

Type locality and age: Buenos Aires Province, Argentina, late Pleistocene.

Observed material: see Appendix II.

Diagnosis: see Esteban (1996) and Czerwonogora & Fariña (2013).

THINOBADISTES HAY, 1919

Notes: The genus *Thinobadistes* was established by Hay (1919), on the basis of a left astragalus (USNM 3333) from the early Hemphillian NALMA Alachua Fm. (central Florida) that was ascribed to the species *Thinobadistes segnis* Hay, 1919. Successively, Webb (1989) described abundant material of this taxon, and erected a younger (middle Hemphillian) species, *T. wetzeli*, again on the basis of an astragalus, UF 93051. The unique diagnostic features of the two species are a difference in size (*T. wetzeli* about 25% larger than *T. segnis*) and the presence/absence of an extra medial atragalo-calcaneal facet (present in *T. segnis* and absent in *T. wetzeli*; see Webb 1989). However, the presence/absence of the latter facet is only recognizable on the holotypes, but it constitutes a poor diagnostic feature in other homologues remains ascribed to both *T. segnis* and *T. wetzeli*. For this reason, *T. segnis* is probably the only valid species for the genus *Thinobadistes*, a lineage that possibly achieved larger size through time and *T. wetzeli* can be probably a junior synonym. In any case, pending a more detailed analysis of this North American lestodontid, the classification proposed by Webb (1989) is maintained herewith but the remains of *Thinobadistes* are treated at the generic level in Chapter 8.

Type species: Thinobadistes segnis Hay, 1919

Other species: Thinobadistes wetzeli Webb, 1989

THINOBADISTES SEGNIS HAY, 1919

Holotype: USNM 3333, left astragalus (Hay 1919; Webb 1989).

Type locality and age: Mixon's Bone Bed, near Williston, Levy County, Florida; Alachua Fm., late Miocene (Hay 1919; Webb 1989).

Known distribution: late Miocene of southeastern North America (Florida and Texas; Webb 1989; Morgan 2008).

Observed material: see Appendix II and Webb (1989).

Diagnosis: see Webb (1989).

THINOBADISTES WETZELI WEBB, 1989

Holotype: UF 93051, left astragalus (Webb 1989).

Type locality and age: Withlacoochee River, site 4X, Citrus County, Florida; late Miocene (Webb 1989).

Known distribution: late Miocene of central Florida and Panhandle of Texas (Webb 1989).

Observed material: see Appendix II and Webb (1989).

Diagnosis: see Webb (1989).

BOLIVARTHERIUM CARLINI, SCILLATO-YANÉ & SÁNCHEZ 2006

Notes: The genus *Bolivartherium* was created by Carlini *et al*. (2006) to include two species: *B. urumaquensis* and *B. codorensis*, formerly ascribed by Linares (2004a) to the genus *Lestodon*. The two species are respectively recovered from the Urumaco (late Miocene) and Codore (Pliocene) Fms (Urumaco, Estado Falcón, Venezuela). However, the two species are difficult to characterize because of the scanty (and largely nonhomologous) remains and more materials are necessary for an exhaustive revision. For this reason, even if the classification is maintained, the genus *Bolivartherium* is hereafter treated in this work as *Bolivartherium* sp.

Type species: *Bolivartherium urumaquensis* (Linares, 2004a)

Other species: *Bolivartherium codorensis* (Linares, 2004a)

BOLIVARTHERIUM URUMAQUENSIS (LINARES, 2004A)

Holotype: MCN 170-72v, right maxillary fragment with alveoli of the Cf1-Mf4; posterior part of the cranium with the occipital, right occipital condyle, and fragments of the parietals, part of the mandible with both rami joined at the symphysis, without ascending ramus, with the alveoli of cf1-mf3, and damaged left ulna (Carlini *et al.* 2006).

Type locality and age: Urumaco, Estado Falcón, Venezuela; Urumaco Fm., late Miocene (Carlini *et al.* 2006).

Known distribution: same as for the type material (Carlini *et al.* 2006).

Observed material: see Appendix II and Carlini *et al.* (2006).

Diagnosis: see Carlini *et al.* (2006).

BOLIVARTHERIUM CODORENSIS (LINARES, 2004A)

Holotype: AMU-CURS 130 (MPU 015 of Linares 2004a), diagenetic skull without dentition (Carlini *et al.* 2006).

Type locality and age: Urumaco, Estado Falcón, Venezuela; Codore Fm., Pliocene (Carlini *et al.* 2006).

Known distribution: same as for the type material (Carlini *et al.* 2006).

Observed material: see Appendix II and Carlini *et al.* (2006).

Diagnosis: see Carlini *et al.* (2006).

LESTOBRADYS RINDERKNECHT *ET AL.*, 2010

Type (and only) species: *Lestobradys sprechmanni* Rinderknecht *et al.*, 2010

LESTOBRADYS SPRECHMANNI RINDERKNECHT *ET AL.*, 2010

Holotype: FCDPV 1826, anterior portion of the skull with left Cf1 and Mf1 and alveoli of the rest of the toothrows; a nearly complete right mandible lacking the symphyseal region and

the ascending ramus, but preserving the alveoli of cf1-mf2 and the partial alveoli of mf3; five vertebrae (Rinderknecht *et al.* 2010).

Type locality and age: Kiyú beach coastal platform, Department of San José, Uruguay; Camacho Fm., late Miocene (Rinderknecht *et al.* 2010).

Known distribution: same as for the type material (Rinderknecht *et al.* 2010).

Observed material: see Appendix II and Rinderknecht *et al.* (2010).

Diagnosis: see Rinderknecht *et al.* (2010).

SPHENOTHERUS AMEGHINO, 1891B

Notes: The genus *Sphenotherus* was created by Ameghino (1891b) on the basis of a fragment of mandible from the late Miocene of Catamarca (Northwestern Argentina). In the same work, Ameghino also created *S. paranensis* based on an isolated tooth from the Entre Ríos Province, but this species was declared junior synonym of *P. zavaletianus* by Esteban (1999).

Type (and only) species: Sphenotherus zavaletianus Ameghino, 1891b

SPHENOTHERUS ZAVALETIANUS AMEGHINO, 1891B

Previously proposed synonymies: see Esteban (1999).

Holotype: MACN A 802, left mandible lacking ascending ramus and dentition (Ameghino 1891b).

Type locality and age: Valle de Santa María (Catamarca, Argentina); stratigraphic data imprecise, most probably late Miocene (Esteban 1999).

Known distribution: Argentina, provinces of Catamarca and Entre Ríos (Ameghino 1891b; Brandoni 2013).

Observed material: see Appendix II.

Diagnosis: see Esteban (1999).

Chapter 6
SKELETAL ANATOMY OF *SIMOMYLODON UCCASAMAMENSIS*

Fossil remains of extinct terrestrial sloths have been discovered in numerous localities throughout the Americas, but knowledge of these animals remains poor in the tropical latitudes in comparison with the austral ones. Even where Pliocene mylodontine sloths are known from North and South America, well-preserved specimens are extremely rare, hindering reliable assessment of their taxonomic assignment and phylogenetic affinities.

In this chapter, new remains of *Simomylodon uccasamamensis*, from the latest Miocene–Pliocene of the Bolivian Altiplano, are described and compared to those of other Neogene Mylodontinae from South and North America. The resulting morphological observations, combined with morphometric analyses, permit reliable differentiation among these moderate-sized Miocene–Pliocene mylodontids. *Simomylodon uccasamamensis* appears to be the smallest Pliocene mylodontine and an endemic taxon of the Andean highlands during the Pliocene, with a continuous chronological range extending throughout the Montehermosan, Chapadmalalan and (early) Marplatan SALMAs. This terrestrial sloth may have found its ideal ecological conditions in the Bolivian Altiplano, during a span of time falling between the important South American late Miocene–Pliocene faunal turnover and the Great American Biotic Interchange around the Pliocene–Pleistocene transition.

6.1 CRANIODENTAL ANATOMY OF *S. UCCASAMAMENSIS*

6.1.1 Description

Cranium- Only two cranial remains were figured and described in detail by Saint-André *et al.* (2010), namely the holotype MNHN-Bol V 11731 (Fig. 6.1) and the paratype MNHN-Bol V 3321 (Fig. 6.2). The new remains here described allow to significantly increase the knowledge of this taxon. The cranium of *Simomylodon uccasamamensis* appears elongated, with the cranial roof and cranial base roughly horizontal in lateral view. The nasal region is slightly depressed in relationship to the braincase. In dorsal view, MNHN-Bol V 3348 (Fig. 6.3A), 3711 (Fig. 6.4A) and 3726 (Fig. 6.5A) are more slender than MNHN-Bol V 3717 (Fig. 6.6A) and 3718 (Fig. 6.7A) (see measurements in Appendix IV, Datasets S1). The snout is elevated and widened anteriorly and relatively short; the braincase is wide in relationship to the total cranial length (Figs 6.4A, 6.6A, 6.7A).

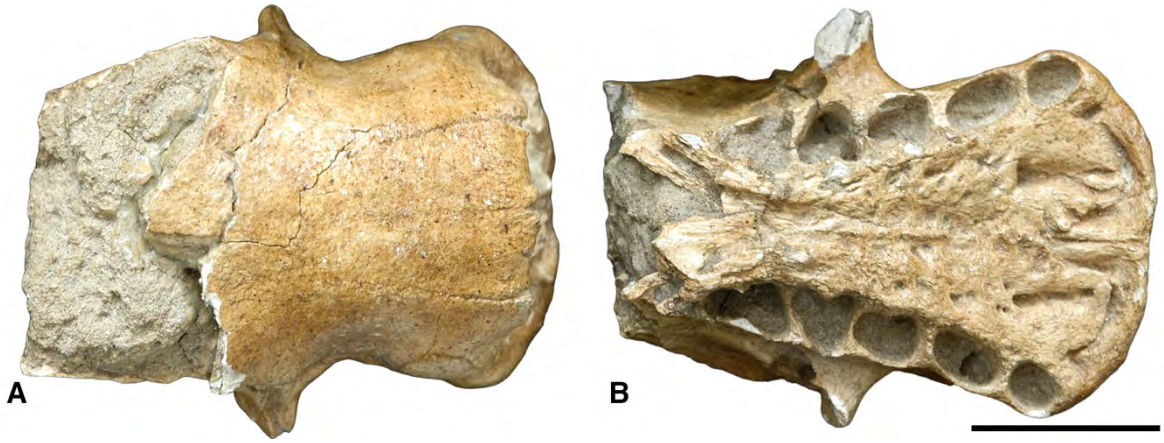

Figure 6.1. Anterior portion of the cranium of *Simomylodon uccasamamensis* (holotype, MNHN-Bol V 11731; ex GB 078) in dorsal (A) and ventral (B) views. Scale bar equals 5 cm.

In dorsal view, the nasals are narrow at the level of the antorbital constriction, and gradually broaden anteriorly and posteriorly (Figs 6.1A, 6.3–6.7A). The nasals are probably wider in MNHN-Bol V 3718 (Fig. 6.7A) than in the other specimens as a result of diagenetic dorsoventral compression of this skull. A V-shaped, posteriorly-pointed nasofrontal suture is present in all specimens examined. The anterior border of the nasals is strongly convex in MNHN-Bol V 3711 and 3726 (Figs 6.4–6.5A) and straighter in MNHN-Bol V 11731, 3717 and 3718 (Figs 6.1A, 6.6–6.7A); in MNHN-Bol V 3348 (Fig. 6.3A), the nasals are strongly convex but with a narrow, anteriorly-projecting median process.

The temporal fossa and the temporal lines are not clearly observable in all the specimens, owing to breakage and/or diagenetic deformation (Figs 6.5–6.6). In general, the temporal lines appear straight and roughly parallel to one another, diverging anteriorly as they approach the postorbital processes of the frontal bones. The temporal lines curve laterally and ventrally at their posterior limit, extending parallel and slightly anterior to the nuchal crest (Figs 6.3, 6.4, 6.7).

In lateral view, the anterior part of the cranium is dominated by the maxilla. This bone contacts the nasal and the frontal dorsally, the lacrimal in its middle part, and the palatine and the alisphenoid posteriorly. The premaxillae are preserved in six specimens. They are V-shaped in MNHN-Bol V 3348, 3711 and 3726 (Figs 6.3–6.5C), whereas they show a more arched profile (and even flatten anteriorly as they approach their midline junction) in MNHN-Bol V 11731, 3717 and 3718 (Figs 6.1B, 6.6–6.7C). Their medial and lateral rami are nearly equivalent in size, with the lateral ramus slightly longer than the medial one, in MNHN-Bol V 3348, 3711 and 3726 (Figs 6.3–6.5C), whereas the lateral ramus is substantially longer than the medial ramus in MNHN-Bol V 11731, 3717 and 3718 (Figs 6.1B, 6.6–6.7C). The palate is

rugose and strongly widened anteriorly, especially in MNHN-Bol V 11731, 3321, 3717 and 3718 (Figs 6.1–6.2B, 6.6–6.7C); whereas it is narrower in MNHN-Bol V 3348, 3711 and 3726 (Figs 6.3–6.5C; see also Morphometric analyses below). In lateral view, the palate is concave at the level of Cf1-Mf1 and convex posteriorly at the level of Mf2-Mf4. The anterior palatal foramina (*sensu* De Iuliis *et al.* 2011) are always clearly delineated (Figs 6.1–6.2B, 6.3–6.7C), and continue into distinct anterior grooves that extend medially to connect with the incisive foramina (not visible in ventral view). Also, enlarged postpalatal foramina (*sensu* Gaudin 2011) are observable in all specimens (Figs 6.1–6.2B, 6.3–6.7C).

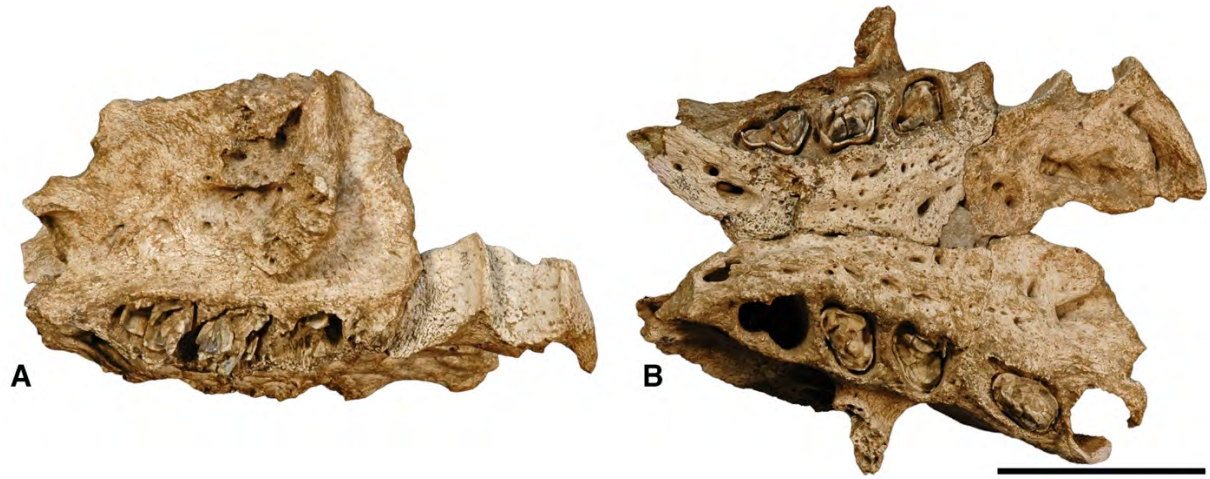

Figure 6.2. Maxillary and premaxillary fragments of *Simomylodon uccasamamensis* (paratype, MNHN-Bol V 3321) in lateral (A) and ventral (B) views. Scale bar equals 5 cm.

The sphenorbital fissure and the optic and sphenopalatine foramina are visible in MNHN-Bol V 3711, 3717 and 3718 (Figs 6.4, 6.6, 6.7). These foramina open into a common depression and are approximately aligned horizontally. The sphenorbital fissure is the posteriormost and largest of the three foramina mentioned above. The optic foramen is adjacent to the sphenorbital fissure and the sphenopalatine foramen is farther anterior, at the anterior margin of the common depression. Posteriorly and ventrally, the foramen ovale is located between the squamosal and the lateral plate of the pterygoid and opens onto the lateral wall of the cranium.

In ventral view, the structures of the middle region of the basicranium are difficult to observe, owing to poor preservation and complete fusion of the sutures. The pterygoids are inflated at their base (Fig. 6.4). The descending laminae of the pterygoid are broad and deep, but only preserved fully in MNHN-Bol V 3711 and 3717 (Figs 6.4, 6.6).

In lateral view, the lacrimal is more elongated anteroposteriorly than dorsoventrally, and is pierced by a rounded lacrimal foramen. The orbital portion of the bone is larger than its facial

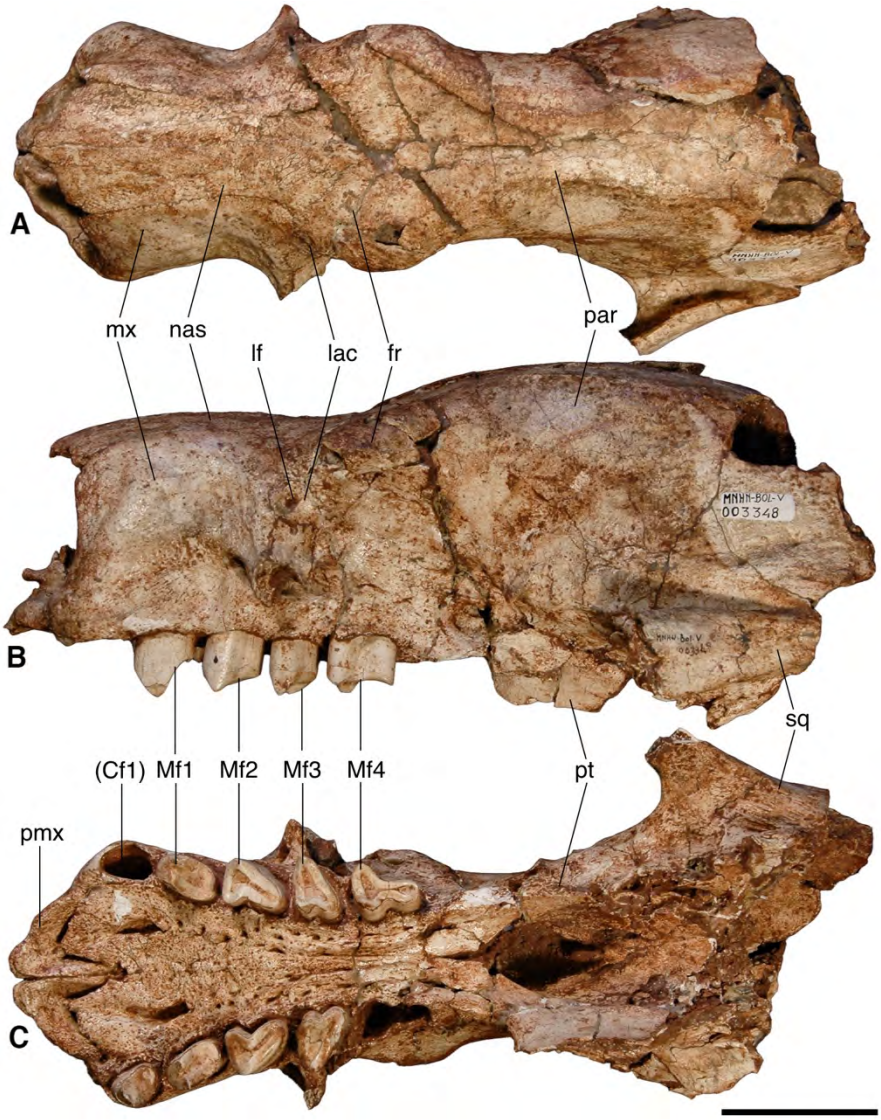

Figure 6.3. Cranium of *Simomylodon uccasamamensis* (MNHN-Bol V 3348) in dorsal (A), lateral (B), and ventral (C) views. Abbreviations: Cf, upper caniniform; fr, frontal; lac, lacrimal; lf, lacrimal foramen; Mf, upper molariform; mx, maxilla; nas, nasal; par, parietal; pmx, premaxilla; pt, pterygoid; sq, squamosal. Scale bar equals 5 cm.

portion. The jugal is firmly attached to the lacrimal and possesses ascending, descending and middle processes (Figs 6.4E, 6.5–6.7B), as is typical for sloths (Gaudin 2004). The ascending process is the longest of the three. It is wide at its base, becoming narrower posteriorly, and ends as a rounded tip located at the level of the anteroposterior midpoint of the zygomatic process of the squamosal. Ascending and middle processes are strongly divergent in MNHN-Bol V 3717 and 3718 (Figs 6.6–6.7B) and more convergent in MNHN-Bol V 3711 and 3726 (Figs 6.4E, 6.5B). The ascending process of the jugal is marked by a weak postorbital process near its base (Figs 6.4E, 6.5–6.7B). The middle process of the jugal is triangular in shape and closely approaches the zygomatic process of the squamosal posteriorly. The descending process of the jugal bears a posteriorly or posteromedially extended hook in MHNH-Bol V 3717 and

3718 (Figs 6.6–6.7) that is not present in MNHN-Bol V 3711 and 3726 (Figs 6.4–6.5). The long zygomatic process of the squamosal is almost horizontal in lateral view, and anterolaterally directed in dorsal view (Figs 6.3–6.7).

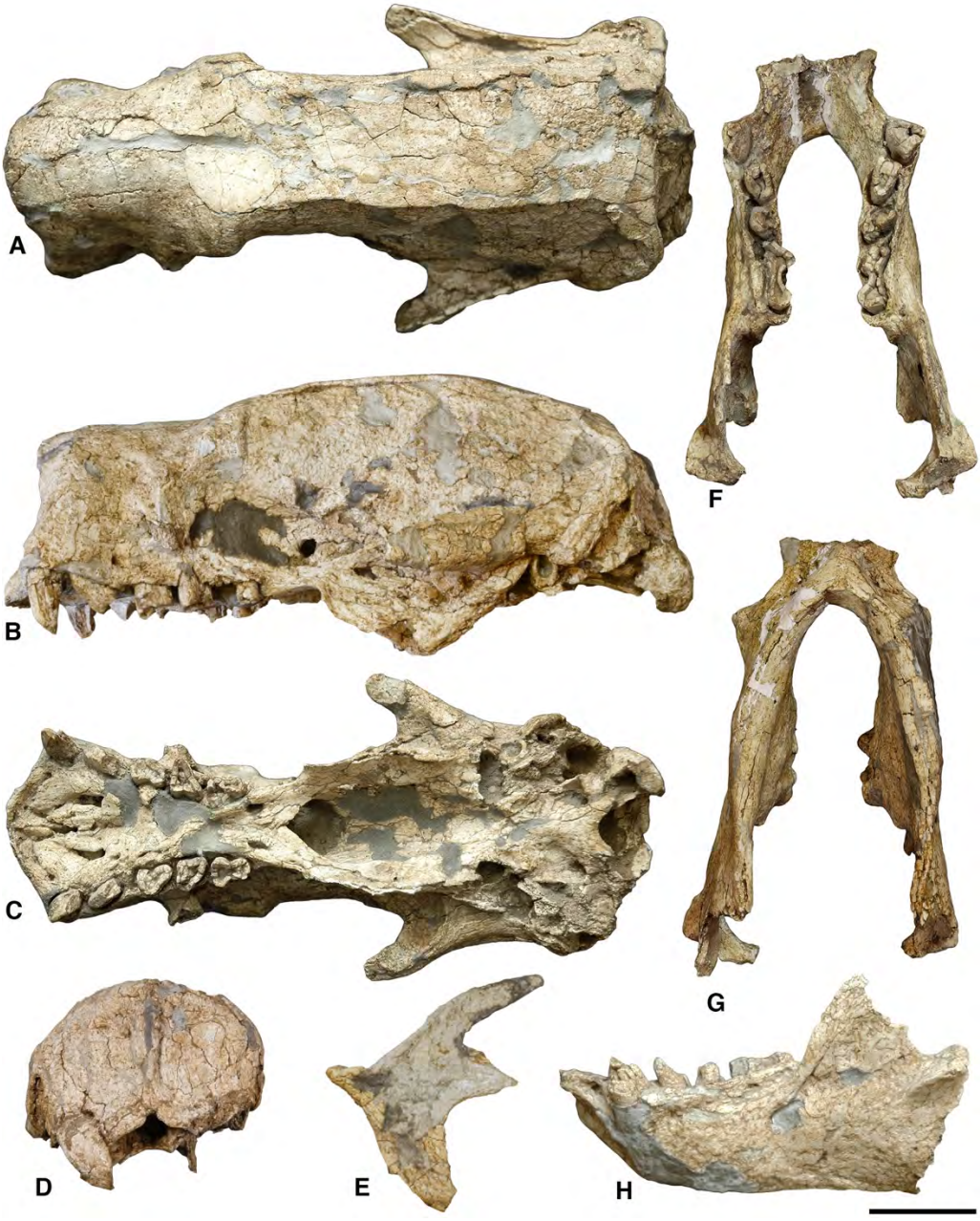

Figure 6.4. Cranium of *Simomylodon uccasamamensis* (MNHN-Bol V 3711) in dorsal (A), lateral (B), ventral (C), and posterior (D) views and (E) isolated jugal in lateral view. Mandibles in occlusal (F), ventral (G) and lateral (H) views. Scale bars equal 5 cm.

In lateral view, the occipital is inclined anteriorly in MNHN-Bol V 3711 (Fig. 6.4B), whereas it appears more vertical in MNHN-Bol V 3718 (Fig. 6.7B). In posterior view (Fig. 6.4D), its transverse breadth exceeds its dorsoventral height. The occipital is marked by a slight median external occipital crest that does not continue dorsally into a sagittal crest and

culminates ventrally in a well-marked notch on the posterior edge of the foramen magnum (Fig. 6.4D). The nuchal crests are strongly developed and clearly visible in dorsal, lateral and posterior views (Figs 6.4, 6.7). The occipital condyles, in ventral view, are roughly triangular in shape with a slightly concave medial edge, and are slightly more elongated mediolaterally than anteroposteriorly (Fig. 6.7C). In lateral view they appear more prominent in MNHN-Bol V 3711 (Fig. 6.4B) than in MNHN-Bol V 3718 (Fig. 6.7B), a difference that is probably related with the inclination of the occiput previously discussed.

Figure 6.5. Cranium and mandibles of *Simomylodon uccasamamensis* (MNHN-Bol V 3726) in dorsal (A), lateral (B), and ventral (C) views. Mandibles in occlusal (D), lateral (E), and ventral (F) views. Scale bars equal 5 cm.

Figure 6.6. Cranium and mandibles of *Simomylodon uccasamamensis* (MNHN-Bol V 3717) in dorsal (A), lateral (B), ventral (C), and anterior (D) views. Mandibles in occlusal (E) and ventral (F) views. Scale bars equal 5 cm.

Upper dentition- The upper tooth rows of *S. uccasamamensis*, composed of five teeth, are divergent anteriorly. The most mesial tooth is caniniform, whereas the remaining four are molariform (Figs 6.3–6.7). There is no diastema between Cf1 and Mf1 (Figs 6.1–6.7). Cf1 is roughly semicircular in cross section in most specimens: MNHN-Bol V 3711 and 3726 (Figs 6.4–6.5), a shape that is also observable in the alveoli of MNHN-Bol V 11731 (Fig. 6.1). The straight side, corresponding ideally to the diameter of this semicircle, faces linguomesially, whereas the arched outline faces labiodistally. Variations of this shape are observable in the

almost triangular caniniform of MNHN-Bol V 3717 (Fig. 6.6) and the nearly circular Cf1 (or correspondent alveoli) of MNHN-Bol V 3718 and 3321 (Figs 6.2, 6.7). In all the specimens where it is preserved, the occlusal surface is almost vertical in lateral view, and directed lingually and distally in occlusal view.

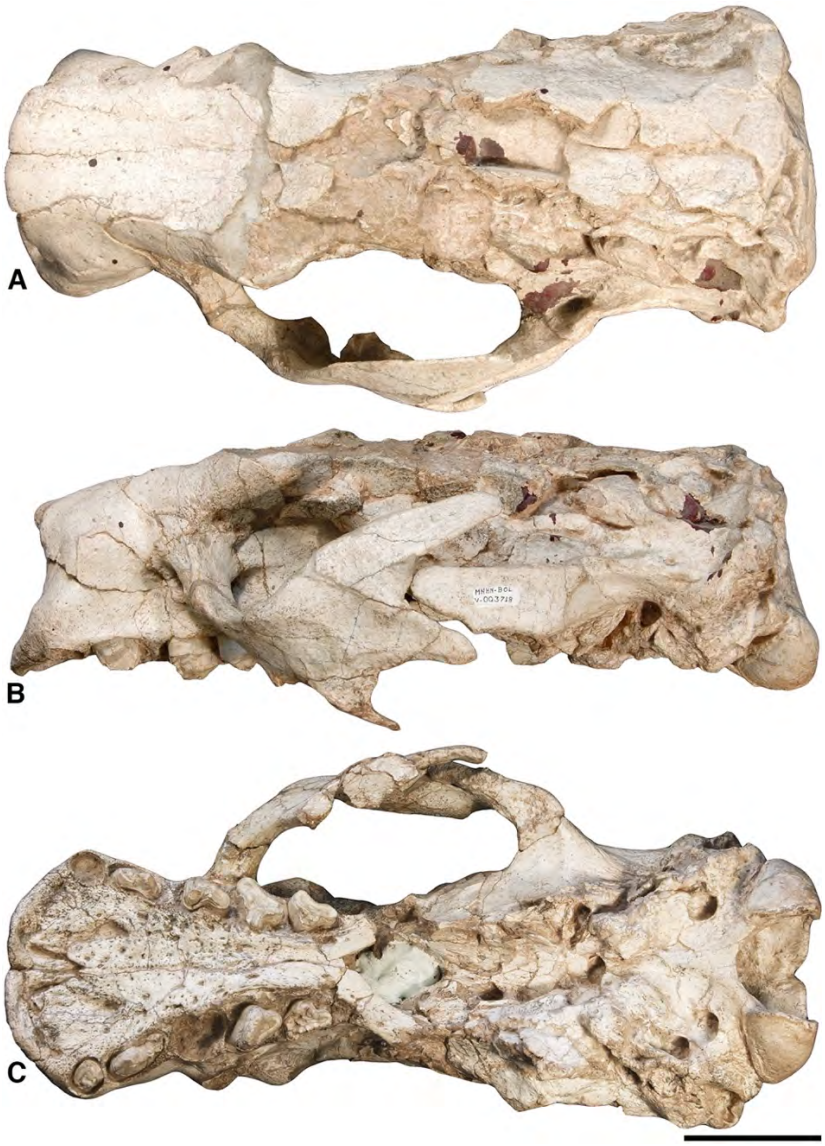

Figure 6.7. Cranium of *Simomylodon uccasamamensis* (MNHN-Bol V 3718) in dorsal (A), lateral (B), and ventral (C) views. Scale bar equals 5 cm.

Mf1 is ovate in cross section, elongated along the main axis of the tooth row. This tooth bears a lingual apicobasal sulcus in MNHN-Bol V 3718 (Fig. 6.7), absent in MNHN-Bol V 11371, 3321, 3711 and 3726 (Figs 6.1–6.2, 6.4–6.5). In MNHN-Bol V 3717 (Fig. 6.6), the lingual sulcus of Mf1 is slightly marked on the left and absent on the right, indicative of the great variability of this character. Mf1 bears a beveled occlusal surface, with a mesial wear facet that is larger than the distal facet.

Mf2 and Mf3 are bilobate and exhibit a deep lingual apicobasal sulcus (Figs 6.2–6.7). In occlusal view, these two teeth are roughly triangular in cross section, with the orthogonal angle disposed mesiolingually (Figs 6.2–6.7). Mf2 and Mf3 vary in their occlusal outlines, but Mf2 is generally longer mesiodistally than transversely, whereas in Mf3 the transverse width is equal to or exceeds the mesiodistal length. The wear facet of Mf2 is more pronounced distally than mesially, whereas in Mf3, it is more pronounced in the central part of the tooth than its labial and lingual extremities (e.g., MNHN-Bol V 3711 and 3717; Figs 6.4, 6.6).

Mf4 is T-shaped in occlusal view, with the distal lobe clearly narrower transversely than the mesial one. The last upper tooth presents both lingual and labial longitudinal sulci, the latter more pronounced than the former (e.g., MNHN-Bol V 11731, 3321, 3711 and 3717; Figs 6.1–6.2, 6.4, 6.6).

Mandible and lower dentition- The lower caniniform, as the upper one, is also generally semicircular in cross section, with some exceptions represented by the triangular shape of MNHN-Bol V 3296 (Fig. 6.8A) and the ovate shape in MNHN-Bol V 3711 and 3371 (Figs 6.4F, 6.9D). It appears as the highest tooth of the lower tooth row, and is nearly equal in size to mf1 (Figs 6.4–6.6, 6.8–6.11). The cf1 is beveled, with the mesial wear facet broader than the distal one. It also presents a slight lingual apicobasal sulcus in MNHN-Bol V 3726 (Fig. 6.5), 3296 (Fig. 6.8) and the juvenile mandibles (Fig. 6.11), a feature not observable in the other specimens (Figs 6.4, 6.6, 6.9–6.10).

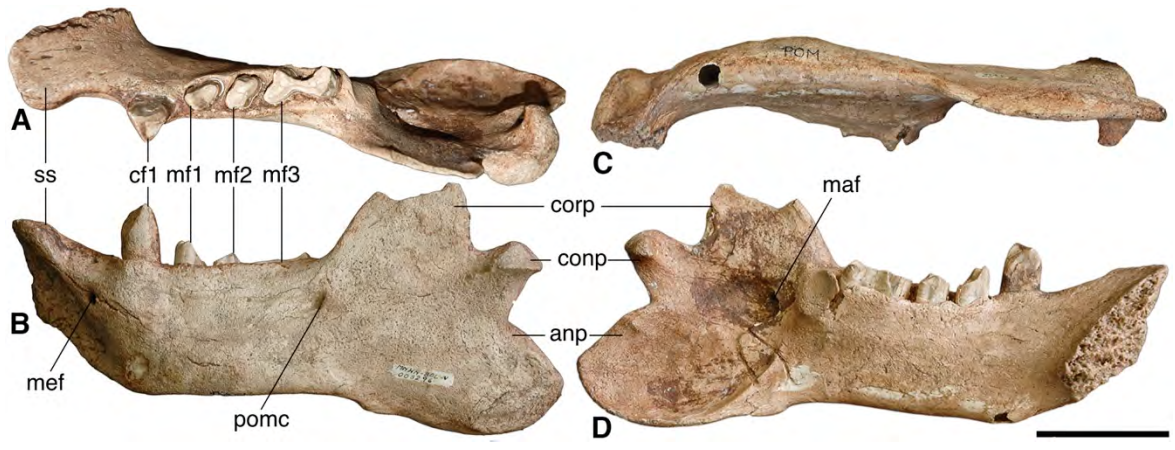

Figure 6.8. Left dentary of *Simomylodon uccasamamensis* (MNHN-Bol V 3296) in occlusal (A), lateral (B), ventral (C), and medial (D) views. Abbreviations: anp, angular process; cf, lower caniniform; conp, condyloid process; corp, coronoid process; maf, mandibular foramen; mef, mental foramen; mf, lower molariform; pomc, posteroexternal opening of the mandibular canal; ss, symphyseal spout. Scale bar equals 5 cm.

A lingual apicobasal sulcus is a consistent feature of mf1. This tooth is transversely wider mesially than distally and bears an oblique, distally inclined wear facet (Figs 6.4–6.6, 6.8–6.11). The irregular cross section of mf2 resembles a parallelogram (Figs 6.4–6.6, 6.8–6.11). The presence of longitudinal sulci on this tooth is variable among the observed specimens. In MNHN-Bol V 3296 (Fig. 6.8), sulci are present on all four sides, whereas in MNHN-Bol V 3371 (Fig. 6.9D) they are almost absent. These two morphologies represent the extremes of the observable variation for mf2.

In occlusal view, mf3 is strongly bilobate, with the mesial lobe wider transversely than the distal lobe (Figs 6.4–6.6, 6.8–6.9, 6.11). The mesial lobe is extended mesiolabially with an apicobasal sulcus that faces mesiolingually. The distal lobe of mf3 is rounded distally. The two lobes are separated by a thin isthmus accompanied lingually by a deep and broad apicobasal sulcus, absent on the labial side (Figs 6.4–6.6, 6.8–6.9, 6.11).

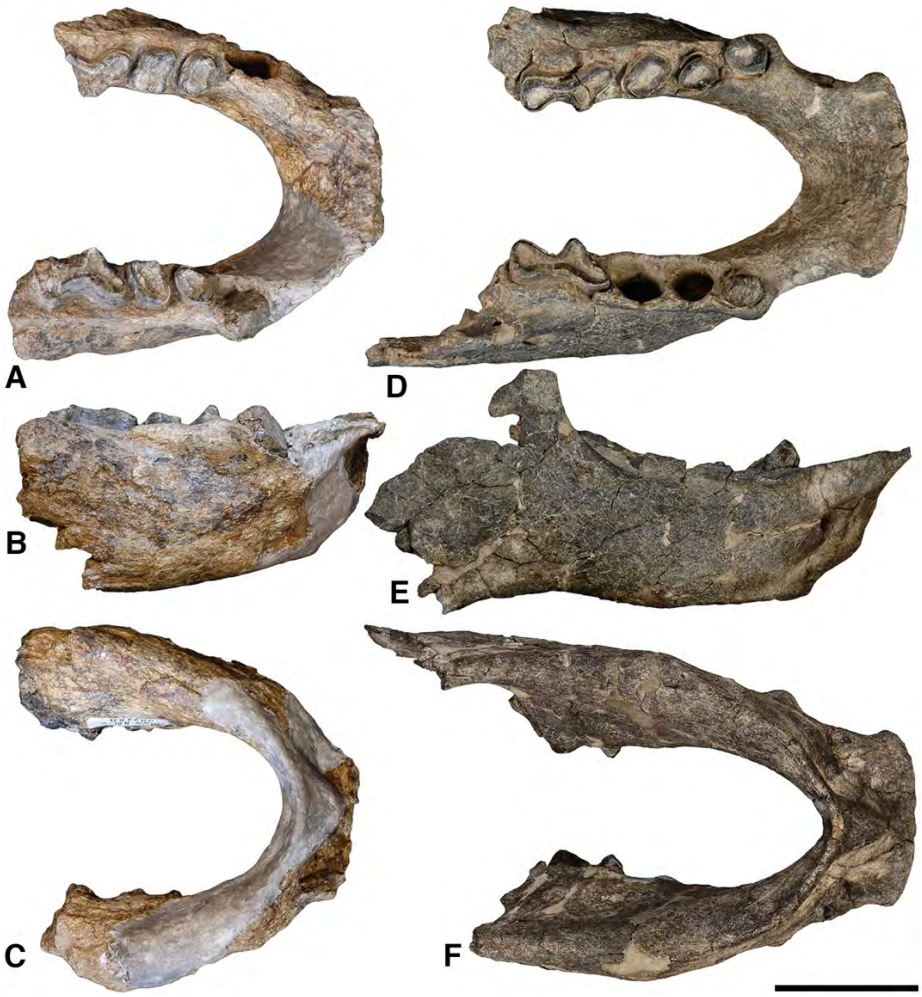

Figure 6.9. Mandibular fragments of *Simomylodon uccasamamensis* (A-C, MNHN-Bol V 3358; D-F, MNHN-Bol V 3371) in occlusal (A, D), lateral (B, E), and ventral (C, F) views. Scale bar equals 5 cm.

The mandible of *S. uccasamamensis* is short and deep, with the ventral border of the horizontal ramus nearly horizontal in lateral view (Figs 6.4–6.6, 6.8–6.9, 6.11). The tooth row is aligned in occlusal view, with the exception of the cf1, which is slightly displaced laterally. The dorsoventral depth of the horizontal ramus of the mandible is constant along the tooth row, becoming narrower towards the symphyseal spout and deepening posteriorly at the base of the ascending ramus. The profile of the symphyseal spout in lateral view is irregular, with a strong convexity flanked by marked dorsal and ventral concavities (Figs 6.4–6.6, 6.8–6.10). In occlusal view, the symphysis is wider distally than proximally, with a visible constriction anterior to the caniniforms. The mandibular foramen is located on the medial side of the mandible, well posterior and slightly ventral to the base of mf3. The posteroexternal opening of the mandibular canal (a characteristic feature of sloths among xenarthrans – see Gaudin 2004; De Iuliis *et al.* 2011) faces laterally at the level of the posterior edge of the root of mf3, well ventral to the dorsal edge of the horizontal ramus. The mandibular canal emerges anteriorly through the mental foramina situated on the anterolateral surface of the symphyseal spout. The mental foramina are highly variable in size and number (e.g., a single one in MNHN-Bol V 3296 and six in MNHN-Bol V 3298; Figs 6.8, 6.10A–C), even in the two dentaries of a single individual (e.g., MNHN-Bol V 3717, 3371).

Figure 6.10. Left anterior mandibular corpus fragment of *Simomylodon uccasamamensis* (A-C, MNHN-Bol V 3298) in occlusal (A), lateral (B), and ventral (C) views, and anterior mandibular symphysis of *Simomylodon uccasamamensis* (D-F, MNHN-Bol V 12518) in occlusal (D), anterior (E), and ventral (F) views. Scale bar equals 5 cm.

Figure 6.11. Juvenile mandibular remains of *Simomylodon uccasamamensis*. A-C, left anterior mandibular fragment (MNHN-Bol V 12001) in lateral (A), occlusal (B), and medial (C) views; D-F, right mandibular fragment (MNHN.F.AYO165) in lateral (D), occlusal (E), and medial (F) views; G-I, left mandibular fragment with complete dentition (MNHN-Bol V 3359) in lateral (G), occlusal (H), and medial (I) views; J-L, right mandibular fragment (MNHN-Bol V 11758) in lateral (J), occlusal (K), and medial (L) views. Scale bar equals 5 cm.

On the ascending ramus, the angular, condyloid and coronoid processes are equally divergent (Fig. 6.8). The angular process is deeply concave medially, with a strongly convex ventral edge that is clearly demarcated from the ventral edge of the horizontal ramus (Fig. 6.8). The transverse width of the mandibular condyle is much greater than its anteroposterior length. It has a hooked aspect in dorsal view, and its lateral portion is oriented horizontally in posterior view, whereas the medial portion is downturned ventrally. The coronoid process is tall, with its posterior edge orthogonal to the main mandibular axis in lateral view (Figs 6.5E, 6.8B, 6.11G). It is somewhat hooked posteriorly in MNHN-Bol V 3726 and 3359 (Figs 6.5E, 6.11G), but not in MNHN-Bol V 3296 (Fig. 6.8B). However, a complete coronoid process belonging to an adult individual is lacking in the present sample and therefore this feature cannot be assessed properly.

No important differences have been detected among the mandibular features of the specimens of *S. uccasamamensis*. In general, the mandibles MNHN-Bol V 3717, 3358 and 3298 (Figs 6.6, 6.9A–C, 6.10A–C) are more robust than the specimens MNHN-Bol V 3711, 3726, 3296, 3371 and 12518 (Figs 6.4, 6.5, 6.8, 6.9D–F, 6.10D–F). This greater robustness is exemplified by the two specimens MNHN-Bol V 3358 and 3371 illustrated in Figure 6.9, with the former (Fig. 6.9A–C) showing a more robust dentition and more anteriorly divergent, thicker and deeper horizontal rami than the latter (Fig. 6.9D–F). These variations were treated by Anaya & MacFadden (1995) as possible indicators of different ontogenetic stages and/or the existence of sexual dimorphism.

The *S. uccasamamensis* sample also includes four mandibular corpora of juvenile individuals (i.e., MNHN-Bol V 3359, 11758, 12001 and MNHN.F.AYO165; Fig. 6.11). In juvenile specimens of *Simomylodon*, cf1 is larger and wider than mf1–mf2. The cf1 also shows a semicircular section and a feeble apicobasal sulcus in the lingual side (Fig. 6.11A–I). The mf1 and mf2 are somewhat more rounded and simple, but already show the same occlusal pattern described above for adults. Additionally, mf3 already shows the same peculiar shape as the adult tooth, with a wide mesial and narrow distal lobe and the presence of a single lingual apicobasal sulcus (Fig. 6.11A–I). Also, the coronoid and condyloid processes appear simpler, without the small incisura on the posteriormost tip of the coronoid process (Fig. 6.11G–I). In posterior view, the condyle appears to be inclined laterally, rather than medially. Overall, the juvenile specimens of *S. uccasamamensis* already display the diagnostic features of the adults, appearing largely as smaller scale versions of the adult bone.

6.1.2 Comparison

Cranium and upper dentition- In *Simomylodon uccasamamensis*, the presence of a high braincase, a deep and anteriorly elevated snout, and an approximately horizontal cranial base in lateral view, are typical features of Mylodontidae (Gaudin 2004). The width of the braincase relative to total skull length is comparable to *Pleurolestodon acutidens* (FMNH P14495; Rovereto 1914), and is greater than *Glossotheridium chapadmalense, Glossotherium robustum*, *Mylodon darwinii* or *Paramylodon harlani* (Owen 1842; Kraglievich 1925, 1934; Stock 1925; McAfee 2009; Brandoni *et al*. 2010).

Other features, above all in the rostral region, allow assignment of *Simomylodon* to the Mylodontinae. In particular, the snout is relatively short, widened anteriorly in dorsal view, and depressed in lateral view (Figs 6.1, 6.3–6.7).

The wide rostrum of *S. uccasamamensis* is also accompanied by an anterior enlargement of the nasals. The nasal becomes narrower posteriorly and widens again at the level of the nasofrontal suture (Figs 6.1, 6.3–6.7). This expansion is a recurrent feature in mylodontids, as is the great enlargement of the external nares (Gaudin 2004). The characters observed on the rostrum are closely related to the morphology of the palate. Indeed, *S. uccasamamensis* shows a V-shaped palate (Figs 6.1–6.7), comparable with all the mylodontines and lestodontines (Gaudin 2004) except *Mylodon*, which has secondarily lost Cf1s, and consequently reduced anterior palatal width (Kraglievich 1934; Brandoni *et al*. 2010). The medial anterior palatal processes of the maxilla are projected farther anteriorly than the lateral ones (Figs 6.1–6.7). This characteristic is also observed in *Glossotheridium*, *Glossotherium*, *Paramylodon*, *Pleurolestodon* and *Mylodon* (Owen 1842; Rovereto 1914; Kraglievich 1925, 1934; Stock 1925; McAfee 2009; Brandoni *et al*. 2010). The extension of the medial palatal processes of the maxilla is moderate anteroposteriorly, but the processes are broad mediolaterally (Figs 6.1–6.7). In this respect, *Simomylodon uccasamamensis* resembles more *Pleurolestodon acutidens* (FMNH P14495) than *Glossotheridium chapadmalense* (Kraglievich 1925).

On the lateral cranial wall, the lacrimal is wide, with its orbital portion larger than its facial portion. The lacrimal is pierced by a small lacrimal foramen (Figs 6.3B, 6.6B), the diminutive size of this opening being a feature of all mylodontines and lestodontines (Gaudin 2004).

All members of Mylodontidae are characterized by complex jugals with distinct ascending, descending and middle processes. The middle process is elongated and triangular, and the descending process is hooked posteriorly (Gaudin 2004). All these features have been observed in the specimens attributed to *Simomylodon* (Figs 6.4E, 6.5–6.7B). Moreover, this taxon presents

a weak postorbital process of the zygomatic arch, as in *Glossotheridium*, *Paramylodon*, *Pleurolestodon* and the lestodontines (Kraglievich 1925; Stock 1925; Webb 1989; Gaudin 2004; McAfee 2009). This is situated at the base of the ascending process, which is long and slender (Figs 6.4E, 6.5–6.7B), resembling that of *Glossotheridium*, *Glossotherium*, *Paramylodon* and *Mylodon* (Kraglievich 1925, 1934; Stock 1925; McAfee 2009; Brandoni *et al.* 2010). In contrast, *Pleurolestodon*, *Lestodon* and *Thinobadistes* have shorter and more robust ascending processes of the jugal (Rovereto 1914; Webb 1989; Bargo *et al.* 2006b). Finally, the ascending process of *S. uccasamamensis* is nearly horizontal, as in most mylodontids (Figs 6.4E, 6.5–6.7B; Gaudin 2004).

The length of the zygomatic process of the squamosal is peculiar in *Simomylodon* because it is the longest (relative to the total cranial length) ever observed among mylodontids. However, its almost horizontal orientation and its broad and flattened tip (Figs 6.3–6.7) are common features of mylodontines and lestodontines (Gaudin 2004).

In dorsal view, the frontals and parietals are anteroposteriorly and mediolaterally flattened and the sagittal crest is absent (Figs 6.3–6.7). This morphology is present in all mylodontines and lestodontines except *Lestodon* (Gaudin 2004). The presence of a flat temporal fossa, delimited by non-connecting temporal lines, is shared with *Pleurolestodon*, *Glossotherium*, *Paramylodon* and *Mylodon* (Owen 1842; Rovereto 1914; Stock 1925; Kraglievich 1934; McAfee 2009; Brandoni *et al.* 2010).

The strongly developed nuchal crest of constant width and aligned with the posterior surface of the occiput (this latter showing a median external occipital crest connecting the nuchal crest to the dorsal edge of the foramen magnum) are features of *Simomylodon* shared with all mylodontids (Gaudin 2004). *Simomylodon* also exhibits a detached notch on the dorsal border of the foramen magnum, comparable with that observed in *Pleurolestodon* (FMNH P14495) and *Mylodon* (Kraglievich 1934). In posterior view, the foramen magnum is limited laterally by roughly triangular occipital condyles that lie at the level of the dentition in lateral view (Figs 6.4B, 6.7B); both are common conditions in Mylodontidae (Gaudin 2004). As in all mylodontines and lestodontines, the occipital condyles extend posteriorly to the posteriormost edge of the foramen magnum in ventral view (Figs 6.4C, 6.7C). The condyles are widely separated from one another, in this respect resembling *Glossotherium*, *Pleurolestodon* and *Thinobadistes*; also, they are mediolaterally elongated in ventral view, to an extent that is comparable with *Mylodon*, *Pleurolestodon* and the lestodontines *Thinobadistes* and *Lestodon* (Owen 1842; Rovereto 1914; Stock 1925; Kraglievich 1934; Webb 1989; McAfee 2009; Brandoni *et al.* 2010). In ventral view, the occipital condyles are well-separated from the hypoglossal foramina (Figs 6.4C, 6.7C) as in *Pleurolestodon* (FMNH P14495).

The upper dentition of *S. uccasamamensis* is similar to the other representatives of Mylodontidae, with five teeth on each side aligned in two anteriorly divergent tooth rows (Figs 6.1–6.7; Gaudin 2004). Exceptions to this pattern are represented by Scelidotheriinae, which have parallel tooth rows (McDonald 1987) and *Octomylodon* and *Mylodon*, which exhibit anterior tooth loss (Scillato-Yané 1977; Brandoni *et al.* 2010).

The Cf1-Mf1 diastema is absent or extremely reduced (Figs 6.4C, 6.7C), as in most mylodontids. Exceptions to this mylodontid pattern are represented by *Mylodon* and *Octomylodon* (Scillato-Yané 1977; Brandoni *et al.* 2010), in which Cf1 is secondarily lost, and *Lestodon,* which shows a derived and extremely elongated diastema (Czerwonogora & Fariña 2013).

In *Simomylodon*, the most mesial upper tooth is strongly caniniform, as observed in all mylodontines and lestodontines with the exception of *Pseudoprepotherium* (Hirschfeld 1985). Cf1 is also the smallest of the upper tooth row (Figs 6.3–6.7), a feature in which *Simomylodon* closely resembles *Pleurolestodon*, *Glossotheridium*, *Glossotherium* and *Paramylodon* (Owen 1842; Rovereto 1914; Kraglievich 1925; Stock 1925; Robertson 1976; McAfee 2009). In occlusal view, Cf1 of *Simomylodon* is located at the anterior edge of the maxilla (Figs 6.1–6.7) as in *Pleurolestodon*, *Thinobadistes*, the megalonychid sloths, and the extant *Bradypus* (Gaudin 2004). The posterior curvature of Cf1 (Figs 6.1–6.7) is present in all mylodontines, whereas the alignment of both Cf1 and cf1 with the remainder of the tooth row is a feature of both mylodontines and scelidotheriines, though absent in *Lestodon* (McDonald 1987; Gaudin 2004; Czerwonogora & Fariña 2013). The Cf1 of *S. uccasamamensis* exhibits almost vertical wear (Figs 6.4–6.6) like that found only in *Pleurolestodon acutidens* (FMNH P14495), among Neogene mylodontines. This condition is absent in *Paramylodon garbanii* (Robertson 1976), *Glossotheriopsis pascuali* (Scillato-Yané 1976), and *Glossotheridium chapadmalense* (Kraglievich 1925).

Mf1 is also recurved posteriorly (Figs 6.2–6.6) as in several Mylodontidae but not in *Mylodon*, *Pseudoprepotherium*, *Lestodon*, and Scelidotheriinae, where Mf1 is nearly straight (Gaudin 2004). The ovate cross-section and the anteroposterior elongation of Mf1 observed in *Simomylodon* (Figs 6.1–6.7) is widespread in Mylodontidae, lacking only in *Octomylodon*, *Catonyx* and *Scelidotherium* (Scillato-Yané 1977; Gaudin 2004). Mf2 is longer mesiodistally than transversely, as is typical among mylodontines and lestodontines. Mf2 and Mf3 present some peculiar features highly similar to the condition in *Pleurolestodon acutidens* and *Paramylodon garbanii*, such as their marked lingual sulcus and the almost orthogonal mesiolingual corner (Figs 6.2–6.6). In contrast, a marked lingual apicobasal sulcus is only found on Mf2, with a weak sulcus on Mf3, in *Glossotheridium chapadmalense* (Kraglievich 1925). Finally, Mf4 is T-shaped (Figs 6.2–6.7), a

peculiar feature of all members of the family Mylodontidae except *Octomylodon,* which possesses a bilobate Mf4 (Scillato-Yané 1977; Gaudin 2004).

Mandible and lower dentition- In occlusal view, cf1 is equivalent in size to mf1 (Figs 6.4–6.6, 6.8–6.11), and mf3 is the largest lower tooth, an invariant trait of Mylodontidae also known to occur in Bradypodidae (Gaudin 2004). The cf1 is roughly semicircular in cross section in most specimens, exceptionally displaying ovate or triangular cross-sections (Figs 6.4–6.6, 6.8–6.11). The latter two conformations are typical among Mylodontinae and Lestodontini, respectively (Gaudin 2004). The caniniform of *Simomylodon* has a beveled occlusal surface (Figs 6.4–6.6, 6.8–6.9, 6.11), resembling that of *Pleurolestodon acutidens* (Rovereto 1914) and *Paramylodon garbanii* (Robertson 1976). The cf1 is beveled also in *Glossotheridium chapadmalense*, but both wear facets are well developed in *Simomylodon* and *Pleurolestodon*, whereas the distal facet is extremely reduced in *G. chapadmalense* (Kraglievich 1925). Whereas cf1 of *Paramylodon garbanii* projects strongly mesially and labially (Robertson 1976), that of *S. uccasamamensis* and *G. chapadmalense* is implanted vertically (Kraglievich 1925). The irregularly lobate mf1 and mf2 (Figs 6.4–6.6, 6.8–6.11) are very similar to those of *P. acutidens*, *G. chapadmalense* and *P. garbanii*, but in *Simomylodon* they are significantly smaller in size. Moreover, *Paramylodon garbanii* shows deeper apicobasal sulci on the lingual and distal sides of mf2 (Robertson 1976), whereas *G. chapadmalense* has a more elongated and almost straight-walled mf2 (Kraglievich 1925). The elongated and bilobate mf3 is a recurrent feature in Mylodontinae and Lestodontini (Gaudin 2004). As already noted, mf3 has asymmetrically developed lingual and labial apicobasal sulci in *S. uccasamamensis*, with the former markedly deeper than the latter (Figs 6.4–6.6, 6.8–6.9, 6.11). Among late Miocene–Pliocene Mylodontinae, the pattern of *S. uccasamamensis* is very similar to that of *G. chapadmalense*, but differs from that of *P. acutidens* (FMNH P14495, 14521), in which both labial and lingual apicobasal sulci are well developed, and *P. garbanii* (UF 10922), which displays an extra bulge on the labial side of mf3.

The mandible of *Simomylodon* presents some typical mylodontid features, such as the straight horizontal ventral edge of the horizontal ramus in lateral view, and a condyle located at the same level as the tooth row (Figs 6.4–6.6, 6.8–6.9, 6.11) (Gaudin 2004; Saint-André *et al.* 2010). In general, the mandible of *Simomylodon* is smaller than that of all the other late Miocene–Pliocene mylodontids (i.e., *P. acutidens*, *P. garbanii* and *G. chapadmalense*; Rovereto 1914; Kraglievich 1925; Robertson 1976). The articular condyle of *Simomylodon* is convex and medially hooked in dorsal view, as in many Mylodontidae, in contrast to the condyle of lestodontines, which is extended both laterally and medially (Gaudin 2004).

The angular process is the posteriormost process of the mandible (Fig. 6.8), another common mylodontid trait. Among Mylodontidae, only *Nematherium* and *Octomylodon* show an equally posterior extension of the condyloid process (Gaudin 2004). In medial view, the mandible of *Simomylodon* shows a detached oblique ridge that extends from the anteroventral edge of the angular process towards the root of the last tooth (Fig. 6.8D). This last condition is shared with *Pleurolestodon*, *Glossotherium*, *Paramylodon* (Gaudin 2004) and specimen MACN Pv 8675 of *G. chapadmalense*. In lateral view, the ascending ramus does not cover mf3 (Figs 6.5E, 6.8B, 6.9E, 6.11D, G), resembling the condition observed in *G. chapadmalense* and *P. garbanii* (Kraglievich 1925; Robertson 1976). This partial coverage of mf3 is observed in some other mylodontid genera, such as *Octodontotherium*, *Pseudoprepotherium*, *Mylodon*, and *Pleurolestodon* (Gaudin 2004). The anterior edge of the mandibular spout is broad and flat in occlusal view, as it is in *Glossotherium*, *Glossotheridium*, and *Lestodon* (Owen 1842; Kraglievich 1925; McAfee 2009; Czerwonogora & Fariña 2013) (Figs 6.4–6.6, 6.8–6.9). Other mylodontine genera such as *Mylodon*, *Paramylodon*, and *Pleurolestodon* possess anteriorly rounded mandibular spouts (Stock 1925; Kraglievich 1934; McAfee 2009; Brandoni *et al*. 2010).

Four mandibles can be ascribed to juvenile individuals of *Simomylodon uccasamamensis,* based on their reduced size and lack of wear on the lower dentition (Fig. 6.11). These remains already display the main diagnostic features that have been found in the adults (e.g., a straight ventral margin, the absence of a diastema between cf1 and mf1, and the extreme reduction of the labial apicobasal sulcus on mf3; Fig. 6.11). All these features strongly contrast with those observed in the juvenile mandibular fragment described by Oliva & Brandoni (2012) and tentatively attributed to a "mylodontid cf. *Simomylodon*" (Huayquerian SALMA, Buenos Aires Province, Argentina). The present data suggests that the specimen described by Oliva & Brandoni (2012) does not belong to *Simomylodon*, but rather is more compatible with the genus *Pleurolestodon*, also recognized in the Huayquerian SALMA of Argentina (Rovereto 1914). However, given that no juvenile mandibular remains are known for this taxon, the latter specimen should be considered as Mylodontinae indet.

6.1.3 Morphometric analyses

The results of Principal Component Analyses (PCA) among the Neogene Mylodontinae are depicted in Figures 6.12 and 6.13, respectively, showing the two distinct modules: cranium and upper dentition (Fig. 6.12) versus mandible and lower dentition (Fig. 6.13). This approach was followed in order to overcome the problem of the paucity of the data, thus maximizing the

number of specimens that could be included in the analyses (see Materials and Methods and Appendix IV, Datasets S1 for further details).

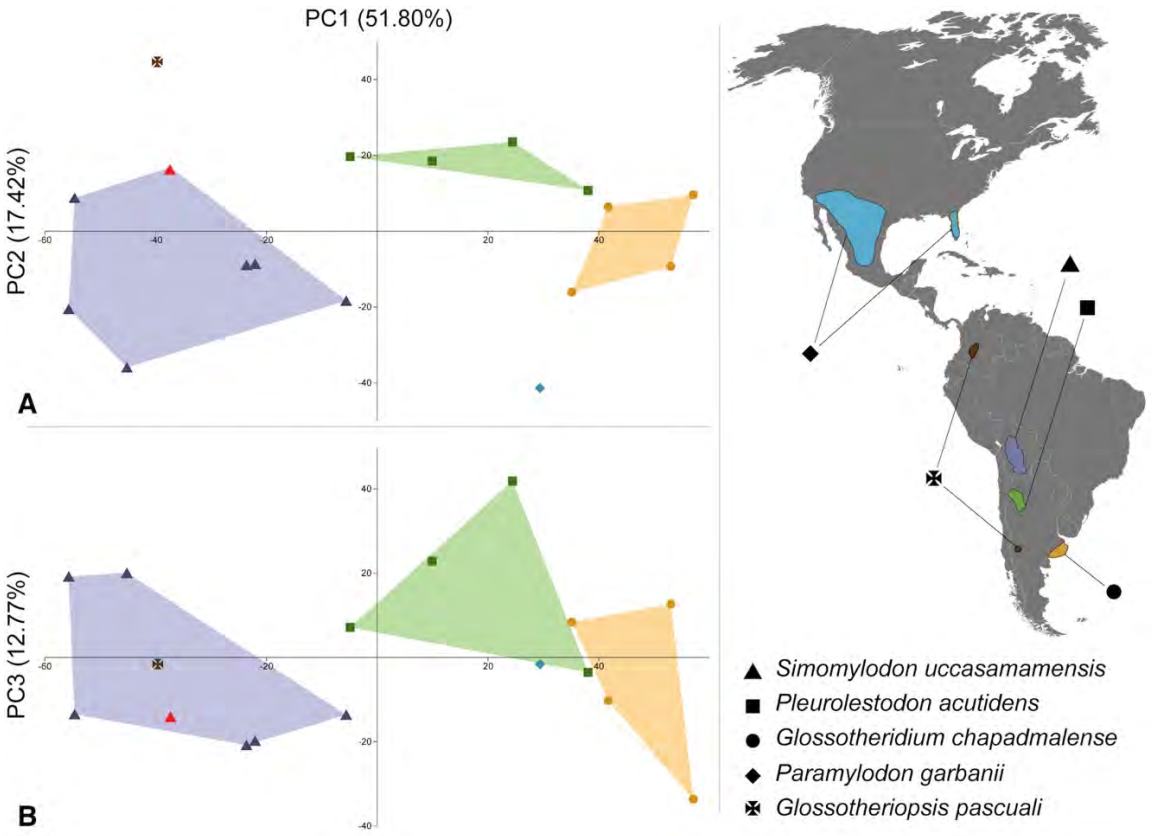

Figure 6.12. Principal component analysis performed on the cranial and upper dentition measurements subset (see Appendix IV, Datasets S1), showing the shape differentiation among the Miocene–Pliocene Mylodontinae. A, principal components 1 and 2 and B, principal components 1 and 3 (together explaining the 81.99% of the among-group variance). On the right: associated paleobiogeographic distribution of the taxa considered.

In the cranial dataset (Fig. 6.12), PC1 explains 51.80% of the variance and, given that all the variables have positive loadings, it likely reflects body size. Size is lower on the left side and higher on the right. PC2 (Fig. 6.12A) explains 17.42% of the variance. Positive values on this axis reflect skulls that have slender palates and thin rostra relative to total skull lengths, whereas negative values represent skulls with relatively wider palates and rostra. Finally, PC3 (Fig. 6.12B), explains 12.77% of the total variance. Positive values for PC3 are associated with robust dentitions and a long and deep snout relative to total skull lengths, whereas negative values correlate with a reduced dental series and a short and slender snout (in relation with total length). The Miocene–Pliocene sloths are well segregated along PC1 (Fig. 6.12), with *Simomylodon uccasamamensis* and *Glossotheriopsis pascuali* as the smallest taxa, and *Glossotheridium*

chapadmalense as the largest taxon in the dataset. *Pleurolestodon acutidens* and *Paramylodon garbanii* occupy intermediate positions (Fig. 6.12).

On PC2, the extreme morphologies are represented by *Glossotheriopsis pascuali* in the positive range and *Paramylodon garbanii* in the negative range (Fig. 6.12A). However, these morphologies must be treated cautiously, because the result may be affected by the lack of total skull length measurements for both species, since neither is represented by complete skulls. *Simomylodon* shows important variation along PC2, whereas *P. acutidens* and *G. chapadmalense* do not overlap (Fig. 6.12A). This means that *G. chapadmalense* exhibits a wider palate and rostrum relative to total skull length than is the case for *P. acutidens*.

On PC3, *S. uccasamamensis* still shows high variation, including *Glossotheriopsis pascuali* from southern Argentina in its morphometric range (Fig. 6.12B). The most extreme morphologies are represented by *P. acutidens* (the highest values) and *G. chapadmalense* (the lowest values). These two taxa, together with *P. garbanii*, partially overlap along PC3 (Fig. 6.12B).

In Figure 6.12, the *Simomylodon uccasamamensis* specimen MNHN-Bol V 3348 (Fig. 6.3) is represented by a red triangle. This cranium was previously attributed to the species *Pleurolestodon dalenzae* by Saint-André *et al*. (2010). The present dataset shows that this specimen falls far outside the morphometric range of the genus *Pleurolestodon*, but well within the range of variation for *Simomylodon* (Fig. 6.12).

Similarly, a second PCA (Fig. 6.13) was performed on the variables of the mandible and lower dentition, yielding the same general pattern as the cranial analysis. PC1, which explains 57.96% of the total variance, is again a representation of size, and *Simomylodon* occupies the lowest positions on the left side of the graph (Fig. 6.13). *Glossotheridium chapadmalense* shows the largest mandibular values, whereas *P. acutidens* and *P. garbanii* are recovered in intermediate positions.

PC2 explains 19.42% of the variance. Higher values are correlated with a long dental series and a deep mandibular ramus at the level of the dentition, relative to total mandibular length, whereas lower values correspond to a shorter dental series and less robust mandible.

Finally, PC3 explains 9.45% of the variance and reflects mandibles with a long horizontal ramus and anteroposteriorly narrow ascending ramus (positive values) versus mandibles displaying a shorter horizontal ramus and a more anteroposteriorly enlarged ascending ramus (negative values).

On both PC1 and PC2 (Fig. 6.13A), *Simomylodon* shows the greatest range of variation, probably due to the inclusion of juvenile individuals in the dataset (Fig. 6.11). These specimens are retrieved in the far bottom-left portions of the graph depicting PC1 versus PC2 (Fig. 6.13A),

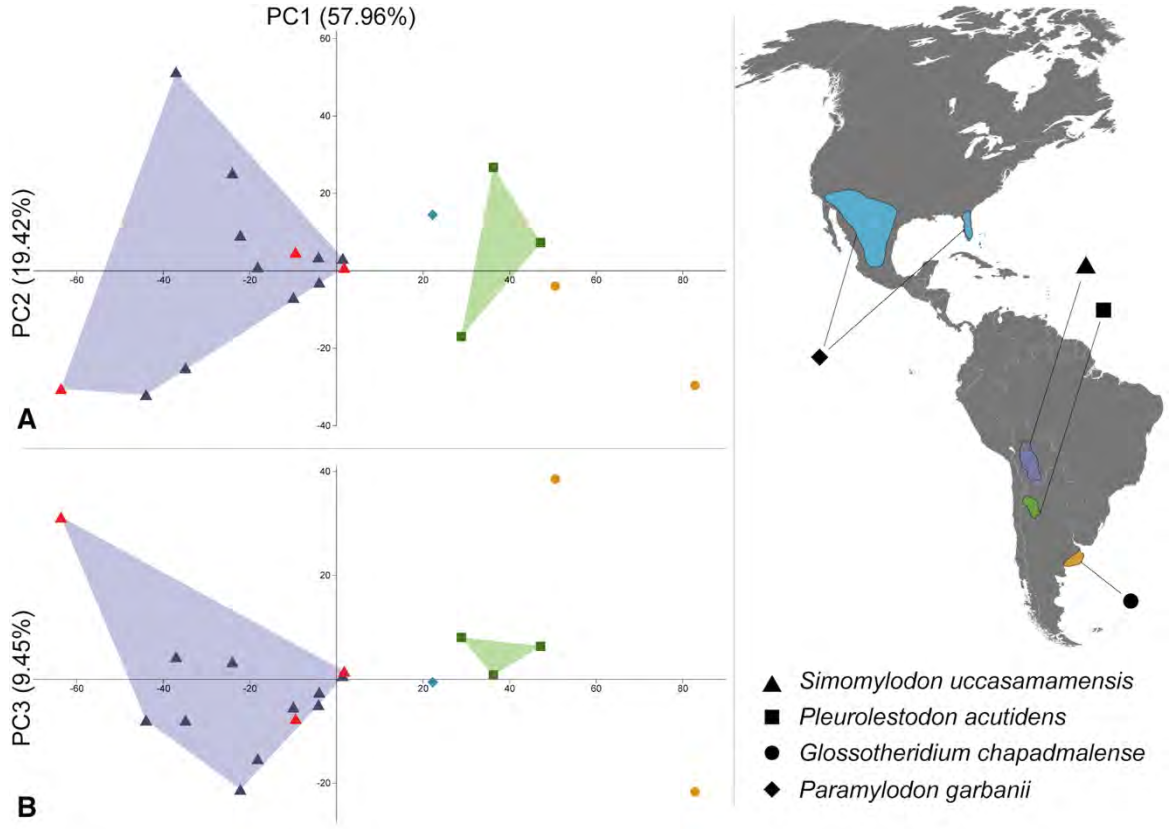

Figure 6.13. Principal component analysis performed on the mandibular and lower dentition measurements subset (see Appendix IV, Datasets S1), showing the shape differentiation among the Miocene–Pliocene Mylodontinae. A, principal components 1 and 2 and B, principal components 1 and 3 (together explaining the 86.83% of the among-group variance). On the right: associated paleobiogeographic distribution of the taxa considered.

corresponding with the lowest values for both principal components. This means that they are the smallest specimens in the dataset (as expected), but they also possess a dental series that is reduced in length and horizontal rami that are of moderate depth relative to total mandibular length. *G. chapadmalense* shows the highest variation on PC3 (Fig. 6.13B), an effect that is probably related to the incompleteness of the dataset for this taxon (no complete mandibles are known).

As before, the red triangles indicate the *Simomylodon uccasamamensis* specimens that were formerly assigned to another taxon. These are the specimens MNHN-Bol V 3358 (Fig. 6.9A–C), 3371 (Fig. 6.9D–F) and 3359 (Fig. 6.11G–I) that Anaya & MacFadden (1995) assigned to *Glossotheridium chapadmalense*. The more extensive data of the present analysis support their inclusion in the genus *Simomylodon* instead.

6.2 EAR REGION ANATOMY OF *S. UCCASAMAMENSIS*

The well-preserved material allows a complete description of the ear region of *Simomylodon uccasamamensis*. The cranium MNHN-Bol V 3718 (Fig. 6.7) shows the best preserved external aspects of the region, and is consequently taken as a reference for the description of this area (Fig. 6.14). In contrast, other specimens (MNHN-Bol V 3711, 3726 and 3717; Figs 6.4–6.6) are somewhat damaged in this region, but breakage allows the observation of some peculiar anatomical traits (Fig. 6.15). Finally, the isolated petrosals MNHN-Bol V 6549 and 9759 are extremely useful for describing the frontal and posteromedial views of the petrosal. MNHN-Bol V 6549 consists of both petrosals, associated with left and right maxillary fragments referable to *Simomylodon uccasamamensis*. The strong similarity between the petrosals of MNHN-Bol V 6549 and 9759, allows the assignment of the second specimen to the latter species (Fig. 6.16). Finally, MNHN-Bol V 3277 (Fig. 6.17) consists of a neurocranium of a small-sized mylodontid sloth that is compatible in size with *Simomylodon uccasamamensis*. This partial skull belongs to the old collection of the MNHN-Bol, dating to the beginning of the 20th century, and its origin is unknown. In this specimen the right incus is preserved, and is therefore discussed here.

6.2.1 Comparative description

Ectotympanic- Left and right ectotympanics are well preserved in MNHN-Bol V 3718 (Fig. 6.14). This bone is horseshoe-shaped in lateral view, elongated dorsoventrally, but also angled anteromedially from the parasagittal plane. Compared with the surrounding bones, its external surface is smooth, a feature typical of the family Mylodontidae (Gaudin 1995: char. 1). This smoothness is variable alongside its arched structure: the distal part is evidently more rugose than the anterior and posterior crura. An incisura tympanica, visible in lateral view, is interposed between the dorsal ends of the anterior and the posterior crura (Fig. 6.14). The anterior crus is connected to the lateral portion of the pterygoid and the squamosal, whereas the posterior crus is only sutured to the post-tympanic process of the squamosal. Other attachment points of the ectotympanic are the pterygoid anteriorly and the tympanohyal posteriorly. Among the Mylodontidae, the ectotympanic-pterygoid contact is also observed in *Glossotherium* and *Paramylodon* (Gaudin 1995: char. 10; Boscaini *et al.* 2018a).

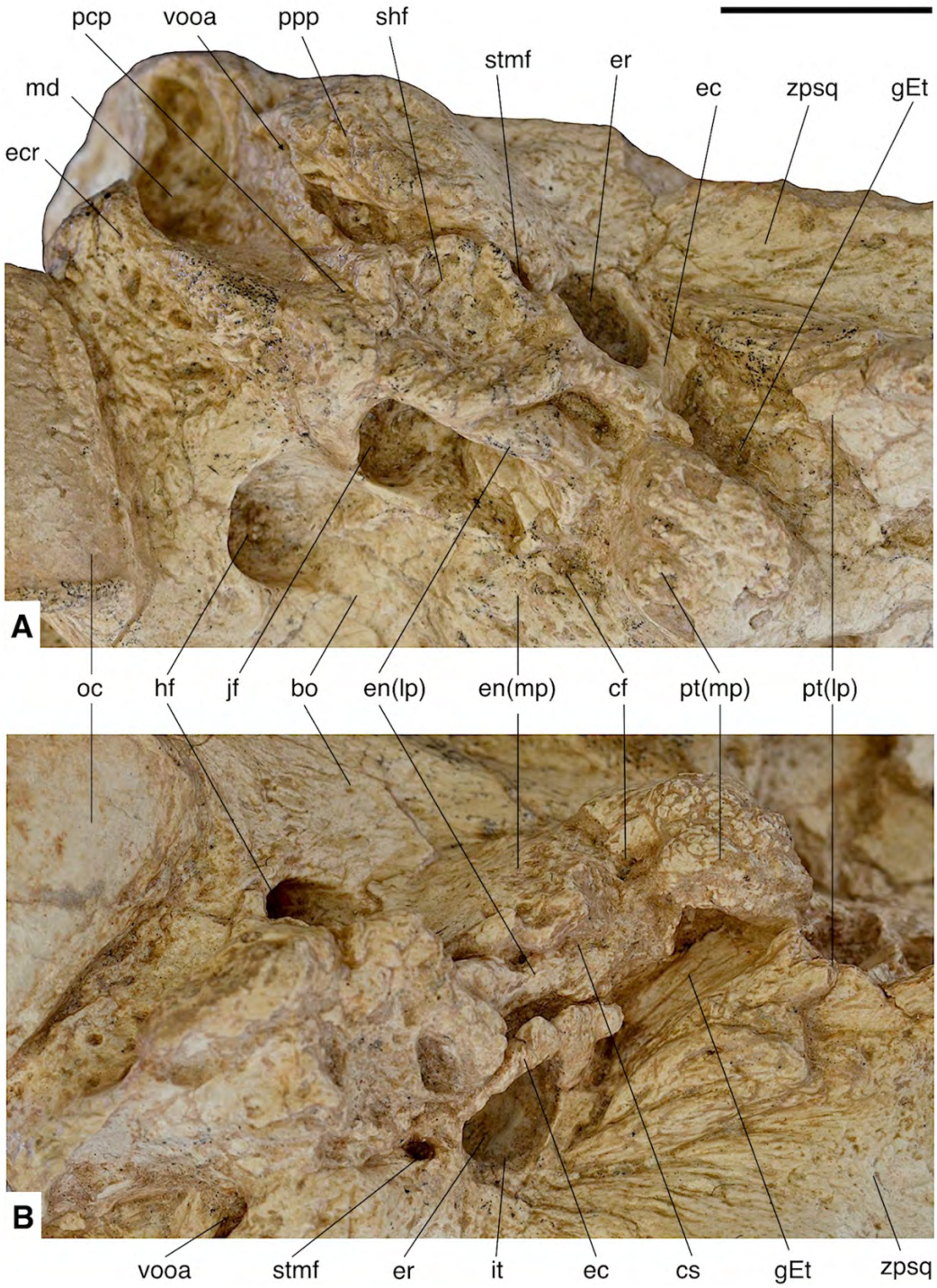

Figure 6.14. Right (A) and left (B) ear region of *Simomylodon uccasamamensis* (MNHN-Bol V 3718) in ventral (A) and ventrolateral (B) views. Abbreviations: bo, basioccipital; cf, carotid foramen; cs, carotid sulcus; ec, ectotympanic; ecr, exoccipital crest; en(lp), entotympanic (lateral plate); en(mp), entotympanic (medial plate); er, epitympanic recess (viewed through the external acoustic meatus); gEt, groove for the Eustachian tube; hf, hypoglossal foramen; it, incisura tympanica; jf, jugular foramen; md, mastoid depression; oc, occipital condyle; pcp, paracondylar process of exoccipital (= paraoccipital process of Patterson *et al.* 1992); ppp, paraoccipital process of petrosal (= mastoid process of squamosal of Patterson *et al.* 1992); pt(lp), pterygoid (lateral portion); pt(mp), pterygoid (medial portion); shf, stylohyal fossa; stmf, stylomastoid foramen; vooa, ventral opening of the canal for the occipital artery (= mastoid foramen of Patterson *et al.* 1992); zpsq, zygomatic process of squamosal. Scale bar equals 2 cm.

Entotympanic- The entotympanic bone is present on both sides of MNHN-Bol V 3718 (Fig. 6.14) and is partially preserved in MNHN-Bol V 3711, 3717 and 3277 (Figs 6.4, 6.6, 6.17). It is an elongated structure, distinctly longer anteroposteriorly than the ectotympanic, as observed also in *Mylodon darwinii* (Gaudin 1995: char. 16) and in *Paramylodon garbanii* (UF 10922). The shape of the entotympanic is variable at the intraspecific level in the mylodontid genera *Paramylodon* and *Glossotherium* (Gaudin 1995: chars 16, 17, 18; Boscaini *et al.* 2018a). The entotympanic of *Simomylodon* is divided into medial and lateral plates of the same anteroposterior length (Fig. 6.14). The carotid sulcus, well preserved only on the left side of MNHN-Bol V 3718 (Fig. 6.14B), divides the medial and the lateral plates, and its roof is pierced posteriorly by a small nutritive foramen. The entotympanic contributes to the roof and the walls, both laterally and medially, of the carotid sulcus (Fig. 6.14B). The medial plate of the entotympanic, sutured to the basioccipital medially and posteriorly as in *Mylodon* (Patterson *et al.* 1992), has a transverse width much greater than that of the lateral plate (Fig. 6.14B). The lateral plate of the entotympanic is connected anteriorly with the medial portion of the pterygoid, and medially with the medial plate of the entotympanic (Fig. 6.14). It is separated from the ectotympanic by a tiny, anteroposteriorly elongated fissure that leads to the middle ear cavity. Posteriorly, the lateral plate of the entotympanic is involved in the formation of the medial edge of the stylohyal fossa (Fig. 6.14). The posterior margin of the lateral plate forms

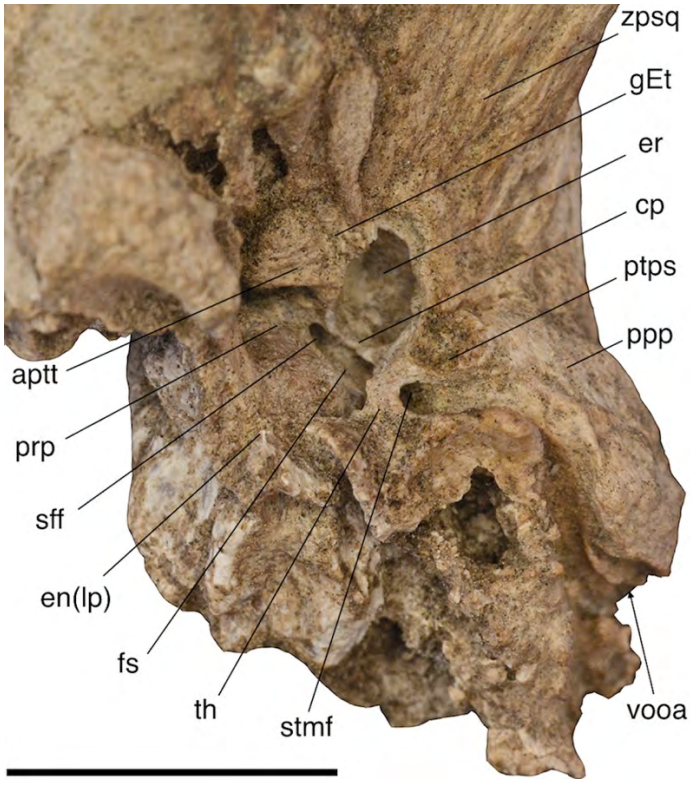

Figure 6.15. Left ear region of *Simomylodon uccasamamensis* (MNHN-Bol V 3717) in ventral view. Abbreviations: aptt, anteroventral process of the tegmen tympani; cp, crista parotica; en(lp), entotympanic (lateral plate); er, epitympanic recess; fs, facial sulcus; gEt, groove for the Eustachian tube; ppp, paraoccipital process of petrosal (= mastoid process of squamosal of Patterson *et al.* 1992); prp, promontorium of petrosal; ptps, post-tympanic process of squamosal; sff, secondary facial foramen; stmf, stylomastoid foramen; th, tympanohyal; vooa, ventral opening of the canal for the occipital artery (= mastoid foramen of Patterson *et al.* 1992); zpsq, zygomatic process of squamosal. Scale bar equals 2 cm.

the anterior wall of the jugular foramen (Fig. 6.14). The lateral plate of the entotympanic is also strongly fused to the ventral part of the promontorium, building a lateral wall involved in the formation of the tympanic cavity. As in *G. robustum* (Boscaini *et al.* 2018a) and unlike *M. darwinii* (Patterson *et al.* 1992), the lateral plate of the entotympanic does not participate in the formation of the floor of the tympanic cavity.

Petrosal and middle ear cavity- The promontorium and the middle ear cavity are clearly discernable in the isolated petrosal of MNHN-Bol V 9759 (Fig. 6.16), but also partially visible in MNHN-Bol V 3718 and 3717 (Figs 6.14–6.15). In lateral view, the promontorium appears typically sloth-like (see Gaudin 1995): it is elongated dorsoventrally, with a rounded anterior border (Fig. 6.16A). In lateral view, the most ventral aperture is the cochlear fossula (with the fenestra cochleae recessed inside: see Wible 2010; Gaudin 2011), which faces laterally, but also ventrally and posteriorly (Fig. 6.16A). The groove extending medially from its margin is a recognized synapomorphy of the family Mylodontidae (Gaudin 2004: char. 47). Posterior and ventral to the cochlear fossula, a strong bony shelf limits the post-tympanic sinus ventrally (Fig. 6.16C). This sinus is furtherly limited by the tympanohyal and the lateral plate of the entotympanic posteriorly and medially, respectively. A strong crista interfenestralis separates the cochlear fossula from the fenestra vestibuli (Fig. 6.16). The latter opening is ovate and faces laterally, but also slightly anteriorly and dorsally. The facial sulcus runs dorsal and lateral to the fenestra vestibuli and extends from the secondary facial foramen anteriorly, to the base of the tympanohyal posteriorly (Fig. 6.16). The facial sulcus is limited laterally by the crista parotica of the petrosal, which in turn culminates anteriorly in the anteroventral process of the tegmen tympani (= processus crista facialis in Patterson *et al.* 1992; Gaudin 1995, 2004; Wible & Gaudin 2004). This structure is damaged in MNHN-Bol V 9759 (Fig. 6.16) but is well-preserved on the left side of MNHN-Bol V 3717 (Fig. 6.15) and on the right side of MNHN-Bol V 3277 (Fig. 6.17). In ventral view, it assumes the shape of an acute isosceles triangle, with its base directed anteromedially (Fig. 6.15). Lateral to the crista parotica there is a large depression, the epitympanic recess, which extends dorsally into the squamosal bone (Figs 6.14–6.17). A small bulge in the posterolateral part of the epitympanic recess is present in MNHN-Bol V 9759 and 6549, which continues anteriorly as a feeble ridge (Fig. 6.16C). This bulge is placed more medially, closer to the crista parotica, in MHNN-Bol V 3277 and 3717, whereas it is absent MNHN-Bol V 3711. In medial view, the petrosal of *Simomylodon* shows an enlarged cerebral surface (Fig. 6.16B–C), more developed than that of *Glossotherium* (Boscaini *et al.* 2018a:

fig. 3). Just ventral to the cerebral surface, the medial wall of the petrosal is strongly concave, forming the sulcus for the internal carotid artery (Fig. 6.16D). Posterior to this concavity, the deep and undivided internal acoustic meatus is the major aperture in medial view. In contrast, the aqueductus vestibuli, which opens into the subarcuate fossa, is extremely reduced (Fig. 6.16B). The aqueductus vestibuli is narrower and the subarcuate fossa is shallower than their homologues in *G. robustum* (Boscaini *et al.* 2018a).

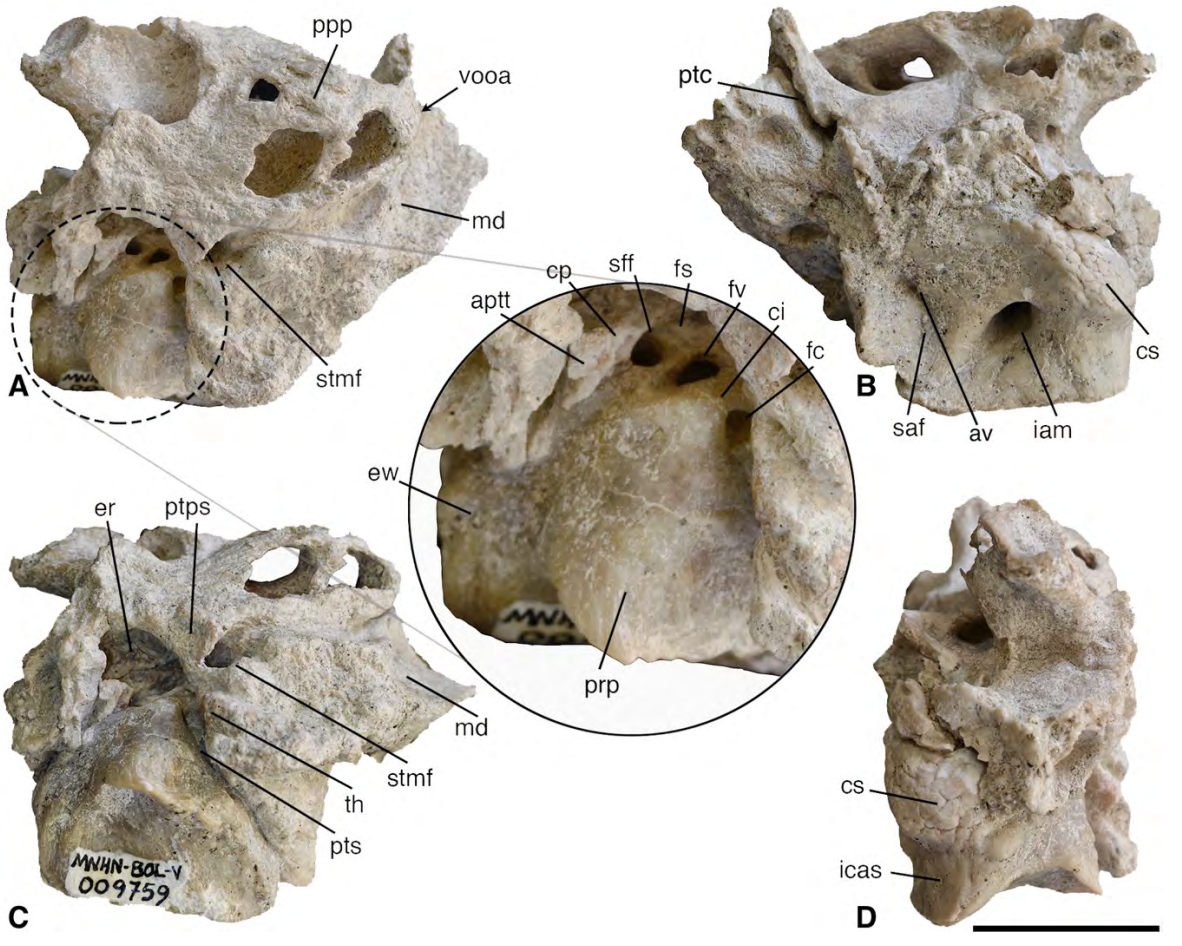

Figure 6.16. Left petrosal of *Simomylodon uccasamamensis* (MNHN-Bol V 9759) in lateral (A), medial (B), ventrolateral (C) and anterior (D) views. Abbreviations: aptt, anteroventral process of the tegmen tympani; ci, crista interfenestralis; cp, crista parotica; cs, cerebral surface; er, epitympanic recess; ew, epitympanic wing of petrosal; fc, cochlear fossula; fs, facial sulcus; fv, fenestra vestibuli; iam, internal acoustic meatus; icas, internal carotid artery sulcus; md, mastoid depression; ppp, paraoccipital process of petrosal (= mastoid process of squamosal of Patterson *et al.* 1992); ptc, post-temporal canal; pts, post-tympanic sinus; prp, promontorium of petrosal; ptps, post-tympanic process of squamosal; saf, subarcuate fossa; sff, secondary facial foramen; stmf, stylomastoid foramen; th, tympanohyal; vooa, ventral opening of the canal for the occipital artery (= mastoid foramen of Patterson *et al.* 1992). Scale bar equals 2 cm.

Tympanohyal and stylohyal fossa- Also the tympanohyal of *S. uccasamamensis* is typically sloth-like: narrow at its base and more enlarged ventrally, where it takes part in the formation of the stylohyal fossa (Fig. 6.15; Gaudin 2011). Its narrow portion appears more sinuous than in *Glossotherium* (Boscaini *et al.* 2018a). The stylohyal fossa is completely preserved only in MNHN-Bol V 3718 and 3277 (Figs 6.14, 6.17). This structure is typical of all sloths excluding the extant genus *Bradypus* (Patterson *et al.* 1992; Gaudin 1995, 2004, 2011). Other bones participating in the formation of the stylohyal fossa are the entotympanic anteromedially, the paracondylar process of the exoccipital posteromedially and the paraoccipital process of petrosal posterolaterally (Fig. 6.14). The stylohyal fossa is slightly elliptical in shape, with its major axis oriented anteromedially and its concave surface facing ventrolaterally. This tilt is characteristic of the majority of Mylodontidae (Gaudin 2004: char 56).

Exoccipital and paraoccipital process of petrosal - The paracondylar process of the exoccipital is directed ventrally and anteriorly and it is markedly more pointed and pyramidal in shape than *Glossotherium* (Fig. 6.14; Boscaini *et al.* 2018a). Its medial margin forms the posterior and lateral borders of the jugular foramen (Fig. 6.14). Its lateral margin merges posteriorly with the exoccipital crest that extends posteriorly and dorsally, proximate to but not contacting the lateral extremity of the occipital condyle. The exoccipital crest is limited anterolaterally by the mastoid portion of the petrosal. The area immediately lateral to the exoccipital crest is markedly concave, forming the so-called mastoid depression (Gaudin 1995; Gaudin & Wible 2006). This depression is more pronounced, more rugose and faces more posteriorly than *Glossotherium robustum* (Boscaini *et al.* 2018a). More anteriorly, the paraoccipital process of petrosal forms a bulge on the lateral side of the braincase, just dorsal to the stylohyal fossa (Fig. 6.14). Two well-marked foramina are situated in this area: the ventral opening of the canal for the occipital artery posteriorly (= mastoid foramen in Patterson *et al.* 1992) and the stylomastoid foramen anteriorly. These two foramina are connected by an open sulcus (Figs 6.14–6.16), a feature also present in the genus *Paramylodon*. In other extinct folivorans like *Mylodon darwinii*, *Glossotherium robustum,* and the lestodontines and scelidotherine sloths, the occipital artery runs in a more elongated enclosed channel. As a result, in these latter sloths, the ventral opening of the canal for the occipital artery and the stylomastoid foramen approach one another more closely. The stylomastoid foramen, which accommodates the facial nerve (VII), is the direct continuation of the facial sulcus of the petrosal already discussed (Figs 6.14–6.16). This opening faces ventrolaterally, a recurrent character in the family Mylodontidae with the exception of *Nematherium*, *Octodontotherium* (Gaudin 1995: char. 58) and *Paramylodon garbanii* (UF 10922). The

position of this foramen is anterolateral to the stylohyal fossa, thus more closely resembling the scelidotherines and *Pseudoprepotherium* than other mylodontids, in which the foramen is situated just anterior to the stylohyal fossa (Gaudin 1995: char. 57). The direction of the internal branch of the occipital artery (i.e., the arteria diploëtica magna) can be observed in MNHN-Bol V 9759 (Fig. 6.16). The arteria diploëtica magna, together with the corresponding vein, were located in the post-temporal canal (Fig. 6.16B; see Rougier *et al.* 1992; Wible & Gaudin 2004; Wible 2010).

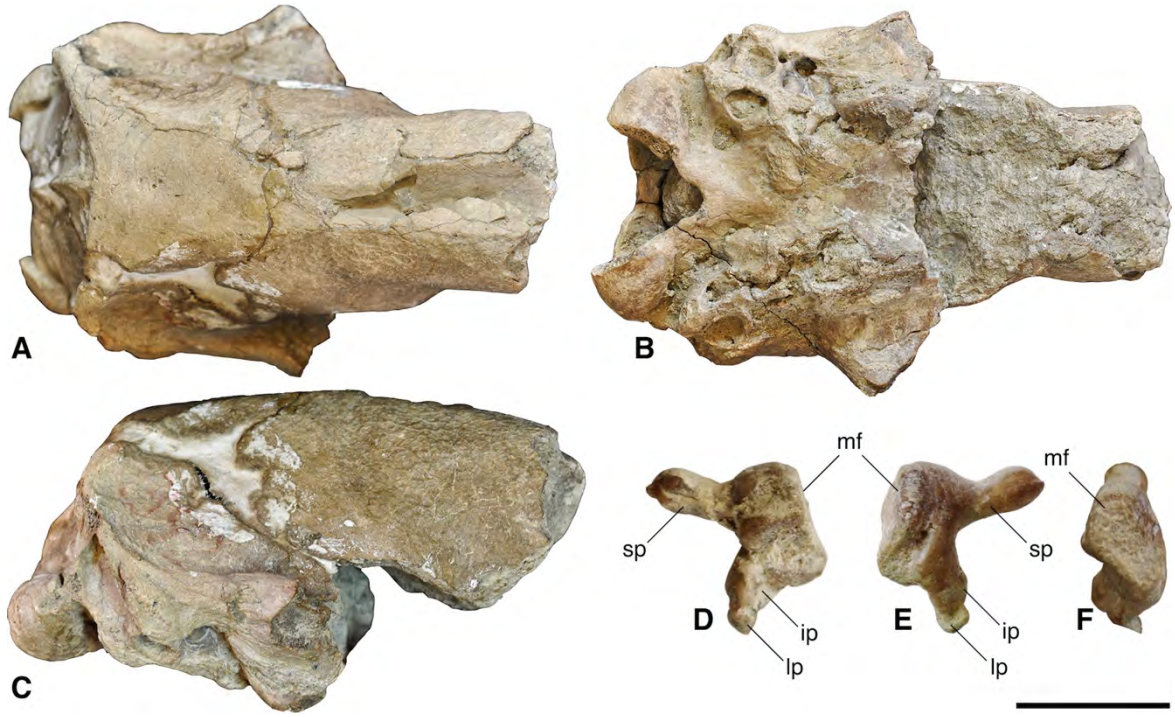

Figure 6.17. Neurocranium and right incus of *Simomylodon uccasamamensis* (MNHN-Bol V 3277). A-C, neurocranium in dorsal (A), ventral (B) and lateral (C) views; D-F, right incus in lateral (D), medial (E) and anterior (F) views. Abbreviations: mf, malleus facet; ip, inferior process; lp, lenticular process; sp, superior process. Scale bar equals 5 cm for A-C, 5 mm for D-F.

Pterygoid- In all the observed specimens, the pterygoids are greatly inflated at their base and are separated into medial and lateral portions by a ventral groove (Fig. 6.14). As in *Mylodon and Glossotherium*, the inflation of the lateral portion of the pterygoid also partially involves the squamosal (Fig. 6.14; Patterson *et al.* 1992; Boscaini *et al.* 2018a). The medial portion of the pterygoid inflation is more globose and less anteroposteriorly enlarged than the lateral one. The lateral inflation also involves partially the basisphenoid, and forms the anterior and medial walls of the carotid foramen (Fig. 6.14). As in all Lestodontinae and Mylodontinae with the exception of *Pseudoprepotherium*, the carotid foramen is fully exposed in ventral view (Gaudin, 1995: char.

15). Like *Glossotherium robustum* (Boscaini *et al.* 2018a), in *Simomylodon* the groove between the medial and lateral portions of the pterygoid housed the Eustachian tube, and a distinct groove for the vidian nerve is apparently lacking.

Basisphenoid and basioccipital- Due to fusion, the sutures between the basisphenoid and the basioccipital cannot be determined in our observed sample. The inflated portion of the basisphenoid is involved in the formation of the medial wall of the carotid foramen, whereas the basioccipital, which extends posteriorly to anteroventral rim of the foramen magnum (Patterson *et al.* 1992; Gaudin 2011), participates in the formation of the jugular and hypoglossal foramina (Fig. 6.14). The basioccipital forms the posteromedial border of the jugular foramen and both the roof and the floor of the hypoglossal foramen (Fig. 6.14). This latter foramen is the posteriormost opening on the ventral side of the braincase. The hypoglossal foramen of *Simomylodon* is directed ventrally and anterolaterally (Fig. 6.14). Its posterior margin has a more rounded and less anteriorly concave border, in comparison with that of *Glossotherium* (Fig. 6.14; Boscaini *et al.* 2018a).

Incus- A single right incus was found embedded in the matrix of the middle ear cavity in MNHN-Bol V 3277 (Fig. 6.17). It bears an articular facet for the malleus that is comprised of two contiguous facets: the main one is flat in lateral and medial views (Fig. 6.17D–E) and teardrop shaped in anterior view (Fig. 6.17F), whereas the secondary facet is concave, smaller and only visible in lateral view (Fig. 6.17D). The inferior process, bearing the lenticular process on its tip, is roughly equivalent in size to the superior process, even if the latter shows a more rounded shape, as in *Paramylodon harlani* (Patterson *et al.* 1992; Blanco & Rinderknecht 2008). In *Mylodon* (Guth 1961) and *Lestododon* (Blanco & Rinderknecht 2008) the superior process appears significantly thicker than the inferior one. The two processes meet at a right angle in *Simomylodon* (Fig. 6.17D–E), as is also observed in *Glossotherium*, *Lestodon* and *Mylodon* (Guth 1961; Blanco & Rinderknecht 2008).

6.3 POSTCRANIAL ANATOMY OF *S. UCCASAMAMENSIS*

The postcranial anatomy of *Simomylodon uccasamamensis* is partially known from the work of Saint-André *et al.* (2010). As with the cranial elements, the presence of many previously undescribed postcranial elements allows for a more complete investigation of the forelimb and hindlimb anatomy of *S. uccasamamensis*. Regarding the axial postcranium, only some isolated and fragmented vertebrae and ribs are currently known, impeding a reliable assessment of the morphology of the unpaired skeletal elements (see Appendix I). On the contrary, for the elements of both the forelimb and the hindlimb, the presence of multiple specimens of the same bone also allows, in some cases, observations regarding their intraspecific variation (see Chapter 7). The large variety of elements present permits an almost total characterization of the appendicular anatomy of this species, making *S. uccasamamensis* the best known early member of Mylodontini. Moreover, *S. uccasamamensis* represents a key taxon for inferring the phylogenetic relationships of Mylodontinae on the basis of postcranial anatomy (see Chapter 8).

6.3.1 Comparative description

Scapula- The anatomy of the scapula of *S. uccasamamensis* was previously unknown (Saint-André *et al.* 2010). The available scapula, MNHN-Bol V 3718 (Fig. 6.18), is associated with a skull (Fig. 6.7), and therefore its assignment to *S. uccasamamensis* is clear. The scapular morphology of mylodontid sloths is very conservative, so that the main differences are essentially size-related. The scapula of *Simomylodon* is very similar in shape not only to the homologous element in *Glossotherium*, *Mylodon* and *Paramylodon*, but also in the lestodontines (e.g., Owen 1842; Stock 1925; Webb 1989). Scapulae of *Catonyx* and *Scelidotherium* appear slightly more elongated dorsoventrally, due to the more acute angle between the vertebral and caudal borders (McDonald 1987).

In lateral view the scapula of *S. uccasamamensis* exhibits a strong scapular spine, which divides the supraspinous fossa anteriorly from the infraspinous fossa posteriorly. The secondary spine is confined to the caudal border, delimiting a very reduced post-scapular fossa (Fig. 6.18). In contrast, the supraspinous and infraspinous fossae are large and roughly the same size. The scapular spine continues anteriorly into the acromion process, which is fused with the coracoid process to form the acromiocoracoid arch typical of sloths (e.g., Engelmann 1985, Rose & Emry 1993, McDonald 2003). This arch bears the articulation for the clavicle (Fig. 6.18B). In ventral

view, the glenoid cavity is pyriform, with its anteriormost end narrower mediolaterally than its posterior end, whereas the facet for the clavicle appears elliptical in outline. All these features are invariably present in Mylodontidae (e.g., Stock 1925; McDonald 1987). In ventral view, the long axes of the glenoid fossa and the clavicular facet form an acute angle in *Simomylodon* (Fig. 6.18), as they do in other mylodontines (e.g., *Glossotherium* MACN Pv 14066 and *Paramylodon* FMNH P14723) and in scelidotheres (e.g., *Catonyx* FMNH P14238 and *Scelidotherium* FMNH P14274). In contrast, this angle is roughly orthogonal in *Lestodon* (MACN Pv 14648). Unfortunately, due to lack of preservation, this feature has not been observed in the genera *Thinobadistes* and *Bolivartherium*, so that it remains unclear whether the morphology in *Lestodon* is typical for lestodontines in general.

In medial view, the scapula of *S. uccasamamensis* MNHN-Bol V 3718 shows a pronounced posterior ridge of the infraspinous fossa, forming a wide and triangular area for the *m. teres minor* (Fig. 6.18C). This feature is common in all the observed Mylodontinae, whereas this fossa is more reduced in size and more posteriorly oriented in Scelidotheriinae.

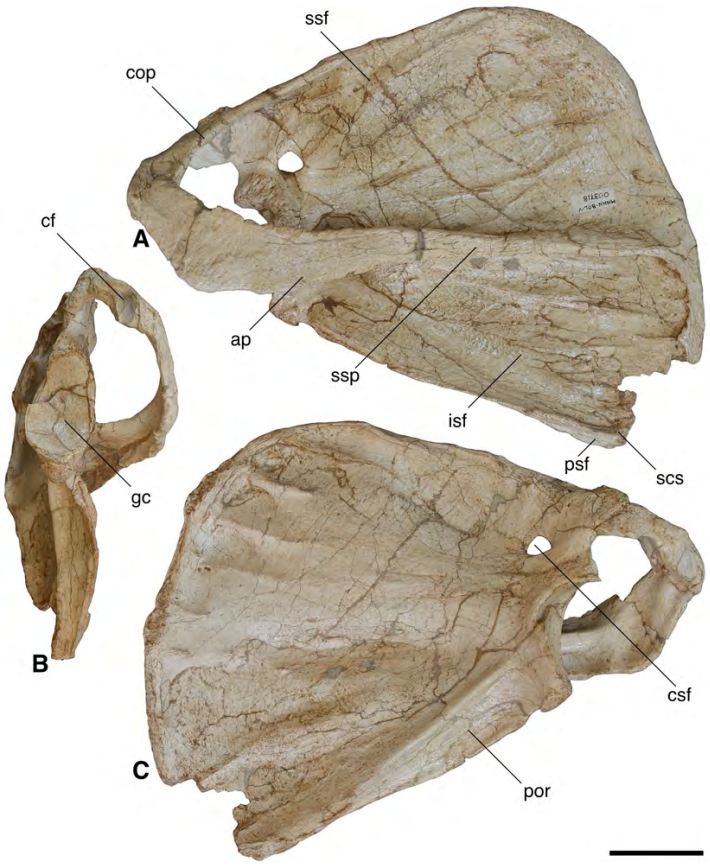

Figure 6.18. Left scapula of *Simomylodon uccasamamensis* (MNHN-Bol V 3718) in lateral (A), proximal (B) and medial (C) views. Abbreviations: ap, acromion process; cf, clavicular fossa; cop, coracoid process; csf, coraco-scapular foramen; gc, glenoid cavity; isf, infraspinous fossa; por, posterior ridge of infraspinous fossa; psf, post-scapular fossa; scs, secondary spine; ssf, supraspinous fossa; ssp, spine of scapula. Scale bar equals 5 cm.

Humerus- Fifteen humeral fragments assigned to *S. uccasamamensis* are available for study (Appendix I). However, none of them is complete, and two uncomplete specimens have been selected in order to show all the features of this element (Fig. 6.19). The humerus of *S. uccasamamensis* is robust, with its distal end, in anterior view, broader mediolaterally than the proximal end (Fig. 6.19). In proximal view (Fig. 6.19A), the humeral head is subspherical in shape, and adjacent anteromedially to the lesser tuberosity and anterolaterally to the greater tuberosity. The latter is more protruded radially than the former (Fig. 6.19A), a widespread feature in Mylodontidae. An exception is represented by *Nematherium* (YPM-PU 15374), in which the opposite condition is present. The latter conformation is also observed in *Hapalops* and *Bradypus*, suggesting that this condition is primitive for sloths.

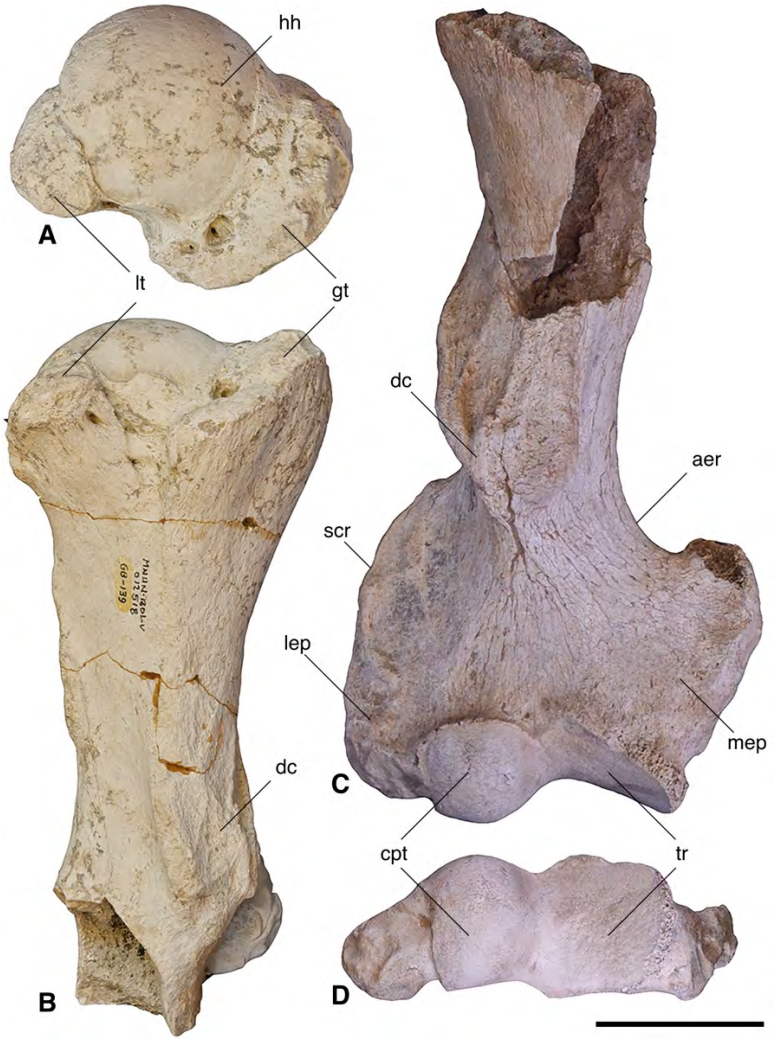

Figure 6.19. Humeral fragments of *Simomylodon uccasamamensis*. A-B, proximal fragment of left humerus (MNHN-Bol V 12518) in proximal (A) and cranial (B) views; C-D, distal fragment of right humerus (MNHN.F.AYO110) in cranial (C) and distal (D) views. Abbreviations: aer, ascending entepicondylar ridge; cpt, capitulum; dc, deltoid crest; gt, greater tuberosity; hh, humeral head; lep, lateral epicondyle; lt, lesser tuberosity; mep, medial epicondyle; scr, supinator crest, tr, trochlea. Scale bar equals 5 cm.

The greater tuberosity continues ventrally into the deltopectoral crest, which shows a rugose surface for muscular attachments (Fig. 6.19B–C). The deltopectoral crest faces anterolaterally and has an oblique distal margin, as is typical in Mylodontinae. In contrast, in *Nematherium*, *Scelidotherium* and *Catonyx*, the deltopectoral crest has a more horizontal distal margin and faces more anteriorly. Moreover, in these taxa, the deltopectoral crest is more expanded medially and overlaps the ascending entepicondylar ridge in anterior view.

In anterior view, the lateral epicondyle is expanded laterally, and delimited by a laterally convex supinator crest (Fig. 6.19C). The supinator crest is curved in proximity of the deltopectoral crest, as observed in *Thinobadistes*, *Pseudoprepotherium* and *Nematherium* (see also Chapter 8: char. 303). In the other Mylodontidae, the profile of the supinator crest is less regular and its most distal portion is proximodistally vertical. As is typical for mylodontids, the medial epicondyle shows a distinct proximodistal process (see also Chapter 8: char. 307). Furthermore, as in all Mylodontinae, the entepicondylar foramen is lacking (Fig. 6.19C) (McDonald & De Iuliis 2008; see also Chapter 8: char. 306). The medial and lateral epicondyle extend transversely to approximately the same degree (Fig. 6.19C), a condition that is also observed in *Thinobadistes* (Webb 1989) and *Pseudoprepotherium* (Hirschfeld 1985). In *Nematherium*, *Catonyx* and *Scelidotherium*, the medial epicondyle is wider than the lateral epicondyle, whereas it is the opposite in the rest of Mylodontinae (see also Chapter 8: char. 308).

In distal view, both epicondyles are directed posteriorly, as is also observed in *G. robustum*, *P. harlani*, *M. darwinii*, and *G. chapadmalensis*. In *Pseudoprepotherium* the medial epicondyle is directed medially, whereas in *Lestodon* it is directed anteriorly. In *Thinobadistes*, the humerus varies in this feature: both epicondyles are either directed posteriorly or mediolaterally in distal view (see also Chapter 8: chars 311–312). In the same view, the capitulum and the trochlea of *Simomylodon* have approximately the same anteroposterior depth (Fig. 6.19D), a widespread mylodontid feature, with the exception of *Scelidotherium* and *Catonyx*, in which the trochlea is consistently anteroposteriorly deeper than the capitulum. However, the trochlea of *S. uccasamamensis* appears transversely wider than the capitulum (Fig. 6.19D), in this way more closely resembling *G. chapadmalensis* and *P. harlani*, rather than *M. darwinii* and *G. robustum*. In the latter species, in fact, the relative mediolateral expansion of capitulum and trochlea is equivalent (see also Chapter 8: chars 309–310).

Radius- Features on the radius of *S. uccasamamensis* can be observed in eight specimens, two of which are complete: MNHN.F.AYO180 (Saint-André *et al.* 2010: fig. 11) and MNHN-Bol V 3375 (Fig. 6.20). The general morphology of the radius of *S. uccasamamensis* is more similar to

that of *Pseudoprepotherium* (Hirschfeld 1985) and the lestodontines (Webb 1989), rather than the remaining Mylodontinae. In fact, the ratio between the anteroposterior radial length, measured at midshaft, and the total length reaches its maximum values in the genera *Pseudoprepotherium*, *Thinobadistes*, *Lestodon* and *Simomylodon* (see also Chapter 8: char. 314). This is due to the presence of a well-developed pronator ridge that makes the anterior border of the radius anteriorly convex, in lateral view (Fig. 6.20B). On the contrary, the posterior border is straight, in lateral view (Fig. 6.20B). This combination of features is observed in *Simomylodon*, *Pseudoprepotherium*, *Thinobadistes* and *Lestodon* (Hirschfeld 1985; Webb 1989). In other Pleistocene Mylodontinae, like *Mylodon*, *Glossotherium* and *Paramylodon,* the radius has a more straight and stocky structure, lacking a well-developed pronator crest (Owen 1842; Stock 1925; McAfee 2016). In contrast, *Nematherium*, *Scelidotherium* and *Catonyx* possess an anteriorly concave posterior border that, together with the anteriorly convex anterior border, give a sinuous aspect to the radius of the latter genera, in lateral view. This latter morphology results into a bend in the shaft that is typical of scelidotheres (McDonald 1987; see also Chapter 8: chars 316–317).

In *Simomylodon* the shape of the radial head is ovoid, as in the majority of Mylodontidae. In contrast, the radial head is generally more rounded in *Nematherium*, *Scelidotherium*, *Catonyx* and *Thinobadistes*. However, the proportions of the distal articulation of the radius do not vary conspicuously among mylodontids (see also Chapter 8: char. 315). The distal radius carries two

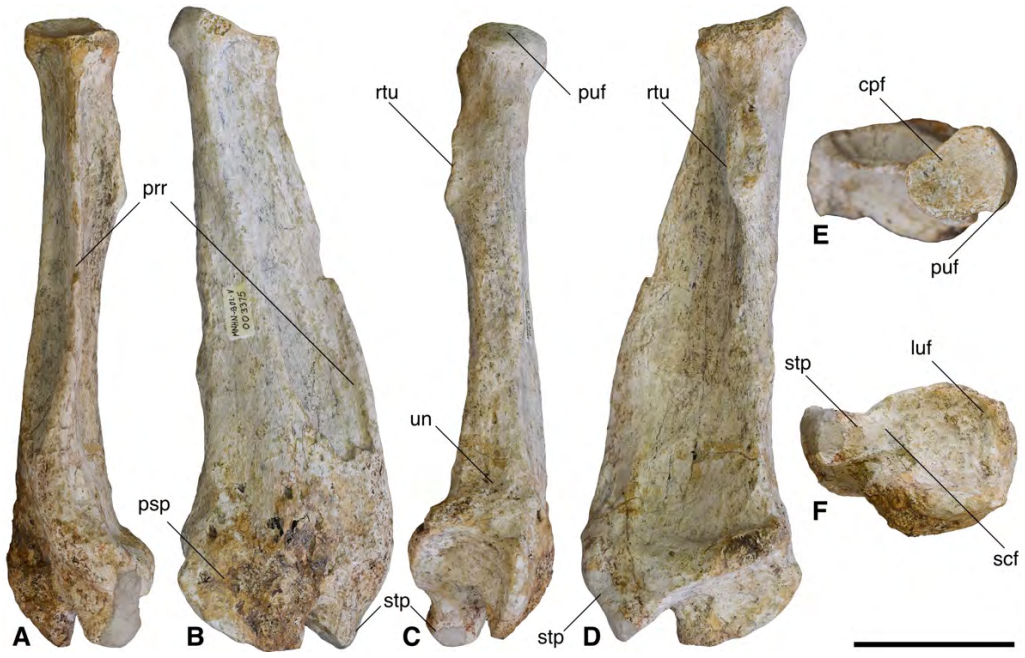

Figure 6.20. Right radius of *Simomylodon uccasamamensis* (MNHN-Bol V 3375) in cranial (A), lateral (B), caudal (C), medial (D), proximal (E) and distal (F) views. Abbreviations: cpf, capitular facet; luf, lunar facet; psp, pseudostyloid process; prr, pronator ridge; puf, proximal ulnar facet; rtu, radial tuberosity; scf, scaphoid facet; stp, styloid process; un, ulnar notch. Scale bar equals 5 cm.

distinct facets for the scaphoid and the lunar in MNHN.F.AYO180 (Saint-André *et al.* 2010), whereas they are confluent in MNHN-Bol V 3375 (Fig. 6.20F). The former condition is widespread in Mylodontidae, whereas the latter condition is typical of *Pseudoprepotherium* and the scelidotheres (Hirschfeld 1985; McDonald 1987).

Ulna- Only one ulnar fragment, lacking part of the olecranon and the distal epiphysis, is available for description: MNHN-Bol V 3717 (Fig. 6.21; Appendix I). The ulna was previously unknown for *S. uccasamamensis* (Saint-André *et al.* 2010) and its recovery in association with a complete cranium (Fig. 6.6), allows a definitive assignment to the latter species. This element is relatively short proximodistally and deep anteroposteriorly, as in other Mylodontinae, with the exception of *Pseudoprepotherium* (Hirschfeld 1985). In the latter taxon, but also in *Nematherium*, *Scelidotherium* and *Catonyx*, the ulna is relatively narrower anteroposteriorly and more proximodistally elongated (see also Chapter 8: char. 322). The olecranon meets the posterior edge of the ulna at a wide angle, comparable to all Mylodontinae with the exception of *Thinobadistes* (Webb 1989). In this latter taxon, the proximal and posterior borders of the ulna meet at an almost orthogonal angle, a feature also observed in *Scelidotherium* and *Catonyx* (McDonald 1987; see also Chapter 8: char 323).

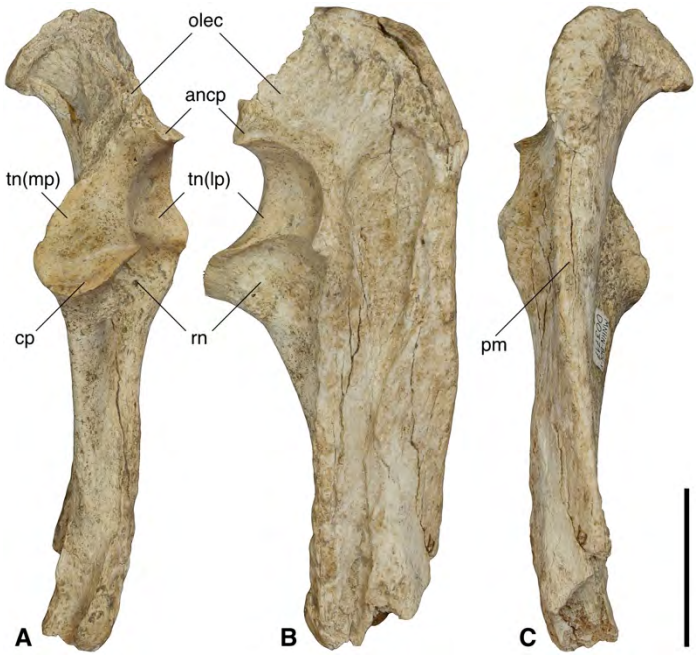

Figure 6.21. Proximal fragment of left ulna of *Simomylodon uccasamamensis* (MNHN-Bol V 3717) in cranial (A), lateral (B) and caudal (C) views. Abbreviations: ancp, anconeal process; cp, coronoid process; olec, olecranon; pm, posterior margin; rn, radial notch; tn(lp), trochlear notch (lateral portion); tn(mp), trochlear notch (medial portion). Scale bar equals 5 cm.

In anterior view, the trochlear notch shows, in *Simomylodon*, two well defined lateral and medial facets, which both culminate at the same height at the level of the anconeal process (Fig. 6.21A), as in *Paramylodon harlani and P. garbanii*. The lateral portion is more proximally extended

than the medial portion in *G. robustum*, *M. darwinii* and *L. armatus*, whereas the opposite condition is observed in *Thinobadistes*, *Nematherium*, *Catonyx* and *Scelidotherium*. The radial notch is also well-defined and its area is relatively wider in *Simomylodon* (in comparison with the trochlear notch) than in *Mylodon*, *Glossotherium* and *Paramylodon* (see also Chapter 8: chars 324–325).

In posterior view (Fig. 6.21C), the width of the ulna decreases from proximal to distal, as observed in all Mylodontinae with the exception of *Pseudoprepotherium*. In the latter genus, but also in *Nematherium*, *Scelidotherium* and *Catonyx*, the ulna is columnar in posterior view, with a uniform transverse width along its whole length (see also Chapter 8: char. 326). These four latter genera also differ from mylodontines in the inclination of the distal articular facet for the cuneiform. In these taxa, the long axis of the facet is oblique, so that in lateral view its anterior margin is more proximal than the posterior (McDonald 1987). In all the other Mylodontidae, however, the distal articular facet is at a right angle to the long axis of the shaft in lateral view (see also Chapter 8: chars 327–328). Unfortunately, this latter feature cannot be observed in *S. uccasamamensis* because the distal ulnar epiphysis is not preserved (Fig. 6.21).

Manus- In general, the manus of *S. uccasamamensi*s has the typical mylodontid conformation, with five metacarpals and three ungual phalanges on the first three digits. This pattern is present in the manus of all known mylodontid sloths, with the exception of *Scelidotherium*, in which the ungual on the first digit is secondarily lost (McDonald 1987).

Several elements of the manus of *S. uccasamamensis* are available (Figs 6.22–6.24), allowing an exhaustive characterization of its morphology. Two of these elements, the scaphoid and the trapezium, were described by Saint-André *et al.* (2010) and subsequently glued into an assembled manus, rendering it impossible to observe all of their features in detail. For this reason, photos of these two elements (Fig. 6.22) were taken directly from Saint-André *et al.* (2010).

The scaphoid of *Simomylodon* (Fig. 6.22A–B) is similar in shape to that of other mylodontids. It bears an elongated medial process that supports the facet for the co-ossified trapezium and first metacarpal (carpal-metacarpal complex). This latter facet is separated from the facet for the trapezoid, as in all Mylodontinae and in contrast with the Scelidotheriinae, in which the two facets are contiguous (McDonald 1987). In *Nematherium*, *Scelidotherium*, and *Catonyx* the medial process is relatively less elongated, and the scaphoid generally shows a blockier aspect than in other Mylodontidae. Accordingly, the former three genera exhibit a higher ratio between the minimum and maximum diameters of the scaphoid (see also Chapter 8: char. 331).

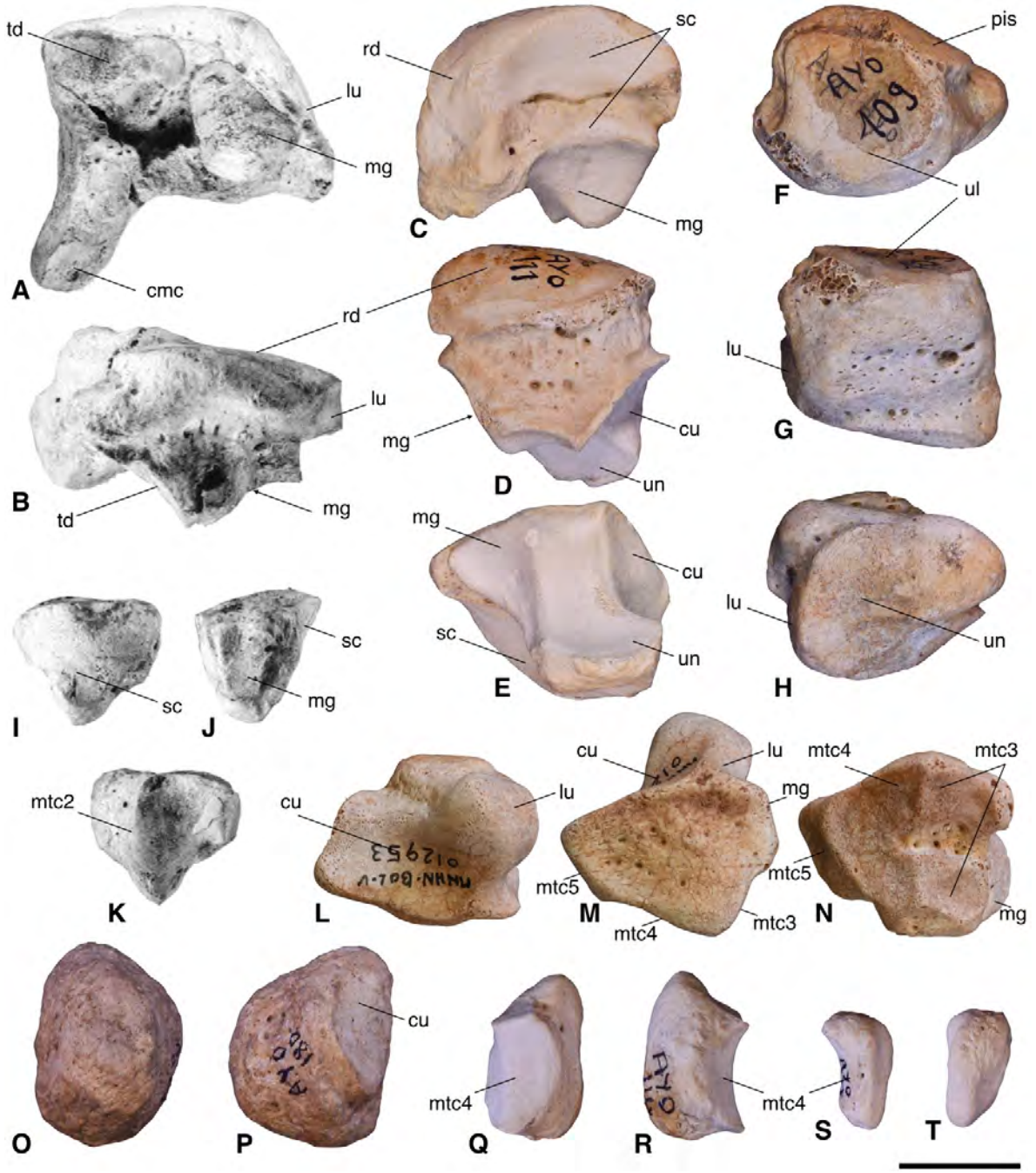

Figure 6.22. Carpals (A-P) and sesamoids (Q-T) of *Simomylodon uccasamamensis*. A-B, left scaphoid (MNHN.F.AYO180) in distal (A) and dorsal (B) views; C-E, left lunar (MNHN.F.AYO111) in cranial (C), dorsal (D) and distal (E) views; F-H, left cuneiform (MNHN.F.AYO109) in proximal (F), dorsal (G) and distal (H) views; I-K, left trapezoid (MNHN.F.AYO180) in proximal (I), caudal (J) and distal (K) views; L-N, right unciform (MNHN-Bol V 12953) in proximal (L), dorsal (M) and distal (N) views; O-P, right pisiform (MNHN.F.AYO180) in palmar (O) and oblique-palmar (P) views; Q-R, right medial sesamoid of mtc4 (MNHN.F.AYO114) in medial (Q) and lateral (R) views; S-T, right lateral sesamoid of mtc4 (MNHN.F.AYO111) in medial (S) and palmar (T) views; Black and white photos have been taken from St-André *et al.* (2010). Abbreviations refer to articular facets for the indicated bones, as follows: cmc, carpal-metacarpal complex; cu, cuneiform, lu, lunar; mg, magnum; mtc (2-3-4-5), metacarpal (2-3-4-5); pis, pisiform; rd, radius; sc, scaphoid; td, trapezoid; ul, ulna; un, unciform. Scale bar equals 2 cm.

The facets for the trapezoid and magnum are separated and almost the same size in MNHN.F.AYO180, the only available scaphoid of S. *uccasamamensis* (Fig. 6.22A–B). However, in larger samples from other mylodontines, such as *Thinobadistes* and *Paramylodon* (AMNH, FMNH, UF collections), the arrangement of these facets is highly variable.

The lunar morphology is extremely conservative in Mylodontidae (McDonald 1987). In the 33 mylodontid lunars measured in this work, no reliable differences in proportions have been detected. The lunar-scaphoid contact is separated into two distinct facets in MNHN.F.AYO111 (Fig. 6.22C), with the proximal one clearly larger than the distal one. In MNHN.F.AYO180 the distal facet is absent (Saint-André *et al.* 2010). The shape of the facets of the lunar-scaphoid contact, and their mutual interconnection, are also variable in the genera *Paramylodon*, *Thinobadistes* and several scelidotheres (McDonald 1987). On the proximal lunar side, the facet for the radius is rounded and forms a wide and convex surface (Fig. 6.22D), whereas on the distal side three contiguous facets can be differentiated (Fig. 6.22E). These are for connection with the magnum medially, unciform centrally and cuneiform laterally (Fig. 6.22E).

The general shape of the mylodontid cuneiform is that of a cube with a flat proximal facet for the ulna and a more complex distal facet for the unciform (McDonald 1987). However, the cuneiform differs significantly in some proportions among the Mylodontidae. In *Simomylodon* (Fig. 6.22F–H), together with all the other mylodontines, the ratio of its dorsopalmar and transverse widths is quite uniform. This ratio is intermediate between those registered for *Nematherium* (which shows the lowest) and *Catonyx*, *Scelidotherium* and *Thinobadistes* (which show the highest). The ratio between the proximodistal length and mediolateral width of the cuneiform only differentiates *Nematherium* from the rest of the mylodontids. However, the ratio between the proximodistal and dorsopalmar widths differentiates between the Mylodontinae and Scelidotherinae, with the former having the higher ratios. In this latter feature, *Thinobadistes* and *Paramylodon* show a certain degree of variation (see also Chapter 8: chars 333–335). In the cuneiform of scelidotheres, the lunar facet is positioned on a process (McDonald 1987), with the consequent marked separation of the cuneiform and the lunar. In contrast, this process is absent in Mylodontinae, so that the facet adjacent to the medial surface of the cuneiform (see also Chapter 8: char. 332). This latter conformation is also observed in *Simomylodon* (Fig. 6.22G–H).

The trapezoid of *S. uccasamamensis* (Fig. 6.22I–K) contacts the scaphoid, the magnum and the second metacarpal, as in all mylodontid sloths. For this reason, the arrangement of the facets is similar in all the taxa considered in the present study. However, in *S. uccasamamensis* the

mediolateral width of the trapezoid is greater than its dorsopalmar length, a feature already noted by Saint-Andre *et al.* (2010). The opposite condition is found in the other observed Mylodontidae, including *S. leptocephalum*, *T. segnis*, *G. robustum*, *P. harlani* and *M. darwinii* (Appendix II), suggesting that the condition of *Simomylodon* is an autopomorphic trait.

No isolated magnums are currently known for *S. uccasamamensis*. The magnum is fused with the third metacarpal in two over five specimens. This fusion is present in MNHN.F.AYO179 (Fig. 6.23I–M) and MNHN.F.AYO180, whereas it is absent in the three isolated third metacarpals MNHN.F.VIZ27 (Fig. 6.23F–H), MNHN.F.VIZ5, and MNHN-Bol V 12927. The fused specimens do not belong to the same individual (both of them are left hand elements) and do not exhibit bone regrowth on either side of the fused elements. This suggests that this connection is not related with any pathology, but represents instead a peculiar trait of *Simomylodon*, that sometimes occurs in the available sample. At present, this condition is unknown in any other mylodontid. Even if the two elements are fused, a transverse nutritive foramen is present at the level of their connection, allowing visual identification of the plane of separation (Fig. 6.23K, M). In this way, it is possible to observe that the magnum has no visible connection with the second metacarpal in dorsal view. The connection between the magnum and the second metacarpal is confined to a single facet on the palmar edge, a typical feature of Mylodontinae (McDonald 1987). On the contrary, an extensive contact between these two elements is visible on the dorsal side of the manus in the scelidotherine sloths (see also Chapter 8: char. 339).

In proximal view, the unciform of *S. uccasamamensis* has a strong process for the lunar and a relatively short lateral platform for the cuneiform (Fig. 6.22L). The proximodistal width of the element exceeds the transverse width, a condition also observed in *M. darwinii*, *G. robustum*, *P. harlani* and some specimens of *T. segnis*. The opposite pattern is observed in all the other mylodontids (see also Chapter 8: char. 336). In distal view the unciform displays well-developed facets for metacarpals three, four, and five (Fig. 6.22N). The former is located medially and divided into two articular surfaces. Immediately lateral to these two facets is the facet for the fourth metacarpal, which is undivided, and abuts an even further laterally positioned and well-developed facet for the fifth metacarpal (Fig. 6.22N). The extensive unciform/fifth metacarpal contact is common in Mylodontinae, reaching an extreme condition in *M. darwinii,* in which the cuneiform also contacts the fifth metacarpal (Haro *et al.* 2016). However, a significant reduction of the unciform-fifth metacarpal facet is observed in *Catonyx*, and the contact complete disappears in *Scelidotherium*, where the fifth metacarpal articulates only with the fourth metacarpal (McDonald 1987; see also Chapter 8: char. 342).

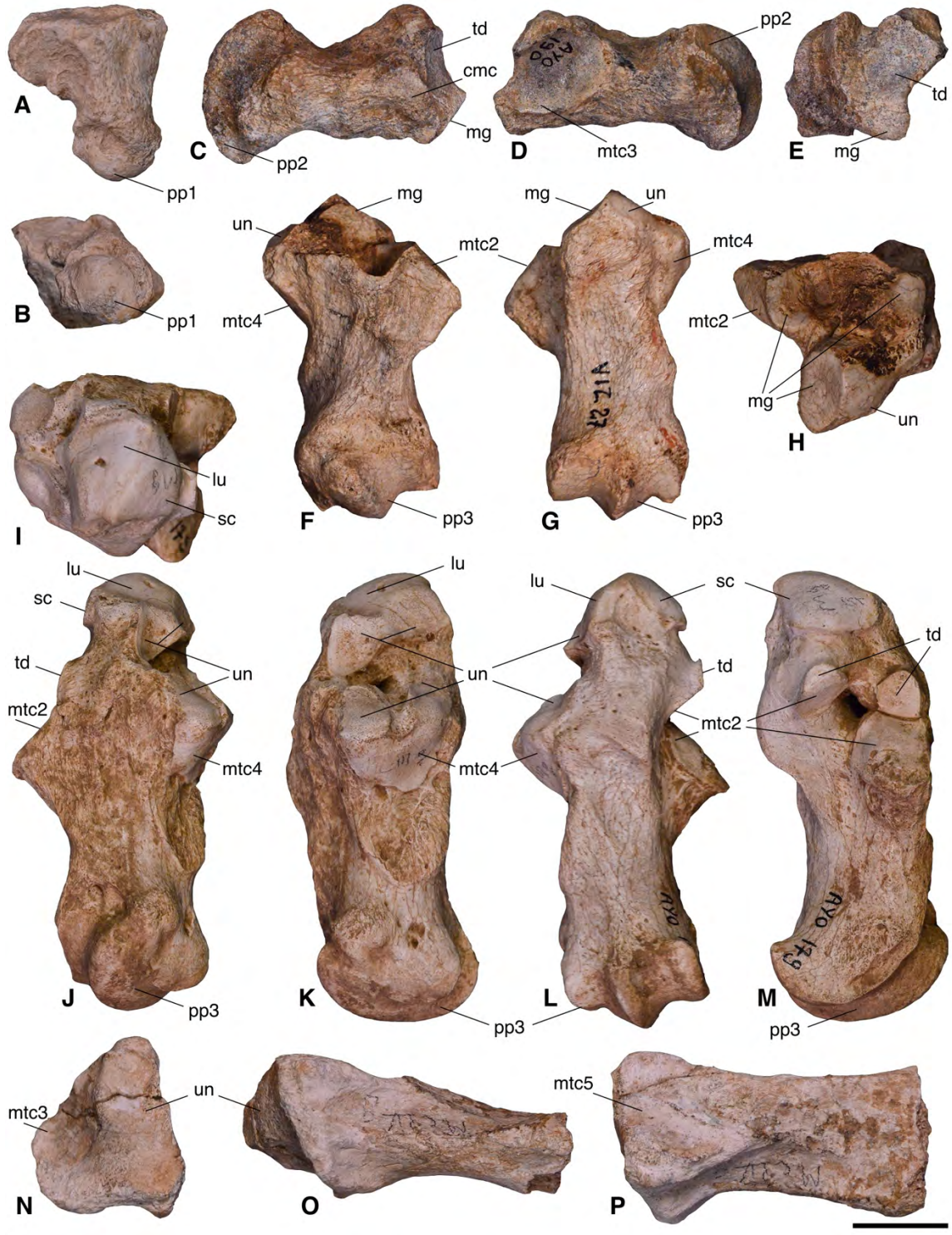

Figure 6.23. Metacarpal elements of *Simomylodon uccasamamensis*. A-B, right carpal-metacarpal complex (MNHN.F.VIZ32) in dorsal (A) and distal (B) views; C-E, right metacarpal II (MNHN.F.AYO190) in cranial (C), caudal (D) and proximal (E) views; F-H, right metacarpal III (MNHN.F.VIZ27) in dorsal (F), palmar (G) and proximal (H) views; I-M, left metacarpal III fused with magnum (MNHN.F.AYO179) in proximal (I), dorsal (J), caudal (K), palmar (L) and cranial (M) views; N-P, proximal fragment of left metacarpal IV (MNHN.F.VIZ33) in proximal (N), dorsal (O) and caudal (P) views. Abbreviations refer to articular facets for the indicated bones, as follows: cmc, carpal-metacarpal complex; lu, lunar; mg, magnum; mtc (2-3-4-5), metacarpal (2-3-4-5); pp (1-2-3), proximal phalanx (1-2-3); sc, scaphoid; td, trapezoid; un, unciform. Scale bar equals 2 cm.

The trapezoid and the first metacarpal are fused in *S. uccasamamensis* (Fig. 6.23A–B), forming the carpal-metacarpal complex, a feature observed in the majority of mylodontids (see also Chapter 8: char 337). The two elements are separate in *Octodontotherium grande* (MNHN.F.DES231), and in some specimens of *Paramylodon harlani* (Stock 1925). The carpal-metacarpal complex possesses two separate proximal facets: a larger one for articulation with the scaphoid and a smaller one for articulation with the second metacarpal. As in all Mylodontinae, there is no facet for the trapezoid on the carpal-metacarpal complex (McDonald 1987). Distally, the element carries a subspherical facet for the proximal phalanx of the first digit (Fig. 6.23A–B).

The second metacarpal of *S. uccasamamensis* (Fig. 6.23C–E) is relatively elongated and narrow mediolaterally. In proximal view, the second metacarpal bears a large articular surface for the trapezoid and a smaller one for the magnum. The latter, as noted above, is confined to the palmar side of the bone (Fig. 6.23C–E). The facet for the carpal-metacarpal complex on the lateral side is reduced, whereas the facet for the third metacarpal is wide and medially concave (Fig. 6.23C–D).

As described above, the third metacarpal of *S. uccasamamensis* can be found either isolated (Fig. 6.23F–H) or fused with the magnum (Fig. 6.23I–M). In the isolated condition, the third metacarpal appears relatively long proximodistally and thin mediolaterally, especially near midshaft, resembling *O. grande*, *Ps. confusum*, *Pa. garbanii* and *M. darwinii* in this respect, whereas in the other mylodontids this element is relatively shorter and thicker (see also Chapter 8: char. 341). The articular surface for with the second metacarpal is convex (Fig. 6.23) and the two metacarpals are separated by a moderately developed proximomedial process on the third metacarpal. This feature in *S. uccasamamensis* is similar to the condition in lestodontines. It is intermediate between the morphology of *Nematherium*, *Catonyx*, *Scelidotherium*, *Pseudoprepotherium*, and *Octodontotherium*, in which the process is shorter and the two metacarpals are closer together, and that of *Mylodon*, *Paramylodon* and *Glossotherium*, in which the two elements show an even greater separation due to the presence of a longer process (see also Chapter 8: char. 340).

Only a proximal fragment of the fourth metacarpal of *S. uccasamamensis* is available (Fig. 6.23N–P). In proximal view, the contacts with the third metacarpal and the unciform are contiguous, with the latter more extended dorsopalmarly than the former (Fig. 6.23N). On the lateral side, the facet for the fifth metacarpal (an element which is unknown in *S. uccasamamensis*) is flat and triangular in outline (Fig. 6.23P).

The proximal and distal phalanges of MNHN-Bol V 3313 (Fig. 6.24A–G) are very similar in shape to those of *G. robustum* and *P. harlani* (Owen 1842; Stock 1925) and likely belonged to

the right third digit of *S. uccasamamensis*. Also, the three ungual phalanges of MNHN.F.AYO180 (Fig. 6.24H–P) likely represent the claws on the first three digits of the left hand, based on their relative size. The ungual phalanges are covered proximally by bony sheaths, which show different stages of completeness, and are pierced by paired foramina on their ventral sides for the insertion of tendons (Fig. 6.24H–P). The claws are almost circular in cross-section, as in *G. robustum* and *P. harlani* (Owen 1842; Stock 1925). As in *P. harlani* (Stock 1925), two symmetrical concavities mark the ventral side of the claw core, and are more marked in the second (Fig. 6.24K–M) than the third (Fig. 6.24N–P) ungual phalanx. As already noticed, the presence of three clawed digits on the manus is a widespread mylodontid feature, not observed in *Scelidotherium* (McDonald 1987; see also Chapter 8: char. 343).

The ungual phalanx described in Anaya & MacFadden (1995) and assigned to an indeterminate mylodontine, coincides in both shape and size with the second ungual phalanx of *S. uccasamamensis* (Fig. 6.24K–M) described and figured herein.

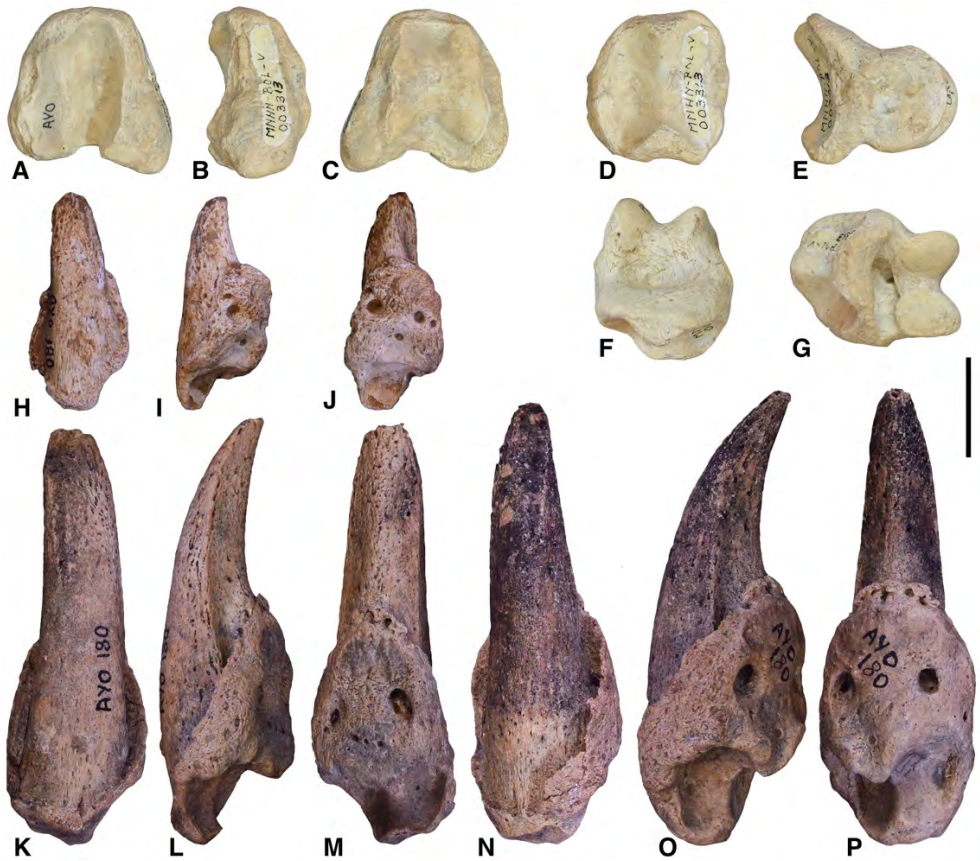

Figure 6.24. Phalanges of the hand of *Simomylodon uccasamamensis*. A-C, right proximal phalanx of third digit (MNHN-Bol V 3313) in proximal (A), lateral (B) and distal (C) views; D-G, right distal phalanx of third digit (MNHN-Bol V 3313) in proximal (D), lateral (E), dorsal (F) and palmar (G) views; H-J, left ungual phalanx of first digit (MNHN.F.AYO180) in dorsal (H), medial (I) and palmar (J) views; K-M, left ungual phalanx of second digit (MNHN.F.AYO180) in dorsal (K), medial (L) and palmar (M) views; N-P, left ungual phalanx of third digit (MNHN.F.AYO180) in dorsal (N), medial (O) and palmar (P) views. Scale bar equals 2 cm.

Femur- Twenty femoral fragments of *S. uccasamamensis* have been recovered, but only eight of them are relatively complete (Appendix I). Of these eight, five appear larger and more robust than the other three. However, the present descriptions and comparisons are valid for all the available femoral remains, whereas intraspecific differences are treated in Chapter 7.

The femur of *S. uccasamamensis* (Fig. 6.25) is similar in shape to that of the other Mylodontinae. The ratio between the mediolateral width at midshaft and total length is similar among mylodontines, but is consistently higher in the scelidotheres (see also Chapter 8: char. 344). Accordingly, this relatively pronounced mediolateral enlargement of the femur is a diagnostic trait for Scelidotheriinae (McDonald 1987), a feature that inspired Owen (1839) to coin the generic name *Scelidotherium* (etymologically "femur beast"). As in all mylodontines, the femur of *Simomylodon* is narrower distally than proximally in anterior view. In *Simomylodon*, the ratio between maximum femoral condylar width and the total femoral length is similar to that of most other Mylodontinae. This ratio is intermediate between the lowest value recorded for mylodontids, that of *Pseudoprepotherium*, *Urumacotherium* and *Mirandabradys*, and the largest value recorded, that of the scelidotheres (see also Chapter 8: char. 345). Also, the ratio between the intertrochanteric width and the total length of the femur is consistent among Mylodontidae, with an exception represented by the scelidotheres, which show the greatest observed values (see also Chapter 8: char. 347). In contrast, the ratio between the anteroposterior depth and mediolateral widths measured at the femoral midshaft is similar in all Mylodontidae, but *Catonyx* and *Scelidotherium* represent an exception and show the lowest values (see also Chapter 8: char. 348).

In *Simomylodon*, the greater trochanter is both broad mediolaterally and deep anteroposteriorly, but is not elongated proximodistally (Fig. 6.25). In fact, it doesn't reach the proximal level of the femoral head. Among Mylodontidae, a nearly equivalent proximal extension of the femoral head and the greater trochanter is only observed in *Pseudoprepotherium*, a morphology resembling that of the basal megatherioid genus *Hapalops* (see also Chapter 8: char. 350).

The femoral neck is moderately extended proximomedially in *Simomylodon* (Fig. 6.25). In anterior view, the neck gradually decreases in mediolateral width from its base to its contact with the proximal edge of the femoral head. This same morphology is observed in *Lestodon*, *Mylodon*, *Glossotherium*, and *Paramylodon* (see also Chapter 8: chars 351–352). In contrast, *Thinobadistes* and *Bolivartherium* show a more distinct sulcus surrounding the articular surface of the femoral head, whereas *Catonyx* and *Scelidotherium* lack a real femoral neck (McDonald 1987; Webb 1989).

In posterior view, all mylodontids exhibit a well-developed intertrochanteric fossa, but a real intertrochanteric ridge connecting the trochanters is present only in *Baraguatherium takumara* (Rincón *et al.* 2016), resembling in this regards the Santacrucian *Hapalops* (see also Chapter 8: char. 349).

The femur of *Simomylodon* possesses a third trochanter that is elongated proximodistally, but is not as laterally prominent as that in *Baraguatherium*, *Pseudoprepotherium*, and *Bolivartherium* (see also Chapter 8: char. 353). This results in a relatively strait, vertical lateral edge of the femoral shaft, similar to the most commonly encountered condition in mylodontids, as represented, e.g., by *Glossotherium* and *Paramylodon* (Fig. 6.25; Owen 1842; Stock 1925). The third trochanter is absent in *Catonyx* and *Scelidotherium* (McDonald 1987).

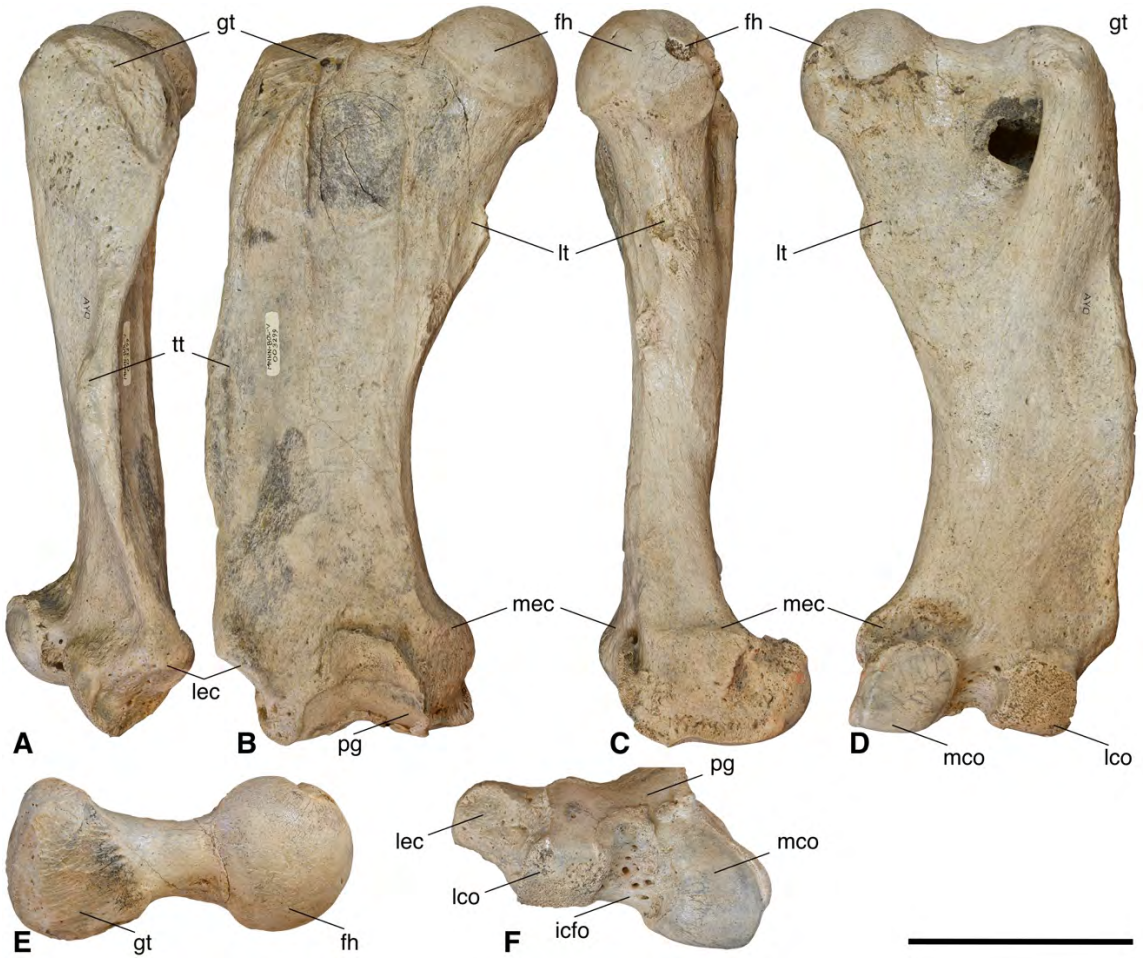

Figure 6.25. Right femur of *Simomylodon uccasamamensis* (MNHN-Bol V 3299) in lateral (A), cranial (B), medial (C), caudal (D), proximal (E) and distal (F) views. Abbreviations: fh, femoral head; gt, greater trochanter; icfo, intercondylar fossa; lco, lateral condyle; lec, lateral epicondyle; lt, lesser trochanter; mco, medial condyle; mec, medial epicondyle; pg, patellar groove; tt, third trochanter. Scale bar equals 10 cm.

The femoral specimen MNHN-Bol V 3365, described by Anaya & MacFadden (1995) and identified only as an "indeterminate Mylodontinae," agrees with all the observed features already discussed for *S. uccasamamensis*. This specimen also resembles the femoral measurements of *S. uccasamamensis* provided in the present study (including sizes, general proportions, and ratios; Appendix IV, Datasets S2 and Appendix VI, Data S2). Anaya & MacFadden (1995) recognized the peculiarity of the mylodontine femoral remains from Inchasi, but the incomplete nature of the material impeded, at that time, a more specific taxonomic identification (Anaya & MacFadden 1995). Based on Saint-André *et al.* (2010) and the descriptions and illustrations from the present study, the femoral specimen discussed in Anaya & MacFadden (1995) is reassigned to *S. uccasamamensis.*

Tibia- The tibia of *S. uccasamamensis* is known from sixteen specimens, ten of which are relatively complete (Appendix I). As was the case with the femora, the complete tibiae appear to differ in their general aspect: three of them are larger and more robust than the remaining ones (see Chapter 7). However, the descriptions and comparisons of the tibiae of *S. uccasamamensis* are conducted considering the whole available sample.

The tibia of *S. uccasamamensis* (Fig. 6.26A–F) is similar, in its general aspect, to its homologous element in *Mylodon*, *Glossotherium* and *Paramylodon,* but also shares several common features with *Lestodon* and *Thinobadistes* (e.g., Owen 1842; Stock 1925; Webb 1989). In lateral and medial views, (Fig. 6.26A, C) the tibia of *S. uccasamamensis* is straight, a common mylodontid feature (see also Chapter 8: char. 355). However, the diaphysis is fairly uniform in anteroposterior depth, as it is in *Mylodon*, *Glossotherium* and *Paramylodon*, whereas the diaphysis decreases in anteroposterior depth from the proximal to the distal end in the lestodontines (Webb 1989). The latter morphology is also observed in *Pseudoprepotherium* (Hirschfeld 1985), *Octodontotherium* (FMNH P13517) and the scelidotheres (McDonald 1987).

The ratio between the anteroposterior depth of the proximal epiphysis and the total tibial length is greater than 0.35 in *Simomylodon,* as it is in all Mylodontidae, with the exceptions of *Pseudoprepotherium*, *Octodontotherium*, *Mirandabradys* and *Urumacotherium*, in which the ratio is lower (see also Chapter 8: char. 357). At the distal end, the ratio between anteroposterior depth and the total tibial length is high in *Simomylodon*, *Mylodon*, *Paramylodon* and *Glossotherium* (greater than 0.74). Lower values (between 0.60 and 0.74) are consistently observed in *Scelidotherium*, *Catonyx*, *Pseudoprepotherium* and *Octodontotherium*. *Lestodon* and *Thinobadistes* show values that fall in between these ranges (see also Chapter 8: char. 358). The ratio between the maximum mediolateral width of the proximal epiphysis and total tibial length is always less than 0.6 in *Simomylodon*, as

it is in *Catonyx*, *Pseudoprepotherium*, *Octodontotherium* and *Thinobadistes*, whereas it is higher than 0.6 in *Mylodon*, *Glossotherium* and *Paramylodon*. This feature is variable in *Lestodon* and *Scelidotherium* (see also Chapter 8: char. 359).

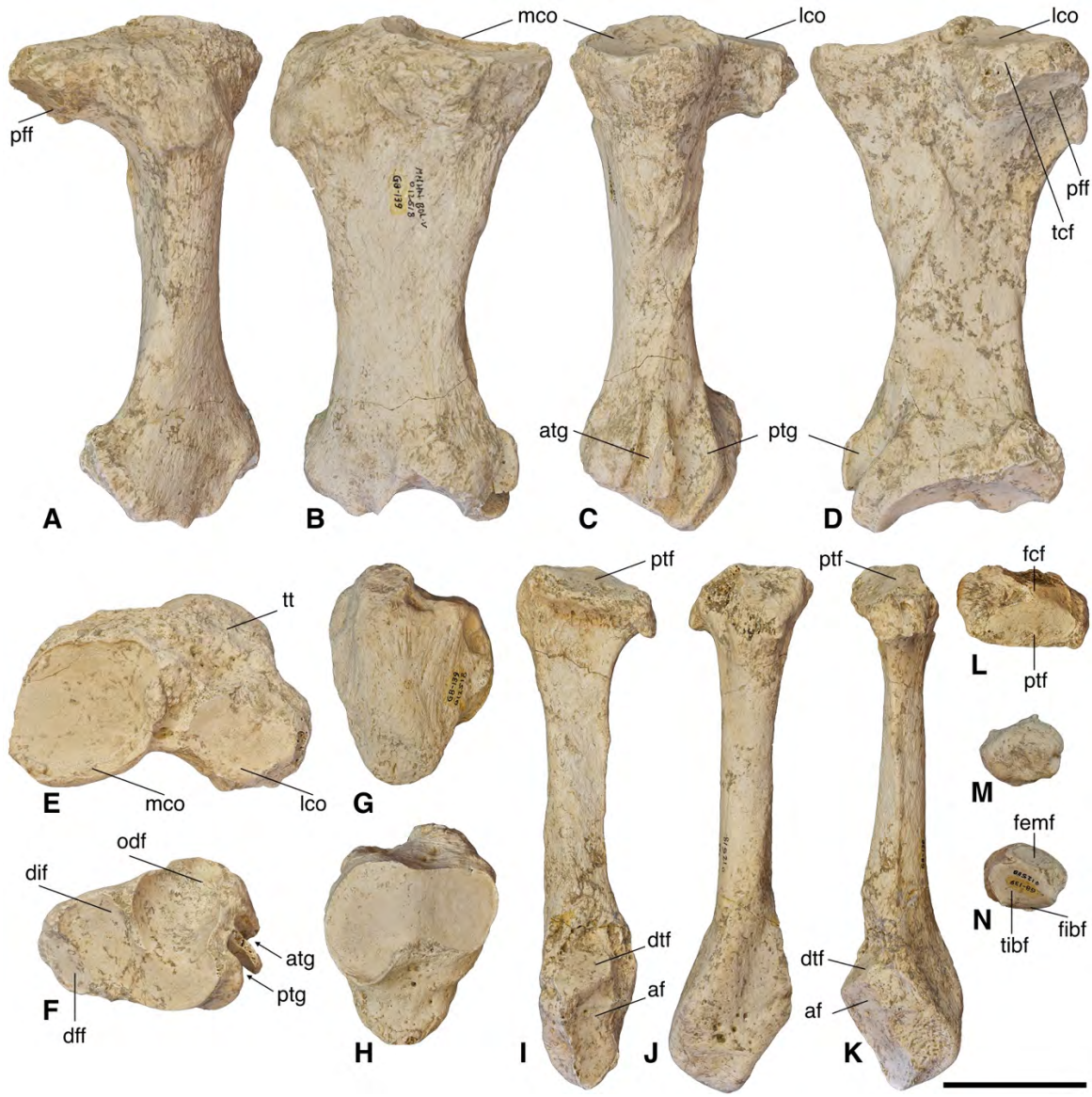

Figure 6.26. Tibia, patella, fibula and cyamella of *Simomylodon uccasamamensis* (MNHN-Bol V 12518). A-F, right tibia in lateral (A), cranial (B), medial (C), caudal (D), proximal (E) and distal (F) views; G-H, right patella in cranial (G) and caudal (H) views; I-L, right fibula in medial (I), lateral (J), caudal (K) and proximal (L) views; M-N, right cyamella in lateral (M) and articular (N) views. Abbreviations: af, astragalar facet; atg, anterior tibial groove (for *m. tibialis caudalis*); dff, distal fibular facet; dif, discoid process facet; dtf, distal tibial facet; fcf, fibular cyamella facet; femf, femoral facet; fibf, fibular facet; lco, lateral condyle; mco, medial condyle; odf, odontoid process facet; pff, proximal fibular facet; ptf, proximal tibial facet; ptg, posterior tibial groove (for *m. flexor digitorum longus* and *m. flexor hallucis longus*); tcf, tibial cyamella facet; tibf, tibial facet; tt, tibial tuberosity. Scale bar equals 5 cm.

In proximal view (Fig. 6.26E), the medial and lateral tibial condyles of *Simomylodon* are markedly unequal in size, with the former much larger than the latter, a typical mylodontid

feature (see also Chapter 8: chars 361–361). Like *Pseudoprepotherium*, *Octodontotherium*, and the scelidotheres, the tibia of *Simomylodon* lacks any trace of a groove anterior to the lateral condyle, a feature characteristic of all the other Mylodontidae (see also Chapter 8: char. 362). This groove faces laterally and probably accommodated the tendon of origin of the *m. extensor digitorum longus* (Evans 1993).

The medial intercondylar eminence is not particularly evident in mylodontid sloths, but it is moderately developed in *Octodontotherium*, *Pseudoprepotherium* and *Mirandabradys*, resembling the megatherioid *Hapalops* in this regard (see also Chapter 8: char. 363).

In medial, posterior and distal views (Fig. 6.26C, D, F), two grooves for tendons are visible on the distal tibia of *S. uccasamamensis*. This condition is also observed in *Pseudoprepotherium*, *Thinobadistes* and *Lestodon*. In *Octodontotherium*, the scelidotheres, but also in the megalonychid and nothrotherid sloths, three distinct grooves are present (McDonald 1987). In the latter sloth groups, these grooves accommodated, respectively (from anterior to posterior), the tendons for the *tibialis posterior*, *flexor digitorum longus* and *flexor hallucis longus* muscles (McDonald 1987). in contrast, *Mylodon*, *Glossotherium* and *Paramylodon* exhibit only a single trough in this area, and the three tendons were likely located in this same groove. The condition of *Simomylodon*, *Pseudoprepotherium* and the lestodontines therefore appears to be intermediate between the other two conformations (see also Chapter 8: char. 365). Given that the posterior groove is larger than the anterior one in *Simomylodon* (Fig. 6.26C), the tendons for the *flexor digitorum longus* and *flexor hallucis longus* muscles were probably housed together in this groove, whereas the tendon the *tibialis posterior* muscle likely maintained its anterior and independent position.

In distal view (Fig. 6.26F), the facet for the astragalus dominates the articular surface of the distal tibia. As in all mylodontids, it is composed of two surfaces, one subspherical for the articulation with the odontoid process, and one flat, for the articulation with the discoid process of the astragalus. The distal fibular facet is located in the posteromedial corner of the distal tibia, a position that is typical in Mylodontinae, with the exception of *Pseudoprepotherium* and *Octodontotherium*. In these latter genera, as in the scelidotheres (McDonald 1987), the distal tibial facet for the fibula is more anteroposteriorly extended (see also Chapter 8: char. 364).

Patella, fibula and cyamella- The patella is represented by two specimens assigned to *S. uccasamamensis*: MNHN-Bol V 3300 (Saint-André *et al.* 2010: fig. 17) and MNHN-Bol V 12518 (Fig. 6.26G–H). This bone is triangular in shape and very similar to that of *Glossotherium* and *Paramylodon* (Owen 1842; Stock 1925). However, the patella of *Lestodon* and *Thinobadistes* is more proximodistally elongated, and with a more pronounced ventral process (Webb 1989). In

posterior view, the articular surface with the femur is transversely convex in the vicinity of its midpoint, but becomes medially and laterally concave, as it does in all Mylodontidae. In *S. uccasamamensis* these latter areas appear equal in proximodistal extent in MNHN-Bol V 3300 (Saint-André *et al.* 2010: fig. 17) whereas they are more asymmetric in MNHN-Bol V 12518 (Fig. 6.26H), with the medial facet elongated distally. Intraspecific variation in the articular surface of the patella has been observed in the analyzed specimens of *Lestodon* and *Thinobadistes* (Appendix II).

Six fibulae of *S. uccasamamensi*s (Fig. 6.26I–L) are available for observation (Appendix I). The fibula is conservative in its morphology among Mylodontidae (McDonald 1987). The ratio between the proximodistal length of the distal articular surface and the total length of the fibula is, for example, similar in all Mylodontidae (see also Chapter 8: char. 366). This bone is mediolaterally narrow and anteroposteriorly broad as in all Mylodontinae, in contrast to the condition of the scelidotheres, in which it is more rounded in cross section (McDonald 1987). Proximally and medially, the fibula carries a flat, anteroposteriorly elongate facet for the tibia and, more posteriorly, a smaller and more convex facet for the cyamella.

The presence of a cyamella (or fabella, or cyamo-fabella) has been inferred in some mylodontids, such as *Catonyx*, *Scelidotherium*, *Paramylodon*, *Pseudoprepotherium*, and *Thinobadistes*, by the presence of articulation surfaces on the proximal epiphyses of either the tibia, the fibula, or both (Stock 1925; Hirschfeld 1985; McDonald 1987; Webb 1989). However, the element itself is apparently not available for any of these taxa, and consequently it is still not figured nor described in detail for any of them. In *S. uccasamamensis,* both right and left cyamellae are available in MNHN-Bol V 12518 (Fig. 6.26M–N, 6.27). The cyamella is roughly spherical and, on its medial side, it shows three contiguous but individualized facets (Fig. 6.26N). These are, respectively (from proximal to distal), for the articulation with femur, tibia and fibula. The facet for the tibia is the largest of the three (Fig. 6.26N). In proximal view, the femoral facet on the

Figure 6.27. Left tibia, fibula and cyamella of *Simomylodon uccasamamensis* (MNHN-Bol V 12518) showing connections between the three elements, in lateral (A), caudal (B) and proximal (C) views. Scale bar equals 5 cm.

cyamella creates a continuous articular surface with the lateral condyle of the tibia for the articulation with the femur (Fig. 6.27C).

Pes- Several tarsal bones of *S. uccasamamensis* are available for description, but the majority of the metatarsals (with the exception of a proximal fragment of the fourth metatarsal) and phalanges of the pes, are currently lacking (Appendix I).

In *S. uccasamamensis*, only a single complete calcaneum has been recovered: MNHN-Bol V 8541 (Fig. 6.28A–D). The posterior portion of the calcaneum corresponds to the tuber calcis, which was modified for the contact with the ground. This area is enlarged anteroposteriorly and mediolaterally, forming a triangular surface that is typical in Mylodontinae (Fig. 6.28A–C). Only *Pseudoprepotherium* exhibits a tuber calcis in which the anteroposterior length is not markedly enlarged (Hirschfeld 1985; see also Chapter 8: char. 374). However, the tuber calcis of *S. uccasamamensis* resembles *Pseudoprepotherium*, the lestodontines and the scelidotheres, in lacking the strong mediolateral expansion of *G. robustum* and *P. harlani* (Owen 1842; Stock 1925; see also Chapter 8: char. 373). As in all mylodontids, the tuber calcis of *S. uccasamamensis* is connected with the anterior articular portion by a neck region that is constricted dorsoventrally and mediolaterally (Fig. 6.28A–C). This neck in *S. uccasamamensis* is clearly shorter than that of scelidotheres, which also lack a tendinous groove on the lateral and ventral sides (Fig. 6.28B–C). This groove probably housed the tendon of the *m. fibularis brevis* (McDonald 1987), a common feature of Mylodontinae (Webb 1989). Just anterior to this groove, the articular portion of the calcaneum contacts the astragalus (Fig. 6.28E–H) and the cuboid (Fig. 6.29D–G). The calcanear-astragalar contact is divided into two separate facets, the ectal and the sustentacular, being the former larger than the latter (Fig. 6.28D). In *S. uccasamamensis*, the sustentacular facet is located on a distinct medial process (Fig. 6.28A–D). This process is not observed in *Glossotherium* and *Paramylodon* (Owen 1842; Stock 1925; see also Chapter 8: char. 375).

Nine astragali of *S. uccasamamensis* have been recovered (Appendix I). The general astragalar proportions in *Simomylodon*, quantified by the ratio between the proximodistal and anteroposterior lengths (between 0.8 and 1.0), are similar to those of most Mylodontinae. Lowest values (< 0.8) are obtained in the basal mylodontines *Octodontotherium* and *Pseudoprepotherium*, and the higher values (> 1.0) in the scelidotheres *Catonyx* and *Scelidotherium* (see also Chapter 8: char. 367). In *Simomylodon*, the astragalar medial and lateral trochlear surfaces are modified, as in all mylodontid sloths, to form a raised and globose odontoid process and a flat, horizontal semicircular discoid facet (Fig. 6.28E, F, H). However, the angle formed

by the odontoid process and the discoid facet, observed in either anterior or posterior view, is quite different among various Mylodontidae (see also Chapter 8: char. 368). The odontoid-discoid angle is markedly obtuse (> 115°) in the scelidotheres, as it is in the basal mylodontine

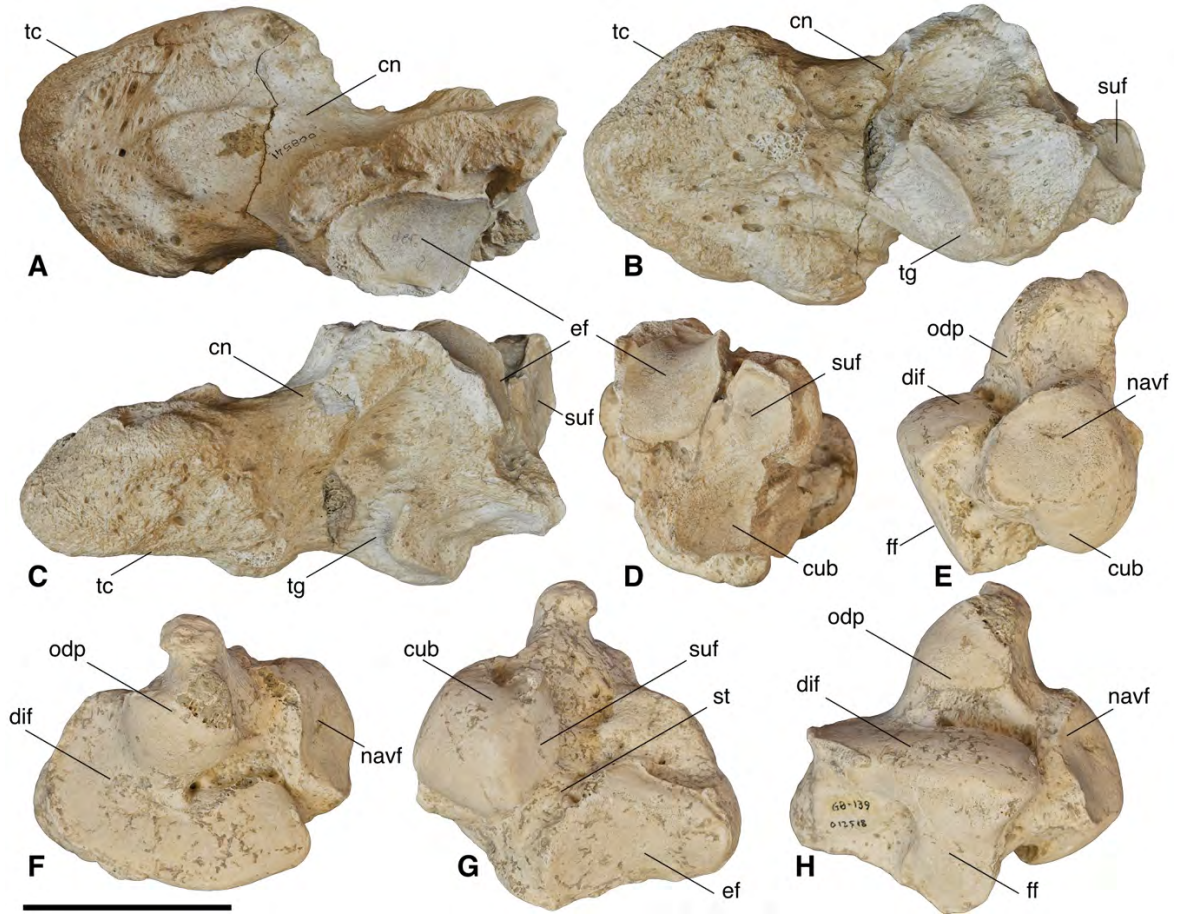

Figure 6.28. Calcaneum and astragalus of *Simomylodon uccasamamensis*. A-D, right calcaneum (MNHN-Bol V 8541) in proximal (A), distal (B), lateral (C) and anterior (D) views; E-H, right astragalus (MNHN-Bol V 12518) in cranial (H), proximal (F), medial (G) and lateral (H) views. Abbreviations: cn, calcaneal neck; cub, cuboid facet; dif, discoid facet; ef, ectal facet; ff, fibular facet, navf, navicular facet; odp, odontoid process; st, sulcus tali; suf, sustentacular facet; tc, tuber calcis; tg, tendinal groove. Scale bar equals 5 cm.

O. grande and the Pliocene North American species *Pa. garbanii*. It is moderately obtuse (> 90° but < 115°) in most Mylodontinae, including *G. robustum*, *M. darwinii*, *Pa. harlani*, *Ps. confusum*, *Pl. acutidens*, and *S. uccasamamensis*. In contrast, this angle is orthogonal or acute (≤ 90°) in the lestodontines. In the mylodontid astragalus, the discoid facet surrounds the odontoid process both laterally and posteriorly. In lateral view, this facet has an anteroposterior curvature in *Nematherium*, *Octodontotherium*, as well as in the scelidotheres and the lestodontines, whereas it is essentially flat in *Glossotherium*, *Mylodon*, *Paramylodon*, *Pleurolestodon*, *Pseudoprepotherium*, and *Simomylodon* (see also Chapter 8: char. 369). As in all Mylodontidae, the astragalus of *S.*

uccasamamensis exhibits a proximodistally elongated facet for the fibula, located at the anteriormost limit of the discoid facet and visible in lateral view (Fig. 6.28H). The shape of this facet is quite variable intraspecifically in *S. uccasamamensis*, as has also been observed in the large samples of the genera *Paramylodon* and *Thinobadistes*.

As stated above, the ectal and sustentacular facets of the calcaneum are separated in *S. uccasamamensis*. The same pattern is observed on the astragalus (Fig. 6.28G), in which the two facets are divided by a deep sulcus tali. This feature is considered primitive among sloths (McDonald 1987). In the genera *Glossotherium*, *Mylodon* and *Paramylodon*, these two facets coalesce into a uniform surface for the articulation with the calcaneum. The primitive condition is found not only in *Simomylodon,* but also in *Nematherium*, *Octodontotherium*, *Pseudoprepotherium*, *Pleurolestodon*, as well as all lestodontines and scelidotheres (see also Chapter 8: char. 370). In *S. uccasamamensi*s, the sustentacular facet is confluent anteriorly with the facet for the cuboid anteriorly (Fig. 6.28G), as is typical for Mylodontinae (McDonald 1987). The facet for the cuboid is anteriorly convex as in most Mylodontidae, whereas it is markedly concave in *Nematherium* and in the scelidotheriine sloths (McDonald 1987). The anteriormost portion of the astragalar head of *S. uccasamamensis* bears the articular surface for the navicular (Fig. 6.28E, F, H). This surface is flat to slightly concave in *S. uccasamamensis* (Fig. 6.28E, F, H), as it is in all mylodontines, whereas in the scelidotheres it is more strongly concave (McDonald 1987). The intraspecific differences observed in *S. uccasamamensis* in the surface contour of this facet have been reported for other taxa, like *P. harlani* (Stock 1925), and directly observed in *T. segnis*.

The navicular of *S. uccasamamensis* (Fig. 6.29A–C) has a typical mylodontine shape, being more enlarged mediolaterally than dorsoventrally. The proximal surface is entirely occupied by a wide facet for the astragalus (Fig. 6.29B–C). On the distal surface, a wide elliptic facet for the ectocuneiform (and probably also for the mesocuneiform) is located along the ventralmost border (Fig. 6.29A, C). Adjacent and ventral to the latter facet, on the slender lateral surface of the bone, there is an anteroposteriorly narrow articulation for the cuboid (Fig. 6.29C).

The cuboid of *S. uccasamamensis* (Fig. 6.29D–G) is very similar to the homologous element in the large-sized mylodontines *G. robustum* and *P. harlani* (Owen 1842; Stock 1925). In proximal view, there is a concave and almost circular surface for the contact with the astragalus (Fig. 6.29E, G). The cuboid of *S. uccasamamensis* is delimited anteriorly by an anteroposteriorly narrow articulation for the navicular (Fig. 6.29E, G) and posteriorly by a dorsoventrally enlarged surface for the calcaneum (Fig. 6.29D). On the distal surface, there are two facets divided by an oblique ridge, for articulation with the fifth metatarsal posteriorly and the fourth metatarsal anteriorly (Fig. 6.29F). Anterodorsally to the latter, there is a smaller rectangular

facet for the third metatarsal that faces anteromedially (Fig. 6.29G). The cuboid-third metatarsal contact is absent in the scelidotheres (McDonald 1987). Another difference among the cuboid of mylodontids is the presence/absence of the cuboid-ectocuneiform contact (see also Chapter 8: char. 376). This contact is extensive in the scelidotheres and clearly visible in the articulated pes in lateral view, whereas it is very reduced in *Pseudoprepotherium* and the lestodontines and absent in the other mylodontines such as *G. robustum*, *P. harlani* and *S. uccasamamensis* (Fig. 6.29D–I). According to Stock (1925), an extremely reduced cuboid-ectocuneiform facet is rarely present in some specimens of *P. harlani*.

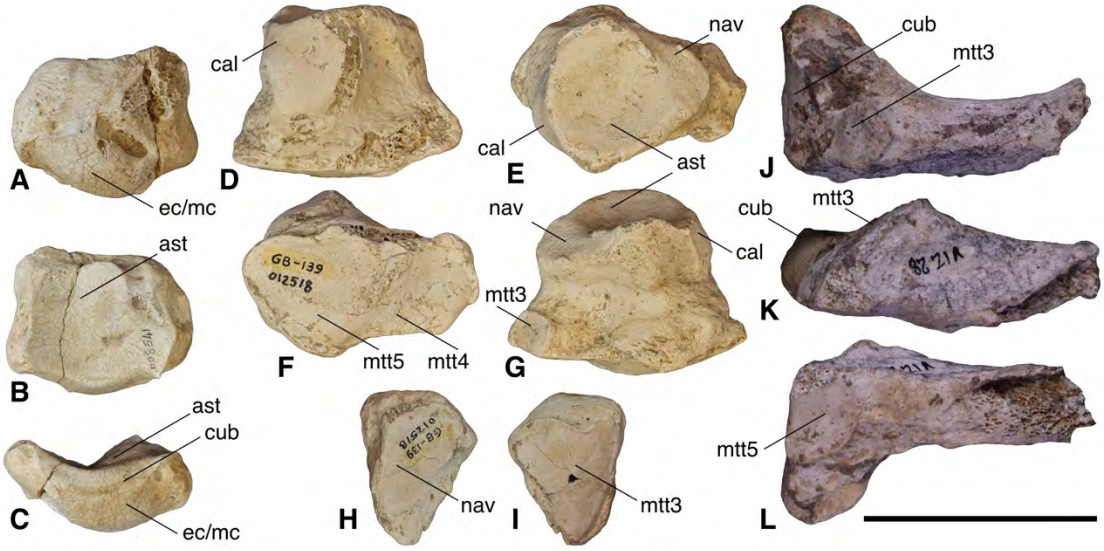

Figure 6.29. Tarsal and metatarsal elements of *Simomylodon uccasamamensis*. A-C, right navicular (MNHN-Bol V 8541) in distal (A), proximal (B) and lateral (C) views; D-G, right cuboid (MNHN-Bol V 12518) in dorsal (D), proximal (E), distal (F) and palmar (G) views; H-I, right ectocuneiform (MNHN-Bol V 12518) in proximal (H) and distal (I) views; J-L, proximal fragment of right metatarsal IV (MNHN.F.VIZ28) in proximal (J), lateral (K) and distal (L) views. Abbreviations refer to articular facets for the indicated bones, as follows: ast, astragalus, cal, calcaneum; cub, cuboid; ec/mc, ectocuneiform and mesocuneiform; mtt (3-4-5), metatarsal (3-4-5); nav, navicular. Scale bar equals 5 cm.

Therefore, the ectocuneiform of *S. uccasamamensis* (Fig. 6.29H–I) bears only two large facets: a concave surface for the navicular proximally, and a convex surface for the third metatarsal distally. The bone is triangular in outline in proximal and distal views, with its longest border facing laterally. In this regard, it is very similar to the ectocuneiforms of *G. robustum* and *P. harlani* (Stock 1925).

The metatarsal series of *S. uccasamamensis* is only known by a proximal fragment of the fourth metatarsal (Fig. 6.29J–L). It is smaller in size than the homologous element of *G. robustum*, *P. harlani*, *T. segnis* and *L. armatus,* resembling more closely that of *O. grande* and *P. garbanii*. A peculiarity of the fourth metatarsal of *S. uccasamamensis* is the reduced facet for the fifth

metatarsal (Fig. 6.29L; Saint-André *et al.* 2010). A similar conformation is observed, among Mylodontidae, only in *O. grande*, whereas in other mylodontid sloths this facet is more dorsopalmarly elongate.

6.4 DISCUSSION

The new material of *Simomylodon uccasamamensis* includes several complete craniodental and postcranial remains, which help to assess morphological features previously unknown for this taxon. The new specimens provide information on anatomical areas that were missing in the specimens previously described by Saint-André *et al.* (2010), such as the cranial roof, the posterior portion and the lateral walls of the cranium, the jugals, several regions of the dentition, the ear region and many postcranial bones previously unknown.

The new craniodental specimens allow a better understanding of the taxonomy of *Simomylodon* and *Pleurolestodon*. For example, the skull MNHN-Bol V 3348 (Fig. 6.3) considered by Saint-André *et al.* (2010) as the holotype of *Pleurolestodon dalenzae*, appears to be extremely similar, in both shape and size, to MNHN-Bol V 3711 (Fig. 6.4) and 3726 (Fig. 6.5). These two latter specimens preserve mandibular characters that are inconsistent with features of the genus *Pleurolestodon* (e.g., the flat anterior symphyseal spout in occlusal view and the lack of coverage of the mf3 by the ascending ramus in lateral view; Figs 6.4–6.5; Rovereto 1914). This hypothesis is further confirmed by the morphometric data. In fact, the genera *Simomylodon* and *Pleurolestodon* are clearly separated in both PCAs (i.e., in both the cranial and mandibular data subsets; Figs 6.12–6.13), revealing consistent differences in size and shape between the two taxa. For these reasons, the skull MNHN-Bol V 3348 from the late Miocene of Choquecota (Fig. 6.3), previously attributed to *Pleurolestodon dalenzae* (Saint-André *et al.* 2010), is here ascribed to the species *S. uccasamamensis*, and represents the most ancient remains attributed to this species. The morphological and morphometric data (Figs 6.12–6.13) agrees with the previous revision of Saint-André *et al.* (2010) regarding the existence, in the Neogene of Argentina, of a single species of the genus *Pleurolestodon* (i.e., *P. acutidens*).

The new enlarged cranial sample of *S. uccasamamensis* also allowed to assess intraspecific variation within this species. The morphology observed in this new material fills an anatomical gap between the specimens MNHN-Bol V 11731 and 3321 (Figs 6.1–6.2) and MNHN-Bol V 3348 (Fig. 6.3), previously assigned to distinct species (Saint-André *et al.* 2010). Moreover, Saint-

André *et al.* (2010) noted the strong similarity of MNHN-Bol V 3348 and the craniodental remains of *S. uccasamamensi*s.

Similarly, the *S. uccasamamensis* mandibular remains described here (Figs 6.4F–H, 6.5D–F, 6.6E–F, 6.8, 6.10, 6.11A–F, J–L) show the same features observed in mandibles from Inchasi described and illustrated by Anaya & MacFadden (1995: figs. 3–5) (Figs 6.9, 6.11G–I). This is further supported by the morphometric data (Fig. 6.13), and therefore the assignment of the specimens MNHN-Bol V 3358 (Fig. 6.9A–C), 3371 (Fig. 6.9D–F) and 3359 (Fig. 6.11G–I) is amended from *Glossotheridium chapadmalense* (Anaya & Macfadden 1995) to *Simomylodon uccasamamensis*. The differences between the Pliocene Andean mylodontid (i.e., *Simomylodon*) and the southern genus *Glossotheridium* are also mentioned by Hoffstetter (1986). Moreover, differences between *Glossotheridium chapadmalense* from the Buenos Aires region (Kraglievich 1925) and the North-American species *Paramylodon garbanii* (Robertson 1976) are recognized on both morphological and morphometric (Figs 6.12–6.13) grounds, further confirming the taxonomic assignment of Morgan (2008) and McDonald & Morgan (2011).

Finally, the morphology observed in the mandibular sample of juvenile individuals (Fig. 6.11) from the present study are inconsistent with the juvenile mandibular corpus from the Huayquerian of Buenos Aires Province, tentatively placed in the genus *Simomylodon* by Oliva & Brandoni (2012). As a consequence, the geographic distribution of *S. uccasamamensis* is for the moment strictly limited to the Bolivian Altiplano. This species can therefore be considered endemic to the Andes, reinforcing the biogeographic assertions of Saint-André *et al.* (2010).

The new well-preserved cranial remains of *S. uccasamamensis* also permitted a detailed characterization of the features of the ear region (Figs 6.14–6.17). This anatomical region is highly diagnostic for sloths (e.g., Gaudin 1995, 2004; De Iuliis 2018) but it is still poorly known for Neogene Mylodontinae such as *Pleurolestodon*, *Glossotheridium* and *Glossotheriopsis*. As demonstrated by Gaudin (1995, 2004), the use of the ear region features into phylogenetic analyses is extremely informative for elucidating the evolutionary history of sloths, and for this reason the codification of these features of *Simomylodon*, as well as for other Mylodontidae, has been conducted for the enlarged matrix of the present thesis (see Chapter 8). Peculiar features of the ear region of *S. uccasamamensis* include: the presence of a fairly deep and narrow mastoid depression, the stylomastoid foramen located anterolaterally to the stylohyal fossa, and the marked separation between the stylomastoid foramen and the ventral opening of the canal for the occipital artery (Figs 6.14–6.17). All these features have been recovered as autapomorphies of *S. uccasamamensis* in the phylogenetic study of Chapter 8.

In a similar way, also the postcranial remains described and compared herewith, significantly extend the knowledge of the skeletal anatomy of *Simomylodon uccasamamensis*. The new data allows for a reconsideration of previously described remains, and attributed to an "indeterminate Mylodontinae" by Anaya & MacFadden (1995). These include a partial femur, MNHN-Bol V 3365 and an ungual phalanx MNHN-Bol V 3355 from the locality of Inchasi. These remains coincide in both shape and size with the material of *S. uccasamamensis* here presented, allowing to ascribe both of them to the latter taxon.

Overall, as noticed by Saint-André *et al.* (2010), the postcranial anatomy of *Simomylodon uccasamamensis*, closely resembles that of Pleistocene larger-sized taxa, such as *Glossotherium robustum* or *Paramylodon harlani*. However, several bony elements of *S. uccasamamensis* show plesiomorphic features that are not observed in more derived Mylodontini. Primitive features in the postcranium of *Simomylodon* can be observed at the level of the humerus, radius, ulna, tibia, astragalus and calcaneum. Among them, the most important are the lack of a proximodistally vertical supinator crest on the humerus, the convexity of the anterior margin of the radius, the presence of two large depressions for tendons in the posteromedial margin of the distal epiphysis of the tibia, the presence of both the sustentacular process of the calcaneum and the sulcus tali of the astragalus. All these features contribute to place *S. uccasamamensis* in a basal position among Mylodontini, further clarifying many previously obscure aspects of the phylogenetic relationships among Mylodontinae (see Chapter 8). In light of the present new information, *S. uccasamamensis* can be considered, at present, the best-known early member of Mylodontini.

Mylodontid remains are extremely rare in the Bolivian Altiplano before the Huayquerian–Montehermosan transition (Saint-André *et al.* 2010). *Simomylodon uccasamamensis* appears for the first time just before the Miocene–Pliocene transition, in the Choquecota deposits, and it persists at several localities from the Altiplano until the late Pliocene, the last occurrence being Ayo Ayo-Viscachani (Saint-André 1994; Saint-André *et al.* 2010). Chronologically, the presence of *Simomylodon uccasamamensis* in the Bolivian Altiplano encompasses two faunal turnover events that are particularly evident in the Bolivian deposits (Hoffstetter 1986). The former occurred at the Miocene–Pliocene boundary, and is coeval with the Quechua tectonic phase (Steinmann 1929). It consisted of a folding event, associated with strong volcanic activity, that brought about an uplift of the Altiplano and resulted in drastic ecological changes, namely drier and colder environments than those of the late Miocene (e.g., Marshall *et al.* 1983; Hoffstetter 1986; Marshall & Sempéré 1991; Saint-André 1994; Saint-André *et al.* 2010). The late Miocene fauna, dominated by the mesotheriids (e.g., *Plesiotypotherium*) and toxodontid

notoungulates, is replaced by a Pliocene assemblage, with macraucheniid litopterns (cf. *Promacrauchenia*), the xotodontine notoungulate *Posnanskytherium*, large hydrochoerine rodents (e.g., *Phugatherium*), and several armored xenarthrans, including sclerocalyptine glyptodonts, pampatheriine armadillos, and megatheriid, nothrotheriid, and mylodontid sloths (Marshall *et al.* 1983; Hoffstetter 1986; Pujos *et al.* 2016). The younger and more dramatic faunal turnover in the Bolivian highlands occurred by the Pliocene–Pleistocene transition (ca. 2.58 Ma) and was driven by the increasing influx of North American immigrants and a further rise of the Andes (e.g., Marshall *et al.* 1983; Hoffstetter 1986; Marshall & Sempéré 1991). This event ended the isolation of the Pliocene faunas of the Altiplano, in which no North American immigrants have been reported to date (Anaya & MacFadden 1995). The chronological distribution of *Simomylodon uccasamamensis* is bracketed between these two major faunal turnover events. During the Pliocene, the central Andes had already attained an altitude of 2,000–2,850 m (MacFadden *et al.* 1994; Saint-André 1994; Saint-André *et al.* 2010) and probably acted as faunal refuge or an "Andean island". The existence of such a refugium is indicated by the absence of North American immigrants from the Bolivian Altiplano, despite the fact that these immigrants have been reported from a number of more southerly localities in Argentina during the Huayquerian, Montehermosan, and Chapadmalalan SALMAs (Marshall *et al.* 1983; Reguero & Candela 2011). Therefore, *Simomylodon uccasamamensis* may have been specifically adapted for an isolated, cold, and dry environment on the Bolivian Altiplano during the Pliocene.

6.5 CONCLUSIONS

- The moderate-sized Miocene–Pliocene mylodontids (i.e., *Glossotheridium chapadmalense*, *Glossotheriopsis pascuali*, *Paramylodon garbanii*, *Pleurolestodon acutidens*, and *Simomylodon uccasamamensis*) can be separated both morphologically and morphometrically.
- *Simomylodon uccasamamensis* and the poorly known *Glossotheriopsis pascuali* are smaller in size than *Glossotheridium chapadmalense*, *Paramylodon garbanii*, and *Pleurolestodon acutidens*.
- *Glossotheridium chapadmalense* and *Paramylodon garbanii*, from the Chapadmalalan SALMA of South America and the late Blancan NALMA of North America, respectively, can be reliably differentiated on both morphological and morphometric grounds, following the assertions of Morgan (2008) and McDonald & Morgan (2011).
- The species *Pleurolestodon dalenzae* (Saint-André *et al.* 2010) is considered a junior synonym of *Simomylodon uccasamamensis*. The genus *Pleurolestodon* is therefore

monospecific, with the Argentinean species *Pleurolestodon acutidens* as the only valid species recognized to date.

- The mandibular fragments from Inchasi assigned to *G. chapadmalense*, and the postcranial remains ascribed to "Mylodontinae indet." by Anaya & MacFadden (1995) are extremely similar to those of *S. uccasamamensis* in both shape and size, and therefore assigned to the latter species.
- The juvenile mylodontid mandible from the Huayquerian SALMA of the Buenos Aires region was erroneously identified as "cf. *Simomylodon"* by Oliva & Brandoni (2012); it does not possess the diagnostic features of the juvenile *S. uccasamamensis* specimens from Bolivia.
- *Simomylodon uccasamamensis* is, to date, the only recognized mylodontid sloth from the Pliocene deposits of the Bolivian Altiplano. This species is endemic to this region during the Montehermosan, Chapdamalalan, and (early) Marplatan SALMAs.
- *Simomylodon uccasamamensis* may have been specifically adapted to the ecologic conditions that prevailed in the isolated, cold and dry ecosystems of the Bolivian Altiplano during the Pliocene epoch, without competition or predation from North American immigrants.

Chapter 7
SEXUAL DIMORPHISM IN *SIMOMYLODON UCCASAMAMENSIS*

Sexual dimorphism (SD) can be expressed phenotypically as differences in size (i.e. sexual size dimorphism, SSD), shape and/or particular traits between the two sexes of the same species (Lammers *et al.* 2001; Isaac 2005). SD is extremely common in species in which reproductive roles are segregated into separate sexes, and it has been recognized in several mammalian lineages, both extant and extinct (e.g., Kurtén 1955; Gingerich 1981; Krishtalka *et al.* 1990).

Sexual dimorphism is low to moderate in living sloths, but it is supposed to have played a more important role for extinct sloth taxa. The presence of SD in extinct sloths was first suggested at the end of the nineteenth century (Lydekker 1894) and nowadays it is commonly advocated as a possible explanation of high intraspecific variation in many extinct sloth species. In this Chapter, the presence of SD in *Simomylodon uccasamamensis* from the Bolivian Altiplano is proposed. Indication of SD is observable in the morphology of cranial and postcranial remains, representing the earliest proposed occurrence of size-based SD in an extinct sloth. Differences between sexes are mainly detected in the morphology of the feeding apparatus and general body size. Comparisons with extant large mammals allow to hypothesize different food selection between the two sexes, with probable divergent habitat use and concomitant niche separation. This, in turn, could have represented an important selective factor for adaptation of *S. uccasamamensis* to environmental changes experienced by the Bolivian Altiplano in late Neogene times.

7.1 MORPHOMETRIC ANALYSES RESULTS

7.1.1 Cranium and upper dentition

As in several other extinct sloths (Lydekker 1894; Cartelle & Bohórquez 1982; McDonald 2006; Miño-Boilini & Zurita 2015; Cartelle *et al.* 2019), two distinct morphs are observed in the craniodental remains of *Simomylodon uccasamamensis*, as typified by the two skulls in Figure 7.1 (see Chapter 6 for other figures). The main differences largely coincide with those observed in other mylodontid species like *Glossotherium* (Lydekker 1894; Cartelle *et al.* 2019) and *Paramylodon* (McDonald 2006) that possess gracile and robust morphs. Compared with total length, some cranial remains appear mediolaterally wider than others, a feature that is particularly evident in the muzzle region (Fig. 7.1).

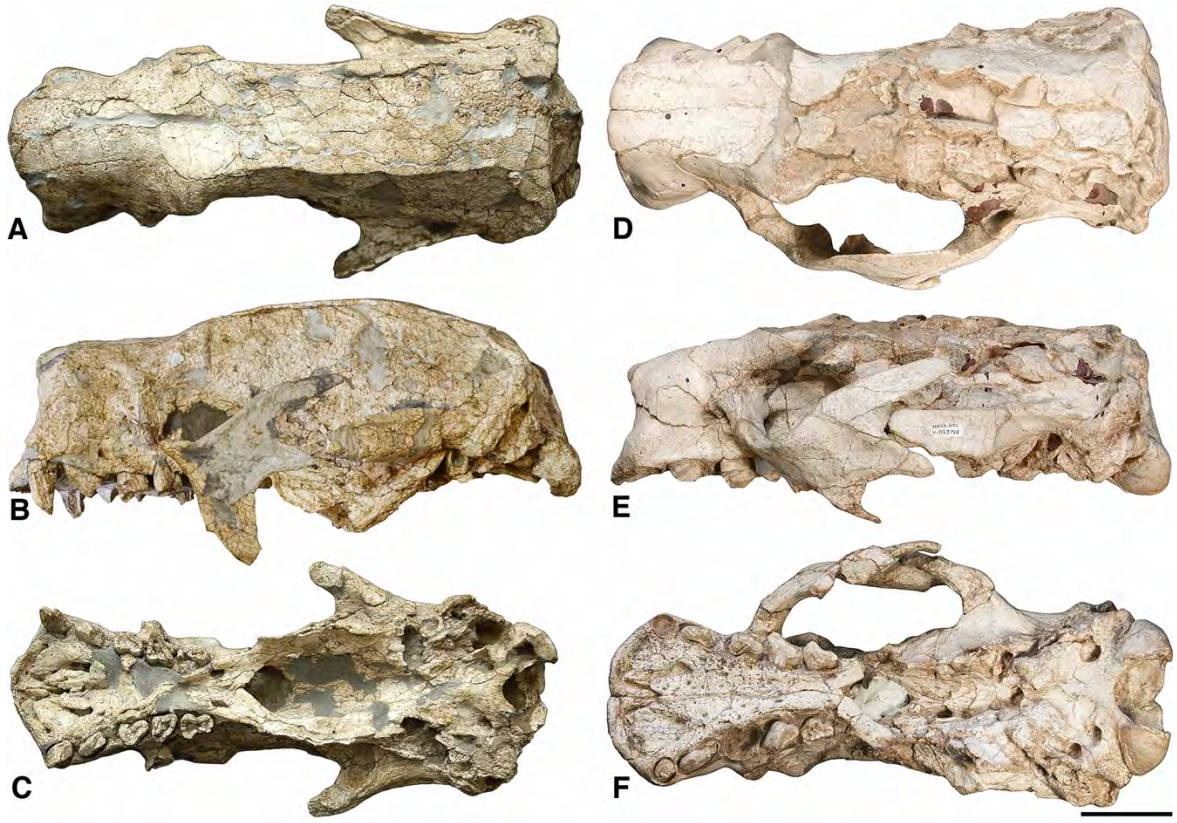

Figure 7.1. Skulls of a gracile specimen MNHN-Bol V 3711 (A–C) and a robust specimen MNHN-Bol V 3718 (D–F) of the extinct sloth *Simomylodon uccasamamensis* from the latest Miocene–late Pliocene of Bolivian Altiplano, in dorsal (A, D), left lateral (B, E) and ventral (C, F) views. Scale bar equals 5 cm.

In the PCA conducted on the cranium and upper dentition dataset (Fig. 7.2A), two groups separate on PC1, which explains the 61.91% of total variance and mainly reflects morphological changes at the level of the muzzle. Thus, negative values of PC1 indicate gracile specimens that show narrow muzzles and palates that are relatively long and narrow, whereas positive values of PC1 characterize robust specimens displaying wider muzzles but also wider and shorter palates (Fig. 7.2A). This shape difference is also partially related to allometry (accounting for 56.26% of total craniodental shape variation), with low and high values of PC1 respectively related to smaller and larger size (Fig. 7.2A). Gracile and robust specimens cluster into well-separated groups (Fig. 7.2B) that are significantly different (NPMANOVA: $F = 6.39$; $p = 0.028$).

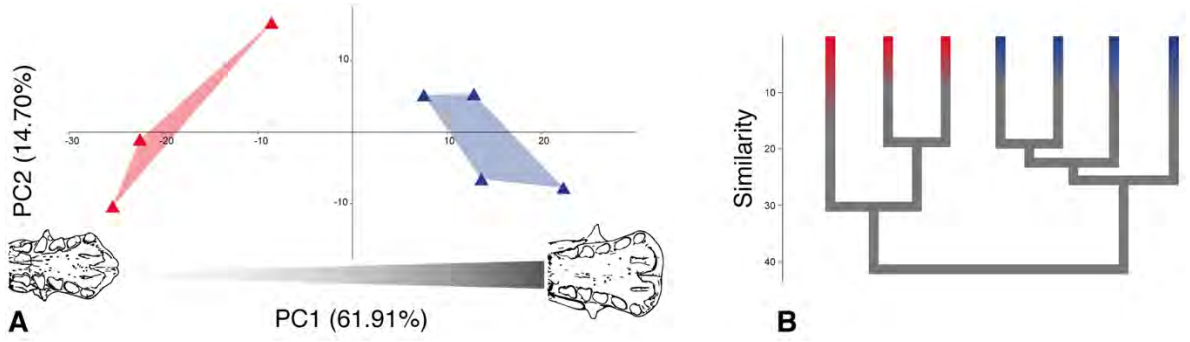

Figure 7.2. Multivariate analyses of the cranial and upper dentition dataset showing the morphological differentiation among the gracile (red) and robust (blue) morphs of the extinct sloth *Simomylodon uccasamamensis* from the latest Miocene–late Pliocene of Bolivian Altiplano. A, PCAs showing PC1 and PC2, with related percentages of explained variance and the main morphological transformations related to PC1 and B, associated hierarchical cluster analyses showing squared Euclidean distances among all specimens analyzed.

7.1.2 Mandible and lower dentition

An analogous separation of mandibular remains into two groups can be detected qualitatively (Anaya & MacFadden 1995; see Chapter 6).

Some *S. uccasamamensis* mandibles have more robust dentition and more anteriorly divergent, thicker, and deeper horizontal rami than others (see Chapter 6). However, this *a priori* separation of the sample is not confirmed by the PCA performed on this dataset on either PC1 or PC2 (Fig. 7.3A).

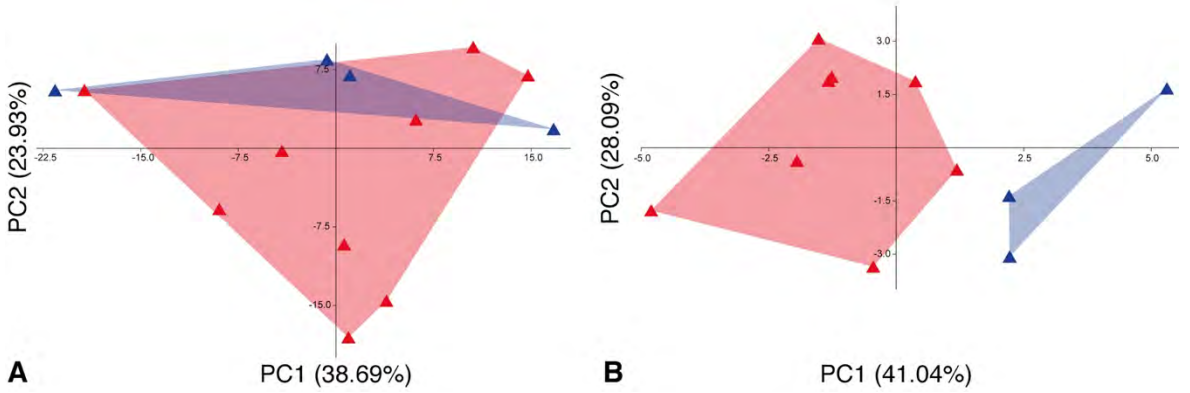

Figure 7.3. PCAs conducted on the mandible and lower dentition dataset (A) and exclusively the lower dentition dataset (B), showing the morphological differentiation among the gracile (red) and robust (blue) morphs of *Simomylodon uccasamamensis*. Percentages of explained variance of PC1 and PC2 are reported. In both cases (A and B) PC1 is a representation of general body size.

Robust specimens tend to group together at positive values of PC2 (23.93% of total variance explained), which is related to the dorsoventral depth of the horizontal ramus of the mandible at the level of dentition. Positive and negative values of PC2 respectively indicate specimens with deeper and shallower mandibular horizontal rami. In contrast, when analyzing only lower dentition (Fig. 7.3B), two groups separate along PC1, which explains 41.04% of total variance (NPMANOVA: $F = 3.59$; $p = 0.008$). Given that lower dentition variables have similar positive loadings in PC1 (Appendix V, Tables S2) this axis likely correlates with size. Smaller and larger lower dentitions are reflected by negative and positive values of PC1, respectively.

7.1.3 Femur and tibia

The PCA performed on the femoral dataset shows a marked separation between robust and gracile specimens along PC1, which explains 65.49% of the total variance (Fig. 7.4A). Also in this case, PC1 likely represents an approximation of body size, because the femoral variables display similar positive loadings (see Appendix V, Tables S2). For this reason, the two clusters group together smaller specimens on negative values of PC1, and larger specimens on positive values (Fig. 7.4A). The departure of the gracile and robust specimens is also confirmed by the cluster analysis (Fig. 7.4B), and their distinction is statistically significant (NPMANOVA: $F = 19.78$; $p = 0.019$). A very similar result is obtained from the tibiae dataset (Fig. 7.5A). Gracile and robust tibiae segregate on the basis of size, reflected in PC1, which represents 69.66% of total variance. The significant difference between the two groups (NPMANOVA: $F = 9.13$; $p = 0.008$) is further confirmed by cluster analysis (Fig. 7.5B).

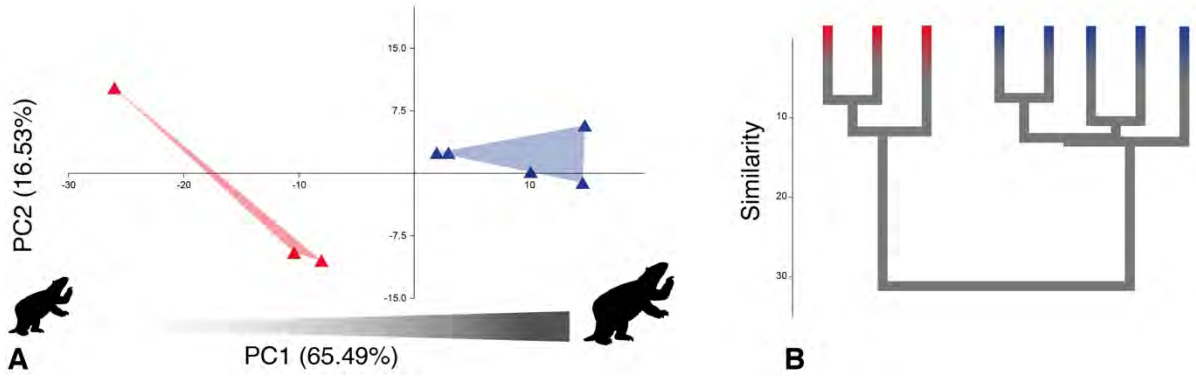

Figure 7.4. Multivariate analyses of the femoral dataset showing the morphological differentiation among the gracile (red) and robust (blue) morphs of the extinct sloth *Simomylodon uccasamamensis* from the latest Miocene–late Pliocene of Bolivian Altiplano. A, PCAs showing PC1 and PC2, with related percentages of explained variance and the main morphological transformations related to PC1 and B, associated hierarchical cluster analyses showing squared Euclidean distances among all specimens analyzed.

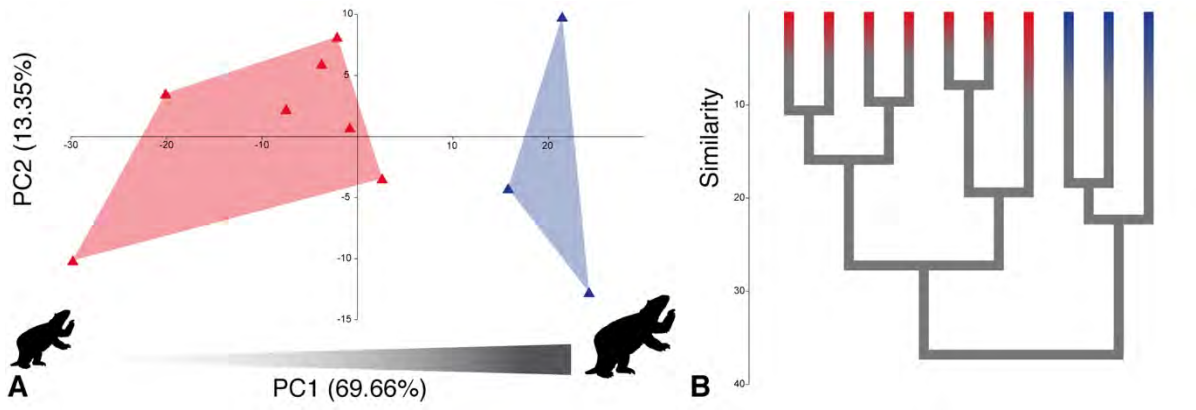

Figure 7.5. Multivariate analyses conducted on the tibial dataset, showing the morphological differentiation among the gracile (red) and robust (blue) morphs of *Simomylodon uccasamamensis*. A, PCA showing principal components 1 and 2, with related percentages of explained variance and the main morphological transformations related to PC1. B, associated hierarchical cluster analysis showing squared Euclidean distances among all specimens analyzed.

7.2 DISCUSSION

7.2.1 Sexing up *Simomylodon*'s variation

In *Simomylodon uccasamamensis*, differences observed in cranial shape, and typified by the two morphs in Figure 1, are consistent with features observed in later mylodontid sloths, which were previously attributed to sexual dimorphism (Lydekker 1894; McDonald 2006; Cartelle *et al.* 2019). In particular, individuals with mediolaterally wide muzzles relative to total cranial length also show rounded or flat anterior margins of the premaxillae, accompanied by more vertical occipital bones and occipital condyles closely appressed to the basicranium (Fig. 7.1D–F; McDonald 2006). In contrast, gracile skulls show longer and narrower palates with pointed anterior margins of the premaxillae and a more pronounced slope of the occiput, with a marked posterior projection of the occipital condyles (Fig. 7.1A–C; McDonald 2006). Differences in general cranial width, particularly noticeable at the level of the muzzle, appear to be at least partially related to body size.

The presence of SD in *S. uccasamamensis* was first suggested on the basis of general robustness differences of two preserved mandibles (i.e., MNHN-Bol V 3358 and 3371; Anaya & MacFadden 1995; Chapter 6: fig. 6.9), in which it was also possible to observe differences in the grade of divergence between toothrows. The PCA of the mandibular dataset cannot reliably differentiate the two morphs (Fig. 7.3A), probably due to the lack of complete mandibular

remains in which both horizontal rami are complete and undeformed. In fact, the current extended dataset is enriched with many mandibular remains, but most are incomplete. However, gracile/robust groups are visually identifiable based on the general size of the lower dentition (Fig. 7.3B).

The quantitative assessment of this study confirms the separation of the two morphs previously recognized qualitatively. The robust and gracile morphs of *S. uccasamamensis* specimens differ in: i) the shape of the anterior portion of the skull, ii) the general size of the lower dentition, and iii) the size of femora and tibiae. These clusters are well-segregated and consistent across the different datasets (i.e., the five specimens that present associated remains included in different datasets are unequivocally assigned to a single morphotype). Moreover, gracile and robust remains are related neither with fossil locality provenance, nor with the stratigraphical age of the corresponding deposits. Robust and gracile morphs are well represented in all the early and late Pliocene localities of the Bolivian Altiplano from which remains have been recovered (with the exception of Choquecota, where only a single skull is known so far; Fig. 7.6). In this regard, stratigraphical and geographical overlapping record of both morphs could indicate that alternative hypotheses such as considering them as sympatric species or geographical varieties should be considered less parsimonious than SD. Therefore, SD implies fewer ad-hoc explanations for considering coexisting robust and gracile morphs than their assignment to local geographical or chronological variants.

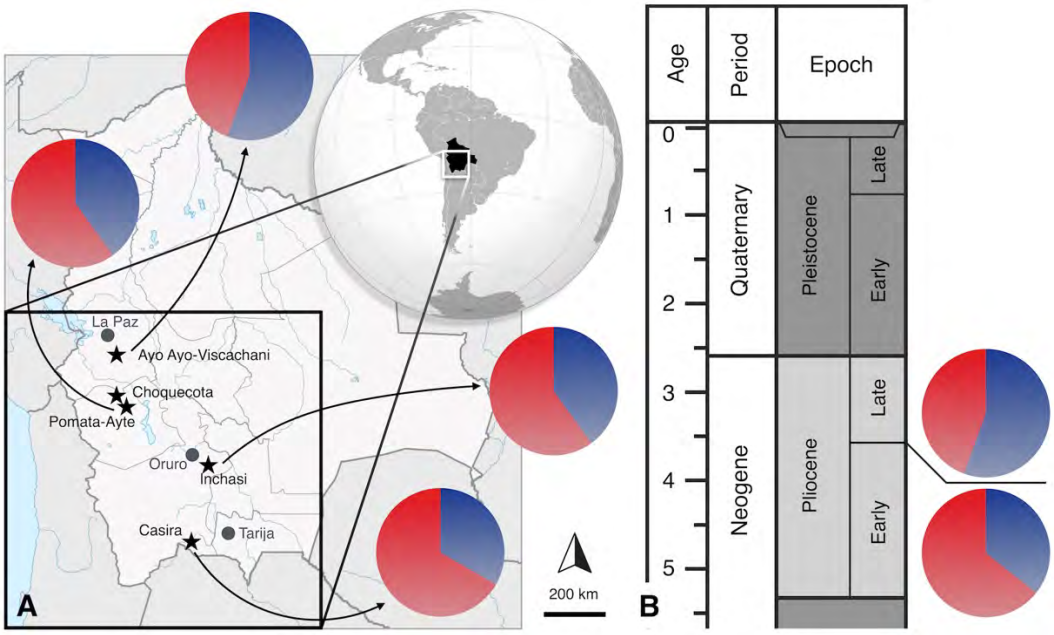

Figure 7.6. Geographical (A) and chronological (B) distribution of the gracile (red) and robust (blue) morphs of *Simomylodon uccasamamensis*. In the (latest Miocene-earliest Pliocene?) locality of Choquecota only a single skull of *S. uccasamamensis* was recovered (n=1) and it is therefore not considered here.

Other sexually dimorphic features observed on the posterior portion of the cranial roof in other extinct sloths (Cartelle & Bohórquez 1982; Miño-Boilini & Zurita 2015) are not clearly observable in *S. uccasamamensis* due to preservation biases (see Chapter 6). Moreover, differences in the occlusal wear of the caniniforms are not notable (see Chapter 6), or at least not as remarkable as in *Paramylodon harlani* (McDonald 2006). Data from the present study attest to the existence of SD in the latest Miocene–late Pliocene mylodontid sloth *Simomylodon uccasamamensis*, thus representing the earliest well-documented occurrence of SD in an extinct sloth (Fig. 7.7).

Figure 7.7. Hypothetical life reconstruction of the extinct sloth *Simomylodon uccasamamensis*, from the latest Miocene–late Pliocene of Bolivian Altiplano. The robust morph (putatively the male) is depicted in the background, and the gracile morph (putatively the female) in the foreground. General darker tones on the dorsum of the male's pelage are inspired by those observed in the extant three-toed sloths (see Lara-Ruiz & Chiarello 2005; Chiarello 2008). Credits: Jorge A. González.

7.2.2 Who's who?

In extinct sloths, an objective assignment of the robust and gracile morphs to either the male or the female sex is difficult (McDonald 2006; Miño-Boilini & Zurita 2015). In mammals, skulls of males are typically more robust than those of females (McDonald 2006), and SSD is generally male-biased (see Isaac 2005; Fairbairn *et al.* 2007). This is also the case for extant xenarthrans (Ralls 1977) and living anteaters, the sister group of sloths, in which males are generally larger than females (Nowak 1999). By contrast, SSD in extant folivorans is female-biased (Richard-Hansen *et al.* 1999; Lara-Ruiz & Chiarello 2005; Chiarello 2008), a pattern that is uncommon among mammals as a whole (Isaac 2005; Fairbairn *et al.* 2007). Female skulls of extant sloths tend to be more elongated in relation to width (Hautier *et al.* 2014), thus supporting in part the identification of the gracile morph as belonging to females. However, differences related to sex in extant sloths are not significant in multivariate analyses (Hautier *et al.* 2014), indicating that intersex SSD is indeed reduced. Moreover, the small body size and highly specialized life habits of living sloths makes them poor models for paleobiological reconstructions of their extinct, much larger-sized relatives (Vizcaíno *et al.* 2016, 2018). For many features, comparisons with extinct sloths and more generally with living and extinct large mammals are more promising (e.g., Vizcaíno *et al.* 2004a, 2018; Bargo *et al.* 2006b; see also Chapters 9 and 10).

Even if not conclusive, the "larger/robust=male, smaller/gracile=female" hypothesis is the most compelling, and the most plausible explanation for sexually-related differences among extinct sloths, as it is embraced by many authors (e.g., Lydekker 1894; Cartelle & Bohórquez 1982; Christiansen & Fariña 2003; McDonald 2006; Cartelle *et al.* 2019).

7.2.3 Functional attributes of sexually dimorphic features

The two morphs of *Simomylodon uccasamamensis* segregate on the basis of body size, but they also show clear differences in the morphology of the anterior and posterior portions of the skull (Figs 7.1, 7.2), in line with previous observations on Pleistocene mylodontines from both South and North America (i.e., *Glossotherium robustum*, *G. phoenesis* and *Paramylodon harlani*; Lydekker 1894; McDonald 2006; Cartelle *et al.* 2019). In xenarthrans, the shape of the muzzle and nuchal protrusion are related to feeding habits and the normal position of the head, and their adaptive role has been investigated at the interspecific level (Bargo *et al.* 2006b; Coutier *et al.* 2017).

The width of the muzzle is related to food intake and dietary habits (McDonald 1997; Bargo *et al.* 2006). The dietary habits of extinct sloths were reconstructed through comparisons with the feeding apparatus of both extant and extinct ungulates (e.g., Janis & Ehrhardt 1988; Janis 1990; Solounias *et al.* 1988; Solounias & Moelleken 1993). Wide-muzzled sloths like *Glossotherium* and *Lestodon* were most likely grazing bulk-feeders, whereas narrow-muzzled sloths such as *Mylodon*, *Scelidotherium*, and *Megatherium* were probably more mixed or selective feeders (McDonald 1997; Bargo *et al.* 2006b; Czerwonogora *et al.* 2011). This is supported by marked differences in the shape of the palate and the premaxillae: wide muzzles with premaxillae that have rounded or flat anterior margins are indicative of grazing diets, whereas narrow muzzles with premaxillae that have pointed anterior margins are usually linked to browsing habits (McDonald 1997; Bargo *et al.* 2006b). The latter results are also consistent with previously published coprolite analyses (Moore 1978).

Among xenarthrans, extant and extinct pilosans show a greater protrusion of the occipital condyles (and a lesser protrusion of the nuchal area) than that of extant cingulates (Coutier *et al.* 2017). Morphology of the nuchal area appears to covary with the angle formed by the lateral semicircular canal and the basicranium, suggesting that the conformation of the nuchal area may serve as an indicator of the usual head posture (Coutier *et al.* 2017). Accordingly, extant pilosans tend to show a wider range of head positions than the typical, armadillo-like nose-down head posture (Coutier *et al.* 2017). Conversely, in extant xenarthrans, protruded nuchal areas and occipital condyles closely associated to the basicranium are related with nose-down normal postures and a limited range of movement of the head.

In a more moderate way, the morphs of *Simomylodon uccasamamensis* show intraspecific differences in both the rostrum and the occipital region, and these shape differences appear to covary with size. More precisely, and like in other mylodontid species (Lydekker 1894; McDonald 2006; Cartelle *et al.* 2019), the large-sized morph has a wider muzzle with flat or curved premaxillae and a vertical orientation of the occiput. In contrast, the smaller-sized morph has a narrower muzzle with pointed premaxillae and a more inclined occiput.

7.2.4 Feeding structures and niche divergence

The idea that sexual dimorphism, and particularly SSD, may have evolved among animals in part for ecological reasons (e.g., intraspecific niche divergence) was first suggested by Darwin (1874). This idea has been long overshadowed by the success of the "sexual selection" hypothesis (i.e., SSD arising from differences in mating success) also treated in Darwin's

classical reviews on the subject (Darwin 1871, 1874). This latter explanation has been preferred on the basis of parsimony and predictive value (Shine 1989). In fact, differences in the two sexes in traits not closely linked with reproductive functions (i.e., reflecting adaptations to different ecologies more than reproductive roles) are less readily explained (Fairbairn *et al.* 2007). Nevertheless, recent studies have documented the presence of several ecological factors influencing sexual size dimorphism in mammals (Shine 1989; Isaac 2005; Ruckstuhl & Neuhaus 2005), such as different predation risks and different foraging requirements between the two sexes (Ruckstuhl & Neuhaus 2005).

Sexual differences in diet selection and food intake rates have been observed in several extant herbivore species and they are often related to differing nutritional demands for the two sexes (for a review see Ruckstuhl & Neuhaus 2005). In general, large males have almost constant high energetic costs in order to maintain their large size, and therefore they tend to accept diets higher in fibre, maximizing food quantity. Females, in contrast, bear the nutritional demands of pregnancy and lactation, tending to prefer more nutritional food and privileging food quality (Ruckstuhl & Neuhaus 2005, and references therein). As a result, for large herbivore species, when both sexes occur in the same habitat, adult females usually feed more selectively and show more browsing habits than males (Clutton-Brock *et al.* 1982). The intersexual niche partitioning in sexual dimorphic species can ultimately lead to habitat, spatial and/or social segregation (Ruckstuhl & Neuhaus 2005).

Trophically-related morphological sexual dimorphism is common in both extant invertebrate and vertebrate lineages and, in some groups, it represents the rule rather than the exception (Shine 1989). Variation of this kind commonly occurs in the feeding apparatus of extant sexually-dimorphic ungulates, in accordance with the forage-selection hypothesis, with females having significantly narrower muzzles than males (Pérez-Barbería & Gordon 1998, 1999).

In *Simomylodon uccasamamensis*, the two forms differ on the basis of general size, but also in the morphology of the feeding apparatus, strongly suggesting trophically-related sexual dimorphism, in accordance with that observed in extant large herbivorous mammals. Additionally, the different occipital inclination and protrusion of the occipital condyles may have had affected the range of movement of the head, thereby shaping differential feeding behaviors in the two sexes of this mylodontine sloth. More precisely, the larger-sized robust morph may have fed mainly on less nutritious herbs than the female. This is suggested by its wider muzzle shape, indicative of more grazing habits, also reinforced by the

supposedly more constrained nose-down posture deduced from its occipital shape. The opposite features are observed in the smaller-sized gracile morph.

In extant mammals, different diets between males and females can ultimately lead to sexual spatial segregation (SSS), a common phenomenon among dimorphic species (Main *et al.* 1996). In grazing species, SSS tends to occur "horizontally", with the males displacing to other feeding patches than those occupied by females (Ruckstuhl & Neuhaus 2005).

SSS between males and females of the extinct sloth *Paramylodon harlani* was suspected on the basis of differences in the relative numbers of individuals assigned to both sexes recovered in the various Rancho La Brea tar pits (McDonald 2006). Males are consistently more abundant than females, probably reflecting a greater territorial range and a differential habitat use (McDonald 2006). Morphofunctional data on *S. uccasamamensis* from the present study are consistent with different habitat uses between the two sexes, suggesting a possible SSS in this taxon.

Bimodal differences between the sexes, involving habitat partitioning through dietary divergence in *S. uccasamamensis*, may have had an adaptive role. SD may have allowed more efficient habitat use, and therefore it may have constituted an advantage for *S. uccasamamensis* during the Miocene-Pliocene faunal turnover (Hoffstetter 1986; Marshall & Sempéré 1991). Around this transition, the Bolivian Altiplano underwent important changes in both altitude and climate (Garzione *et al.* 2008). Pliocene ecosystems of this region turned dryer and colder relative to late Miocene climes, with a consequent decrease of vegetation cover (Marshall & Sempéré 1991; Lamb & Hoke 1997). This process led to both the displacement of faunal elements, with notoungulates largely replaced by xenarthran lineages, and the appearance of local adaptations (Hoffstetter 1986; Marshall & Sempéré 1991; Vizcaíno *et al.* 2012a). The capacity of both males and females to efficiently feed in changing environments, avoiding intraspecific competition, can be regarded as a possible cause of the spread of *S. uccasamamensis* on the Bolivian Altiplano during the Pliocene. More generally, and although this can be hardly testable, it might also have been a driver for the widespread dispersal of Mylodontinae during Pliocene and Pleistocene times throughout the entire American continent (McNab 1985; McDonald & Pelikan 2006).

7.3 CONCLUSIONS

The material of latest Miocene–late Pliocene sloth *Simomylodon uccasamamensis* from the Bolivian Altiplano analyzed in this chapter sheds light on the intraspecific variation of this taxon. Two well-segregated morphs can be recognized in both cranial and postcranial remains and the main differences observed concern the morphology of the skulls, particularly in the rostral region, and the relative size of femora and tibiae. In the analyzed sample, these differences appear to be neither geographically nor chronologically related. By analogy with a similar segregation of features previously attributed to SD in several Pleistocene sloths from both South and North America, the presence of SD can be hypothesized for *S. uccasamamensis*, further corresponding to the earliest occurrence of SD in extinct sloths. The differences between sexes relate to size (i.e., gracile and robust morphs are recognized) but also to the shape of the muzzle, strongly suggesting the presence of differences in feeding habits between males and females. To some extent, this may have contributed to the existence of intraspecific niche partitioning and/or ultimately to a certain grade of intersexual spatial segregation. In this way, mylodontine sloths, widely distributed during Pliocene and Pleistocene times in both South and North America, would have benefitted from a non-competitive habitat use between the two sexes.

Chapter 8
PHYLOGENY OF MYLODONTIDAE

The phylogeny of the Mylodontidae sloths has recently been the object of intense studies. However, in some cases, contrasting hypotheses have been proposed, especially for the relationships among late Miocene–Pleistocene mylodontines and lestodontines. In this chapter, a new and detailed phylogenetic analysis is conducted, after adding new characters and taxa, previously unexplored from a phylogenetic point of view.

New features, added to the craniodental analysis of Gaudin (2004), are derived from postcranial skeletal anatomy. In this way, the current reappraisal represents the first exhaustive phylogenetic study on the Mylodontidae that incorporates features coded for the entire skeleton. When available, multiple specimens of each bony element are observed for each OTU, both qualitatively and quantitatively, in order to take into account intraspecific variation.

The taxonomic sample of this study follows the revision of Mylodontinae in Chapter 5, considering, for the first time, the members of this group at the specific level. However, many other Mylodontidae are considered, and their phylogenetic relationships tested. The taxonomic sample of this study is enriched with new taxa from central and northern South America, with the aim of compensating for the knowledge bias in favor of austral mylodontids, which have historically been more extensively studied than those from tropical latitudes.

Special emphasis is also given to the Mylodontini–Lestodontini split, which is supposed to have occurred at the Middle–Late Miocene transition, giving rise to independent adaptive radiations across South and North America.

8.1 RESULTS

8.1.1 Description of the new characters and their states

The following postcranial features, here numbered 287–383, were added to the craniodental characters list (1–286) of Gaudin (2004). Characters marked with double asterisks are multistate and ordered. Some of the features were modified from Gaudin & Branham (1998), McDonald & Muizon (2002), Pujos (2002), Pujos *et al.* (2007), De Iuliis *et al.* (2011), Rincón *et al.* (2015), Amson *et al.* (2016) and Haro *et al.* (2016). The complete list of characters of the present study is reported in Appendix VI, Data S1, and for characters that include ratios, the raw data is available in Appendix VI, Data S2. The complete matrix analyzed in this thesis (see section 8.1.2) is included as Appendix VI, Data S4.

Scapula (Fig. 8.1)

287 – Ratio SW/SL: (0) < 0.16; (1) ≥ 0.16.

288 – General shape of scapula: (0) broad and rectangular; (1) roughly triangular.

289 – Suprascapular ossification: (0) present; (1) absent.

290 – Post-scapular fossa (= teres major fossa): (0) small and located on the posterior scapular border; (1) posteriorly expanded.

291 – Accessory scapular spine: (0) short spine located on the posterior scapular border; (1) well-developed and laterally projecting.

292 – Vertebral border of scapula: (0) convex; (1) straight.

293 – Supraspinous fossa and infraspinous fossa: (0) roughly the same size; (1) supraspinous fossa greater in area than the infraspinous fossa.

294 – Acromion process: (0) at the level of the glenoid fossa in lateral view, or fails to reach ventrally to level of glenoid; (1) extended ventral to glenoid in lateral view.

295 – Acromion process fused with the coracoid process: (0) absent; (1) present.

296 – Coraco-scapular foramen: (0) absent; (1) present. [Modified from Gaudin & Branham (1998): ch. 72].

297 – Glenoid fossa, shape of outline: (0) ovoid-piriform; (1) semicircular.

298 – Glenoid fossa and facet for clavicle in ventral view: (0) long axes disposed at acute angle (around 45 degrees); (1) long axes disposed almost perpendicularly.

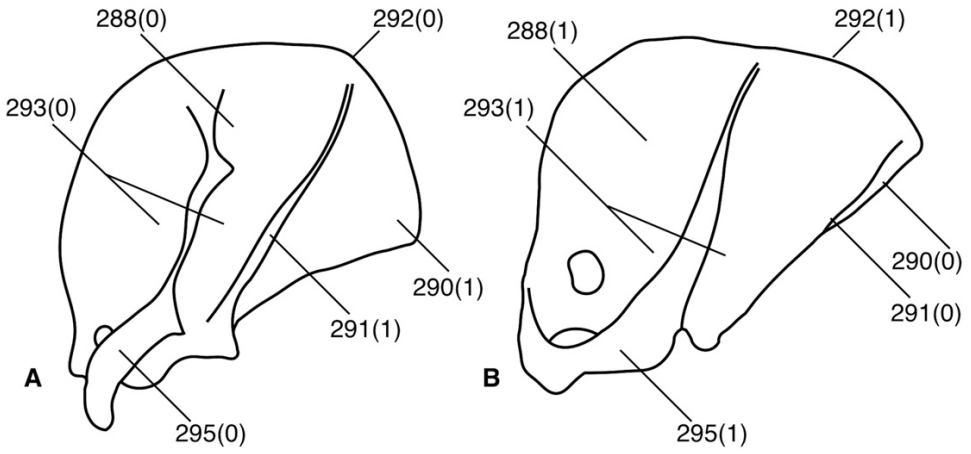

Figure 8.1. Comparison of left scapulae of *Tamandua* sp. MACN Ma 10.8 (A) and *Glossotherium robustum* MACN Pv 14066 (B) in lateral view, depicting differing morphologies and phylogenetically significant characters and character states. Images are not to scale.

Humerus (Fig. 8.2)

299 – Ratio HHW/HHL, (0) < 0.80; (1) ≥ 0.80.

300 – Ratio HEMP/HDEW, (0) ≥ 0.36; (1) < 0.36.

301 – Deltoid crest in anterior view: (0) faces laterally, occupies part of the anterior view; (1) faces anteriorly, reaching the medial side.

302 – Distal border of deltoid crest in anterior view: (0) oblique; (1) nearly horizontal.

303 – ** Supinator crest in anterior view: (0) without lateral extension (lateral margin oblique proximodistally); (1) with moderate lateral extension (convex profile of lateral margin); (2) with well-developed lateral extension (lateral margin vertical proximodistally).
304 – ** Degree of radial protrusion of greater tuberosity versus lesser tuberosity in proximal view: (0) lt>gt; (1) lt≈gt; (2) lt<gt. [Modified from De Iuliis *et al.* (2011): ch. 37].
305 – Olecranon fossa: (0) distinct, deep; (1) shallow depression.
306 – Entepicondylar foramen: (0) present; (1) absent. [From Pujos (2002): ch. 20; Pujos *et al.* (2007): ch. 27; Amson *et al.* (2016): ch. 4].
307 – Distinct proximodistally vertical process on the ascending entepicondylar ridge: (0) absent; (1) present.
308 – ** Lateral epicondyle versus medial epicondyle in anterior view: (0) lateral epicondyle less mediolaterally expanded than the medial epicondyle; (1) lateral epicondyle and medial epicondyle equally expanded; (2) lateral more expanded than the medial epicondyle.
309 – Capitulum vs trochlear mediolateral width in distal view: (0) trochlea wider transversely than the capitulum; (1) width roughly equivalent.
310 – Capitulum vs trochlear anteroposterior depth in distal view: (0) same anteroposterior depth; (1) trochlea deeper.
311 – Lateral epicondyle in distal view: (0) directed posteriorly; (1) directed laterally.
312 – ** Medial epicondyle in distal view: (0) directed medially; (1) directed posteriorly; (2) directed anteriorly.
313 – Capitular tail (*sensu* Sargis 2002): (0) present; (1) absent.

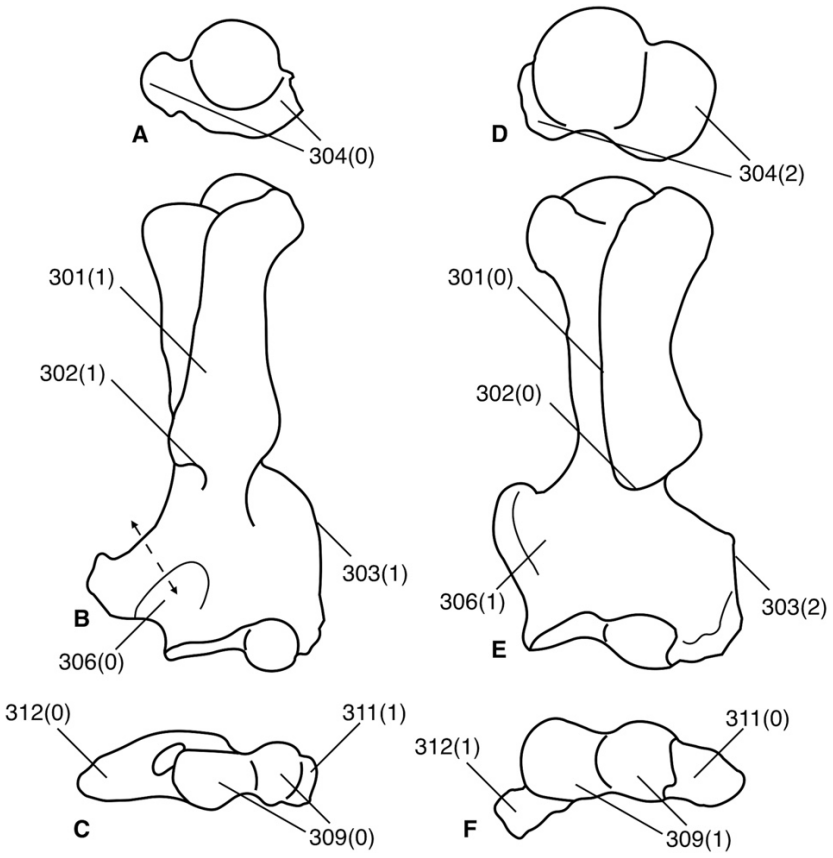

Figure 8.2. Comparison of left humeri of *Nematherium* sp. YPM-PU 15374 (A–C) and *Glossotherium robustum* (based on Owen 1842) (D–F), in proximal (A, D), anterior (B, E), and distal (C, F) views, depicting differing morphologies and phylogenetically significant characters and character states. Images are not to scale.

Radius (Fig. 8.3)

314 – ** Ratio APDR/RL: (0) ≤ 0.160; (1) > 0.160, ≤ 0.245; (2) > 0.245.

315 – ** Radial head shape: (0) deep anteroposteriorly and narrow transversely, RHW/RHL ≤ 0.63; (1) ovoid, RHW/RHL > 0.63, ≤ 0.82; (2) circular or approximately so, RHW/RHL > 0.82, ≤ 1.0.

316 – Posterior border of radius in lateral view: (0) straight; (1) concave anteriorly.

317 – Anterior border of radius in lateral view: (0) convex anteriorly; (1) straight.

318 – Anterior border of radius in anterior view: (0) not inflected medially; (1) inflected medially.

319 – Dorsolateral sulcus on styloid process (*m. abductor pollicis longus* groove): (0) absent; (1) present.

320 – Distal articulation of radius: (0) with one single facet for scaphoid and lunar; (1) with distinct facets.

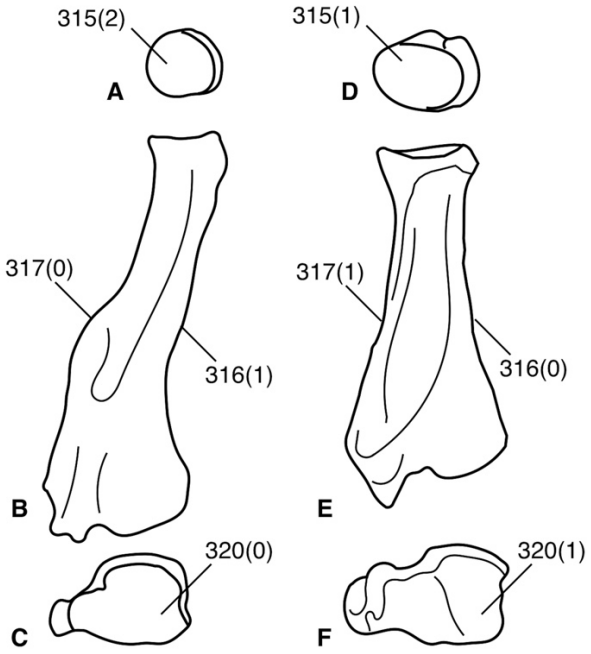

Figure 8.3. Comparison of left radii of *Scelidotherium* sp. MACN Pv 8854 (A–C) and *Glossotherium robustum* (based on Owen 1842) (D–F) in proximal (A, D), lateral (B, E) and distal (C, F) views, depicting differing morphologies and phylogenetically significant characters and character states. Images are not to scale.

Ulna (Fig. 8.4)

321 – ** Ratio UPCDE/UL: (0) ≤ 0.55; (1) > 0.55, ≤ 0.75; (2) > 0.75.

322 – ** Ratio THU/UL: (0) < 0.12; (1) ≥ 0.12, < 0.20; (2) ≥ 0.20, ≤ 0.26; (3) > 0.26.

323 – ** Angle between olecranon and posterior border of the ulna in lateral view: (0) acute (less than 90 degrees); (1) roughly orthogonal (around 90 degrees); (2) obtuse (more than 90 degrees).

324 – ** Medial (trochlear) and lateral (capitular) portions of the trochlear notch in anterior view: (0) medial portion extends proximal to lateral; (1) medial and lateral portion with roughly equivalent proximal extent; (2) lateral portion extends proximal to medial.

325 – Radial notch: (0) facet occupying the whole fossa; (1) facet occupying only part of the fossa.

326 – Posterior border of the ulna in posterior view: (0) columnar, with uniform transverse width along whole length; (1) decreasing transverse thickness from proximal to distal.
327 – Styloid process: (0) pedunculated; (1) sessile.
328 – Styloid process: (0) with oblique articular surface; (1) with horizontal articular facet.

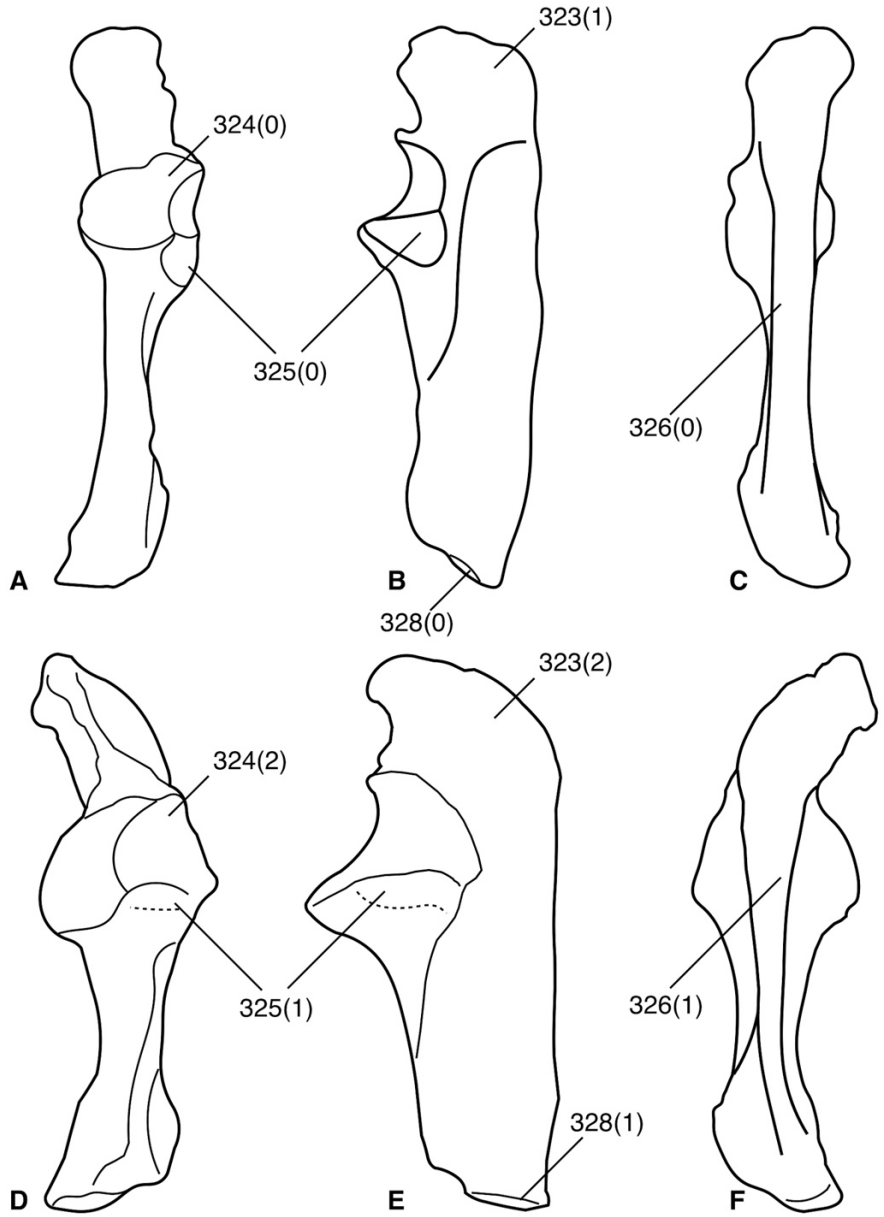

Figure 8.4. Comparison of left ulnae of *Catonyx tarijensis* FMNH P14238 (A–C) and *Glossotherium robustum* (based on Owen 1842) (D–F), in anterior (A, D), lateral (B, E), and posterior (C, F) views, depicting differing morphologies and phylogenetically significant characters and character states. Images are not to scale.

Manus (Fig. 8.5)
329 – Scaphoid and lunar: (0) fused; (1) separate.
330 – Ungual phalanges: (0) bifid, with forked distal tip; (1) single distal point.
331 – Scaphoid, ratio between its minimum and maximum diameters: (0) < 0.64; (1) ≥ 0.64.

332 – Cuneiform-lunar contact, in proximal view: (0) pedunculated; (1) sessile.

333 – ** Cuneiform shape, ratio between dorsopalmar and mediolateral widths: (0) < 0.65; (1) ≥ 0.65, < 0.87; (2) ≥ 0.87.

334 – Cuneiform shape, ratio between proximodistal length and mediolateral width: (0) < 0.65; (1) ≥ 0.65. [Modified from Haro *et al.* (2016): ch. 326].

335 – Cuneiform shape, ratio between proximodistal and dorsopalmar widths: (0) < 0.95; (1) ≥ 0.95. [Modified from Haro *et al.* (2016): ch. 324].

336 – Unciform shape, ratio between proximodistal and mediolateral widths: (0) < 1.0; (1) ≥ 1.0.

337 – Trapezium and metacarpal I: (0) unfused; (1) fused, forming the carpal-metacarpal complex. [Modified from De Iuliis *et al.* (2011): ch. 50].

338 – Contact between trapezium (or carpal-metacarpal complex) and trapezoid: present (0); absent (1) [Modified from Haro *et al.* (2016): ch. 330].

339 – Exposure of contact between metacarpal II and magnum in dorsal view of articulated manus: absent (0); present (1) [From Haro *et al.* (2016): ch. 331].

340 – Metacarpal 2 - Metacarpal 3 facet: (0) sessile and flat; (1) pedunculated and concavo-convex.

341 – ** Metacarpal 3 shape (ratio between mediolateral width at the middle of shaft and total length): (0) ≤ 0.37; (1) > 0.37, < 0.52; (2) ≥ 0.52 [Modified from Haro *et al.* (2016): ch. 339].

342 – Mediolateral extension of the facet of metacarpal 5 on unciform in dorsal view: (0) well-developed (comparable to the extent of the metacarpal 4-unciform facet); (1) extremely reduced (less than the half of the extent of the metacarpal 4-unciform facet) or absent.

343 – ** Number of claws on manus: (0) 5-4; (1) 3; (2) 2 [From Gaudin & Branham (1998): ch. 92].

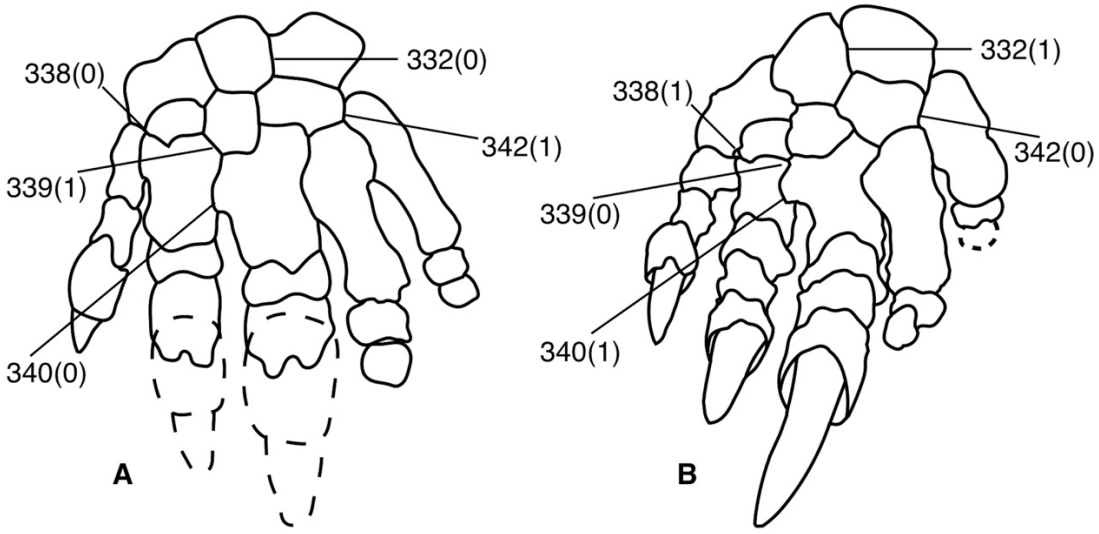

Figure 8.5. Comparison of left manus of *Catonyx tarijensis* FMNH P14247 (after McDonald 1987) (A) and *Glossotherium robustum* (based on Owen 1842) (B), in dorsal view, depicting differing morphologies and phylogenetically significant characters and character states. Images are not to scale.

Femur (Fig. 8.6)

344 – ** Femur shape (ratio between mediolateral width at midshaft and total length): (0) long and narrow, TDF/FL < 0.20; (1) intermediate, TDF/FL ≥ 0.20, < 0.35; (2) short and broad, TDF/FL ≥ 0.35. [Modified from Pujos *et al.* (2007): ch. 33; De Iuliis *et al.* (2011): ch. 58; Amson *et al.* (2016): ch. 26].

345 – ** Ratio FCW/FL: (0) ≤ 0.27; (1) > 0.27, ≤ 0.36; (2) > 0.36.

346 – Ratio LCL/MCL: (0) ≥ 0.75; (1) < 0.75.

347 – ** Ratio Wtroc/FL: (0) ≤ 0.30; (1) > 0.30, ≤ 0.47; (2) > 0.47.

348 – ** Ratio APDF/TDF: (0) ≥ 0.54; (1) < 0.54, ≥ 0.32; (2) < 0.32. [Modified from De Iuliis *et al.* (2011): ch. 57].

349 – Intertrochanteric ridge: (0) present; (1) absent.

350 – ** Femoral head in anterior view: (0) greater trochanter extends proximal to head; (1) proximal extent of head and greater trochanter equivalent; (2) head extends further proximally than the greater trochanter. [Modified from Rincón *et al.* (2015): ch. 13].

351 – Femoral head protrusion: (0) well-developed (with distinct neck); (1) sessile (without a distinct neck). [Modified from Rincón *et al.* (2015): ch. 11].

352 – Detached sulcus delimitating, both medially and laterally, the articular surface of the femoral head in anterior view: (0) present; (1) absent.

353 – ** Third trochanter: (0) absent; (1) prominent but relatively short proximodistally; (2) prominent and proximodistally elongate, forming a lateral blade. [Modified from McDonald & Muizon (2002): ch. 29; Pujos (2002): ch. 25; Pujos *et al.* (2007): ch. 31; Amson *et al.* (2016): ch. 28].

354 – Position of proximal and distal epiphyses of femur in distal view: (0) on the same plane of main axis; (1) twisted with respect to the main axis.

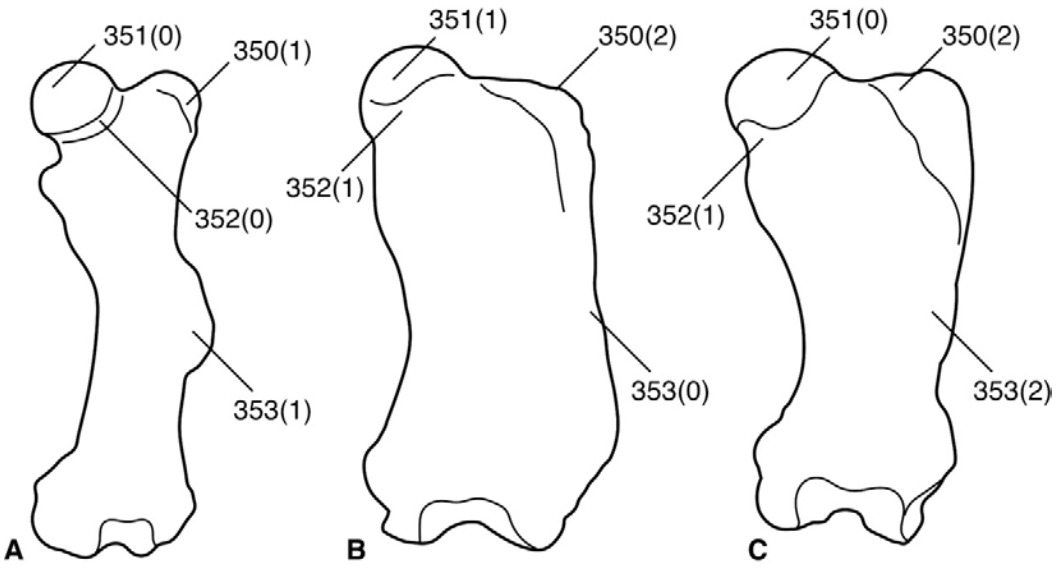

Figure 8.6. Comparison of left femora of *Hapalops* sp. FMNH P13209 (A), *Catonyx tarijensis* FMNH P14238 (B) and *Glossotherium robustum* (based on Owen 1842) (C), in anterior view, depicting differing morphologies and phylogenetically significant characters and character states. Images are not to scale.

Tibia and fibula (Fig. 8.7)

355 – Tibial shaft in lateral view: (0) anteriorly convex; (1) straight. [Modified from Rincón *et al.* (2015), ch. 18.]

356 – ** Ratio TDT/TL: (0) < 0.18; (1) ≥ 0.18, < 0.30; (2) ≥ 0.30.

357 – ** Ratio TPEL/TL: (0) ≤ 0.25; (1) > 0.25, ≤ 0.35; (2) > 0.35.

358 – ** Ratio TML/TPEL: (0) < 0.60; (1) ≥ 0.60, < 0.74; (2) ≥ 0.74.

359 – ** Ratio TPEW/TL: (0) < 0.40; (1) ≥ 0.40, < 0.60; (2) ≥ 0.60.

360 – Ratio LTFL/MTFL: (0) ≥ 0.83; (1) < 0.83.

361 – Ratio LTFW/MTFW: (0) ≥ 0.86; (1) < 0.86.

362 – Groove anterior to the tibial lateral condyle in proximal view (pit for attachment of medial meniscal ligament?): (0) absent; (1) present.

363 – Tibia, medial intercondylar eminence: (0) well-developed; (1) reduced or absent.

364 – Tibia, fibular facet in distal view: (0) extended anteroposteriorly; (1) occupying only the posteromedial corner of the tibia's distal surface.

365 – ** Grooves for the tendons of the *m. flexor hallucis longus*, *m. flexor digitorum longus* and *m. tibialis caudalis*, on the distomedial edge of the posterior tibial surface: (0) three well-marked grooves present; (1) two well-marked grooves; (2) single large depression present.

366 – Ratio EFFL/FiTL of fibula: (0) < 0.20; (1) ≥ 0.20.

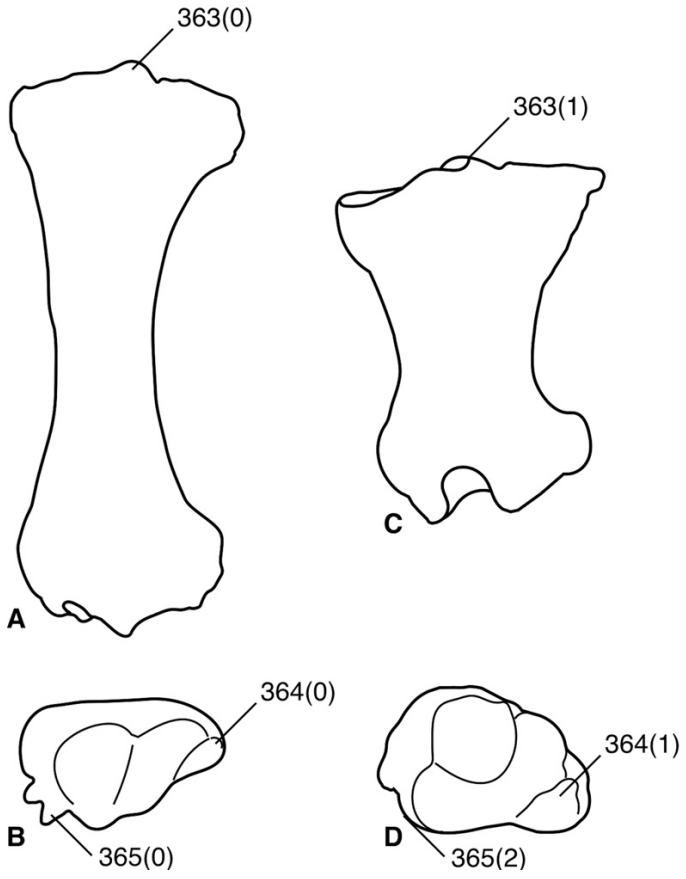

Figure 8.7. Comparison of left tibiae of *Octodontotherium grande* FMNH P13517 (A–B) and *Glossotherium robustum* (based on Owen 1842) (C–D), in anterior (A, C) and distal (B–D) views, depicting differing morphologies and phylogenetically significant characters and character states. Images are not to scale.

Pes (Fig. 8.8)

367 – ** Ratio between the maximum proximodistal and anteroposterior length of the astragalus: (0) < 0.80; (1) ≥ 0.80, < 1.00; (2) ≥ 1.00.

368 – ** Astragalus, odontoid process-discoid angle in either anterior or posterior view: (0) markedly obtuse (> 115°); (1) moderately obtuse (> 90°, ≤ 115°); (2) orthogonal or acute (≤ 90°). [Modified from Pujos (2002): ch. 29; Pujos *et al.* (2007): ch. 37; Amson *et al.* (2016): ch. 36].

369 – ** Astragalus, surface contour of discoid process in lateral view: (0) proximally convex; (1) essentially flat.

370 – Astragalus, sulcus tali: (0) present; (1) absent.

371 – Astragalus, sustentacular facet surface contour: (0) flat; (1) convex.

372 – Astragalus, cuboid facet surface contour: (0) convex; (1) concave.

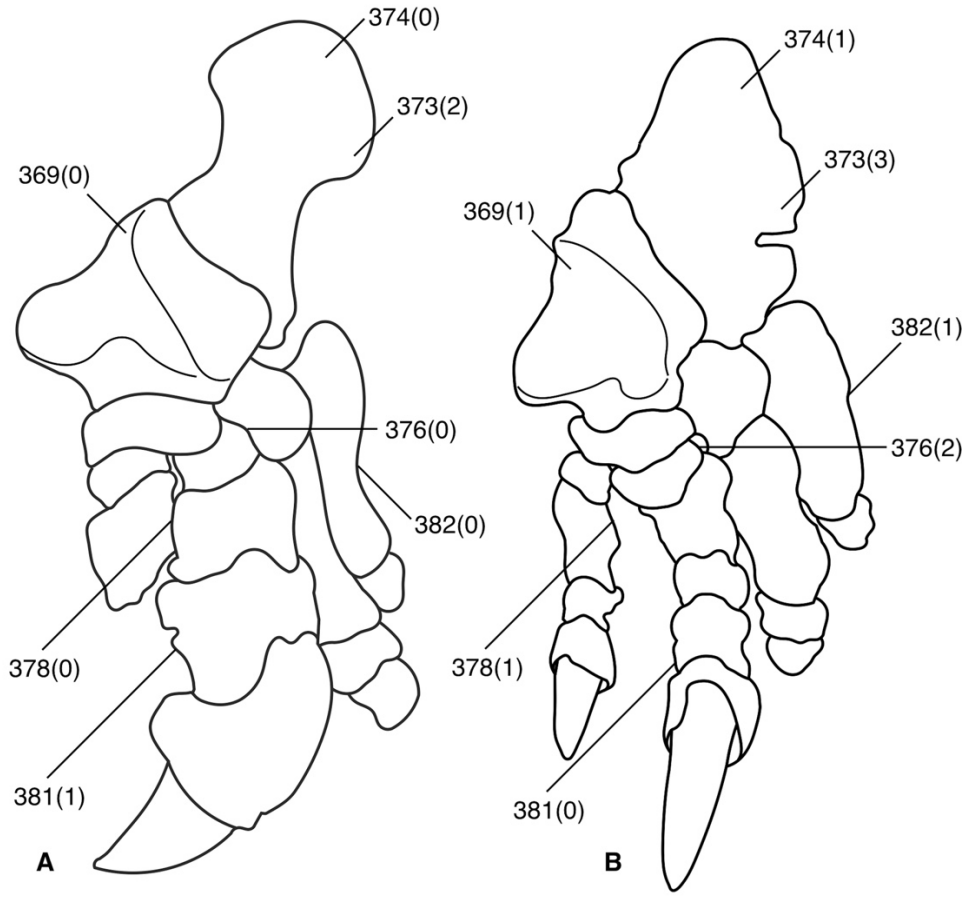

Figure 8.8. Comparison of left pedes of *Catonyx tarijensis* FMNH P14238 (A) and *Glossotherium robustum* (based on Owen 1842) (B), in proximal view, depicting differing morphologies and phylogenetically significant characters and character states. Images are not to scale.

373 – ** Calcaneal posterior mediolateral enlargement: (0) absent; (1) present, forming an arched posterior profile; (2) present, forming a broad surface touching the ground (mediolateral width/total length < 0.55); (3) present, forming a very broad surface touching the ground (mediolateral width/total length ≥ 0.55).

374 – Calcaneum, tuber calcis, distal development of proximal processes: (0) weak; (1) strong (reaching at least the proximal third of the bone). [From Amson *et al.* (2016): ch. 40].
375 – Sustentacular process of the calcaneum: (0) present; (1) absent.
376 – ** Contact of ectocuneiform with cuboid in lateral view: (0) large, nearly twice the size of the navicular-cuboid contact; (1) small, roughly the same size as the navicular-cuboid contact; (2) absent.
377 – Metatarsal 2 fusion with mesocuneiform: (0) absent; (1) present.
378 – Metatarsal 3 and metatarsal 2 contact: (0) present; (1) absent.
379 – ** Metatarsal 3 shape (ratio between minimum dorsopalmar depth of shaft and total length): (0) ≤ 0.40; (1) > 0.40, ≤ 0.46; (2) > 0.46, ≤ 0.56; (3) ≥ 0.56.
380 – ** Metatarsal 4 shape (ratio between minimum mediolateral width of shaft and total length): (0) ≤ 0.25; (1) > 0.25, ≤ 0.40; (2) > 0.40. [Modified from Amson *et al.* (2016): ch. 45].
381 – Digit III of pes, proximal and intermediate phalanges: (0) free; (1) co-ossified. [Modified from Pujos *et al.* (2007): ch. 41; Amson *et al.* (2016): ch. 44].
382 – Constriction of metatarsal 5 at midshaft: (0) present; (1) absent, distal border forming a continuous surface contacting the ground.
383 – Osteoderms: (0) absent; (1) present. [See McDonald (2018)].

8.1.2 Phylogenetic analyses results

The analysis of the total matrix, using 40 taxa, resulted in 87 most parsimonious trees [MPTs]. A strict consensus (tree length [TL] = 1157 steps; consistency index [CI] = 0.502; retention index [RI] = 0.864) is shown in Figure 8.9. Even if support values are low to moderate in some cases (Fig. 8.9), the strict consensus still yields the main clades of mylodontids that were recovered in the previous most comprehensive phylogenetic analysis of Gaudin (2004). These clades include Pilosa (node A), Vermilingua (node B), Folivora (node D), Eufolivora (node F) [the latter term is a substitution of the term Eutardigrada used by Gaudin 2004, and was introduced by Varela *et al.* (2018), following the proposal of Delsuc *et al.* (2001)], Mylodontidae (node H), Scelidotheriinae (node L), and Lestodontini (node O). Moreover, other groups are observed, like [*Octomylodon* sp. + *Baraguatherium takumara* + *Octodontobradys puruensis*] (node I), [*Urumacotherium* sp. + *Pseudoprepotherum confusum* + *P. venezuelanum*] (node J), and Mylodontini (node S; *sensu* Saint-André 1994). Lestodontini and Mylodontini form a monophyletic group (node N) that constitutes the sister group of *Brievabradys laventensi*s (all together forming a clade at node M). A complete list of the synapomorphies and autapomorphies that are common to all the 87 MPTs is available in Appendix VI, Data S5.

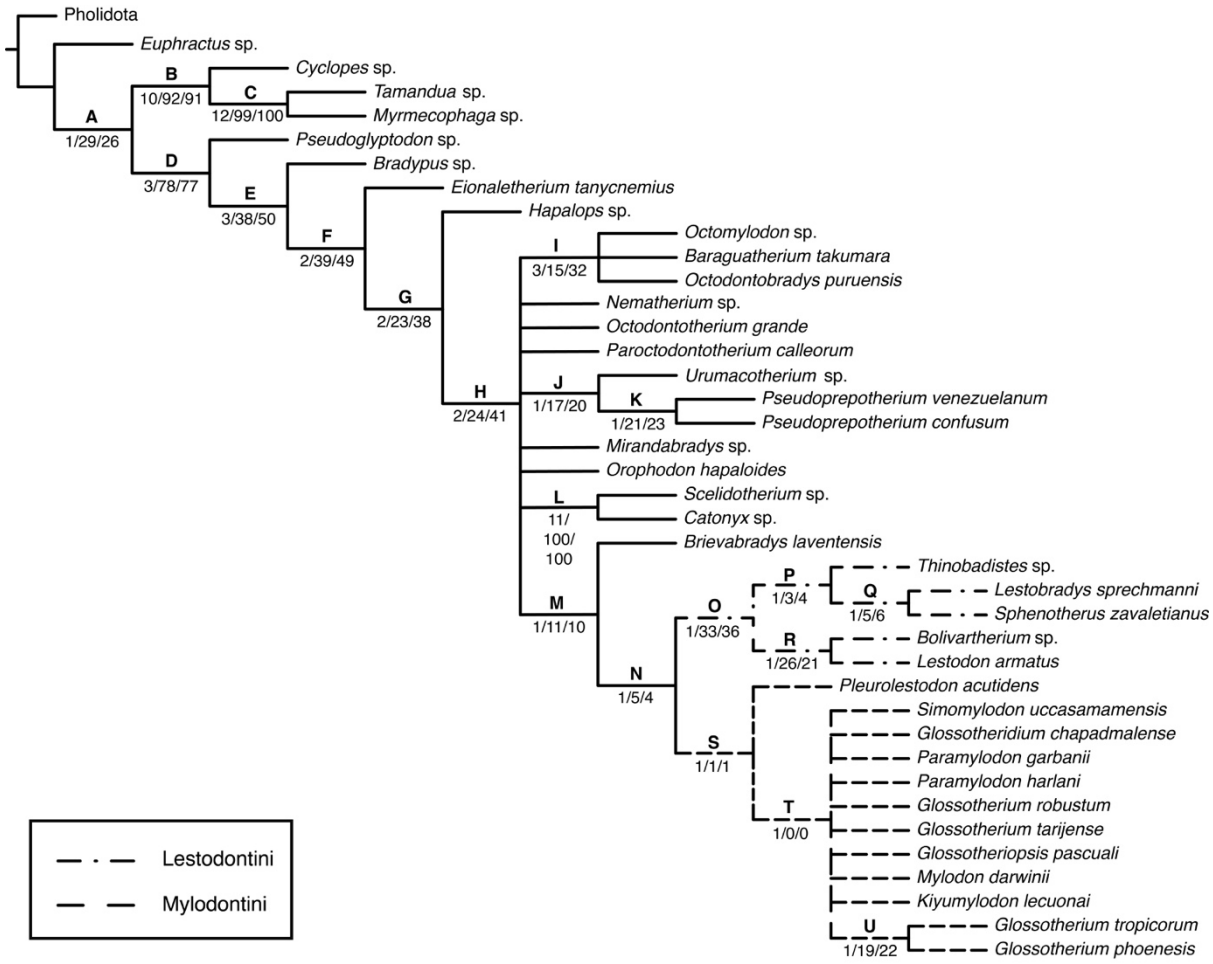

Figure 8.9. Strict consensus (TL = 1157 steps; CI = 0.502; RI = 0.864) of 87 most parsimonious trees, obtained from the analysis of the entire matrix (40 taxa and 383 characters). Capital letters are used to define nodes in the text. Numbers underneath each node represent Bremer, bootstrap and jackknife support values, respectively.

Pseudoglyptodon (from the Tinguiririan and Deseadan SALMAs of Bolivia, Argentina, and Chile, Engelmann 1987; McKenna *et al.* 2006; Pujos & De Iuliis 2007) is generally considered the earliest South American sloth (McKenna *et al.* 2006; Gaudin & Croft 2015). Varela *et al.* (2018) recently tested its phylogenetic position using Bayesan searching methods, and recovered *Pseudoglyptodon* as the sister taxon of all the other sloths. In the present parsimony-based analysis, the position of *Pseudoglyptodon* is confirmed and well-supported (Fig. 8.9: node D). However, as stressed by Varela *et al.* (2018) the position of *Pseudoglyptodon* may represent an artefact, due to the limited knowledge of this taxon. The phylogenetic position of *Eionaletherium tanycnemius* (from the late Miocene of northwestern Venezuela, Rincón *et al.* 2015) is also a probable artefact. This "mylodontoid" species is only known by some isolated hindlimb bones (i.e., both femora, tibiae, and one fibula; see Appendix II; Rincón *et al.* 2015). More fossil remains are needed in order to reliably discern its precise phylogenetic position. The modern three-toed sloth *Bradypus*

is placed between these latter two genera, representing the sister taxon of Eufolivora (Fig. 8.9: node F). The genera *Octomylodon*, *Baraguatherium*, and *Octodontobradys* form a moderately well-supported clade (Fig. 8.9: node I). This group includes early and late Miocene forms, latitudinally spanning South America. Also *Pseudoprepotherium* (i.e., *P. confusum* and *P. venezuelanum*) appears to be monophyletic (Fig. 8.9: node K), and its closest relative is *Urumacotherium* sp., forming a moderately well-supported clade of Miocene taxa from northern South America (Fig. 8.9: node J). All the synapomorphies supporting these associations are discussed below.

As in Gaudin (2004), the most strongly supported group is Scelidotheriinae (Fig. 8.9: node L). Even if the clade Mylodontinae is not recovered in this preliminary analysis (Fig. 8.9), several groups inside Mylodontinae are common to all 87 MPTs (Fig. 8.9: nodes M–U) with varying support values. Among them, Lestodontini (Fig. 8.9: node O) appears with fully resolved internal relationships among the five genera included. In contrast, the only relationships that is consistently recovered among Mylodontini is the placement of *Pleurolestodon acutidens* as sister taxon to all the other Mylodontini (Fig. 8.9: node S), and the monophyly of the group constituted by *Glossotherium tropicorum* and *G. phoenesis* (Fig. 8.9: node U), as in Cartelle *et al.* (2019). In fact, in the strict consensus (Fig. 8.9), large polytomies are observed at the base of Mylodontidae (i.e., at node H) and inside Mylodontini (i.e., at node T).

TNT software allows the automatic detection of unstable taxa, and recovery of the highest number of stable nodes by pruning the lowest number of terminal taxa. Using this "pruning" calculation, a substantial recovery of phylogenetic signal can be obtained by removing the taxa *Orophodon hapaloides* and *Glossotheriopsis pascuali*. This is consistent with the large amount of missing information that these taxa exhibit in the data matrix (see Appendix VI, Data S4). *Orophodon hapaloides* and *Glossotheriopsis pascuali* are each known only by scant remains. *O. hapaloides* is represented by some teeth, mandibular fragments, and isolated autopodial bones (Hoffstetter 1956; see also Appendix II), whereas only a rostral fragment of the cranium with some isolated teeth is known for *G. pascuali* (Scillato-Yané 1976; Appendix II). These two taxa are mainly responsible for the polytomy observed in the strict consensus tree of Figure 8.9. *Orophodon hapaloides* tends to occupy several different positions at the base of Mylodontidae, whereas the variable position of *Glossotheriopsis pascuali* is primarily responsible for the polytomy inside Mylodontini. This is consistent with previous suprageneric attributions proposed for these taxa: *Orophodon* has been considered a generalized "mylodontoid," and has been recently placed into Mylodontoidea as a probable basal member of the clade (Carlini & Scillato-Yané 2004). In contrast, *Glossotheriopsis* has been considered a member of Mylodontinae since its

original description, but without more precise information on its phylogenetic relationships (Scillato-Yané 1976). The present study testifies the need of more complete remains in order to clarify the relationships of these latter taxa.

A second analysis was performed after inactivating *Orophodon hapaloides* and *Glossotheriopsis pascuali*. The analysis of this subset of 38 taxa resulted in 2 MPTs, which differ in the relationships among the *Glossotherium* species. A strict consensus (TL = 1153 steps; CI = 0.551; RI = 0.888) is depicted in Figure 8.10, together with support values at every node.

As expected, the latter analysis recovers a higher number of nodes, as well as higher support values than the previous search (Fig. 8.10). Again, a complete list of the synapomorphies and autapomorphies common to both MPTs is available in Appendix VI, Data S6. In this latter analysis, all the major clades recovered in the previous search (Fig. 8.9) are present and well-supported (Fig. 8.10). This is particularly evident for the groups outside Mylodontidae (i.e., before node H in Figure 8.9 or node 8 in Figure 8.10) which show, in both cases, the same configuration. It is noteworthy that this result is obtained without applying any *a priori* constraint to major nodes such as Pilosa, Vermilingua, and Folivora, as used by Gaudin (2004).

The monophyly of Pilosa, Vermilingua, and Folivora, corresponding to nodes 1, 2, and 4 in Figure 8.10, are corroborated by 15, 19, and four unequivocal synapomorphies, respectively (Appendix VI, Data S6). The majority of these synapomorphies are craniodental features and have been treated in detail by Gaudin (2004). However, some new postcranial features corroborate the monophyly of pilosans, such as the presence of a coraco-scapular foramen (296: 0→1), a spherical shape of the humeral head (299: 0→1), a shallow olecranon fossa (305: 0→1), the absence of the capitular tail on the distal articulation of the humerus (313: 0→1), and a relatively long and anteroposteriorly narrow radius (314: 1→0) and ulna (322: 1→0).

Only a few synapomorphies are recovered at the base of Folivora (Fig. 8.10: node 4) and subsequent nodes (Fig. 8.10: nodes 5–7). The arrangement of taxa at the base of Folivora is corroborated by four (node 4), five (node 5), three (node 6) and two (node 7) unambiguous synapomorphies, respectively (Appendix VI, Data S6). The low number of synapomorphies defining both Folivora (Fig. 8.10: node 4) and Eufolivora (Fig. 8.10: node 6), in comparison to the homologous nodes of Gaudin's (2004) analysis, can be explained in part by the absence of *a priori* constraints in the present analysis, but also by the inclusion of poorly-known taxa such as *Pseudoglyptodon* (McKenna *et al.* 2006) and *Eionaletherium* (Rincón *et al.* 2015). In fact, if *Pseudoglyptodon* and *Eionaletherium* are temporarily deactivated, the number of unambiguous synapomorphies of Folivora and Eufolivora increases to 34 and 25, respectively. Moreover, nodes 6 and 7 are supported by synapomorphies that are exclusive to the hindlimb (i.e., femur,

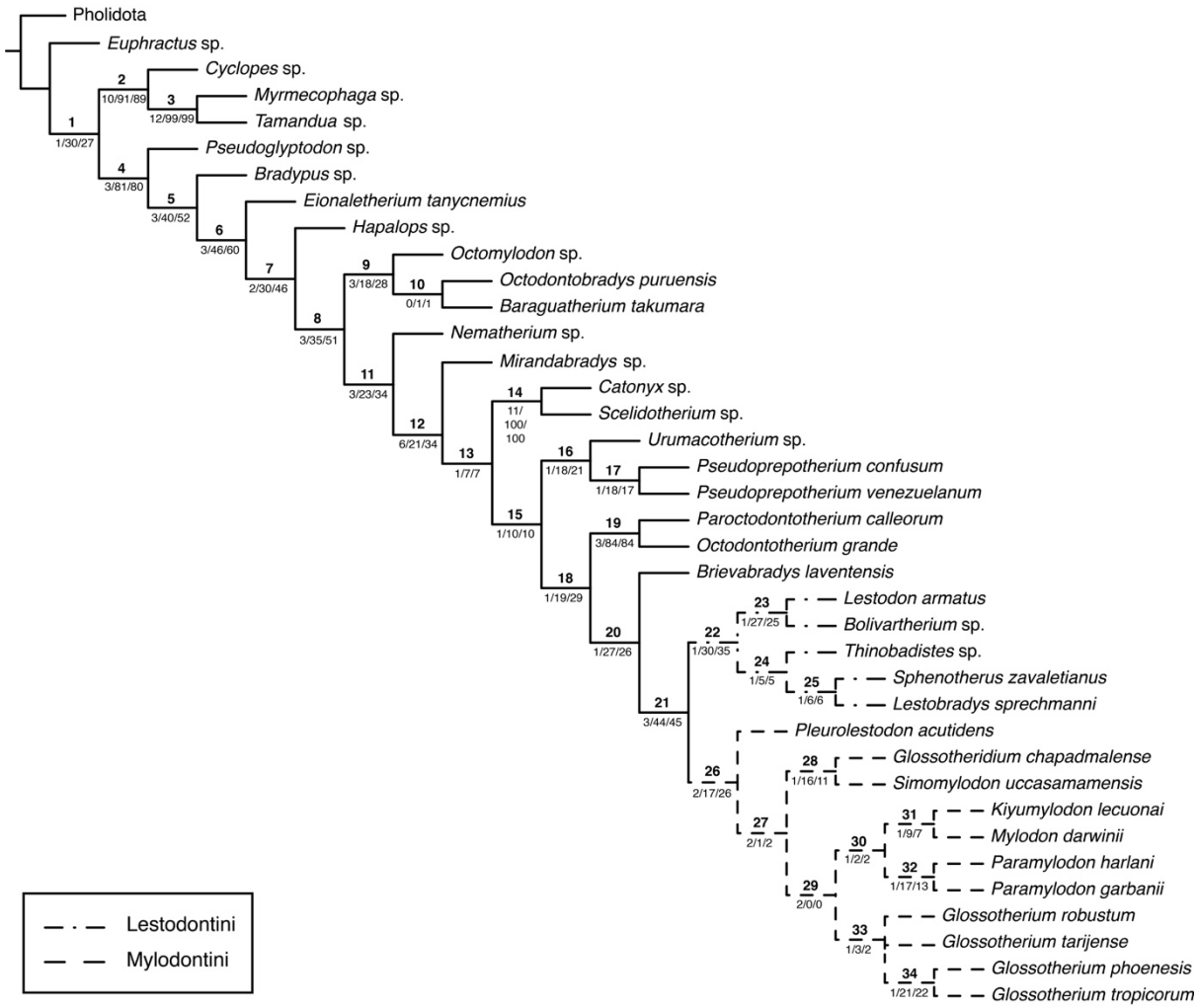

Figure 8.10. Strict consensus (TL = 1153 steps; CI = 0.551; RI = 0.888) of two most parsimonious trees, obtained from the analysis of the pruned matrix (38 taxa and 383 characters), after removing *Orophodon hapaloides* and *Glossotheriopsis pascuali*. Bold numbers are used to define nodes in the text. Numbers underneath each node represent Bremer, bootstrap and jackknife support values, respectively.

tibia and fibula), the only remains that are known for *Eionaletherium tanycnemius* (Rincón *et al.* 2015). In the present analysis, the latter taxon occupies the most basal position among Eufolivora (Fig. 8.10: node 6), due to the primitive features of its femur and tibia, as discussed by Rincón *et al.* (2015). Unambiguous synapomorphies of Eufolivora are: a more mediolaterally wide femur in relation to total length, both in its middle point (344: 0→1) and at the level of the distal articular surface (345: 0→1), and an high mediolateral diameter of the femoral shaft in relation to its anteroposterior depth (348: 0→1). At node 7, the unambiguous synapomorphies are: a short tibia in relation to the anteroposterior length of its proximal epiphysis (357: 0→1), and a highly unequal mediolateral width between the two femoral articular surfaces on the proximal epiphysis of the tibia (361: 0→1). Even if synapomorphies

are limited in number, *Eionaletherium* is consistently recovered as the outgroup of a clade including *Hapalops* and Mylodontidae (Fig. 8.10). However, the fragmented remains of *Eionaletherium* were thought to belong to a general "mylodontoid" by Rincón *et al.* (2015). It is highly probable that the discovery of more remains of the latter taxon would bring about a clarification of its phylogenetic position.

Mylodontidae (Fig. 8.10: node 8) is supported in the present study by nine unambiguous synapomorphies - eight of them are craniodental and only one is postcranial (Appendix VI, Data S1 and S6). This node is more strongly corroborated by the present study than was the case in Gaudin (2004), in which Mylodontidae was supported by six characters, five of which were unambiguous (Gaudin 2004). The unambiguous synapomorphies of Mylodontidae in the present study are: enlargement of the occlusal size of Cf1 (13: 0→2), molariform aspect of the first tooth of both the upper and lower dental series (19: 1→0), Cf1 and cf1 respectively oblique and beveled in their wear surface (20: 1→2), Mf4 showing a T-shaped cross-section in occlusal view (35: 2→7), absence of the medial ridge running along the anterior edge of the coronoid process (46: 1→0), condyle orthogonal to the long axis of the mandible in dorsal view (59: 0→1), mandibular symphysis extending posterior to the first lower tooth (63: 0→1), glenoid fossa well-separated from the epitympanic recess (283: 0→2), and ratio between the anteroposterior lengths of the lateral and medial femoral distal condyles lower than 0.75 (346: 0→1). The low number of mylodontid synapomorphies recovered by Gaudin (2004) was attributed to the position of *Octomylodon* sp. (from the late Miocene of southern Argentina; Scillato-Yané 1977), a poorly-known taxon lacking many traditionally-recognized mylodontid features, as the most basal member of the clade (Gaudin 2004). However, in the present study (Figs 1–3), *Octomylodon* is recovered in a monophyletic group that also includes *Octodontobradys puruensis* (from Brazil, late Miocene–early Pliocene, Santos *et al.* 1996) and *Baraguatherium takumara* (from northwestern Venezuela, early Miocene, Rincón *et al.* 2016), also poorly known taxa. In the strict consensus of Figure 8.10, the latter two taxa also appear to be more closely related to one another than to *Octomylodon*, but their monophyly is too weakly supported to be considered reliable (Fig. 8.10: node 10) and no synapomorphies are recovered for this node (see Appendix VI, Data S6). In contrast, the monophyly of the clade comprising the genera *Octomylodon*, *Octodontobradys*, and *Baraguatherium* is corroborated by five unambiguous synapomorphies, namely: left and right toothrows parallel in occlusal view (4: 1→0), bilobate cross-section of several teeth, such as mf1 (32: 0→5), mf2 (34: 0→6), Mf2 and Mf3 (33: 0→6), and the presence of an elongated mandibular symphysis (62: 2→3). These features are therefore recovered in Miocene taxa

spanning a broad latitudinal range within South America. The peculiarity of these features induced some authors to erect distinct mylodontid subgroups such as Octomylodontinae (Scillato-Yané 1977) and Octodontobradyinae (Santos *et al.* 1996). However, since cranial remains are currently lacking for both *Octodontobradys* and *Baraguatherium*, further data is necessary to properly characterize (and eventually name) the latter clade.

All the other Mylodontidae are grouped together in the various analyses of the present study, forming a monophyletic group (Fig. 8.10: node 11), with *Nematherium* as the most basal taxon. A similar topology was obtained by Gaudin (2004) and recently by Haro *et al.* (2016, 2017). This latter clade is supported by four unambiguous synapomorphies, mostly detected on the mandible, namely: short and broad coronoid process (47: 0→2), short and deep angular process (48: 2→0), posterior border of the condyloid process almost vertical in lateral view (52: 0→1), and palate moderately extended posteriorly (124: 0→1). The poorly known genus *Mirandabradys* (from middle–late Miocene sediments of northwestern Venezuela; Carlini *et al.* 2006) is recovered at Node 12 (Fig. 8.10), representing the sister group of the clade including all the Scelidotheriinae and Mylodontinae of the present study (Fig. 8.10: node 13). However, node 12 is consistently better-supported than node 13 (Fig. 8.10). This, again, may be due to the scant knowledge of *Mirandabradys*, which consists of a highly diagenetically modified skull and a few postcranial remains (Carlini *et al.* 2006). In fact, the initial taxonomic assignment of *Mirandabradys* was as a general "mylodontoid" by Carlini *et al.* (2006), and the specimens were difficult to code for many features in the present study (see Appendix VI, Data S4). Rincón *et al.* (2015), analyzing a mylodontid matrix exclusively built on femoral features, recovered the genus *Mirandabradys* together with *Pseudoprepotherium venezuelanum* (from the late Miocene of Venezuela and Brazil; Collins 1934; Hirschfeld 1985) as sister taxa, suggesting that the phylogenetic position of *Mirandabradys* may be prone to change if better-preserved craniodental materials are found. The support values of nodes 12 and 13 (Fig. 8.10), suggest that *Mirandabradys* is more derived than *Nematherium*, but also that stronger affinities of *Mirandabradys* with the Mylodontinae cannot currently be ruled out (see also Discussion).

The monophyly of Scelidotheriinae (Fig. 8.10: node 14) is strongly supported, in accordance with the previous analyses performed by Gaudin (2004) and Haro *et al.* (2016, 2017). *Scelidotherium* (from Argentina, Pliocene–Pleistocene; McDonald 1987) and *Catonyx* (from southern South America, Pleistocene; McDonald 1987), the two scelidotheres considered in this work, constitute a monophyletic group supported by 49 unambiguous synapomorphies, 17 of which are postcranial. Postcranial features that are unique to these scelidotheres include:

humeral trochlea deeper anteroposteriorly than the capitulum in ventral view (310: 0→1), short and broad third metacarpal of the manus (341: 1→2), reduced contact between fifth metacarpal and unciform (342: 0→1), mediolaterally broad femur both at midshaft (344: 1→2) and at the distal femoral articulation (345: 1→2) in relation to total femoral length, large intertrochanteric width in relation to total femoral length (347: 1→2), femur relatively broad mediolaterally and narrow anteroposteriorly at midshaft (348: 1→2), femoral head sessile (351: 0→1) and lacking a well-developed sulcus in anterior view (352: 0→1), absence of the third trochanter of femur (353: 1→0), proximal epiphysis of tibia anteroposteriorly narrow in relation to total tibial length (357: 1→2), astragalus more elongated proximodistally than anteroposteriorly (367: 0→2), extended contact between the ectocuneiform and cuboid in lateral view (376: 1→0), and co-ossified proximal and intermediate phalanges of the third digit of the pes (381: 0→1).

Mylodontinae (Fig. 8.10: node 15) is a monophyletic clade that represents the sister group of Scelidotheriinae (Engelmann 1985; Gaudin 2004). Even if support values are quite low for this clade (Fig. 8.10: node 15), the present analysis recovers 16 unambiguous synapomorphies for this node, nine of which are craniodental, with the remaining seven derived from the postcranial skeleton. These are: further enlargement of the occlusal size of Cf1 (13: 2→1), mediolateral inclination of the condylar articular surface on the mandible (60: 0→1), increase in the mediolateral width of mandibular symphysis (67: 0→1) and the snout (86: 1→2), depression of the snout region relative to the braincase in lateral view (91: 0→1), presence of a fossa lateral to external nares on the anterior edge of maxilla (103: 0→1), palate elongate and strongly widened anteriorly (122: 1→3), dorsoventral depth of occipital condyles slightly exceeds mediolateral width in posterior view (191: 2→1), well-developed medial groove of fenestra cochleae (248: 0→1), lateral and medial epicondyle of humerus equally expanded in anterior view (308: 0→1), posterior border of radius roughly straight in lateral view (316: 1→0), anterior border of radius not inflected medially in anterior view (318: 1→0), obtuse angle between olecranon and posterior border of the ulna in lateral view (323: 1→2), lack of contact between second metacarpal and magnum in dorsal view of articulated manus (339: 1→0), third metacarpal mediolaterally narrow relative to total length (341: 1→0), and convex contour of the sustentacular facet of the astragalus (371: 0→1).

The two species of *Pseudoprepotherium* currently known, *P. confusum* (Colombia, middle Miocene; Hirschfeld 1985) and *P. venezuelanum*, constitute a monophyletic clade (Fig. 8.10: node 17). They share two unambiguous apomorphies: the ascending ramus of the mandible partially

covers the posteriormost teeth of the mandible in lateral view (40: 0→1), and a significant elongated mandibular symphysis relative to total mandibular length (62: 2→3). According to the results of the present study, the closest relative of *Pseudoprepotherium* is *Urumacotherium* (Peru, Brazil and Venezuela, middle Miocene to early Pliocene; Bocquentin-Villanueva 1984; Negri *et al.* 2010; Tejada-Lara *et al.* 2015) (Fig. 8.10: node 16). This latter genus, widely distributed both geographically and chronologically, share with *Pseudoprepotherium* four unambiguous synapomorphies: condyloid process of the mandible inclined posterodorsally in lateral view (52: 1→0), distal femoral articulation mediolaterally narrow relative to total femoral length (345: 1→0), proximal and distal femoral epiphyses on the same transverse plane (354: 1→0), and a flat surface contour of the astragalar discoid process in lateral view (369: 0→1 [a convergence on the Mylodontini, see below]).

All the remaining Mylodontinae constitute a monophyletic group (Fig. 8.10: node 18) supported by 10 unambiguous craniodental synapomorphies. These include: first tooth of both upper and lower dental series caniniform in shape (19: 0→1), loss of fossa anterior to Cf1 (22: 1→0), Mf1 recurved posteriorly (28: 0→1), mandibular symphysis very wide transversely at midpoint (67: 1→2), lateral edge of symphyseal spout not everted (71: 1→0), small lacrimal foramen (142: 2→0), elongation of the zygomatic process of squamosal (168: 1→2), occipital condyles not conspicuously elongated anteroposteriorly in ventral view (195: 1→0), well-developed lateral exposure of fenestra cochleae (247: 0→1), and stylomastoid foramen located directly anterior to tympanohyal/stylohyal fossa (258: 1→2).

Paroctodontotherium calleorum (Bolivia, late Oligocene; Shockey & Anaya 2011) and *Octodontotherium grande* (Argentina, late Oligocene; Ameghino 1894; Hoffstetter 1956; Pujos & De Iuliis 2007; Shockey & Anaya 2011) form a well-supported clade (Fig. 8.10: node 19) whose monophyly is corroborated by six unambiguous craniodental synapomorphies. These are: Cf1 is the smallest tooth of the upper toothrow (13: 1→0 [a convergence on the Mylodontini, see below]), bilobate cross-section of both Mf2 and Mf3 (33: 0→6), skull moderately short and wide (82: 2→3), braincase low and broad (83: 0→1), mediolaterally broad snout relative to total cranial length (86: 2→3), and temporal lines converging but not contacting on dorsal midline of braincase (93: 0→1).

The enigmatic and poorly known *Brievabradys laventensis* (Colombia, middle Miocene; Villarroel 2000) is recovered at Node 20 (Fig. 8.10), and shares only three unambiguous craniodental synapomorphies with Mylodontini and Lestodontini. These include: Cf1 positioned right at the anterior edge of maxilla in occlusal view (21: 1→0), trigonal cross-section

of cf1 (30: 0→1), and mandible fairly short and deep (37: 2→4). Despite the scarce material available for *Brievabradys laventensis* (see Chapter 5, Appendix II; Villarroel 2000), in both analyses this taxon is reliably recovered as the sister group of the clade comprised by Mylodontini and Lestodontini (Fig. 8.9: node N; Fig. 8.10: node 21). There are five unambiguous synapomorphies supporting the latter node, all of them craniodental features: long axis of posterior molariform teeth oblique to long axis of toothrow (16: 0→1), Mf2 and Mf3 with lobate cross-sections, and with anteroposterior length greater than transverse width (33: 0→4), profile of anterior edge of mandibular symphysis convex in lateral view (65: 1→0), temporal fossa flat anteroposteriorly and dorsoventrally (92: 0→1), and descending process of the jugal wide in lateral view (159: 1→0).

Both Lestodontini (Fig. 8.10: node 22) and Mylodontini (Fig. 8.10: node 26) are also well-supported, with eight and seven unambiguous synapomorphies corroborating their monophyly, respectively (see Appendix VI, Data S6). Moreover, as already observed, the monophyly of both clades is retrieved in all analyses, even without the pruning procedure described above (Figs 8.9–8.10).

Unambiguous synapomorphies of Lestodontini include six craniodental features: Cf1/cf1 with oblique/nearly vertical wear facet (20: 2→0), intermediate development of both the coronoid process (47: 2→1) and the angular process (48: 0→1) (i.e., both mandibular processes are neither elongate and narrow nor short and broad), moderate length of the mandibular condyloid process (51: 0→1), mandibular condyle extending both medially and laterally in dorsal view (57: 2→1), and mandible with weakly developed fossa posterior to cf1 (76: 0→1). There are also two unambiguous hindlimb synapomorphies that serve to diagnose Lestodontini: orthogonal or acute odontoid process-discoid angle of the astragalus (368: 1→2), and fusion of the mesocuneiform and second metatarsal (377: 0→1). Relationships inside Lestodontini are less strongly supported, but are nonetheless fully resolved in both the analyses reported in the present study (Figs 8.9–8.10). These relationships are defined by unambiguous synapomorphies, all of which are craniodental traits (see Appendix VI, Data S1 and S6). *Lestodon* (Argentina, Bolivia and Uruguay, Pliocene–Pleistocene; Czerwonogora & Fariña 2013) and *Bolivartherium* (northwestern Venezuela, late Miocene–early Pliocene; Carlini *et al.* 2006) constitute a monophyletic group (Fig. 8.10: node 23), defined by four unambiguous synapomorphies: the presence of an elongated diastema between Cf1 and Mf1 (6: 0&1→2), Cf1 and cf1 displaced laterally relative to the molariform toothrow (24: 0→1), presence of a well-developed buccinator fossa of maxilla (106: 1→2), and strong development of the postorbital

process of the frontal (175: 1→2). All the other lestodontines considered in this analysis are grouped together (Fig. 8.10: node 24), with *Sphenotherus* (Argentina, late Miocene; Ameghino 1891b) and *Lestobradys* (Uruguay, late Miocene; Rinderknecht *et al.* 2010) more closely related to each other than either is to *Thinobadistes* (southeastern North America, late Miocene; Webb 1989) (Fig. 8.10: node 25). Two unambiguous synapomorphies serve to diagnose Node 24: the presence of a moderate diastema between Mf1 and Mf2 (25: 0→1), and the relatively shallow and elongate shape of the mandible (37: 4→2). The affinity of *Sphenotherus* and *Lestobradys* is only supported by a single unambiguous synapomorphy, which is also a convergence on the Mylodontini, namely the irregularly lobate cross-section of mf2 (34: 0→4).

The monophyly of Mylodontini (Fig. 8.10: node 26) is corroborated by seven unambiguous synapomorphies, two of which are postcranial, including: Cf1 is the smallest tooth of the upper toothrow (13: 1→0), Mf2 and Mf3 with square outline in cross-section (32: 0→3), irregularly lobate cross-section of mf2 (34: 0→4), presence of an oblique medial ridge on the ascending ramus of the mandible (44: 0→1), lateral and medial palatal processes of maxilla of equivalent anterior extent (111: 1→0), flat surface contour of the astragalar discoid process in lateral view (369: 0→1), and the presence of osteoderms (383: 0→1). Among Mylodontini, *Pleurolestodon* (Argentina, late Miocene; Rovereto 1914) is recovered as the most basal taxon of the clade in both analyses (Figs 8.9–8.10). In fact, all the other Mylodontini constitute a monophyletic clade (Fig. 8.10: node 27) supported by three unequivocal synapomorphies: ovate cross-section of cf1 (30: 1→0), flat anterior edge of mandibular symphysis in dorsal view (70: 1→0), and the presence of a contact between the ectotympanic and the pterygoid (211: 0→1).

Glossotheridium chapadmalense (Argentina, early Pliocene; Kraglievich 1925) and *Simomylodon uccasamamensis* (Bolivia, late Miocene–Pliocene; Saint-André *et al.* 2010) together form a moderately well-supported monophyletic group (Fig. 8.10: node 28). The relationship of these two species is corroborated by four unambiguous synapomorphies: condyloid process of mandible oriented posterodorsally in lateral view (52: 1→0), mandibular symphysis anteroposteriorly short (62: 2→1), descending process of jugal strongly tapering toward the tip (151: 0→1), and greatly elongate zygomatic process of squamosal relative to total cranial length (168: 2→3).

More derived Mylodontini are grouped into another clade (Fig. 8.10: node 29). This node shows low support values but is defined by eight unequivocal synapomorphies, all postcranial features. These are: well-developed supinator crest of humerus in anterior view (303: 1→2), humeral lateral epicondyle more expanded than the medial epicondyle (308: 1→2), straight

anterior border of radius in lateral view (317: 0→1), radial notch on the ulna occupying only part of the radial fossa (325: 0→1), proximal epiphysis of tibia mediolaterally wide relative to total length of tibia (359: 1→2), single large depression for the tibial tendons on the posterior distal tibial surface (365: 1→2), absence of astragalar sulcus tali (370: 0→1), and absence of a detached sustentacular process of the calcaneum (375: 0→1).

This latter clade is further divided into a dichotomy, leading on one side to a group including the genera *Kïyumylodon* (Uruguay, late Miocene, Rinderknecht *et al.* 2007), *Mylodon* (southern South America, Pleistocene, Kraglievich 1934; Brandoni *et al.* 2010) and *Paramylodon* (Central and North America, Pliocene–Pleistocene, McDonald 1995; McAfee 2009) (Fig. 8.10: node 30) and, on the other, to the genus *Glossotherium* (South America, Pleistocene, McAfee 2009), also recovered as a monophyletic group (Fig. 8.10: node 33).

Synapomorphies that serve to diagnose the former node include: skull elongate and narrow in shape, with maximum width of braincase less than 25% of total cranial length (82: 2→0), lateral and medial rami of premaxilla nearly equivalent in size (116: 0→1), occipital condyles moderately well separated, with distance between condyles between 5-10% of total cranial length (186: 0→1), butterfly shaped basisphenoid (198: 1→2), and anteroposteriorly elongate stapedius fossa (245: 0→1). Two other monophyletic groups are included in the latter clade: in the former *Kïyumylodon* and *Mylodon* are grouped as sister taxa (Fig. 8.10: node 31), and their relationship is supported by three unequivocal synapomorphies, whereas the other links the two *Paramylodon* species (Fig. 8.10: node 31), and is corroborated by one ambiguous and one unambiguous synapomorphy. The three apomorphies shared by *Kïyumylodon* and *Mylodon* relate mainly to the shape of mf1 and mf2, which are both ovate anteroposteriorly in cross-section (32: 3→0; 34: 4→0), as well as the partial covering of the posteriormost lower tooth by the coronoid process of the mandible in lateral view (40: 0→1). According to the present study, the only two synapomorphies that serve to diagnose the genus *Paramylodon* are: dorsoventral depth of occipital condyles slightly greater than mediolateral width in posterior view (191: 0→1 [ambiguous]) and the absence of a venous sinus in the foramen magnum (271: 1→0 [unambiguous]).

The genus *Glossotherium* (Fig. 8.10: node 33) is diagnosed by three unambiguous synapomorphies and one ambiguous synapomorphy. The former include: intermediate depth of mandible (37: 4→3), auditory bulla poorly ossified (213: 1→2), and intermediate shape of third metacarpal (neither elongate and narrow nor short and broad, 341: 0→1). The ambiguous feature that helps define the genus *Glossotherium* is the reduction in size of the entotympanic

(219: 1→0). However, whereas this feature is invariably observed in *G. tarijense* and *G. tropicorum*, it shows intraspecific variation in both *G. robustum* (Boscaini *et al*. 2018a) and *G. phoenesis* (Cartelle *et al*. 2019) (see also Appendix VI, Data S4). The relationships among the four species of *Glossotherium* are still unresolved. In fact, the differences between the two MPTs obtained in the pruned analysis of the present study (Fig. 8.10) are related to different arrangements of the species inside this genus (Fig. 8.11). In one, *G. robustum* and *G. tarijense* represent progressive sister taxa to a group uniting *G. phonenesis* and *G. tropicorum* (Fig. 8.11A). In the other case, *G. robustum* and *G. tarijense* are grouped together in a monophyletic clade that is the sister group of (*G. phonenesis* + *G. tropicorum*) (Fig. 8.11B). Both scenarios are equally parsimonious, and additional anatomical data, especially for *G. tarijense*, are likely necessary to resolve this conflict. However, the phylogenetic relationship of *G. tropicorum* and *G. phoenesis* is more reliable, since this relationship is recovered in all the analyses of the present study (Figs 8.9–8.11). These two species have been recently reviewed by De Iuliis *et al*. (2017) and Cartelle *et al*. (2019) and joined in a monophyletic group by the latter study. Based on the results of the present analyses (Figs 8.9–8.11), the rounded profile of the anterior edge of the mandibular symphysis is the only unambiguous synapomorphy for the node linking *G. tropicorum* and *G. phoenesis*. Three other ambiguous synapomorphies that might also diagnose this clade include: presence of a moderate diastema between Mf1 and Mf2 (25: 0→1), intermediate development of the coronoid process (47: 2→1), and occipital condyles well-separated from condyloid foramina (194: 1→2).

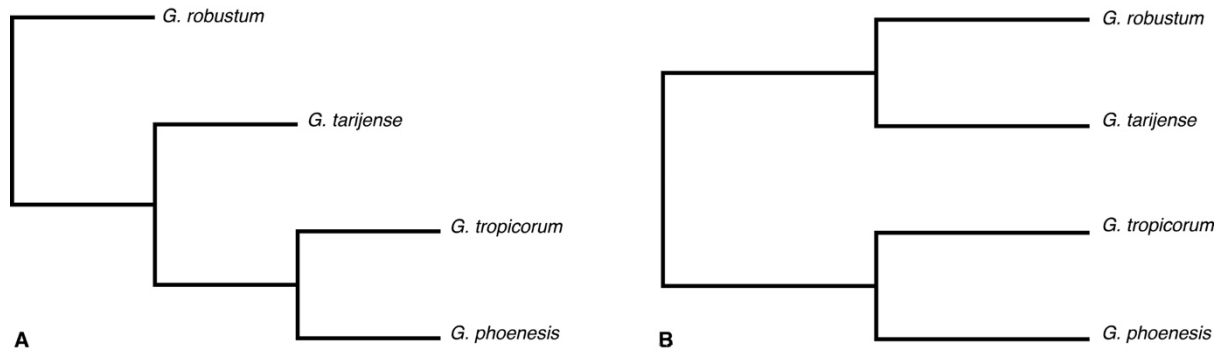

Figure 8.11. Equiparsimonious scenarios for the relationships among the *Glossotherium* species, obtained from the analysis of the pruned matrix (38 taxa and 383 characters), after removing *Orophodon hapaloides* and *Glossotheriopsis pascuali*.

8.2 DISCUSSION

The present analysis constitutes the first attempt to clarify the phylogenetic relationships among Mylodontidae, based on morphological features of the whole skeleton. Also, the inclusion of several new mylodontid taxa allows novel testing of their phylogenetic positions, unexplored in prior studies, further enhancing the value of this, the first species-level phylogeny of the Mylodontinae.

The set of postcranial features included in this study (i.e., characters 287–383) consistently help in defining many aspects of mylodontid phylogeny. In fact, if the postcranial features are removed from the analyses (together with the taxon *Eionaletherium tanycnemius*, that is known only from postcranial remains; Rincón *et al.* 2015), some of the relationships previously discussed lack significant resolution, as illustrated in Figure 8.12. This figure shows a strict consensus of six MPTs (TL = 905 steps; CI = 0.555; RI = 0.902) that resulted from an analysis in which *Eionaletherium tanycnemius* and the postcranial characters were omitted.

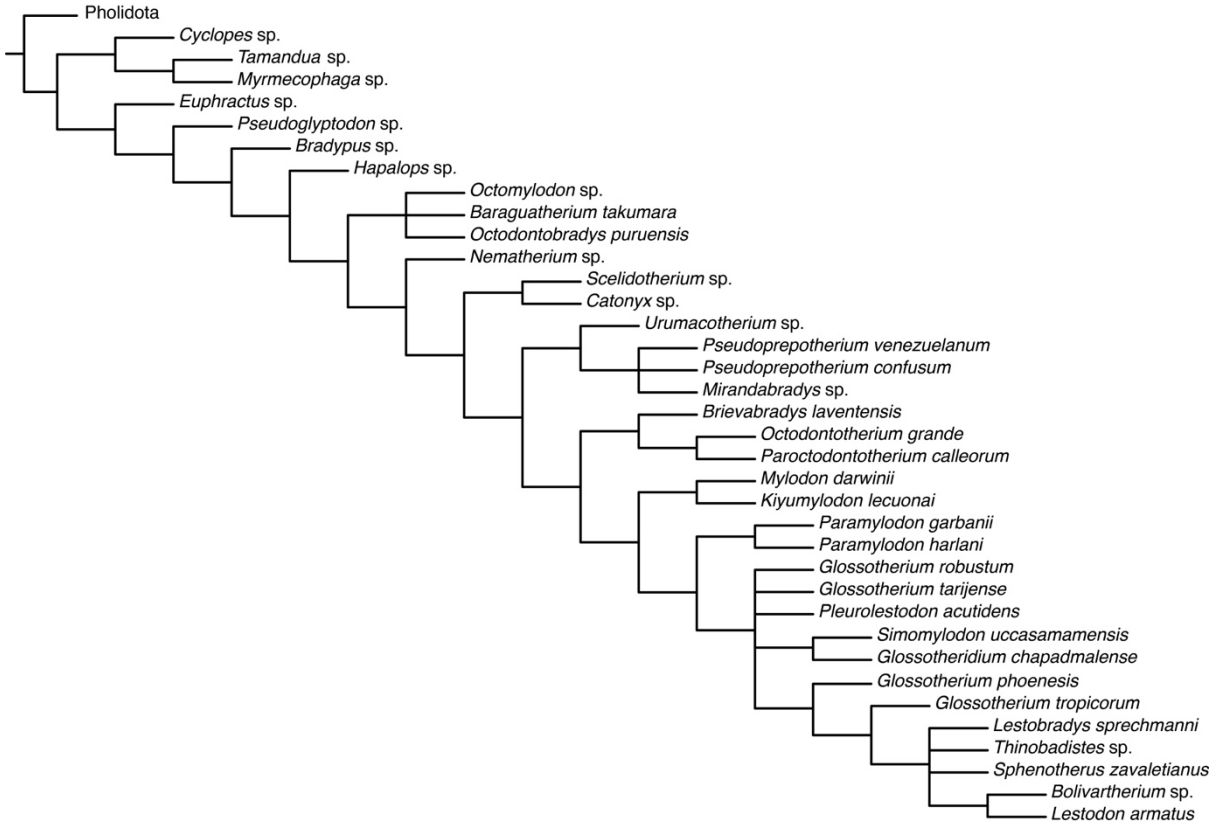

Figure 8.12. Strict consensus (TL = 905 steps; CI = 0.555; RI = 0.902) of six most parsimonious trees, obtained from the analysis of the craniodental set of features, after the inactivation of *Eionaletherium tanycnemiu*s, which is only known from postcranial remains (37 taxa and 286 characters).

As one might expect, the results illustrated in Figure 8.12 are quite similar to those obtained by the craniodental analysis of Gaudin (2004), and yet important differences are observed. For example, in Figure 8.12, Pilosa appears not to be monophyletic (as expected from the lack of both the *a priori* constraints and the postcranial data), and the relationships among Mylodontinae are significantly less resolved. Even if several clades inside Mylodontidae are still recovered after the removal of *Eionaletherium* and the postcranial characters, such as [*Octomylodon* sp. + *Baraguatherium takumara* + *Octodontobradys puruensis*], [*Octodontotherium grande* + *Paroctodontotherium calleorum*], [*Paramylodon harlani* + *Paramylodon garbanii*], [*Simomylodon uccasamamensis* + *Glossotheridium chapadmalense*], and [*Bolivartherium* sp. + *Lestodon armatus*], other relationships show substantial changes. One of them involves the phylogenetic position of *Mirandabradys*, which is recovered in a monophyletic group including *Pseudoprepotherium* and *Urumacotherium* in Figure 8.12, quite distinct from its position as sister to Scelidotheriinae + Mylodontinae as illustrated in Figure 8.10. This may attest to a certain degree of affinity between these three taxa from the Neogene of tropical northwestern South America. Another difference is the phylogenetic position of *Brievabradys laventensis*, which shows a close relationship, on the basis of craniodental data, with the Desedean species *Octodontotherium grande* and *Paroctodontotherium calleorum* (Fig. 8.12), but occupies a more derived position than those two taxa when postcranial data is included (Fig. 8.10). Again, these incongruences among results reflect the need for more fossil remains of these poorly characterized taxa, and consequently more paleontological efforts in the central and northern latitudes of South America.

However, the greatest differences between the results obtained from analysis of the total matrix and analysis of the craniodental characters only (Figs 8.10, 8.12) lie within Mylodontinae. When analyzing craniodental features alone, the genus *Glossotherium* is no longer monophyletic (Fig. 8.12). Moreover, Mylodontini and Lestodontini are both monophyletic, but the latter is nested inside the former, thus constituting the most derived mylodontid clade (Fig. 8.12). This result is similar to that of Gaudin (2004), and could be related to the peculiar craniodental modifications achieved by lestodontines during their evolutionary history (e.g., Gervais 1855; Webb 1989).

The inclusion of the postcranial features in the present study provides increased resolution of the phylogenetic relationships inside Mylodontinae, especially for late Miocene–Pleistocene taxa (Fig. 8.13). The resolution of these relationships has always been among the most problematic issues in sloth phylogenetic studies, in part due to the wide morphological range encompassed by *Paramylodon* and *Glossotherium* (Engelmann 1985; MacAfee 2009), as well as other late Miocene–Pleistocene mylodontines (Gaudin 2004). This was reflected in Gaudin's

(2004) phylogenetic results, which failed to unambiguously resolve relationships in the section of the tree occupied by late Miocene–Pleistocene mylodontines.

The present result is consistent with the hypotheses of Engelmann (1985) on the probable strong affinity between *Paramylodon* and *Mylodon*, both showing a tendency toward the reduction of the dentition, with the loss, partial or definitive, of Cf1s (Engelmann 1985; McDonald 1995). Moreover, Engelmann (1985) predicted, on the basis of observations of the whole skeleton of certain mylodontines, that *Paramylodon*, *Glossotherium*, and *Mylodon* might be more derived than the lestodontines, the latter maintaining some primitive features, mainly in their postcranial anatomy (Engelmann 1985). This observation was supported and extended by Webb (1989), who also considered the lestodontines to be a monophyletic group. As detailed below, many observations of the latter author have been confirmed by the present parsimony-based analysis.

Lestodontini and Mylodontini show opposite trends in the development of their upper caniniforms (Webb 1989). The large occlusal size of Cf1 is recovered as a synapomorphy of Mylodontinae (Fig. 8.10: node 15), and a true caniniform morphology for Cf1 is one of the synapomorphies that serve to diagnose Node 20 (i.e., *Brievabradys* + Mylodontini + Lestodontini). Both features are therefore plesiomorphic for both Lestodontini and Mylodontini. Lestodontines later experienced a sharpening of Cf1s, as the almost vertical wear facet of Cf1/cf1 is recovered as a synapomorphy of the clade (Fig. 8.10: node 22). In *Lestodon* and *Bolivartherium* (Fig. 8.10: node 23), Cf1s are also displaced anteriorly and laterally from the molariform toothrow by a long diastema. In contrast, Mylodontini went through a reduction of the upper caniniforms, a feature that represents a synapomorphy of the latter clade. In some species, such as *Mylodon darwinii* and *Paramylodon harlani*, a partial or definitive loss of Cf1s is recorded.

Lestodontini are also characterized by two synapomorphies of the hindlimb: the fusion between the mesocuneiform and the second metatarsal (Webb 1989), and the presence of an orthogonal or acute odontoid process-discoid angle on the astragalus. The former feature is typical of *Thinobadistes* and *Lestodon* (Webb 1989) but it is occassionally observed also in *Paramylodon harlani* (Stock 1925). The latter feature, the angle between the odontoid process and the discoid, is orthogonal-acute in Lestodontini, whereas it is generally moderately obtuse (between 90° and 115°) in Mylodontini. Among Mylodontini, an exception is represented by *Paramylodon garbanii*, in which the odontoid process-discoid angle is wider than 115°, thus maintaining the plesiomorphic condition of Mylodontidae. The astragalus of Mylodontini also shows a flat surface contour of the astragalar discoid process, observed in lateral view. This surface is proximally convex in Lestodontini, a primitive condition for Mylodontidae.

Mylodontini are also characterized by the presence of osteoderms, a feature that independently evolved in this clade and appears not to be plesiomorphic for Pilosa (McDonald 2018). In fact, among pilosans, osteoderms have been reliably detected only among Mylodontidae (McDonald 2018; Cartelle *et al*. 2019). Based on the present dataset, the presence of osteoderms appears to be a synapomorphy of Mylodontini and, outside this clade, they have only been reported for the scelidothere *Valgipes bucklandi* (Brazil, Pleistocene; Cartelle *et al*. 2009; 2019). The probable earliest occurrence of osteoderms is from *Pleurolestodon*, a late Miocene taxon from Argentina (Rovereto 1914). Dermal ossicles are reported for the latter taxon by Rovereto (1914), but are currently missing from the vertebrate paleontological collection of MACN (Curator A. Kramarz, pers. comm.). The earliest well-documented osteoderms in mylodontids are those of *Simomylodon uccasamamensis*, which have been recovered in association with an almost complete skull (MNHN-Bol V 3726) from the early Pliocene of Casira (southern Bolivia). The presence of dermal ossicles is invariably reported for later well-known mylodontines, such as the genera *Paramylodon*, *Glossotherium*, and *Mylodon*, but also for *Ocnotherium*, *Oreomylodon*, and *Mylodonopsis*, whose phylogenetic affinities are still under study (McDonald 2018; Cartelle *et al*. 2019). Osteoderms have never been detected in any other mylodontid lineage (with the exception of *Valgipes*, as noted above), including lestodontine sloths (Webb 1989; McDonald 2018; Cartelle *et al*. 2019).

Eight postcranial synapomorphies serve to diagnose node 29 (Fig. 8.10), strongly contributing to the definition of the phylogenetic relationships among Mylodontini. In fact, when postcranial features are removed from the analysis (Fig. 8.12), the collapse of the latter node appears to be mainly responsible for the polytomy observed inside Mylodontini. The synapomorphies recovered at node 29 are located on several elements of the skeleton, including the humerus, radius, ulna, tibia, astragalus, and calcaneum, all of which retain more primitive morphologies in *Pleurolestodon acutidens*, *Glossotheridium chapadmalense*, and *Simomylodon uccasamamensis*. However, in *P. acutidens* and *G. chapadmalense*, the appendicular anatomy is known only for an astragalus and a humerus respectively, whereas almost the entire postcranial anatomy is observable in *S. uccasamamensis*. At present, *S. uccasamamensis* can be therefore considered the best known early member of Mylodontini.

Postcranial transformations occurring at node 29 include, on the humerus, an expansion of the lateral epicondyle and the presence of an almost vertical supinator crest. The radius of the most derived Mylodontini displays a blockier structure, lacking an expansion of its anterior margin in lateral view. Also, the tibia shows a single large depression for tendons on the posteromedial margin of the distal epiphysis, whereas the tibial proximal epiphysis is relatively

wider mediolaterally. In the pes, both the sustentacular process of the calcaneum and the sulcus tali of the astragalus disappear at node 29. This latter feature, first noticed by Gervais (1873), has been long considered useful for separating lestodontines and mylodontines, in combination with the development of caniniforms (e.g., Kraglievich 1926; Webb 1989; Rinderknecht *et al.* 2010). However, in the early members of Mylodontini, *Pleurolestodon* and *Simomylodon*, the astragalo-calcaneal contact is still clearly separated into its ectal and sustentacular facets (Saint-André *et al.* 2010). Consequently, this feature is not reliable, if taken alone, to assign fossil remains to either one of the two clades. According to the present data, the reduction of the size of the caniniforms is not coupled with the fusion of the ectal and a sustentacular astragalar facets - the former (Fig. 8.10: node 26) was achieved prior to than the latter (Fig. 8.10: node 29). The complete fusion of the two calcaneal facets on the astragalus is observed in the genera *Mylodon*, *Paramylodon*, *Mylodonopsis*, and *Glossotherium* (Owen 1842; Stock 1925; Robertson 1976; Cartelle 1991; McAfee 2016).

The present phylogenetic study offers a new and more complex scenario for the evolutionary history of mylodontid sloths than those proposed in recent years (e.g., Gaudin 2004; Varela *et al.* 2018). For example, the Miocene genera *Octomylodon*, *Baraguatherium*, and *Octodontobradys* are recovered as a monophyletic group at the base of Mylodontidae (Fig. 8.13). *Mirandabradys*, from the Miocene of Venezuela, is recovered as the sister taxon to Scelidotheriinae + Mylodontinae (Fig. 8.13). However, a certain degree of affinity of *Mirandabradys* with the mylodontines *Urumacotherium* and *Pseudoprepotherium* from the Miocene of northwestern South America may be indicated based on craniodental data (Fig. 8.12). Despite their early age, the sister taxa *Paroctodontotherium* and *Octodontotherium* share more derived features, forming a monophyletic clade of late Oligocene age (Fig. 8.13). *Brievabradys,* from the middle Miocene of Colombia, is the sister taxon of the lestodontine and mylodontine sloths (Fig. 8.13).

As appears evident from the phylogenetic relationships recovered in this study, in association with the chronostratigraphic and paleobiogeographic data (Fig. 8.13; Appendix VI, Table S7), taxa from northern South America occupy basal positions for Mylodontidae (i.e., *Octodontobradys*, *Baraguatherium*), Mylodontinae (i.e., *Urumacotherium*, *Pseudoprepotherium*), and also represent the closest sister group to Mylodontini and Lestodontini (i.e., *Brievabradys*). These taxa

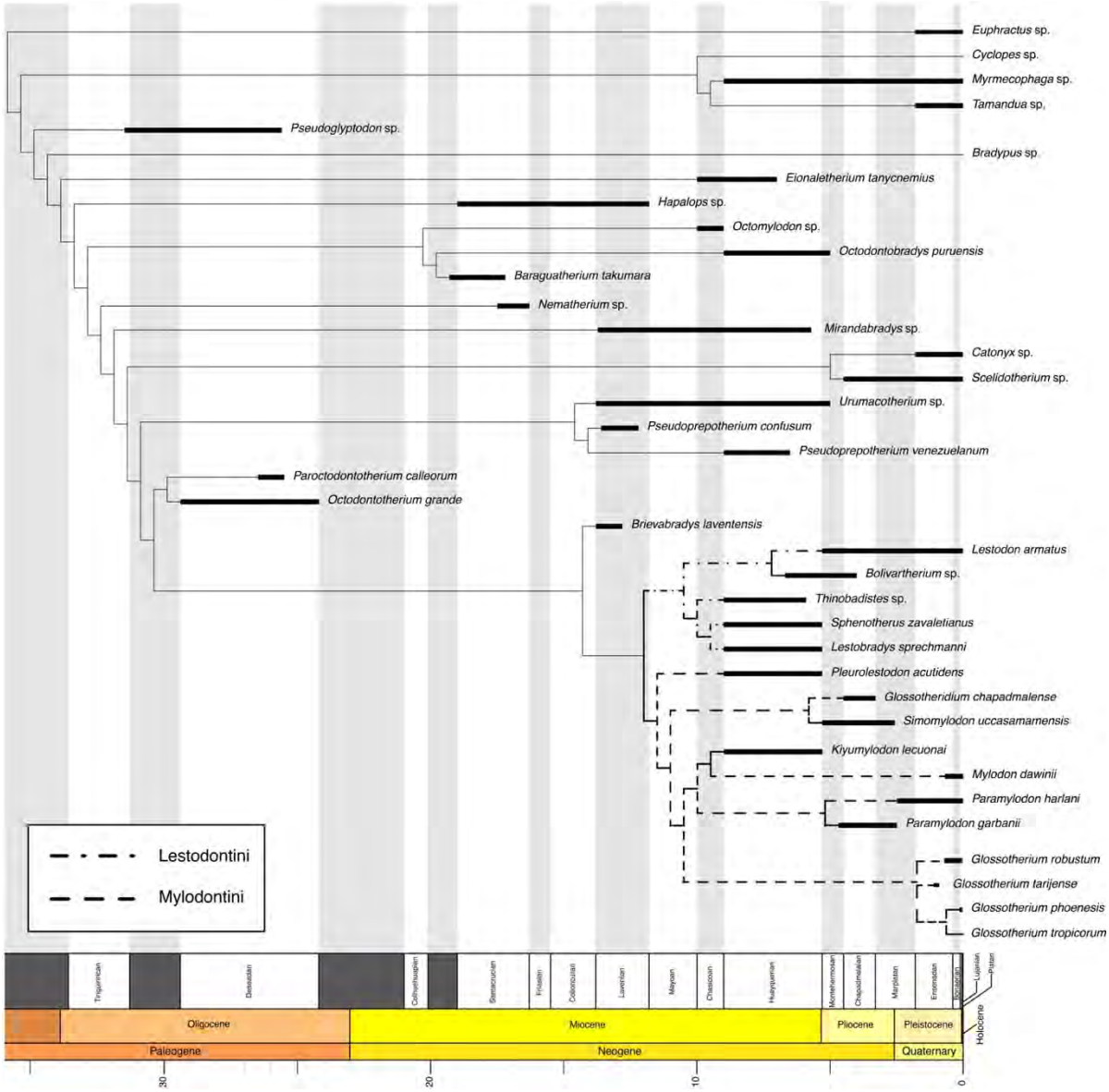

Figure 8.13. Strict consensus of figure 8.10 illustrated in chronostratigraphic context, following the known stratigraphic ranges of the taxa (for further information see Appendix VI, Tables S4 and S5).

attest to the presence of early mylodontid members all over South America, starting from the early Miocene.

With the exception of *Mirandabradys*, the phylogenetic position of all the basal mylodontids discussed here (i.e., *Octomylodon*, *Baraguatherium*, *Octodontobradys, Urumacotherium*, *Pseudoprepotherium, Paroctodontotherium*, *Octodontotherium,* and *Brievabradys*) were tested by Varela *et al.* (2018) based on Bayesian inference methods. The latter authors recovered the majority of these taxa in a single monophyletic group, tentatively identified as the Orophodontinae (Varela *et al.* 2018). However, the low probability associated with the basal node of Orophodontinae (Varela *et al.* 2018: fig. 1) suggests that the latter clade may not represent a natural group. Moreover,

Orophodontinae is not recovered when the matrix assembled by Varela *et al.* (2018) is analyzed using parsimony-based methods, much like the results from the present study (Fig. 8.10).

Varela *et al.* (2018) obtained two monophyletic clades similar to the Mylodontini and Lestodontini of the present study, but with the genus *Mylodon* external to both (Varela *et al.* 2018: fig. 1). An analogous result has been also recently obtained by Cartelle *et al.* (2019: fig. 15). The first phylogenetic study to recover both Mylodontini and Lestodontini as sister clades is that of Saint-André (1994), but with *Pleurolestodon* as their sister taxon. Saint-André (1994) is also the first work in which the term Mylodontini is used extensively. Even though Saint-André (1994) does not formally establish the taxon, it has been subsequently adopted by some authors (e.g., Saint-André *et al.* 2010; Pujos *et al.* 2016).

The results presented here support the monophyly of both Lestodontini and Mylodontini, with *Brievabaradys laventensis* as their closest sister taxon (Figs 8.10, 8.13). Contrary to Saint-André (1994) and Varela *et al.* (2018), both *Mylodon darwinii* and *Pleurolestodon acutidens* are included in the latter clade. Lestodontini and Mylodontini comprise a large number of taxa, ranging chronologically from the late Miocene to the late Pleistocene (Huayquerian to Lujanian SALMAs) (Fig. 8.13). In accordance with the present calibration (Fig. 8.13), the divergence of both groups took place at the middle–late Miocene transition (ca. 12 Ma). The two clades diversified soon thereafter, expanding throughout most of South America in the early late Miocene (ca. 11.8–9.0 Ma; Mayoan and Chasicoan SALMAs). Lestodontini represents the first mylodontid group to expand northward, with the genus *Thinobadistes* recovered in North America in the late Miocene (Webb 1989). In contrast, the first mylodontine to reach Central and North America is *Paramylodon*, during the Pliocene (and persisting to the end of the Pleistocene; McDonald 1995; Morgan 2008; McDonald & Morgan 2011). Both groups therefore had some representatives that expanded into North America, migrating northward before and during the Great American Biotic Interchange (McNab 1985; Webb 1989; McDonald & Pelikan 2006; McDonald & De Iuliis 2008).

This widespread dispersal of the clade may be related to the peculiar feeding adaptations of mylodontines, the only folivorans that displayed morphological traits that are indicative of grazing habits (Bargo *et al.* 2006; Bargo & Vizcaíno 2008; Pujos *et al.* 2012). Also, trophically-related sexual dimorphism has been proposed for several mylodontines, and its adaptive value can be regarded as an additional possible driver for the wide distribution of the clade (Boscaini *et al.* 2019b).

8.3 CONCLUSIONS

The phylogenetic analysis of this chapter represents the first comprehensive, species-level study of the phylogenetic relationships within the sloth family Mylodontidae, based on morphological features taken from the entire skeletal anatomy. The results obtained imply a more complex scenario for the phylogenetic relationships among mylodontid sloths, relative to those proposed in other recent studies. The postcranial features included in this extended matrix provide increased resolution relative to previous phylogenetic studies, especially for Mylodontinae from the late Miocene to Pleistocene of both South and North America.

In accordance with previous analyses, the monophyly of both Mylodontini and Lestodontini is recovered in the present dataset. Mylodontine and lestodontine sloths diverged around the middle – late Miocene transition and later evolved independently, expanding in both South and North America during the Neogene and the Quaternary. In this period, the two clades experienced large-scale adaptive radiations, occupying environments at both austral and tropical latitudes throughout the Americas.

Chapter 9
THE INNER EAR OF *GLOSSOTHERIUM ROBUSTUM*

Several detailed studies of the external morphology of the ear region in extinct sloths have been published in the past few decades, and this anatomical region has proved extremely helpful in elucidating the phylogenetic relationships among the members of this mammalian clade. Few studies of the inner ear anatomy in these peculiar animals were conducted historically, but these are increasing in number in recent years, in both the extinct and extant representatives, due to wider access to CT-scanning facilities, which allow non-destructive access to internal morphologies. In the present chapter, the inner ear of the extinct ground sloth *Glossotherium robustum* is reconstructed, providing the first data from this anatomical region for the family Mylodontidae. The anatomy of the bony labyrinth of the genus *Glossotherium* is here compared at the level of the superorder Xenarthra, including all available extant and extinct representatives, using geometric morphometric methods. In light of the new data, the evolution of inner ear anatomy in the xenarthran clade, and most particularly in sloths, is discussed, considering the influence of phylogeny, allometry and physiology on the shape of this highly informative region of the skull. These analyses show that the inner ear of *Glossotherium* more closely resembles that of the extant anteaters, and to a lesser extent those of the giant ground sloth *Megatherium* and euphractine armadillos, than those of the extant sloths *Bradypus* and *Choloepus*, further demonstrating the striking morphological convergence between the two extant sloth genera.

9.1 THE BONY LABYRINTH OF *GLOSSOTHERIUM ROBUSTUM*

9.1.1 Description and comparison

The inner ear of *G. robustum* MACN Pv 13553 appears very small relative to skull size (Fig. 9.1), in this sense more closely resembling the labyrinth of *Megatherium*, the only inner ear of an extinct sloth available for comparison (Billet *et al.* 2013: fig. 1), than those of the extant sloths (Billet *et al.* 2012: fig. 1). This was to be expected, given the allometric relationship between the inner ear and petrosal and the skull (Billet *et al.* 2015b), as well as the allometry between body mass and the size of the inner ear and petrosal (Jones & Spells 1963; Muller 1999; Spoor *et al.* 2007). The visualization of the inner ear within the surrounding posterior cranium (Fig. 9.1) also shows that the lateral semicircular canal is very obliquely oriented relative to the horizontal plane of the skull base, as observed for extinct sloths and extant armadillos (Coutier *et al.* 2017).

As observed for *Megatherium* (Billet *et al.* 2013) and reported for *Lestodon* and *Catonyx* in a published abstract (Varela *et al.* 2016), the semicircular canals in *Glossotherium* are thin (i.e., with a small cross-sectional diameter) with a large radius of curvature with respect to the vestibular region (Figs 9.1–9.2), whereas they are thicker with a smaller radius of curvature in extant sloths (Billet *et al.* 2012, 2013, 2015a). Among xenarthrans, semicircular canals with a reduced radius of curvature are only observed in extant sloths and in the pink fairy armadillos (i.e., *Chlamyphorus*; Billet *et al.* 2015a: char. 10). However, there are some remarkable

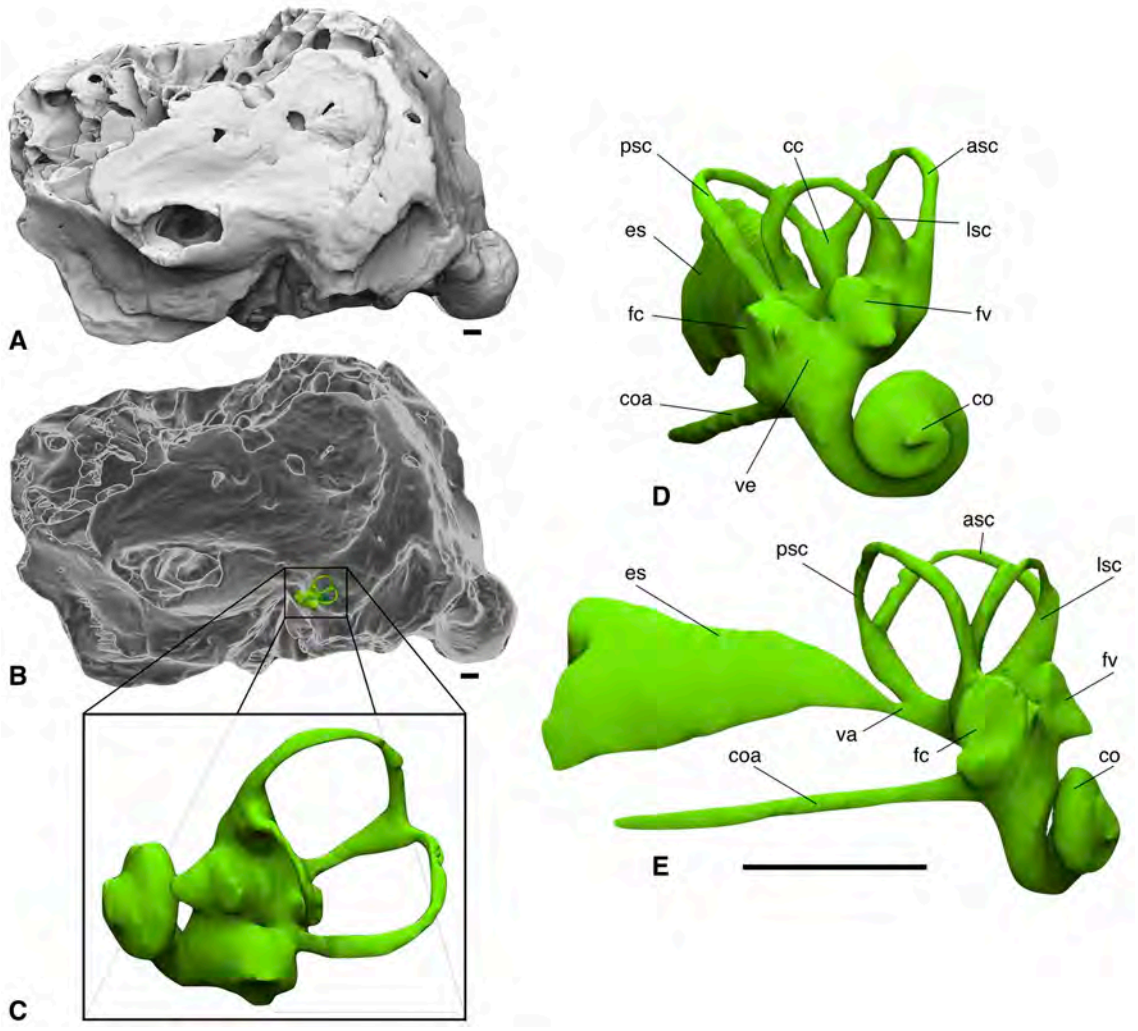

Figure 9.1. Three-dimensional reconstructions of the neurocranium and the bony labyrinths of *Glossotherium robustum* (MACN Pv 13553). (A, B) neurocranium in lateral view (B, transparency, showing the bony labyrinth of the inner ear in opaque green) (anterior towards left); (C) close-up of the left bony labyrinth of the inner ear (anterior towards left, dorsal towards top); (D, E) right inner ear of the same specimen in (D) frontolateral and (E) ventrolateral views. Abbreviations: asc, anterior semicircular canal; cc, crus commune; coa, cochlear aqueduct; co, cochlea; es, endolymphatic sac; fc, fenestra cochleae (= fenestra rotunda); fv, fenestra vestibuli (= fenestra ovalis); lsc, lateral semicircular canal; psc, posterior semicircular canal; va, vestibular aqueduct; ve, vestibulum. Scale bar equals 1 cm.

differences between *Glossotherium* and other sloths. For example, the angle between the anterior and posterior semicircular canals is acute in *Glossotherium* (78.2º), but is obtuse (>90º) in all the extant sloths and in *Megatherium.* Among the other xenarthrans here considered, the latter condition is only observed in *Chaetophractus* (Billet *et al.* 2015a: char. 12).

The two extinct sloths also differ in the arrangement of the posterior root and arch of the lateral semicircular canal. In *Glossotherium* (Fig. 9.1D–E), the posterior root of the lateral semicircular canal lies at the level of the ampullar entrance of the posterior semicircular canal, whereas in *Megatherium* it is situated much further dorsally (Billet *et al.* 2015a: char. 1). The latter condition is variably observed in *Bradypus* and is characteristic of the cingulate genus *Dasypus*, whereas the former condition is shared by all the other xenarthrans observed. The lateral semicircular canal of *Glossotherium* (Fig. 9.1D–E) presents only a weak torsion (Billet *et al.* 2015a: char. 4), as observed in almost all the xenarthrans with the exception of *Megatherium* and *D. novemcinctus,* in which the torsion is more pronounced (Billet *et al.* 2015a). The *G. robustum* specimen MACN Pv 13553 also possesses an entrance into the posterior limb of the lateral semicircular canal from the posterior ampulla, a condition only observed in the pygmy anteater *Cyclopes* and *Chlamyphorus* (Billet *et al.* 2015a: char. 5). The lack of the bulge in the utricular region of *Glossotherium* (Fig. 9.1D–E) is another marked difference with *Megatherium*. This bulge is also variably developed in *Choloepus,* but is absent in *Bradypus* and all other xenarthrans (Billet *et al.* 2015a: char. 16).

A feature that could link all the sloths considered here is the absence of the secondary bony (basilar) lamina sulcus on the cochlear endocast (Fig. 9.1D–E), a condition that is also observed in *Chlamyphorus* (Billet *et al.* 2015a: char. 11).

Plesiomorphic features shared by all the sloths considered here are the presence of a small fenestra vestibuli (Billet *et al.* 2015a: char. 3), and the orientation of the vestibular aqueduct and cochlear canaliculus, which are subparallel or slightly oblique relative to the crus commune (Fig. 9.1D–E; Billet *et al.* 2015a: char. 9). These conditions are invariably present in pilosans, whereas derived states of these features are observed among the armadillos (Billet *et al.* 2015a).

Finally, a labyrinthine feature linking *Glossotherium* with the giant anteater *Myrmecophaga* involves the cochlear canal, which is particularly short relative to inner ear size. Both taxa also have fewer than two cochlear coils (Fig. 9.1D–E; Billet *et al.* 2015a: char. 7).

9.1.2 Morphometric geometric results

The overall shape similarity between the bony labyrinth of the genus *Glossotherium* and those of anteaters is further reinforced by morphometric data analysis, conducted on the 80 semilandmark dataset. The PCA based on the entire bony labyrinth (Fig. 9.2) reveals that *Glossotherium* most closely resembles the extant anteaters, and to a lesser degree *Megatherium* and the armadillos. The similarity of the bony labyrinth of *Glossotherium* to those of extant anteaters is recovered on both PC1 (positive values) and PC2 (negatives values), and it is correlated with an enlargement of the semicircular canals, smaller cochlea, and more acute angle between the anterior and the posterior semicircular canals (PC1, positive values), as well as a longer crus commune and reduced separation between the anterior and posterior semicircular canals dorsal to the crus commune (PC2, negative values) (Fig. 9.2A). On PC3, armadillos and anteaters are not clearly separated, and *Glossotherium* is again closely associated with the anteaters and, to a lesser degree, with the dasypodid armadillos and *Megatherium* (Fig. 9.2B).

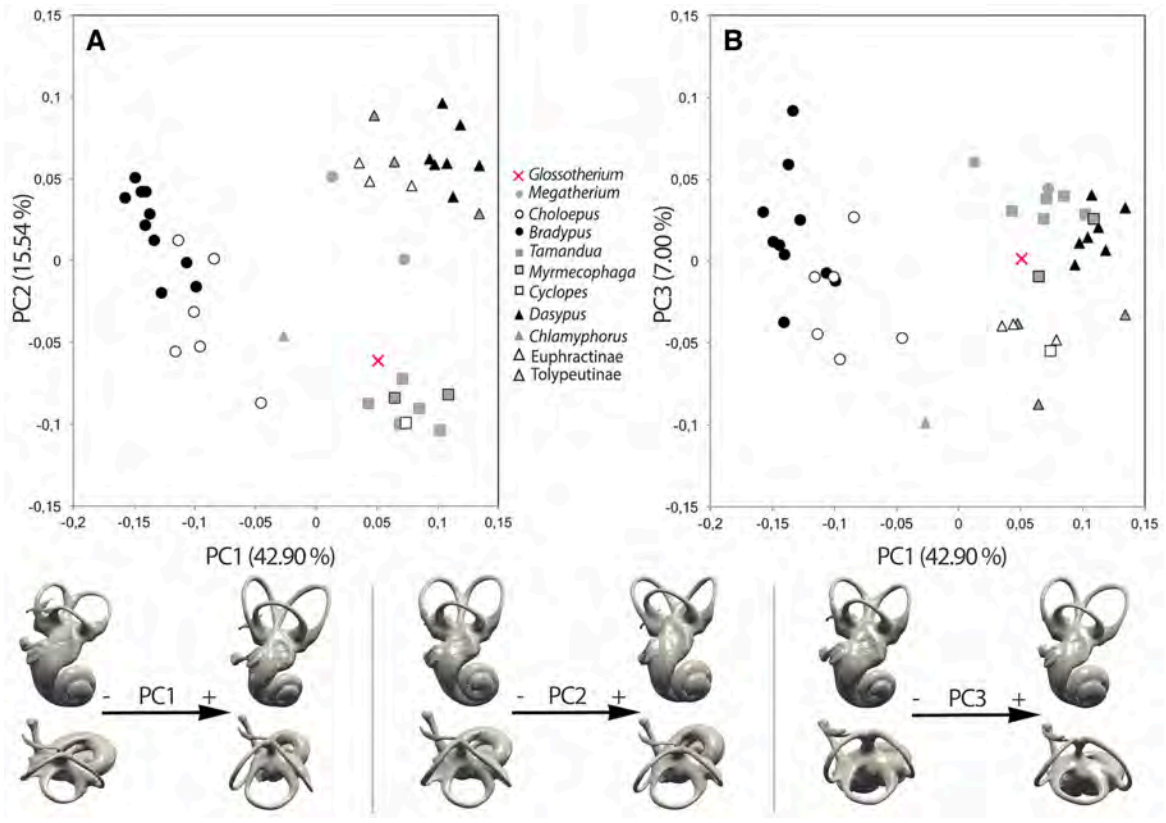

Figure 9.2. Principal component analysis performed on the total set of 80 semilandmarks, showing the shape differentiation of the bony labyrinth among extant xenarthrans, as well as the two extinct sloths *Glossotherium* and *Megatherium*. (A) principal components 1 and 2 and (B) principal components 1 and 3. At the bottom: associated patterns of morphological transformation on the first 3 axes (65.44% of the among-group variance).

A second PCA was performed exclusively on the semicircular canal semilandmark subset (Fig. 9.3), and showed results very similar to the first PCA (Fig. 9.2), with *Glossotherium* even closer to *Myrmecophaga* and *Tamandua* (the lesser or collared anteater) than any other xenarthran. The genera *Myrmecophaga*, *Tamandua*, and *Glossotherium* fall into the higher values of PC1, associated with larger semicircular canals, a less inclined crus commune and a reduced angle between the anterior and posterior semicircular canals; and, into the lower values of PC2, corresponding, in its most extreme values (e.g., *Cyclopes*), to a dorsoventrally elongated posterior semicircular canal smaller than the rounded anterior semicircular canal, and a narrower crus commune (Fig. 9.3A). As in the former analysis (Fig. 9.2B), the PC3 doesn't reliably separate any group, and the genus *Glossotherium* is more closely associated with the anteaters, the euphractine armadillos and *Megatherium* than any other xenarthran (Fig. 9.3B).

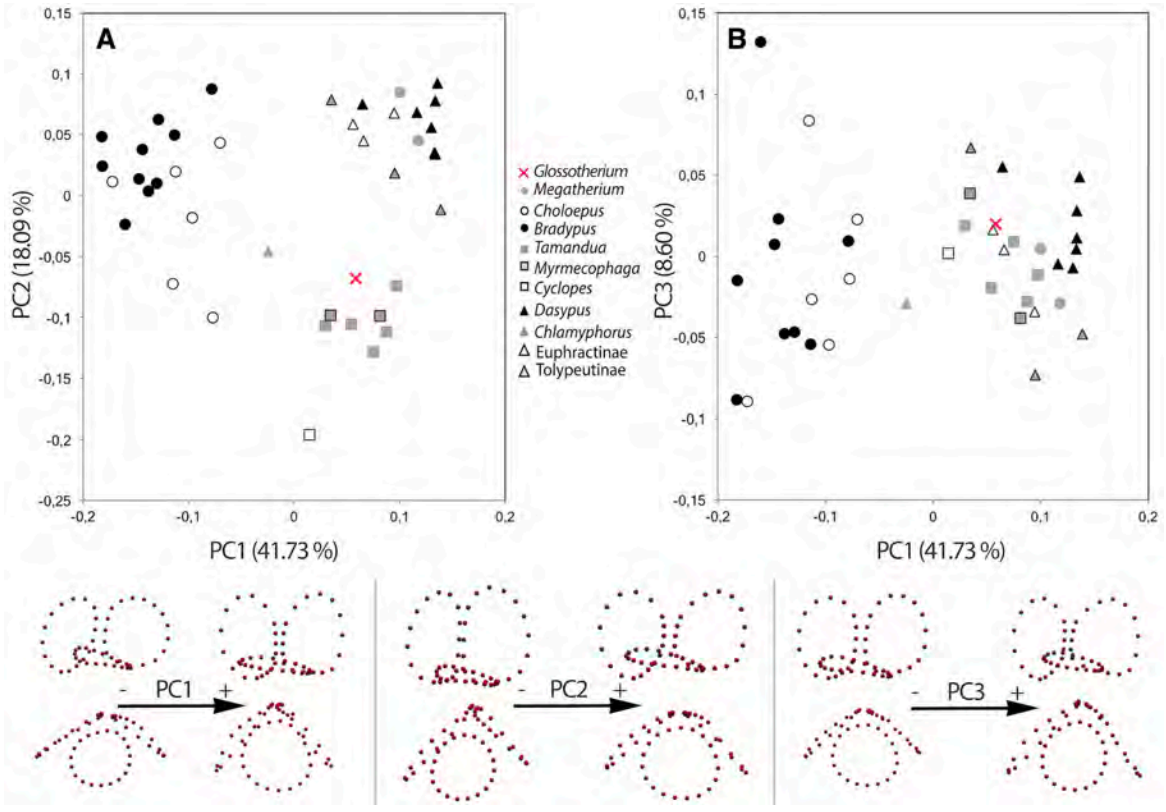

Figure 9.3. Principal component analysis performed on a subset of 60 semilandmarks, showing the shape differentiation of semicircular canals among extant xenarthrans, as well as the two extinct sloths *Glossotherium* and *Megatherium*. (A) principal components 1 and 2 and (B) principal components 1 and 3. At the bottom: associated patterns of morphological transformation on the first 3 axes (68.42% of the among-group variance).

Similarly, a third PCA was performed, this time considering only the cochlear semilandmark data set (Fig. 9.4). In this PCA, *Glossotherium* sits close to *Megatherium*,

Myrmecophaga and the euphractine armadillos, and falls into higher values of PC1 and slightly negative values of PC2 (Fig. 9.4A), which correspond to a low spired and asymmetrically-convoluted cochlea. Along PC3 (Fig. 9.4B), *Glossotherium* falls in the middle of the shape range, close to anteaters, euphractine armadillos and two-toed sloths.

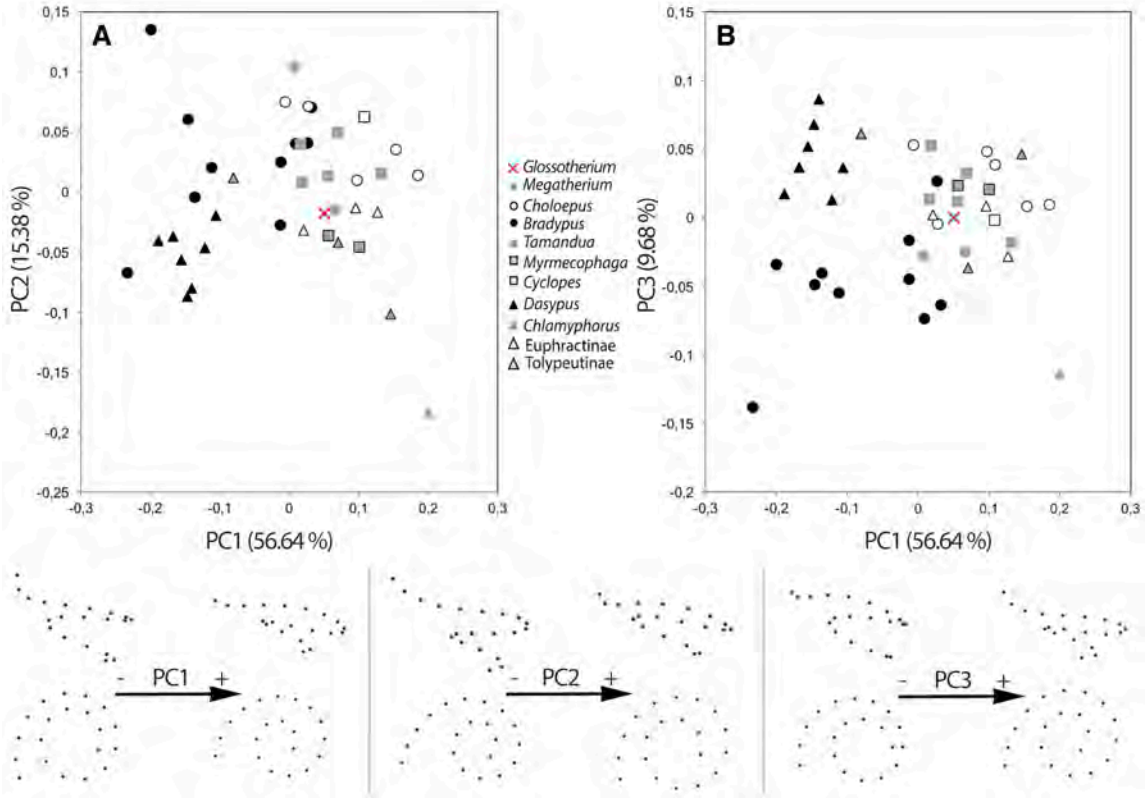

Figure 9.4. Principal component analysis performed on a subset of 20 semilandmarks, showing the shape differentiation of the cochlea among extant xenarthrans, as well as the two extinct sloths *Glossotherium* and *Megatherium*. (A) principal components 1 and 2 and (B) principal components 1 and 3. At the bottom: associated patterns of morphological transformation on the first 3 axes (81.70% of the among-group variance).

The same PCAs were also conducted with the shape data corrected for allometry, using either body mass (Appendix VII, Figure S2) or centroid size (Appendix VII, Figure S3) as estimators of size, which respectively explain the 10.25% and 8.63% of the labyrinthine shape variation. Given the low influence of allometry (see Billet *et al.* 2015a), these PCAs are very similar to the previous ones (Figs 9.2–9.4) and the results are available in Appendix VII (Figures S2–S3). The allometric shape vector (ASV) and partial least square (PLS) analyses are also similar to those of Billet *et al.* (2015a).

The ASV analyses enable to observe the transformations of the whole labyrinth that are related to allometry (Appendix VII, Figures S4–S5). Regarding the two extinct sloths considered, *Megatherium* tends to be separated from the extant xenarthrans, a probable

consequence of its extreme weight and size (Billet *et al.* 2015a). However, despite its large body mass (less than 30% of *Megatherium*, but around 37 times the mass of the largest extant xenarthran), *Glossotherium* sits among the higher values for the allometric shape vectors that are typical of the extant anteaters (Appendix VII, Figures S4–S5).

Covariation between the semicircular canals and the cochlea was also examined by performing a PLS analysis (Appendix VII, Figure S6). On the first singular warp (SW1; Appendix VII, Figure S6), the same association of cochlear and semicircular canal features described by Billet *et al.* (2015a: fig 7a) is observed: small semicircular canals (i.e., with a small radius of curvature) with an obtuse angle between the anterior and the posterior canals are associated with a long and convoluted cochlea, oriented obliquely relative to the lateral semicircular canal. *Glossotherium* is close again to the anteaters, the euphractine armadillos, and *Megatherium*. On the second singular warp (SW2; Appendix VII, Figure S6) the short crus commune and the small semicircular canals with divergent anterior and posterior canals, are associated with a cochlea that has a larger diameter and a taller spire. *Glossotherium* is recovered near the boundary between the extant sloth *Choloepus* and anteaters in this analysis.

9.2 DISCUSSION

9.2.1 Internal anatomy: the bony labyrinth of the inner ear

Billet *et al.* (2015a) discussed in detail both the weak influence of allometry and the strong imprint of phylogeny in their sample of bony labyrinths among xenarthrans. The inclusion of the genus *Glossotherium* in the present dataset allowed to extend Billet *et al.*'s (2015a) observations to a sample now including a member of the diverse extinct sloth family Mylodontidae. Regarding allometry, even if the influence of size is rather low in the new dataset (accounting for 10.25% and 8.63% of labyrinthine shape variation using body mass and centroid size corrections, respectively), it is slightly higher than the values for the previous dataset (9.94% and 7.64% respectively; Billet *et al.* 2015a). An increase in allometric effect was also observed by removing *Megatherium* from the extant dataset (Billet *et al.* 2015a). The stronger allometric effect with the inclusion of *Glossotherium* suggests that further integration of other large to medium-sized extinct xenarthrans will enable more reliable evaluation of the effect of allometry.

In contrast, the imprint of phylogeny on labyrinthine shape is remarkable in the previous dataset, with the exceptions of the genera *Chlamyphorus* and *Megatherium* (Billet *et al.* 2015a). This scenario is further complicated with the inclusion of *Glossotherium*, since it is strongly associated with extant anteaters (and to a lesser degree *Megatherium* and the extant armadillos) in the first three axes of all PCAs in these results. This suggests that functional factors might also be responsible for the observed distribution. For this reason, some of the methods linking inner ear morphology with particular functional attributes were tentatively applied to *Glossotherium* and critically reviewed.

9.2.2 Functional considerations for the semicircular canals

As already noted by Billet *et al.* (2015a), most of the morphological transformations of the xenarthran bony labyrinth are ascribable to changes in the configuration of the semicircular canals (Figs 9.2–9.3). The semicircular canals, together with the utricle, helps in detecting the angular acceleration and deceleration of the head, stabilizing the gaze during locomotion, and aid in the coordination of body movements (e.g., Spoor *et al.* 2007; Sipla & Spoor 2008; Silcox *et al.* 2009; David *et al.* 2010; Ekdale 2016).

Spoor *et al.* (2007) assigned six agility categories to a mammalian sample, from extra slow (e.g., extant sloths) to fast (e.g., bats), and observed that agile mammals have significantly larger semicircular canals (i.e., with a larger radius of curvature) relative to body mass than those that move more slowly. In the graph depicted in Figure 9.5, modified after Spoor *et al.* (2007) and Billet *et al.* (2013), *Glossotherium* falls in the top-right corner, close to *Megatherium* and modern mammals of similar size, most of which were classified as medium-slow animals by Spoor *et al.* (2007). Elephants are the extant mammals that best approximate the relative size of the semicircular canals and body mass of *Megatherium* (Billet *et al.* 2013), whereas for *Glossotherium* the hippopotamus is the closest taxon (see the grey circles in Figure 9.5 close to *Megatherium* and *Glossotherium,* respectively). However, this association is probably much more strongly influenced by the correlation between semicircular canal length and body size than it is by the (weaker) correlation with agility (Malinzak *et al.* 2012). In fact, graphical comparisons can only be made at a given body mass (Billet *et al.* 2013; Ruf *et al.* 2016), and the method of Spoor *et al.* (2007) and the predictive equations of Silcox *et al.* (2009) are difficult to apply for extremely small-sized and large-sized mammals (Billet *et al.* 2013). Even more so, a direct comparison of the extinct sloths with the extremely slow extant sloths cannot be undertaken at the moment, due to the striking difference in body size (Billet *et al.* 2013; Vizcaíno *et al.*

2018). However, what is evident in the graph in Figure 9.5 is that *Glossotherium*, like *Megatherium* but in contrast to extant sloths, has semicircular canals of similar or perhaps slightly greater length, relative to those of similar-sized mammals.

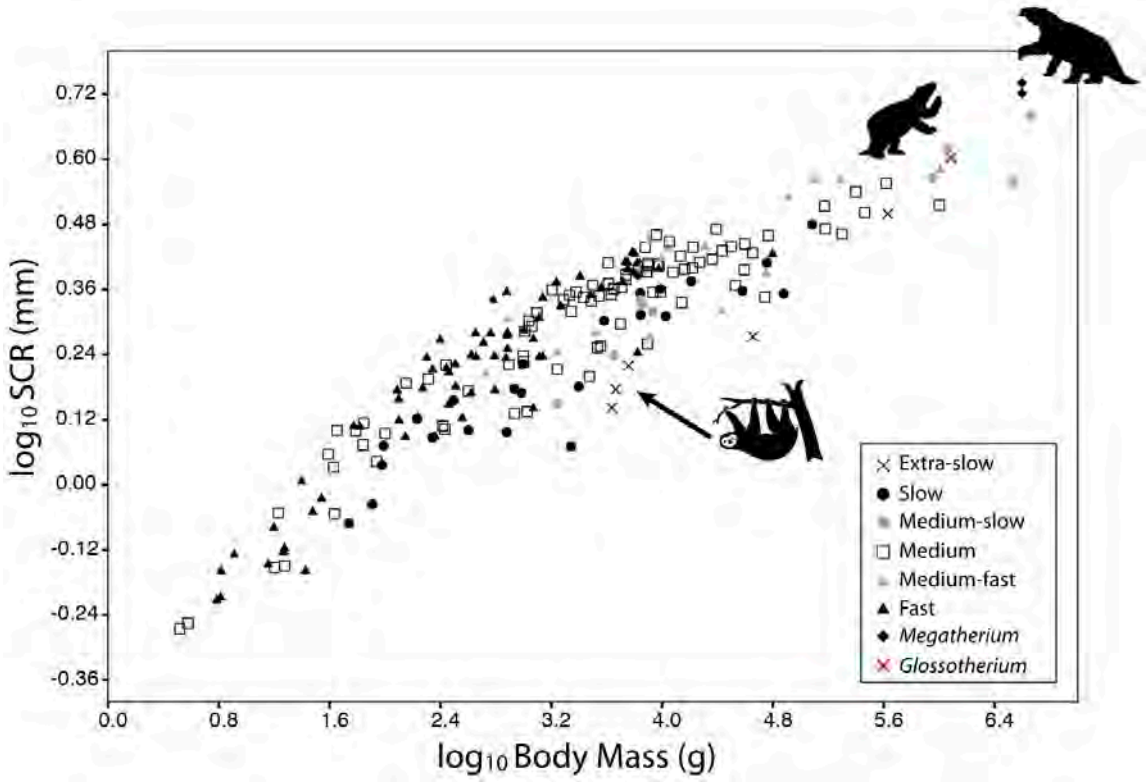

Figure 9.5. Double logarithmic plot of average semicircular canal radius (SCR) against body mass for 210 mammals, after Spoor *et al.* (2007) and Billet *et al.* (2013), showing the graphical relationship among semicircular canal sizes, body mass and agility.

The orientation of the semicircular canals relative to one another has been linked to the sensitivity of the equilibrium system (Malinzak *et al.* 2012; Berlin *et al.* 2013). Malinzak *et al.* (2012) proposed that the closer the angles among the semicircular canal planes are to orthogonality (90°), the higher the sensitivity to head rotations (Malinzak *et al.* 2012; Berlin *et al.* 2013). The bony labyrinth of *Glossotherium* shows a pronounced deviation from orthogonality: following the protocol of Berlin *et al.* (2013) the 90_{var} is 12.28 ($\log_{10}90_{var}$=1.09), which is close to the lowest values for average sensitivity in the dataset of Berlin *et al.* (2013). These values, in turn, are associated by Berlin *et al.* (2013) with fossorial habits. The average 90_{var} value for the fossorial taxa in that sample (mean=11.0°; st. dev.=3.2°) is twice that of non-fossorial taxa (mean=5.5°; st. dev.=1.8°). Despite the fact that large Pleistocene "burrows" in the Pampean region have repeatedly been attributed to the activity of mylodontid sloths (e.g., Zárate *et al.* 1998; Bargo *et al.* 2000; Vizcaíno *et al.* 2001; Blanco &

Rinderknecht 2012), *G. robustum* was almost certainly not an obligate fossorial taxon like those included in Berlin *et al.*'s (2013) dataset. Moreover, among extant xenarthrans, the $\log_{10}90_{var}$ calculated for *G. robustum* (1.09), is closer to the range calculated for the non-fossorial *Tamandua tetradactyla* (1.42–2.63) and *Bradypus variegatus* (1.73–3.08) than those calculated for *Dasypus novemcinctus* (2.25–2.49) (Billet *et al.* 2012; Ruf *et al.* 2016). Among the extant xenarthrans for which this value was calculated in Ruf *et al.* (2016), *Dasypus novemcinctus* is the only taxon that displays burrowing habits (Gaudin & Biewener 1992), and it is, indeed, the most distant data point from *Glossotherium*. This data shows that burrowers do not necessarily display lower degrees of canal orthogonality and confirm that, to date, "it is not functionally clear why lower degrees of canal orthogonality would be associated with a burrowing lifestyle" (Berlin *et al.* 2013: p. 14). Ruf *et al.* (2016) also stressed the fact that the correlation coefficients of the regressions in Berlin *et al.* (2013) are quite modest, and that both Malinzak *et al.* (2012) and Berlin *et al.* (2013) do not take into account non-negligible intraspecific variation.

Recent studies (e.g., Billet *et al.* 2012; Perier *et al.* 2016; Ruf *et al.* 2016) have been considering the intraspecific variation of the bony labyrinth as a useful tool to properly characterize distinct morphologies, but also as an important parameter for inferring function. Billet *et al.* (2012) noticed that the extant sloths show a surprisingly high degree of intraspecific variation, particularly in their semicircular canals, compared with other mammals. This higher amount of intraspecific variation of the bony labyrinth was related with a possible relaxation of the selective pressure on its morphology, as a consequence of the reduced functional demand for rapid postural adjustments (Billet *et al.* 2012). This idea was reinforced by Perier *et al.* (2016), who concluded that the bony labyrinths of slow-moving primates show higher amounts of intraspecific variation than the fast-moving ones, though to a much lesser extent than in extant sloths. In other words, the slower an animal is, the more the bony labyrinth may vary intraspecifically (Perier *et al.* 2016). The latter authors, while not necessarily invalidating the results obtained by studies that include the radius or the orthogonality of the semicircular canals (e.g., Spoor *et al.* 2007; Malinzak *et al.* 2012), explicitly warn against the interpretation of measurements based on one or a few individuals per species (Perier *et al.* 2016).

At present, it is clear that extinct sloths and living armadillos and anteaters have relatively longer semicircular canals (i.e., with a larger radius of curvature; Figs 9.2–9.3) than the living tree sloths. From a phylogenetic point of view, this data confirms the previous hypothesis of Billet *et al.* (2013) that the strange morphology of the extant sloths' semicircular canals is due

to convergence, probably related with the parallel acquisition of their slow and suspensory locomotion (e.g., Gaudin 2004; Nyakatura 2012).

9.2.3 Functional considerations for the cochlea

The cochlea is related to the sense of hearing, and many of its macroscopic features have been associated with auditory physiology (for a review see Ekdale 2016). For example, Manoussaki *et al.* (2008) demonstrated that the ratio of the radius of curvature in the basal cochlear spiral relative to that of the apical spiral (Radii ratio=R_{base}/R_{apex}) is correlated with low frequency hearing limits in both land and aquatic mammals. More precisely, the higher the ratio (i.e., the more asymmetric the coiling in perpendicular view), the lower the low frequency limit of hearing (Manoussaki *et al.* 2008). Even if this relationship is highly significant (Manoussaki *et al.* 2008), the procedure proposed by the authors is not straightforward. Indeed, the obtained low frequency limit values range from 100 to 20 Hz, depending on the measurement. Danilo *et al.* (2015), Ekdale & Racicot (2015) and Orliac & O'Leary (2016) reported similar repeatability issues. Despite this operational limit, it seems that low-spired cochleae in mammals have lower frequency limits, as suggested by Gosselin-Ildari (2006, in Ekdale & Rowe 2011) who found a positive correlation between the cochlear ratio (height divided by width, in lateral view) and the low frequency limit in primates. In fact, the cochlea of *Glossotherium* is one of the most low-spired and asymmetrically-coiled among xenarthrans (Fig. 9.4). Other morphological features that support specialization for low frequency hearing in *Glossotherium* include the overlapping turns in vestibular view and the absence of the secondary bony lamina (Ekdale & Racicot 2015). Moreover, specialized low frequency hearing has already been proposed for *G. robustum* by Blanco & Rinderknecht (2008, 2012) on the basis of middle ear ossicle size-estimations. They suggested a low-frequency limit of 44 Hz for *G. robustum*, somewhat higher than that of modern elephants. This limit could be related to specific ecological adaptations, such as long-range communication via infrasound, and fossoriality (Blanco & Rinderknecht 2008, 2012). However, the association of *Glossotherium* with *Megatherium*, the anteaters and the euphractine armadillos, rather than with extant sloths, is consistently weaker in the cochlear dataset (Fig. 9.4) than in the semicircular canals dataset (Fig. 9.3), and more data is needed to properly evaluate if this similarity is due to functional considerations.

9.3 CONCLUSIONS

In this chapter, the first inner ear of an extinct mylodontid sloth is reconstructed and compared with that of the extant xenarthrans and the genus *Megatherium*.

After including *Glossotherium* in the morphometric analyses, it appears that folivorans do not cluster together in the morphospace. In fact, the effect of phylogeny, though strong (Billet *et al.* 2015a), cannot explain all the observed variation. Given that allometry has a limited influence on the shape of the bony labyrinth in xenarthrans (Billet *et al.* 2015a), functional aspects should be taken into account when trying to explain the observed distribution. However, methods linking geometric features with functional aspects have recently been questioned, in part due to the strong phylogenetic signals (Lebrun *et al.* 2010; Benoit *et al.* 2013) and in some cases to the relatively weak correlation between subjective categories of agility and the bony labyrinth morphology (Malinzak *et al.* 2012). These effects are often hard to tease apart, and their interrelationships can vary among different mammalian clades. Other criticisms were expressed by David *et al.* (2010, 2016), who concluded that "since the degree to which the canals reflect the size and shape of the ducts inside is highly variable, such studies cannot provide the essential information for functional analyses" (David *et al.* 2016: p. 2). This suggests that most methods currently employed are not reliable enough for predicting functional abilities in extinct species based on the semicircular canal morphology, even if some progress is being made among extant species (David *et al.* 2010, 2016).

Moreover, the limited attention to intraspecific variation has been recently stressed (Perier *et al.* 2016; Ruf *et al.* 2016). This is particularly true for extinct species, for which there is often a strong temptation to estimate habits based on the bony labyrinthine morphology of a single individual (Perier *et al.* 2016).

For the time being, the peculiar conformation of the semicircular canals in living sloths, coupled with their unusual locomotory habits, has not been observed in any other xenarthran, which reinforces the hypothesis that the two extant genera have undergone striking levels of convergence.

The addition of other extinct xenarthrans (especially but not exclusively limited to sloths) to the present dataset, may allow clarification of the timing of these evolutionary changes.

Chapter 10
DIGITAL ENDOCASTS OF *GLOSSOTHERIUM ROBUSTUM*

The internal cranial morphology of the terrestrial sloth *Glossotherium robustum* is described here based on a neurocranium from the late Pleistocene of the Pampean region of Buenos Aires, northeastern Argentina. The first published data on the morphology of the brain cavity of this species date back to the latest nineteenth century. The novel techniques of CT scanning and digital reconstructions enable non-destructive access to the internal cranial features of both extinct and extant vertebrates, and thus improve our knowledge of anatomical features that had previously remained obscure. Therefore, CT scans have been performed on the posterior half of a skull of *G. robustum* and digital models of the endocasts and internal structures were created. The results reveal the morphology of the brain cavity itself, as well as the cranial sinuses and the trajectory of several cranial nerves and blood vessels. These features have been compared with the two extant folivoran genera, the two-toed sloth *Choloepus* and the three-toed sloth *Bradypus*. For many characteristics, especially those related to the paranasal pneumaticity and the brain cavity, a closer similarity between *Glossotherium* and *Choloepus* is observed, in accordance with the most widely accepted phylogenetic scenarios. However, other features are only shared by the two extant genera, but are probably related to allometric effects and the convergence that affected the two modern lineages. This study, which represents the first exhaustive analysis of digital endocasts of an extinct sloth, reveals the importance of the application of new methodologies, such as CT scans, for elucidating the evolutionary history of this peculiar mammalian clade.

10.1 DESCRIPTIONS AND COMPARISONS

10.1.1 Brain endocast

The 3D model of the brain digital endocast of *Glossotherium robustum* is almost complete, with the exception of the dorsal portion of the left olfactory bulb, which was impossible to reconstruct due to the lack of bony material (Fig. 10.1A–D). In general, the external surface is well preserved and the pattern of convolutions and the majority of blood vessels and nerves are recognizable. As expected, the brain of *Glossotherium* was considerably larger than that of the extant forms *Choloepus* and *Bradypus*, both in terms of linear measures and volume (Fig. 10.1). At first glance, the patterns of convolutions in the cerebral hemisphere of these three genera are different, with *Glossotherium* showing a higher level of complexity than the endocasts of the two extant taxa (Fig. 10.1).

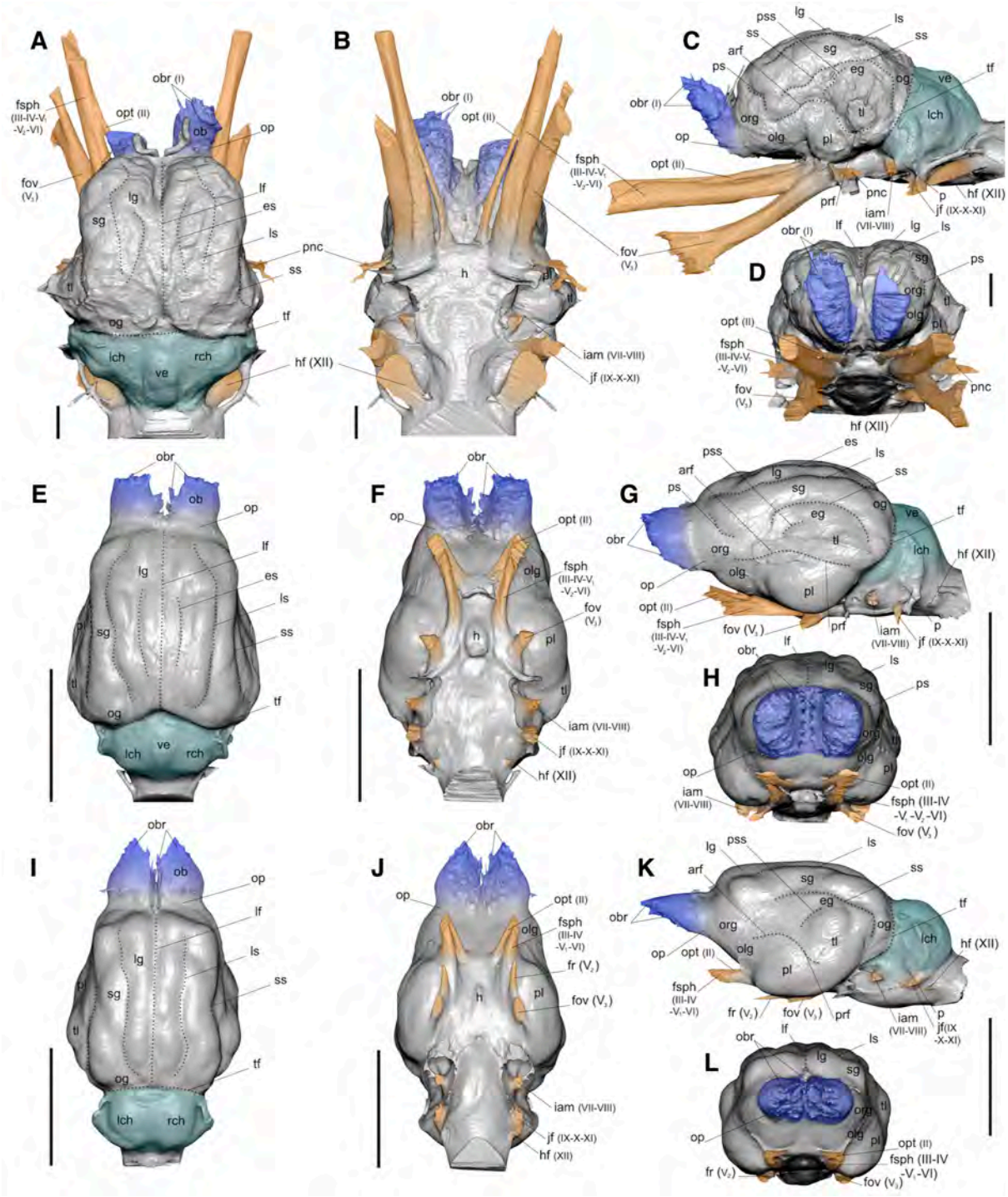

Figure 10.1. Brain endocasts of *Glossotherium* (MACN Pv 13553) (A–D), *Choloepus* (AMNH 30765) (E–H), and *Bradypus* (AMNH 95105) (I–L), in dorsal (A, E, I), ventral (B, F, J), lateral (C, G, K), and anterior (D, H, L) views. Abbreviations: arf, anterior rhinal fissure; eg, ectosylvian gyrus; es, entolateral sulcus; fov, foramen ovale; fr, foramen rotundum; fsph, sphenorbital fissure; h, hypophysis; hf, hypoglossal foramen; iam, internal acoustic meatus; jf, jugular foramen; lch, left cerebellar hemisphere; lf, longitudinal fissure; lg, lateral gyrus; ls, lateral sulcus; ob, olfactory bulb; obr, olfactory bulb ramifications; og, occipital gyrus; olg, olfactory gyrus; op, olfactory peduncle; opt, optic nerve; org, orbital gyrus; p, paraflocculus; pl, pyriform lobe; pnc, petrosal nerve complex; prf, posterior rhinal fissure; ps, presylvian sulcus; pss, pseudosylvian sulcus; rch, right cerebellar hemisphere; sg, suprasylvian gyrus; ss, suprasylvian sulcus; tf, transverse fissure; tl, temporal lobe; ve, vermis. Colors indicate: grey, cerebrum; blue, olfactory bulbs; turquoise, cerebellum; orange, neurovascular connections. Roman numeral designations indicate cranial nerves. Scale bars equal 2 cm.

However, the seemingly higher degree of complexity is not related to an increase in number of the convolutions, but to the presence of surface irregularities. These latter are in fact small recesses and protrusions of irregular shape and limited extent, not compatible with the morphology of convolutions mentioned in the literature (e.g., Barone & Bortolami 2004). A similar high degree of complexity is observed in other extinct giant extinct sloth genera such as *Lestodon*, *Megatherium*, *Mylodon*, *Oreomylodon*, and *Scelidotherium* (Gervais 1869; Dechaseaux 1958, 1962a, b, 1971), and to a lesser extent in the small-sized extinct early sloths *Hapalops* and *Eucholoeops* (Dozo 1987, 1994).

In *Glossotherium*, the cerebrum is globular. The cerebral hemispheres arch strongly dorsally, and are separated by a very deep longitudinal fissure (Fig. 10.1A–D). In dorsal view the fissure is especially deep and wide anteriorly, imparting a peculiar "walnut kernel" shape to the brain. In *Choloepus* and *Bradypus*, the hemispheres are less arched and the longitudinal fissure less prominent than in *Glossotherium* (Fig. 10.1E–L). The morphology of the extant sloths more closely resembles that of *Hapalops* and *Eucholoeops* (Dozo 1987, 1994).

In dorsal view (Fig. 10.1A, E, I), the symmetric convolutions are represented mainly by the lateral and suprasylvian gyri, arranged similarly anteroposteriorly in *Glossotherium*, *Choloepus*, and *Bradypus*. The occipital gyri are oriented mediolaterally, emphasizing the transverse fissure that separates the telencephalon from the cerebellum. The entolateral sulcus, which divides the lateral gyrus anteroposteriorly into medial and lateral portions, is a feature shared only by *Glossotherium* and *Choloepus*. It is absent in *Bradypus* (Fig. 10.1A, E, I).

The dorsal surface of the telencephalon of *Lestodon*, *Megatherium*, *Mylodon*, *Oreomylodon*, *Scelidotherium* (Gervais 1869; Dechaseaux 1958, 1962a, b, 1971), and the *Glossotherium* specimen figured in Dechaseaux (A10.263; 1958, 1971) is extremely similar to that of *Glossotherium* MACN Pv 13553. It comprises two globose hemispheres divided by a deep longitudinal fissure. The well-developed suprasylvian gyri are always present in these extinct genera. A deep entolateral sulcus is visible in A10.263 of *Glossotherium* (Dechaseaux 1958, 1971) and also in *Lestodon*, *Megatherium*, *Mylodon*, *Oreomylodon*, and *Scelidotherium* (Gervais 1869; Dechaseaux 1958, 1962a, 1971), whereas it seems to be absent in *Hapalops* and *Eucholoeops* (Dozo 1987, 1994).

In *Glossotherium*, *Oreomylodon*, *Lestodon*, and *Megatherium*, the entire dorsal brain surface is strongly arched and the anterior portion is very wide, bulging mediolaterally (Gervais 1869; Dechaseaux 1958, 1962a, b, 1971). However, the width of the *Megatherium* brain (Gervais 1869) strongly decreases along the pseudosylvian sulci, in contrast to the condition observed in the mylodontids mentioned above (Gervais 1869; Dechaseaux 1958, 1962a, 1971). In all these genera (including *Megatherium*), the large olfactory gyrus is delimited by a deep rhinal fissure,

which is curved dorsally, its apex approaching the nearly vertical pseudosylvian sulcus (Fig. 10.1C; Dechaseaux 1958, 1962a, b, 1971). A well-developed pyriform lobe is delimited by the rhinal fissure in *Glossotherium* (Fig. 10.1C) and *Oreomylodon* (Dechaseaux 1971: fig. 13) as well as in both the extant taxa (Fig. 10.1G, K). This fissure is generally used as an indication of the ventral limit of the neocortex, which is considered the newest portion of the cerebral hemisphere in mammals (Jerison 1991).

The olfactory bulbs of *Glossotherium* are prominent and extend strongly dorsally, with a wide and flat anterior surface covered by the ramifications of the olfactory nerve (I) (Fig. 10.1A–D). In anterior view, these bulbs appear "teardrop-shaped" with the dorsal part wider than the ventral one (Fig. 10.1D). Both bulbs are flanked by two large symmetrical blood vessels and some additional tiny vessels, which make the architecture of the olfactory bulbs in *Glossotherium* very similar to that observed in other terrestrial sloths such as *Oreomylodon* (Dechaseaux 1971). Unfortunately, a detailed comparison with the olfactory bulbs of *G. robustum* A10.263 (Dechaseaux 1958, 1971) is not possible, due to the quality of the cast of the latter. However, based on what is preserved, the morphology of the whole brain would seem to be almost identical in the two *Glossotherium* specimens.

The olfactory bulbs of *Choloepus* and *Bradypus* differ in shape. In *Choloepus*, the olfactory bulbs are well separated and their outline is rectangular in dorsal view (Fig. 10.1E). In lateral view, the ventral surface (bearing the ramifications of the olfactory nerve and lying on the cribriform plate) is inclined anterodorsally (Fig. 10.1G), but the dorsal edge is horizontal, in contrast to the inclined orientation present in *Glossotherium*. The olfactory bulbs are reniform in anterior view, unlike the teardrop-shaped bulbs in *Glossotherium* (Fig. 10.1H). On the other hand, the olfactory bulbs in *Bradypus* are situated closer together. They are anteroposteriorly elongated and triangular in outline in lateral view, its margins converging to form a distinct point anteriorly, and with a horizontal dorsal edge like that of *Choloepus* (Fig. 10.1I). A similar condition is also observed in *Hapalops* (Dozo 1987) and *Eucholoeops* (Dozo 1994). Moreover, in anterior view, the dorsoventral height of the olfactory bulbs is greater than the transverse width in *Glossotherium* and *Choloepus* (Fig. 10.1D, H), whereas the opposite is observed in *Bradypus* (Fig. 10.1L). The general shape of the olfactory bulbs in *Glossotherium* is more similar to *Choloepus* than to *Bradypus*, *Hapalops*, or *Eucholoeops*.

The cerebellum of *Oreomylodon*, *Lestodon*, *Mylodon*, *Scelidotherium*, *Megatherium*, and especially *Glossotherium* is large with both cerebellar hemispheres laterally expanded (Fig. 10.1A, C; Gervais 1869; Dechaseaux 1958, 1962a, 1971). In these taxa, the cerebellum is sub-triangular in dorsal view with the apex formed by the posterior portion of the vermis. The latter structure

is well delineated (Fig. 10.1A; Gervais 1869; Dechaseaux 1958, 1962a, 1971). Along the transverse fissure of all these genera (with the exception of *Scelidotherium* and *Megatherium*), the cerebellum is as wide as the posterior portion of the cerebral hemisphere (Fig. 10.1A). The paraflocculus is the lateral expansion of the cerebellum that is housed in the subarcuate fossa of the petrosal bone (Dechaseaux 1971; Macrini *et al.* 2007a, b). In *Glossotherium* MACN Pv 13553, the bulge that comprises the paraflocculus is clearly recognizable on the surface of the endocast (Fig. 10.1C), as it is in the endocasts of *Oreomylodon* and *Glossotherium* figured in Dechaseaux (1971). In both extant forms, the cerebellum is roughly oval in shape with the maximal width always less than that of the telencephalon (Fig. 10.1E, I). The lateral cerebellar hemispheres have rounded and smooth surfaces. The vermis is well developed in *Choloepus,* whereas it leaves no distinctive impression on the endocast surface of *Bradypus* (Fig. 10.1E, I). The parafloccular areas are poorly marked in the extant sloths, and are located just dorsal to the jugular foramen (Fig. 10.1G, K), as in *Glossotherium* and *Oreomylodon* (Dechaseaux 1971).

10.1.2 Cranial nerves

In *Glossotherium*, the emergence of the cranial nerves is visible in ventral, lateral, and anterior views (Fig. 10.1), and has been identified following Dechaseaux (1971) and Gaudin *et al.* (2015).

The anteriormost nerve leaving the base of the encephalic cavity corresponds to the optic nerve (II), which extends through the optic foramen (Fig. 10.1B). The optic nerve opens into the sphenorbital fissure in all the observed specimens of *Glossotherium*, *Choloepus*, and *Bradypus*. The confluence of the optic nerve and the sphenorbital fissure is located anterior to the olfactory bulbs in *Glossotherium* (Fig. 10.1B–C), whereas it is posteriorly located in *Choloepus* (Fig. 10.1F–G) and *Bradypus* (Fig. 10.1J–K). In all the sloths, the optic foramen and the sphenorbital fissure share a common external aperture in lateral view (Gaudin 2004).

The sphenorbital fissure transmits several nerves (i.e., III-IV-V_1-V_2-VI) and is, therefore, the largest foramen in the skull wall of all the observed specimens. In *Glossotherium* MACN Pv 13553 (Fig. 10.1B–D) and *Choloepus* AMNH 30765 (Fig. 10.1F–H), both the ophthalmic (V_1) and the maxillary (V_2) divisions of the trigeminal nerve pass through the sphenorbital fissure, whereas in *Bradypus* AMNH 95105 (Fig. 10.1J–L), the maxillary division extends through the foramen rotundum. This feature, observed in the encephalic cavity of *Glossotherium*, *Choloepus*, and *Bradypus*, agrees with the observations of Gaudin (2004) on the external surface of the skull in lateral view. In fact, the foramen rotundum is confluent with the sphenorbital fissure in most Mylodontidae (excluding *Nematherium* and *Pseudoprepotherium*) and also in *Choloepus*, *Eremotherium*,

Megatherium, and *Thalassocnus*, whereas these two openings are separate in all the other sloths.

The foramen ovale, which accommodates the mandibular division of the trigeminal (V_3), is present posterior and lateral to the sphenorbital fissure in all the examined specimens (Fig. 10.1).

More posteriorly, at the level of the petrosal bone, the internal acoustic meatus is pierced by the facial (VII) and vestibulocochlear (VIII) nerves (Fig. 10.1). The latter ends at the level of the inner ear, whereas the facial nerve has a more convoluted trajectory that has been reconstructed for *Glossotherium* (Fig. 10.2). Emerging from the primary facial foramen of the petrosal, the facial nerve enlarges into the geniculate ganglion, which is enclosed in the cavum supracochleare, just medial to the anteroventral process of the tegmen tympani, and anterior to the rostral end of the crista parotica. From this point, the facial nerve turns posteriorly, travels through the secondary facial foramen into the facial sulcus and, passing through the stylomastoid foramen, it leaves the cranium ventrally (Fig. 10.2). Anterior to the geniculate ganglion, the greater petrosal nerve turns medially and, after passing through the hiatus Fallopii, extends in a distinct sulcus on the epitympanic wing of the petrosal, before turning ventrally at the level of the trigeminal ganglion (Fig. 10.2). The greater petrosal nerve then enters in the foramen located in the anterior wall of the carotid foramen, piercing the ventral surface of the medial portion of the pterygoid and emerging anteriorly in the groove of the vidian nerve (Fig. 10.2). The lesser petrosal nerve is an anterior extension of the tympanic nerve (a branch of the glossopharyngeal nerve, cranial nerve IX, that forms a sensory tympanic plexus on the ventral surface of the promontorium; Clemente 1985; Evans 1993; Wible 2010). The tympanic nerve leaves no trace on the petrosal surface, but the lesser petrosal nerve enters a canal that extends parallel with but dorsal to the greater petrosal nerve (Fig. 10.2). The lesser petrosal nerve then follows the mandibular branch of the trigeminal nerve, and leaves the cranium through the foramen ovale.

More posteriorly, cranial nerves IX, X, and XI leave the braincase through the jugular foramen (Figs. 10.1–2).

The hypoglossal nerve (XII) is the most posterior cranial nerve, and is extremely well developed in *Glossotherium* (Fig. 10.1A–C), but very reduced in the extant sloths (Fig. 10.1E–L).

In general, *Glossotherium* exhibits great enlargement of the sphenorbital fissure, the foramen ovale, and the hypoglossal foramen, in comparison with of all the other nerve-transmitting foramina (Fig. 10.1A–D). On the contrary, more homogeneity in the size of the foramina is observed in the extant sloths *Choloepus* (Fig. 10.1E–H) and *Bradypus* (Fig. 10.1I–L).

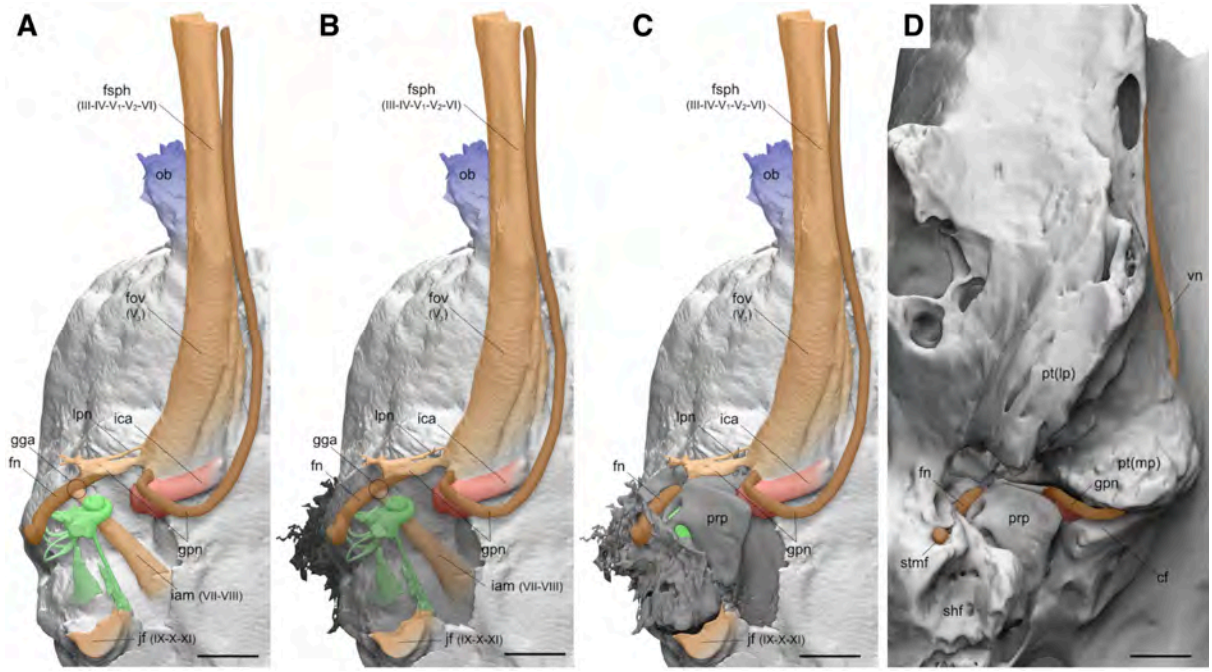

Figure 10.2. Digital reconstruction of (A–C) the right side endocasts in ventrolateral view, with the petrosal represented in decreasing degrees of opacity, and (D) the right side braincase in ventrolateral view, of *Glossotherium robustum* (MACN Pv 13553). Abbreviations: cf, carotid foramen; fn, facial nerve; fov, foramen ovale; fsph, sphenorbital fissure; gga, geniculate ganglion area; gpn, greater petrosal nerve; iam, internal acoustic meatus; ica, internal carotid artery; jf, jugular foramen; lpn, lesser petrosal nerve; ob, olfactory bulb; prp, promontorium of petrosal; pt(lp), pterygoid (lateral portion); pt(mp), pterygoid (medial portion); shf, stylohyal fossa; stmf, stylomastoid foramen; vn, vidian nerve. Colors indicate: blue, olfactory bulbs; green, bony labyrinth; orange, neurovascular connections; red, arterial vessels. Darker tones of red and orange indicate inferred structures on the outer surface of the skull. Roman numeral designations indicate cranial nerves. Scale bars equal 2 cm.

10.1.3 Blood vessels

As already observed, the surface of the brain endocast of *Glossotherium* is more rugose and convoluted than in the extant sloths. Not only are sulci and gyri more evident in *Glossotherium* than in the extant genera, but grooves for the blood vessels are also more clearly marked. In fact, some vessels have left marks that we attribute to both arteries and veins (Fig. 10.3).

Arteries- The main arterial vessel leading to the brain is the internal carotid artery, entering in the cranial cavity through the carotid foramen, located at the anteromedial corner of the petrosal. In *Glossotherium*, the track of the internal carotid artery is particularly enlarged at the base of the trigeminal ganglion, and is visible on both sides of the ventral surface of the endocast, at the level of the hypophyseal region (Fig. 10.3B–D). This vessel is partially visible in the ventral

endocast of *Choloepus* (Fig. 10.3F) but not detectable in *Bradypus*. In both *Glossotherium* and *Choloepus*, the internal carotid artery shows a strong posterolateral to anteromedial trajectory, following a detached sulcus on the internal side of the petrosal (Patterson *et al.* 1992; Boscaini *et al.* 2018a). In *Glossotherium* (Fig. 10.3A, B, D), two paired arteries diverge toward the olfactory bulbs (= internal ethmoidal arteries, according to Evans 1993: 626). These are partially preserved in *Glossotherium* MACN Pv 13553 along the medial margin of the olfactory bulbs, and are oriented largely dorsoventrally (Fig. 10.3A, B, D).

These vessels are attributed to arteries on the basis of their large size, which is more compatible with the anteriormost termination of the ventral arterial system of the brain than any vein draining the region. Moreover, this pattern is typical in mammals and appears to be plesiomorphic in xenarthrans, as it is observed in the extant armadillos, anteaters, and sloths (Hyrtl 1854; Tandler 1901; Bugge 1979).

Veins- The venous circulation is partially preserved in MACN Pv 13553. In dorsal view, some tiny vessels, the branches of the frontal meningeal veins, depart from the olfactory bulbs and are posteriorly directed (Fig. 10.3A, C, D). More posteriorly, the branches of the parietal meningeal vein are thicker than the frontal meningeal veins and are irregularly distributed. All these veins are confluent with the dorsal sagittal sinus, the posteriormost portion of which is represented in MACN Pv 13553 (Fig. 10.3A). This latter sinus is observable along nearly its entire length in *Oreomylodon* (Dechaseaux 1971). The dorsal sagittal sinus connects posteriorly to the paired transverse sinuses at the level of their median divergence (Fig. 10.3; Evans 1993: 709). The grooves for these latter vessels, located at the boundary between the cerebral hemispheres and the cerebellum (and thus along the transverse fissure), are the largest on the dorsal surface of the endocast, a condition that is also observed in other extinct sloths such as *Megatherium*, *Mylodon*, *Oreomylodon*, *Scelidotherium*, and *Eucholoeops* (Gervais 1869; Dechaseaux 1958, 1962a, 1971; Dozo 1994).

In lateral view, the transverse sinus divides laterally into two anteriorly directed lesser veins: the ventral cerebral vein and the dorsal petrosal sinus (Fig. 10.3C). The former has a wider diameter than the latter, and extends partially in the caudal suprasylvian sulcus, whereas the latter is narrower, lies in a more ventral position (on the pyriform lobe), and projects farther anteriorly (Fig. 10.3C).

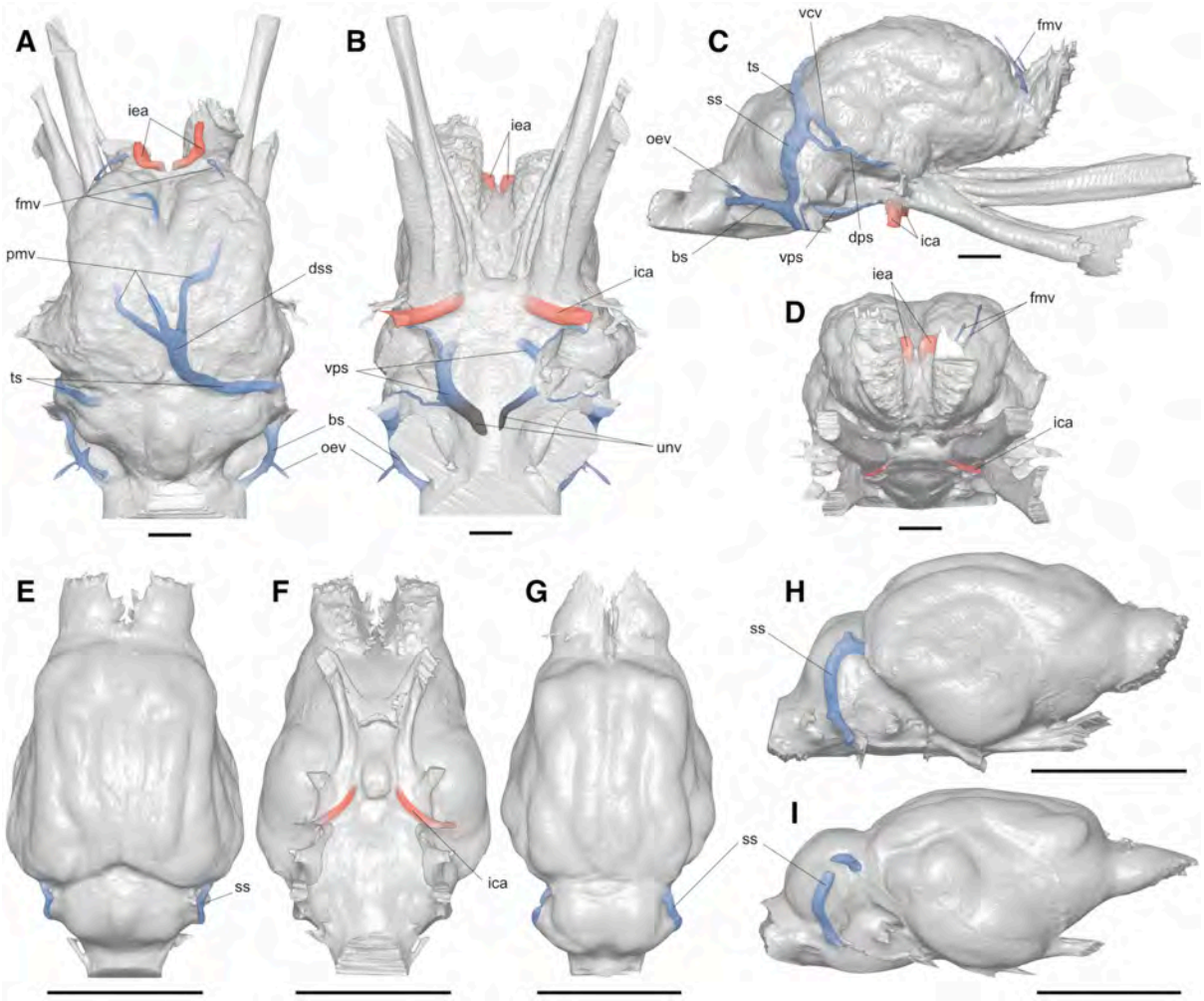

Figure 10.3. Brain endocasts of *Glossotherium* (MACN Pv 13553) (A–D), *Choloepus* (AMNH 30765) (E, F, H), and *Bradypus* (AMNH 95105) (G, I), in dorsal (A, E, G), ventral (B, F), lateral (C, H, I), and anterior (D) views, showing the arterial vessels (red) and venous vessels (blue). Abbreviations: bs, basilar sinus; dps, dorsal petrosal sinus; dss, dorsal sagittal sinus; fmv, branches of the frontal meningeal vein; ica, internal carotid artery; iea, internal ethmoidal artery; oev, occipital emissary vein; pmv, branches of the parietal meningeal vein; ss, sigmoid sinus; ts, transverse sinus; unv, unknown vessel; vcv, ventral cerebral vein; vps, ventral petrosal sinus. Scale bars equal 2 cm.

The greater part of the transverse sinus flows laterally and ventrally into the sigmoid sinus, which leaves the cranium through the jugular foramen (Fig. 10.3B–C). The sigmoid sinus is the only vein that is recognizable on the endocasts of the extant sloths *Choloepus* (Fig. 10.3E, H) and *Bradypus* (Fig. 10.3G, I). In its most ventral portion, the sigmoid sinus of *Glossotherium* MACN Pv 13553 is joined by two veins, the ventral petrosal sinus and the basilar sinus (= ventral occipital sinus; Reinhard *et al.* 1992) (Fig. 10.3B–C). In ventral view (Fig. 10.3B), the ventral petrosal sinus extends anteroposteriorly through a fissure that lies between the petrosal and the basioccipital. In its anteriormost portion, the ventral petrosal sinus passes through a second opening in the posterior wall of the carotid foramen, whereas posteriorly it emerges in the

anterior wall of the jugular foramen, where it joins the sigmoid sinus ultimately leaving the skull through the jugular vein (Fig. 10.3B–C). There is a large venous branch of the ventral petrosal sinus that extends posteroventromedially, the left and right sides converging toward the floor of the foramen magnum. As it is not known a large vein that would occupy such a position in xenarthrans, or indeed in other mammals, for the time being, this branch has been labeled as an unknown vessel (Fig. 10.3B). The basilar sinus merges with the sigmoid sinus more dorsally than the ventral petrosal sinus, and extends through the condyloid canal (Fig. 10.3A–C). At its posterior end, the basilar sinus turns into the internal vertebral venous plexus as it leaves the foramen magnum (Evans 1993: 711). This condition was previously observed in the genus *Mylodon* by Patterson *et al.* (1992), who suggested that the "very large groove running from the inside of the foramen lacerum posterium to the foramen magnum" was pierced by an unidentified "venous sinus" (Patterson *et al.* 1992: 6). In accordance with the CT scans performed in the present study and the recent veterinary *Nomina Anatomica* (Clemente 1985; Evans 1993), this vein is likely the basilar sinus. The groove that housed this vessel is absent in all living xenarthrans (Patterson *et al.* 1989, 1992).

The condyloid canal, which connects the jugular foramen with the foramen magnum, has a dorsoposteriorly directed branch near its caudal end (Fig. 10.3A–C). This branch emerges posteriorly at the mastoid foramen, located just dorsal to the occipital condyle. This latter canal accommodated the occipital emissary vein, draining the external surface of the occipital bone.

10.1.4 Cranial pneumaticity

The paranasal sinuses, a characteristic feature of placental mammals (e.g., Moore 1981; Novacek 1993), are air-filled chambers that form within a variety of cranial bones and are connected to the nasal cavity. The paranasal sinuses are commonly divided into maxillary, frontal, and sphenoidal sinuses, of which the maxillary sinuses are the most basal and widespread among eutherian mammals (Moore 1981). The maxillary sinuses are also invariably present in xenarthrans (Moore 1981). Unfortunately, due to breakage of the anterior portion of MACN Pv 13553 (see Chapter 3, Fig. 3.1), the maxillary sinuses cannot be observed. Thus, the description and comparison that follow will be limited to the frontal and sphenoidal sinuses. These sinuses are so named because they are typically found within the frontal and sphenoidal bones (specifically the presphenoid; Evans 1993), but sometimes they extend into other cranial bones (Moore 1981). For this reason, and following this scheme, the description of the cranial pneumatization pattern in *Glossotherium* and the extant sloth genera will be based on the bony

elements directly involved (e.g., "orbitosphenoid sinus"). In mammals, the number and extent of the chambers differ among species, but their development also varies greatly during ontogeny, producing intraspecific variation among individuals of different ages, particularly during the later stages of growth and in adult life (Moore 1981; Farke 2008). Moreover, minor differences occur between the right and left sides of a single individual (Moore 1981). Therefore, the descriptions are limited to symmetrically observed aspects of sinus morphology, and the inter-taxon comparison is made only among adult specimens, in order to avoid differences related to different ontogenetic stages.

The three genera considered in this chapter (i.e., *Glossotherium*, *Choloepus*, and *Bradypus*) possess both frontal and orbitosphenoid sinuses. In *Bradypus*, the frontal sinuses are smooth walled and shallow in lateral view (Fig. 10.4G–I). These sinuses are approximately rectangular in dorsal view and more elongated anteroposteriorly than mediolaterally. They are composed of a single chamber that covers the olfactory bulbs dorsally and is limited posteriorly by the fronto-parietal suture (Fig. 10.4G–H). Ventral to, and separate from the frontal sinuses, some small sinuses open into the orbitosphenoid. These orbitosphenoid sinuses are located just ventral to the olfactory bulbs and posterior to the ethmoid. Their most lateral portions project anteriorly towards the nasopharynx (Fig. 10.4G). Another highly pneumatized part of the skull is the zygomatic process of the squamosal, which contains the epitympanic sinus, passing dorsally from its posterior connection to the tympanic cavity into the squamosal, and then extending anteriorly to the level of the glenoid fossa (Fig. 10.4G–H). The epitympanic sinus is the only observable paratympanic space (i.e., "any significant pneumatic excavation within the confines of the middle ear but outside the bounds of the tympanic cavity proper"; Forasiepi *et al.* 2019: 63). Also, large pterygoid sinuses have been described in the maned sloth, *B. torquatus* (e.g., Guth 1961), but are not evident in this specimen of *B. variegatus*, and are not known to be developed in other *Bradypus* species (Patterson *et al.* 1992; Hayssen 2008, 2010). The frontal, orbitosphenoid, and zygomatic sinuses are distinct and well separated in lateral, dorsal, and anterior views (Fig. 10.4G–I).

In *Choloepus* (Fig. 10.4D–F), the frontal sinuses are much larger, more complex, more convoluted, and display more bilateral asymmetry than those of *Bradypus* (Fig. 10.4G–I). In the two-toed sloth, these sinuses are composed of several chambers extending dorsally over the olfactory bulbs (Fig. 10.4D–F). In dorsal view (Fig. 10.4E), they extend posterior to the fronto-parietal suture into the parietal, following an irregular pattern that is not observed in *Bradypus* (Fig. 10.4H).

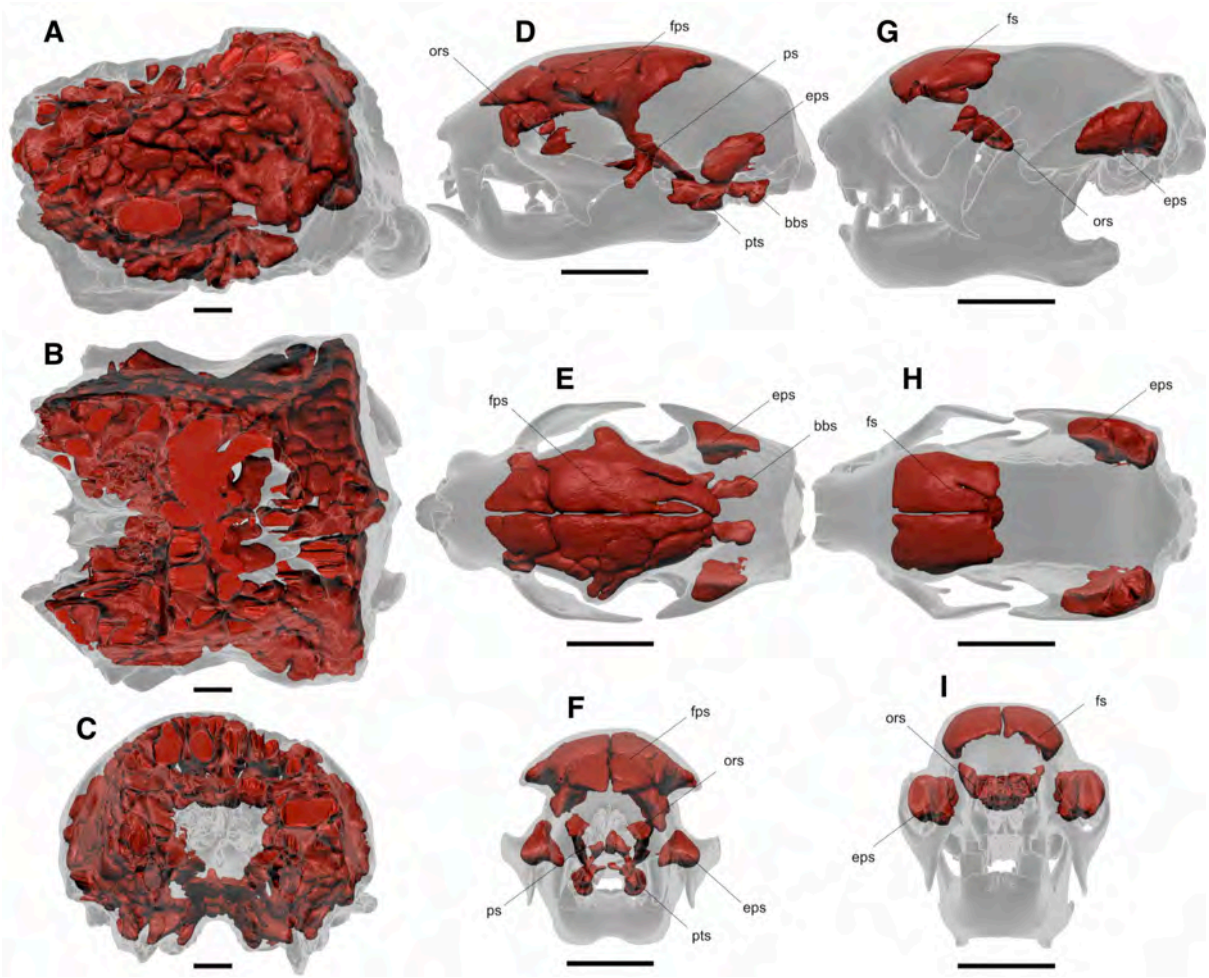

Figure 10.4. Cranial pneumaticity in the skulls of *Glossotherium* (MACN Pv 13553) (A–C), *Choloepus* (AMNH 30765) (D–F), and *Bradypus* (AMNH 95105) (G–I), in lateral (A, D, G), dorsal (B, E, H), and anterior (C, F, I) views. Abbreviations: bbs, basisphenoid-basioccipital sinuses; eps, epitympanic sinuses; fps, fronto-parietal sinuses; fs, frontal sinuses; ors, orbitosphenoid sinuses; ps, palatine sinuses; pts, pterygoid sinuses. Scale bars equal 2 cm.

Choloepus has small orbitosphenoid sinuses that are visible in lateral and anterior views, just ventral to the olfactory bulbs (Fig. 10.4D, F). These are separated from the frontal sinuses, as in *Bradypus*. In their most lateral parts they project anteriorly, but are quite asymmetric (Fig. 10.4D, F). In contrast with *Bradypus*, the frontal sinuses of *Choloepus* project markedly posteroventrally in lateral and anterior views. This extension merges with the palatine sinuses (Fig. 10.4D, F). On the right side of *Choloepus* AMNH 30765, the pneumatization is continuous, whereas it is separated by a thin septum on the left side (Fig. 10.4D, F). More ventrally, the pneumatization of the palatine is in contact with the pterygoid sinuses in both the right and the left sides. The inflation of the pterygoid is more pronounced in *Choloepus* than in *Bradypus* (except in *B. torquatus*, see preceding paragraph) or *Glossotherium* (Gaudin 2004: char. 137). The

basicranial pneumatization extends posteriorly into the basisphenoid and the basioccipital, again with a sinuous and irregular pattern comparable to the irregularities observed in the other sinuses of *Choloepus*. As in *Bradypus*, the zygomatic process of the squamosal is also well pneumatized, housing an extensive epitympanic sinus (Fig. 10.4D–F). The pneumatized region extends from the tympanic cavity dorsally into the squamosal and anteriorly to the level of the glenoid fossa, but it tapers in width posteriorly, terminating before reaching the posterior end of the zygomatic process. Therefore, the epitympanic sinus is somewhat smaller and more anteriorly restricted than that of *Bradypus* (Fig. 10.4D–E, G–H). *Choloepus* displays more pneumatized areas than *Bradypus*, as well as more communication among them (Fig. 10.4D–F, G–I).

In *Glossotherium* (MACN Pv 13553; Fig. 10.4A–C) the pneumatization is so pervasive that the sinuses mirror the external morphology of the cranium and are not separable into well-defined areas as in *Choloepus* (Fig. 10.4D–F) and *Bradypus* (Fig. 10.4G–I). Pneumatization in *Glossotherium* affects the whole braincase, from the occipital to the parietals and frontals, extending ventrally into the side walls of the braincase and the basicranium, and supported throughout by internal struts (Fig. 10.4A–C). This condition is comparable to the extent of pneumatization in other extinct giant sloths in which this feature has been observed, such as the mylodontid *Oreomylodon* and the megalonychids *Megalocnus* and *Megistonyx* (Dechaseaux 1971; Patterson *et al.* 1992; McDonald *et al.* 2013). However, such pneumatization may not be universal in giant extinct sloths, as suggested by the genus *Eremotherium* (see sectioned skull in Patterson *et al.* 1992: 35). In lateral view, air-filled chambers are missing from only a few areas of the skull of *Glossotherium*. These include the paraoccipital process of the petrosal and the exoccipital crest, both involved in the formation of the stylohyal fossa (Fig. 10.4A–B). Also, the bones surrounding the foramen magnum are not pneumatized, including the most distal portion of the basioccipital and the most ventral limit of the occipital, along with the occipital condyles (Fig. 10.4A–B). This is probably related to the robustness necessary in these areas that articulate with the hyoid apparatus and the vertebral column, respectively. A reduction of the sinuses in the vicinity of the foramen magnum is also observed in modern elephants, the cranium of which is otherwise highly pneumatized (Van der Merwe *et al.* 1995). Left and right portions of the cranium in *Glossotherium* display similar pneumatization, but there is considerable shape variation. Some tubular structures are detectable among the rounded air-filled spaces, both on the internal and external sides of the pneumatized layer. These structures are neurovascular in nature, but their limits frequently cannot be traced because of breakage or structural discontinuities.

10.2 DISCUSSION

The recent increase in paleoneurological studies of extant and extinct vertebrates reflects the fact that brain endocasts represent an important source of anatomical, morpho-functional, and, in particular cases, ethological information, which help researchers in their attempt to better understand the paleobiology of extinct mammals (e.g., Sakai *et al.* 2011; Cunningham *et al.* 2014; Thiery & Ducrocq 2015; Dozo & Martínez 2016; Vinuesa *et al.* 2016; Bertrand *et al.* 2017). Unfortunately, our knowledge of extinct sloth brain morphology and its functional implications are based on only a very few, dated studies (e.g., Gervais 1869; Dechaseaux 1971; Dozo 1987, 1994). In addition, endocasts from this group of mammals have been obtained from only a limited number of genera, almost always represented by very few specimens. Despite these limitations, the descriptions and comparisons of the endocast features in the present study allow for some preliminary analysis.

Brain endocast- According to Dechaseaux (1971) and Dozo (1987), all the extinct sloth taxa discussed above show a very similar brain morphology, and this similarity involves not only the general shape of the brain, but also the pattern of convolutions, which are highly conservative in both extinct and extant sloth species. However, the apparent roughness of the external surface is shared exclusively among the large-bodied extinct sloths, suggesting that this feature might be related to allometric factors. The pattern of convolutions apparently remained fairly stable during the evolutionary history of sloths and the number, and arrangement, of the identified convolutions is almost the same (Fig. 10.1). In both *Glossotherium* MACN Pv 13553 and A10.263, the entolateral sulcus is clearly visible, but this is also true in the extinct genera *Lestodon*, *Megatherium, Mylodon, Oreomylodon*, and *Scelidotherium* (Gervais 1869; Dechaseaux 1958, 1962a, 1971), and in the extant two-toed sloth *Choloepus*. However, this sulcus is absent in the extant three-toed sloth *Bradypus* and in the middle Miocene forms *Hapalops* and *Eucholoeops* (Dozo 1987, 1994). The distribution of this feature accords with the most recent phylogenetic scenarios based on morphological evidence (Gaudin 1995, 2004), which propose that *Choloepus* and *Glossotherium* are more closely related to one another than either is to *Bradypus*. However, the condition in *Bradypus* is present in *Hapalops* and *Eucholoeops*, even though the latter two are more closely related to *Choloepus* than *Glossotherium* according to Gaudin (2004). The simplified pattern of *Bradypus*, *Hapalops*, and *Eucholoeops*, along with the phylogenetic position of *Bradypus* as the putative sister-taxon to all other sloths, suggests that *Bradypus* has maintained the plesiomorphic condition probably since the Oligocene (Dozo 1987, 1994; Gaudin & Croft

2015), but it may also imply that the similarity between *Glossotherium* and *Choloepus* evolved convergently.

The complexity of convolutions is generally higher in large-sized mammals than in medium- to small-sized mammals, because the convolutions increase the amount of cortical surface area, compensating for reductions in surface area to volume ratio for brains of increasing size (e.g., Prothero & Sundsten 1984; Roth & Dicke 2005; Macrini *et al.* 2007b). Folivorans seemingly do not follow this rule. In fact, the apparent complexity of the telencephalic surface in *Glossotherium* and other large-sized species is related to the presence of several surface irregularities, consisting of a high number of recesses and protrusions (Fig. 10.1). Their irregular shape, small size, and, especially, uniform distribution on the brain surface (they are even observed on surfaces of the blood vessels) allow to exclude the possibility that these structures are convolutions. They are more likely interpreted as traces of meninges. In large extant mammals of similar size (e.g., pachyderms and cetaceans), meninges, cisterns, and other soft-tissue structures tend to fill the spaces in the sulci of the brain, obscuring the pattern of sulci and gyri (Macrini *et al.* 2007b and references therein) and this phenomenon can be partially responsible for the reduced sulcation in *Glossotherium*. In any case, in extant and extinct sloths the basic pattern of convolutions is always observable, independent of body size. This basic pattern closely resembles that of carnivorans, which display the simplest arrangement of convolutions among gyrencephalic mammals (Barone & Bortolami 2004). This similarity is particularly strong for the dorsal surface of the telencephalon, and has been previously reported by Gervais (1869), Elliot-Smith (1898), and Anthony (1953).

The olfactory bulbs in *Glossotherium* strongly project dorsally (Fig. 10.1A–D), with an enlarged anterior surface covered by the many ramifications of the olfactory nerve. In the specimens of *Oreomylodon* and *Glossotherium* figured by Dechaseaux (1958, 1971), the olfactory bulbs are also directed and enlarged dorsally. Even though the splanchnocranial portion is missing in *Glossotherium* MACN Pv 13553, a fragment of the ethmoid bone is preserved, in which the cribriform plate appears vertical, exceeding in height the dorsal portion of the olfactory peduncles. This condition is also observed in *Oreomylodon* (Dechaseaux 1971: fig. 5), but it does not occur in the extant sloth taxa, where the cribriform plate ends at the dorsal limit of the olfactory peduncles, thus conferring a horizontal dorsal profile to the bulbs in lateral view. In *Glossotherium*, the dorsal projection of the olfactory bulbs can be related to the dorsoventral expansion of the nasal cavities, which can affect the horizontal development of the cribriform plate and, consequently, the vertical profile of the bulbs. It is currently difficult to assess if, and how, this peculiar morphology of the olfactory bulbs relates to the olfactory sensitivity in this

extinct sloth. For example, the expansion of the nasal cavities may represent an adaptation to particular environmental conditions, or may be related to thermoregulation, water balance, or even sound production (or a combination of them). A larger set of cranial and paleoneurological data is needed to better understand the correlation between morphology and function of the olfactory bulbs in these taxa. A dorsal projection of the olfactory bulbs is not present in *Choloepus*, but like *Glossotherium*, it has anteroposteriorly short bulbs that are deep dorsoventrally and narrow transversely. The olfactory bulbs of *Bradypus* are shallow dorsoventrally, elongated anteroposteriorly, and pointed at their anterior tip, with a broad olfactory peduncule, imparting a morphology quite different from that observed in *Glossotherium* and *Choloepus*. The shape of the olfactory bulbs in *Bradypus* does resemble that of *Hapalops* (Dozo 1987), and to a lesser extent of *Eucholoeops* (Dozo 1994), which again likely represents the retention of a plesiomorphic condition in these taxa.

If the telencephalon shows a fairly uniform pattern of convolutions in both extinct and extant sloths, the cerebellum (together with the olfactory bulbs) represents the most variable portion of the sloth endocasts. In dorsal view, *Glossotherium* has a sub-triangular cerebellum with the apex formed by the posterior portion of the vermis. This shape is the result of a lateral expansion of the two cerebellar hemispheres, which reach a maximum transverse width equivalent to that of the posterior portions of the cerebral hemispheres. This latter is a common feature in large-bodied extinct sloths, and is generally accompanied by the presence of a well-developed paraflocculus. The presence of large paraflocculi is considered a plesiomorphic character within therian mammals (Kielan-Jaworowska 1986; Macrini *et al.* 2007b). In *Glossotherium*, the paraflocular areas are proportionally wider than in the small-bodied extant sloths *Bradypus* and *Choloepus*, in which they appear as tiny swellings just dorsal to the jugular foramen (Fig. 10.1). The former condition was previously illustrated by Dechaseaux (1971) for both *Glossotherium* and *Oreomylodon*. The latter condition is here reported for the two extant genera *Choloepus* and *Bradypus,* but was also recognized in the late early Miocene sloths *Hapalops* and *Eucholoeops* (Dozo 1987, 1994). Further studies should investigate the possible allometric and functional significance of this feature.

Cranial nerves- The main trajectories of the cranial nerves have been reconstructed for *Glossotherium robustum* MACN Pv 13553 (Figs. 10.1–2) and the extant sloths *Bradypus* and *Choloepus* (Fig. 10.1). The cranial nerve pathways through the sphenorbital fissure, foramen rotundum, and foramen ovale are similar in *Glossotherium* and *Choloepus*, and differ significantly from the pattern in *Bradypus*, consistent with their proposed closer phylogenetic affinity (Gaudin

1995, 2004). In *Glossotherium*, the grooves for the sphenorbital fissure, the foramen ovale, and the hypoglossal foramen are enlarged relative to other foramina transmitting cranial nerves, confirming initial observations by Owen (1839, 1842). The presence of these deep furrows is probably related to a greater development of the trigeminal and hypoglossal nerves (and accompanying vasculature), compared to other nerves, in the extinct sloth *Glossotherium*, than in *Bradypus* and *Choloepus*, where the nerve-transmitting foramina are more uniform in size. This probably can be related to larger relative sizes of tongue and jaw muscles in the extinct genus *Glossotherium* than the extant forms, in accordance with their different dietary habits (Bargo *et al*. 2006b; Pujos *et al*. 2012). The large sphenorbital fissure and foramen ovale also could be partially related to an increased sensory innervation and vasculature coming from the elongated rostrum and enlarged nasal cavity of *Glossotherium*.

Blood vessels- Blood vessels are more difficult to observe in the small-sized extant sloths than the large-sized *Glossotherium* (Fig. 10.3). In the latter (Fig. 10.3A–D) many blood vessels are discernible, and the general pattern is similar to that observed in other extinct sloths (Gervais 1869; Dechaseaux 1958, 1962a, 1971; Dozo 1994) and comparable with the plesiomorphic condition in xenarthrans (Hyrtl 1854; Tandler 1901; Bugge 1979). This suggests a conservative conformation of the blood circulation. The sigmoid sinus is the only vessel that is invariably observed in *Glossotherium*, *Choloepus*, and *Bradypus*, whereas the impression of the internal carotid artery is another feature only found in *Glossotherium* and *Choloepus* (Fig. 10.3).

Cranial pneumatization- Many hypotheses concerning the function of the paranasal sinuses have been proposed (exhaustive reviews are available in Blanton & Biggs 1969; Moore 1981; Blaney 1990). The idea that cranial pneumatization is basically functionless (Weidenreich 1924, 1941; Edinger 1950; Witmer 1997) has become the most widely accepted hypothesis over the last decade (Farke 2008, 2010). The possible existence of "opportunistic pneumatization," which implies that the sinuses do not have any apparent function and are merely the result of the removal of structurally unnecessary bone, has been gaining support over the last few years and was recently advocated by Farke (2007, 2008, 2010) who conducted the "broadest and most comprehensive quantitative analysis of sinus morphology ever attempted" (Farke 2010: 1010). The same author demonstrated that the size and complexity of paranasal sinuses in bovids are not related with their ramming behavior, as previously thought (Farke 2010). On the contrary, they seem to be partially related to the size of the frontals (and consequently the whole skull), and consistent with a role for the sinuses in weight reduction (Farke 2010).

However, this is true only in those groups that already possess pneumatized frontal bones, suggesting both a positive allometry with skull size and a strong phylogenetic component. In this sense, Farke (2010) recognized that the presence of a frontal sinus is the ancestral condition in Bovidae and has been lost several times during the evolution of the clade. In different bovid taxa, Farke (2010) also detected several pneumaticity patterns, which include: i) sinuses extending up to the fronto-parietal suture (i.e., sinuses that do not cross the suture and even conform to its morphology), ii) sinuses extending beyond the fronto-parietal suture to pneumatize the parietal, and occasionally also the occipital bone, and iii) sinuses widely extended and pneumatizing large regions of the cranium (e.g., including the entirety of the horn cores).

These preliminary data suggest that similarities between bovids and sloths can be recognized regarding the development of the sinuses. Generally, sinus morphology in Xenarthra seems to have a strong phylogenetic component, given that frontal sinuses have been demonstrated to be diagnostic even at the subspecific level for different morphotypes of the nine-banded armadillo *Dasypus novemcinctus* (Billet *et al*. 2017). In contrast, frontal sinuses are lacking in anteaters, in which only some basicranial pneumatizations are observed, mainly in the alisphenoid, palatine, and the pterygoid bones, along with an epitympanic sinus in the squamosal (Moore 1981; Storch & Habersetzer 1991; Patterson *et al*. 1992; Gaudin 1995, 2004).

In the three sloth genera described in the present chapter, the frontal sinuses are invariably present. *Bradypus*, the putative sister group to all the other extant and extinct sloths (e.g., Gaudin 2004) presents the simplest observed pattern, with the fronto-parietal suture limiting the extent of the frontal sinuses posteriorly (Fig. 10.4G–I). On the other hand, *Glossotherium* and *Choloepus*, which are more closely related phylogenetically according to Gaudin (2004), also show similarities exclusive of *Bradypus* in the morphology of their cranial sinuses. For example, both exhibit a continuous pneumatization, from the frontals to the basicranium (Fig. 10.4A–F). This pneumatization is extremely exaggerated in *Glossotherium,* so that it involves a series of interconnected chambers invading nearly every posterior cranial bone. Total body size must be taken into account, and it is noteworthy that *Bradypus* is the smallest of the three genera, followed closely by *Choloepus*, whereas *Glossotherium* is much larger, approaching the size of the largest modern bovids. This suggests the presence of a corresponding positive allometry in sinus size relative to skull size. As Farke (2010) observed in bovids, it appears that in the sloth clade, the different patterns observed are likely related to both phylogenetic effects and the influence of body size.

10.3 CONCLUSIONS

The digital cranial endocasts of *G. robustum* have been described and compared with representative specimens of extant sloths, providing an anatomical characterization of the main features of the brain cavity, cranial nerves, blood vessels, and sinuses.

Among these structures, some features could have a phylogenetic signal, such as the general shape of the brain endocast, the presence/absence of the entolateral sulcus, and the shape of the olfactory bulbs and the vermis. However, the general pattern of sulci and gyri on the brain endocast appeared to be extremely conservative in the folivoran clade, confirming its simple organization, independent of body size, if compared with other mammals. Similarly, the arterial and venous circulation appeared to be conservative in sloths, even if blood vessel features are more difficult to observe in smaller- rather than larger-sized sloths. Other characters, such as the apparent roughness of the external surface of the brain endocast and the mediolaterally expanded cerebellum, may be related, instead, to allometric factors. In contrast, the relative size of the foramina through which the trigeminal and hypoglossal nerves passed suggests a probable physiological influence, related with food processing and sensory information.

Finally, paranasal pneumatization shows evidence of mixed signals, i.e., it is mainly affected by phylogeny and allometry, even if a functional influence related to body size increase cannot be currently refuted.

Chapter 11
CONCLUSIONS

In the present thesis, several aspects of the evolutionary history of Mylodontidae have been investigated, using different approaches and applying different methodologies, depending on the proposed specific objectives (see Chapter 2 for further details).

In this concluding section, the main aspects of each chapter are summarized, and some possible future directions of the research are proposed.

11.1 GEOGRAPHY AND GEOLOGY (Chapter 4)

The localities of the Bolivian Altiplano explored during the last decades (i.e., Ayo Ayo-Viscachani, Casira, Choquecota, Inchasi, and Pomata-Ayte) provided a large number of fossil remains of several extinct mammals, and particularly xenarthran sloths. From a geographical perspective, these localities span a large portion of the Bolivian Altiplano, from the La Paz Province in the North to the Argentinian-Bolivian border in the South. Bibliographic information on absolute ages, combined with novel data, allowed for a revision of the fossil sites. These localities are almost exclusively Pliocene in age, but the locality of Choquecota also contains latest Miocene deposits. In some of these localities (i.e., Choquecota and Pomata-Ayte), the presence of the volcanic tuff "Toba 76" is useful to mark the Miocene–Pliocene transition in the Neogene series of the central Altiplano, and its absolute age has been recently recalculated at 5.26 ± 0.02 Ma (Boscaini *et al.* 2019a). The oldest remains of Neogene mylodontine sloths from the Bolivian Altiplano have been found fifteen meters below "Toba 76" in the Choquecota locality, whereas the youngest occur at the top of the Umala Formation in the deposits of Ayo Ayo-Viscachani.

11.2 SYSTEMATIC REVISION OF MYLODONTINAE (Chapter 5)

In recent years, multiple paleontological collections were visited in order to obtain information on both South and North American mylodontid taxa, and to facilitate a taxonomic revision of the members of Mylodontinae. The collections visited in South America (Argentina, Bolivia, and Venezuela), North America (USA and Canada), and Europe (France), together with photographic and bibliographic data, provided extensive information on the anatomy of mylodontid remains, which has been fundamental for comparisons with the Bolivian fossil

specimens (Chapter 6), but also for conducting a detailed phylogenetic analysis of the clade (Chapter 8).

Overall, at least twenty-nine species under twenty-one genera within Mylodontinae are considered valid. Some of these species, such as *Urumacotherium garciai* and *U. campbelli*, *Bolivartherium urumaquensis* and *B. codorensis*, and *Thinobadistes wetzeli*, are known only by a limited number of specimens, and for this reason their identifications have been confirmed only at the generic level. For Neogene mylodontine taxa, some synonymies and changes of taxonomic attributions have been proposed on the basis of the comparative study of the fossil remains from the Bolivian Altiplano (see next section).

11.3 DESCRIPTION AND COMPARISON OF THE SKELETAL ANATOMY OF *SIMOMYLODON UCCASAMAMENSIS* (Chapter 6)

Simomylodon uccasamamensis is, to date, the only recognized mylodontid sloth from the late Miocene–Pliocene deposits of the Bolivian Altiplano. This species is endemic to this region during the Montehermosan, Chapdamalalan, and (early) Marplatan SALMAs. In fact, the moderate-sized Miocene–Pliocene mylodontids (i.e., *Glossotheridium chapadmalense*, *Glossotheriopsis pascuali*, *Paramylodon garbanii*, *Pleurolestodon acutidens*, and *Simomylodon uccasamamensis*) can be separated both morphologically and morphometrically. *Simomylodon uccasamamensis* and the Miocene species *Pleurolestodon acutidens* have a wide braincase in relation to the total cranial length, occipital condyles that are well-separated from the condyloid foramina, and a medial palatal process of the maxilla with a transverse width greater than its anteroposterior length. The foramen magnum of *S. uccasamamensis* shows a well-developed notch located on its dorsal border, similar to that observed in *Pleurolestodon* and *Mylodon* and, in lateral view, the ascending process of the jugal is long and slender, strongly resembling that of *Glossotheridium chapadmalense*.

At the level of the dentition, the diastema between Cf and Mf1 is absent or extremely reduced in *S. uccasamamensis* and, in lateral view, the Cf presents an almost vertical wear facet, similar to the condition in *Pleurolestodon acutidens*. Mf2 and Mf3 possess a marked lingual sulcus, comparable to *Pleurolestodon acutidens* and *Paramylodon garbanii*. Also, in *S. uccasamamensis* the lower caniniforms are beveled, with well-developed mesial and distal wear surfaces, the mf3 is marked by a deep apicobasal sulcus on its lingual side absent in the labial side, and is not covered by the ascending ramus of the mandible in lateral view (like *G. chapadmalense* and unlike *P. acutidens*

and *P. garbanii*). In the mandible, the symphyseal spout is anteriorly flat in *S. uccasamamensis,* as in *G. chapadmalense,* and not rounded as in *P. acutidens* and *P. garbanii*.

On morphometric grounds, *Simomylodon uccasamamensis* and *Glossotheriopsis pascuali* are of similar body size, and both of them are smaller than *Glossotheridium chapadmalense*, *Paramylodon garbanii*, and *Pleurolestodon acutidens*.

All the mylodontine specimens from the Inchasi locality described by Anaya & MacFadden (1995) are consistent in both shape and size with *S. uccasamamensis*, and are consequently ascribed to the latter taxon. These include both the mandibular fragments from Inchasi assigned to *G. chapadmalense*, and the postcranial remains ascribed to "Mylodontinae indet." (Anaya & MacFadden 1995). Likewise, the species *Pleurolestodon dalenzae* (Saint-André *et al*. 2010) is considered a junior synonym of *Simomylodon uccasamamensis*. The genus *Pleurolestodon* is therefore monospecific, with the Argentinean species *Pleurolestodon acutidens* as the only valid species recognized to date. In contrast, a juvenile mylodontid mandible from the Huayquerian SALMA of the Buenos Aires Province (Oliva & Brandoni 2012), does not possess the diagnostic features of the juvenile *S. uccasamamensis* specimens from Bolivia. Consequently, its taxonomic attribution as "cf. *Simomylodon"* (Oliva & Brandoni 2012) is changed to "Mylodontinae indet."

Moreover, the late Blancan *Paramylodon garbanii* from North America appears to be distinct from *Glossotheridium chapadmalense,* from the Chapadmalalan SALMA of South America, being differentiable on both morphological and morphometric grounds, reflecting the assertions of Morgan (2008) and McDonald & Morgan (2011).

Overall, *Simomylodon uccasamamensis* is a constant element of the late Miocene – Pliocene localities of the Bolivian Altiplano, and has still not been recovered from outside this region. Accordingly, *S. uccasamamensis* may have been specifically adapted to the ecologic conditions that prevailed in the cold and dry ecosystems of the Bolivian Altiplano during the Pliocene epoch.

11.4 SEXUAL DIMORPHISM IN *SIMOMYLODON UCCASAMAMENSIS* (Chapter 7)

Analysis of the abundant material of *Simomylodon uccasamamensis* from the late Miocene–Pliocene of the Bolivian Altiplano shows the presence of two well-segregated morphs. These two robust and gracile morphotypes are recognizable in both cranial and postcranial elements. The main bimodal differences regard the morphology of the muzzle, the inclination of the occiput, and the relative size of long bones such as femora and tibiae.

The remains previously designated as the holotypes of *Simomylodon uccasamamensis* and *Pleurolestodon dalenzae* by Saint-André *et al*. (2010) appear, in the analyses of the present study, to be members of the robust and the gracile forms of *S. uccasamamensis*, respectively.

The differences between gracile and robust morphs appear to be neither geographically nor chronologically related, strongly suggesting that the two forms are likely different sexes, rather than different taxa. Moreover, a similar segregation of features was previously attributed to sexual dimorphism in several other Pleistocene sloths from both South and North America, suggesting the same condition occurs in *S. uccasamamensis*. This type of intraspecific variation constitutes the earliest well-documented occurrence of sexual dimorphism in extinct sloths. The size-based differences between sexes are accompanied by distinct morphologies of the muzzle, strongly suggesting the presence of distinct feeding habits between males and females. As in extant large herbivores, this may have contributed to the existence of intraspecific niche partitioning and a certain grade of intersexual spatial segregation. In this way, males and females of *S. uccasamamensis*, would have probably avoided intraspecific competition for food resources. This, in turn, may have constituted an adaptation to the changing conditions and the decreasing resources of the Bolivian Altiplano at the Miocene–Pliocene transition. More generally, sexual dimorphism in mylodontine sloths may have been an important contributor to the widespread distribution of the clade during the Quaternary.

11.5 PHYLOGENY OF MYLODONTIDAE (Chapter 8)

In this thesis, a reappraisal of the phylogeny of Mylodontidae has been treated in Chapter 8. This phylogeny of Mylodontidae is the first conducted on morphological features derived from the entire skeleton, and is the largest such analysis to date, incorporating 40 taxa. To increase resolution, Mylodontinae have been treated at the species-level, and special attention has been paid to those taxa from northern areas of South America, previously unexplored from a phylogenetic perspective. The added taxonomic and anatomical coverage, with the new taxa and postcranial features included in this extended matrix, allow for increased resolution relative to previous phylogenetic studies, especially for late Miocene to Pleistocene Mylodontinae from both South and North America.

Among Mylodontinae, *Urumacotherium* and *Pseudoprepotherium* form a monophyletic clade, comprised of Miocene forms from northwestern South America. Despite their older (i.e., Oligocene) age, *Octodontotherium* and *Paroctodontotherium* appear to be more derived, and also to

constitute a monophyletic group. *Brievabradys* from the middle Miocene of Colombia appears to be one step more derived, and the sister taxon of all the other Mylodontinae considered in this analysis. These latter, in turn, are grouped in two monophyletic groups, Mylodontini and Lestodontini, in accordance with the previous analysis of Saint-André (1994). The latter result is not obtained when postcranial features are removed from the analysis, stressing the importance of using the total anatomical evidence available for investigating the phylogenetic relationships of this folivoran clade.

Among Mylodontini, the genera *Pleurolestodon*, *Glossotheridium* and *Simomylodon* represent the most basal members of the clade. Species of the genera *Paramylodon* and *Glossotherium,* respectively, also appear to be monophyletic. From a chronologic point of view, mylodontine and lestodontine sloths diverged around 12 Ma and later diversified independently, expanding in both South and North America during the Neogene and the Quaternary. In this period, the two clades experienced large-scale adaptive radiations, occupying environments at both temperate and tropical latitudes throughout the Americas.

11.6 THE INNER EAR OF *GLOSSOTHERIUM ROBUSTUM* (Chapter 9)

Endocranial structures are another important source of information, with the potential for resolving crucial aspects of the evolutionary history of Folivora. For this reason, the first inner ear of an extinct mylodontid sloth was digitally reconstructed and compared with that of the extant xenarthrans and the giant megatheriine genus *Megatherium*.

However, when analyzing the general labyrinthine shapes with morphometric analyses, the bony labyrinth of *Glossotherium* shows stronger affinities with that of the extant anteaters than the extant sloths. In this extended dataset, folivorans do not cluster together in the morphospace, demonstrating that the effect of phylogeny, even if strong (Billet *et al.* 2015a), cannot explain all the observed variation. Given that allometry has a limited influence on the shape of the bony labyrinth in xenarthrans (Billet *et al.* 2015a), functional aspects should be considered when trying to explain the observed distribution. Nonetheless, current methods linking geometric features with functional aspects of the inner ear have recently been questioned, and are difficult to apply to extinct species, especially without considering intraspecific variation.

In the future, more efficient models linking the morphology of the bony labyrinth with functional attributes in mammals, may shed light on the peculiar association of the labyrinthine

shape in *Glossotherium* and the anteaters. Moreover, the addition of other extinct xenarthrans to the present dataset will be necessary, in order to clarify the timing of the evolutionary changes that occurred in the inner ear of Xenarthra.

11.7 ENDOCRANIAL CASTS OF *GLOSSOTHERIUM ROBUSTUM* (Chapter 10)

The digital cranial endocasts of *Glossotherium robustum* have been described and compared with those of the extant genera *Bradypus* and *Choloepus*, providing the first anatomical characterization of the main features of the brain cavity, cranial nerves, blood vessels, and sinuses in a mylodontid sloth.

Among these structures, the general shape of the brain endocast, the presence/absence of the entolateral sulcus, and the shape of the olfactory bulbs and of the vermis show some phylogenetic signal. Other features, such as the general pattern of sulci and gyri on the brain endocast, and the arterial and venous circulation, appear to be extremely conservative in the folivoran clade. These latter features show a simple organization, independent of body size, when compared with other non-xenarthran mammals as well.

The relative size of the foramina through which the trigeminal and hypoglossal nerves passed is consistently greater in *Glossotherium* than in *Bradypus* and *Choloepus*. These proportions suggest a probable physiological influence, related with food processing and sensory information. In contrast, other features, such as the roughness of the external surface of the brain endocast and the mediolaterally expanded cerebellum, may be related to allometric factors.

Finally, paranasal pneumatization shows evidence of mixed phylogenetic and allometric signals. However, a functional influence related to increased body size cannot currently be discounted.

The digital models reconstructed in this thesis for *G. robustum* represent the first exhaustive anatomical characterization of the endocranial cavities of an extinct sloth. In the future, the analysis of other models, spanning across extinct and extant pilosans and cingulates, will shed light on many of the questions that arose from the present study. The anatomical regions of *G. robustum* analyzed in this work under 3D imaging techniques show the great potential of these methodologies for elucidating the evolutionary history of this peculiar mammalian clade.

APPENDIX I

Appendix I. Table S1. *Simomylodon uccasamamensis* – Referred material.

CODE	SITE	SALMA	DESCRIPTION	PREVIOUS ATTRIBUTION - REFERENCE	FIGURE
MNHN-Bol V 11731 (=GB 078)	Viscachani	Marp.	Anterior part of cranium without dentition	*Simomylodon uccasamamensis* (Holotype) - Saint-André *et al.* (2010)	Fig. 6.1
MNHN-Bol V 3321	Ayo-Ayo	Marp.	Maxillary and premaxillary fragments with upper dentition	*Simomylodon uccasamamensis* (Paratype) - Saint-André *et al.* (2010)	Fig. 6.2
MNHN-Bol V 3348	Choquecota	Huay./Mont.?	Cranium lacking the posterior part	*Pleurolestodon dalenzae* (Holotype) - Saint-André *et al.* (2010)	Fig. 6.3
MNHN-Bol V 3711	Inchasi	Chap.	Cranium and mandibles with complete dentition and atlas	None - This work	Fig. 6.4
MNHN-Bol V 3726	Casira	Mont.-Chap.	Complete cranium (lacking the posterior portion) and mandibles, associated with osteoderms	None - This work	Fig. 6.5
MNHN-Bol V 3717	Casira	Mont.-Chap.	Cranium and mandibles with almost complete dentition and proximal left ulnar fragment	None - This work	Figs 6.6; 6.15; 6.21
MNHN-Bol V 3718	Inchasi	Chap.	Complete cranium lacking the right zygomatic arch and associated left scapula	None - This work	Figs 6.7; 6.14; 6.18
MNHN-Bol V 3296	Pomata-Ayte	Mont.	Left mandible with complete dentition	*Simomylodon uccasamamensis* - Saint-André *et al.* (2010)	Fig. 6.8
MNHN-Bol V 3358	Inchasi	Chap.	Two mandibular fragments with incomplete dentition	*Glossotheridium chapadmalense* - Anaya & MacFadden (1995)	Fig. 6.9A-C
MNHN-Bol V 3371	Inchasi	Chap.	Two mandibular fragments with incomplete dentition	*Glossotheridium chapadmalense* - Anaya & MacFadden (1995)	Fig. 6.9D-F
MNHN-Bol V 3298	Pomata-Ayte	Mont.	Left anterior mandibular fragment with cf-mf2	*Simomylodon uccasamamensis* - Saint-André *et al.* (2010)	Fig. 6.10A-C
MNHN-Bol V 12518 (=GB 139)	Viscachani	Marp.	Mandibular symphysis with right cf1; part of atlas, axis and caudal vertebrae; proximal part of left humerus; left and right femora, tibiae, fibulae and astragali; right cuboid and calcaneal fragment	None - This work	Figs 6.10D-F; 6.19A-B; 6.26-27; 6.28E-H; 6.29D-I
MNHN-Bol V 12001 (= VIZ357)	Viscachani	Marp.	Left mandibular corpus fragment and dentition (juvenile)	None - This work	Fig. 6.11A-C
MNHN.F.AYO165	Ayo-Ayo	Marp.	Right mandible (juvenile)	*Simomylodon uccasamamensis* - Saint-André *et al.* (2010)	Fig. 6.11D-F
MNHN-Bol V 3359	Inchasi	Chap.	Left mandible with complete dentition (juvenile)	*Glossotheridium chapadmalense* - Anaya & MacFadden (1995)	Fig. 6.11G-I
MNHN-Bol V 11758 (= GB 105)	Viscachani	Marp.	Right mandibular fragment with alveoli of mf1-mf2 and partial alveoli of cf and mf3 (juvenile)	None - This work	Fig. 6.11J-L
MNHN-Bol V 3714	Casira	Mont.-Chap.	Fragment of right mandible with cf to partial mf3	None - This work	-
MNHN-Bol V 6567	Casira	Mont.-Chap.	Fragment of right maxilla with Mf4	None - This work	-
MNHN-Bol V 6549	Pomata-Ayte	Mont.	Two maxillary fragments with dentition and two petrosal remains	None - This work	-
MNHN-Bol V 9759	Casira	Mont.-Chap.	Two petrosal remains and various basicranial fragments	None - This work	Fig. 6.16
MNHN-Bol V 12002 (= VIZ0358)	Viscachani	Marp.	Right Mf2	None - This work	-
MNHN-Bol V 6560	Casira	Mont.-Chap.	Left mandible fragment with roots of mf1 and mf2	None - This work	-
MNHN-Bol V 3716	Casira	Mont.-Chap.	Upper right Mf1, Mf4 and other tooth fragments	None - This work	-
MNHN-Bol V 3277	?	?	Neurocranium and right incus	None - This work	Fig. 6.17
MNHN.F.AYO133	Ayo-Ayo	Marp.	Fragment of mandible	*Simomylodon uccasamamensis* - Saint-André *et al.* (2010)	-
MNHN.F.AYO135	Ayo-Ayo	Marp.	Fragment of right maxillary with partial alveoli of Mf2-Mf3-Mf4	*Simomylodon uccasamamensis* - Saint-André *et al.* (2010)	-

MNHN.F.AYO164	Ayo-Ayo	Marp.	Right mf2 and mf3	*Simomylodon uccasamamensis* - Saint-André *et al.* (2010)	-
MNHN.F.AYO181	Ayo-Ayo	Marp.	Proximal part of right mandible with mf3 and alveoli of mf2	*Simomylodon uccasamamensis* - Saint-André *et al.* (2010)	-
MNHN.F.AYO185	Ayo-Ayo	Marp.	Right mandible fragment with cf1 and alveoli of mf1-mf3	*Simomylodon uccasamamensis* - Saint-André *et al.* (2010)	-
MNHN.F.AYO186	Ayo-Ayo	Marp.	Mandibular symphysis with right cf1	*Simomylodon uccasamamensis* - Saint-André *et al.* (2010)	-
MNHN.F.AYO188	Ayo-Ayo	Marp.	Complete upper left dental series (modified from Saint-André *et al.* (2010))	*Simomylodon uccasamamensis* - Saint-André *et al.* (2010)	-
MNHN.F.AYO208	Ayo-Ayo	Marp.	Mandibular symphysis	*Simomylodon uccasamamensis* - Saint-André *et al.* (2010)	-
MNHN.F.AYO209	Ayo-Ayo	Marp.	Fragment of left mandible without dentition	*Simomylodon uccasamamensis* - Saint-André *et al.* (2010)	-
MNHN.F.VIZ1	Viscachani	Marp.	Fragment of left mandible with mf1-mf3	*Simomylodon uccasamamensis* - Saint-André *et al.* (2010)	-
MNHN.F.VIZ18	Viscachani	Marp.	Occipital condyle	*Simomylodon uccasamamensis* - Saint-André *et al.* (2010)	-
MNHN.F.VIZ35	Viscachani	Marp.	Right Cf and fragments of other teeth	*Simomylodon uccasamamensis* - Saint-André *et al.* (2010)	-
MNHN.F.AYO102	Ayo-Ayo	Marp.	Left humerus with damaged epiphyses	*Simomylodon uccasamamensis* - Saint-André *et al.* (2010)	-
MNHN.F.AYO109	Ayo-Ayo	Marp.	Left cuneiform	*Simomylodon uccasamamensis* - Saint-André *et al.* (2010)	Fig. 6.22F-H
MNHN.F.AYO110	Ayo-Ayo	Marp.	Right humerus without proximal epiphysis	*Simomylodon uccasamamensis* - Saint-André *et al.* (2010)	Fig. 6.19C-D
MNHN.F.AYO111	Ayo-Ayo	Marp.	Left lunar and lateral sesamoid of right mtc4	*Simomylodon uccasamamensis* - Saint-André *et al.* (2010)	Fig. 6.22C-E, S-T
MNHN.F.AYO112	Ayo-Ayo	Marp.	Two rib fragments	*Simomylodon uccasamamensis* - Saint-André *et al.* (2010)	-
MNHN.F.AYO113	Ayo-Ayo	Marp.	Proximal rib fragment	*Simomylodon uccasamamensis* - Saint-André *et al.* (2010)	-
MNHN.F.AYO114	Ayo-Ayo	Marp.	Medial sesamoid of right mtc4	None - This work	Fig. 6.22Q-R
MNHN.F.AYO121	Ayo-Ayo	Marp.	Right humeral head	*Simomylodon uccasamamensis* - Saint-André *et al.* (2010)	-
MNHN.F.AYO126	Ayo-Ayo	Marp.	Proximal epiphysis of right radius	*Simomylodon uccasamamensis* - Saint-André *et al.* (2010)	-
MNHN.F.AYO128	Ayo-Ayo	Marp.	Right cuboid	*Simomylodon uccasamamensis* - Saint-André *et al.* (2010)	-
MNHN.F.AYO129	Ayo-Ayo	Marp.	Proximal articulation of right femur	*Simomylodon uccasamamensis* - Saint-André *et al.* (2010)	-
MNHN.F.AYO132	Ayo-Ayo	Marp.	Rib fragment	*Simomylodon uccasamamensis* - Saint-André *et al.* (2010)	-
MNHN.F.AYO148	Ayo-Ayo	Marp.	Sacrum fragments with cotyloid cavities and incomplete lumbar vertebra	*Simomylodon uccasamamensis* - Saint-André *et al.* (2010)	-
MNHN.F.AYO156	Ayo-Ayo	Marp.	Cervical vertebra	*Simomylodon uccasamamensis* - Saint-André *et al.* (2010)	-
MNHN.F.AYO166	Ayo-Ayo	Marp.	Diaphysis of left femur (without both epiphyses)	*Simomylodon uccasamamensis* - Saint-André *et al.* (2010)	-
MNHN.F.AYO167	Ayo-Ayo	Marp.	Right femur without femoral head and distal epiphysis	*Simomylodon uccasamamensis* - Saint-André *et al.* (2010)	-
MNHN.F.AYO168	Ayo-Ayo	Marp.	Distal fragment of right femur	*Simomylodon uccasamamensis* - Saint-André *et al.* (2010)	-
MNHN.F.AYO169	Ayo-Ayo	Marp.	Distal articulation of left femur with ectepicondyle	*Simomylodon uccasamamensis* - Saint-André *et al.* (2010)	-
MNHN.F.AYO170	Ayo-Ayo	Marp.	Incomplete axis	*Simomylodon uccasamamensis* - Saint-André *et al.* (2010)	-
MNHN.F.AYO171	Ayo-Ayo	Marp.	Centre of vertebra	*Simomylodon uccasamamensis* - Saint-André *et al.* (2010)	-

MNHN.F.AYO172	Ayo-Ayo	Marp.	Centre of caudal vertebra	*Simomylodon uccasamamensis* - Saint-André *et al.* (2010)	-
MNHN.F.AYO178	Ayo-Ayo	Marp.	Right radius without proximal epiphysis	*Simomylodon uccasamamensis* - Saint-André *et al.* (2010)	-
MNHN.F.AYO179	Ayo-Ayo	Marp.	Proximal fragment of right radius, left mtc3 fused to magnum, proximal phalanx	*Simomylodon uccasamamensis* - Saint-André *et al.* (2010)	Fig. 6.23I-M
MNHN.F.AYO180	Ayo-Ayo	Marp.	Left radius, scaphoid, lunar, trapezoid, mtc2, mtc3 fused to magnum, 1 distal phalanx, sesamoid, 4 ungual phalanges, fragments of ribs, vertebrae and sternebrae	*Simomylodon uccasamamensis* - Saint-André *et al.* (2010)	Figs 6.22A-B, I-K, O-P; 6.24H-P
MNHN.F.AYO182	Ayo-Ayo	Marp.	Left astragalus	*Simomylodon uccasamamensis* - Saint-André *et al.* (2010)	-
MNHN.F.AYO183	Ayo-Ayo	Marp.	Complete caudal vertebra	*Simomylodon uccasamamensis* - Saint-André *et al.* (2010)	-
MNHN.F.AYO184	Ayo-Ayo	Marp.	Fragment of right humerus of a juvenile individual	*Simomylodon uccasamamensis* - Saint-André *et al.* (2010)	-
MNHN.F.AYO187	Ayo-Ayo	Marp.	Dorsal vertebra	*Simomylodon uccasamamensis* - Saint-André *et al.* (2010)	-
MNHN.F.AYO190	Ayo-Ayo	Marp.	Right mtc2	*Simomylodon uccasamamensis* - Saint-André *et al.* (2010)	Fig. 6.23C-E
MNHN.F.AYO196	Ayo-Ayo	Marp.	Diaphysis of left femur of a juvenile individual	*Simomylodon uccasamamensis* - Saint-André *et al.* (2010)	-
MNHN.F.AYO197	Ayo-Ayo	Marp.	Diaphysis of right femur (without both epiphyses)	*Simomylodon uccasamamensis* - Saint-André *et al.* (2010)	-
MNHN.F.AYO198	Ayo-Ayo	Marp.	Dorsal vertebra	*Simomylodon uccasamamensis* - Saint-André *et al.* (2010)	-
MNHN.F.AYO200	Ayo-Ayo	Marp.	Distal fragment of right tibia	*Simomylodon uccasamamensis* - Saint-André *et al.* (2010)	-
MNHN.F.AYO201	Ayo-Ayo	Marp.	Distal portion of left tibia	*Simomylodon uccasamamensis* - Saint-André *et al.* (2010)	-
MNHN.F.AYO205	Ayo-Ayo	Marp.	Corpus of dorsal vertebra	*Simomylodon uccasamamensis* - Saint-André *et al.* (2010)	-
MNHN.F.AYO206	Ayo-Ayo	Marp.	Caudal vertebra	*Simomylodon uccasamamensis* - Saint-André *et al.* (2010)	-
MNHN.F.AYO207	Ayo-Ayo	Marp.	Incomplete caudal vertebra	*Simomylodon uccasamamensis* - Saint-André *et al.* (2010)	-
MNHN.F.AYO217	Ayo-Ayo	Marp.	Caudal vertebra	*Simomylodon uccasamamensis* - Saint-André *et al.* (2010)	-
MNHN.F.AYO218	Ayo-Ayo	Marp.	Centre of dorsal vertebra	*Simomylodon uccasamamensis* - Saint-André *et al.* (2010)	-
MNHN.F.AYO219	Ayo-Ayo	Marp.	Caudal vertebra	*Simomylodon uccasamamensis* - Saint-André *et al.* (2010)	-
MNHN.F.AYO220	Ayo-Ayo	Marp.	Caudal vertebra	*Simomylodon uccasamamensis* - Saint-André *et al.* (2010)	-
MNHN.F.AYO222	Ayo-Ayo	Marp.	Distal part of right humerus	*Simomylodon uccasamamensis* - Saint-André *et al.* (2010)	-
MNHN.F.AYO223	Ayo-Ayo	Marp.	Left radius without proximal epiphysis	*Simomylodon uccasamamensis* - Saint-André *et al.* (2010)	-
MNHN.F.AYO227	Ayo-Ayo	Marp.	Proximal articulation of left humerus	*Simomylodon uccasamamensis* - Saint-André *et al.* (2010)	-
MNHN.F.AYO228	Ayo-Ayo	Marp.	Distal articulation of left humerus	*Simomylodon uccasamamensis* - Saint-André *et al.* (2010)	-
MNHN.F.AYO229	Ayo-Ayo	Marp.	Distal articulation of right humerus	*Simomylodon uccasamamensis* - Saint-André *et al.* (2010)	-
MNHN.F.POM20	Pomata-Ayte	Mont.	Incomplete cervical vertebra	*Simomylodon uccasamamensis* - Saint-André *et al.* (2010)	-
MNHN.F.POM25	Pomata-Ayte	Mont.	Left humerus without epiphyses of a juvenile individual	*Simomylodon uccasamamensis* - Saint-André *et al.* (2010)	-
MNHN.F.POM26	Pomata-Ayte	Mont.	Caudal vertebra	*Simomylodon uccasamamensis* - Saint-André *et al.* (2010)	-

MNHN.F.POM56	Pomata-Ayte	Mont.	Incomplete caudal vertebra	*Simomylodon uccasamamensis* - Saint-André *et al.* (2010)	-
MNHN.F.POM57	Pomata-Ayte	Mont.	Atlas	*Simomylodon uccasamamensis* - Saint-André *et al.* (2010)	-
MNHN.F.POM58	Pomata-Ayte	Mont.	Lumbar vertebra	*Simomylodon uccasamamensis* - Saint-André *et al.* (2010)	-
MNHN.F.POM60	Pomata-Ayte	Mont.	Incomplete cervical vertebra	*Simomylodon uccasamamensis* - Saint-André *et al.* (2010)	-
MNHN.F.POM61	Pomata-Ayte	Mont.	Centre of cervical vertebra	*Simomylodon uccasamamensis* - Saint-André *et al.* (2010)	-
MNHN.F.POM62	Pomata-Ayte	Mont.	Right tibia	*Simomylodon uccasamamensis* - Saint-André *et al.* (2010)	-
MNHN.F.POM63	Pomata-Ayte	Mont.	Incomplete left astragalus	*Simomylodon uccasamamensis* - Saint-André *et al.* (2010)	-
MNHN.F.POM64	Pomata-Ayte	Mont.	Right astragalus	*Simomylodon uccasamamensis* - Saint-André *et al.* (2010)	-
MNHN.F.POM65	Pomata-Ayte	Mont.	Proximal fragment of left fibula	*Simomylodon uccasamamensis* - Saint-André *et al.* (2010)	-
MNHN.F.POM66	Pomata-Ayte	Mont.	Right cuboid	*Simomylodon uccasamamensis* - Saint-André *et al.* (2010)	-
MNHN.F.POM79	Pomata-Ayte	Mont.	Distal fragment of left mtc3	*Simomylodon uccasamamensis* - Saint-André *et al.* (2010)	-
MNHN.F.VIZ13	Viscachani	Marp.	Centre of dorsal vertebra	*Simomylodon uccasamamensis* - Saint-André *et al.* (2010)	-
MNHN.F.VIZ14	Viscachani	Marp.	Centre of dorsal vertebra	*Simomylodon uccasamamensis* - Saint-André *et al.* (2010)	-
MNHN.F.VIZ16	Viscachani	Marp.	Proximal epiphysis of left radius	*Simomylodon uccasamamensis* - Saint-André *et al.* (2010)	-
MNHN.F.VIZ17	Viscachani	Marp.	Left semilunar	*Simomylodon uccasamamensis* - Saint-André *et al.* (2010)	-
MNHN.F.VIZ22	Viscachani	Marp.	Distal epiphysis of left tibia	*Simomylodon uccasamamensis* - Saint-André *et al.* (2010)	-
MNHN.F.VIZ23	Viscachani	Marp.	Centre of caudal vertebra with transversal apophyses	*Simomylodon uccasamamensis* - Saint-André *et al.* (2010)	-
MNHN.F.VIZ24	Viscachani	Marp.	Left mtc4 proximal fragment	*Simomylodon uccasamamensis* - Saint-André *et al.* (2010)	-
MNHN.F.VIZ26	Viscachani	Marp.	Caudal vertebra	*Simomylodon uccasamamensis* - Saint-André *et al.* (2010)	-
MNHN.F.VIZ27	Viscachani	Marp.	Right mtc3 not fused to magnum	*Simomylodon uccasamamensis* - Saint-André *et al.* (2010)	Fig. 6.23F-H
MNHN.F.VIZ28	Viscachani	Marp.	Right mtt4 without distal end	*Simomylodon uccasamamensis* - Saint-André *et al.* (2010)	Fig. 6.29J-L
MNHN.F.VIZ29	Viscachani	Marp.	Caudal vertebra	*Simomylodon uccasamamensis* - Saint-André *et al.* (2010)	-
MNHN.F.VIZ3	Viscachani	Marp.	Incomplete distal epiphysis of left humerus	*Simomylodon uccasamamensis* - Saint-André *et al.* (2010)	-
MNHN.F.VIZ30	Viscachani	Marp.	Fragment of rib	*Simomylodon uccasamamensis* - Saint-André *et al.* (2010)	-
MNHN.F.VIZ31	Viscachani	Marp.	Incomplete atlas and axis	*Simomylodon uccasamamensis* - Saint-André *et al.* (2010)	-
MNHN.F.VIZ32	Viscachani	Marp.	Right mtc1	*Simomylodon uccasamamensis* - Saint-André *et al.* (2010)	Fig. 6.23A-B
MNHN.F.VIZ33	Viscachani	Marp.	Left mtc4 proximal fragment	*Simomylodon uccasamamensis* - Saint-André *et al.* (2010)	Fig. 6.23N-P
MNHN.F.VIZ34	Viscachani	Marp.	Centre of caudal vertebra	*Simomylodon uccasamamensis* - Saint-André *et al.* (2010)	-
MNHN.F.VIZ39	Viscachani	Marp.	Right astragalus	None - This work	-
MNHN.F.VIZ4	Viscachani	Marp.	Ventral part of scapula with part of the glenoid cavity	*Simomylodon uccasamamensis* - Saint-André *et al.* (2010)	-

MNHN.F.VIZ5	Viscachani	Marp.	Left mtc3 not fused to magnum	*Simomylodon uccasamamensis* - Saint-André *et al.* (2010)	-
MNHN.F.VIZ7	Viscachani	Marp.	Corpus of dorsal vertebra	*Simomylodon uccasamamensis* - Saint-André *et al.* (2010)	-
MNHN.F.VIZ8	Viscachani	Marp.	Centre of caudal vertebra	*Simomylodon uccasamamensis* - Saint-André *et al.* (2010)	-
MNHN.F.VIZ9	Viscachani	Marp.	Vertebral corpus	*Simomylodon uccasamamensis* - Saint-André *et al.* (2010)	-
MNHN-Bol V 10919	Ayo-Ayo	Marp.	Distal part of right femur	None - This work	-
MNHN-Bol V 11673	Ayo-Ayo	Marp.	Proximal part of right femur	None - This work	-
MNHN-Bol V 11766	Viscachani	Marp.	Proximal fragment of left humerus	None - This work	-
MNHN-Bol V 11767	Viscachani	Marp.	Left fibula	None - This work	-
MNHN-Bol V 11772	Viscachani	Marp.	Proximal fragment of left tibia	None - This work	-
MNHN-Bol V 11776	Viscachani	Marp.	Proximal fragment of right humerus	None - This work	-
MNHN-Bol V 11777	Viscachani	Marp.	Distal fragment of right tibia	None - This work	-
MNHN-Bol V 11778	Viscachani	Marp.	Ungual phalanx	None - This work	-
MNHN-Bol V 11779	Viscachani	Marp.	Right astragalus	None - This work	-
MNHN-Bol V 11780	Viscachani	Marp.	Left navicular	None - This work	-
MNHN-Bol V 11784	Viscachani	Marp.	Right lunar	None - This work	-
MNHN-Bol V 11788	Viscachani	Marp.	Left astragalus	None - This work	-
MNHN-Bol V 11789	Viscachani	Marp.	Caudal vertebra	None - This work	-
MNHN-Bol V 11795	Viscachani	Marp.	Distal fragment of left humerus	None - This work	-
MNHN-Bol V 11876	Pomata-Ayte	Mont.	Left tibia	None - This work	-
MNHN-Bol V 12277	Viscachani	Marp.	Right femur	None - This work	-
MNHN-Bol V 12507	Viscachani	Marp.	Tibio-fibula fused proximally	None - This work	-
MNHN-Bol V 12927	Pomata-Ayte	Mont.	Left mtc3 not fused to magnum	None - This work	-
MNHN-Bol V 12949	Pomata-Ayte	Mont.	Right humerus of a juvenile individual	None - This work	-
MNHN-Bol V 12953	Pomata-Ayte	Mont.	Complete left femur and right unciform	None - This work	Fig. 6.22L-N
MNHN-Bol V 13215	Pomata-Ayte	Mont.	Distal fragment of right tibia	None - This work	-
MNHN-Bol V 13216	Pomata-Ayte	Mont.	Complete right tibia	None - This work	-
MNHN-Bol V 13217	Pomata-Ayte	Mont.	Juvenile fibula	None - This work	-
MNHN-Bol V 13218	Ayo-Ayo	Marp.	Right mandible without dentition	None - This work	-
MNHN-Bol V 13219	Ayo-Ayo	Marp.	Mandibular symphysis with alveoli of right caniniform	None - This work	-
MNHN-Bol V 13220	Ayo-Ayo	Marp.	Complete right tibia	None - This work	-

MNHN-Bol V 13221	Ayo-Ayo	Marp.	Complete left tibia	None - This work	-
MNHN-Bol V 13222	Choquecota	Huay./Mont.?	Thoracic vertebra incomplete (juvenile)	None - This work	-
MNHN-Bol V 3299	Ayo-Ayo	Marp.	Right femur	*Simomylodon uccasamamensis* - Saint-André *et al.* (2010)	Fig. 6.25
MNHN-Bol V 3300	Ayo-Ayo	Marp.	Left patella and left tibia	*Simomylodon uccasamamensis* - Saint-André *et al.* (2010)	-
MNHN-Bol V 3301	Ayo-Ayo	Marp.	Distal part of left femur	*Simomylodon uccasamamensis* - Saint-André *et al.* (2010)	-
MNHN-Bol V 3303	Ayo-Ayo	Marp.	Distal epiphysis of left humeus	*Simomylodon uccasamamensis* - Saint-André *et al.* (2010)	-
MNHN-Bol V 3305	Ayo-Ayo	Marp.	Proximal epiphysis of right tibia	*Simomylodon uccasamamensis* - Saint-André *et al.* (2010)	-
MNHN-Bol V 3313	Ayo-Ayo	Marp.	Proximal, distal and ungual phalanges of the same finger	*Simomylodon uccasamamensis* - Saint-André *et al.* (2010)	Fig. 6.24A-G
MNHN-Bol V 3318	Ayo-Ayo	Marp.	Left mtc2	*Simomylodon uccasamamensis* - Saint-André *et al.* (2010)	-
MNHN-Bol V 3355	Inchasi	Chap.	Ungual phalanx	Mylodontinae indet. - Anaya & MacFadden (1995)	-
MNHN-Bol V 3365	Inchasi	Chap.	Right femoral fragment	Mylodontinae indet. - Anaya & MacFadden (1995)	-
MNHN-Bol V 3375	Inchasi	Chap.	Complete right radius	None - This work	Fig. 6.20
MNHN-Bol V 3773	Ayo-Ayo	Marp.	Fragment of right femur without epiphyses	None - This work	-
MNHN-Bol V 3774	Ayo-Ayo	Marp.	Proximal part of left ulna	None - This work	-
MNHN-Bol V 3792	Ayo-Ayo	Marp.	Distal part of left humerus	None - This work	-
MNHN-Bol V 6562	Casira	Mont.-Chap.	Left fibula	None - This work	-
MNHN-Bol V 6564	Casira	Mont.-Chap.	Right Lunar, two ungual phalanges, left mc3, fragment of mtc5, vertebral and rib fragments	None - This work	-
MNHN-Bol V 6573	Inchasi	Chap.	Distal part of left humerus, proximal part of left radius, left lunar, cuneiform, fragments of mtc1-2-3-4	None - This work	-
MNHN-Bol V 8541	Ayo-Ayo	Marp.	Fragment of right femur and tibia; complete right fibula, calcaneum, navicular	None - This work	Figs 6.28A-D; 6.29A-C
UF 312843	Ayo-Ayo	Marp.	Right astragalus	None - This work	-

Appendix I. Table S2. *Simomylodon uccasamamensis* – Reduced list of material, with the homologous elements employed for the study of intraspecific variation.

Age	Locality	Collection	Code	Description	Morph
Early Pliocene	Pomata-Ayte	MNHN-Bol V	3296	Left mandible with complete dentition	Gracile
Early Pliocene	Pomata-Ayte	MNHN-Bol V	3298	Left mandibular fragment with caniniform and molariforms 1 and 2	Robust
Late Pliocene	Ayo Ayo-Viscachani	MNHN-Bol V	3299	Right femur	Robust
Late Pliocene	Ayo Ayo-Viscachani	MNHN-Bol V	3300	Left patella and tibia	Robust
Late Pliocene	Ayo Ayo-Viscachani	MNHN-Bol V	3301	Distal part of left femur	Robust
Late Pliocene	Ayo Ayo-Viscachani	MNHN-Bol V	3305	Proximal epiphysis of right tibia	Gracile
Late Pliocene	Ayo Ayo-Viscachani	MNHN-Bol V	3321	Maxillary and premaxillary fragments with upper dentition	Robust
Latest Miocene to Early Pliocene	Choquecota	MNHN-Bol V	3348	Cranium lacking the posterior portion	Gracile
Early Pliocene	Inchasi	MNHN-Bol V	3358	Two mandibular fragments with incomplete dentition	Robust
Early Pliocene	Inchasi	MNHN-Bol V	3365	Right femoral and tibial fragments	Gracile
Early Pliocene	Inchasi	MNHN-Bol V	3371	Two mandibular fragments with incomplete dentition	Gracile
Early Pliocene	Inchasi	MNHN-Bol V	3711	Cranium and mandibles with complete dentition and atlas	Gracile
Early Pliocene	Casira	MNHN-Bol V	3714	Fragment of right mandible with caniniform to partial molariform 3	Gracile
Early Pliocene	Casira	MNHN-Bol V	3717	Cranium and mandibles with almost complete dentition and proximal left ulnar fragment	Robust
Early Pliocene	Inchasi	MNHN-Bol V	3718	Complete cranium lacking the right zygomatic arch and left scapula	Robust
Early Pliocene	Casira	MNHN-Bol V	3726	Cranium lacking the posterior portion and mandibles	Gracile
Late Pliocene	Ayo Ayo-Viscachani	MNHN-Bol V	11731	Anterior portion of cranium without dentition	Robust
Late Pliocene	Ayo Ayo-Viscachani	MNHN-Bol V	11772	Proximal fragment of left tibia	Robust
Early Pliocene	Pomata-Ayte	MNHN-Bol V	11876	Left tibia	Gracile
Late Pliocene	Ayo Ayo-Viscachani	MNHN-Bol V	12277	Right femur	Robust
Late Pliocene	Ayo Ayo-Viscachani	MNHN-Bol V	12507	Tibia and fibula fused proximally	Gracile
Late Pliocene	Ayo Ayo-Viscachani	MNHN-Bol V	12518	Mandibular symphysis with right caniniform; part of atlas, axis and caudal vertebrae; proximal part of left humerus; left and right femora, tibiae, fibulae, cyamellae and astragali; right cuboid and calcaneal fragment; right ectocuneiform	Gracile
Early Pliocene	Pomata-Ayte	MNHN-Bol V	12953	Left femur and right unciform	Robust
Early Pliocene	Pomata-Ayte	MNHN-Bol V	13216	Right tibia	Gracile
Late Pliocene	Ayo Ayo-Viscachani	MNHN-Bol V	13218	Right mandible without dentition	Gracile
Late Pliocene	Ayo Ayo-Viscachani	MNHN-Bol V	13219	Mandibular symphysis with alveoli of right caniniform	Robust
Late Pliocene	Ayo Ayo-Viscachani	MNHN-Bol V	13220	Right tibia	Robust
Late Pliocene	Ayo Ayo-Viscachani	MNHN-Bol V	13221	Left tibia	Gracile
Late Pliocene	Ayo Ayo-Viscachani	MNHN.F.AYO	168	Distal fragment of right femur	Gracile
Late Pliocene	Ayo Ayo-Viscachani	MNHN.F.AYO	169	Distal articulation of left femur with ectepicondyle	Robust
Late Pliocene	Ayo Ayo-Viscachani	MNHN.F.AYO	185	Right mandibular fragment with caniniform and alveoli of molariforms	Gracile
Late Pliocene	Ayo Ayo-Viscachani	MNHN.F.VIZ	1	Fragment of left mandible with molariforms	Gracile

APPENDIX II

Appendix II. Total list of materials observed for the present thesis. Asterisks represent specimens observed through high-quality photographs.

TAXON	CODE	COUNTRY	SITE/AGE	DESCRIPTION
Baraguatherium takumara	IVIC-P-1828	Venezuela	Cerro la Cruz - Early Miocene	Right mandibular fragment with mf1-mf3; isolated right Mf2
Baraguatherium takumara	IVIC-P-2917	Venezuela	Cerro la Cruz - Early Miocene	Right femur without proximal epiphisis
Baraguatherium takumara	MBLUZ-P-5043/5044	Venezuela	Cerro la Cruz - Early Miocene	Two teeth fragments
Bolivartherium codorensis	AMU-CURS 130	Venezuela	Codore Fm. - Pliocene	Cranium
Bolivartherium urumaquensis	MCN 170-72V	Venezuela	Urumaco - Late Miocene	Canial fragment, two maxillary fragments, mandibles, ulna, astragalus, sacrum and other fragments (type)
Bolivartherium urumaquensis	MCN 85-72V	Venezuela	Urumaco - Late Miocene	Left and right femora
Bradypus sp.	AMNH 16871	?	Extant	Complete skeleton
Bradypus sp.	MACN Ma 50.119	Bolivia	Extant	Cranium and mandibles
Bradypus sp.	MACN Ma 50.120	Bolivia	Extant	Cranium and mandibles
Bradypus sp.	MACN Ma 2.71	Brazil	Extant	Cranium and mandibles
Bradypus sp.	MACN Ma 20.7	Brazil	Extant	Cranium and mandibles
Bradypus sp.	MACN Ma 31.167	Ecuador	Extant	Cranium and mandibles
Bradypus sp.	MACN Ma 4.125	Paraguay	Extant	Complete skeleton
Bradypus tridactylus	MACN Ma 4.52	?	Extant	Cranium and mandibles
Bradypus tridactylus	MACN Ma 4.260	Brazil	Extant	Cranium
Brievabradys laventensis	LV-4-12*	Colombia	La Venta - middle Miocene	Partial cranium and mandibles
Catonyx sp.	MACN Pv 16639	Argentina	Buenos Aires - Pleistocene	Two femures, left ulna, partially reconstructed right scapula, left tibia, calcaneum
Catonyx tarijensis	FMNH P14225	Bolivia	Tarija - Pleistocene	Left radius, ulna, scaphoid, lunar, cuneiform and magnum
Catonyx tarijensis	FMNH P14238	Bolivia	Tarija - Pleistocene	Complete skeleton
Choloepus hoffmanni	AMNH 245516	?	Extant	Half cranium and mandible
Choloepus hoffmanni	AMNH 26906	Panamá	Extant	Cranium and mandible
Eionaletherium tanycnemius	IVIC-P-2870	Venezuela	Urumaco - Late Miocene	Femur, tibia, fibula
Euphractus sexcintus	AMNH 1661	?	Extant	Complete skeleton
Euphractus sexcintus	AMNH 1663	?	Extant	Complete skeleton
Euphractus sexcintus	AMNH 1682	?	Extant	Complete skeleton
Glossotheridium chapadmalense	MLP 3-151	Argentina	Chapadmalal - Pliocene	Cranium without the distal part and with both mandibles
Glossotheridium chapadmalense	MACN Pv 8675	Argentina	Miramar - Baliza Chica - Pliocene	Cranium, mandible and part of the atlas (Type)
Glossotheridium chapadmalense	MACN Pv 10156	Argentina	Miramar - Pliocene	Left humerus
Glossotheridium chapadmalense	MMP S-273	Argentina	Playa los Lobos - Chapadmalal - Pliocene	Complete cranium with only one molar
Glossotheridium chapadmalense	MMP M-245	Argentina	Punta lobería - Chapadmalal - Pliocene	Complete cranium without right Cf1, left Cf1, Mf1, Mf5
Glossotheriopsis pascuali	MLP 76-VIII-30-1	Argentina	Rio Negro - early middle Miocene	Rostral part of cranium with C1f and Mf1-2, mandibular fragments and two isolated teeth
Glossotherium robustum	MACN Pv 62	Argentina	Pleistocene - no locality	Left humerus
Glossotherium robustum	AMNH 11271	Argentina	Arroyo Balta - Pleistocene	Mounted skeleton
Glossotherium robustum	MACN Pv 10606	Argentina	Balcarce - Arroyo Grande - Pleistocene	Proximal fragment of radius
Glossotherium robustum	MACN Pv 993	Argentina	Buenos Aires - Pleistocene	Left and right mandibles
Glossotherium robustum	MACN Pv 999	Argentina	Buenos Aires - Pleistocene	Complete skeleton
Glossotherium robustum	AMNH 11273	Argentina	Buenos Aires - Pleistocene	Cranium and mandible, highly reconstructed

Glossotherium robustum	AMNH 11275	Argentina	Buenos Aires - Pleistocene	Complete forelimb and manus (mounted specimen)
Glossotherium robustum	AMNH 11276	Argentina	Buenos Aires - Pleistocene	Left femur
Glossotherium robustum	AMNH 11278	Argentina	Buenos Aires - Pleistocene	Rostral part of cranium and mandible
Glossotherium robustum	AMNH 11307	Argentina	Buenos Aires - Pleistocene	Left humerus
Glossotherium robustum	MACN A 1159	Argentina	Buenos Aires - Pleistocene	Maxillary fragment
Glossotherium robustum	MACN Pv 12095	Argentina	Buenos Aires - Pleistocene	Right ulna
Glossotherium robustum	MACN Pv 18656	Argentina	Buenos Aires - Pleistocene	Right humerus, fragment of femur, proximal fragment of ulna, caudal vertebrae and other fragments
Glossotherium robustum	MACN Pv 2652	Argentina	Buenos Aires - Pleistocene	Cranium without the occipital region, teeth present
Glossotherium robustum	MACN Pv 4423	Argentina	Buenos Aires - Pleistocene	Right humerus
Glossotherium robustum	MLP 3-136	Argentina	Buenos Aires - Pleistocene	Cranium and mandibles
Glossotherium robustum	MLP 3-237	Argentina	Buenos Aires - Pleistocene	Proximal fragment of left ulna
Glossotherium robustum	MLP M-85	Argentina	Buenos Aires - Pleistocene	Fragment of left mandible with dentition
Glossotherium robustum	MLP M-87	Argentina	Buenos Aires - Pleistocene	Fragment of left mandible with dentition
Glossotherium robustum	MLP M-88	Argentina	Buenos Aires - Pleistocene	Fragment of left mandible with dentition
Glossotherium robustum	MNHN.F.PAM 116	Argentina	Buenos Aires - Pleistocene	Two mandibles without dentition but complete alveoli
Glossotherium robustum	MNHN.F.PAM 117	Argentina	Buenos Aires - Pleistocene	Two mandibles with complete dentition
Glossotherium robustum	MNHN.F.PAM 123	Argentina	Buenos Aires - Pleistocene	Right humerus
Glossotherium robustum	MNHN.F.PAM 125	Argentina	Buenos Aires - Pleistocene	Right femur
Glossotherium robustum	MNHN.F.PAM 128	Argentina	Buenos Aires - Pleistocene	Right femur
Glossotherium robustum	MNHN.F.PAM 132	Argentina	Buenos Aires - Pleistocene	Right tibia
Glossotherium robustum	MNHN.F.PAM 135	Argentina	Buenos Aires - Pleistocene	Left tibia
Glossotherium robustum	MNHN.F.PAM 141	Argentina	Buenos Aires - Pleistocene	Almost complete four autopodia
Glossotherium robustum	MNHN.F.PAM 141 (A.C. 7069)	Argentina	Buenos Aires - Pleistocene	Left ulna
Glossotherium robustum	MNHN.F.PAM 141 (A.C. 7111)	Argentina	Buenos Aires - Pleistocene	Right fibula
Glossotherium robustum	MNHN.F.PAM 141 (A.C. 7112)	Argentina	Buenos Aires - Pleistocene	Left fibula
Glossotherium robustum	MNHN.F.PAM 142	Argentina	Buenos Aires - Pleistocene	Cranium without dentition
Glossotherium robustum	MNHN.F.PAM 144	Argentina	Buenos Aires - Pleistocene	Uncomplete right pes
Glossotherium robustum	MACN Pv 14760	Argentina	Cordoba - Pleistocene	Proximal fragment of left scapula
Glossotherium robustum	MACN Pv 17572	Argentina	Entre Ríos - Pleistocene	Two incomplete humeri, fragment of femur, tibia, radius, astragalus, scapula and bones of manus and pes
Glossotherium robustum	MACN Pv 12715	Argentina	Gorchs, Rio Salado - Pleistocene	Cranium without dentition
Glossotherium robustum	MACN Pv 14726	Argentina	Gramilla - Sant. del Estero - Pleistocene	Left mandibular fragment with dentition
Glossotherium robustum	MNHN.F.PAM 1881-35	Argentina	La Plata - Pleistocene	Left mandibular fragment without dentition
Glossotherium robustum	AMNH 11270	Argentina	Luján - Buenos Aires - Pleistocene	Cranium and mandibles (juvenile)
Glossotherium robustum	MLP 3-140	Argentina	Luján - Buenos Aires - Pleistocene	Complete skeleton
Glossotherium robustum	MNHN.F.PAM 547 (A.C.7209)	Argentina	Luján - Buenos Aires - Pleistocene	Left mandible with dentition
Glossotherium robustum	MACN Pv 7993	Argentina	Monte Hermoso - Pleistocene	Right mandible with dentition
Glossotherium robustum	MLP 3-762b	Argentina	Olavarría - late Pleistocene	Complete cranium
Glossotherium robustum	MLP 3-139	Argentina	Olavarría - Upper Pleistocene	Complete skeleton (juvenile)
Glossotherium robustum	MACN Pv 6856	Argentina	Punta Hermengo - Miramar - Pleistocene	Isolated molariform
Glossotherium robustum	MNHN.F.R 269	?	Pleistocene - no locality	Left tibia

Glossotherium robustum	MMP M-1489	Argentina	Pleistocene - no locality	Complete cranium without left-right Cf1 and right Mf1
Glossotherium robustum	MMP M-1490	Argentina	Pleistocene - no locality	Complete cranium without left-right Cf1
Glossotherium robustum	MACN Pv 1321	Argentina	Pleistocene - no locality	Several appendicular bones (juvenile)
Glossotherium robustum	MACN Pv 14055	Argentina	Pleistocene - no locality	Left and right mandibles with dentition
Glossotherium robustum	MACN Pv 14066	Argentina	Pleistocene - no locality	Left scapula
Glossotherium robustum	MACN Pv 14070	Argentina	Pleistocene - no locality	Left ulna
Glossotherium robustum	MACN Pv 14911a	Argentina	Pleistocene - no locality	Cranium (partial) with mandible
Glossotherium robustum	MACN Pv 91	Argentina	Pleistocene - no locality	Atlas, axis, patella, ulna, radius, calcaneum and bones of the pes
Glossotherium robustum	MACN Pv 990	Argentina	Pleistocene - no locality	Mandibles with dentition
Glossotherium robustum	MACN Pv 996	Argentina	Pleistocene - no locality	Cranium and mandibles, highly restored
Glossotherium robustum	MLP 3-114	Argentina	Pleistocene - no locality	Right tibia
Glossotherium robustum	MLP 3-128	Argentina	Pleistocene - no locality	Right tibia
Glossotherium robustum	MLP 3-137	Argentina	Pleistocene - no locality	Left and right mandibles with dentition
Glossotherium robustum	MLP 3-188	Argentina	Pleistocene - no locality	Complete skeleton
Glossotherium robustum	MLP 3-252	Argentina	Pleistocene - no locality	Atlas
Glossotherium robustum	MLP 35-III-10-1	Argentina	Pleistocene - no locality	Right tibia
Glossotherium robustum	MNHN.F.PAM 141 (A.C. 7068)	Argentina	Pleistocene - no locality	Right humerus
Glossotherium robustum	MNHN.F.PAM 118	Argentina	Pleistocene - no locality	Left humerus
Glossotherium robustum	MNHN.F.PAM 119	Argentina	Pleistocene - no locality	Left humerus
Glossotherium robustum	MNHN.F.PAM 122	Argentina	Pleistocene - no locality	Left humerus
Glossotherium robustum	MNHN.F.PAM 141 (A.C. 7067)	Argentina	Pleistocene - no locality	Left humerus
Glossotherium robustum	MNHN.F.PAM 141 (A.C. 7070)	Argentina	Pleistocene - no locality	Right ulna
Glossotherium robustum	MNHN.F.PAM 259	Argentina	Pleistocene - no locality	Right mandible with complete dentition
Glossotherium robustum	MNHN.F.PAM 280	Argentina	Pleistocene - no locality	Fragment of right mandible with cf1-mf2 and partial alveoli of mf3
Glossotherium robustum	MNHN.F.PAM s/n	Argentina	Pleistocene - no locality	Proximal fragment of both mandibles with left mf1, mf2 and alveoli of cf1
Glossotherium robustum	MNHN.F.PAM s/n (1)	Argentina	Pleistocene - no locality	Left radius
Glossotherium robustum	MNHN.F.PAM s/n (2)	Argentina	Pleistocene - no locality	Right radius
Glossotherium robustum	MMP S-207	Argentina	Pleistocene - no locality	Maxillary fragment with complete dentition
Glossotherium robustum	MACN Pv 10120	Argentina	Río Carcarañá - Santa Fe - Pleistocene	Various manus fragments
Glossotherium robustum	MACN Pv 11331	Argentina	Río Carcarañá - Santa Fe - Pleistocene	Various manus and pes fragments
Glossotherium robustum	MACN Pv 11421	Argentina	Río Carcarañá - Santa Fe - Pleistocene	Various manus and pes fragments
Glossotherium robustum	MACN Pv 14401	Argentina	Río Carcarañá - Santa Fe - Pleistocene	Left maxillary fragment with two molars
Glossotherium robustum	MACN Pv 854	Argentina	Río de la Plata - Pleistocene	Left mandible with dentition
Glossotherium robustum	MACN Pv 14714	Argentina	Río Quequén - Buenos Aires - Pleistocene	Left mandibular fragment with dentition
Glossotherium robustum	MACN Pv 9651	Argentina	Río Quequén - Buenos Aires - Pleistocene	Rostral part of cranium
Glossotherium robustum	MNHN.F.PAM 141 (A.C. 7061)	Argentina	Seguin - Pleistocene	Cranium and complete mandibles
Glossotherium robustum	MACN Pv 11769	Argentina	Tornsquist - Buenos Aires - Pleistocene	Cranium
Glossotherium robustum	MACN Pv 13553	Argentina	Zandil - Pleistocene	Occipital region of cranium
Glossotherium tarijensis	FMNH P14204	Bolivia	Tarija - Pleistocene	Cranium (with occipital portion reconstructed) and mandible
Glossotherium tarijensis	MACN Pv 1002	Bolivia	Tarija - Pleistocene	Cranium with partial dentition (Type)
Glossotherium tarijensis	MNHN-Bol V 3279	Bolivia	Tarija - Pleistocene	Cranium with dentition

Glossotherium tarijensis	MNHN.F.TAR 2013	Bolivia	Tarija - Pleistocene	Fragment of right mandible with mf1, mf2 and part of mf3
Glossotherium tarijensis	MNHN.F.TAR 2025	Bolivia	Tarija - Pleistocene	Two mandibles with complete dentition
Glossotherium tarijensis	MNHN.F.TAR 767	Bolivia	Tarija - Pleistocene	Right humerus
Glossotherium tarijensis	MNHN.F.TAR 784	Bolivia	Tarija - Pleistocene	Cranium with part of dentition
Glossotherium tarijensis	MNHN.F.TAR 787	Bolivia	Tarija - Pleistocene	Right tibia
Glossotherium tarijensis	MNHN.F.TAR 788	Bolivia	Tarija - Pleistocene	Right tibia
Glossotherium tarijensis	MNHN.F.TAR 789	Bolivia	Tarija - Pleistocene	Right tibia
Glossotherium tarijensis	MNHN.F.TAR 790	Bolivia	Tarija - Pleistocene	Left tibia
Glossotherium tarijensis	MNHN.F.TAR 792	Bolivia	Tarija - Pleistocene	Right tibia
Glossotherium tarijensis	MNHN.F.TAR 793	Bolivia	Tarija - Pleistocene	Right tibia
Glossotherium tarijensis	MNHN.F.TAR 794	Bolivia	Tarija - Pleistocene	Right humerus
Glossotherium tropicorum	ROM 12674	Ecuador	Corralito - Pleistocene	Ear region
Glossotherium tropicorum	ROM 3146	Ecuador	Corralito - Pleistocene	Skull and left mandible with dentition
Glossotherium tropicorum	VF-11	Venezuela	Muaco - late Pleistocene	Left femur
Glossotherium tropicorum	VF-188	Venezuela	Muaco - late Pleistocene	Proximal part of cranium
Glossotherium tropicorum	VF-205	Venezuela	Muaco - late Pleistocene	Right mandible
Glossotherium tropicorum	VF-24	Venezuela	Muaco - late Pleistocene	Right ulna
Glossotherium tropicorum	VF-26	Venezuela	Muaco - late Pleistocene	Right humerus
Glossotherium tropicorum	VF-28	Venezuela	Muaco - late Pleistocene	Right radius
Hapalops cf. *ruetemeyeri*	FMNH P13128	Argentina	Santa Cruz Fm. - late Early Miocene	Mandibles, proximal fragment of humerus, left femur, tibia, fibula
Hapalops elongatus	MACN Pv 11766	Argentina	Chubut - Pampa del Castillo	Distal part of right humerus
Hapalops elongatus	FMNH P13121	Argentina	Santa Cruz Fm. - late Early Miocene	Mandibles
Hapalops elongatus	FMNH P13123	Argentina	Santa Cruz Fm. - late Early Miocene	Radius, proximal fragment of ulna and complete patella, tibia, fibula, calcaneum, astragalus, navicular, cuboid, and phalanges
Hapalops elongatus	FMNH P13133	Argentina	Santa Cruz Fm. - late Early Miocene	Cranium, mandible, left and right humeri, scapula, radius, ulna
Hapalops ruetemeyeri	FMNH P13130	Argentina	Santa Cruz Fm. - late Early Miocene	Mandibles, right humerus, ulna, radius, left femur, tibia, one vertebra, phalanges and mtc4
Hapalops ruetemeyeri	FMNH P13132	Argentina	Santa Cruz Fm. - late Early Miocene	Cranium and mandible
Hapalops sp.	FMNH P13136	Argentina	Santa Cruz Fm. - late Early Miocene	Mandibles
Kiyumylodon lecuonai	FCDPV 1829*	Uruguay	Camacho Fm. - Late Miocene	Right mandible
Lestobradys sprechmanni	FCDPV 1826*	Uruguay	Camacho Fm. - Late Miocene	Fragmented cranium, right mandible and some vertebrae
Lestobradys sprechmanni	FCDPV 462*	Uruguay	Camacho Fm. - Late Miocene	Left mandible
Lestobradys sprechmanni	MNHN 1641*	Uruguay	Camacho Fm. - Late Miocene	Right astragalus
Lestodon armatus	MACN Pv 10747	Argentina	Barrancas Mar del Plata - early Pleistocene	Left cuboid
Lestodon armatus	MACN Pv 10748	Argentina	Barrancas Mar del Plata - early Pleistocene	Right cuboid
Lestodon armatus	MACN Pv 10749	Argentina	Barrancas Mar del Plata - early Pleistocene	Right navicular
Lestodon armatus	MACN Pv 10750	Argentina	Barrancas Mar del Plata - early Pleistocene	Mtt3 right
Lestodon armatus	MACN Pv 10751	Argentina	Barrancas Mar del Plata - early Pleistocene	Mtt3 right
Lestodon armatus	MACN Pv 10752	Argentina	Barrancas Mar del Plata - early Pleistocene	Mtt4 left
Lestodon armatus	MACN Pv 10754	Argentina	Barrancas Mar del Plata - early Pleistocene	Mtc4 left
Lestodon armatus	MACN Pv 10755	Argentina	Barrancas Mar del Plata - early Pleistocene	Mtc3 right

Lestodon armatus	MACN Pv 10756	Argentina	Barrancas Mar del Plata - early Pleistocene	Right unciform
Lestodon armatus	MACN Pv 10757	Argentina	Barrancas Mar del Plata - early Pleistocene	Left lunar
Lestodon armatus	MACN Pv 10758	Argentina	Barrancas Mar del Plata - early Pleistocene	Right lunar
Lestodon armatus	MACN Pv 10759	Argentina	Barrancas Mar del Plata - early Pleistocene	Mtc3 right
Lestodon armatus	MACN Pv 10760	Argentina	Barrancas Mar del Plata - early Pleistocene	Mtc5 left
Lestodon armatus	MACN Pv 10761	Argentina	Barrancas Mar del Plata - early Pleistocene	Left unciform
Lestodon armatus	MACN Pv 10762	Argentina	Barrancas Mar del Plata - early Pleistocene	Left magnum
Lestodon armatus	MACN Pv 10763	Argentina	Barrancas Mar del Plata - early Pleistocene	Left magnum
Lestodon armatus	MACN Pv 10789	Argentina	Barrancas Mar del Plata - early Pleistocene	Mtt2 right
Lestodon armatus	MACN Pv 10826	Argentina	Barrancas Mar del Plata - early Pleistocene	Left mandible with dentition (juvenile)
Lestodon armatus	MACN Pv 10827	Argentina	Barrancas Mar del Plata - early Pleistocene	Left and right mandibles with dentition, juvenile
Lestodon armatus	MACN Pv 10828	Argentina	Barrancas Mar del Plata - early Pleistocene	Left and right mandibles with dentition
Lestodon armatus	MACN Pv 10829	Argentina	Barrancas Mar del Plata - early Pleistocene	Left and right mandibles with dentition
Lestodon armatus	MACN Pv 10833	Argentina	Barrancas Mar del Plata - early Pleistocene	Occipital and maxillary fragment with dentition
Lestodon armatus	AMNH 11272	Argentina	Buenos Aires - Pleistocene	Rostral part of cranium highly damaged and isolated petrosal
Lestodon armatus	AMNH 11310	Argentina	Buenos Aires - Pleistocene	Postcranial elements (atlas, astragalus, humerus, tibia)
Lestodon armatus	AMNH 96233	Argentina	Buenos Aires - Pleistocene	Postcranial elements (scaphoid, unciform, cuneiform, mtc3, mtc4, navicular, cuboid, lunar)
Lestodon armatus	MACN Pv 14615	Argentina	Buenos Aires - Pleistocene	Left radius
Lestodon armatus	MACN Pv 14616	Argentina	Buenos Aires - Pleistocene	Right radius
Lestodon armatus	MACN Pv 14648	Argentina	Buenos Aires - Pleistocene	Complete right scapula
Lestodon armatus	MACN Pv 14653	Argentina	Buenos Aires - Pleistocene	Right radius
Lestodon armatus	MACN Pv 14663	Argentina	Buenos Aires - Pleistocene	Left radius
Lestodon armatus	MACN Pv 17182	Argentina	Buenos Aires - Pleistocene	Left humerus, dorsal vertebra, calcaneum, fragment of scapula
Lestodon armatus	MACN Pv 9398	Argentina	Buenos Aires - Pleistocene	Right mandibular fragment with dentition
Lestodon armatus	MACN Pv 9479	Argentina	Buenos Aires - Pleistocene	Right ulna
Lestodon armatus	MACN Pv 9480	Argentina	Buenos Aires - Pleistocene	Left ulna
Lestodon armatus	MLP 3-47	Argentina	Buenos Aires - Pleistocene	Right calcaneum
Lestodon armatus	MLP 3-48	Argentina	Buenos Aires - Pleistocene	Left tibia
Lestodon armatus	MLP 3-58	Argentina	Buenos Aires - Pleistocene	Distal part of left femur
Lestodon armatus	MNHN.F.PAM 100	Argentina	Buenos Aires - Pleistocene	Fragment of left ulna
Lestodon armatus	MNHN.F.PAM 101	Argentina	Buenos Aires - Pleistocene	Right ulna
Lestodon armatus	MNHN.F.PAM 105	Argentina	Buenos Aires - Pleistocene	Left femur
Lestodon armatus	MNHN.F.PAM 107	Argentina	Buenos Aires - Pleistocene	Left tibia
Lestodon armatus	MNHN.F.PAM 90	Argentina	Buenos Aires - Pleistocene	Proximal fragment of both mandibles with dentition
Lestodon armatus	MNHN.F.PAM 91	Argentina	Buenos Aires - Pleistocene	Left maxillary fragment with Cf1 and Mf1
Lestodon armatus	MNHN.F.PAM 98	Argentina	Buenos Aires - Pleistocene	Right humerus
Lestodon armatus	ROM 51756	Argentina	Buenos Aires - Pleistocene	Left tibia
Lestodon armatus	ROM 263	Argentina	Buenos Aires - Pleistocene	Cranium broken in two fragments
Lestodon armatus	ROM 51757	Argentina	Buenos Aires - Pleistocene	Left fibula
Lestodon armatus	ROM 51758	Argentina	Buenos Aires - Pleistocene	Right astragalus
Lestodon armatus	ROM 51760	Argentina	Buenos Aires - Pleistocene	Left humerus

Lestodon armatus	ROM 51761	Argentina	Buenos Aires - Pleistocene	Left radius
Lestodon armatus	MACN Pv 10710	Argentina	Mar del Plata - Pleistocene	Proximal fragment of right ulna
Lestodon armatus	MACN Pv 10830	Argentina	Mar del Plata - Pleistocene	Cranium and mandible
Lestodon armatus	MACN Pv 10834	Argentina	Mar del Plata - Pleistocene	Fragment of cranium with dentition (juvenile)
Lestodon armatus	MACN Pv 9470	Argentina	Playa del Barco - Buenos Aires - Pleistocene	Cranium and mandibles with almost complete dentition
Lestodon armatus	MACN Pv 5749	Argentina	Playa del Barco - Pleistocene	Mandibles and dentition
Lestodon armatus	MACN Pv 14911b	Argentina	Pleistocene - no locality	Posterior portion of cranium
Lestodon armatus	MACN Pv 4950	Argentina	Pleistocene - no locality	Proximal part of right humerus
Lestodon armatus	MACN Pv 94	Argentina	Pleistocene - no locality	Right mandible with mf1
Lestodon armatus	MLP 3-133	Argentina	Pleistocene - no locality	Complete right ulna
Lestodon armatus	MLP 3-17	Argentina	Pleistocene - no locality	Left femur (juvenile)
Lestodon armatus	MLP 3-18	Argentina	Pleistocene - no locality	Left humerus, atlas and other fragments
Lestodon armatus	MLP 3-20	Argentina	Pleistocene - no locality	Left tibia
Lestodon armatus	MLP 3-30	Argentina	Pleistocene - no locality	Complete cranium and mandibles
Lestodon armatus	MLP 3-33	Argentina	Pleistocene - no locality	Proximal and distal parts of cranium
Lestodon armatus	MLP 3-49	Argentina	Pleistocene - no locality	Left tibia
Lestodon armatus	MLP 3-59	Argentina	Pleistocene - no locality	Proximal part of left left femur
Lestodon armatus	MLP 3-62	Argentina	Pleistocene - no locality	Left tibia
Lestodon armatus	MLP 3-64	Argentina	Pleistocene - no locality	Left astragalus
Lestodon armatus	MLP 3-65	Argentina	Pleistocene - no locality	Left calcaneum
Lestodon armatus	MLP 3-66	Argentina	Pleistocene - no locality	Left patella
Lestodon armatus	MLP 3-73	Argentina	Pleistocene - no locality	Right fibula
Lestodon armatus	MLP 3-797	Argentina	Pleistocene - no locality	Atlas
Lestodon armatus	MLP 3-822	Argentina	Pleistocene - no locality	Proximal fragment of right ulna
Lestodon armatus	MLP 3-824	Argentina	Pleistocene - no locality	Right astragalus
Lestodon armatus	MLP 3-826	Argentina	Pleistocene - no locality	Left astragalus
Lestodon armatus	MLP 3-83	Argentina	Pleistocene - no locality	Right and left ulna, right radius, right mandibular corpus fragment, three vertebras and other manus and pes fragments
Lestodon armatus	MLP 3-831	Argentina	Pleistocene - no locality	Left humerus, right tibia, left patella
Lestodon armatus	MLP 40-IV-26-1	Argentina	Pleistocene - no locality	Left radius
Lestodon armatus	MLP 50-VII-1-5	Argentina	Pleistocene - no locality	Right astragalus
Lestodon armatus	MLP 56-XII-12-2	Argentina	Pleistocene - no locality	Left tibia
Lestodon armatus	MLP S.N.	Argentina	Pleistocene - no locality	Left astragalus
Lestodon armatus	MLP s/n1	Argentina	Pleistocene - no locality	Distal part of left femur
Lestodon armatus	MLP s/n2	Argentina	Pleistocene - no locality	Distal part of right femur
Lestodon armatus	MLP SN13	Argentina	Pleistocene - no locality	Left tibia
Lestodon armatus	MLP SN19	Argentina	Pleistocene - no locality	Left patella
Lestodon armatus	MLP SN22	Argentina	Pleistocene - no locality	Left astragalus
Lestodon armatus	MLP SN23	Argentina	Pleistocene - no locality	Right astragalus
Lestodon armatus	MLP SN25	Argentina	Pleistocene - no locality	Right astragalus
Lestodon armatus	MNHN.F.PAM 141 (A.C. 7167-7165)	Argentina	Pleistocene - no locality	Scaphoid and lunar (left)
Lestodon armatus	MNHN.F.PAM 141 (A.C. 7178)	Argentina	Pleistocene - no locality	Right navicular
Lestodon armatus	MNHN.F.PAM s/n (3)	Argentina	Pleistocene - no locality	Left radius

Lestodon armatus	MACN Pv 11687	Argentina	Río Carcarañá - Santa Fe - Pleistocene	Cranium
Lestodon armatus	MLP 3-3	Argentina	San Antonio de Areco - Buenos Aires - Pleistocene	Complete skeleton
Lestodon armatus	FMNH P13713	Bolivia	Tarija - Pleistocene	Left lunar, left cuboid
Lestodon armatus	FMNH P13727	Bolivia	Tarija - Pleistocene	Rostral part of cranium, highly damaged
Lestodon armatus	FMNH P13732	Bolivia	Tarija - Pleistocene	Right mandible with complete dentition
Lestodon armatus	FMNH P14226	Bolivia	Tarija - Pleistocene	Mtt4, navicular, magnum and other postcranial remains
Lestodon armatus	FMNH P14228	Bolivia	Tarija - Pleistocene	Skull, mandibles and some postcranial bones (ectocunieform, astragalus, mtt3, mtt4, radius, tibia, calcaneum)
Lestodon armatus	FMNH P14229	Bolivia	Tarija - Pleistocene	Two scapular fragments, humerus and pelvis, tibia
Lestodon armatus	FMNH P14247	Bolivia	Tarija - Pleistocene	Right fibula, left mtt5 and other bones
Lestodon armatus	FMNH P15492	Bolivia	Tarija - Pleistocene	Left radius
Lestodon armatus	MNHN.F.TAR 771	Bolivia	Tarija - Pleistocene	Right tibia
Lestodon armatus	MNHN.F.TAR 773	Bolivia	Tarija - Pleistocene	Proximal fragment of both mandibles with left cf1, mf1, mf2, mf3 and right cf1
Lestodon armatus	MNHN.F.TAR 775	Bolivia	Tarija - Pleistocene	Right humerus
Lestodon armatus	MNHN.F.TAR 776	Bolivia	Tarija - Pleistocene	Right tibia
Lestodon armatus	MNHN.F.TAR 778	Bolivia	Tarija - Pleistocene	Left humerus
Lestodon armatus	MNHN.F.TAR 808	Bolivia	Tarija - Pleistocene	Left tibia with fused fibula
Lestodon armatus	UF 92431	Bolivia	Tarija - Pleistocene	Left mandible with mf1-mf3 and alveoli of cf1
Lestodon armatus	UF 92432	Bolivia	Tarija - Pleistocene	Right scapula
Lestodon armatus	UF s/n	Bolivia	Tarija - Pleistocene	Left mandible and symphysis
Manis gigantea	AMNH 53855	?	Extant	Complete skeleton
Mirandabradys socorrensis	AMU-CURS 29	Venezuela	Socorro Fm. - middle Miocene	Cranium, femur, tibia and fibula fused, ulnar fragment
Mirandabradys urumaquensis	AMU-CURS 157	Venezuela	Urumaco Fm. - late Miocene	Left femur
Mirandabradys zabasi	AMU-CURS 109	Venezuela	Codore Fm. - Pliocene	Mtc3
Mirandabradys zabasi	AMU-CURS 127	Venezuela	Codore Fm. - Pliocene	Femur (almost complete)
Mirandabradys zabasi	AMU-CURS 128	Venezuela	Codore Fm. - Pliocene	Femur distal part
Mylodon darwinii	MLP 36-VIII-12-1	Argentina	Buenos Aires - early Pleistocene	Cranium without dentition
Mylodon darwinii	MACN Pv 15348	Argentina	Buenos Aires - Pleistocene	Cranium
Mylodon darwinii	MLP 94-VIII-10-3	Chile	Cueva del Mylodon - late Pleistocene	Posterior part of cranium and maxillary fragment
Mylodon darwinii	MACN Pv 5980	Argentina	Miramar - early Pleistocene	Left mandibular fragment with mf2 and mf3
Mylodon darwinii	MNHN-Bol V 6457	Bolivia	Mojotorillo - Pleistocene	Left mandible with alveoli of dentition
Mylodon darwinii	MNHN-Bol V 6472	Bolivia	Mojotorillo - Pleistocene	Left mandibular fragment with alveoli of dentition
Mylodon darwinii	MNHN-Bol V 6473	Bolivia	Mojotorillo - Pleistocene	Left mandibular fragment
Mylodon darwinii	MACN Pv 13882	Argentina	Necochea - Pleistocene	Cranium with left and right mf1s
Mylodon darwinii	MLP 3-762a	Argentina	Olavarría - late Pleistocene	Complete cranium with only one molar
Mylodon darwinii	MLP 3-764	Argentina	Olavarría - late Pleistocene	Complete cranium and mandibles
Mylodon darwinii	MLP 54-III-8-1	Argentina	Olavarría - late Pleistocene	Posterior portion of cranium
Mylodon darwinii	MACN Pv 14106	Argentina	Pleistocene - no locality	Right ulna
Mylodon darwinii	MLP 3-122	Argentina	Pleistocene - no locality	Cranium without dentition
Mylodon darwinii	FMNH P14288	Argentina	Río Quequén - Buenos Aires - Pleistocene	Cranium, atlas, radius, ulna, astragalus, almost complete left manus
Mylodon darwinii	MACN Pv 13797	Argentina	Buenos Aires - Pleistocene	Right and left humeri
Mylodon darwinii	MACN Pv 14678	Argentina	Buenos Aires - Pleistocene	Left humerus
Mylodon darwinii	MACN Pv 14681	Argentina	Buenos Aires - Pleistocene	Right humerus

Mylodon darwinii	MACN Pv 6866	Chile	Última Espereanza - late Pleistocene	Left tibia, distal part of left femur, part of left scapula, three fused vertebrae
Myrmecophaga sp.	MACN Ma 31.132	Argentina	Pleistocene - no locality	Complete skeleton
Myrmecophaga sp.	AMNH 1414	?	Extant	Complete skeleton
Myrmecophaga sp.	AMNH 2414	?	Extant	Complete skeleton
Nematherium angulatum	FMNH P13129	Argentina	Santa Cruz Fm. - late Early Miocene	Cranium (reconstructed), left radius, ulna and carpals
Nematherium angulatum	FMNH P13258	Argentina	Santa Cruz Fm. - late Early Miocene	Mtc3 and calcaneum
Nematherium angulatum	MACN A 9318	Argentina	Santa Cruz Fm. - late Early Miocene	Distal part of right radius
Nematherium angulatum	MNHN SCZ 121	Argentina	Santa Cruz Fm. - late Early Miocene	Cranium and mandibles
Nematherium angulatum	ROM 6081	Argentina	Santa Cruz Fm. - late Early Miocene	Cranium and left mandible, and fragments of right mandible
Nematherium angulatum	ROM 6082	Argentina	Santa Cruz Fm. - late Early Miocene	Mandibles with dentition
Nematherium birdi	AMNH 32652	Chile	Cañadon la leona - Palomares - late Miocene	Partial cranium
Nematherium longirostris	MACN A 4660	Argentina	Monte Observación - Santa Cruz - late Early Miocene	Cranium almost complete (Type)
Nematherium sp.	MACN A 4669	Argentina	Corriguen - Santa Cruz - late Early Miocene	Left and right mandibles with complete dentition
Nematherium sp.	MACN A 5781	Argentina	Monte Observación - Santa Cruz - late Early Miocene	Cranium with complete dentition
Nematherium sp.	MACN A 5782	Argentina	Monte Observación - Santa Cruz - late Early Miocene	Right mandibular fragment
Nematherium sp.	MACN A 5783	Argentina	Monte Observación - Santa Cruz - late Early Miocene	Maxilla with left and right molariform series
Nematherium sp.	MACN A 5784	Argentina	Monte Observación - Santa Cruz - late Early Miocene	Right mandibular fragment with mf2 and partial mf1 and mf3
Nematherium sp.	MACN A 5785	Argentina	Monte Observación - Santa Cruz - late Early Miocene	Left mandibular fragment with complete dentition
Nematherium sp.	MACN A 5786	Argentina	Monte Observación - Santa Cruz - late Early Miocene	Left portion of cranium
Nematherium sp.	MACN A 5787	Argentina	Monte Observación - Santa Cruz - late Early Miocene	Rostral part of cranium with dentition
Nematherium sp.	YPM-PU 15374*	Argentina	Santa Cruz Fm. - late Early Miocene	Left humerus
Nematherium sp.	YPM-PU 15965*	Argentina	Santa Cruz Fm. - late Early Miocene	Astragalus, calcaneum and part of calcaneum
Octodontobradys puruensis	UFAC PV 1803*	Brazil	Acre - late Miocene/early Pliocene	Left and right mandibles with dentition
Octodontobradys puruensis	UFAC PV 2108*	Brazil	Acre - late Miocene/early Pliocene	Right maxillary fragment without dentition
Octodontobradys puruensis	UFAC PV 5643*	Brazil	Acre - late Miocene/early Pliocene	Left and right fragmented mandibles without dentition
Octodontotherium grande	MNHN.F.DES 191-201	Argentina	Deseado Fm. - late Oligocene	Various phalanges
Octodontotherium grande	MNHN.F.DES 202	Argentina	Deseado Fm. - late Oligocene	Right lunar
Octodontotherium grande	MNHN.F.DES 203	Argentina	Deseado Fm. - late Oligocene	Left lunar
Octodontotherium grande	MNHN.F.DES 204-211	Argentina	Deseado Fm. - late Oligocene	Ungual phalanges
Octodontotherium grande	MNHN.F.DES 212	Argentina	Deseado Fm. - late Oligocene	Left astragalus without proximal articulation
Octodontotherium grande	MNHN.F.DES 213	Argentina	Deseado Fm. - late Oligocene	Right astragalus
Octodontotherium grande	MNHN.F.DES 214	Argentina	Deseado Fm. - late Oligocene	Right scaphoid (fragmented)
Octodontotherium grande	MNHN.F.DES 215	Argentina	Deseado Fm. - late Oligocene	Left scaphoid (fragmented)
Octodontotherium grande	MNHN.F.DES 216	Argentina	Deseado Fm. - late Oligocene	Right unciform
Octodontotherium grande	MNHN.F.DES 217	Argentina	Deseado Fm. - late Oligocene	Right mtt4 without proximal end

Octodontotherium grande	MNHN.F.DES 218	Argentina	Deseado Fm. - late Oligocene	Right mtt4 without distal end
Octodontotherium grande	MNHN.F.DES 219	Argentina	Deseado Fm. - late Oligocene	Distal fragment of left mtt4
Octodontotherium grande	MNHN.F.DES 220	Argentina	Deseado Fm. - late Oligocene	Left mtt3
Octodontotherium grande	MNHN.F.DES 221	Argentina	Deseado Fm. - late Oligocene	Left mtt3
Octodontotherium grande	MNHN.F.DES 223	Argentina	Deseado Fm. - late Oligocene	Right mtc2
Octodontotherium grande	MNHN.F.DES 224	Argentina	Deseado Fm. - late Oligocene	Right mtt3
Octodontotherium grande	MNHN.F.DES 225	Argentina	Deseado Fm. - late Oligocene	Left mtc2
Octodontotherium grande	MNHN.F.DES 228	Argentina	Deseado Fm. - late Oligocene	Proximal fragment of left mtt4
Octodontotherium grande	MNHN.F.DES 229	Argentina	Deseado Fm. - late Oligocene	Left unciform
Octodontotherium grande	MNHN.F.DES 230	Argentina	Deseado Fm. - late Oligocene	Left lunar
Octodontotherium grande	MNHN.F.DES 231(1)	Argentina	Deseado Fm. - late Oligocene	Left mtc1
Octodontotherium grande	MNHN.F.DES 231(2)	Argentina	Deseado Fm. - late Oligocene	Left scaphoid
Octodontotherium grande	MNHN.F.DES 232	Argentina	Deseado Fm. - late Oligocene	Left mf1
Octodontotherium grande	MNHN.F.DES 233	Argentina	Deseado Fm. - late Oligocene	Isolated molariform, probable left Mf2
Octodontotherium grande	MNHN.F.DES 234	Argentina	Deseado Fm. - late Oligocene	Isolated molariform, probable right Mf2
Octodontotherium grande	MNHN.F.DES 235	Argentina	Deseado Fm. - late Oligocene	Right Mf4
Octodontotherium grande	MNHN.F.DES 236	Argentina	Deseado Fm. - late Oligocene	Right mf3 (juvenile)
Octodontotherium grande	MNHN.F.DES 237	Argentina	Deseado Fm. - late Oligocene	Left mf3
Octodontotherium grande	MNHN.F.DES 238	Argentina	Deseado Fm. - late Oligocene	Left mf2
Octodontotherium grande	MNHN.F.DES 239	Argentina	Deseado Fm. - late Oligocene	Right Mf3
Octodontotherium grande	MNHN.F.DES 240	Argentina	Deseado Fm. - late Oligocene	Left Mf2
Octodontotherium grande	MNHN.F.DES 241	Argentina	Deseado Fm. - late Oligocene	Right Mf2
Octodontotherium grande	MNHN.F.DES 242	Argentina	Deseado Fm. - late Oligocene	Left cf1
Octodontotherium grande	MNHN.F.DES 243	Argentina	Deseado Fm. - late Oligocene	Right Mf4
Octodontotherium grande	MNHN.F.DES 244	Argentina	Deseado Fm. - late Oligocene	Left Mf1
Octodontotherium grande	MNHN.F.DES 245	Argentina	Deseado Fm. - late Oligocene	Left Mf4
Octodontotherium grande	MNHN.F.DES 246	Argentina	Deseado Fm. - late Oligocene	Proximal fragment of left mandible with mf2 and alveoli of cf1-mf1 and partial alveoli of mf3
Octodontotherium grande	MNHN.F.DES 247	Argentina	Deseado Fm. - late Oligocene	Left cf1 (or mf1)
Octodontotherium grande	MNHN.F.DES 248	Argentina	Deseado Fm. - late Oligocene	Right cf1
Octodontotherium grande	MNHN.F.DES 250	Argentina	Deseado Fm. - late Oligocene	Left maxillary and lacrimal fragment of a juvenile with Mf1-3
Octodontotherium grande	MNHN.F.DES 251	Argentina	Deseado Fm. - late Oligocene	Frgament of molariform, probably mf2 or mf3
Octodontotherium grande	MNHN.F.DES 252	Argentina	Deseado Fm. - late Oligocene	Right Mf3
Octodontotherium grande	MNHN.F.DES 253	Argentina	Deseado Fm. - late Oligocene	Fragment of right mandible with cf1-mf1 and partial alveoli of mf2
Octodontotherium grande	MNHN.F.DES 261	Argentina	Deseado Fm. - late Oligocene	Left Mf1
Octodontotherium grande	MNHN.F.DES 272	Argentina	Deseado Fm. - late Oligocene	Ungual phalanx
Octodontotherium grande	MNHN.F.DES 273	Argentina	Deseado Fm. - late Oligocene	Ungual phalanx
Octodontotherium grande	MACN Pv 9294	Argentina	Pico Truncado - Santa Cruz - late Oligocene	Isolated molariform
Octodontotherium grande	MACN Pv 9296	Argentina	Pico Truncado - Santa Cruz - late Oligocene	Upper Mf4

Octodontotherium grande	MACN Pv 9297	Argentina	Pico Truncado - Santa Cruz - late Oligocene	Right mf1
Octodontotherium grande	FMNH P13363	Argentina	Pico Truncado/La Flecha - late Oligocene	Left and right mandibles and astragalus
Octodontotherium grande	FMNH P13368	Argentina	Pico Truncado/La Flecha - late Oligocene	Two left unciforms and one vertebra
Octodontotherium grande	FMNH P13388	Argentina	Pico Truncado/La Flecha - late Oligocene	Right maxillary fragment with Cf1-Mf3-Mf4 and alveoli of Mf1-Mf2
Octodontotherium grande	FMNH P13468	Argentina	Pico Truncado/La Flecha - late Oligocene	Right mtc2, left mtc3, left mtc4 and various phalanges
Octodontotherium grande	FMNH P13506	Argentina	Pico Truncado/La Flecha - late Oligocene	Tooth (right Cf1)
Octodontotherium grande	FMNH P13507	Argentina	Pico Truncado/La Flecha - late Oligocene	Right mandibular fragment with mf1
Octodontotherium grande	FMNH P13512	Argentina	Pico Truncado/La Flecha - late Oligocene	Maxillary fragment with M2-M3
Octodontotherium grande	FMNH P13517	Argentina	Pico Truncado/La Flecha - late Oligocene	Right tibia
Octodontotherium grande	FMNH P13560	Argentina	Pico Truncado/La Flecha - late Oligocene	Tooth (Cf1)
Octodontotherium grande	FMNH P13583	Argentina	Pico Truncado/La Flecha - late Oligocene	Teeth
Octodontotherium grande	FMNH P13616	Argentina	Pico Truncado/La Flecha - late Oligocene	Skull
Octodontotherium grande	FMNH P15072	Argentina	Pico Truncado/La Flecha - late Oligocene	Left mtc3 (distal part), two mtt4 (right damaged, left complete), two left mtt4, one vertebra, several phalanges
Octodontotherium grande	FMNH P15073	Argentina	Pico Truncado/La Flecha - late Oligocene	Teeth
Octodontotherium grande	MACN A 52 - 340	Argentina	Santa Cruz? - late Oligocene	Left mandibular fragment with mf2, partial alveoli of mf1 and mf3. Part of ungual phalanx.
Octodontotherium grande	MACN A 52 - 341	Argentina	Santa Cruz? - late Oligocene	Right mandibular fragment with cf1, alveoli of mf1, and partial alveoli of mf2
Octodontotherium grande	MACN A 52 - 342	Argentina	Santa Cruz? - late Oligocene	Isolated tooth
Octodontotherium grande	MACN A 52 - 342a	Argentina	Santa Cruz? - late Oligocene	Isolated tooth
Octodontotherium grande	MACN A 52 - 342b	Argentina	Santa Cruz? - late Oligocene	Isolated tooth
Octodontotherium grande	MACN A 52 - 343	Argentina	Santa Cruz? - late Oligocene	Left mf2
Octodontotherium grande	MACN A 52 - 343a	Argentina	Santa Cruz? - late Oligocene	Isolated teeth
Octodontotherium grande	MACN A 52 - 344	Argentina	Santa Cruz? - late Oligocene	Isolated teeth
Octodontotherium grande	MACN Pv 12777	Argentina	Santa Cruz? - late Oligocene	Left mandibular fragment with complete dentition
Octomylodon robertoscagliai	M-977	Argentina	Arroyo Chasicó - late Miocene	Cranium and mandible (only left half)
Orophodon hapaloides	MNHN.F.DES 254	Argentina	Deseado Fm. - late Oligocene	Right mtc2
Orophodon hapaloides	MNHN.F.DES 255	Argentina	Deseado Fm. - late Oligocene	Right mtc3
Orophodon hapaloides	MNHN.F.DES 256	Argentina	Deseado Fm. - late Oligocene	Right mtc1
Orophodon hapaloides	MNHN.F.DES 258	Argentina	Deseado Fm. - late Oligocene	Lunar
Orophodon hapaloides	MNHN.F.DES 259	Argentina	Deseado Fm. - late Oligocene	Right astragalus
Orophodon hapaloides	MNHN.F.DES 260	Argentina	Deseado Fm. - late Oligocene	Left mf1 (or mf2)
Orophodon hapaloides	MNHN.F.DES 262-266	Argentina	Deseado Fm. - late Oligocene	Various phalanges
Orophodon hapaloides	MNHN.F.DES 267	Argentina	Deseado Fm. - late Oligocene	Right mf3 of a juvenile
Orophodon hapaloides	MNHN.F.DES 268	Argentina	Deseado Fm. - late Oligocene	Right Mf1
Orophodon hapaloides	MNHN.F.DES 269	Argentina	Deseado Fm. - late Oligocene	Left Mf2 (or Mf3)
Orophodon hapaloides	MNHN.F.DES 277	Argentina	Deseado Fm. - late Oligocene	Fragment of left mandible with mf1-3
Orophodon hapaloides	MNHN.F.DES 281	Argentina	Deseado Fm. - late Oligocene	Right Mf4
Orophodon hapaloides	AMNH 96292	Argentina	Las Cascadas - Chubut - late Oligocene	Left mandibular fragment with cf1-mf1
Orophodon hapaloides	MACN A 52 - 345	Argentina	Pico Truncado/La Flecha - late Oligocene	Upper caniniform

Orophodon hapaloides	MACN A 52 - 346	Argentina	Santa Cruz? - late Oligocene	Two molariforms
Paramylodon garbanii	UF 10922	USA	Alachua Co. - Haile 15A - Florida - Pliocene	Palate with dentition and both petrosals, mandibles, and many postcranial elements
Paramylodon garbanii	AMNH F:AM 96370	USA	Gila R. Bridge of Duncan - Arizona - Pliocene	Astragalus, some phalanges, part of scapula, vertebrae and other fragments
Paramylodon garbanii	UF 24725	USA	Kissimmee River - Florida - Pliocene	Left mf1
Paramylodon garbanii	UF 52651	USA	Kissimmee River - Florida - Pliocene	Isolated caniniform
Paramylodon garbanii	UF 52652	USA	Kissimmee River - Florida - Pliocene	Right mf1
Paramylodon garbanii	UF 52653	USA	Kissimmee River - Florida - Pliocene	Part of tooth
Paramylodon garbanii	UF 52654	USA	Kissimmee River - Florida - Pliocene	Part of tooth
Paramylodon garbanii	AMNH F:AM 11693	USA	Las cruces - New Mexico - Plio/Pleistocene	Cranium (highly damaged)
Paramylodon garbanii	UF 101453	USA	Macasphalt - Florida - Pliocene	Head of left femur
Paramylodon garbanii	UF 104464	USA	Macasphalt - Florida - Pliocene	Two falanges
Paramylodon garbanii	UF 104466	USA	Macasphalt - Florida - Pliocene	Fragment of left femur
Paramylodon garbanii	UF 94625	USA	Macasphalt - Florida - Pliocene	Left mandible with cf1-mf2 (juvenile)
Paramylodon garbanii	UF/TRO 37	USA	Macasphalt - Florida - Pliocene	Right femur
Paramylodon harlani	UF 240075	USA	Alachua Co. - Haile 7C - latest Pliocene	Left mandible with mf4 (juvenile)
Paramylodon harlani	UF 224000	USA	Alachua Co. - Haile 7G - late Pliocene	Proximal part of right femur, patella, left tibia, dermal bones
Paramylodon harlani	AMNH 2780	USA	Hay Springs, Nebraska - Pleistocene	Cranium and mandble
Paramylodon harlani	UF 115735	USA	Leisey Shell Pit 1a - early Pleistocene	Right mandible without dentition
Paramylodon harlani	UF 127402	USA	Leisey Shell Pit 1a - early Pleistocene	Right femur
Paramylodon harlani	UF 219969	USA	Leisey Shell Pit 1a - early Pleistocene	Left mandible without dentition
Paramylodon harlani	UF 239312	USA	Leisey Shell Pit 1a - early Pleistocene	Right mandible without dentition
Paramylodon harlani	UF 239334	USA	Leisey Shell Pit 1a - early Pleistocene	Left ectocuneiform
Paramylodon harlani	UF 312801	USA	Leisey Shell Pit 1a - early Pleistocene	Right skull fragment with ear region (subadult)
Paramylodon harlani	UF 64358	USA	Leisey Shell Pit 1a - early Pleistocene	Skull fragment with ear region
Paramylodon harlani	UF 64361	USA	Leisey Shell Pit 1a - early Pleistocene	Left femur
Paramylodon harlani	UF 64362	USA	Leisey Shell Pit 1a - early Pleistocene	Fragmented femur
Paramylodon harlani	UF 64363	USA	Leisey Shell Pit 1a - early Pleistocene	Right femur distal fragment
Paramylodon harlani	UF 64365	USA	Leisey Shell Pit 1a - early Pleistocene	Left tibia
Paramylodon harlani	UF 64366	USA	Leisey Shell Pit 1a - early Pleistocene	Left astragalus
Paramylodon harlani	UF 64368	USA	Leisey Shell Pit 1a - early Pleistocene	Right mtc2
Paramylodon harlani	UF 64373	USA	Leisey Shell Pit 1a - early Pleistocene	Fragmented neurocranium
Paramylodon harlani	UF 64400	USA	Leisey Shell Pit 1a - early Pleistocene	Fragmented neurocranium
Paramylodon harlani	UF 65831	USA	Leisey Shell Pit 1a - early Pleistocene	Left mtc3
Paramylodon harlani	UF 65833	USA	Leisey Shell Pit 1a - early Pleistocene	Left mtt5
Paramylodon harlani	UF 65835	USA	Leisey Shell Pit 1a - early Pleistocene	Right cuboid
Paramylodon harlani	UF 65836	USA	Leisey Shell Pit 1a - early Pleistocene	Right cuneiform
Paramylodon harlani	UF 65837	USA	Leisey Shell Pit 1a - early Pleistocene	Left magnum
Paramylodon harlani	UF 65838	USA	Leisey Shell Pit 1a - early Pleistocene	Left magnum
Paramylodon harlani	UF 65839	USA	Leisey Shell Pit 1a - early Pleistocene	Left ectocuneiform

Paramylodon harlani	UF 65840	USA	Leisey Shell Pit 1a - early Pleistocene	Right navicular
Paramylodon harlani	UF 65844	USA	Leisey Shell Pit 1a - early Pleistocene	Right ectocuneiform
Paramylodon harlani	UF 65851	USA	Leisey Shell Pit 1a - early Pleistocene	Right humerus
Paramylodon harlani	UF 65857	USA	Leisey Shell Pit 1a - early Pleistocene	Right ulna
Paramylodon harlani	UF 65859	USA	Leisey Shell Pit 1a - early Pleistocene	Left femur
Paramylodon harlani	UF 65860	USA	Leisey Shell Pit 1a - early Pleistocene	Left tibia
Paramylodon harlani	Uf 65861	USA	Leisey Shell Pit 1a - early Pleistocene	Left tibia
Paramylodon harlani	Uf 65862	USA	Leisey Shell Pit 1a - early Pleistocene	Left tibia
Paramylodon harlani	UF 65865	USA	Leisey Shell Pit 1a - early Pleistocene	Skull fragment with ear region
Paramylodon harlani	UF 65866	USA	Leisey Shell Pit 1a - early Pleistocene	Right skull fragment with ear region
Paramylodon harlani	UF 67425	USA	Leisey Shell Pit 1a - early Pleistocene	Left lunar
Paramylodon harlani	UF 80039	USA	Leisey Shell Pit 1a - early Pleistocene	Left femur distal fragment
Paramylodon harlani	UF 80085	USA	Leisey Shell Pit 1a - early Pleistocene	Right skull fragment with ear region
Paramylodon harlani	UF 80163	USA	Leisey Shell Pit 1a - early Pleistocene	Left radius
Paramylodon harlani	UF 80164	USA	Leisey Shell Pit 1a - early Pleistocene	Right femur distal fragment
Paramylodon harlani	UF 80176	USA	Leisey Shell Pit 1a - early Pleistocene	Left tibia
Paramylodon harlani	UF 80367	USA	Leisey Shell Pit 1a - early Pleistocene	Left mandible with m3
Paramylodon harlani	UF 80782	USA	Leisey Shell Pit 1a - early Pleistocene	Left scaphoid
Paramylodon harlani	UF 81737	USA	Leisey Shell Pit 1a - early Pleistocene	Left calcanuem fragment
Paramylodon harlani	UF 82207	USA	Leisey Shell Pit 1a - early Pleistocene	Right scaphoid
Paramylodon harlani	UF 83335	USA	Leisey Shell Pit 1a - early Pleistocene	Right mandible with complete dentition
Paramylodon harlani	UF 83769	USA	Leisey Shell Pit 1a - early Pleistocene	Skull
Paramylodon harlani	UF 84136	USA	Leisey Shell Pit 1a - early Pleistocene	Right humerus
Paramylodon harlani	UF 84848/87048	USA	Leisey Shell Pit 1a - early Pleistocene	Left and right mandibles with left cf1 and right mf3
Paramylodon harlani	UF 86700	USA	Leisey Shell Pit 1a - early Pleistocene	Right ectocuneiform
Paramylodon harlani	UF 86869	USA	Leisey Shell Pit 1a - early Pleistocene	Right lunar
Paramylodon harlani	UF 87024	USA	Leisey Shell Pit 1a - early Pleistocene	Left mtc4
Paramylodon harlani	UF 87087	USA	Leisey Shell Pit 1a - early Pleistocene	Left femur distal fragment
Paramylodon harlani	UF 87100	USA	Leisey Shell Pit 1a - early Pleistocene	Right astragalus
Paramylodon harlani	UF 87101	USA	Leisey Shell Pit 1a - early Pleistocene	Left unciform and right scaphoid
Paramylodon harlani	UF 87103	USA	Leisey Shell Pit 1a - early Pleistocene	Right scaphoid
Paramylodon harlani	UF 87104	USA	Leisey Shell Pit 1a - early Pleistocene	Left unciform
Paramylodon harlani	UF 87105	USA	Leisey Shell Pit 1a - early Pleistocene	Right mtt3
Paramylodon harlani	UF 87106	USA	Leisey Shell Pit 1a - early Pleistocene	Left magnum
Paramylodon harlani	UF 88722	USA	Leisey Shell Pit 1a - early Pleistocene	Fragmented neurocranium
Paramylodon harlani	UF 88724	USA	Leisey Shell Pit 1a - early Pleistocene	Right mtc5
Paramylodon harlani	UF 88726	USA	Leisey Shell Pit 1a - early Pleistocene	Left lunar
Paramylodon harlani	MACN Pv 8735	USA	Oregon - Pleistocene	Right humerus
Paramylodon harlani	AMNH 16896	USA	Rancho la Brea - middle/late Pleistocene	Almost complete skeleton

Paramylodon harlani	FMNH P12519	USA	Rancho la Brea - middle/late Pleistocene	Cranium
Paramylodon harlani	FMNH P12521	USA	Rancho la Brea - middle/late Pleistocene	Almost complete skeleton
Paramylodon harlani	FMNH P12522	USA	Rancho la Brea - middle/late Pleistocene	Mandible highly reconstructed
Paramylodon harlani	FMNH P14723	USA	Rancho la Brea - middle/late Pleistocene	Almost complete skeleton
Paramylodon harlani	FMNH PM3646	USA	Rancho la Brea - middle/late Pleistocene	Cranium
Paroctodontotherium calleorum	UATF-V-127	Bolivia	Salla - late Oligocene	Fragmented cranium
Pleurolestodon acutidens	FMNH P14495	Argentina	Catamarca - late Miocene	Cranium, mandibles, vertebrae, and other fragments
Pleurolestodon acutidens	FMNH P14521	Argentina	Catamarca - late Miocene	Right mandible with complete dentition
Pleurolestodon acutidens	MACN Pv 2784	Argentina	Catamarca - late Miocene	Upper right maxillary with three molars
Pleurolestodon acutidens	MACN Pv 2785	Argentina	Catamarca - late Miocene	Cranium highly diagenetic
Pleurolestodon acutidens	MACN Pv 2816	Argentina	Catamarca - late Miocene	Right astragalus
Pleurolestodon acutidens	MACN Pv 8205	Argentina	Catamarca - late Miocene	Two lower molariforms
Pseudoglyptodon sp.	MNHN-Bol V 9623	Bolivia	Salla - late Oligocene	Left mandibular fragment with mf1-mf2
Pseudoglyptodon sp.	SGO PV 2995*	Chile	Tinguiririca River Valley - early Oligocene	Rostral part of cranium
Pseudoprepotherium confusum	FMNH PM54786	Colombia	La Venta - middle Miocene	Two mandibular fragments
Pseudoprepotherium confusum	UCMP 117525*	Colombia	La Venta - middle Miocene	Left femur
Pseudoprepotherium confusum	UCMP 37919*	Colombia	La Venta - middle Miocene	Two left tibiae, scapular fragment, phalanx, mtt4
Pseudoprepotherium confusum	UCMP 37996*	Colombia	La Venta - middle Miocene	Mtt4 and two phalanges
Pseudoprepotherium confusum	UCMP 37999*	Colombia	La Venta - middle Miocene	Navicular
Pseudoprepotherium confusum	UCMP 38000*	Colombia	La Venta - middle Miocene	Fragmented skull, tibia, patella, astragalus, proximal phalanx, scaphoid
Pseudoprepotherium confusum	UCMP 38003*	Colombia	La Venta - middle Miocene	Mtt3
Pseudoprepotherium confusum	UCMP 38006*	Colombia	La Venta - middle Miocene	Left and right mandibles with dentition
Pseudoprepotherium confusum	UCMP 380108*	Colombia	La Venta - middle Miocene	Left humerus and epiphysis of left femur
Pseudoprepotherium confusum	UCMP 38046*	Colombia	La Venta - middle Miocene	Carpals, tarsals, ungual pahalanx and isolated tooth
Pseudoprepotherium confusum	UCMP 38841*	Colombia	La Venta - middle Miocene	Carpals, tarsals, ungual pahalanx and metapods
Pseudoprepotherium confusum	UCMP 38843*	Colombia	La Venta - middle Miocene	Fragment of astragalus
Pseudoprepotherium confusum	UCMP 38846*	Colombia	La Venta - middle Miocene	Fragments of tibia, vertebra and mtt3
Pseudoprepotherium confusum	UCMP 38853*	Colombia	La Venta - middle Miocene	Mtt3
Pseudoprepotherium confusum	UCMP 38854*	Colombia	La Venta - middle Miocene	Fragment of mtt3
Pseudoprepotherium confusum	UCMP 38887*	Colombia	La Venta - middle Miocene	Isolated tooth
Pseudoprepotherium confusum	UCMP 38914*	Colombia	La Venta - middle Miocene	Fragments of mandible with dentition
Pseudoprepotherium confusum	UCMP 38928*	Colombia	La Venta - middle Miocene	Patella, mtt3 and centre of vertebra
Pseudoprepotherium confusum	UCMP 38965*	Colombia	La Venta - middle Miocene	Left and right astragali and other fragments
Pseudoprepotherium confusum	UCMP 39903*	Colombia	La Venta - middle Miocene	Isolated tooth
Pseudoprepotherium confusum	UCMP 39957*	Colombia	La Venta - middle Miocene	Skull (damaged)
Pseudoprepotherium confusum	UCMP 40043*	Colombia	La Venta - middle Miocene	Left mandible and isolated teeth
Pseudoprepotherium confusum	UCMP 41137*	Colombia	La Venta - middle Miocene	Left femur
Scelidotherium leptocephalum	AMNH 11287	Argentina	Buenos Aires - Pleistocene	Skull, mandibles, most of skeleton
Scelidotherium leptocephalum	FMNH P14274	Argentina	Buenos Aires - Pleistocene	Scapula, left and right humeri, ulna, almost complete manus
Scelidotherium sp.	MACN Pv 7116	Argentina	Buenos Aires - late Pleistocene	Various autopodial fragments

Scelidotherium sp.	MACN Pv 13825	Argentina	Buenos Aires - Pleistocene	Right ulna
Scelidotherium sp.	MACN Pv 13927	Argentina	Buenos Aires - Pleistocene	Right ulna
Scelidotherium sp.	MACN Pv 18547	Argentina	Buenos Aires - Pleistocene	Incomplete cranium (subadult)
Scelidotherium sp.	MACN Pv 6964	Argentina	Buenos Aires - Pleistocene	Right humerus, ulna, radius, left ulna and various fragments of manus and pes
Scelidotherium sp.	MACN Pv 7150	Argentina	Buenos Aires - Pleistocene	Almost entire skeleton
Scelidotherium sp.	MACN Pv 8854	Argentina	Buenos Aires - Pleistocene	Left radius
Scelidotherium sp.	MLP 3-401	Argentina	Buenos Aires - Pleistocene	Complete skeleton
Scelidotherium sp.	MLP 3-521	Argentina	Buenos Aires - Pleistocene	Two tibias, fibulae and astragali
Scelidotherium sp.	MLP 3-522	Argentina	Buenos Aires - Pleistocene	Right tibia
Scelidotherium sp.	MLP 3-524	Argentina	Buenos Aires - Pleistocene	Right tibia with partial fibula fused
Scelidotherium sp.	MLP 3-526	Argentina	Buenos Aires - Pleistocene	Left tibia
Scelidotherium sp.	MLP 3-528	Argentina	Buenos Aires - Pleistocene	Left tibia and fibula
Scelidotherium sp.	MLP 3-532	Argentina	Buenos Aires - Pleistocene	Left tibia
Scelidotherium sp.	MLP 3-843	Argentina	Buenos Aires - Pleistocene	Right tibia
Scelidotherium sp.	MACN Pv 2749	Argentina	Chascomús - Buenos Aires - early Pleistocene	Right astragalus
Scelidotherium sp.	MACN Pv 9619	Argentina	Chascomús - Buenos Aires - late Pleistocene	Right astragalus
Scelidotherium sp.	MACN Pv 2213	Argentina	Laguna Adela - Buenos Aires - Pleistocene	Cranium with dentition
Scelidotherium sp.	AMNH 45910	Argentina	Mar del Plata - early Pleistocene	Cranium
Scelidotherium sp.	MLP 3-484	Argentina	Mar del Plata - Pleistocene	Right femur, radius and ulna
Scelidotherium sp.	MACN Pv 6149	Argentina	Miramar - early Pleistocene	Left calcaneum
Scelidotherium sp.	MACN Pv 5742	Argentina	Miramar - late Pleistocene	Right calcaneum
Scelidotherium sp.	MACN Pv 7023	Argentina	Miramar - late Pleistocene	Left astragalus
Scelidotherium sp.	MLP 3-671	Argentina	Olavarría - late Pleistocene	Complete cranium and mandibles
Scelidotherium sp.	MACN Pv 9376	Argentina	Playa del Barco - Buenos Aires - Pleistocene	Right calcaneum
Scelidotherium sp.	MACN Pv 79	Argentina	Pleistocene - no locality	Right radius
Scelidotherium sp.	MLP 08-V-29-1	Argentina	Pleistocene - no locality	Left tibia
Scelidotherium sp.	MLP 3-766	Argentina	Pleistocene - no locality	Left ulna
Scelidotherium sp.	MLP 41-V-16-3	Argentina	Pleistocene - no locality	Left femur
Scelidotherium sp.	MACN Pv 7014	Argentina	Puerto Nuevo - Buenos Aires - Pleistocene	Various bones without epiphyses (juvenile)
Scelidotherium sp.	MACN Pv 2215	Argentina	Rio de la Plata - early Pleistocene	Cranium with dentition
Scelidotherium sp.	MACN Pv 10856	Argentina	Rio de la Plata - Pleistocene	Left astragalus
Scelidotherium sp.	MACN Pv 856	Argentina	Rio de la Plata - Pleistocene	Left astragalus
Scelidotherium sp.	UF 162357	Bolivia	Ñuapua - Late Pleistocene	Right mandible
Scelidotherium sp.	FMNH P14301	Argentina	Río Quequén - Buenos Aires - Pleistocene	Humeri, ulnae, right radius, right manus, femur, tibia, patella and other fragments
Sphenotherus zavaletianus	MACN A 802	Argentina	Catamarca - late Miocene	Left mandibular fragment with alveoli of dentition (Type)
Sphenotherus zavaletianus	MACN Pv 13488	Argentina	Paraná - Entre Ríos - late Miocene	Right mf3
Sphenotherus zavaletianus	MACN Pv 13504	Argentina	Paraná - Entre Ríos - late Miocene	Left mf3
Tamandua sp.	MACN Ma 10.8	Argentina	Extant	Complete skeleton
Tamandua sp.	MACN Ma 25911	Argentina	Extant	Complete skeleton
Tamandua sp.	MACN Ma 33.255	Argentina	Extant	Complete skeleton
Thinobadistes cf *wetzeli*	UF 201320	USA	Tyner farm - Florida - late Miocene	Left Mf1
Thinobadistes cf *wetzeli*	UF 201321	USA	Tyner farm - Florida - late Miocene	Right mf4

Thinobadistes cf *wetzeli*	UF 201322	USA	Tyner farm - Florida - late Miocene	Right scapula
Thinobadistes cf *wetzeli*	UF 201323	USA	Tyner farm - Florida - late Miocene	Right fibula
Thinobadistes cf *wetzeli*	UF 201324	USA	Tyner farm - Florida - late Miocene	Right tibia
Thinobadistes cf *wetzeli*	UF 201327	USA	Tyner farm - Florida - late Miocene	Right astragalus
Thinobadistes cf *wetzeli*	UF 209900	USA	Tyner farm - Florida - late Miocene	Left humerus
Thinobadistes cf *wetzeli*	UF 215589	USA	Tyner farm - Florida - late Miocene	Left cuboid
Thinobadistes cf *wetzeli*	UF 215593	USA	Tyner farm - Florida - late Miocene	Right mf2
Thinobadistes cf *wetzeli*	UF 225079	USA	Withlacoochee river - Florida - late Miocene	Left navicular
Thinobadistes cf *wetzeli*	UF 23588	USA	Withlacoochee river - Florida - late Miocene	Right mtc2
Thinobadistes cf *wetzeli*	UF 23589	USA	Withlacoochee river - Florida - late Miocene	Palate with caniniforms (juvenile)
Thinobadistes cf *wetzeli*	UF 93059	USA	Withlacoochee river - Florida - late Miocene	Upper caniniform (juvenile)
Thinobadistes cf *wetzeli*	UF 93060	USA	Withlacoochee river - Florida - late Miocene	Upper caniniform (juvenile)
Thinobadistes cf *wetzeli*	UF 93061	USA	Withlacoochee river - Florida - late Miocene	Upper caniniform (juvenile)
Thinobadistes cf *wetzeli*	UF 93062	USA	Withlacoochee river - Florida - late Miocene	Upper caniniform (juvenile)
Thinobadistes segnis	UF 19235	USA	McGehee Farm - Florida - late Miocene	Two broken fragments of right mf3
Thinobadistes segnis	AMNH (FLA 218-3320)	USA	Mixon's bone bed - Florida - late Miocene	Maxillary fragments with part of dentition
Thinobadistes segnis	AMNH F:AM 102658	USA	Mixon's bone bed - Florida - late Miocene	Cranium and mandible
Thinobadistes segnis	AMNH F:AM 102659 to 102661	USA	Mixon's bone bed - Florida - late Miocene	Fagmented crania and mandibles
Thinobadistes segnis	AMNH F:AM 102662 to 102678	USA	Mixon's bone bed - Florida - late Miocene	Maxillary, mandibular fragments, isolated teeth
Thinobadistes segnis	AMNH F:AM 102664	USA	Mixon's bone bed - Florida - late Miocene	Mandible with dentition
Thinobadistes segnis	AMNH F:AM 102679 to 102702	USA	Mixon's bone bed - Florida - late Miocene	Mandibular fragments, isolated teeth
Thinobadistes segnis	AMNH F:AM 102711 to 102719	USA	Mixon's bone bed - Florida - late Miocene	Vertebrae, ribs, sternebrae
Thinobadistes segnis	AMNH F:AM 102720 to 102731	USA	Mixon's bone bed - Florida - late Miocene	Humeri and fragments of humeri
Thinobadistes segnis	AMNH F:AM 102732 to 102740	USA	Mixon's bone bed - Florida - late Miocene	Radii and fragments of radii
Thinobadistes segnis	AMNH F:AM 102741 to 102744	USA	Mixon's bone bed - Florida - late Miocene	Ulnae and fragments of ulnae
Thinobadistes segnis	AMNH F:AM 102745 to 102803	USA	Mixon's bone bed - Florida - late Miocene	Carpals
Thinobadistes segnis	AMNH F:AM 102804 to 102853	USA	Mixon's bone bed - Florida - late Miocene	Metacarpals
Thinobadistes segnis	AMNH F:AM 102854 to 103006	USA	Mixon's bone bed - Florida - late Miocene	Phalanges of manus
Thinobadistes segnis	AMNH F:AM 103010 to 103016	USA	Mixon's bone bed - Florida - late Miocene	Femora and fragments of femora
Thinobadistes segnis	AMNH F:AM 103017 to 103020	USA	Mixon's bone bed - Florida - late Miocene	Patellae and fragments of patellae
Thinobadistes segnis	AMNH F:AM 103021 to 103030	USA	Mixon's bone bed - Florida - late Miocene	Tibiae and fragments of tibae
Thinobadistes segnis	AMNH F:AM 103031 to 103034	USA	Mixon's bone bed - Florida - late Miocene	Fibulae and fragments of fibulae
Thinobadistes segnis	AMNH F:AM 103035 to 103050	USA	Mixon's bone bed - Florida - late Miocene	Astragali
Thinobadistes segnis	AMNH F:AM 103051 to 103058	USA	Mixon's bone bed - Florida - late Miocene	Calcanea and fragments of calcanea
Thinobadistes segnis	AMNH F:AM 103059 to 103074	USA	Mixon's bone bed - Florida - late Miocene	Cuboids
Thinobadistes segnis	AMNH F:AM 103075 to 103081	USA	Mixon's bone bed - Florida - late Miocene	Naviculars
Thinobadistes segnis	AMNH F:AM 103082-103083	USA	Mixon's bone bed - Florida - late Miocene	Ectocuneiforms
Thinobadistes segnis	AMNH F:AM 103084	USA	Mixon's bone bed - Florida - late Miocene	Left mesocuneiform
Thinobadistes segnis	AMNH F:AM 103085-103086	USA	Mixon's bone bed - Florida - late Miocene	mtt1s

Thinobadistes segnis	AMNH F:AM 103087 to 103096	USA	Mixon's bone bed - Florida - late Miocene	mtt2s
Thinobadistes segnis	AMNH F:AM 103097 to 103107	USA	Mixon's bone bed - Florida - late Miocene	mtt3s
Thinobadistes segnis	AMNH F:AM 103108 to 103122	USA	Mixon's bone bed - Florida - late Miocene	mtt4s
Thinobadistes segnis	AMNH F:AM 103123 to 103130	USA	Mixon's bone bed - Florida - late Miocene	mtt5s
Thinobadistes segnis	AMNH F:AM 103131 to 103199	USA	Mixon's bone bed - Florida - late Miocene	Phalanges of pes
Thinobadistes segnis	UF 21509	USA	Mixon's bone bed - Florida - late Miocene	Skull and complete skeleton (mounted)
Thinobadistes segnis	UF 93064 cast of USNM 3333	USA	Mixon's bone bed - Florida - late Miocene	Left astragalus (Type)
Thinobadistes segnis	UF 201326	USA	Tyner farm - Florida - late Miocene	Left astragalus
Thinobadistes wetzeli	AMNH F:AM 102525	USA	Box T. Ranch - Texas - late Miocene	Left astragalus
Thinobadistes wetzeli	AMNH F:AM 77813	USA	Box T. Ranch - Texas - late Miocene	Left mandible (juvenile)
Thinobadistes wetzeli	UF 201325	USA	Tyner farm - Florida - late Miocene	Left tibia distal epiphysis
Thinobadistes wetzeli	UF 224229	USA	Tyner farm - Florida - late Miocene	Right jugal
Thinobadistes wetzeli	UF 17397	USA	Withlacoochee river - Florida - late Miocene	Right humerus
Thinobadistes wetzeli	UF 93051	USA	Withlacoochee river - Florida - late Miocene	Left astragalus (Type)
Thinobadistes wetzeli	UF 93052	USA	Withlacoochee river - Florida - late Miocene	Left ulna
Thinobadistes wetzeli	UF 93053	USA	Withlacoochee river - Florida - late Miocene	Left mtt3
Urumacotherium campbelli	LACM 117502*	Brazil	Acre - late Miocene/early Pliocene	Cranium without dentition
Urumacotherium campbelli	UFAC PV 1679*	Brazil	Acre - late Miocene/early Pliocene	Isolated molariform
Urumacotherium campbelli	UFAC PV 1804*	Brazil	Acre - late Miocene/early Pliocene	Left mandible with complete dentition
Urumacotherium campbelli	UFAC PV 3730*	Brazil	Acre - late Miocene/early Pliocene	Isolated molariform
Urumacotherium campbelli	UFAC PV 3961*	Brazil	Acre - late Miocene/early Pliocene	Left mandible with complete dentition
Urumacotherium campbelli	UFAC PV 3962*	Brazil	Acre - late Miocene/early Pliocene	Left maxillary fragment with Mf1-4 and alveoli of Cf1
Urumacotherium campbelli	UFAC PV 4987*	Brazil	Acre - late Miocene/early Pliocene	Left maxillary fragment with alveoli of Mf1-2
Urumacotherium garciai	CIAAP 443/443-1*	Venezuela	Urumaco Fm. - late Miocene	Fragment of cranium, mandibles, femur, humerus, tibia, astragalus, etc

APPENDIX III

Appendix III. Description and depiction of the measurements used in this thesis. Modified from Esteban (1996) and Toledo *et al*. (2014).

CRANIODENTAL MEASUREMENTS

Skull (A–D):
basw, basicranial width (at the level of the epitympanic recesses);
Cew, condyle external width;
Ciw, condyle internal width;
DSl, upper dental series length;
FMh, foramen magnum height;
mae, maxillary extension (anterior to Cf1);
mcl, maxillo-condylar length;
mPOw, minimum post-orbital width;
MfSl, upper molariform series length;
MSNw, maximum snout width;
mSNw, minimum snout width;
OCh, occipital height;
OCw, occipital width;
pl, palatal length (excluding the premaxilla);
pMf4l, post-Mf4 length;
pwCf1, palatal width (at the level of Cf1);
pwMf1, palatal width (at the level of Mf1);
pwMf4, palatal width (at the level of Mf4);
SNh, snout height;
SNl, snout length;
tl, total length.

Mandible (E–F):
cah, condyle-angle height;
conl, condyle length;
conw, condyle width;
cpl, coronoid process anteroposterior length;
csl, condyle-spout length;
dsl, lower dental series length;
hrcf1, height of ramus at the level of cf1;
hrmf1, height of ramus at the level of mf1;
hrmf2, height of ramus at the level of mf2;
hrmf3, height of ramus at the level of mf3;
lm(cf1), length of mandible (from the anterior tip to the anteriormost limit of cf1);
lm(mf3), length of mandible (from the anterior tip to the posteriormost limit of mf3);
mfsl, lower molariform series length;
scw, symphyseal constriction width;
ssl, symphyseal spout length;
ssw, symphyseal spout width;
tlm, total length of mandible.

Dentition (G–H):
a, anterior;
cf, lower caniniform;
Cf, upper caniniform;
d, lower diastema;
D, upper diastema;
l, mesiodistal length;
mf, lower molariform;
Mf, upper molariform;
p, posterior;
w, buccolingual width.

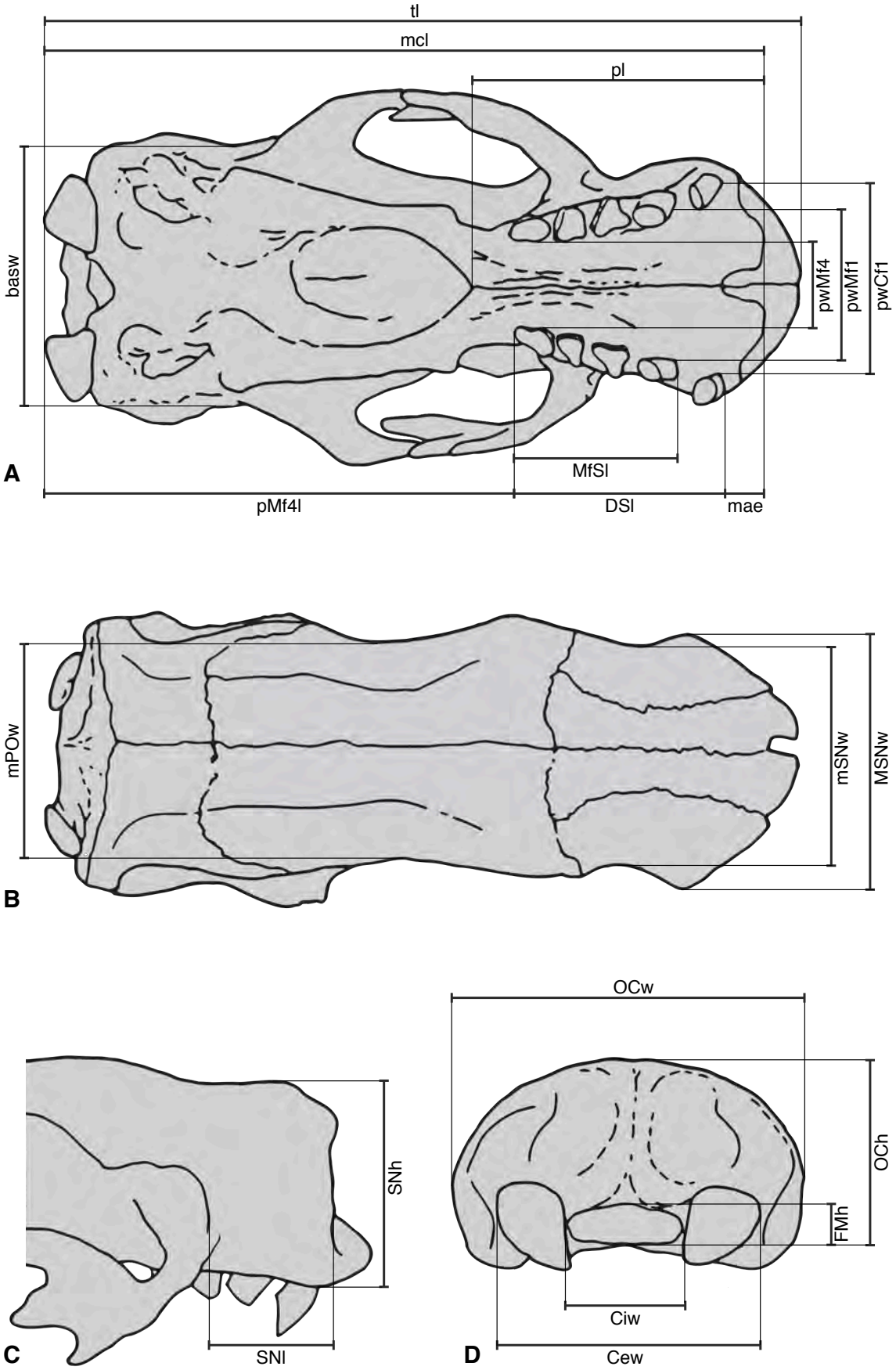
tl
mcl
pl
basw
pwMf4
pwMf1
pwCf1
A
MfSl
pMf4l
DSl
mae
mPOw
mSNw
MSNw
B
OCw
SNh
OCh
FMh
Ciw
C
SNl
D
Cew

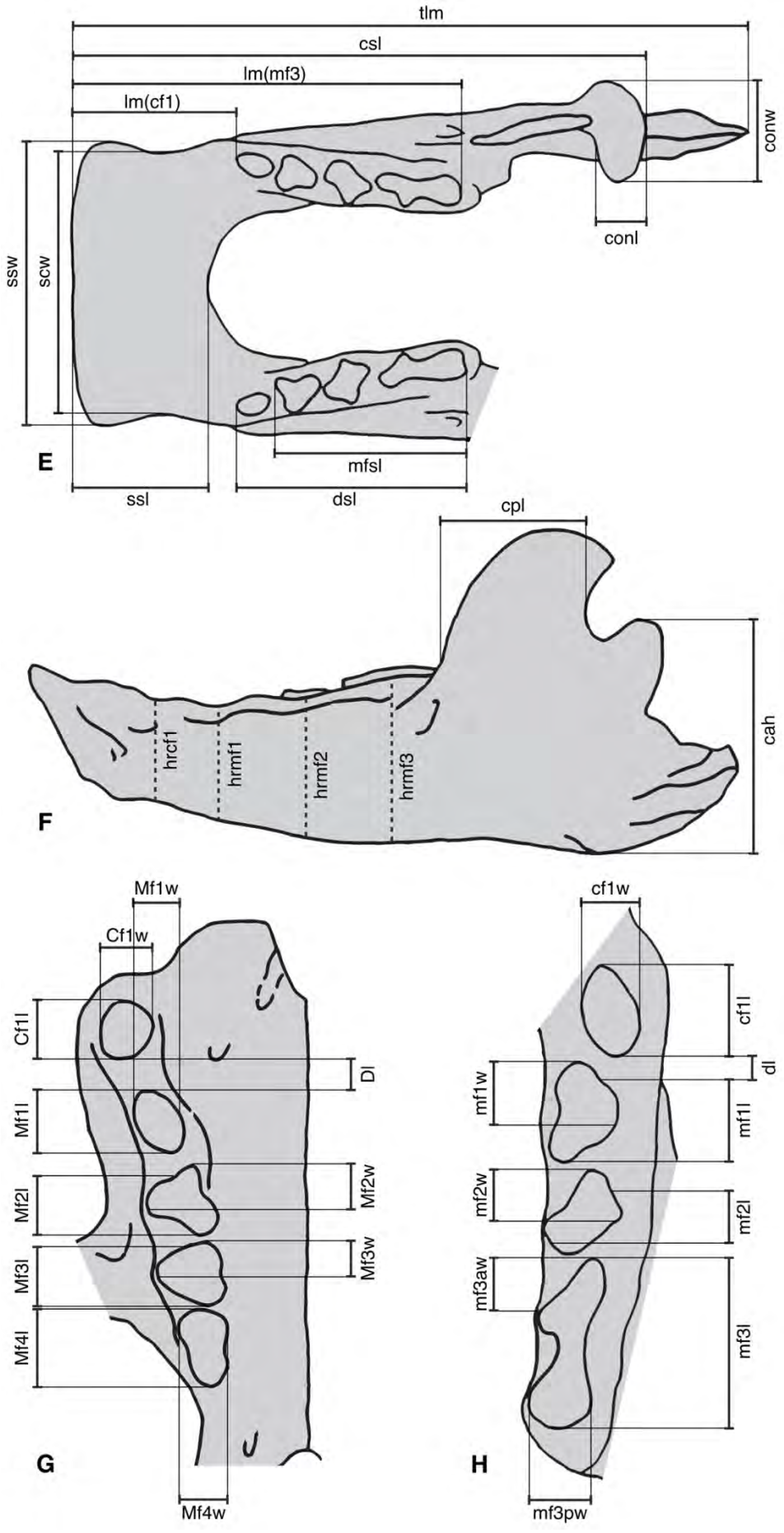
tlm
csl
lm(mf3)
lm(cf1)
conw
conl
ssw
scw
mfsl
ssl
dsl
E
cpl
cah
hrcf1
hrmf1
hrmf2
hrmf3
F
Mf1w
Cf1w
Cf1l
Dl
Mf1l
Mf2l
Mf2w
Mf3l
Mf3w
Mf4l
Mf4w
G
cf1w
cf1l
dl
mf1w
mf1l
mf2w
mf2l
mf3aw
mf3l
mf3pw
H

POSTCRANIAL MEASUREMENTS

Scapula (I–J):
SL, Scapular Length (supraglenoid tubercle to dorso-posterior border of scapula at end of spine);
SW, Scapular Glenoid Fossa Width (maximum transverse width of glenoid fossa).

Humerus (K–L):
HDEW, Humeral Distal Epiphysis Width;
HEMP, Humeral Entepicondyle Medial Protrusion;
HHL, Humeral Head Length;
HHW, Humeral Head Width.

Radius (M–N):
APDR, Antero-Posterior Diameter of Radius at midshaft;
RHL, Radial Head Length;
RHW, Radial Head Width;
RL, Radius Length.

Ulna (O):
THU, Transverse Height of Ulna at midshaft;
UCPDE, Ulnar Coronoid Process to Distal End;
UL, Ulnar Length.

Femur (P–R):
APDF, Antero-Posterior Diameter of Femur at midshaft;
FCW, Femoral Maximum Condylar Width;
ICFW, Inter-Condylar Femoral Width;
FHL, Femoral Head Length;
FHW, Femoral Head Width;
FL, Femoral Length, between head and medial condyle;
FMDEW, Femoral Maximum Distal Epiphysis Width;
PGW, Patellar Groove Width;
LCL, Lateral Condyle Length;
MCL, Medial Condyle Length;
TDF, Transverse Diameter of Femur at midshaft;
Wtroc, Width across trochanters.

Tibia (S–U):
APDT, Antero-Posterior Diameter of Tibia at midshaft;
LTFL, Lateral Tibial Facet Length;
LTFW, Lateral Tibial Facet Width;
MTFL, Medial Tibial Facet Length;
MTFW, Medial Tibial Facet Width;
TDT, Transverse Diameter of Tibia at midshaft;
TL, Tibial Length, from interfacet eminence to tibial malleolus;
TML, Tibial Mortise Length;
TMW, Tibial Mortise Width;
TPEL, Tibial Proximal Epiphysis Length;
TPEW, Tibial Proximal Epiphysis Width.

Fibula (V):
FiTL: Fibular Total Length
EFFL: Ectal Fibular Facet Length

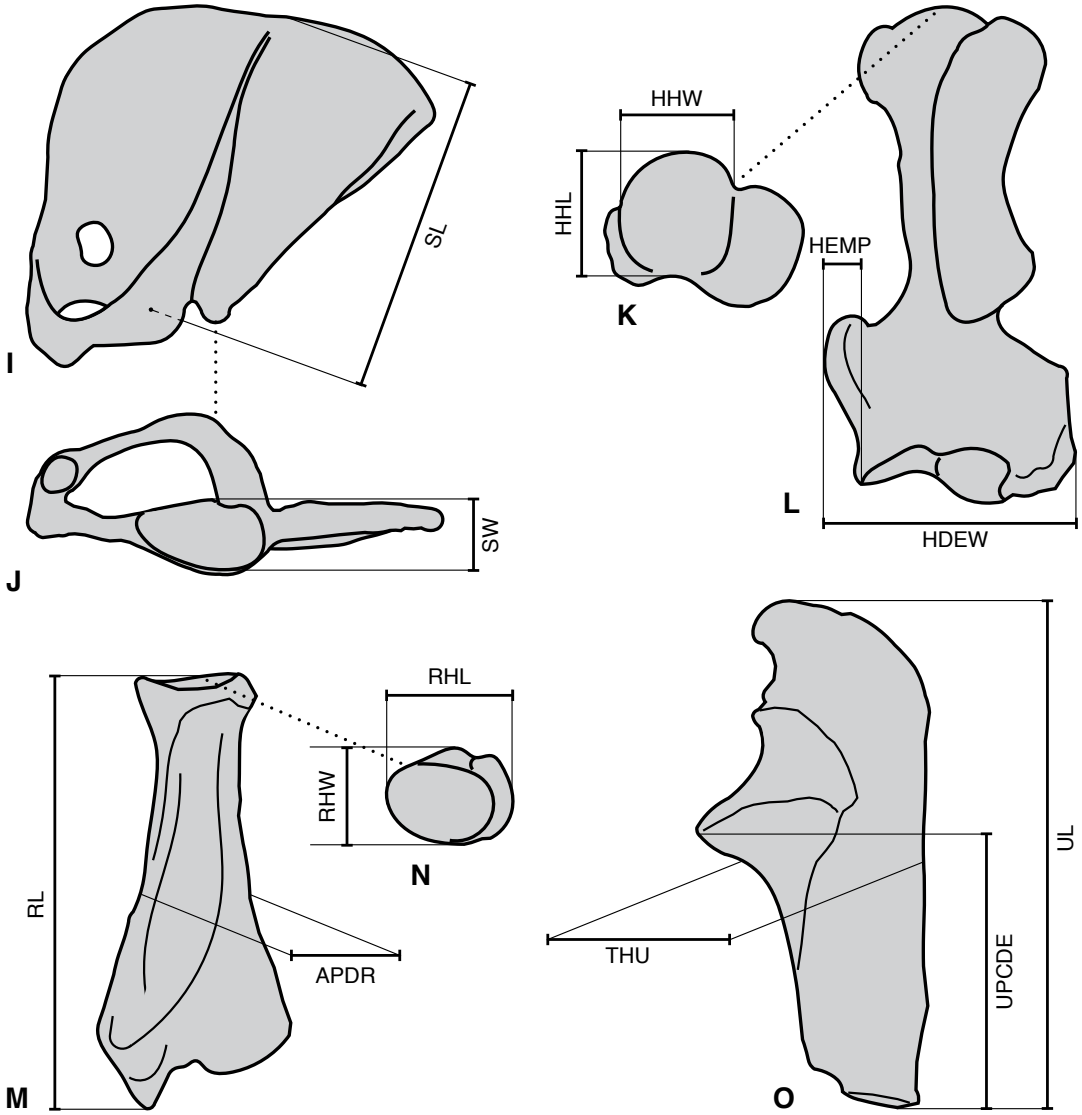
SL
I
SW
J
HHW
HHL
K
HEMP
L
HDEW
RHL
RHW
N
RL
APDR
M
UL
THU
UPCDE
O

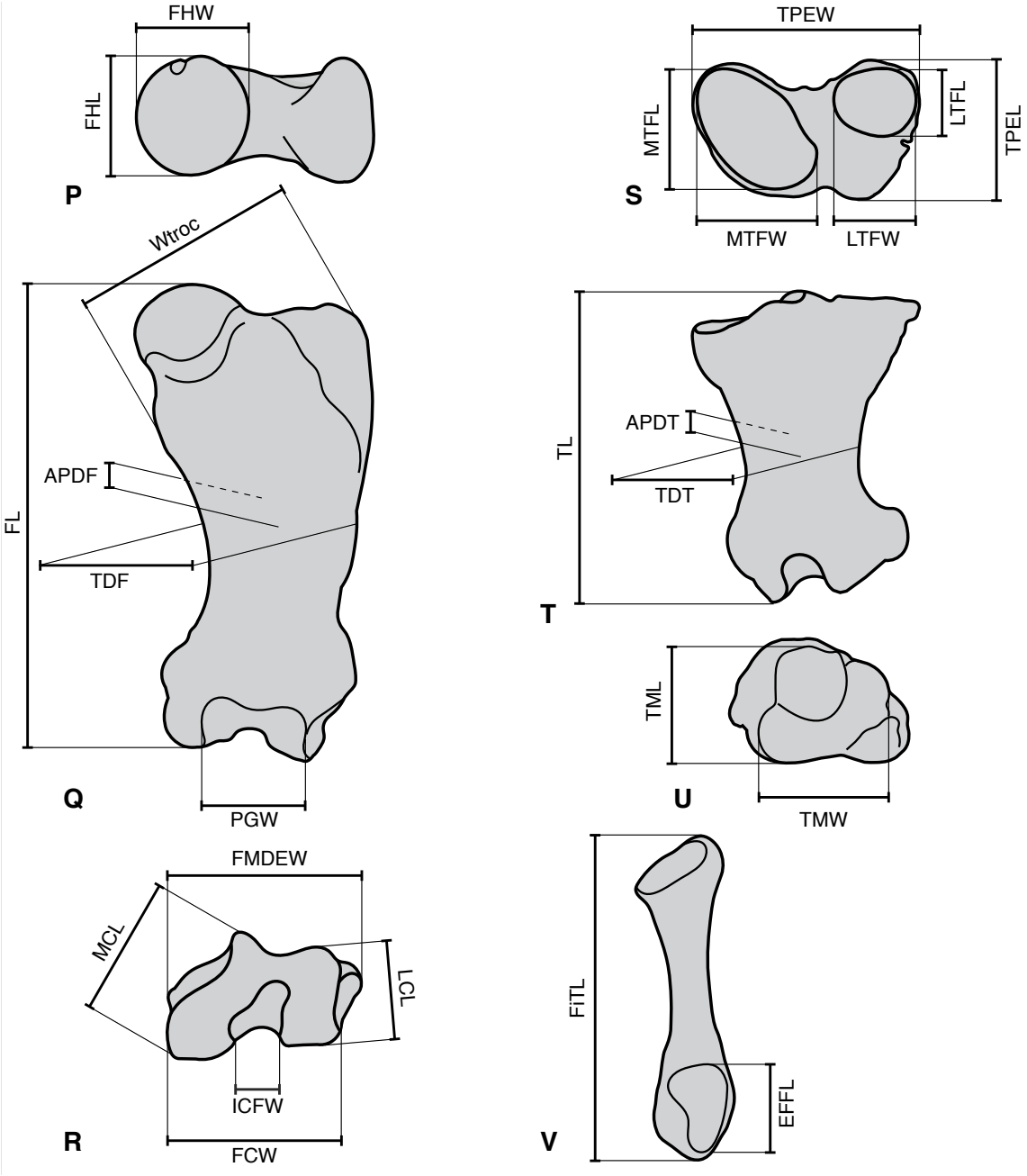
FHW
FHL
P
TPEW
MTFL
LTFL
TPEL
S
MTFW
LTFW
Wtroc
FL
APDF
TDF
Q
PGW
TL
APDT
TDT
T
TML
U
TMW
FMDEW
MCL
LCL
ICFW
R
FCW
FiTL
EFFL
V

APPENDIX IV

Appendix IV. Datasets S1. Tables of measurements of the craniodental remains of *Simomylodon uccasamamensis*, employed for the morphometric analyses of Chapter 6. Remains and variables excluded form the morphometric analysis are marked with an asterisk.

	CRANIUM															
	tl*	**mcl**	**pl**	**pMf4l**	**DSl**	**MfSl***	**OCw**	**basw**	**pwCf1**	**pwMf1**	**pwMf4**	**mPOw**	**MSNw**	**mSNw**	**SNh**	**SNl**
MNHN-BOL V 11731			111,3		90,5	74,9			78,3	65,2	28,4		90	71,4	76,5	47,2
MNHN-BOL V 3321			114,1		103,3	84,2			85,7	80,2	32,8			80,4		52,2
MNHN-BOL V 3348			133,5		100,3	84			62,1	52,1	25,7	58,1	81,9	64,2	61,6	57,6
MNHN-BOL V 3711	302,1	291,7	124,2	186,1	99,4	83,3	115	102,8	66,7	57,4	19,9	60,5	89,3	65	76,4	46,4
MNHN-BOL V 3726			121,3		94,9	78,8	100,3	88,2	59,1	53,4	21	52,9	80,6	64,2	61	52,5
MNHN-BOL V 3717			112,6		99,9	80,6			80,8	65,5	25,9	70,8	97,9	76,8	59,4	51,8
MNHN-BOL V 3718	306,2	290,3	121,2	178,4	98,6	83,3	115,8	104,9	82,2	69,3	25,8	65,1	94,8	74,6	68,8	49,1
MNHN-BOL V 6567*																
MNHN-BOL V 6549*																
MNHN-BOL V 12002*																
MNHN-BOL V 3716*																
MNHN AYO 188*																
MNHN VIZ 35*																

	UPPER DENTITION															
	OCh*	**FMh***	**Ciw***	**Cew***	**mae**	**Dl**	**Cf1l**	**Cf1w**	**Mf1l**	**Mf1w**	**Mf2l**	**Mf2w**	**Mf3l**	**Mf3w**	**Mf4l**	**Mf4w**
MNHN-BOL V 11731					10,4	3	14,5	11,2	18,1	10,4	16,5	12,7	18	15,7	21,2	14,1
MNHN-BOL V 3321					5,4	3,3	16,2	14,1	19,5	11,1	16,7	13,8	19,4	13,5	16,7	13,3
MNHN-BOL V 3348					12	3,4	14,3	10,6	18,7	11,4	18,8	14,1	18,2	13,8	21,2	14,9
MNHN-BOL V 3711	80,3	26,7	36,6		8,1	3,3	17,3	12,5	18,8	8,4	17,6	13,6	18,8	14,4	18,1	14,4
MNHN-BOL V 3726					13,2	5,3	11,3	8,5	18,9	8,9	17,9	13,1	17,1	14,5	18,8	14,9
MNHN-BOL V 3717					8,7	3	17,3	13,7	16,4	11,2	19,5	15,3	19,2	13,7	18	17
MNHN-BOL V 3718	76,8	31,9	37,8	85,3	11	4	13,1	10,2	21,6	9,7	18,8	14,4	20,1	15,5	18,2	15,4
MNHN-BOL V 6567*															17,7	14,3
MNHN-BOL V 6549*											18	15,1	20,1	15,3	18,9	16,8
MNHN-BOL V 12002*											15,6	11,1				
MNHN-BOL V 3716*									19,7	11,2					18,9	17,8
MNHN AYO 188*							11,6	8,1	12,6	7	12,3	9,8	13,7	10,2	11,9	11,5
MNHN VIZ 35*							12,4	9,3								

	MANDIBLE													
	dsl	**mfsl***	**lm(mf3)**	**lm(cf1)**	**ssl**	**csl**	**tlm***	**conl**	**conw**	**ssw**	**scw**	**hrcf1**	**hrmf1**	**hrmf2**
MNHN-BOL V 3711	86,9	64,6	118,8	32,6	29	200,8		24,5	36,6	55,2	52,5	51,2	50,6	52,5
MNHN-BOL V 3726	84,5	64,6	127,3	46,8	46,3					54,9	50,4	37,8	38,9	44,4
MNHN-BOL V 3717	84,5	62,3	109,8	31,3	40,8	187,8				58,8	55,7	51,7	51,8	51
MNHN-BOL V 3296	84,1	62	125,1	46,5	43,2	224,1	241	21,8	36,2			55,1	53,1	49,5
MNHN-BOL V 3358	86,9	65,5										46,3	54,5	56,1
MNHN-BOL V 3371	85,2	67,1	131,7	46,8	42,8					62,5	59,4	47,5	48,9	52,4
MNHN-BOL V 12518				39,8	40						51,5			
MNHN-BOL V 3298				46,4								51,9	51,1	53,5
MNHN-BOL V 11758*													33,1	33,8
MNHN-BOL V 12001	52,3	43,1										28,5	31,8	33,5
MNHN-BOL V 3359	47,9	36						13,4	18,2					27,1
MNHN AYO 165	64,9	49,2										29,3	31,5	35,3
MNHN-BOL V 3714												42,5	42,1	42,6
MNHN-BOL V 6560*														
MNHN AYO 164*														
MNHN AYO 181*								18,1	38,8					56,1
MNHN AYO 185	83,3	63,8	120	37,8	33,3			20,9	29,2			46,7	43	47,8
MNHN AYO 186*					50					76,9	70,8	56,7		
MNHN AYO 209*													47,6	45,3
MNHN VIZ 1*		65										36,3	36,2	40,8

	LOWER DENTITION												
	hrmf3	**cpl**	**cah**	**dl**	**cf1l**	**cf1w**	**mf1l**	**mf1w**	**mf2l**	**mf2w**	**mf3l**	**mf3aw**	**mf3pw**
MNHN-BOL V 3711	53,1	55	74,9	4,1	18,5	13,7	14,4	11,1	17,1	11,6	33,3	17,7	13,7
MNHN-BOL V 3726	49,2			5	15,2	10,6	15	11,2	17,5	12,8	31,8	16,3	13,7
MNHN-BOL V 3717	51,8	53,7	80,1	4,7	19,1	14,6	16,5	10,5	18,8	12,3	30	19,3	13,6
MNHN-BOL V 3296	51,8	60,9	81,2	6,5	16,6	11	14,2	8,5	14,7	10,4	29,5	15,9	11,6
MNHN-BOL V 3358	56,9			4,8	16,5	14,2	16,1	13,4	16,5	13,3	33,6	21,1	16,3
MNHN-BOL V 3371	52,8			3,3	14,8	10,4	13,8	9	18,7	12,1	33,7	18,8	13,1
MNHN-BOL V 12518					16,7	14,2	16	10			28,3	17,8	12,7
MNHN-BOL V 3298				8,8	17,3	14,6	16,6	11,8	17,8	12,8			
MNHN-BOL V 11758*							13,7	8,7	13,3	10,2			
MNHN-BOL V 12001	35,6			3,3	8,3	6,2	10,3	7,3	11,6	6,9	17,8	11,5	8
MNHN-BOL V 3359	30,8	33,8	44,3		9,1	7,7	8,2	6,6	9,6	7	15,5	9,2	7,2
MNHN AYO 165	37			5	11,6	8,4	10,7	8	12.1	8.8	21,5	11,6	10,4
MNHN-BOL V 3714				5,2	15,7	10,7	15,7	13,2	17,1	12,7			

MNHN-BOL V 6560*							17,3	11,7	19,6	13,8			
MNHN AYO 164*									15,2	11	30,1	16,2	12,5
MNHN AYO 181*	54,2		99,5						17,6	12,7	33,5	17,1	12
MNHN AYO 185	46,3	63,8		6,2	14,3	10,8	16,1	12,1	17	14	29,4	18,5	13,1
MNHN AYO 186*					14,9	13,6							
MNHN AYO 209*							14,2	11,1	15,9	13,3			
MNHN VIZ 1*	47,2						15	9,8	17	9	32,6	17,4	12,2

Appendix IV. Datasets S2. Tables of measurements employed in Chapter 7 for the study of sexual dimorphism in *S. uccasamamensis*.

					CRANIUM															UPPER DENTITION									
Age	**Locality**	**Collection**	**Code**	**Morph**	**mcl**	**pl**	**pMf4l**	**DSl**	**Ocw**	**basw**	**pwCf1**	**pwMf1**	**pwMf4**	**mPOw**	**MSNw**	**mSNw**	**SNh**	**SNl**	**mae**	**Dl**	**Cf1l**	**Cf1w**	**Mf1l**	**Mf1w**	**Mf2l**	**Mf2w**	**Mf3l**	**Mf3w**	**Mf4l**	**Mf4w**
L.P.	A-V	MNHN-Bol V	3321	R		114,1		103,3			85,7	80,2	32,8			80,4		52,2	5,4	3,3			19,5	11,1	16,7	13,8	19,4	13,5	16,7	13,3
E.P.	CHO	MNHN-Bol V	3348	G		133,5		100,3			62,1	52,1	25,7	58,1	81,9	64,2	61,6	57,6	12	3,4	14,3	10,6	18,7	11,4	18,8	14,1	18,2	13,8	21,2	14,9
E.P.	INC	MNHN-Bol V	3711	G	291,7	124,2	186,1	99,4	115	102,8	66,7	57,4	19,9	60,5	89,3	65	76,4	46,4	8,1	3,3	17,3	12,5	18,8	8,4	17,6	13,6	18,8	14,4	18,1	14,4
E.P.	CAS	MNHN-Bol V	3717	R		112,6		99,9			80,8	65,5	25,9	70,8	97,9	76,8	59,4	51,8	8,7	3	17,3	13,7	16,4	11,2	19,5	15,3	19,2	13,7	18	17
E.P.	INC	MNHN-Bol V	3718	R	290,3	121,2	178,4	98,6	115,8	104,9	82,2	69,3	25,8	65,1	94,8	74,6	68,8	49,1	11	4	13,1	10,2	21,6	9,7	18,8	14,4	20,1	15,5	18,2	15,4
E.P.	CAS	MNHN-Bol V	3726	G		121,3		94,9	100,3	88,2	59,1	53,4	21	52,9	80,6	64,2	61	52,5	13,2	5,3	11,3	8,5	18,9	8,9	17,9	13,1	17,1	14,5	18,8	14,9
L.P.	A-V	MNHN-Bol V	11731	R		111,3		90,5			78,3	65,2	28,4		90	71,4	76,5	47,2												

					LOWER DENTITION									MANDIBLE														
Age	**Locality**	**Collection**	**Code**	**Morph**	**cf1l**	**cf1w**	**mf1l**	**mf1w**	**mf2l**	**mf2w**	**mf3l**	**mf3aw**	**mf3pw**	**dsl**	**lm(mf3)**	**lm(cf1)**	**ssl**	**csl**	**conl**	**conw**	**ssw**	**scw**	**hrcf1**	**hrmf1**	**hrmf2**	**hrmf3**	**cpl**	**cah**	**dl**
L.P.	A-V	MNHN.F.VIZ	1	G			15	9,8	17	9	32,6	17,4	12,2										36,3	36,2	40,8	47,2			
L.P.	A-V	MNHN.F.AYO	185	G	14,3	10,8								83,3	120	37,8	33,3		20,9	29,2			46,7	43	47,8	46,3	63,8		6,2
E.P.	P-A	MNHN-Bol V	3296	G	16,6	11	14,2	8,5	14,7	10,4	29,5	15,9	11,6	84,1	125,1	46,5	43,2	224,1	21,8	36,2			55,1	53,1	49,5	51,8	60,9	81,2	6,5
E.P.	P-A	MNHN-Bol V	3298	R	17,3	14,6	16,6	11,8	17,8	12,8						46,4							51,9	51,1	53,5				8,8
E.P.	INC	MNHN-Bol V	3358	R	16,5	14,2	16,1	13,4	16,5	13,3	33,6	21,1	16,3	86,9									46,3	54,5	56,1	56,9			4,8
E.P.	INC	MNHN-Bol V	3371	G	14,8	10,4	13,8	9	18,7	12,1	33,7	18,8	13,1	85,2	131,7	46,8	42,8				62,5	59,4	47,5	48,9	52,4	52,8			3,3
E.P.	INC	MNHN-Bol V	3711	G	18,5	13,7	14,4	11,1	17,1	11,6	33,3	17,7	13,7	86,9	118,8	32,6	29	200,8	24,5	36,6	55,2	52,5	51,2	50,6	52,5	53,1	55	74,9	4,1
E.P.	CAS	MNHN-Bol V	3714	G	15,7	10,7	15,7	13,2	17,1	12,7													42,5	42,1	42,6				5,2
E.P.	CAS	MNHN-Bol V	3717	R	19,1	14,6			18,8	12,3	30	19,3	13,6	84,5	109,8	31,3	40,8	187,8			58,8	55,7	51,7	51,8	51	51,8	53,7	80,1	4,7
E.P.	CAS	MNHN-Bol V	3726	G	15,2	10,6	15	11,2	17,5	12,8	31,8	16,3	13,7	84,5	127,3	46,8	46,3				54,9	50,4	37,8	38,9	44,4	49,2			5
L.P.	A-V	MNHN-Bol V	12518	G	16,7	14,2	16	10			28,3	17,8	12,7			39,8	40					51,5							
L.P.	A-V	MNHN-Bol V	13218	G										83,7	136,8	52,2	51,3						51,2	55,2					3,3
L.P.	A-V	MNHN-Bol V	13219	R												50,2	60,3				71,1	66,6							4,3

					FEMORAL MEASUREMENTS											
Age	**Locality**	**Collection**	**Code**	**Morph**	**FL**	**TDF**	**APDF**	**Wtroc**	**FHL**	**FHW**	**FMDEW**	**PGW**	**FCW**	**ICFW**	**MCL**	**LCL**
L.P.	A-V	MNHN.F.AYO	168	G							115,4	50,7	94,6	23,9	75	51,7
L.P.	A-V	MNHN.F.AYO	169	R								58,7	105,2	25,2		60,6
L.P.	A-V	MNHN-Bol V	3299	R	343,6	94	41,6	136,2	66,9	64,7	134	58,4	101,9	21,6	85,2	55,1
L.P.	A-V	MNHN-Bol V	3301	R								59,8	98,8	20,5	83,8	59,5
E.P.	INC	MNHN-Bol V	3365	G		82,1	35,4				121,8	53,3	93,2	21	71,6	52,8
L.P.	A-V	MNHN-Bol V	12277	R	337,8	99,7	38,7	135,4	65,5	61,6	128	60,1	103,2	28,2	82,3	54,6
L.P.	A-V	MNHN-Bol V	12518	G	307,2	83,95	37,45	133,4	62	60	122,25	55,65	95,95	18,7	75,75	48,95
E.P.	P-A	MNHN-Bol V	12953	R	337	95,3	43,3	140,8	74,4	69,1	132,1	64,6	105,4	22,8	84,6	56,8

					TIBIAL MEASUREMENTS										
Age	**Locality**	**Collection**	**Code**	**Morph**	**TL**	**TDT**	**APDT**	**TPEW**	**TPEL**	**MTFL**	**MTFW**	**LTFL**	**LTFW**	**TMW**	**TML**
L.P.	A-V	MNHN-Bol V	3300	R	188,5	51	30	102,6	73,9	65,7	60,4	39,1	40,6	75	62,4
L.P.	A-V	MNHN-Bol V	3305	G		47,3	27,7	95,7	60,1	57,8	53,4	33,1	39,2		
E.P.	INC	MNHN-Bol V	3365	G		43,8	23,2	82,9			54,2				
L.P.	A-V	MNHN-Bol V	11772	R		54,9	32,2	107,9	85,4	67,2	60,6	42	48		
E.P.	P-A	MNHN-Bol V	11876	G	168,8	43,9	23,5	87,6	61,6	46,4	54,7	27,1	27,7	64,8	49,6
L.P.	A-V	MNHN-Bol V	12507	G	173,5	46,4	23,5	99,1	74,6	56,8	57,8	34,1	37,4	68,1	52
L.P.	A-V	MNHN-Bol V	12518	G	173,85	48,55	26,55	100,3	67,2	50,5	58,3	34,1	37,2	69,1	52,85
E.P.	P-A	MNHN-Bol V	13216	G	154,1	40,2	23,9	85,8	62,7	44,1	43,9	28,3	33,2	63,7	46,2
L.P.	A-V	MNHN-Bol V	13220	R	180	54,4	31,3	103,7	84,7	53,4	53,8	36,2	37,1	75,9	58,2
L.P.	A-V	MNHN-Bol V	13221	G	177,6	50,3	28	96,5	63,8	55,3	51,5	28,8	35,2	69,6	57,4

AGE: E.P., Early Pliocene; L.P., Late Pliocene.
LOCALITY: A-V, Ayo Ayo-Viscachani; CAS, Casira; CHO, Choquecota; INC, Inchasi; P-A, Pomata-Ayte.
MORPH: G, Gracile; R, Robust.

APPENDIX V

Appendix V. Tables S1. PCAs additional information (eigenvalues and loadings) of the morphometric analyses of Chapter 6.

Cranium and upper dentition (Fig. 6.12)

Eigenvalues:

PC	Eigenvalue	% variance
1	1514.63	51.803
2	509.451	17.424
3	373.222	12.765
4	188.711	6.4542
5	104.66	3.5795
6	670.195	2.2922
7	495.394	1.6943
8	399.276	1.3656
9	251.448	0.85999
10	158.833	0.54323
11	129.933	0.44439
12	985.047	0.3369
13	567.973	0.19426
14	370.829	0.12683
15	23.585	0.080664
16	105.522	0.03609

Loadings:

	PC 1	PC 2	PC 3	PC 4	PC 5	PC 6	PC 7	PC 8
mcl	0.37259	0.38638	-0.54315	0.10693	-0.21969	0.021535	-0.16764	0.28972
pl	0.23903	0.13575	0.09784	-0.43068	0.017574	0.49853	-0.27638	-0.42449
pMf4l	0.19	0.24442	-0.36849	0.21063	-0.29039	-0.14077	0.16531	-0.37541
DSl	0.25358	0.3323	0.50309	0.44717	0.09564	0.0077698	-0.2268	-0.10772
OCw	0.18351	0.097667	-0.13498	0.034097	0.48516	0.0060899	0.22683	-0.12216
basw	0.16875	0.049415	-0.13044	0.0055439	0.52796	0.17306	0.27186	-0.071017
pwCf1	0.30103	-0.46332	-0.14414	0.26816	0.069611	0.26254	0.26924	-0.020955
pwMf1	0.17862	-0.38922	0.0046107	0.31789	0.0055346	-0.27085	-0.2773	0.0030231
pwMf4	0.16877	0.12939	0.028389	-0.043069	0.20335	-0.23165	-0.31447	-0.051489
mPOw	0.28251	0.019093	0.037402	-0.33923	0.26008	-0.22967	-0.01034	0.54539
MSNw	0.38157	-0.41002	0.054696	0.046129	-0.19229	0.28599	-0.2126	0.10022
mSNw	0.33439	-0.08437	0.014474	-0.27304	0.0035925	-0.27337	-0.11793	-0.11665
SNh	0.31622	-0.07611	0.25907	-0.20053	-0.23453	-0.40586	0.45103	-0.24734
SNl	0.094832	0.20138	0.1873	0.1498	-0.13034	0.23635	0.27738	0.23833
Cf1l	0.048779	0.046642	0.051218	0.024043	0.025621	-0.072594	0.13987	-0.080426
Cf1w	0.018132	0.041758	0.049073	0.074227	0.082627	-0.084776	0.015711	0.0067782
Mf1l	0.060489	0.042867	0.14071	0.083755	0.02096	-0.040161	-0.09901	-0.060867
Mf1w	0.052998	0.056968	0.058326	-0.020438	0.029058	0.017775	-0.03712	0.12555
Mf2l	0.074173	0.071653	0.09	0.02232	-0.013005	0.089302	0.068785	0.0099151
Mf2w	0.066727	0.05182	0.10257	0.050071	-7,40E-01	0.092887	0.014399	0.098494
Mf3l	0.053308	0.060046	0.11312	0.10425	0.040234	0.040566	0.080268	0.053356
Mf3w	0.018697	0.056983	0.15343	0.12345	-0.040457	-0.008148	0.067545	0.13504
Mf4l	0.054178	0.12116	0.16972	0.11271	-0.036875	0.0012572	0.10023	0.092512
Mf4w	0.029017	0.049883	0.079849	0.047043	-0.017802	0.039684	0.081766	0.08103
mae	0.1326	0.056389	0.15377	-0.26335	-0.32452	0.16661	0.19435	0.19943
Dl	0.024044	0.035642	0.029675	-0.037832	-0.042485	-0.11532	-0.04569	-0.097074

	PC 9	PC 10	PC 11	PC 12	PC 13	PC 14	PC 15	PC 16
mcl	-0.32171	0.08675	-0.18519	0.14878	0.14464	-0.11723	-0.02182	-0.049957
pl	-0.21006	-0.13665	0.10207	0.13605	0.068847	0.10452	-0.02874	-0.19621
pMf4l	0.41477	-0.15594	0.1462	-0.11256	-0.11717	0.22848	-0.01607	0.046463
DSl	0.13989	0.10751	-0.27901	-0.06581	-0.091616	-0.027299	-0.04388	-0.086166
OCw	0.20364	-0.22363	0.34555	0.097371	0.17368	-0.28635	-0.05737	0.0020153
basw	-0.11756	0.047014	-0.24678	-0.06141	0.035596	-0.11685	0.20992	0.24457
pwCf1	-0.05759	0.35296	-0.023797	0.17045	-0.2885	0.28073	0.032453	-0.14303
pwMf1	-0.2473	-0.20683	0.35573	0.10108	0.15453	-0.19257	0.19336	-0.23168
pwMf4	0.15202	-0.07453	0.15555	0.15233	-0.37894	0.16473	0.2902	0.006859
mPOw	0.15242	-0.17657	-0.066826	-0.04010	-0.064632	0.34583	-0.1248	-0.073828
MSNw	0.3251	-0.29931	-0.19243	-0.19496	0.18595	-0.095913	-0.11524	0.32396
mSNw	-0.05552	0.53461	0.2211	-0.38077	-0.0955	-0.2282	-0.15083	0.09705
SNh	-0.27417	-0.26052	-0.27264	0.16236	0.023173	0.013715	-0.03672	-0.051434
SNl	-0.30916	-0.27538	0.27104	-0.49927	-0.27949	-0.10528	0.18459	-0.022228
Cf1l	0.15768	0.16061	-0.069777	-0.15749	0.45695	-0.021448	0.071569	-0.2492
Cf1w	0.10047	0.10895	-0.23159	-0.05996	0.095774	-0.25121	-0.01626	-0.30983
Mf1l	-0.15625	0.10837	-0.038356	0.19919	-0.11999	0.0023377	0.05673	0.28027
Mf1w	0.015544	-0.00489	0.0054569	-0.00539	0.069857	-0.099399	0.14323	0.025382
Mf2l	-0.01363	0.1445	0.11602	-0.05777	0.0030419	0.12397	-0.20823	0.070542
Mf2w	0.040271	0.060229	0.16475	0.02553	0.2908	0.25907	-0.01753	-0.23629
Mf3l	-0.07336	0.073741	0.1356	-0.03069	0.21959	0.37198	0.061059	-0.11959
Mf3w	0.017948	0.059731	0.076692	0.22284	0.22054	0.14387	0.16754	0.19582
Mf4l	-0.01778	0.011417	0.1881	0.4278	0.022926	-0.16323	-0.30517	0.34562
Mf4w	-0.02912	0.076124	0.2854	0.015327	0.014921	-0.000717	-0.53007	-0.040631
mae	0.3592	0.23245	0.16419	0.25949	-0.053509	-0.28819	0.42031	-0.094633
Dl	-0.13351	0.14003	0.13267	-0.18199	0.34822	0.25856	0.29005	0.46006

Mandible and lower dentition (Fig. 6.13)

Eigenvalues:

PC	Eigenvalue	% variance
1	1360.44	57.964
2	455.868	19.423
3	221.825	9.4512
4	102.277	4.3577
5	842.757	3.5907
6	453.922	1.934
7	238.298	1.0153
8	17.346	0.73905
9	130.659	0.55669
10	624.276	0.26598
11	573.283	0.24426
12	373.473	0.15912
13	254.117	0.10827
14	173.914	0.074099
15	117.152	0.049914
16	0.727868	0.031012
17	0.672909	0.02867
18	0.174011	0.007414

Loadings:

	PC 1	PC 2	PC 3	PC 4	PC 5	PC 6	PC 7	PC 8	PC 9
cf1l	0.068736	0.12325	-0.025261	0.012826	-0.18717	0.097775	-0.091009	-0.009362	0.13239
cf1w	0.059841	0.065584	-0.01906	-0.011688	-0.13249	0.14507	-0.16831	0.14977	0.27853
mf1l	0.11749	0.046032	0.0092446	0.028499	-0.078107	0.048642	-0.043865	0.22273	0.12995
mf1w	0.09773	0.01948	0.0058672	0.0051301	-0.004962	0.14398	-0.074944	0.1731	0.080062
mf2l	0.1096	0.010038	-0.0048386	-0.001363	0.089965	0.014254	0.059311	0.25527	0.12328
mf2w	0.050516	0.022794	-0.03993	-0.043273	0.049177	0.055315	0.022924	0.30059	0.10272
mf3l	0.21428	0.14764	0.00074529	0.038781	-0.10548	0.020309	0.13821	0.17603	0.11131
mf3aw	0.10722	0.045868	-0.010656	-0.009901	0.12655	0.11391	-0.032613	0.26289	-0.06232
mf3pw	0.067677	0.033714	0.017868	0.048242	0.086014	0.1415	-0.015908	0.33824	0.026445
dsl	0.51336	0.39684	-0.015708	0.083577	-0.41819	-0.006212	0.024815	-0.17575	-0.43602
lm(mf3)	0.34207	-0.41397	0.48463	0.23548	0.090008	-0.068905	-0.60204	-0.071382	-0.01656
lm(cf1)	0.18419	-0.26556	0.21835	0.12187	0.029952	-0.075496	0.52738	-0.20841	0.40329
ssl	0.10707	-0.16281	0.28183	0.32432	0.023125	0.45348	0.41654	0.032338	-0.31736
csl	0.32868	-0.63573	-0.36617	-0.4588	-0.25569	0.029587	0.094889	0.087072	-0.08682
conl	0.050404	0.013435	-0.076274	0.12211	0.092114	0.054506	-0.010883	-0.020351	0.21024
conw	0.069215	0.055067	-0.12108	0.16997	0.16492	-0.042471	0.069001	-0.37239	0.19068
ssw	0.017188	-0.006414	0.16006	-0.002920	0.0078081	-0.78643	0.16421	0.22977	-0.18749
scw	0.036912	-0.040701	0.12374	0.055297	0.050595	-0.11947	0.24078	0.10219	-0.07447
hrcf1	0.14314	0.16667	0.15859	-0.47106	0.254	0.13754	0.068308	-0.16811	-0.05161
hrmf1	0.17697	0.12103	0.22095	-0.45756	0.29559	0.016706	-0.018342	-0.21298	0.045798
hrmf2	0.26642	0.16697	0.053428	-0.088424	0.45235	-0.002979	0.046384	0.24091	-0.08161
hrmf3	0.33945	0.21187	0.063066	-0.001071	-0.25925	-0.14807	0.0045936	-0.029574	0.46548
cpl	0.14705	0.010014	-0.29882	0.20368	0.23156	-0.039118	0.048679	0.11999	0.10171
cah	0.29845	-0.04583	-0.51448	0.26865	0.36165	-0.10227	-0.091165	-0.18757	-0.12766
dl	0.011071	0.0032388	0.06593	0.022051	0.0037394	-0.044484	0.004209	0.23538	-0.03990

	PC 10	PC 11	PC 12	PC 13	PC 14	PC 15	PC 16	PC 17	PC 18
cf1l	0.15468	0.11936	-0.027912	0.15393	0.34579	0.14424	-0.10212	-0.035811	-0.35588
cf1w	0.16027	0.10507	0.18388	0.35307	0.39878	-0.021045	0.033873	-0.055652	0.12825
mf1l	0.014808	0.21546	-0.02694	-0.15565	-0.073505	-0.2511	-0.20914	-0.34176	0.13811
mf1w	-0.13762	0.029347	-0.36523	-0.29972	-0.14699	-0.19994	-0.11391	0.32244	0.14955
mf2l	-0.32503	-0.13347	0.39676	0.02442	-0.30674	0.13811	-0.094276	-0.30831	-0.11807
mf2w	-0.03076	-0.010855	0.085007	-0.18144	-0.060768	0.090125	0.23994	0.49559	-0.27532
mf3l	-0.24806	-0.17245	-0.22507	0.08503	0.20058	0.45703	-0.45409	-0.004315	0.07773
mf3aw	-0.14134	-0.09989	-0.17353	0.061836	0.0030069	0.28107	0.45091	-0.17434	0.56152
mf3pw	-0.04617	-0.11854	-0.075528	-0.10237	0.16803	0.11015	0.30075	0.090053	-0.39908
dsl	-0.24945	-0.01516	0.11311	-0.00151	0.057218	-0.20396	0.19764	0.030623	-0.04065
lm(mf3)	-0.09972	0.052218	0.026233	0.042793	-0.026971	0.059376	0.0010374	0.015246	-0.05325
lm(cf1)	-0.32039	0.0096327	-0.067617	-0.16748	0.26792	-0.21994	0.068935	-0.058547	-0.03811
ssl	0.4432	-0.006696	0.11412	-0.07638	-0.065646	0.19504	-0.054136	-0.052346	0.011561
csl	0.088259	-0.080412	0.077298	0.10063	-0.017838	-0.013065	0.010184	0.048794	0.033625
conl	-0.08039	-0.11553	0.19179	0.20821	-0.15644	0.034004	-0.025106	0.11973	-0.06749
conw	-0.00586	-0.18356	0.30962	0.16128	0.0097559	0.1151	0.15057	0.31194	0.26213
ssw	0.15698	-0.027891	0.10828	-0.08165	0.094002	0.19271	0.024874	-0.033533	-0.02712
scw	-0.06188	0.36392	-0.37564	0.65579	-0.20289	-0.054158	0.052981	0.20399	-0.03594
hrcf1	-0.16271	0.4678	0.21625	-0.03922	-0.17581	0.25168	-0.12355	0.046171	-0.07610
hrmf1	0.20039	-0.11188	-0.2156	-0.10484	0.26222	0.046455	0.17043	-0.10563	0.013667
hrmf2	0.16741	-0.35066	0.085343	0.23169	0.019871	-0.48868	-0.22427	0.029653	-0.02389
hrmf3	0.47008	0.0022213	-0.076708	-0.10321	-0.41845	0.085762	0.0485	0.0389	0.066339
cpl	0.059639	0.44002	0.071392	-0.05389	0.049123	-0.1048	0.32013	-0.27179	-0.08093
cah	0.078052	0.087727	-0.2042	-0.13586	0.062995	0.18607	-0.23531	0.027904	-0.05406
dl	0.041195	0.33208	0.32316	-0.17993	0.30269	-0.071225	-0.19206	0.37582	0.37707

Appendix V. Tables S2. PCAs additional information (eigenvalues and loadings) of the morphometric analyses of Chapter 7.

Cranium and upper dentition (Fig. 7.2A)

Eigenvalues:

PC	Eigenvalue	% variance
1	353.894	61.916
2	84.0119	14.698
3	63.6207	11.131
4	43.8958	7.6799
5	16.3645	2.8631
6	9.78198	1.7114

Loadings:

	PC 1	PC 2	PC 3	PC 4	PC 5	PC 6
mcl	-0.007122	0.014023	-0.011176	-0.002994	-0.083257	0.026918
pl	-0.30937	0.19606	0.52571	0.37403	0.15851	-0.082903
pMf4l	-0.039171	0.077129	-0.061467	-0.016467	-0.45791	0.14805
DSl	0.050048	-0.064348	0.39116	0.21225	-0.49032	-0.25346
Ocw	0.13416	0.41325	0.26202	0.072946	0.045636	0.060776
basw	0.14551	0.41557	0.28171	0.078321	0.12288	0.038555
pwCf1	0.56452	-0.031402	0.044797	0.031755	0.244	0.07584
pwMf1	0.49423	-0.17011	-0.072307	0.42666	-0.097535	-0.26766
pwMf4	0.16523	-0.1685	0.011675	0.26689	0.13635	0.59159
mPOw	0.22375	0.085669	0.27458	-0.41683	-0.019248	0.15404
MSNw	0.27107	0.16248	0.15666	-0.45056	0.030972	-0.21077
mSNw	0.33587	-0.20676	0.072613	0.032784	-0.027893	-0.045332
SNh	0.090872	0.61438	-0.45291	0.25072	-0.045304	0.15604
SNl	-0.077242	-0.26616	0.26917	0.11949	0.058507	0.34443
mae	-0.10263	-0.031845	0.0061389	-0.093111	0.39868	-0.091773
Dl	-0.020978	-0.027765	-0.045648	0.0051248	0.074413	-0.1224
Cf1l	0.040445	0.10508	0.070479	-0.11518	-0.3262	0.22284
Cf1w	0.041703	0.058639	0.062893	-0.11649	-0.21354	0.16263
Mf1l	0.0095666	0.046474	-0.011483	0.14358	0.21302	-0.21409
Mf1w	0.022454	-0.061644	0.072875	0.012448	0.022951	0.23649
Mf2l	-0.003913	0.0023617	0.054431	-0.10216	0.10318	0.050182
Mf2w	0.020144	-0.000704	0.046008	-0.059034	0.023907	0.059979
Mf3l	0.043343	0.036419	0.040058	0.0091186	0.035565	-0.02732
Mf3w	-0.002555	0.031576	-0.007381	-0.006252	0.10423	-0.13684
Mf4l	-0.05436	0.0089599	0.060303	-0.005834	0.12131	0.18288
Mf4w	0.0021933	-0.008313	0.040977	-0.15395	0.070559	0.01402

Mandible and lower dentition (Fig. 7.3A)

Eigenvalues:

PC	Eigenvalue	% variance
1	133.406	38.688
2	82.5284	23.933
3	60.5771	17.567
4	28.1313	8.1581
5	12.9349	3.7511
6	10.1375	2.9399
7	6.80427	1.9732
8	3.14769	0.91283
9	2.56332	0.74336
10	2.20299	0.63887
11	1.30906	0.37963
12	1.08487	0.31461

Loadings:

	PC 1	PC 2	PC 3	PC 4	PC 5	PC 6	PC 7	PC 8	PC 9	PC 10	PC 11	PC 12
cf1l	-0.056785	0.067324	0.047069	-0.019393	-0.19471	0.047447	-0.12681	0.1523	0.1633	0.10591	-0.20288	-0.010419
cf1w	-0.060653	0.08176	0.074324	0.025314	-0.1062	0.081217	0.095964	0.17434	0.56828	0.065327	-0.27327	-0.041309
mf1l	-0.004237	0.0012376	0.027074	0.011548	-0.022005	0.02019	0.20809	0.044143	0.23429	0.21215	0.04168	0.084272
mf1w	-0.022696	-0.005281	0.058378	0.072064	0.023687	0.16118	0.24539	-0.024731	-0.074546	0.61963	0.12826	-0.03862
mf2l	-0.029286	-0.013326	0.083572	0.06587	0.064592	-0.096362	-0.015893	0.10901	-0.045543	-0.15841	0.16419	0.20634
mf2w	-0.010253	0.036996	0.044015	0.081782	0.031762	0.042747	0.23072	-0.013103	-0.18571	0.10493	0.49797	0.00018995
mf3l	0.0040573	-0.017283	0.020638	0.12569	0.2503	0.20507	-0.12924	0.22037	-0.33264	0.13863	-0.37519	-0.075056
mf3aw	-0.029385	0.049923	0.08328	0.06026	0.15218	0.12361	0.10848	-0.20629	0.059938	0.06941	-0.19036	0.24352
mf3pw	-0.019314	0.026884	0.048258	0.087002	0.074898	0.16906	0.17417	-0.08937	-0.10141	0.12152	-0.04573	-0.18636
dsl	-0.026912	0.026207	0.0079504	0.055474	0.033305	0.26713	-0.091572	0.072108	0.094373	0.046077	0.053142	-0.035256
lm(mf3)	0.44128	-0.014053	-0.16449	0.61318	0.22178	-0.23257	-0.23891	-0.12686	0.21797	0.023553	0.068704	0.052714
lm(cf1)	0.5298	-0.002727	0.018784	0.18524	0.0028373	-0.060262	0.19204	0.3902	-0.1131	0.069664	-0.072285	0.19085

ssl	0.5265	0.0097795	0.52691	-0.13414	-0.42269	0.067976	0.1218	-0.08104	-0.09187	-0.11928	0.017527	-0.26707
csl	0.3938	0.082454	-0.70543	-0.37092	-0.090829	0.31255	-0.008628	-0.050161	0.010112	-0.009578	-0.005772	-0.075919
conl	-0.0209	0.014709	0.0084333	0.055118	-0.045846	0.090046	-0.17222	0.13075	0.048831	0.080706	0.094022	-0.14263
conw	0.00999	0.064129	-0.030297	0.036885	-0.26615	0.23123	-0.35319	0.18121	0.025913	8.409E-05	0.094528	0.12246
ssw	0.19173	0.068189	0.23603	-0.35792	0.36935	0.018935	-0.11411	-0.14294	0.48803	0.026867	0.25607	0.076428
scw	0.16837	0.091104	0.2646	-0.34835	0.44777	0.059988	-0.30684	0.10608	-0.22587	0.13926	-0.16672	0.12936
hrcf1	-0.0444	0.56213	-0.090377	-0.17892	-0.088393	-0.48016	-0.12931	0.1908	-0.13884	0.17289	0.23232	0.0075804
hrmf1	0.014815	0.64856	0.029014	0.14472	-0.10601	-0.039084	0.037684	-0.33133	0.0093413	0.14181	-0.32135	-0.040842
hrmf2	-0.063697	0.42155	0.033319	0.13938	0.29346	0.26058	0.27545	0.30634	0.032614	-0.53835	0.082615	-0.18979
hrmf3	-0.004305	0.20372	0.037347	0.14584	-0.033312	0.48556	-0.055735	-0.23558	-0.068818	0.035577	0.27297	0.33719
cpl	0.089386	-0.051857	-0.15723	-0.12742	0.29312	-0.16617	0.37103	-0.18692	-0.008413	0.033137	-0.080235	-0.24112
cah	0.044098	0.010199	0.0013987	-0.10861	-0.11185	-0.0829	0.19856	-0.23295	-0.13115	-0.25731	-0.2058	0.58502
dl	-0.008945	0.0041607	-0.061787	-0.10552	-0.037108	-0.024156	0.32537	0.42861	0.12817	0.15422	-0.018283	0.34651

Lower dentition (Fig. 7.3B)

Eigenvalues:

PC	Eigenvalue	% variance
1	7.22908	41.038
2	4.94874	28.093
3	2.26662	12.867
4	1.32672	7.5316
5	0.81795	4.6434
6	0.576646	3.2735
7	0.345104	1.9591
8	0.0934957	0.53076
9	0.0110876	0.062942

Loadings:

	PC 1	PC 2	PC 3	PC 4	PC 5	PC 6	PC 7	PC 8	PC 9
cf1l	0.22425	-0.49955	0.32752	-0.14776	0.45405	-0.36018	-0.31198	0.10709	0.35548
cf1w	0.46249	-0.54686	0.1993	-0.029005	-0.16414	0.24025	0.44727	-0.030768	-0.40103
mf1l	0.19838	-0.090977	-0.30576	-0.10086	-0.10199	0.5228	0.14146	0.2228	0.7038
mf1w	0.45536	0.19245	-0.37553	-0.39666	0.31477	0.23636	-0.421	-0.070108	-0.34661
mf2l	0.14741	0.052624	0.12152	0.77305	0.37976	0.36271	-0.14314	-0.25739	0.024682
mf2w	0.29905	0.154	-0.41284	0.29093	0.27783	-0.44796	0.41177	0.42682	-0.046907
mf3l	0.21085	0.57503	0.64404	-0.21438	0.17218	0.14455	0.24007	0.22857	0.060944
mf3aw	0.43457	0.10773	0.12641	0.27574	-0.62119	-0.15643	-0.46597	0.28247	0.016286
mf3pw	0.38031	0.19321	-0.050338	-0.074675	-0.14313	-0.32523	0.20139	-0.74335	0.30089

Femora (Fig. 7.4A)

Eigenvalues:

PC	Eigenvalue	% variance
1	199.564	65.494
2	50.3763	16.533
3	21.5795	7.0821
4	14.5845	4.7864
5	9.98225	3.276
6	6.24448	2.0493
7	2.37451	0.77928

Loadings:

	PC 1	PC 2	PC 3	PC 4	PC 5	PC 6	PC 7
FL	0.6837	-0.64775	0.083881	-0.20196	-0.093673	0.0094933	-0.012964
TDF	0.33744	0.10046	-0.62296	0.10635	0.34485	-0.14783	-0.16027
APDF	0.12566	0.10945	0.052196	0.10309	0.30066	-0.21635	0.49908
Wtroc	0.09267	-0.017394	0.21496	0.27021	0.19433	0.051829	-0.075949
FHL	0.15767	-0.033545	0.35573	0.44206	0.31914	0.08404	-0.12067
FHW	0.11993	-0.030069	0.32932	0.26567	0.2347	-0.0066326	0.13849
FMDEW	0.32357	0.38926	0.27945	-0.55449	-0.010803	0.35011	0.041572
PGW	0.2142	0.40092	0.1174	0.12371	-0.0018645	0.1355	-0.62978
FCW	0.26683	0.3384	-0.14804	0.24629	-0.19411	0.37873	0.52961
ICFW	0.11175	-0.096041	-0.43608	0.23009	-0.083994	0.41308	-0.076542
MCL	0.29517	0.33677	-0.060164	-0.15032	0.04533	-0.61283	0.011324
LCL	0.1835	0.081317	0.11563	0.37323	-0.73505	-0.30149	-0.027082

Tibiae (Fig. 7.5A)

Eigenvalues:

PC	Eigenvalue	% variance
1	296.454	69.66
2	56.8082	13.349
3	28.1641	6.6179
4	23.5168	5.5259
5	13.4984	3.1718
6	3.52399	0.82805
7	2.34551	0.55114
8	1.01943	0.23954
9	0.245556	0.0577

Loadings:

	PC 1	PC 2	PC 3	PC 4	PC 5	PC 6	PC 7	PC 8	PC 9
TL	0.40883	0.64999	-0.22425	-0.16366	-0.10687	0.0030319	-0.046158	-0.18591	-0.11353
TDT	0.25175	-0.019342	-0.16072	0.24308	0.13564	-0.2864	0.58406	-0.32988	-0.17093
APDT	0.16331	-0.040031	-0.04914	0.22584	0.33291	-0.028945	0.50385	0.52574	0.039252
TPEW	0.42212	-0.15691	-0.078294	0.75853	-0.1673	0.038265	-0.42906	0.025117	0.035459
TPEL	0.42577	-0.59115	-0.42624	-0.46499	-0.057035	-0.19638	-0.09602	-0.026437	0.069469
MTFL	0.37203	0.091363	0.6179	-0.1794	0.15997	-0.49505	-0.2147	0.22092	-0.22515
MTFW	0.22237	0.10007	0.1679	-0.064997	-0.76552	0.089151	0.3524	0.077425	0.10615
LTFL	0.24871	-0.14987	0.19203	-0.14435	-0.027485	0.55644	0.083454	0.38231	0.0022335
LTFW	0.23975	-0.19877	0.46058	-0.016201	0.24493	0.35555	0.11987	-0.60765	0.15738
TMW	0.18062	0.14592	-0.23949	-0.089019	0.25799	0.43279	-0.10381	0.043254	-0.53972
TML	0.20866	0.31596	-0.13152	-0.078201	0.29865	0.026795	-0.084771	0.082569	0.75646

APPENDIX VI

Appendix VI. Data S1. Characters and character states employed for the phylogenetic analyses of Chapter 8 (1–201: Gaudin (2004); 202–286: Gaudin (1995); 287–383: present thesis). Characters marked with a single asterisk (*) are multistate, those marked with two asterisks (**) are multistate and ordered. For abbreviations and references in characters 1–201 see Gaudin (2004); 202–286 see Gaudin (1995); 287–383 see "References" and Appendix III.

1 – Teeth: (0) absent; (1) present [Gaudin 2004: ch. 1].
2 – ** Dental formula: (0) typical mammalian dentition, with true incisors, canines, and postcanines; (1) identifiable incisors, canines, etc. absent, at least 7 upper teeth, 8 lower teeth; (2) 5 upper teeth, 4 lower teeth; (3) 4 uppers, 4 lowers; (4) 4 uppers, 3 lowers [Gaudin 2004: ch. 2].
3 – * Toothrow: (0) horizontal in lateral view; (1) upper toothrow concave, lower toothrow convex; (2) Cf1 and cf1 slightly depressed ventrally relative to the remaining molariforms; (3) Cf1 and cf1 strongly depressed [Wetzel 1985; Gaudin 2004: ch. 3].
4 – Left and right toothrows: (0) parallel in occlusal view; (1) anteriorly divergent [Gaudin 2004: ch. 4].
5 – Inclination of teeth: (0) teeth implanted vertically; (0) upper teeth slant labially posteriorly, lower lingually posteriorly [Naples 1982; Gaudin 2004: ch. 5].
6 – * Diastema between Cf1 and Mf1: (0) absent; (1) moderate (<1/2 of the anteroposterior length of the Cf1); (2) elongated (>1/2 of the anteroposterior length of the Cf1).
7 – Teeth: (0) brachydont; (1) hypsodont [Gaudin 2004: ch. 7].
8 – Enamel: (0) absent; (1) present [Gaudin 2004: ch. 8].
9 – ** Modified orthodentine core of teeth: (0) absent; (1) present, small, typically avascular; (2) present, large, typically well-vascularized [Ferigolo 1985; Gaudin 2004: ch. 4].
10 – Thickness of orthodentine: (0) thick layer, thickness greater than or equal to the thickness of outer layer of enamel or cementum; (1) thin layer, thickness less than outer layer of cementum [Gaudin 2004: ch. 10].
11 – ** Outer layer of cementum: (0) absent; (1) forms thin layer around outside of tooth; (2) forms thick layer around outside of tooth; (3) greatly hypertrophied, nearly as thick as core of modified orthodentine [Ferigolo 1985; Gaudin 2004: ch. 11].
12 – Premaxillary teeth: (0) absent; (1) present [Gaudin 2004: ch. 12].
13 – * Size of Cf1: (0) smallest tooth; (1) greatly enlarged; (2) neither the smallest nor enlarged [Gaudin 2004: ch. 13].
14 – * Size of cf1: (0) smallest tooth; (1) greatly enlarged; (2) neither the smallest nor enlarged [Gaudin 2004: ch. 14].
15 – * Size of mf3: (0) smallest molariform; (1) largest molariform, or equivalent in size to the largest; (2) neither the smallest nor largest molariform [Gaudin 2004: ch. 15].
16 – * Long axis of molariform teeth: (0) parallel or orthogonal to long axis of the toothrow; (1) oblique to long axis in posterior portion of toothrow; (2) oblique along entire length of toothrow; (3) oblique to long axis in anterior portion of toothrow [Gaudin 2004: ch. 16].
17 – * Occlusal surface of molariforms: (0) beveled, at times worn flat; (1) with large anterior and posterior step-like facets [Hoffstetter 1956]; (2) with strong transverse crests; (3) flat [Gaudin 2004: ch. 17].
18 – Anterior extent of upper and lower toothrow: (0) lower toothrow extends anterior to upper; (1) upper toothrow extends anterior to lower [Gaudin 2004: ch. 18].
19 – * Morphology of Cf1/cf1: (0) molariform; (1) caniniform; (2) incisiform [Gaudin 2004: ch. 19].
20 – * Wear surface on Cf1/cf1: (0) oblique, nearly vertical wear facet; (1) oblique facet; (2) lower tooth beveled, upper tooth oblique; (3) upper tooth beveled, lower tooth oblique; (4) both teeth worn flat; (5) teeth with strong transverse crests [Gaudin 2004: ch. 20].
21 – ** Position of Cf1 relative to the anterior edge of the maxilla: (0) right at the edge [separation <3% BNL]; (1) near the edge [separation >3%, <10% BNL]; (2) well-separated from the anterior edge [separation >10% BNL] [Gaudin 2004: ch. 21].
22 – Fossa anterior to Cf1: (0) absent; (1) present [Gaudin 2004: ch. 22].
23 – Fossa on palatal surface of maxilla posterior to Cf1: (0) absent; (1) present [Gaudin 2004: ch. 23].
24 – Alignment of Cf1/cf1: (0) in line with other molariforms; (1) displaced laterally relative to molariform toothrow [Kraglievich 1928; Gaudin 2004: ch. 24].
25 – Diastema between Mf1 and Mf2: (0) absent; (1) moderate (<1/2 of the anteroposterior length of the Mf1).
26 – Curvature of Cf1: (0) straight; (1) recurved posteriorly [Gaudin 2004: ch. 26].
27 – Mf4 curvature, in lateral view: (0) straight; (1) curved anteriorly [Scott 1903–4; Gaudin 2004: ch. 27].
28 –Mf1 curvature, in lateral view: (0) straight; (1) recurved posteriorly [Gaudin 2004: ch. 28].
29 – * Cf1 cross-section: (0) ovate; (1) trigonal; (2) rectangular; (3) ovate, with posterior bulge; (4) square; (5) reniform [Gaudin 2004: ch. 29].
30 – * cf1 cross-section: (0) ovate; (1) trigonal, apex anterior; (2) meniscoid; (3) ovate, with posterior bulge; (4) v-shaped, apex directed laterally; (5) rectangular; (6) trigonal, apex posterior; (7) reniform [Gaudin 2004: ch. 30].
31 – * Mf1 cross-section: (0) circular; (1) ovate, elongate anteroposteriorly; (2) rectangular; (3) lobate, transverse width > anteroposterior length; (4) bilobate; (5) reniform; (6) trilobate [Modified from Gaudin (2004): ch. 31].
32 – * mf1 cross-section: (0) ovate anteroposteriorly; (1) rectangular; (2) square; (3) irregularly lobate; (4) irregularly lobate and elongate anterolabially to posterolingually, compressed perpendicular to long axis; (5) bilobate; (6) reniform; (7) trilobate [Modified from Gaudin (2004): ch. 32].

33 – * Mf2 and Mf3 cross-section: (0) ovate anteroposteriorly; (1) rectangular; (2) trapezoidal; (3) square; (4) lobate, anteroposterior length ≥ transverse width; (5) lobate, transverse width > anteroposterior length; (6) bilobate; (7) trilobate [Gaudin 2004: ch. 33].
34 – * mf2 cross-section: (0) ovate anteroposteriorly; (1) rectangular; (2) trapezoidal; (3) square; (4) irregularly lobate; (5) irregularly lobate and elongate anterolabially to posterolingually, compressed perpendicular to long axis; (6) bilobate; (7) reniform; (8) trilobate [Modified from Gaudin (2004): ch. 34].
35 – * Mf4 cross-section: (0) ovate, long axis orientated anteroposteriorly; (1) circular; (2) rectangular; (3) trigonal; (4) reniform; (5) irregular; (6) bilobate; (7) T-shaped; (8) trilobate [Gaudin 2004: ch. 35].
36 – * mf3 cross-section: (0) ovate, long axis orientated anteroposteriorly; (1) circular; (2) trapezoidal; (3) bilobate; (4) elongate and irregularly lobate; (5) S-shaped; (6) trilobate [Gaudin 2004: ch. 36].
37 – ** Depth of mandible: (0) shallow & elongate, maximum depth of horizontal ramus ≤17.5% of MML; (1) >17.5%, ≤20% of MML; (2) >20%, ≤22.5% of MML; (3) >22.5%, ≤25% of MML; (4) >25%, ≤27.5% of MML; (5) short and deep, maximum depth of horizontal ramus >27.5% of MML [Gaudin 2004: ch. 37].
38 – ** Inferior edge of mandible: (0) concave in lateral view; (1) straight, horizontal; (2) weakly, uniformly convex; (3) with strong convex ventral bulge [Gaudin 2004: ch. 38].
39 – Horizontal ramus of mandible bulges mediolaterally at toothrow: (0) absent; (1) present [Scott 1903–4; Gaudin 2004: ch. 39].
40 – * Ascending ramus of mandible covers posterior teeth in lateral view: (0) no; (1) partially; (2) yes [Gaudin 2004: ch. 40].
41 – ** Relative position of processes of ascending ramus: (0) condyle posterior to coronoid and angle; (1) condyle and angle subequal, both posterior to coronoid; (2) angle posterior to condyle posterior to coronoid [Gaudin 2004: ch. 41].
42 – ** Distance between processes of ascending ramus: (0) condyle closer to angle than coronoid; (1) three processes equidistant; (2) condyle closer to coronoid [Gaudin 2004: ch. 42].
43 – Junction between ascending and horizontal ramus of mandible: (0) horizontal ramus blends into ascending ramus; (1) distinct constriction at junction, ascending ramus indented below anterior to base of angular process, joins horizontal ramus well dorsal to ventral margin of horizontal ramus [Gaudin 2004: ch. 43].
44 – Ascending ramus with internal ridge running obliquely vertically from ventral edge, near the base of the angle, toward the last tooth: (0) absent; (1) present [Gaudin 2004: ch. 44].
45 – Coronoid process hooked posteriorly: (0) absent; (1) present [Gaudin 2004: ch. 45].
46 – Coronoid process with medial ridge running along anterior edge: (0) absent or rudimentary; (1) present [Gaudin 2004: ch. 46].
47 – ** Shape of coronoid process: (0) elongate & narrow, ratio of maximum height to anteroposterior length measured at mid-height >1.25; (1) intermediate development, ratio of height to length ≤1.25, >1.0; (2) short and broad, ratio of height to length ≤1.0 [Scott 1903–4]; (3) rudimentary or absent [Gaudin 2004: ch. 47].
48 – ** Shape of angular process: (0) short and deep, ratio of maximum length to depth measured at midlength < 1.0; (1) intermediate development, ratio of length to depth >1.0, <1.25; (2) elongate and narrow, ratio of length to depth ≥1.5 [Gaudin 2004: ch. 48].
49 – Medial fossa of angular process: (0) absent or rudimentary; (1) present [Gaudin 2004: ch. 49].
50 – Tip of angular process inflected medially: (0) absent; (1) present [Scott 1903–4; Gaudin 2004: ch. 50].
51 – ** Length of condyloid process: (0) short, <10% of MML; (1) moderate length, ≥10%, <15% of MML; (2) elongate, ≥15% of MML [Gaudin 2004: ch. 51].
52 – Condyloid process orientation: (0) inclined posterodorsally in lateral view; (1) posterior edge nearly vertical [Gaudin 2004: ch. 52].
53 – Position of condyle relative to dentition: (0) dorsal to toothrow; (1) at or just above level of toothrow [Gaudin 2004: ch. 53].
54 – ** Shape of condyle in dorsal view: (0) expanded mediolaterally; (1) ovate, slightly wider than long; (2) elongate anteroposteriorly, narrow mediolaterally [Naples 1982; Webb 1985; Gaudin 2004: ch. 54].
55 – * Shape of condyle in posterior view: (0) concave; (1) flat; (2) evenly convex; (3) convex medially, concave laterally [Sicher 1944; Naples 1982; Webb 1985; Gaudin 2004: ch. 55].
56 – ** Inclination of condyle in lateral view: (0) inclined posterodorsally; (1) nearly horizontal; (2) inclined posteroventrally [Gaudin 2004: ch. 56].
57 – ** Condyle: (0) hooks laterally in dorsal view; (1) extends medially and laterally; (2) hooks medially; (3) medial and lateral hook rudimentary or absent [Gaudin 2004: ch. 57].
58 – ** Condylar articular surface: (0) forms single smoothly confluent surface; (1) with distinct but confluent medial and lateral surfaces; (2) with medial and lateral surfaces separated by groove [Naples 1982, 1987; Gaudin 2004: ch. 58].
59 – ** Condyle orientation in dorsal view: (0) directed posteromedially; (1) orientated orthogonal to long axis of mandible; (1) directed posterolaterally [Sicher 1944; Gaudin 2004: ch. 59].
60 – Plane of condylar articular surface changes mediolaterally, rolling in corkscrew fashion so that the lateral end of the facet faces more anterior or dorsal than the medial end: (0) absent; (1) present [Gaudin 2004: ch. 60].
61 – Mandibular symphysis: (0) unfused; (1) fused [Gaudin 2004: ch. 61].

62 – ** Length of symphysis: (0) very short, <10% of MML; (1) short, ≥10%, <20% of MML; (2) moderate length, ≥20%, <27% of MML; (3) elongate, >28% of MML [Gaudin 2004: ch. 62].
63 – Position of posterior end of symphysis vs. dentition: (0) symphysis ends anterior to first lower tooth; (1) symphysis extends posterior to first lower tooth [Gaudin 2004: ch. 63].
64 – Symphysis inclination: (0) anterodorsal; (1) anteroventral [Gaudin 2004: ch. 64].
65 – ** Profile of anterior edge of symphysis in lateral view: (0) convex; (1) straight; (2) concave.
66 – * Symphyseal keel: (0) absent; (1) present along whole length of symphysis; (2) present on symphyseal spout only [Gaudin 2004: ch. 65].
67 – ** Width of symphysis at midpoint: (0) narrow, ≤15% of MML; (1) moderately wide, >16%, <19% of MML; (2) very wide, >20% of MML [Gaudin 2004: ch. 66].
68 – ** Length of symphyseal spout: (0) rudimentary or very short, <10% of MML; (1) moderately developed, >10%, <30% of MML; (2) elongate, >30% of MML [Gaudin 2004: ch. 67].
69 – Junction of symphysis and lower edge of horizontal ramus: (0) forms sharp or rounded angle; (1) no clear demarcation between symphysis and horizontal ramus [Gaudin 2004: ch. 68].
70 – Profile of anterior edge of symphysis in dorsal view: (0) flat; (1) rounded or pointed [Gaudin 2004: ch. 69].
71 – Lateral edge of symphyseal spout everted: (0) absent; (1) present [Scott 1903–4; Gaudin 2004: ch. 71].
72 – Lateral edges of spout: (0) parallel; (1) converge anteriorly [Scott 1903–4; Gaudin 2004: ch. 26].
73 – Orientation of spout in lateral view: (0) horizontal; (1) inclined anterodorsally [Gaudin 2004: ch. 73].
74 – Posterior external opening of mandibular canal: (0) absent; (1) present [Gaudin 2004: ch. 74].
75 – ** Position of posterior external opening of mandibular canal: (0) canal opens laterally on horizontal ramus; (1) canal opens anterolaterally, on ascending ramus; (2) canal opens anteromedially, on internal side of ascending ramus [Gaudin 2004: ch. 75].
76 – ** Mandible with fossa posterior to cf1: (0) absent; (1) weakly developed; (2) strongly developed [Scott 1903–4; Gaudin 2004: ch. 76].
77 – Length of stylohyal: (0) short, roughly equivalent in length to epihyal or less than 20% of BNL; (1) elongate, longer than epihyal or greater than 20% of BNL [Flower 1885; Naples 1986; Gaudin 2004: ch. 77].
78 – * Shape of stylohyal shaft in lateral view: (0) curved, concave dorsally; (1) curved, concavoconvex; (2) curved, concave ventrally; (3) straight [Flower 1885; Naples 1986; Gaudin 2004: ch. 78].
79 – Stylohyal with posterior process: (0) absent; (1) present [Flower 1885; Naples 1986; Gaudin 2004: ch. 79].
80 – Ossified larynx: (0) absent; (1) present [Naples 1986; Gaudin 2004: ch. 80].
81 – ** Ratio of length of skull to length of humerus: (0) ≥1.2; (1) approximately 1.0; (2) <1.0 [Reed 1954; Gaudin 2004: ch. 81].
82 – ** Skull shape: (0) skull elongate and narrow, maximum width of braincase < 25% of BNL; (1) braincase width ≥25%, <30% of BNL; (2) braincase width ≥30%, <35% of BNL; (3) braincase width ≥35%, <40% of BNL; (4) skull short and wide, braincase width ≥40% of BNL [Gaudin 2004: ch. 82].
83 – Shape of braincase: (0) high and narrow, globose or tubular; (1) low and broad [Gaudin 2004: ch. 83].
84 – Position of orbit in lateral view: (0) in typical mammalian position; (1) displaced ventrally, lies at or below level of toothrow [Gaudin 2004: ch. 84].
85 – ** Length of snout (preorbital length measured to tip of Nasal): (0) snout elongate, preorbital length >45% of BNL; (1) preorbital length < 40%, ≥27%; (2) preorbital length < 27%, ≥25%; (3) preorbital length <25%, ≥15%; (4) snout short, preorbital length <15% of BNL [Gaudin 2004: ch. 85].
86 – ** Width of snout measured at midpoint: (0) snout narrow, width < 20% of BNL; (1) width >20%, ≤25% of BNL; (2) width >25%, ≤30% of BNL; (3) snout broad, width >30% of BNL [Gaudin 2004: ch. 86].
87 – Height of snout: (0) snout depressed anteriorly; (1) deep, elevated anteriorly [Gaudin 2004: ch. 87].
88 – Shape of snout in dorsal view: (0) uniform, or slightly tapered anteriorly; (1) widened anteriorly [Gaudin 2004: ch. 88].
89 – Depth of nasopharynx: (0) shallow, depth ≤10% of BNL; (1) deep, depth >10% of BNL [Gaudin 2004: ch. 89).
90 – * Basicranial/basifacial angle: (0) parallel, but whole cranial base concave in lateral view; (1) parallel, cranial base roughly horizontal; (2) reflexed [Webb 1985; Gaudin 2004: ch. 90].
91 – * Profile of dorsal surface of the skull in lateral view: (0) horizontal or irregular; (1) profile of nasal region and braincase relatively horizontal, but nasal region depressed relative to braincase; (2) evenly convex [Patterson *et al.* 1992; Gaudin 2004: ch. 91].
92 – Temporal fossa: (0) curved anteroposteriorly and dorsoventrally; (1) flat [Gaudin 2004: ch. 92].
93 – ** Sagittal crest: (0) absent or rudimentary; (1) temporal lines converge but do not contact; (2) crest present [Gaudin 2004: ch. 93].
94 – ** Supraoccipital exposure on cranial roof: (0) absent; (1) small; (2) large [Gaudin 2004: ch. 94].
95 – Zygomatic arch: (0) incomplete; (1) complete [Gaudin 2004: ch. 95].
96 – Fossa behind root of zygoma, lying anterodorsal to mastoid process: (0) absent; (1) present [Gaudin 2004: ch. 96].
97 – * Temporal lines: (0) are confluent with sagittal crest or with nuchal crest posteriorly; (1) do not meet, curve ventrally and run anterior but parallel to nuchal crest; (2) temporal fossa reduced, temporal lines lie far forward of nuchal crest [Gaudin 2004: ch. 97].
98 – External nares: (0) moderate; (1) greatly enlarged [Gaudin 2004: ch. 98].

99 – ** Inclination of lateral wall of external nares: (0) anteroventral; (1) vertical; (2) anterodorsal [Flower 1885; Gaudin 2004: ch. 99].
100 – ** Length and width of nasal: (0) short and wide, ratio of maximum length to width measured at midpoint < 3.0; (1) ratio of length to width >3.0, <4.0; (2) elongate and narrow, ratio of length to width >4.0 [Gaudin 2004: ch. 100].
101 – Nasal width: (0) uniform along entire length; (2) expands anteriorly and/or posteriorly [Webb 1989; Gaudin 2004: ch. 101].
102 – * Anterior edge of nasal: (0) with lateral process and medial process separated by distinct notch; (1) evenly convex; (2) straight or concave [Scott 1903–4; Gaudin 2004: ch. 102].
103 – Anterior edge of maxilla with fossa lateral to external nares: (0) absent; (1) present [Gaudin 2004: ch. 103].
104 – Anterior edge of palatal process of maxilla extends under external nares: (0) absent; (1) present [Kraglievich 1928; Gaudin 2004: ch. 104].
105 – *. Maxilla elevated for dental alveoli: (0) not elevated; (1) elevated in the middle, along the length of the molariform row; (2) elevated posteriorly only; (3) elevated anteriorly only; (4) elevated anteriorly and posteriorly [Gaudin 2004: ch. 105].
106 – ** Antorbital or buccinator fossa of maxilla: (0) absent; (1) weak; (2) well-developed [Gaudin 2004: ch. 106].
107 – Maxilla contacts frontal dorsally: (0) excluded by nasal/lacrimal contact; (1) present [Wetzel 1985; Gaudin 2004: ch. 107].
108 – Maxilla with orbital exposure: (0) absent or rudimentary; (1) present [Novacek 1986; Gaudin 2004: ch. 108].
109 – Maxilla contacts lacrimal within orbit: (0) present; (1) excluded by orbital exposure of jugal [Gaudin 2004: ch. 109].
110 – Jugal participation in rim of maxillary foramen: (0) absent; (1) present [Gaudin 2004: ch. 110].
111 – ** Anterior extent of lateral and medial palatal processes of maxilla: (0) medial process anterior; (1) two processes of equivalent length; (2) lateral process anterior [Scott 1903–4; Gaudin 2004: ch. 111].
112 – Maxilla with fossa behind last upper tooth: (0) absent; (1) present [Gaudin 2004: ch. 112].
113 – Attachment of premaxilla to skull: (0) tightly sutured; (1) loosely attached [Gaudin 2004: ch. 113].
114 – ** Dorsal process of premaxilla: (0) very large; (1) narrow anteroposteriorly, but contacts nasal dorsally; (2) reduced in height, does not contact nasal; (3) absent [Gaudin 2004: ch. 114].
115 – * Shape of palatal process of premaxilla: (0) Vshaped, narrow mediolaterally; (1) V-shaped, wide; (2) rectangular plate, left and right halves separate, converge anteriorly; (3) oval plate, left and right halves sutured in midline; (4) Y-shaped, with elongate anterior process and medial and lateral rami posteriorly; (5) with elongate anterior process and posterior medial and lateral rami, but squared, thickened mediolaterally and dorsoventrally; (6) wide elongate flat surface [Gaudin 2004: ch. 115].
116 – Relative size of medial and lateral rami of premaxilla: (0) lateral ramus much larger; (1) lateral and medial ramus of nearly equivalent size [Gaudin 2004: ch. 116].
117 – Shape of incisive foramen: (0) ovate or triangular; (1) slit-like, hidden in ventral view by medial palatal process of maxilla [Gaudin 2004: ch. 117].
118 – Septomaxilla: (0) absent; (1) present [McKenna 1975; Gaudin 2004: ch. 118].
119 – ** Length of nasoturbinal vs. maxilloturbinal: (0) nasoturbinal shorter; (1) equal length; (2) nasoturbinal longer [Gaudin 2004: ch. 119].
120 – Mediolateral contour of palate: (0) concave between toothrows; (1) flat to convex between toothrows [Paula Couto 1971; Gaudin 2004: ch. 120].
121 – * Anteroposterior contour of palate: (0) evenly concave; (1) flat; (2) flat posteriorly, concave anteriorly; (3) convex posterior to dentition, concave anteriorly; (4) convex along length of toothrow, concave anteriorly; (5) evenly convex [Gaudin 2004: ch. 121].
122 – * Length and width of palate: (0) elongate and narrow, widened at zygomatic processes of maxilla; (1) elongate and narrow; (2) elongate, slightly widened anteriorly; (3) elongate, strongly widened anteriorly; (4) short, uniformly wide [Gaudin 2004: ch. 122].
123 – Palate rugose, with many pits and grooves: (0) absent; (1) present [Gaudin 2004: ch. 123].
124 – ** Palate extends posteriorly and dorsally as a shelf that runs alongside the inner edge of descending laminae of the pterygoids: (0) absent; (1) present, shelf ends at midpoint of descending lamina; (2) present, shelf extends posteriorly all the way back to the level of the tympanic cavity [Gaudin 2004: ch. 124].
125 – Palate with paired anterior foramina that open into distinct grooves that run anteriorly toward the incisive foramina: (0) absent; (1) present [Gaudin 2004: ch. 125].
126 – Postpalatine foramina: (0) small to absent; (1) enlarged [Stock 1913; Gaudin 2004: ch. 126].
127 – ** Palate posterior extent: (0) palate ends at level of sphenopalatine foramen; (1) palate slightly elongate posteriorly, ends at level of orbital foramina; (2) elongate posteriorly, extends to level of glenoid fossa; (3) greatly elongated, extends posteriorly to level of tympanic cavity.
128 – Pterygoid exposure in palate: (0) absent; (1) present [Gaudin 2004: ch. 128].
129 – Pterygoids contact in ventral midline: (0) absent; (1) present [Gaudin 2004: ch. 129].
130 – ** Width of interpterygoid region: (0) narrow, maximum width ≤10% of BNL; (1) widened, width >10%, ≤ 15% of BNL; (2) very broad, width >15% of BNL [Gaudin 2004: ch. 130].
131 – Pterygoid exposure in roof of nasopharynx: (0) small to absent; (1) large;

132 – Pterygoid/vomer contact: (0) absent; (1) present [Gaudin 2004: ch. 132].
133 – Lateral surface of pterygoid: (0) relatively smooth; (1) rugose laterally [Gaudin 2004: ch. 133].
134 – ** Pterygoid hamulus: (0) present, extends posterior to anterior edge of tympanic; (1) present, short; (2) absent [Gaudin 2004: ch. 134].
135 – ** Pterygoid descending lamina: (0) absent; (1) small; (2) broad, deep [Gaudin 2004: ch. 135].
136 – * Inclination of posterior edge of pterygoid in lateral view: (0) concave posterior border; (1) straight, nearly vertical posterior edge; (2) straight, anteriorly inclined posterior edge [Kraglievich 1928; Gaudin 2004: ch. 136].
137 – ** Pterygoid inflation: (0) uninflated; (1) inflated only at base; (2) large sinus present [Gaudin 2004: ch. 137].
138 – * Pterygoid fenestra: (0) absent; (1) present anteriorly; (2) present posteriorly [Gaudin 2004: ch. 138].
139 – Size of lacrimal: (0) small to absent; (1) large [Gaudin 2004: ch. 139].
140 – Relative size of facial and orbital portions of lacrimal: (0) orbital larger than facial; (1) facial greater than or equal to orbital exposure [Gaudin 2004: ch. 140].
141 – Number of lacrimal foramina: (0) one; (1) two [Gaudin 2004: ch. 141].
142 – ** Size of lacrimal foramen: (0) small, maximum dorsoventral diameter <2% of BNL; (1) moderate, diameter ≥2%, <2.5% of BNL; (2) large, diameter ≥2.5%, <3% of BNL; (3) greatly enlarged, diameter ≥3% of BNL [Gaudin 2004: ch. 142].
143 – Lacrimal eminence: (0) absent; (1) present [Gaudin 2004: ch. 143].
144 – * Lacrimal foramen with prominent lateral walls: (0) absent; (1) present; (2) foramen opens into ventrally directed canal [Owen 1856; Scott 1903–4; Gaudin 2004: ch. 144].
145 –** Shape of jugal: (0) simple, no processes; (1) with large descending process; (2) with large ascending and descending processes; (3) with ascending, descending, and middle processes [Gaudin 2004: ch. 145].
146 – ** Postorbital process of zygomatic arch (jugal or squamosal): (0) absent; (1) weak; (2) present [Gaudin 2004: ch. 146].
147 – Jugal and lacrimal overlap facial portion of maxilla anteriorly in lateral view: (0) absent; (1) present [Gaudin 2004: ch. 147].
148 – Middle process of jugal: (0) elongate, triangular; (1) short, deep dorsoventrally [Gaudin 2004: ch. 148].
149 – ** Width of ascending process of jugal: (0) wide; (1) narrow, slender; (2) rod-like; (3) rod-like proximally, with large, flat distal expansion [Scott 1903–4; Gaudin 2004: ch. 149].
150 – Orientation of ascending process of jugal in lateral view: (0) oblique to nearly horizontal; (1) nearly vertical [Webb 1985; Gaudin 2004: ch. 150].
151 – Relative lengths of ascending and descending processes of jugal: (0) ascending process less than or equal to descending process; (1) ascending process longer [Gaudin 2004: ch. 151].
152 – ** Width of descending process of jugal: (0) wide; (1) wide at base, tapers strongly toward tip; (2) narrow [Gaudin 2004: ch. 152].
153 – Descending process of jugal hooked posteriorly: (0) absent; (1) present [Scott 1903–4].
154 – Number of posteriorly projecting points on distal portion of descending process of jugal: (0) one; (1) two [Gaudin 2004: ch. 154].
155 – Attachment of jugal to skull: (0) firmly sutured; (1) loosely attached [Webb 1985; Gaudin 2004: ch. 155].
156 – ** Position of infraorbital canal: (0) canal short, ventrally situated; (1) canal elongate and ventral; (2) canal elongate and displaced dorsally [Gaudin 2004: ch. 156].
157 – Infraorbital foramen exposure in ventral view: (0) unexposed; (1) exposed [Gaudin 2004: ch. 157].
158 – * Relationship of foramen ovale to orbital bones: (0) foramen surrounded by the alisphenoid; (1) foramen between the alisphenoid and squamosal; (2) foramen between alisphenoid, pterygoid and squamosal, or between squamosal and pterygoid externally, with alisphenoid surrounding the opening internally; (3) foramen between alisphenoid and pterygoid [Gaudin 2004: ch. 158].
159 – Foramen rotundum: (0) confluent with the sphenorbital fissure; (1) separate [Gaudin 2004: ch. 159].
160 – Optic foramen vs. sphenorbital fissure: (0) two foramina clearly separate, with distinct external openings; (1) optic foramen empties into sphenorbital canal, two foramina share common external aperture [Gaudin 2004: ch. 160].
161 – * Position of sphenopalatine foramen relative to sphenorbital fissure/optic foramen: (0) situated well anterior and ventral to these openings; (1) just anteroventral to orbital foramina, situated in common fossa; (2) displaced posteriorly, lies between optic foramen and foramen ovale [Gaudin 2004: ch. 161].
162 – ** Bony ridge lateral to orbital foramina: (0) absent; (1) anterior ridge extending from wall of sphenorbital fissure/optic foramen anteriorly, foramina open into anterior groove; (2) ridge continues posteriorly from sphenorbital fissure/optic foramen toward glenoid, often with large muscular process [Gaudin 2004: ch. 162].
163 – Orbital exposure of orbitosphenoid: (0) small to absent; (1) well-developed [Gaudin 2004: ch. 163].
164 – * Orbital exposure of palatine: (0) low, elongate anteroposteriorly; (1) higher, more rectangular or square; (2) L-shaped, with tall anterior portion, low long posterior portion; (3) very tall, narrow anteroposteriorly [Gaudin 2004: ch. 164].
165 – Alisphenoid contacts parietal dorsally: (0) absent; (1) present [Novacek & Wyss 1986; Novacek *et al.* 1988; Gaudin 2004: ch. 165].
166 – Alisphenoid and pterygoid: (0) unfused or fused only in adults; (1) fuse very early in ontogeny.

167 – Squamosal with lateral bulge at root of zygoma for epitympanic sinus: (0) absent or rudimentary; (1) present [Gaudin 2004: ch. 167].
168 – ** Length of zygomatic process of squamosal: (0) reduced, length ≤5% of BNL; (1) moderate, length >5%, ≤10% of BNL; (2) elongate, length >10%, ≤15% of BNL; (3) greatly elongate, length >15% of BNL [Gaudin 2004: ch. 168].
169 – Inclination of zygomatic process in lateral view: (0) ventral; (1) horizontal or slightly dorsal [Gaudin 2004: ch. 169].
170 – ** Depth of zygomatic process: (0) narrow dorsoventrally, depth measured at midpoint < 5% of BNL; (1) moderately deep, depth ≥5%, <10% of BNL; (2) deep, depth ≥10% of BNL [Gaudin 2004: ch. 170].
171 – * Shape of free end of zygomatic process: (0) rounded; (1) broad and somewhat flattened; (2) pointed [Gaudin 2004: ch. 171].
172 – ** Position of frontal/parietal suture: (0) anterior to glenoid fossa; (1) at anterior edge of glenoid; (2) well posterior to front of glenoid [Naples 1982; Gaudin 2004: ch. 172].
173 – * Frontal and parietal dorsal shape: (0) convex anteroposteriorly and mediolaterally; (1) flattened anteroposteriorly and mediolaterally; (2) flattened mediolaterally, though strongly convex anteroposteriorly [Gaudin 2004: ch. 173].
174 – * Frontal sinus: (0) confluent with maxillary sinus and nasal cavity; (1) absent; (2) small, restricted to frontal; (3) large, extends into parietal and nasal [Gaudin 2004: ch. 174].
175 – ** Postorbital process of frontal: (0) absent (1) weakly developed; (2) strongly developed.
176 – Supraorbital foramen: (0) absent; (1) present [Gaudin 2004: ch. 175].
177 – Postorbital constriction: (0) absent or rudimentary; (1) strongly developed [Gaudin 2004: ch. 177].
178 – ** Position of postorbital process: (0) well posterior to maxillary foramen; (1) displaced anteriorly to level of maxillary foramen; (2) strongly displaced anteriorly, lies anterior to maxillary foramen [Gaudin 2004: ch. 178].
179 – Parietal with distinct anteroventral process extending towards orbital foramina: (0) absent; (1) present [Gaudin 2004: ch. 179].
180 – Parietal eminence: (0) absent or rudimentary; (1) present [Scott 1903–4; Gaudin 2004: ch. 180].
181 – Inclination of occiput in lateral view: (0) inclined anteriorly; (1) vertical, or slightly inclined posteriorly [Gaudin 2004: ch. 181].
182 – ** Nuchal crest: (0) absent; (1) weakly developed; (2) strong [Gaudin 2004: ch. 182].
183 – Nuchal crest: (0) uniform width; (1) splits dorsally into anterior and posterior occipital crests, which together outline a raised triangular area in the dorsal surface of the skull roof [Gaudin 2004: ch. 183].
184 – Nuchal crest position vs. occiput: (0) in line with the posterior surface of the occiput; (1) overhangs occiput posteriorly [Gaudin 2004: ch. 184].
185 – Median ridge of occiput: (0) extends from foramen magnum dorsally to the nuchal crest; (1) extends dorsally onto the roof of the skull (Scott 1903–4; Gaudin 2004: ch. 185].
186 – ** Distance between occipital condyles: (0) widely separate, minimum distance between condyles (in ventral view) >10% of BNL; (1) moderately well separated, distance between condyles ≤10%, >5% of BNL; (2) close to one another, distance between condyles ≤5% of BNL [Scott 1903–4; Gaudin 2004: ch. 186].
187 – ** Condyloid foramen size: (0) small, maximum diameter <2% of BNL; (1) moderate, diameter ≥2%, <3% of BNL; (2) enlarged, diameter ≥3% of BNL [Gaudin 2004: ch. 187].
188 – Position of occipital condyles relative to dentition: (0) at nearly the same level as the dentition; (1) situated well dorsal to the dentition [Gaudin 2004: ch. 188].
189 – Posterior edge of occipital condyles: (0) protrudes posterior to posterior edge of foramen magnum; (1) ends at or anterior to posterior foramen magnum [Gaudin 2004: ch. 189].
190 – Exoccipital crest vs. occipital condyles: (0) crest separated from lateral edge of condyles; (1) crest abuts lateral edge of condyles [Gaudin 2004: ch. 190].
191 – ** Occipital condyle proportions in posterior view: (0) mediolaterally elongate, ratio of maximum width to maximum height ≥1.0; (1) ratio of width to height <1.0, ≥0.75; (2) mediolaterally compressed, dorsoventrally elongate, ratio of width to height <0.75 [Gaudin 2004: ch. 191].
192 – * Occipital condyle shape in posterior view: (0) rhomboid, quadrangular; (1) roughly triangular, with straight or slightly concave medial edge, strongly convex lateral margin; (2) roughly triangular but extended far medioventrally; (3) roughly triangular but extended laterally; (4) irregularly shaped [Gaudin 2004: ch. 192].
193 – Occipital condyles: (0) sessile; (1) with distinct neck [Scott 1903–4; Gaudin 2004: ch. 193].
194 – ** Position of occipital condyles vs. condyloid foramina: (0) condyles lie just posterior to foramina, minimum distance between condyles and foramina <1.0% of BNL; (1) distance between condyles and foramina >1.0, <2.5% of BNL; (2) condyles well-separated from foramina, distance >2.5% of BNL [Gaudin 2004: ch. 194].
195 – Occipital condyle shape in ventral view: (0) condyles not conspicuously elongated anteroposteriorly; (1) condyles elongated anteroposteriorly [Gaudin 2004: ch. 195].
196 – Rectus capitis fossae: (0) absent; (1) present [Scott 1903–4, Gaudin 2004: ch. 196].
197 – Shape of basioccipital: (0) wide and flat; (1) narrow and convex mediolaterally [Gaudin 2004: ch. 197].
198 – Shape of basisphenoid: (0) uniformly narrow; (1) triangular, narrows anteriorly; (2) butterfly shaped, with two posterior processes and three anterior processes, two extending laterally and one in the middle [Gaudin 2004: ch. 198].

199 – * Ethmoid exposure in nasopharynx: (0) vomerine wings separate exposing intervening ethmoid; (1) vomerine wings fused, leaving overlying ethmoid unexposed; (2) ethmoid unexposed, covered by posterior extension of hard palate [Gaudin 2004: ch. 199].
200 – Vomer: (0) with short, straight ventral keel, or with keel lacking altogether; (1) with elongate asymmetrical ventral keel extending posteriorly into nasopharynx [Lull 1929; Patterson *et al.* 1992; Gaudin 2004: ch. 200].
201 – Exposure of vomer in nasopharynx: (0) small, presphenoid and basisphenoid broadly exposed; (1) very large, covers presphenoid and much of basisphenoid [Gaudin 2004: ch. 201].
202 – Tympanic external surface: (0), smooth; (1) rugose [Gaudin 1995: ch. 1].
203 – Tympanic directed: (0) anteromedially; (1) anteroposteriorly; (2) anterolaterally [Gaudin 1995: ch. 2].
204 – Tympanic attachment: (0) loose dorsal attachment; (1) fused dorsally [Gaudin 1995: ch. 3].
205 – Attachment of posterior crus of tympanic: (0), squamosal, tympanohyal and mastoid; (1) squamosal/mastoid bridge [Gaudin 1995: ch. 4].
206 – Medial expansion of tympanic: (0) absent; (1) present [Gaudin 1995: ch. 5].
207 – ** Shape of tympanic: (0) elongate dorsoventrally; (1) circular; (2) elongate anteroposteriorly [Gaudin 1995: ch. 6].
208 – Styliform process: (0) absent; (1) present [Gaudin 1995: ch. 7].
209 – Recessus meatus: (0) absent; (1) present [Gaudin 1995: ch. 8].
210 – Sulcus and crista tympanica: (0) prominent; (1) reduced [Gaudin 1995: ch. 9].
211 – Tympanic/pterygoid contact: (0) absent; (1) present [Gaudin 1995: ch. 10].
212 – Tympanic forms posterior wall of glenoid fossa: (0) no; (1) yes [Gaudin 1995: ch. 11].
213 – * Auditory bulla: (0) bulla completely ossified or nearly so, membranous bulla absent or rudimentary, entotympanic and tympanic attached along entire length, petrosal hidden in ventral view; (1) membranous bulla small, entotympanic and tympanic unattached or attached only posterior, petrosal narrowly exposed ventrally; (2) bulla poorly ossified, membranous bulla large, entotympanic and tympanic unattached, petrosal widely exposed ventrally [Guth 1961; Webb 1985; Gaudin 1995: ch. 12].
214 – Ossified external auditory meatus (i.e., a tubular extension of the tympanic lateral to crista tympanica): (0) absent; (1) present [Gaudin 1995: ch. 13].
215 – Fissura Glaseri: (0) opens in typical xenarthran position; (1) opens into distinct groove in squamosal lying medial to entoglenoid process [Gaudin 1995: ch. 14].
216 – * Median lacerate foramen: (0) fully exposed in ventral view; (1) partially covered ventrally by entotympanic and tympanic; (2) fully covered ventrally [Gaudin 1995: ch. 15].
217 – * Entotympanic length vs. tympanic length: (0) tympanic longer; (1) two nearly equal in length; (2) entotympanic longer [Gaudin 1995: ch. 16].
218 – * Ventral extent of entotympanic vs. tympanic: (0) entotympanic dorsal; (1) ventral extent of two bones roughly equivalent; (2) entotympanic ventral [Gaudin 1995: ch. 17].
219 – Size of entotympanic: (0) reduced to a small plate or blocky structure, does not extend to anterior end of promontorium; (1) prominent, extends to or beyond female end of promontorium [Gaudin 1995: ch. 18].
220 – Entotympanic form and position: (0) vertical plate situated on medial portion of ventral surface of petrosal; (1) laterally situated vertical plate with horizontal medial expansion dorsally [Gaudin 1995: ch. 19].
221 – Entotympanic lateral plate: (0) thickened mediolaterally; (1) very thin [Gaudin 1995: ch. 20].
222 – Ventral edge of entotympanic: (0) flat in lateral view; (1) extended into anteroventral process [Gaudin 1995: ch. 21].
223 – Entotympanic width: (0) fairly uniform throughout its length; (1) widened posteriorly [Gaudin 1995: ch. 22].
224 – * Entotympanic lateral surface: (0) concave; (1) flat vertical surface ventrally with deep dorsal hollow; (2) flat vertical surface. [Gaudin 1995: ch. 23].
225 – * Entotympanic directed: (0) anteromedially; (1) anteroposteriorly; (2) anterolaterally [Gaudin 1995: ch. 24].
226 – * Dorsal edge of entotympanic. (0) strong concave curvature in lateral view, with dorsal projection at anterior end; (1) weakly curved, without dorsal projection; (2) flat, or nearly so [Gaudin 1995: ch. 25].
227 – * Entotympanic participation in sulcus for internal carotid artery: (0) forms lateral wall of sulcus; (1) forms lateral wall and at least part of the roof; (2) forms lateral wall, roof, and has medial ridge forming at least part of the medial wall [Gaudin 1995: ch. 26].
228 – Lateral process of entotympanic extending above anterior portion of tympanic: (0) absent; (1) present [Gaudin 1995: ch. 27].
229 – Entotympanic lateral extension contacting tympanohyal: (0) absent; (1) present [Gaudin 1995: ch. 28].
230 – * Entotympanic participation in tympanic cavity floor: (0) rudimentary or absent; (1) weak participation in medial portion of floor; (2) strong, forming almost entire medial half of floor [Gaudin 1995: ch. 29].
231 – Position of medial expansion of entotympanic: (0) dorsal to floor of basicranium; (1) at level of basicranium [Gaudin 1995: ch. 30].
232 – Entotympanic/mastoid contact: (0) absent; (1) present [Gaudin 1995: ch. 31].
233 – Mastoid depression: (0) absent; (1) present [Gaudin 1995: ch. 32].
234 – Mastoid lateral exposure: (0) weak; (1) strong [Matthew 1918; Novacek & Wyss 1986; Gaudin 1995: ch. 33].
235 – Depth of mastoid depression: (0) narrow, fairly deep; (1) broadened, shallow [Gaudin 1995: ch. 34].
236 – * Mastoid process: (0) rudimentary or absent; (1) well developed; (1) greatly enlarged [Gaudin 1995: ch. 35].
237 – Mastoid process foramen: (0) absent; (1) present [Gaudin 1995: ch. 36].

238 – ** Nuchal and exoccipital crests (in posterior view): (0) parallel; (1) diverge distally; (2) diverge proximally, converge distally [Gaudin 1995: ch. 37].
239 – * Paroccipital process. (0) weakly developed or rudimentary; (1) well-developed; (2) greatly enlarged, free standing process [Gaudin 1995: ch. 38].
240 – Pterygoid lateral groove: (0) absent; (1) present [Gaudin 1995: ch. 39].
241 – * Pterygoid participation in bony wall of tympanic cavity: (0) absent; (1) present; (2) enlarged to form entire medial wall [Winge 1941; Gaudin 1995: ch. 40].
242 – ** Shape of promontorium: (0) globose; (1) dorsoventrally elongate, flat anteriorly and globose posteriorly; (2) anteroposteriorly elongate, flat anteriorly and globose posteriorly [Gaudin 1995: ch. 41].
243 – ** Processus crista facialis: (0) small, reduced plate; (1) large, concave plate; (2) large, rugose bony mass; (3) enormous, exposed external to tympanic cavity [Gaudin 1995: ch. 42].
244 – Epitympanic sinus: (0) absent; (1) present [Emry 1970; Novacek 1986; Gaudin 1995: ch. 43].
245 – Stapedius fossa: (0) circular, situated directly posterior to fenestra ovalis; (1) anteroposteriorly elongate, bounded by strong ventral ridge, situated lateral to fenestra ovalis in ventral view [Gaudin 1995: ch. 44].
246 – Fossa incudis: (0) situated in posteromedial corner of wide epitympanic recess; (1) occupies entire posteroventral wall of epitympanic recess [Gaudin 1995: ch. 45].
247 – Lateral exposure of fenestra cochleae: (0) small; (1) well-developed [Gaudin 1995: ch. 46].
248 – Medial groove of fenestra cochleae: (0) rudimentary or absent; (1) well-developed [Gaudin 1995: ch. 47].
249 – Internal auditory meatus: (0) shallow fossa perforated by large foramina; (1) deep, undivided canal [Gaudin 1995: ch. 48].
250 – Direction of internal auditory meatus: (0) medial; (1) posteromedial [Gaudin 1995: ch. 49].
251 – Position of subarcuate fossa relative to internal auditory meatus: (0) posterodorsal; (1) dorsal [Gaudin 1995: ch. 50].
252 – ** Direction of tympanohyal: (0) initially posterolateral, then tums distally and runs posteromedial; (1) posterolateral distally; (2) strongly ventral distally [Gaudin 1995: ch. 51].
253 – Width of tympanohyal: (0) roughly uniform along entire length; (1) greatly widened distally [Gaudin 1995: ch. 52].
254 – Stylohyal fossa: (0) absent; (1) present [Gaudin 1995: ch. 53].
255 – Shape of stylohyal fossa: (0) circular; (1) oval [Gaudin 1995: ch. 54].
256 – Stylohyal articulation elements: (0) mostly tympanohyal; (1) tympanohyal, mastoid, entotympanic, and paroccipital process of exoccipital [Gaudin 1995: ch. 55].
257 – ** Direction of stylohyal articulation: (0) ventral; (1) ventrolateral; (2) posterior [Gaudin 1995: ch. 56].
258 – * Position of stylomastoid foramen relative to tympanohyal/stylohyal fossa: (0) posterolateral; (1) lateral or anterolateral; (2) directly anterior [Gaudin 1995: ch. 57].
259 – * Direction of stylomastoid canal: (0) dorsal; (1) posteroventral; (2) posteroventrolateral; (3) ventrolateral [Gaudin 1995: ch. 58].
260 – * Connection of stylomastoid foramen and foramina for occipital a/a. diploetica magna: (0) no connection; (1) stylomastoid foramen connected to widely separate dorsal foramen for a. diploetica magna via open groove for occipital a.; (2) stylomastoid foramen connected to nearby ventral opening of canal for occipital a. by weak groove; (3) stylomastoid foramen connected to nearby ventral opening of canal for occipital a. by strong groove; (4) stylomastoid foramen and ventral opening of canal for occipital a. open into same fossa [Gaudin 1995: ch. 59].
261 – Position of eustachian tube: (0) anteromedial comer of tympanic cavity; (1) posteromedial comer [Gaudin 1995: ch. 60].
262 – ** Elements in eustachian tube opening: (0) entotympanic and tympanic; (1) entotympanic, tympanic, and pterygoid; (2) tympanic, pterygoid, and basioccipital/basisphenoid [Gaudin 1995: ch. 61].
263 – ** Direction of eustachian tube: (0) posteroventral; (1) ventral; (2) anterior [Gaudin 1995: ch. 62].
264 – Size of the posterior lacerate foramen: (0) small; (1) greatly enlarged [Matthew 1918; Novacek 1986, Gaudin 1995: ch. 63].
265 – Shape of posterior lacerate foramen: (0) circular; (1) oval [Gaudin 1995: ch. 64].
266 – Posterior lacerate foramen inset below and behind entotympanic and petrosal: (0) no; (1) yes [Engelmann 1978, 1985; Gaudin 1995: ch. 65].
267 – Position of posterior lacerate foramen relative to condylar foramen: (0) close; (1) well-separated [Gaudin 1995: ch. 66].
268 – Internal carotid artery foramen (within entotympanic or between entotympanic and basicranium): (0) absent; (1) present [Gaudin 1995: ch. 67].
269 – Slope of internal carotid artery sulcus: (0) anterodorsal; (1) saddle-shaped, first anteroventral then anterodorsal [Gaudin 1995: ch. 68].
270 – ** Grooves, canals, and foramina of occipital a. and a. diploetica magna: (0) a. diploetica magna travels along sidewall of braincase, where it enters cranial cavity; (1) occipital a. travels in open groove near petrosquamous suture, a. diploetica magna branches off dorsally to enter foramen leading into braincase; (2) occipital a. travels within partially closed canal; (3) occipital artery completely enclosed within canal; (4) canal for occipital a. short, perforates mastoid process dorsoventrally [Gaudin 1995: ch. 69].
271 – Foramen magnum venous sinus: (0) absent; (1) present [Gaudin 1995: ch. 70].
272 – Shape of mallear head in dorsal view: (0) rounded; (1) parallel-sided [Segall 1976; Gaudin 1995: ch. 71].

273 – Size of dorsal and ventral incudal facets of malleus in lateral view: (0) dorsal > ventral; (1) facets subequal [Gaudin 1995: ch. 72].
274 – Lamina and anterior process of malleus: (0) small; (1) enlarged [Gaudin 1995: ch. 73].
275 – Angle between manubrium and neck of malleus: (0) much less than 180° (ca. 110° to 130°); (1) near 180° [Gaudin 1995: ch. 74].
276 – Glenoid position relative to superficies meatus (the latter defined by Patterson *et al.* (1992:5) as "the groove on the ventral surface of the squamosal 1ateral and dorsal to the tympanum"): (0) glenoid at or above meatus; (1) glenoid ventral [Gaudin 1995: ch. 75].
277 – * Shape of glenoid: (0) elongate anteroposteriorly; (1) hemispherical; (2) widened mediolaterally [Sicher 1944; Naples 1982, 1987; Webb 1985; Gaudin 1995: ch. 76].
278 – * Glenoid inclination: (0) posterodorsal; (1) horizontal; (2) anterodorsal [Naples 1982; Gaudin 1995: ch. 77].
279 – Glenoid medial shelf: (0) absent; (1) present [Naples 1987; Gaudin 1995: ch. 78].
280 – Glenoid lateral shelf: (0) absent; (1) present [Naples 1987; Gaudin 1995: ch. 79].
281 – Glenoid posterior shelf: (0) absent; (1) present [Gaudin 1995: ch. 80].
282 – ** Posterior surface of glenoid: (0) smooth; (1) grooved; (2) rugose [Gaudin 1995: ch. 81].
283 – * Position of glenoid relative to porus acousticus: (0) just anterior; (1) separate; (2) well-separate [Gaudin 1995: ch. 82].
284 – ** Entoglenoid process: (0) rudimentary or absent; (1) weakly developed, appressed against lateral side of descending lamina of pterygoid; (2) weakly developed but free-standing; (3) well-developed [Gaudin 1995: ch. 83].
285 – Postglenoid foramen: (0) reduced or absent; (1) present [Hoffstetter 1958; Engelmann 1978, 1985; Gaudin 1995: ch. 84].
286 – * Direction of root of zygoma: (0) anterior; (1) anterolateral; (2) 1ateral [Gaudin 1995: ch. 85].
287 – Ratio SW/SL: (0) < 0.16; (1) ≥ 0.16.
288 – General shape of scapula: (0) broad and rectangular; (1) roughly triangular.
289 – Suprascapular ossification: (0) present; (1) absent.
290 – Post-scapular fossa (= teres major fossa): (0) small and located on the posterior scapular border; (1) posteriorly expanded.
291 – Accessory scapular spine: (0) short spine located on the posterior scapular border; (1) well-developed and laterally projecting.
292 – Vertebral border of scapula: (0) convex; (1) straight.
293 – Supraspinous fossa and infraspinous fossa: (0) roughly the same size; (1) supraspinous fossa greater in area than the infraspinous fossa.
294 – Acromion process: (0) at the level of the glenoid fossa in lateral view, or fails to reach ventrally to level of glenoid; (1) extended ventral to glenoid in lateral view.
295 – Acromion process fused with the coracoid process: (0) absent; (1) present.
296 – Coraco-scapular foramen: (0) absent; (1) present. [Modified from Gaudin & Branham (1998): ch. 72].
297 – Glenoid fossa, shape of outline: (0) ovoid-piriform; (1) semicircular.
298 – Glenoid fossa and facet for clavicle in ventral view: (0) long axes disposed at acute angle (around 45 degrees); (1) long axes disposed almost perpendicularly.
299 – Ratio HHW/HHL, (0) < 0.80; (1) ≥ 0.80.
300 – Ratio HEMP/HDEW, (0) ≥ 0.36; (1) < 0.36.
301 – Deltoid crest in cranial view: (0) faces laterally, occupies part of the cranial view; (1) faces anteriorly, reaching the medial side.
302 – Distal border of deltoid crest in frontal view: (0) oblique; (1) nearly horizontal.
303 – ** Supinator crest in anterior view: (0) without lateral extension (lateral margin oblique proximodistally); (1) with moderate lateral extension (convex profile of lateral margin); (2) with well-developed lateral extension (lateral margin vertical proximodistally).
304 – ** Degree of radial protrusion of greater tuberosity versus lesser tuberosity in proximal view: (0) lt>gt; (1) lt≈gt; (2) lt<gt. [Modified from De Iuliis *et al.* (2011): ch. 37].
305 – Olecranon fossa: (0) distinct, deep; (1) shallow depression.
306 – Entepicondylar foramen: (0) present; (1) absent. [From Pujos (2002): ch. 20; Pujos *et al.* (2007): ch. 27; Amson *et al.* (2016): ch. 4].
307 – Distinct proximodistally vertical process on the ascending entepicondylar ridge: (0) absent; (1) present.
308 – ** Lateral epicondyle versus medial epicondyle in anterior view: (0) lateral epicondyle less mediolaterally expanded than the medial epicondyle; (1) lateral epicondyle and medial epicondyle equally expanded; (2) lateral more expanded than the medial epicondyle.
309 – Capitulum vs trochlear mediolateral width in distal view: (0) trochlea wider transversely than the capitulum; (1) width roughly equivalent.
310 – Capitulum vs trochlear anteroposterior depth in distal view: (0) same anteroposterior depth; (1) trochlea deeper.
311 – Lateral epicondyle in distal view: (0) directed posteriorly; (1) directed laterally.
312 – **Medial epicondyle in distal view: (0) directed medially; (1) directed posteriorly; (2) directed anteriorly.
313 – Capitular tail (*sensu* Sargis 2002): (0) present; (1) absent.

314 – ** Ratio APDR/RL: (0) ≤ 0.160; (1) > 0.160, ≤ 0.245; (2) > 0.245.
315 – ** Radial head shape: (0) deep anteroposteriorly and narrow transversely, RHW/RHL ≤ 0.63; (1) ovoid, RHW/RHL > 0.63, ≤ 0.82; (2) circular or approximately so, RHW/RHL > 0.82, ≤ 1.0.
316 – Posterior border of radius in lateral view: (0) straight; (1) concave anteriorly.
317 – Anterior border of radius in lateral view: (0) convex anteriorly; (1) straight.
318 – Anterior border of radius in anterior view: (0) not inflected medially; (1) inflected medially.
319 – Dorsolateral sulcus on styloid process (*m. abductor pollicis longus* groove): (0) absent; (1) present.
320 – Distal articulation of radius: (0) with one single facet for scaphoid and lunar; (1) with distinct facets.
321 – ** Ratio UPCDE/UL: (0) ≤ 0.55; (1) > 0.55, ≤ 0.75; (2) > 0.75.
322 – ** Ratio THU/UL: (0) < 0.12; (1) ≥ 0.12, < 0.20; (2) ≥ 0.20, ≤ 0.26; (3) > 0.26.
323 – ** Angle between olecranon and posterior border of the ulna in lateral view: (0) acute (less than 90 degrees); (1) roughly orthogonal (around 90 degrees); (2) obtuse (more than 90 degrees).
324 – ** Medial (trochlear) and lateral (capitular) portions of the trochlear notch in cranial view: (0) medial portion extends proximal to lateral; (1) medial and lateral portion with roughly equivalent proximal extent; (2) lateral portion extends proximal to medial.
325 – Radial notch: (0) facet occupying the whole fossa; (1) facet occupying only part of the fossa.
326 – Posterior border of the ulna in posterior view: (0) columnar, with uniform transverse width along whole length; (1) decreasing transverse thickness from proximal to distal.
327 – Styloid process: (0) pedunculated; (1) sessile.
328 – Styloid process: (0) with oblique articular surface; (1) with horizontal articular facet.
329 – Scaphoid and lunar: (0) fused; (1) separate.
330 – Ungual phalanges: (0) bifid, with forked distal tip; (1) single distal point.
331 – Scaphoid, ratio between its minimum and maximum diameters: (0) < 0.64; (1) ≥ 0.64.
332 – Cuneiform-lunar contact, in proximal view: (0) pedunculated; (1) sessile.
333 – ** Cuneiform shape, ratio between dorsopalmar and mediolateral widths: (0) < 0.65; (1) ≥ 0.65, < 0.87; (2) ≥ 0.87.
334 – Cuneiform shape, ratio between proximodistal length and mediolateral width: (0) < 0.65; (1) ≥ 0.65. [Modified from Haro *et al.* (2016): ch. 326].
335 – Cuneiform shape, ratio between proximodistal and dorsopalmar widths: (0) < 0.95; (1) ≥ 0.95. [Modified from Haro *et al.* (2016): ch. 324].
336 – Unciform shape, ratio between proximodistal and mediolateral widths: (0) < 1.0; (1) ≥ 1.0.
337 – Trapezium and metacarpal I: (0) unfused; (1) fused, forming the carpal-metacarpal complex. [Modified from De Iuliis *et al.* (2011): ch. 50].
338 – Contact between trapezium (or carpal-metacarpal complex) and trapezoid: present (0); absent (1) [Modified from Haro *et al.* (2016): ch. 330].
339 – Exposure of contact between metacarpal II and magnum in dorsal view of articulated manus: absent (0); present (1) [From Haro *et al.* (2016): ch. 331].
340 – Metacarpal 2 - Metacarpal 3 facet: (0) sessile and flat; (1) pedunculated and concavo-convex.
341 – ** Metacarpal 3 shape (ratio between mediolateral width at the middle of shaft and total length): (0) ≤ 0.37; (1) > 0.37, < 0.52; (2) ≥ 0.52 [Modified from Haro *et al.* (2016): ch. 339].
342 – Mediolateral extension of the facet of metacarpal 5 on unciform in dorsal view: (0) well-developed (comparable to the extent of the metacarpal 4-unciform facet); (1) extremely reduced (less than the half of the extent of the metacarpal 4-unciform facet) or absent.
343 – ** Number of claws on manus: (0) 5-4; (1) 3; (2) 2 [From Gaudin & Branham (1998): ch. 92].
344 – ** Femur shape (ratio between mediolateral width at midshaft and total length): (0) long and narrow, TDF/FL < 0.20; (1) intermediate, TDF/FL ≥ 0.20, < 0.35; (2) short and broad, TDF/FL ≥ 0.35. [Modified from Pujos *et al.* (2007): ch. 33; De Iuliis *et al.* (2011): ch. 58; Amson *et al.* (2016): ch. 26].
345 – ** Ratio FCW/FL: (0) ≤ 0.27; (1) > 0.27, ≤ 0.36; (2) > 0.36.
346 – Ratio LCL/MCL: (0) ≥ 0.75; (1) < 0.75.
347 – ** Ratio Wtroc/FL: (0) ≤ 0.30; (1) > 0.30, ≤ 0.47; (2) > 0.47.
348 – ** Ratio APDF/TDF: (0) ≥ 0.54; (1) < 0.54, ≥ 0.32; (2) < 0.32. [Modified from De Iuliis *et al.* (2011): ch. 57].
349 – Intertrochanteric ridge: (0) present; (1) absent.
350 – ** Femoral head in anterior view: (0) greater trochanter extends proximal to head; (1) proximal extent of head and greater trochanter equivalent; (2) head extends further proximally than the greater trochanter. [Modified from Rincón *et al.* (2015): ch. 13].
351 – Femoral head protrusion: (0) well-developed (with distinct neck); (1) sessile (without a distinct neck). [Modified from Rincón *et al.* (2015): ch. 11].
352 – Detached sulcus delimitating, both medially and laterally, the articular surface of the femoral head in frontal view: (0) present; (1) absent.

353 – ** Third trochanter: (0) absent; (1) prominent but relatively short proximodistally; (2) prominent and proximodistally elongate, forming a lateral blade. [Modified from McDonald & Muizon (2002): ch. 29; Pujos (2002): ch. 25; Pujos *et al.* (2007): ch. 31; Amson *et al.* (2016): ch. 28].
354 – Position of proximal and distal epiphyses of femur in distal view: (0) on the same plane of main axis; (1) twisted with respect to the main axis.
355 – Tibial shaft in lateral view: (0) anteriorly convex; (1) straight. [Modified from Rincón *et al.* (2015), ch. 18.]
356 – ** Ratio TDT/TL: (0) < 0.18; (1) ≥ 0.18, < 0.30; (2) ≥ 0.30.
357 – ** Ratio TPEL/TL: (0) ≤ 0.25; (1) > 0.25, ≤ 0.35; (2) > 0.35.
358 – ** Ratio TML/TPEL: (0) < 0.60; (1) ≥ 0.60, < 0.74; (2) ≥ 0.74.
359 – ** Ratio TPEW/TL: (0) < 0.40; (1) ≥ 0.40, < 0.60; (2) ≥ 0.60.
360 – Ratio LTFL/MTFL: (0) ≥ 0.83; (1) < 0.83.
361 – Ratio LTFW/MTFW: (0) ≥ 0.86; (1) < 0.86.
362 – Groove anterior to the tibial lateral condyle in proximal view (pit for attachment of medial meniscal ligament?): (0) absent; (1) present.
363 – Tibia, medial intercondylar eminence: (0) well-developed; (1) reduced or absent.
364 – Tibia, fibular facet in distal view: (0) extended anteroposteriorly; (1) occupying only the posteromedial corner of the tibia's distal surface.
365 – ** Grooves for the tendons of the *m. flexor hallucis longus*, *m. flexor digitorum longus* and *m. tibialis caudalis*, on the distomedial edge of the posterior tibial surface: (0) three well-marked grooves present; (1) two well-marked grooves; (2) single large depression present.
366 – Ratio EFFL/FiTL of fibula: (0) < 0.20; (1) ≥ 0.20.
367 – ** Ratio between the maximum proximodistal and anteroposterior length of the astragalus: (0) < 0.80; (1) ≥ 0.80, < 1.00; (2) ≥ 1.00.
368 – ** Astragalus, odontoid process-discoid angle in either anterior or posterior view: (0) markedly obtuse (> 115°); (1) moderately obtuse (> 90°, ≤ 115°); (2) orthogonal or acute (≤ 90°). [Modified from Pujos (2002): ch. 29; Pujos *et al.* (2007): ch. 37; Amson *et al.* (2016): ch. 36].
369 – ** Astragalus, surface contour of discoid process in lateral view: (0) proximally convex; (1) essentially flat.
370 – Astragalus, sulcus tali: (0) present; (1) absent.
371 – Astragalus, sustentacular facet surface contour: (0) flat; (1) convex.
372 – Astragalus, cuboid facet surface contour: (0) convex; (1) concave.
373 – ** Calcaneal posterior mediolateral enlargement: (0) absent; (1) present, forming an arched posterior profile; (2) present, forming a broad surface touching the ground (mediolateral width/total length < 0.55); (3) present, forming a very broad surface touching the ground (mediolateral width/total length ≥ 0.55).
374 – Calcaneum, tuber calcis, distal development of proximal processes: (0) weak; (1) strong (reaching at least the proximal third of the bone). [From Amson *et al.* (2016): ch. 40].
375 – Sustentacular process of the calcaneum: (0) present; (1) absent.
376 – ** Contact of ectocuneiform with cuboid in lateral view: (0) large, nearly twice the size of the navicular-cuboid contact; (1) small, roughly the same size as the navicular-cuboid contact; (2) absent.
377 – Metatarsal 2 fusion with mesocuneiform: (0) absent; (1) present.
378 – Metatarsal 3 and metatarsal 2 contact: (0) present; (1) absent.
379 – ** Metatarsal 3 shape (ratio between minimum dorsopalmar depth of shaft and total length): (0) ≤ 0.40; (1) > 0.40, ≤ 0.46; (2) > 0.46, ≤ 0.56; (3) ≥ 0.56.
380 – ** Metatarsal 4 shape (ratio between minimum mediolateral width of shaft and total length): (0) ≤ 0.25; (1) > 0.25, ≤ 0.40; (2) > 0.40. [Modified from Amson *et al.* (2016): ch. 45].
381 – Digit III of pes, proximal and intermediate phalanges: (0) free; (1) co-ossified. [Modified from Pujos *et al.* (2007): ch. 41; Amson *et al.* (2016): ch. 44].
382 – Constriction of metatarsal 5 at midshaft: (0) present; (1) absent, distal border forming a continuous surface contacting the ground.
383 – Osteoderms: (0) absent; (1) present. [See McDonald (2018)].

Appendix VI. Data S2. Tables displaying the calculated ratios for the characters which include numerical values. All the measurements are expressed in millimeters. Explanations of abbreviations are available in Appendix III.

Raw data of character 287 – Ratio SW/SL: (0) < 0.16; (1) ≥ 0.16.

CODE	TAXON	SL	SW	SW/SL
MACN Ma 4.125	*Bradypus* sp.	58,9	10,3	0,174872666
FMNH P14238	*Catonyx* sp.	407	81,4	0,2
AMNH 1663	*Euphractus* sp.	55,5	8,4	0,151351351
MACN Pv 14066	*Glossotherium robustum*	323	62	0,191950464
FMNH P13133	*Hapalops* sp.	108,1	19	0,175763182
MACN Pv 14648	*Lestodon armatus*	537	96,7	0,180074488
MACN Pv 6866	*Mylodon darwinii*	343	57	0,166180758
MACN Ma 31.132	*Myrmecophaga* sp.	150,7	22,8	0,151293962
FMNH P14723	*Paramylodon harlani*	357	79	0,221288515
AMNH 16896	*Paramylodon harlani*	329,8	75,3	0,228320194
FMNH P14274	*Scelidotherium* sp.	315	65,6	0,208253968
MACN Pv 7150	*Scelidotherium* sp.	365	63,3	0,173424658
MNHN-Bol V 3718	*Simomylodon uccasamamensis*	227,3	39,6	0,174219094
MACN Ma 33.255	*Tamandua* sp.	86,6	12,2	0,140877598
MACN Ma 10.8	*Tamandua* sp.	78,8	11,8	0,149746193
MACN Ma 25911	*Tamandua* sp.	85,8	13,9	0,162004662
UF 201322	*Thinobadistes* sp.	283	58,7	0,207420495

Raw data of character 299 – Ratio HHW/HHL, (0) < 0.80; (1) ≥ 0.80.

CODE	TAXON	HHW	HHL	HHW/HHL
MACN Ma 4.125	*Bradypus* sp.	13	16	0,8125
AMNH 1663	*Euphractus* sp.	11,5	14,9	0,771812081
MACN Pv 62	*Glossotherium robustum*	93,9	98,6	0,952332657
MACN Pv 17572	*Glossotherium robustum*	98,3	100	0,983
MNHN.F.PAM 119	*Glossotherium robustum*	90,7	110,7	0,819331527
MNHN.F.PAM 118	*Glossotherium robustum*	93,2	109,2	0,853479853
MNHN.F.PAM 122	*Glossotherium robustum*	88,8	100,7	0,88182721
MACN Pv 4423	*Glossotherium robustum*	95,9	104,1	0,921229587
AMNH 11307	*Glossotherium robustum*	87,8	93,1	0,943071966
MNHN.F.PAM 141 (A.C. 7067)	*Glossotherium robustum*	90,5	93,6	0,966880342
MNHN.F.PAM 141 (A.C. 7068)	*Glossotherium robustum*	92,9	95,1	0,976866456
MNHN.F.PAM 123	*Glossotherium robustum*	85,1	85,7	0,992998833
MNHN.F.TAR 794	*Glossotherium tarijense*	77,8	96,2	0,808731809
MNHN.F.TAR 767	*Glossotherium tarijense*	95	101	0,940594059
VF-26	*Glossotherium tropicorum*	82,6	92,5	0,892972973
FMNH P13128	*Hapalops* sp.	17,4	21,3	0,816901408
FMNH P13130	*Hapalops* sp.	23,8	28,1	0,846975089
FMNH P13133	*Hapalops* sp.	21,8	22,1	0,986425339
MNHN.F.TAR 775	*Lestodon armatus*	90,1	108	0,834259259
MNHN.F.PAM 98	*Lestodon armatus*	108,8	129,6	0,839506173
MACN Pv 17182	*Lestodon armatus*	113,4	132,1	0,858440575
MNHN.F.TAR 778	*Lestodon armatus*	108,2	121	0,894214876
MLP 3-831	*Lestodon armatus*	116,5	120,4	0,967607973
FMNH P14229	*Lestodon armatus*	120,7	116,7	1,034275921
MLP 3-18	*Lestodon armatus*	109,6	105,9	1,034938621
FMNH P14228	*Lestodon armatus*	128,1	122	1,05
AMNH 53855	*Manis gigantea*	20	27,8	0,71942446
MACN Pv 14678	*Mylodon darwinii*	91,9	103,4	0,888781431
MACN Pv 14681	*Mylodon darwinii*	90,6	101,2	0,895256917
MACN Pv 13797	*Mylodon darwinii*	100	96,9	1,031991744
MACN Ma 31.132	*Myrmecophaga* sp.	31,6	35,1	0,9002849
UF 68581	*Paramylodon harlani*	88,5	101,5	0,871921182
AMNH 16896	*Paramylodon harlani*	96,2	109,7	0,876937101

MACN Pv 8735 cast	*Paramylodon harlani*	109	120	0,908333333
UF 84136	*Paramylodon harlani*	96,4	105,3	0,915479582
FMNH P14723	*Paramylodon harlani*	97,8	103,6	0,944015444
MACN Pv 7150	*Scelidotherium* sp.	84,5	93,3	0,9056806
FMNH P14274	*Scelidotherium* sp.	89,4	96,9	0,922600619
MACN Pv 6964	*Scelidotherium* sp.	86,8	91,2	0,951754386
FMNH P14301	*Scelidotherium* sp.	124,2	118,9	1,044575273
MNHN-Bol V 11766	*Simomylodon uccasamamensis*	56,1	58	0,967241379
MNHN-Bol V 12518	*Simomylodon uccasamamensis*	58,9	59,8	0,984949833
MNHN.F.AYO 121	*Simomylodon uccasamamensis*	58,9	59,5	0,989915966
MNHN-Bol V 11776	*Simomylodon uccasamamensis*	51,1	49,3	1,036511156
MNHN.F.AYO 102	*Simomylodon uccasamamensis*	65,8	59,9	1,098497496
MACN Ma 33.255	*Tamandua* sp.	16,3	19,4	0,840206186
MACN Ma 10.8	*Tamandua* sp.	18,6	21,5	0,865116279
MACN Ma 25911	*Tamandua* sp.	18,2	21	0,866666667
AMNH 102730	*Thinobadistes segnis*	75,4	83,9	0,898688915
UF 21509	*Thinobadistes segnis*	76,3	82,1	0,929354446
AMNH 102723	*Thinobadistes segnis*	79,4	82,5	0,962424242
AMNH 102724	*Thinobadistes segnis*	81,9	79,6	1,028894472
UF 209900	*Thinobadustes wetzeli*	78,4	80,5	0,973913043
UF 17397	*Thinobadustes wetzeli*	90,5	87,9	1,029579067

Raw data of character 300 – Ratio HEMP/HDEW, (0) ≥ 0.36; (1) < 0.36.

CODE	TAXON	HEMP	HDEW	HEMP/HDEW
MACN Ma 4.125	*Bradypus* sp.	9,6	30,6	0,31372549
FMNH P14238	*Catonyx* sp.	48,3	234,4	0,20605802
AMNH 1663	*Euphractus* sp.	7,9	27,8	0,284172662
MNHN.F.PAM 141 (A.C. 7067)	*Glossotherium robustum*	13,2	189	0,06984127
MNHN.F.PAM 118	*Glossotherium robustum*	19,3	218,5	0,088329519
MNHN.F.PAM 122	*Glossotherium robustum*	34,6	209,1	0,165471066
AMNH 11307	*Glossotherium robustum*	31,9	191,1	0,16692831
MNHN.F.PAM 123	*Glossotherium robustum*	29,2	168,8	0,172985782
MNHN.F.PAM 141 (A.C. 7068)	*Glossotherium robustum*	62,3	177,3	0,351381839
MACN Pv 17572	*Glossotherium robustum*	36,8	193	0,190673575
MNHN.F.TAR 767	*Glossotherium tarijense*	28,4	217,4	0,130634775
VF-26	*Glossotherium tropicorum*	49,4	178,9	0,276131917
FMNH P13130	*Hapalops* sp.	24,4	66,5	0,366917293
MACN Pv 11766	*Hapalops* sp.	24,8	58,6	0,423208191
FMNH P13133	*Hapalops* sp.	25,2	56,4	0,446808511
MNHN.F.PAM 98	*Lestodon armatus*	33,1	265	0,12490566
MLP 3-831	*Lestodon armatus*	41,1	250	0,1644
FMNH P14229	*Lestodon armatus*	47,3	240	0,197083333
FMNH P14228	*Lestodon armatus*	52,6	263	0,2
MACN Pv 17182	*Lestodon armatus*	52,5	235	0,223404255
MLP 3-18	*Lestodon armatus*	54,3	230	0,236086957
MNHN.F.TAR 778	*Lestodon armatus*	69	269,7	0,255839822
AMNH 53855	*Manis gigantea*	20,5	54,5	0,376146789
MACN Pv 13797	*Mylodon darwinii*	35,2	205	0,171707317
MACN Ma 31.132	*Myrmecophaga* sp.	46,5	86,3	0,538818076
FMNH P14723	*Paramylodon harlani*	44,7	248,9	0,179590197
UF 84136	*Paramylodon harlani*	47,1	231,1	0,203807875
AMNH 16896	*Paramylodon harlani*	54,8	238,7	0,229576875
MACN Pv 8735 cast	*Paramylodon harlani*	68,9	290	0,237586207
UF 68581	*Paramylodon harlani*	51,1	201,1	0,254102437
FMNH P14274	*Scelidotherium* sp.	32	239,1	0,133835215
MACN Pv 6964	*Scelidotherium* sp.	30	182	0,164835165
MACN Pv 7150	*Scelidotherium* sp.	40,7	207	0,196618357
FMNH P14301	*Scelidotherium* sp.	82	273	0,3003663
MNHN-Bol V 3792	*Simomylodon uccasamamensis*	17,3	128,9	0,134212568
MNHN.F.AYO 110	*Simomylodon uccasamamensis*	23,9	122	0,195901639
MNHN-Bol V 11795	*Simomylodon uccasamamensis*	21,5	107,9	0,199258573

MNHN-Bol V 3303	*Simomylodon uccasamamensis*	22,9	110,5	0,207239819
MNHN-Bol V 12949	*Simomylodon uccasamamensis*	21,7	103,6	0,209459459
MNHN.F.AYO 222	*Simomylodon uccasamamensis*	27,5	113,2	0,242932862
MACN Ma 25911	*Tamandua* sp.	19,3	50,1	0,385229541
MACN Ma 10.8	*Tamandua* sp.	19,4	42,8	0,453271028
MACN Ma 33.255	*Tamandua* sp.	22,7	47,3	0,479915433
AMNH 102724	*Thinobadistes segnis*	38,5	177,4	0,217023675
AMNH 102730	*Thinobadistes segnis*	40,1	177,9	0,225407532
AMNH 102723	*Thinobadistes segnis*	49,1	182,7	0,268746579
UF 21509	*Thinobadistes segnis*	65,6	203,6	0,322200393
UF 209900	*Thinobadustes* cf *wetzeli*	44,9	179,9	0,249583102

Raw data of character 314 – Ratio APDR/RL: (0) ≤ 0.160; (1) > 0.160, ≤ 0.245; (2) > 0.245.

CODE	TAXON	RL	APDR	APDR/RL
MACN Ma 4.125	*Bradypus* sp.	152,7	7,4	0,048461035
FMNH P14238	*Catonyx* sp.	364,3	82,9	0,227559704
FMNH P14225	*Catonyx* sp.	300,2	72,4	0,241172552
AMNH 1663	*Euphractus* sp.	42	7	0,166666667
MNHN.F.PAM s/n (2)	*Glossotherium robustum*	268,7	54	0,200967622
MNHN.F.PAM s/n (1)	*Glossotherium robustum*	266,8	56,6	0,212143928
MACN Pv 91	*Glossotherium robustum*	264	64,8	0,245454545
VF-28	*Glossotherium tropicorum*	263,5	56	0,212523719
FMNH P13130	*Hapalops* sp.	144,1	21,1	0,146426093
FMNH P13133	*Hapalops* sp.	129,5	19,3	0,149034749
MACN Pv 14616	*Lestodon armatus*	365	86,5	0,236986301
MACN Pv 14615	*Lestodon armatus*	374	92,9	0,248395722
FMNH P14228	*Lestodon armatus*	383	97,8	0,25535248
MLP 40-IV-26	*Lestodon armatus*	362	93,1	0,25718232
MNHN.F.PAM s/n (3)	*Lestodon armatus*	341,5	92,4	0,27057101
MACN Pv 14653	*Lestodon armatus*	378	109,6	0,28994709
MACN Pv 14663	*Lestodon armatus*	345	105,5	0,305797101
FMNH P15492	*Lestodon armatus*	350	107,9	0,308285714
AMNH 53855	*Manis gigantea*	73,4	15,5	0,211171662
FMNH P14288	*Mylodon darwinii*	300	51,5	0,171666667
MACN Ma 31.132	*Myrmecophaga* sp.	177,4	18	0,101465614
FMNH P13129	*Nematherium* sp.	134,4	23,9	0,177827381
UF 80163	*Paramylodon harlani*	253,6	42,2	0,166403785
FMNH P14723	*Paramylodon harlani*	302	67,1	0,22218543
AMNH 16896	*Paramylodon harlani*	287,6	65,7	0,228442281
FMNH P14301	*Scelidotherium* sp.	413	90,2	0,218401937
MACN Pv 6964	*Scelidotherium* sp.	290	68,1	0,234827586
MACN Pv 79	*Scelidotherium* sp.	302	71,4	0,236423841
MACN Pv 8854	*Scelidotherium* sp.	275	54,5	0,198181818
MNHN-Bol V 3375	*Simomylodon uccasamamensis*	201,1	44,7	0,222277474
MNHN.F.AYO 180	*Simomylodon uccasamamensis*	189,2	47,6	0,251585624
MACN Ma 25911	*Tamandua* sp.	79,6	9,6	0,120603015
MACN Ma 33.255	*Tamandua* sp.	78,2	10,8	0,138107417
MACN Ma 10.8	*Tamandua* sp.	71,4	10,8	0,151260504
AMNH 102732	*Thinobadistes* sp.	264,1	65,1	0,246497539
UF 21509	*Thinobadistes* sp.	265,5	66	0,248587571
AMNH 102733	*Thinobadistes* sp.	231,7	61,8	0,266724212

Raw data of character 315 – Radial head shape: (0) deep anteroposteriorly and narrow transversely, RHW/RHL ≤ 0.63; (1) ovoid, RHW/RHL > 0.63, ≤ 0.82; (2) circular or approximately so, RHW/RHL > 0.82, ≤ 1.0.

CODE	TAXON	RHL	RHW	RHW/RHL
MACN Ma 4.125	*Bradypus* sp.	11,7	12,1	1,034188034
FMNH P14225	*Catonyx* sp.	63,3	52	0,821484992
FMNH P14238	*Catonyx* sp.	65,1	57,7	0,886328725
AMNH 1663	*Euphractus* sp.	11,3	5,2	0,460176991
MNHN.F.PAM s/n (2)	*Glossotherium robustum*	68,1	43,3	0,635829662
MACN Pv 10606	*Glossotherium robustum*	61,8	47,1	0,762135922
MACN Pv 91	*Glossotherium robustum*	62,1	50,8	0,818035427
MNHN.F.PAM s/n (1)	*Glossotherium robustum*	63	52	0,825396825
VF-28	*Glossotherium tropicorum*	55	39	0,709090909
FMNH P13123	*Hapalops* sp.	19,6	13,7	0,698979592
FMNH P13130	*Hapalops* sp.	22,6	15,8	0,699115044
FMNH P13133	*Hapalops* sp.	21,3	16,9	0,79342723
MNHN.F.PAM s/n (3)	*Lestodon armatus*	78	49,3	0,632051282
FMNH P15492	*Lestodon armatus*	97,1	67,3	0,693099897
FMNH P14228	*Lestodon armatus*	97,7	71,8	0,734902764
MACN Pv 14616	*Lestodon armatus*	82,5	63,8	0,773333333
MACN Pv 14663	*Lestodon armatus*	82,2	65,5	0,796836983
MACN Pv 14653	*Lestodon armatus*	85,1	69,1	0,811985899
MACN Pv 14615	*Lestodon armatus*	74,9	61,9	0,826435247
MLP 40-IV-26	*Lestodon armatus*	75,6	66,6	0,880952381
AMNH 53855	*Manis gigantea*	18,3	13,3	0,726775956
FMNH P14288	*Mylodon darwinii*	71,6	50,4	0,703910615
MACN Ma 31.132	*Myrmecophaga* sp.	20,5	17,3	0,843902439
FMNH P13129	*Nematherium* sp.	21,9	18,1	0,826484018
AMNH 16896	*Paramylodon harlani*	74,1	55,9	0,754385965
UF 80163	*Paramylodon harlani*	64,4	50	0,776397516
FMNH P14723	*Paramylodon harlani*	70,4	57,8	0,821022727
FMNH P14301	*Scelidotherium* sp.	92	77,4	0,841304348
MACN Pv 6964	*Scelidotherium* sp.	58,5	52,2	0,892307692
MACN Pv 79	*Scelidotherium* sp.	56,4	55,1	0,976950355
MACN Pv 8854	*Scelidotherium* sp.	52,8	52,5	0,994318182
MNHN-Bol V 6573	*Simomylodon uccasamamensis*	39,5	27,7	0,701265823
MNHN.F.AYO 179	*Simomylodon uccasamamensis*	36,5	27,5	0,753424658
MNHN.F.VIZ 16	*Simomylodon uccasamamensis*	33,5	26,9	0,802985075
MNHN.F.AYO 126	*Simomylodon uccasamamensis*	35,7	29,1	0,81512605
MNHN.F.AYO 180	*Simomylodon uccasamamensis*	33,3	27,5	0,825825826
MNHN-Bol V 3375	*SImomylodon uccasamamensis*	33,4	27,6	0,826347305
MACN Ma 10.8	*Tamandua* sp.	12,1	9,1	0,752066116
MACN Ma 33.255	*Tamandua* sp.	11,4	9	0,789473684
MACN Ma 25911	*Tamandua* sp.	13	10,3	0,792307692
AMNH 102732	*Thinobadistes segnis*	50,9	44,1	0,866404715

Raw data of character 321 – Ratio UPCDE/UL: (0) ≤ 0.55; (1) > 0.55, ≤ 0.75; (2) > 0.75.

CODE	TAXON	UL	UPCDE	UPCDE/UL
MACN Ma 4.125	*Bradypus* sp.	163,4	153,5	0,939412485
MACN Pv 16639	*Catonyx* sp.	384	230	0,598958333
FMNH P14238	*Catonyx* sp.	467	299,3	0,640899358
FMNH P14225	*Catonyx* sp.	386,3	255,9	0,662438519
AMNH 1663	*Euphractus* sp.	70,4	38,1	0,541193182
MACN Pv 91	*Glossotherium robustum*	342	210	0,614035088
MACN Pv 12095	*Glossotherium robustum*	345	212	0,614492754
MNHN.F.PAM 141 (A.C. 7069)	*Glossotherium robustum*	350,6	228,2	0,650884199
MNHN.F.PAM 141 (A.C. 7070)	*Glossotherium robustum*	350,3	234,8	0,670282615
MACN Pv 14070	*Glossotherium robustum*	343	232	0,67638484
VF-24	*Glossotherium tropicorum*	314,6	217,3	0,690718373
FMNH P13130	*Hapalops* sp.	163,8	123,4	0,753357753
MACN Pv 9479	*Lestodon armatus*	409	255	0,623471883

MLP 3-83	*Lestodon armatus*	464	290	0,625
MLP 3-133	*Lestodon armatus*	430	272	0,63255814
MACN Pv 9480	*Lestodon armatus*	384	245	0,638020833
MNHN.F.PAM 101	*Lestodon armatus*	500	340	0,68
AMNH 53855	*Manis gigantea*	106,4	75,5	0,709586466
FMNH P14288	*Mylodon darwinii*	380	228	0,6
MACN Pv 14106	*Mylodon darwinii*	366	232	0,633879781
MACN Ma 31.132	*Myrmecophaga* sp.	222,6	166	0,745732255
FMNH P13129	*Nematherium* sp.	152,5	102,6	0,672786885
UF 10922	*Paramylodon garbanii*	269,8	166,4	0,61675315
UF 65857	*Paramylodon harlani*	336,1	199	0,592085689
FMNH P14723	*Paramylodon harlani*	395,4	243	0,614567527
AMNH 16896	*Paramylodon harlani*	378,2	247,5	0,654415653
FMNH P14301	*Scelidotherium* sp.	514	297,2	0,578210117
MACN Pv 13927	*Scelidotherium* sp.	430	255	0,593023256
MACN Pv 13825	*Scelidotherium* sp.	370	220	0,594594595
MLP 3-766	*Scelidotherium* sp.	410	257	0,626829268
FMNH P14274	*Scelidotherium* sp.	407	255,8	0,628501229
MACN Pv 6964	*Scelidotherium* sp.	355	225	0,633802817
MACN Pv 7150	*Scelidotherium* sp.	364	243	0,667582418
MNHN-Bol V 3717	*Simomylodon uccasamamensis*	199,8	118,9	0,595095095
MACN Ma 25911	*Tamandua* sp.	115	76,1	0,66173913
MACN Ma 10.8	*Tamandua* sp.	104,6	71,3	0,681644359
MACN Ma 33.255	*Tamandua* sp.	107,7	76,9	0,714020427
UF 21509	*Thinobadistes segnis*	338	205,3	0,60739645
UF 93052	*Thinobadustes wetzeli*	343,3	206,2	0,600640839

Raw data of character 322 – Ratio THU/UL: (0) < 0.12; (1) ≥ 0.12, < 0.20; (2) ≥ 0.20, ≤ 0.26; (3) > 0.26.

CODE	TAXON	UL	THU	THU/UL
MCN 170-72V	*Bolivartherium urumaquensis*	163,1	51,3	0,314530963
MACN Ma 4.125	*Bradypus* sp.	163,4	5,3	0,032435741
FMNH P14238	*Catonyx* sp.	467	118,4	0,253533191
FMNH P14225	*Catonyx* sp.	386,3	97,2	0,251617914
MACN Pv 16639	*Catonyx* sp.	384	83,5	0,217447917
AMNH 1663	*Euphractus* sp.	70,4	9,7	0,137784091
MACN Pv 91	*Glossotherium robustum*	342	110,5	0,323099415
MACN Pv 12095	*Glossotherium robustum*	345	115,3	0,334202899
MNHN.F.PAM 141 (A.C. 7070)	*Glossotherium robustum*	350,3	101,3	0,289180702
MNHN.F.PAM 141 (A.C. 7069)	*Glossotherium robustum*	350,6	104,7	0,298630918
MACN Pv 14070	*Glossotherium robustum*	343	109,5	0,319241983
VF-24	*Glossotherium tropicorum*	314,6	91,9	0,292116974
FMNH P13130	*Hapalops* sp.	163,8	16,5	0,100732601
MACN Pv 9479	*Lestodon armatus*	409	116,6	0,285085575
MACN Pv 9480	*Lestodon armatus*	384	115,4	0,300520833
MNHN.F.PAM 101	*Lestodon armatus*	500	121,9	0,2438
MLP 3-83	*Lestodon armatus*	464	105,5	0,22737069
MLP 3-133	*Lestodon armatus*	430	124,4	0,289302326
AMNH 53855	*Manis gigantea*	106,4	14,5	0,136278195
FMNH P14288	*Mylodon darwinii*	380	115	0,302631579
MACN Pv 14106	*Mylodon darwinii*	366	96,9	0,264754098
MACN Ma 31.132	*Myrmecophaga* sp.	222,6	21,6	0,09703504
FMNH P13129	*Nematherium* sp.	152,5	18,7	0,122622951
UF 10922	*Paramylodon garbanii*	269,8	80,4	0,297998517
UF 65857	*Paramylodon harlani*	336,1	96,2	0,286224338
AMNH 16896	*Paramylodon harlani*	378,2	135,7	0,358804865
FMNH P14723	*Paramylodon harlani*	395,4	172,8	0,437025797
FMNH P14274	*Scelidotherium* sp.	407	107,2	0,263390663
MACN Pv 13927	*Scelidotherium* sp.	430	92,4	0,214883721
MLP 3-766	*Scelidotherium* sp.	410	89,2	0,217560976
MACN Pv 7150	*Scelidotherium* sp.	364	86,8	0,238461538
MACN Pv 6964	*Scelidotherium* sp.	355	89,6	0,252394366

MACN Pv 13825	*Scelidotherium* sp.	370	97,2	0,262702703
FMNH P14301	*Scelidotherium* sp.	514	136,2	0,264980545
MNHN-Bol V 3717	*Simomylodon uccasamamensis*	199,8	54,6	0,273273273
MACN Ma 10.8	*Tamandua* sp.	104,6	9,3	0,088910134
MACN Ma 25911	*Tamandua* sp.	115	10,9	0,094782609
MACN Ma 33.255	*Tamandua* sp.	107,7	10,6	0,098421541
UF 21509	*Thinobadistes segnis*	338	72	0,213017751
UF 93052	*Thinobadustes wetzeli*	343,3	95,6	0,278473638

Raw data of character 331 – Scaphoid, ratio between its minimum and maximum diameters: (0) < 0.64; (1) ≥ 0.64.

CODE	TAXON	max diam	min diam	min/max
FMNH P14225	*Catonyx* sp.	67,8	44,1	0,650442478
MACN Pv 11331	*Glossotherium robustum*	63	30,6	0,485714286
MNHN.F.PAM 141 (A.C. 7072)	*Glossotherium robustum*	54,3	38	0,699815838
MNHN.F.PAM 141 (A.C. 7089)	*Glossotherium robustum*	51,5	37,6	0,730097087
MNHN.F.PAM 141 (A.C. 7167)	*Lestodon armatus*	77,8	45,8	0,588688946
FMNH P14288	*Mylodon darwinii*	64,7	32,9	0,508500773
FMNH P13129	*Nematherium* sp.	15,1	9,9	0,655629139
MNHN.F.DES 231(2)	*Octodontotherium grande*	55	26,3	0,478181818
UF 10922	*Paramylodon garbanii*	48,7	24,7	0,507186858
UF 87101	*Paramylodon harlani*	60,5	29	0,479338843
UF 80782	*Paramylodon harlani*	59,2	30,1	0,508445946
UF 87103	*Paramylodon harlani*	77,2	40,8	0,528497409
UF 82207	*Paramylodon harlani*	66,7	35,8	0,536731634
AMNH 16896-2	*Paramylodon harlani*	76,2	45,9	0,602362205
FMNH P14723	*Paramylodon harlani*	74,3	45,8	0,616419919
AMNH 16896-1	*Paramylodon harlani*	76,8	48,1	0,626302083
FMNH P14301	*Scelidotherium* sp.	80,9	54,6	0,674907293
FMNH P14274	*Scelidotherium* sp.	63,4	43,9	0,692429022
MNN AYO 180	*Simomylodon uccasamamensis*	50	26,7	0,534
UF 21509	*Thinobadistes segnis*	65,1	30,5	0,468509985
AMNH 102751	*Thinobadistes segnis*	62,7	34,6	0,551834131
AMNH 102753	*Thinobadistes segnis*	61,7	37,5	0,607779579

Raw data of character 333 – Cuneiform shape, ratio between dorsopalmar and mediolateral widths: (0) < 0.65; (1) ≥ 0.65, < 0.87; (2) ≥ 0.87.

CODE	TAXON	Medio-lat	Tran	Dors-palm/Medio-lat
FMNH P14225	*Catonyx* sp.	57	65,4	0,871559633
FMNH P14238	*Catonyx* sp.	59,8	62	0,964516129
MACN Pv 11421	*Glossotherium robustum*	52,9	77,7	0,680823681
MNHN.F.PAM 141 (A.C. 7091)	*Glossotherium robustum*	50,7	60	0,845
MNHN.F.PAM 141 (A.C. 7074)	*Glossotherium robustum*	51,3	57,7	0,889081456
FMNH P13129	*Nematherium* sp.	10,6	16,4	0,646341463
UF 10922	*Paramylodon garbanii*	29,8	36,2	0,82320442
AMNH 16896-2	*Paramylodon harlani*	52,6	66,2	0,794561934
AMNH 16896-1	*Paramylodon harlani*	57,5	69,1	0,832127352
FMNH P14723	*Paramylodon harlani*	59,1	69,5	0,850359712
UF 65836	*Paramylodon harlani*	53,6	61,6	0,87012987
FMNH P14274	*Scelidotherium* sp.	58,3	58,7	0,99318569
MNHN.F.AYO 109	*Simomylodon uccasamamensis*	31,7	37,2	0,852150538
MNHN-Bol V 6573	*Simomylodon uccasamamensis*	27,8	32,5	0,855384615
AMNH 102779	*Thinobadistes segnis*	43,1	49,4	0,872469636
AMNH 102769	*Thinobadistes segnis*	50,5	54,1	0,933456562
UF 21509	*Thinobadistes segnis*	40,1	41,4	0,968599034

Raw data of character 334 – Cuneiform shape, ratio between proximodistal length and mediolateral width: (0) < 0.65; (1) ≥ 0.65.

CODE	TAXON	Medio-lat	Prox-dist	Prox-dist/Medio-lat
FMNH P14225	*Catonyx* sp.	65,4	54,3	0,830275229
FMNH P14238	*Catonyx* sp.	62	52	0,838709677
MACN Pv 11421	*Glossotherium robustum*	77,7	56	0,720720721
MNHN.F.PAM 141 (A.C. 7091)	*Glossotherium robustum*	60	48	0,8
MNHN.F.PAM 141 (A.C. 7074)	*Glossotherium robustum*	57,7	51,7	0,896013865
FMNH P13129	*Nematherium* sp.	16,4	9,3	0,567073171
UF 10922	*Paramylodon garbanii*	36,2	31,4	0,867403315
FMNH P14723	*Paramylodon harlani*	69,5	49,6	0,713669065
AMNH 16896-1	*Paramylodon harlani*	69,1	49,4	0,714905933
UF 65836	*Paramylodon harlani*	61,6	47,1	0,76461039
AMNH 16896-2	*Paramylodon harlani*	66,2	55,2	0,833836858
FMNH P14274	*Scelidotherium* sp.	58,7	48,2	0,821124361
MNHN.F.AYO 109	*Simomylodon uccasamamensis*	37,2	31,3	0,841397849
MNHN-Bol V 6573	*Simomylodon uccasamamensis*	32,5	29,3	0,901538462
AMNH 102769	*Thinobadistes segnis*	54,1	45,3	0,837338262
AMNH 102779	*Thinobadistes segnis*	49,4	43,4	0,87854251
UF 21509	*Thinobadistes segnis*	41,4	37,2	0,898550725

Raw data of character 335 – Cuneiform shape, ratio between proximodistal and dorsopalmar widths: (0) < 0.95; (1) ≥ 0.95.

CODE	TAXON	Dors-palm	Prox-dist	Prox-dist/Dors-palm
FMNH P14238	*Catonyx* sp.	59,8	52	0,869565217
FMNH P14225	*Catonyx* sp.	57	54,3	0,952631579
MNHN.F.PAM 141 (A.C. 7091)	*Glossotherium robustum*	50,7	48	0,946745562
MNHN.F.PAM 141 (A.C. 7074)	*Glossotherium robustum*	51,3	51,7	1,007797271
MACN Pv 11421	*Glossotherium robustum*	52,9	56	1,058601134
FMNH P13129	*Nematherium* sp.	10,6	9,3	0,877358491
UF 10922	*Paramylodon garbanii*	29,8	31,4	1,053691275
FMNH P14723	*Paramylodon harlani*	59,1	49,6	0,839255499
AMNH 16896-1	*Paramylodon harlani*	57,5	49,4	0,859130435
UF 65836	*Paramylodon harlani*	53,6	47,1	0,878731343
AMNH 16896-2	*Paramylodon harlani*	52,6	55,2	1,049429658
FMNH P14274	*Scelidotherium* sp.	58,3	48,2	0,826758148
MNHN.F.AYO 109	*Simomylodon uccasamamensis*	31,7	31,3	0,987381703
MNHN-Bol V 6573	*Simomylodon uccasamamensis*	27,8	29,3	1,053956835
AMNH 102769	*Thinobadistes segnis*	50,5	45,3	0,897029703
UF 21509	*Thinobadistes segnis*	40,1	37,2	0,927680798
AMNH 102779	*Thinobadistes segnis*	43,1	43,4	1,006960557

Raw data of character 336 – Unciform shape, ratio between proximodistal and mediolateral widths: (0) < 1.0; (1) ≥ 1.0.

CODE	TAXON	*Medio-lat*	*Prox-dist*	Prox-dist/Medio-lat
FMNH P14225	*Catonyx* sp.	64,5	57,9	0,897674419
MACN Pv 10120 (R)	*Glossotherium robustum*	62,9	64,5	1,025437202
MACN Pv 17572	*Glossotherium robustum*	49,5	54,3	1,096969697
MNHN.F.PAM 141 (A.C. 7076)	*Glossotherium robustum*	52,4	62,3	1,188931298
MNHN.F.PAM 141 (A.C. 7094)	*Glossotherium robustum*	52,1	62,5	1,199616123
FMNH P14288	*Mylodon darwinii*	55,8	71,7	1,284946237
FMNH P13129	*Nematherium* sp.	13,1	9,9	0,755725191
MNHN.F.DES 216	*Octodontotherium grande*	41,5	29,6	0,713253012
FMNH P13368	*Octodontotherium grande*	41	31,3	0,763414634
FMNH P13368	*Octodontotherium grande*	40	35,1	0,8775
MNHN.F.DES 229	*Octodontotherium grande*	40,3	38,8	0,962779156
FMNH P14723	*Paramylodon harlani*	69,1	68,6	0,99276411
AMNH 16896-2	*Paramylodon harlani*	68,6	73,3	1,06851312

AMNH 16896-1	*Paramylodon harlani*	66,6	73,2	1,099099099
UF 87104	*Paramylodon harlani*	65,1	78,3	1,202764977
UF 87101	*Paramylodon harlani*	56,3	77,8	1,381882771
FMNH P14274	*Scelidotherium* sp.	53,8	48,1	0,894052045
MNHN-Bol V 12953	*Simomylodon uccasamamensis*	33,7	38,5	1,142433234
UF 21509	*Thinobadistes segnis*	51,5	41,8	0,811650485
AMNH 102807	*Thinobadistes segnis*	56,6	57,1	1,008833922
AMNH 102802	*Thinobadistes segnis*	44,1	45,6	1,034013605

Raw data of character 341 – Metacarpal 3 shape (ratio between mediolateral width at the middle of shaft and total length): (0) ≤ 0.37; (1) > 0.37, < 0.52; (2) ≥ 0.52.

CODE	TAXON	Length	MediolatW	MediolatW/Length
FMNH P14238	*Catonyx* sp.	108,5	56,8	0,523502304
FMNH P14225	*Catonyx* sp.	103,6	58,9	0,568532819
MACN Pv 11331	*Glossotherium robustum*	81,8	35,6	0,435207824
MNHN.F.PAM 141 (A.C. 7097)	*Glossotherium robustum*	81,1	37,6	0,463625154
MACN Pv 17572	*Glossotherium robustum*	81,9	40,9	0,499389499
MNHN.F.PAM 141 (A.C. 7078)	*Glossotherium robustum*	81,1	41,4	0,510480888
AMNH 53855	*Manis gigantea*	22,6	10,4	0,460176991
AMU-CURS 109	*Mirandabradys zabasi*	136,2	33,1	0,243024963
FMNH P14288	*Mylodon darwinii*	100,2	29,1	0,290419162
FMNH P13258	*Nematherium* sp.	29,3	13,4	0,457337884
FMNH P13129	*Nematherium* sp.	26	15,2	0,584615385
FMNH P13468	*Octodontotherium grande*	76,8	22,4	0,291666667
MNHN.F.DES 255	*Orophodon hapaloides*	45,7	19,6	0,428884026
UF 10922	*Paramylodon garbanii*	68,3	24,6	0,360175695
AMNH 16896-2	*Paramylodon harlani*	95,8	40,1	0,418580376
UF 65831	*Paramylodon harlani*	93,1	40,3	0,432867884
AMNH 16896-1	*Paramylodon harlani*	102,1	44,8	0,438785504
FMNH P14723	*Paramylodon harlani*	93,4	45,4	0,48608137
FMNH P14274	*Scelidotherium* sp.	108	56	0,518518519
FMNH P14301	*Scelidotherium* sp.	124,6	64,7	0,519261637
MNHN.F.VIZ 5	*Simomylodon uccasamamensis*	67,7	18,7	0,276218612
MNHN-Bol V 12927	*Simomylodon uccasamamensis*	62,1	21	0,338164251
MNHN-Bol V 6573	*Simomylodon uccasamamensis*	64,6	23,1	0,357585139
MNHN.F.VIZ 27	*Simomylodon uccasamamensis*	66,8	23,9	0,357784431
MNHN-Bol V 6564	*Simomylodon uccasamamensis*	71,9	26	0,361613352
UF 21509	*Thinobadistes segnis*	91,3	32,1	0,351588171
AMNH 102820	*Thinobadistes segnis*	89,3	36,7	0,410974244
AMNH 102831	*Thinobadistes segnis*	88,5	42,2	0,476836158

Raw data of character 344 – Femur shape (ratio between mediolateral width at midshaft and total length): (0) long and narrow, TDF/FL < 0.20; (1) intermediate, TDF/FL ≥ 0.20, < 0.35; (2) short and broad, TDF/FL ≥ 0.35.

CODE	TAXON	FL	TDF	TDF/FL
MACN Ma 4.125	*Bradypus* sp.	103,8	11,1	0,106936416
FMNH P14238	*Catonyx* sp.	555	210	0,378378378
MACN Pv 16639	*Catonyx* sp.	440	175	0,397727273
IVIC-P-2870	*Eionaletherium tanycnemius*	507,2	147,5	0,290812303
AMNH 1663	*Euphractus* sp.	78,2	12,4	0,158567775
MNHN.F.PAM 125	*Glossotherium robustum*	485,4	131,9	0,271734652
AMNH 12716	*Glossotherium robustum*	531,8	146,3	0,275103422
MNHN.F.PAM 128	*Glossotherium robustum*	493,7	155,8	0,315576261
VF-11	*Glossotherium tropicorum*	464,7	134,8	0,290079621
FMNH P13128	*Hapalops* sp.	163,1	42,5	0,260576334
MNHN.F.PAM 105	*Lestodon armatus*	758,4	204,6	0,269778481
MLP 3-17	*Lestodon armatus*	560	160	0,285714286
AMNH 53855	*Manis gigantea*	141,1	22,4	0,158752658
AMU-CURS 29	*Mirandabradys socorrensis*	568,6	168,1	0,29563841

AMU-CURS 157	*Mirandabradys urumaquensis*	585,3	148,2	0,253203485
AMU-CURS 127	*Mirandabradys zabasi*	526,3	135,5	0,257457724
MACN Ma 31.132	*Myrmecophaga* sp.	227,7	22,6	0,099253404
UF TRO 37	*Paramylodon garbanii*	341	99,4	0,291495601
UF 10922	*Paramylodon garbanii*	352,5	115,8	0,328510638
UF 64361	*Paramylodon harlani*	503,2	153,8	0,305643879
FMNH P14723	*Paramylodon harlani*	548,3	172,1	0,313879263
UF 127402	*Paramylodon harlani*	539,3	176,4	0,327090673
AMNH 16896	*Paramylodon harlani*	530,1	176,4	0,332767402
UF 65859	*Paramylodon harlani*	455,1	153,5	0,337288508
MLP 3-484	*Scelidotherium* sp.	353	132,4	0,375070822
MLP 41-V-16-3	*Scelidotherium* sp.	430	185	0,430232558
FMNH P14301	*Scelidotherium* sp.	605	233,1	0,385289256
MNHN-Bol V 3299	*Simomylodon uccasamamensis*	343,6	94	0,273573923
MNHN-Bol V 12518	*Simomylodon uccasamamensis*	307,2	85,3	0,277669271
MNHN-Bol V 12953	*Simomylodon uccasamamensis*	337	95,3	0,282789318
MNHN-Bol V 12277	*Simomylodon uccasamamensis*	337,8	99,7	0,295145056
MACN Ma 10.8	*Tamandua* sp.	99	14,3	0,144444444
MACN Ma 25911	*Tamandua* sp.	108,6	16	0,14732965
MACN Ma 33.255	*Tamandua* sp.	105,7	16	0,151371807
UF 21509	*Thinobadistes segnis*	440,3	114,1	0,259141494
AMNH 103010	*Thinobadistes segnis*	441,3	115,9	0,262633129
AMNH 103013	*Thinobadistes segnis*	423,4	117,1	0,276570619

Raw data of character 345 – Ratio FCW/FL: (0) ≤ 0.27; (1) > 0.27, ≤ 0.36; (2) > 0.36.

CODE	TAXON	FL	FCW	FCW/FL
MACN Ma 4.125	*Bradypus* sp.	103,8	20,5	0,197495183
FMNH P14238	*Catonyx* sp.	555	200	0,36036036
MACN Pv 16639	*Catonyx* sp.	440	163	0,370454545
IVIC-P-2870	*Eionaletherium tanycnemius*	507,2	146,1	0,28805205
AMNH 1663	*Euphractus* sp.	78,2	18,2	0,232736573
MNHN.F.PAM 125	*Glossotherium robustum*	485,4	134,5	0,277091059
AMNH 12716	*Glossotherium robustum*	531,8	158,9	0,29879654
MNHN.F.PAM 128	*Glossotherium robustum*	493,7	159	0,32205793
VF-11	*Glossotherium tropicorum*	464,7	136,1	0,292877125
FMNH P13128	*Hapalops* sp.	163,1	45,4	0,278356836
MLP 3-17	*Lestodon armatus*	560	195	0,348214286
MNHN.F.PAM 105	*Lestodon armatus*	758,4	215,7	0,284414557
AMNH 53855	*Manis gigantea*	141,1	37,6	0,266477675
AMU-CURS 29	*Mirandabradys socorrensis*	568,6	160,6	0,282448118
AMU-CURS 157	*Mirandabradys urumaquensis*	585,3	142,5	0,24346489
MACN Ma 31.132	*Myrmecophaga* sp.	227,7	44,8	0,19675011
UF TRO 37	*Paramylodon garbanii*	341	110,8	0,324926686
UF 10922	*Paramylodon garbanii*	352,5	118,8	0,337021277
UF 127402	*Paramylodon harlani*	539,3	176,3	0,326905248
UF 64361	*Paramylodon harlani*	503,2	167	0,331875994
UF 65859	*Paramylodon harlani*	455,1	151,4	0,332674138
FMNH P14723	*Paramylodon harlani*	548,3	193	0,351997082
AMNH 16896	*Paramylodon harlani*	530,1	190	0,358422939
MLP 41-V-16-3	*Scelidotherium* sp.	430	156,4	0,36372093
MLP 3-484	*Scelidotherium* sp.	353	150,4	0,426062323
FMNH P14301	*Scelidotherium* sp.	605	242	0,4
MNHN-Bol V 3299	*Simomylodon uccasamamensis*	343,6	101,9	0,296565774
MNHN-Bol V 12277	*Simomylodon uccasamamensis*	337,8	103,2	0,305506217
MNHN-Bol V 12518	*Simomylodon uccasamamensis*	307,2	94,4	0,307291667
MNHN-Bol V 12953	*Simomylodon uccasamamensis*	337	105,4	0,312759644
MACN Ma 33.255	*Tamandua* sp.	105,7	22,2	0,210028382
MACN Ma 10.8	*Tamandua* sp.	99	22,3	0,225252525
MACN Ma 25911	*Tamandua* sp.	108,6	27,6	0,254143646
AMNH 013010	*Thinobadistes segnis*	441,3	129,7	0,293904373
UF 21509	*Thinobadistes segnis*	440,3	133,3	0,302748126
AMNH 103013	*Thinobadistes segnis*	423,4	132,1	0,311998111

Raw data of character 346 – Ratio LCL/MCL: (0) ≥ 0.75; (1) < 0.75.

CODE	TAXON	MCL	LCL	LCL/MCL
IVIC-P-2917	*Baraguatherium takumara*	87,9	63,3	0,720136519
MACN Ma 4.125	*Bradypus* sp.	14,2	13,6	0,957746479
FMNH P14238	*Catonyx* sp.	144	100,4	0,697222222
IVIC-P-2870	*Eionaletherium tanycnemius*	82,3	80,1	0,97326853
AMNH 1663	*Euphractus* sp.	15,4	12,3	0,798701299
AMNH 12716	*Glossotherium robustum*	138,6	86,9	0,626984127
MNHN.F.PAM 125	*Glossotherium robustum*	128,2	85,6	0,667706708
MNHN.F.PAM 128	*Glossotherium robustum*	143,6	97	0,675487465
VF-11	*Glossotherium tropicorum*	126,2	86,1	0,682250396
FMNH P13128	*Hapalops* sp.	31,4	25,2	0,802547771
FMNH P13130	*Hapalops* sp.	42,8	33	0,771028037
MLP s/n1	*Lestodon armatus*	163	99,3	0,609202454
MLP 3-58	*Lestodon armatus*	180	114,9	0,638333333
MLP 3-17	*Lestodon armatus*	159	104,6	0,657861635
MLP s/n2	*Lestodon armatus*	165	98,1	0,594545455
MNHN.F.PAM 105	*Lestodon armatus*	197,7	119,7	0,605462822
AMNH 53855	*Manis gigantea*	34,2	27,3	0,798245614
AMU-CURS 29	*Mirandabradys socorrensis*	133,9	94,5	0,70575056
AMU-CURS 157	*Mirandabradys urumaquensis*	130	86,2	0,663076923
AMU-CURS 128	*Mirandabradys zabasi*	111,6	79,3	0,710573477
MACN Pv 6866	*Mylodon darwinii*	137,1	79	0,576221736
MACN Ma 31.132	*Myrmecophaga* sp.	44,1	39,5	0,89569161
UF TRO 37	*Paramylodon garbanii*	92,2	56	0,607375271
UF 10922	*Paramylodon garbanii*	93,3	59,6	0,638799571
UF 64362	*Paramylodon harlani*	117,8	70,8	0,601018676
AMNH 16896	*Paramylodon harlani*	153,5	93,7	0,610423453
UF 80039	*Paramylodon harlani*	118,7	72,9	0,614153328
FMNH P14723	*Paramylodon harlani*	155,9	95,8	0,614496472
UF 65859	*Paramylodon harlani*	132,2	83,5	0,631618759
UF 64363	*Paramylodon harlani*	126,8	80,2	0,632492114
UF 64361	*Paramylodon harlani*	130,4	82,5	0,632668712
UF 127402	*Paramylodon harlani*	153,7	99,4	0,646714379
Uf 87087	*Paramylodon harlani*	124,7	81,7	0,655172414
UF 80164	*Paramylodon harlani*	124	83,1	0,67016129
MLP 3-484	*Scelidotherium* sp.	75,4	91,8	1,217506631
MLP 41-V-16-3	*Scelidotherium* sp.	82,6	106,4	1,288135593
FMNH P14301	*Scelidotherium* sp.	163,1	116	0,71122011
MNHN-Bol V 10919	*Simomylodon uccasamamensis*	80,9	49,2	0,60815822
MNHN-Bol V 12518	*Simomylodon uccasamamensis*	77,3	48,7	0,630012937
MNHN-Bol V 3299	*Simomylodon uccasamamensis*	85,2	55,1	0,646713615
MNHN-Bol V 12518(2)	*Simomylodon uccasamamensis*	74,2	49,2	0,663072776
MNHN-Bol V 12277	*Simomylodon uccasamamensis*	82,3	54,6	0,663426488
MNHN-Bol V 12953	*Simomylodon uccasamamensis*	84,6	56,8	0,671394799
MNHN.F.AYO 168	*Simomylodon uccasamamensis*	75	51,7	0,689333333
MNHN-Bol V 3301	*Simomylodon uccasamamensis*	83,8	59,5	0,710023866
MNHN-Bol V 3365	*Simomylodon uccasamamensis*	71,6	52,8	0,737430168
MACN Ma 25911	*Tamandua* sp.	21,8	18,8	0,862385321
MACN Ma 10.8	*Tamandua* sp.	20	18,9	0,945
MACN Ma 33.255	*Tamandua* sp.	18,8	17,8	0,946808511
UF 21509	*Thinobadistes segnis*	122,8	72,5	0,590390879
AMNH 103013	*Thinobadistes segnis*	129,5	84,7	0,654054054
AMNH 103010	*Thinobadistes segnis*	115,6	84,3	0,729238754

Raw data of character 347 – Ratio Wtroc/FL: (0) ≤ 0.30; (1) > 0.30, ≤ 0.47; (2) > 0.47.

CODE	TAXON	FL	Wtroc	Wtroc/FL
MACN Ma 4.125	*Bradypus* sp.	103,8	25,4	0,244701349
FMNH P14238	*Catonyx* sp.	555	264,4	0,476396396
MACN Pv 16639	*Catonyx* sp.	440	220	0,5

IVIC-P-2870	*Eionaletherium tanycnemius*	507,2	198,2	0,390772871
AMNH 1663	*Euphractus* sp.	78,2	30,5	0,390025575
MNHN.F.PAM 125	*Glossotherium robustum*	485,4	197,8	0,40749897
AMNH 12716	*Glossotherium robustum*	531,8	232,9	0,437946596
MNHN.F.PAM 128	*Glossotherium robustum*	493,7	231,3	0,46850314
VF-11	*Glossotherium tropicorum*	464,7	207,7	0,446955025
FMNH P13128	*Hapalops* sp.	163,1	56,8	0,348252606
MLP 3-17	*Lestodon armatus*	560	230	0,410714286
AMNH 53855	*Manis gigantea*	141,1	47,1	0,333805811
AMU-CURS 29	*Mirandabradys socorrensis*	568,6	225,4	0,396412241
AMU-CURS 157	*Mirandabradys urumaquensis*	585,3	226,2	0,386468478
AMU-CURS 127	*Mirandabradys zabasi*	526,3	209,5	0,398061942
MACN Ma 31.132	*Myrmecophaga* sp.	227,7	52,6	0,231005709
UF TRO 37	*Paramylodon garbanii*	341	150,3	0,440762463
UF 64361	*Paramylodon harlani*	503,2	214,4	0,426073132
UF 127402	*Paramylodon harlani*	539,3	250,4	0,464305581
FMNH P14723	*Paramylodon harlani*	548,3	255,5	0,465985774
UF 65859	*Paramylodon harlani*	455,1	219	0,48121292
AMNH 16896	*Paramylodon harlani*	530,1	260,8	0,491982645
MLP 3-484	*Scelidotherium* sp.	353	180	0,509915014
MLP 41-V-16-3	*Scelidotherium* sp.	430	220	0,511627907
FMNH P14301	*Scelidotherium* sp.	605	310	0,512396694
MNHN-Bol V 3299	*Simomylodon uccasamamensis*	343,6	136,2	0,396391153
MNHN-Bol V 12277	*Simomylodon uccasamamensis*	337,8	135,4	0,400828893
MNHN-Bol V 12953	*Simomylodon uccasamamensis*	337	140,8	0,417804154
MNHN-Bol V 12518	*Simomylodon uccasamamensis*	307,2	133,4	0,434244792
MACN Ma 10.8	*Tamandua* sp.	99	23,5	0,237373737
MACN Ma 25911	*Tamandua* sp.	108,6	26,3	0,242173112
MACN Ma 33.255	*Tamandua* sp.	105,7	26,7	0,252601703
AMNH 103010	*Thinobadistes segnis*	441,3	171,3	0,388171312
UF 21509	*Thinobadistes segnis*	440,3	181,5	0,412218942

Raw data of character 348 – Ratio APDF/TDF: (0) ≥ 0.54; (1) < 0.54, ≥ 0.32; (2) < 0.32.

CODE	TAXON	TDF	APDF	APDF/TDF
IVIC-P-2917	*Baraguatherium takumara*	101,8	32,8	0,322200393
MACN Ma 4.125	*Bradypus* sp.	11,1	8,1	0,72972973
FMNH P14238	*Catonyx* sp.	210	60,7	0,289047619
MACN Pv 16639	*Catonyx* sp.	175	53	0,302857143
IVIC-P-2870	*Eionaletherium tanycnemius*	147,5	29,1	0,197288136
AMNH 1663	*Euphractus* sp.	12,4	8,5	0,685483871
MNHN.F.PAM 128	*Glossotherium robustum*	155,8	70	0,449293967
AMNH 12716	*Glossotherium robustum*	146,3	69	0,47163363
MNHN.F.PAM 125	*Glossotherium robustum*	131,9	66	0,500379075
VF-11	*Glossotherium tropicorum*	134,8	54,9	0,40727003
FMNH P13128	*Hapalops* sp.	42,5	16,8	0,395294118
FMNH P13130	*Hapalops* sp.	48,4	20,5	0,423553719
MLP 3-17	*Lestodon armatus*	160	63,6	0,3975
MLP 3-58	*Lestodon armatus*	200	80,4	0,402
MLP 3-59	*Lestodon armatus*	155	68,1	0,439354839
MNHN.F.PAM 105	*Lestodon armatus*	204,6	94,2	0,460410557
AMNH 53855	*Manis gigantea*	22,4	14,8	0,660714286
AMU-CURS 29	*Mirandabradys socorrensis*	168,1	59,6	0,354550863
AMU-CURS 157	*Mirandabradys urumaquensis*	148,2	39,3	0,265182186
AMU-CURS 127	*Mirandabradys zabasi*	135,5	52,9	0,390405904
MACN Pv 6866	*Mylodon darwinii*	150	65	0,433333333
MACN Ma 31.132	*Myrmecophaga* sp.	22,6	19,4	0,85840708
UF 10922	*Paramylodon garbanii*	115,8	41,7	0,360103627
UF TRO 37	*Paramylodon garbanii*	99,4	40,8	0,410462777
UF 80164	*Paramylodon harlani*	141	51,6	0,365957447
AMNH 16896	*Paramylodon harlani*	176,4	67	0,379818594
UF 65859	*Paramylodon harlani*	153,5	59,1	0,385016287

UF 64361	*Paramylodon harlani*	153,8	59,5	0,38686606
UF 127402	*Paramylodon harlani*	176,4	69,2	0,392290249
UF 224000	*Paramylodon harlani*	135	53,2	0,394074074
FMNH P14723	*Paramylodon harlani*	172,1	68,5	0,398024404
UF 64363	*Paramylodon harlani*	152,4	64,2	0,421259843
UF 80039	*Paramylodon harlani*	150,7	64,8	0,429993364
MLP 41-V-16-3	*Scelidotherium* sp.	185	47	0,254054054
MLP 3-484	*Scelidotherium* sp.	132,4	38,9	0,293806647
FMNH P14301	*Scelidotherium* sp.	233,1	72,7	0,311883312
MNHN.F.AYO 197	*Simomylodon uccasamamensis*	96,2	35,6	0,37006237
MNHN-Bol V 10919	*Simomylodon uccasamamensis*	95,7	36,5	0,381400209
MNHN.F.AYO 167	*Simomylodon uccasamamensis*	87,6	33,5	0,382420091
MNHN-Bol V 12277	*Simomylodon uccasamamensis*	99,7	38,7	0,388164493
MNHN.F.AYO 196	*Simomylodon uccasamamensis*	70,2	28,2	0,401709402
MNHN-Bol V 11673	*Simomylodon uccasamamensis*	91	36,6	0,402197802
MNHN-Bol V 8541	*Simomylodon uccasamamensis*	91,1	36,7	0,402854007
MNHN-Bol V 3773	*Simomylodon uccasamamensis*	100,3	42,6	0,424725823
MNHN-Bol V 3365	*Simomylodon uccasamamensis*	82,1	35,4	0,431181486
MNHN-Bol V 12518	*Simomylodon uccasamamensis*	85,3	37,3	0,437280188
MNHN-Bol V 3299	*Simomylodon uccasamamensis*	94	41,6	0,442553191
MNHN-Bol V 12953	*Simomylodon uccasamamensis*	95,3	43,3	0,454354669
MNHN-Bol V 12518(2)	*Simomylodon uccasamamensis*	82,6	37,6	0,455205811
MNHN.F.AYO 166	*Simomylodon uccasamamensis*	77,5	38,4	0,495483871
MACN Ma 25911	*Tamandua* sp.	16	9,3	0,58125
MACN Ma 33.255	*Tamandua* sp.	16	9,3	0,58125
MACN Ma 10.8	*Tamandua* sp.	14,3	8,9	0,622377622
AMNH 103010	*Thinobadistes segnis*	115,9	50,3	0,433994823
AMNH 103013	*Thinobadistes segnis*	117,1	52,8	0,45089667
UF 21509	*Thinobadistes segnis*	114,1	52,5	0,460122699

Raw data of character 356 – Ratio TDT/TL: (0) < 0.18; (1) ≥ 0.18, < 0.30; (2) ≥ 0.30.

CODE	TAXON	TL	TDT	TDT/TL
MACN Ma 4.125	*Bradypus* sp.	94,5	7	0,074074074
MACN Pv 16639	*Catonyx* sp.	258	70,1	0,271705426
FMNH P14238	*Catonyx* sp.	333,5	96,8	0,290254873
IVIC-P-2870	*Eionaletherium tanycnemius*	434,6	70,4	0,161988035
AMNH 1663	*Euphractus* sp.	64,1	5,5	0,085803432
MLP 3-128	*Glossotherium robustum*	290	91,1	0,314137931
MNHN.F.R 269	*Glossotherium robustum*	245,2	77,8	0,317292007
MLP 3-114	*Glossotherium robustum*	260	90,9	0,349615385
MNHN.F.PAM 135	*Glossotherium robustum*	238,1	86,4	0,362872743
MNHN.F.PAM 132	*Glossotherium robustum*	228,3	84,3	0,369250986
MNHN.F.TAR 793	*Glossotherium tarijense*	278,8	83,1	0,298063128
MNHN.F.TAR 790	*Glossotherium tarijense*	287,6	89,8	0,312239221
MNHN.F.TAR 788	*Glossotherium tarijense*	250	78,5	0,314
MNHN.F.TAR 792	*Glossotherium tarijense*	291,9	99,8	0,34189791
MNHN.F.TAR 789	*Glossotherium tarijense*	293,7	101,3	0,344909772
MNHN.F.TAR 787	*Glossotherium tarijense*	252,7	87,3	0,345468935
FMNH P13128	*Hapalops* sp.	125,3	18,4	0,146847566
FMNH P13123	*Hapalops* sp.	132,6	12,8	0,09653092
FMNH P13130	*Hapalops* sp.	150,1	23,8	0,158560959
MNHN.F.TAR 808	*Lestodon armatus*	347,2	104,1	0,299827189
MNHN.F.TAR 771	*Lestodon armatus*	347,5	105,6	0,303884892
MLP 3-48	*Lestodon armatus*	375	114,5	0,305333333
MNHN.F.PAM 107	*Lestodon armatus*	351,4	109,7	0,312179852
MLP 3-831	*Lestodon armatus*	350	110	0,314285714
MLP 56-XII-12-2	*Lestodon armatus*	370	116,6	0,315135135
MLP 3-62	*Lestodon armatus*	300	96,5	0,321666667
MLP SN13	*Lestodon armatus*	290	94,2	0,324827586
MLP 3-20	*Lestodon armatus*	300	100	0,333333333
MLP 3-49	*Lestodon armatus*	315	106,1	0,336825397

MNHN.F.TAR 776	*Lestodon armatus*	301,2	103,6	0,343957503
AMNH 53855	*Manis gigantea*	118,9	17,7	0,148864592
AMU-CURS 29	*Mirandabradys socorrensis*	337,5	77,4	0,229333333
MACN Pv 6866	*Mylodon darwinii*	240	82,1	0,342083333
MACN Ma 31.132	*Myrmecophaga* sp.	187,4	15,7	0,083778015
FMNH P13517	*Octodontotherium grande*	269	54,6	0,202973978
UF 10922	*Paramylodon garbanii*	179,3	62,7	0,349693252
UF 65862	*Paramylodon harlani*	222,7	69,7	0,312977099
UF 64365	*Paramylodon harlani*	211	68,5	0,32464455
UF 65860	*Paramylodon harlani*	195,8	68,2	0,348314607
UF 224000	*Paramylodon harlani*	195,8	70,3	0,359039837
UF 65861	*Paramylodon harlani*	201,6	73,2	0,363095238
UF 80176	*Paramylodon harlani*	203,8	76,5	0,375368008
AMNH 16896	*Paramylodon harlani*	244,9	98,9	0,403838301
FMNH P14723	*Paramylodon harlani*	245,1	105,5	0,430436557
MLP 08-V-29-1	*Scelidotherium* sp.	290	66,2	0,228275862
MLP 3-524	*Scelidotherium* sp.	290	68,5	0,236206897
MLP 3-522	*Scelidotherium* sp.	280	70,8	0,252857143
MLP 3-843	*Scelidotherium* sp.	255	64,6	0,253333333
MLP 3-521	*Scelidotherium* sp.	267	68,6	0,256928839
MLP 3-532	*Scelidotherium* sp.	283	74,4	0,262897527
MLP 3-526	*Scelidotherium* sp.	270	72,5	0,268518519
FMNH P14301	*Scelidotherium* sp.	383	112,1	0,292689295
MNHN-Bol V 11876	*Simomylodon uccasamamensis*	168,8	43,9	0,26007109
MNHN-Bol V 12507	*Simomylodon uccasamamensis*	173,5	46,4	0,267435159
MNHN-Bol V 3300	*Simomylodon uccasamamensis*	188,5	51	0,270557029
MNHN-Bol V 12518	*Simomylodon uccasamamensis*	173,8	48,1	0,276754891
MNHN-Bol V 12518(2)	*Simomylodon uccasamamensis*	173,9	49	0,281771133
MACN Ma 10.8	*Tamandua* sp.	98,8	7,6	0,076923077
MACN Ma 25911	*Tamandua* sp.	104,9	9	0,085795996
MACN Ma 33.255	*Tamandua* sp.	97,9	8,6	0,08784474
UF 201324	*Thinobadistes* cf *wetzeli*	239	64,7	0,270711297
AMNH 103028	*Thinobadistes segnis*	261,7	68,6	0,262132212
AMNH 103023	*Thinobadistes segnis*	252,2	69,8	0,276764473
UF 21509	*Thinobadistes segnis*	250	73,6	0,2944
AMNH 103021	*Thinobadistes segnis*	228,2	69,5	0,304557406
AMNH 103025	*Thinobadistes segnis*	245	79,6	0,324897959

Raw data of character 357 – Ratio TPEL/TL: (0) ≤ 0.25; (1) > 0.25, ≤ 0.35; (2) > 0.35.

CODE	TAXON	TL	TPEL	TPEL/TL
MACN Ma 4.125	*Bradypus* sp.	94,5	16,5	0,174603175
FMNH P14238	*Catonyx* sp.	333,5	158,5	0,475262369
MACN Pv 16639	*Catonyx* sp.	258	124	0,480620155
IVIC-P-2870	*Eionaletherium tanycnemius*	434,6	91,4	0,210308329
AMNH 1663	*Euphractus* sp.	64,1	16	0,249609984
MLP 3-128	*Glossotherium robustum*	290	106,5	0,367241379
MLP 3-114	*Glossotherium robustum*	260	102,6	0,394615385
MNHN.F.PAM 135	*Glossotherium robustum*	238,1	108,2	0,454430911
MNHN.F.R 269	*Glossotherium robustum*	245,2	116	0,473083197
MNHN.F.PAM 132	*Glossotherium robustum*	228,3	112,8	0,494086728
MNHN.F.TAR 789	*Glossotherium tarijense*	293,7	122,1	0,415730337
MNHN.F.TAR 788	*Glossotherium tarijense*	250	106,2	0,4248
MNHN.F.TAR 793	*Glossotherium tarijense*	278,8	128	0,459110473
MNHN.F.TAR 792	*Glossotherium tarijense*	291,9	144	0,49331963
FMNH P13128	*Hapalops* sp.	125,3	36,8	0,293695132
FMNH P13123	*Hapalops* sp.	132,6	37,1	0,279788839
FMNH P13130	*Hapalops* sp.	150,1	44,9	0,299133911
MLP 3-62	*Lestodon armatus*	300	115	0,383333333
MLP 3-20	*Lestodon armatus*	300	120	0,4
MLP SN13	*Lestodon armatus*	290	120	0,413793103
MLP 56-XII-12-2	*Lestodon armatus*	370	155	0,418918919

MNHN.F.TAR 771	*Lestodon armatus*	347,5	146	0,420143885
MNHN.F.TAR 776	*Lestodon armatus*	301,2	127,9	0,424634794
MLP 3-48	*Lestodon armatus*	375	160	0,426666667
MLP 3-831	*Lestodon armatus*	350	150	0,428571429
MLP 3-49	*Lestodon armatus*	315	140	0,444444444
MNHN.F.PAM 107	*Lestodon armatus*	351,4	161,7	0,460159363
MNHN.F.TAR 808	*Lestodon armatus*	347,2	171,7	0,49452765
AMNH 53855	*Manis gigantea*	118,9	26,6	0,22371741
AMU-CURS 29	*Mirandabradys socorrensis*	337,5	107,8	0,319407407
MACN Pv 6866	*Mylodon darwinii*	240	99,3	0,41375
MACN Ma 31.132	*Myrmecophaga* sp.	187,4	34,5	0,184098186
FMNH P13517	*Octodontotherium grande*	269	90,3	0,335687732
UF 10922	*Paramylodon garbanii*	179,3	76,7	0,427774679
UF 224000	*Paramylodon harlani*	195,8	68,6	0,350357508
UF 80176	*Paramylodon harlani*	203,8	90,5	0,444062807
UF 65862	*Paramylodon harlani*	222,7	99,6	0,447238437
UF 64365	*Paramylodon harlani*	211	98,2	0,465402844
UF 65861	*Paramylodon harlani*	201,6	96,3	0,477678571
UF 65860	*Paramylodon harlani*	195,8	94,6	0,483146067
FMNH P14723	*Paramylodon harlani*	245,1	125,4	0,511627907
AMNH 16896	*Paramylodon harlani*	244,9	128,6	0,525112291
MLP 3-526	*Scelidotherium* sp.	270	109,1	0,404074074
MLP 3-521	*Scelidotherium* sp.	267	109,5	0,41011236
MLP 08-V-29-1	*Scelidotherium* sp.	290	120,3	0,414827586
MLP 3-524	*Scelidotherium* sp.	290	121	0,417241379
MLP 3-532	*Scelidotherium* sp.	283	127,3	0,449823322
MLP 3-843	*Scelidotherium* sp.	255	117,3	0,46
MLP 3-522	*Scelidotherium* sp.	280	130	0,464285714
FMNH P14301	*Scelidotherium* sp.	383	186,3	0,486422977
MNHN-Bol V 12518	*Simomylodon uccasamamensis*	173,9	62,8	0,361127085
MNHN-Bol V 11876	*Simomylodon uccasamamensis*	168,8	61,6	0,36492891
MNHN-Bol V 3300	*Simomylodon uccasamamensis*	188,5	73,9	0,39204244
MNHN-Bol V 12518(2)	*Simomylodon uccasamamensis*	173,8	71,6	0,411967779
MNHN-Bol V 12507	*Simomylodon uccasamamensis*	173,5	74,6	0,429971182
MACN Ma 33.255	*Tamandua* sp.	97,9	16	0,163432074
MACN Ma 10.8	*Tamandua* sp.	98,8	16,3	0,164979757
MACN Ma 25911	*Tamandua* sp.	104,9	17,4	0,165872259
UF 201324	*Thinobadistes* cf *wetzeli*	239	104,5	0,437238494
AMNH 103028	*Thinobadistes segnis*	261,7	99,3	0,379442109
AMNH 103025	*Thinobadistes segnis*	245	93,9	0,383265306
AMNH 103023	*Thinobadistes segnis*	252,2	102,8	0,407613006
UF 21509	*Thinobadistes segnis*	250	104,1	0,4164
AMNH 103021	*Thinobadistes segnis*	228,2	113,6	0,49780894

Raw data of character 358 – Ratio TML/TPEL: (0) < 0.60; (1) ≥ 0.60, < 0.74; (2) ≥ 0.74.

CODE	TAXON	TPEL	TML	TML/TPEL
MACN Ma 4.125	*Bradypus* sp.	16,5	10,5	0,636363636
FMNH P14238	*Catonyx* sp.	158,5	99,3	0,626498423
MACN Pv 16639	*Catonyx* sp.	124	77,3	0,623387097
IVIC-P-2870	*Eionaletherium tanycnemius*	91,4	65,6	0,717724289
AMNH 1663	*Euphractus* sp.	16	8,8	0,55
MNHN.F.PAM 135	*Glossotherium robustum*	108,2	81	0,748613678
MNHN.F.PAM 132	*Glossotherium robustum*	112,8	88,7	0,786347518
MNHN.F.R 269	*Glossotherium robustum*	116	93	0,801724138
MLP 3-128	*Glossotherium robustum*	106,5	98,5	0,924882629
MLP 3-114	*Glossotherium robustum*	102,6	103,6	1,009746589
MNHN.F.TAR 792	*Glossotherium tarijense*	144	93	0,645833333
MNHN.F.TAR 793	*Glossotherium tarijense*	128	91,2	0,7125
MNHN.F.TAR 789	*Glossotherium tarijense*	122,1	104,8	0,858312858
MNHN.F.TAR 788	*Glossotherium tarijense*	106,2	104	0,979284369
FMNH P13128	*Hapalops* sp.	36,8	20,5	0,557065217

FMNH P13123	*Hapalops* sp.	37,1	21,2	0,571428571
FMNH P13130	*Hapalops* sp.	44,9	24,9	0,554565702
MNHN.F.PAM 107	*Lestodon armatus*	161,7	104,7	0,647495362
MLP 3-49	*Lestodon armatus*	140	93,4	0,667142857
MNHN.F.TAR 808	*Lestodon armatus*	171,7	116,5	0,678509027
MLP 3-48	*Lestodon armatus*	160	114,7	0,716875
MNHN.F.TAR 771	*Lestodon armatus*	146	110,1	0,754109589
MLP 3-831	*Lestodon armatus*	150	113,4	0,756
MNHN.F.TAR 776	*Lestodon armatus*	127,9	97	0,758405004
MLP 56-XII-12-2	*Lestodon armatus*	155	125,8	0,811612903
MLP 3-20	*Lestodon armatus*	120	102,8	0,856666667
MLP SN13	*Lestodon armatus*	120	104,5	0,870833333
MLP 3-62	*Lestodon armatus*	115	110,9	0,964347826
AMNH 53855	*Manis gigantea*	26,6	18,5	0,695488722
AMU-CURS 29	*Mirandabradys socorrensis*	107,8	72,1	0,668831169
MACN Pv 6866	*Mylodon darwinii*	99,3	87,7	0,883182276
MACN Ma 31.132	*Myrmecophaga* sp.	34,5	18,7	0,542028986
FMNH P13517	*Octodontotherium grande*	90,3	55,1	0,610188261
UF 10922	*Paramylodon garbanii*	76,7	61,2	0,79791395
FMNH P14723	*Paramylodon harlani*	125,4	97,3	0,775917065
UF 65860	*Paramylodon harlani*	94,6	76,8	0,811839323
UF 65861	*Paramylodon harlani*	96,3	80,8	0,839044652
UF 65862	*Paramylodon harlani*	99,6	83,8	0,841365462
AMNH 16896	*Paramylodon harlani*	128,6	108,5	0,8437014
UF 64365	*Paramylodon harlani*	98,2	86,3	0,878818737
UF 224000	*Paramylodon harlani*	68,6	69,8	1,017492711
MLP 08-V-29-1	*Scelidotherium* sp.	120,3	72,5	0,602660017
MLP 3-843	*Scelidotherium* sp.	117,3	71,7	0,611253197
MLP 3-522	*Scelidotherium* sp.	130	86,6	0,666153846
MLP 3-532	*Scelidotherium* sp.	127,3	86,5	0,679497251
MLP 3-524	*Scelidotherium* sp.	121	84	0,694214876
MLP 3-521	*Scelidotherium* sp.	109,5	78,8	0,719634703
MLP 3-526	*Scelidotherium* sp.	109,1	78,8	0,722273144
FMNH P14301	*Scelidotherium* sp.	186,3	115,2	0,618357488
MNHN-Bol V 12507	*Simomylodon uccasamamensis*	74,6	52	0,697050938
MNHN-Bol V 12518	*Simomylodon uccasamamensis*	71,6	53,1	0,741620112
MNHN-Bol V 11876	*Simomylodon uccasamamensis*	61,6	49,6	0,805194805
MNHN-Bol V 12518(2)	*Simomylodon uccasamamensis*	62,8	52,6	0,837579618
MNHN-Bol V 3300	*Simomylodon uccasamamensis*	73,9	62,4	0,844384303
MACN Ma 33.255	*Tamandua* sp.	16	8,4	0,525
MACN Ma 25911	*Tamandua* sp.	17,4	9,7	0,557471264
MACN Ma 10.8	*Tamandua* sp.	16,3	9,6	0,588957055
UF 201324	*Thinobadistes* cf *wetzeli*	104,5	67,1	0,642105263
AMNH 103021	*Thinobadistes segnis*	113,6	75,7	0,666373239
UF 21509	*Thinobadistes segnis*	104,1	70,2	0,674351585
AMNH 103028	*Thinobadistes segnis*	99,3	71,8	0,72306143
AMNH 103023	*Thinobadistes segnis*	102,8	74,8	0,727626459
AMNH 103025	*Thinobadistes segnis*	93,9	71,1	0,757188498

Raw data of character 359 – Ratio TPEW/TL: (0) < 0.40; (1) ≥ 0.40, < 0.60; (2) ≥ 0.60.

CODE	TAXON	TPEW	TL	TPEW/TL
MACN Ma 4.125	*Bradypus* sp.	21,8	94,5	0,230687831
FMNH P14238	*Catonyx* sp.	191,7	333,5	0,574812594
MACN Pv 16639	*Catonyx* sp.	153,4	258	0,594573643
IVIC-P-2870	*Eionaletherium tanycnemius*	150,3	434,6	0,345835251
AMNH 1663	*Euphractus* sp.	18,8	64,1	0,293291732
MNHN.F.PAM 135	*Glossotherium robustum*	145,5	238,1	0,611087778
MLP 3-128	*Glossotherium robustum*	185	290	0,637931034
MNHN.F.R 269	*Glossotherium robustum*	163	245,2	0,664763458
MNHN.F.PAM 132	*Glossotherium robustum*	158,5	228,3	0,694261936
MNHN.F.TAR 793	*Glossotherium tarijense*	173	278,8	0,620516499

MNHN.F.TAR 789	*Glossotherium tarijense*	185,6	293,7	0,631937351
MNHN.F.TAR 792	*Glossotherium tarijense*	191,8	291,9	0,657074341
FMNH P13128	*Hapalops* sp.	46,3	125,3	0,369513168
FMNH P13123	*Hapalops* sp.	46,9	132,6	0,353695324
FMNH P13130	*Hapalops* sp.	56,6	150,1	0,377081945
MNHN.F.TAR 771	*Lestodon armatus*	210,1	347,5	0,604604317
MLP 3-48	*Lestodon armatus*	230	375	0,613333333
MLP 3-831	*Lestodon armatus*	220	350	0,628571429
MLP 3-20	*Lestodon armatus*	190	300	0,633333333
MNHN.F.TAR 776	*Lestodon armatus*	190,9	301,2	0,633798141
MLP 3-49	*Lestodon armatus*	200	315	0,634920635
MNHN.F.PAM 107	*Lestodon armatus*	224,6	351,4	0,639157655
MLP 3-62	*Lestodon armatus*	200	300	0,666666667
MLP SN13	*Lestodon armatus*	195	290	0,672413793
MLP 56-XII-12-2	*Lestodon armatus*	250	370	0,675675676
MNHN.F.TAR 808	*Lestodon armatus*	260	347,2	0,748847926
AMNH 53855	*Manis gigantea*	39,3	118,9	0,330529857
AMU-CURS 29	*Mirandabradys socorrensis*	174,7	337,5	0,51762963
MACN Pv 6866	*Mylodon darwinii*	156,6	240	0,6525
MACN Ma 31.132	*Myrmecophaga* sp.	46,7	187,4	0,249199573
FMNH P13517	*Octodontotherium grande*	117,8	269	0,437918216
UF 10922	*Paramylodon garbanii*	115,2	179,3	0,642498606
UF 65860	*Paramylodon harlani*	131,9	195,8	0,673646578
UF 65861	*Paramylodon harlani*	137,2	201,6	0,680555556
UF 65862	*Paramylodon harlani*	152,4	222,7	0,684328693
UF 64365	*Paramylodon harlani*	146,3	211	0,693364929
UF 224000	*Paramylodon harlani*	136,6	195,8	0,697650664
UF 80176	*Paramylodon harlani*	155,5	203,8	0,763002944
AMNH 16896	*Paramylodon harlani*	188,7	244,9	0,770518579
FMNH P14723	*Paramylodon harlani*	221,6	245,1	0,904120767
MLP 08-V-29-1	*Scelidotherium* sp.	160,2	290	0,552413793
MLP 3-521	*Scelidotherium* sp.	151	267	0,565543071
MLP 3-524	*Scelidotherium* sp.	170	290	0,586206897
MLP 3-522	*Scelidotherium* sp.	175	280	0,625
MLP 3-526	*Scelidotherium* sp.	170	270	0,62962963
MLP 3-532	*Scelidotherium* sp.	180	283	0,636042403
MLP 3-843	*Scelidotherium* sp.	165	255	0,647058824
FMNH P14301	*Scelidotherium* sp.	231,8	383	0,605221932
MNHN-Bol V 11876	*Simomylodon uccasamamensis*	87,6	168,8	0,518957346
MNHN-Bol V 3300	*Simomylodon uccasamamensis*	102,6	188,5	0,544297082
MNHN-Bol V 12507	*Simomylodon uccasamamensis*	99,1	173,5	0,571181556
MNHN-Bol V 12518	*Simomylodon uccasamamensis*	99,3	173,8	0,571346375
MNHN-Bol V 12518(2)	*Simomylodon uccasamamensis*	101,3	173,9	0,582518689
MACN Ma 33.255	*Tamandua* sp.	24,3	97,9	0,248212462
MACN Ma 10.8	*Tamandua* sp.	24,8	98,8	0,251012146
MACN Ma 25911	*Tamandua* sp.	26,8	104,9	0,255481411
UF 201324	*Thinobadistes* cf *wetzeli*	140	239	0,585774059
AMNH 103028	*Thinobadistes segnis*	140,8	261,7	0,538020634
UF 21509	*Thinobadistes segnis*	140,3	250	0,5612
AMNH 103025	*Thinobadistes segnis*	137,5	245	0,56122449
AMNH 103023	*Thinobadistes segnis*	142,4	252,2	0,564631245
AMNH 103021	*Thinobadistes segnis*	136,8	228,2	0,599474145

Raw data of character 360 – Ratio LTFL/MTFL: (0) ≥ 0.83; (1) < 0.83.

CODE	TAXON	MTFL	LTFL	LTFL/MTFL
MACN Ma 4.125	*Bradypus* sp.	12,1	11,3	0,933884298
FMNH P14238	*Catonyx* sp.	110,8	80	0,722021661
MACN Pv 16639	*Catonyx* sp.	81,2	49,4	0,608374384
IVIC-P-2870	*Eionaletherium tanycnemius*	57,5	48,3	0,84
AMNH 1663	*Euphractus* sp.	13,7	11,6	0,846715328
MNHN.F.PAM 132	*Glossotherium robustum*	88,4	60	0,678733032

MNHN.F.PAM 135	*Glossotherium robustum*	87,9	62,8	0,714448237
MNHN.F.R 269	*Glossotherium robustum*	81	63	0,777777778
MNHN.F.TAR 792	*Glossotherium tarijense*	113	77,4	0,684955752
MNHN.F.TAR 793	*Glossotherium tarijense*	89	62	0,696629213
FMNH P13128	*Hapalops* sp.	24,4	24,3	0,995901639
FMNH P13123	*Hapalops* sp.	22,7	18	0,792951542
FMNH P13130	*Hapalops* sp.	32,2	33,3	1,034161491
MLP 3-20	*Lestodon armatus*	104,2	60,8	0,583493282
MLP 3-62	*Lestodon armatus*	107	63,2	0,590654206
MNHN.F.PAM 107	*Lestodon armatus*	113,1	72,7	0,642793988
MLP 56-XII-12-2	*Lestodon armatus*	119,1	79,8	0,670025189
MNHN.F.TAR 808	*Lestodon armatus*	127,9	88,7	0,693510555
MNHN.F.TAR 771	*Lestodon armatus*	110,4	77,7	0,703804348
MLP SN13	*Lestodon armatus*	105,1	78,1	0,743101808
MLP 3-831	*Lestodon armatus*	117,3	87,3	0,744245524
MLP 3-48	*Lestodon armatus*	133,4	104,7	0,784857571
MLP 3-49	*Lestodon armatus*	105,2	83,4	0,792775665
MNHN.F.TAR 776	*Lestodon armatus*	100,2	81,7	0,815369261
AMNH 53855	*Manis gigantea*	22,5	21,2	0,942222222
AMU-CURS 29	*Mirandabradys socorrensis*	78,7	62,3	0,791613723
MACN Pv 6866	*Mylodon darwinii*	95,3	63,6	0,667366212
MACN Ma 31.132	*Myrmecophaga* sp.	28,4	28,5	1,003521127
FMNH P13517	*Octodontotherium grande*	66,5	50,4	0,757894737
UF 10922	*Paramylodon garbanii*	61,9	44,5	0,718901454
UF 65860	*Paramylodon harlani*	81,3	51,5	0,633456335
UF 80176	*Paramylodon harlani*	91,6	59,9	0,653930131
UF 65862	*Paramylodon harlani*	85,3	57,7	0,676436108
AMNH 16896	*Paramylodon harlani*	109,8	74,3	0,676684882
UF 64365	*Paramylodon harlani*	86,7	68,8	0,793540946
FMNH P14723	*Paramylodon harlani*	104,8	83,5	0,796755725
UF 65861	*Paramylodon harlani*	75,3	60,5	0,803452855
MLP 3-532	*Scelidotherium* sp.	102,1	57,3	0,561214496
MLP 3-521	*Scelidotherium* sp.	93,6	54,7	0,584401709
MLP 3-522	*Scelidotherium* sp.	86,5	60,5	0,699421965
MLP 3-526	*Scelidotherium* sp.	87,7	63,4	0,722919042
MLP 08-V-29-1	*Scelidotherium* sp.	88,6	66	0,744920993
MLP 3-843	*Scelidotherium* sp.	75,6	62	0,82010582
MLP 3-524	*Scelidotherium* sp.	84,7	69,5	0,820543093
FMNH P14301	*Scelidotherium* sp.	138,1	96,1	0,695872556
MNHN-Bol V 3305	*Simomylodon uccasamamensis*	57,8	33,1	0,57266436
MNHN-Bol V 11876	*Simomylodon uccasamamensis*	46,4	27,1	0,584051724
MNHN-Bol V 3300	*Simomylodon uccasamamensis*	65,7	39,1	0,595129376
MNHN-Bol V 12507	*Simomylodon uccasamamensis*	56,8	34,1	0,600352113
MNHN-Bol V 11772	*Simomylodon uccasamamensis*	67,2	42	0,625
MNHN-Bol V 12518	*Simomylodon uccasamamensis*	50,4	33,1	0,656746032
MNHN-Bol V 12518(2)	*Simomylodon uccasamamensis*	50,6	35,1	0,693675889
MACN Ma 10.8	*Tamandua* sp.	15,2	12,8	0,842105263
MACN Ma 33.255	*Tamandua* sp.	14,7	12,5	0,850340136
MACN Ma 25911	*Tamandua* sp.	17,2	15	0,872093023
UF 201324	*Thinobadistes* cf *wetzeli*	85,2	60,1	0,705399061
AMNH 103021	*Thinobadistes segnis*	77,7	47,3	0,608751609
AMNH 103023	*Thinobadistes segnis*	82,6	61,1	0,739709443
AMNH 103025	*Thinobadistes segnis*	81,1	61,6	0,759556104
AMNH 103028	*Thinobadistes segnis*	76,2	60,4	0,792650919

Raw data of character 361 – Ratio LTFW/MTFW: (0) ≥ 0.86; (1) < 0.86.

CODE	TAXON	MTFW	LTFW	LTFW/MTFW
MACN Ma 4.125	*Bradypus* sp.	9,9	10,7	1,080808081
FMNH P14238	*Catonyx* sp.	95,3	79,3	0,832109129
MACN Pv 16639	*Catonyx* sp.	76,4	55,6	0,727748691
IVIC-P-2870	*Eionaletherium tanycnemius*	66,1	58,7	0,888048411

AMNH 1663	*Euphractus* sp.	9,3	9,6	1,032258065
MNHN.F.PAM 132	*Glossotherium robustum*	97,7	60	0,614124872
MNHN.F.PAM 135	*Glossotherium robustum*	92,8	61,3	0,660560345
MNHN.F.R 269	*Glossotherium robustum*	105	71	0,676190476
MNHN.F.TAR 792	*Glossotherium tarijense*	119,2	73,6	0,617449664
MNHN.F.TAR 793	*Glossotherium tarijense*	96	66	0,6875
FMNH P13128	*Hapalops* sp.	24,4	17,3	0,709016393
FMNH P13123	*Hapalops* sp.	28,5	24	0,842105263
FMNH P13130	*Hapalops* sp.	29,7	23,8	0,801346801
MLP 56-XII-12-2	*Lestodon armatus*	153,4	90,4	0,589308996
MLP 3-48	*Lestodon armatus*	163,5	96,8	0,59204893
MLP 3-831	*Lestodon armatus*	126,2	81,2	0,643423138
MNHN.F.TAR 771	*Lestodon armatus*	127,2	84	0,660377358
MLP 3-20	*Lestodon armatus*	115,7	76,8	0,663785653
MNHN.F.TAR 776	*Lestodon armatus*	120,6	80,1	0,664179104
MLP SN13	*Lestodon armatus*	117,6	80,6	0,68537415
MNHN.F.TAR 808	*Lestodon armatus*	125,8	87,5	0,69554849
MLP 3-49	*Lestodon armatus*	111,8	78,5	0,702146691
MNHN.F.PAM 107	*Lestodon armatus*	130	92,1	0,708461538
MLP 3-62	*Lestodon armatus*	106	79,5	0,75
AMNH 53855	*Manis gigantea*	20,9	19,9	0,95215311
AMU-CURS 29	*Mirandabradys socorrensis*	91,1	62,3	0,683863886
MACN Pv 6866	*Mylodon darwinii*	95,8	68,3	0,712943633
MACN Ma 31.132	*Myrmecophaga* sp.	21,7	20,4	0,940092166
FMNH P13517	*Octodontotherium grande*	66,2	49,1	0,741691843
UF 10922	*Paramylodon garbanii*	64,8	49,3	0,760802469
FMNH P14723	*Paramylodon harlani*	122,8	71,4	0,581433225
AMNH 16896	*Paramylodon harlani*	118,4	74,4	0,628378378
UF 65860	*Paramylodon harlani*	76,1	48,1	0,632063075
UF 64365	*Paramylodon harlani*	100,2	65	0,648702595
UF 65861	*Paramylodon harlani*	86,3	58,1	0,673232908
UF 80176	*Paramylodon harlani*	96,5	67	0,694300518
UF 65862	*Paramylodon harlani*	93	68,3	0,734408602
MLP 3-521	*Scelidotherium* sp.	83,6	52,7	0,630382775
MLP 3-843	*Scelidotherium* sp.	85	57	0,670588235
MLP 3-522	*Scelidotherium* sp.	85,9	60,1	0,699650757
MLP 3-524	*Scelidotherium* sp.	84	59,3	0,705952381
MLP 08-V-29-1	*Scelidotherium* sp.	81,1	60	0,739827374
MLP 3-532	*Scelidotherium* sp.	81,8	62,3	0,761613692
MLP 3-526	*Scelidotherium* sp.	85,3	69,3	0,812426729
FMNH P14301	*Scelidotherium* sp.	121,3	92,5	0,762572135
MNHN-Bol V 11876	*Simomylodon uccasamamensis*	54,7	27,7	0,506398537
MNHN-Bol V 12518	*Simomylodon uccasamamensis*	60,3	36,9	0,611940299
MNHN-Bol V 12507	*Simomylodon uccasamamensis*	57,8	37,4	0,647058824
MNHN-Bol V 12518(2)	*Simomylodon uccasamamensis*	56,3	37,5	0,6660746
MNHN-Bol V 3300	*Simomylodon uccasamamensis*	60,4	40,6	0,67218543
MNHN-Bol V 3305	*Simomylodon uccasamamensis*	53,4	39,2	0,734082397
MNHN-Bol V 11772	*Simomylodon uccasamamensis*	60,6	48	0,792079208
MACN Ma 33.255	*Tamandua* sp.	13,1	11,7	0,893129771
MACN Ma 10.8	*Tamandua* sp.	12,8	12,1	0,9453125
MACN Ma 25911	*Tamandua* sp.	13,9	14,2	1,021582734
UF 201324	*Thinobadistes* cf *wetzeli*	89,5	59,7	0,667039106
AMNH 103021	*Thinobadistes segnis*	77,3	44,7	0,578266494
AMNH 103025	*Thinobadistes segnis*	86,5	56,7	0,655491329
AMNH 103023	*Thinobadistes segnis*	80,7	60,1	0,744733581
AMNH 103028	*Thinobadistes segnis*	76,3	61,5	0,806028834

Raw data of character 366 – Ratio EFFL/FiTL of fibula: (0) < 0.20; (1) ≥ 0.20.

CODE	TAXON	FiTL	EFFL	EFFL/FiTL
MACN Ma 4.125	*Bradypus* sp.	86,1	10	0,116144019
FMNH P14238	*Catonyx* sp.	378	83,8	0,221693122

IVIC-P-2870	*Eionaletherium tanycnemius*	402,5	55,6	0,138136646
AMNH 1663	*Euphractus* sp.	62,2	12,9	0,207395498
MNHN.F.PAM 141 (A.C. 7111)	*Glossotherium robustum*	233,1	70	0,3003003
MNHN.F.PAM 141 (A.C. 7112)	*Glossotherium robustum*	228,7	73,9	0,323130739
FMNH P13128	*Hapalops* sp.	119,4	17,6	0,147403685
FMNH P13123	*Hapalops* sp.	122,5	31,8	0,259591837
MLP 3-73	*Lestodon armatus*	365	94,8	0,259726027
MNHN.F.TAR 808	*Lestodon armatus*	355,8	70,7	0,198707139
FMNH P14247	*Lestodon armatus*	353,5	110,9	0,313719943
AMNH 53855	*Manis gigantea*	110,3	19,6	0,177697189
MACN Ma 31.132	*Myrmecophaga* sp.	173,4	19,1	0,110149942
UF 10922	*Paramylodon garbanii*	190,5	53,3	0,279790026
AMNH 16896	*Paramylodon harlani*	272,4	83,6	0,306901615
FMNH P14723	*Paramylodon harlani*	263	81,5	0,309885932
MLP 3-528	*Scelidotherium* sp.	293	86,1	0,293856655
MNHN-Bol V 12507	*Simomylodon uccasamamensis*	176,5	35,4	0,200566572
MNHN-Bol V 11767	*Simomylodon uccasamamensis*	183,9	37,6	0,204458945
MNHN-Bol V 8541	*Simomylodon uccasamamensis*	164,9	36,3	0,220133414
MNHN-Bol V 12518	*Simomylodon uccasamamensis*	180,3	40	0,221852468
MNHN-Bol V 12518(2)	*Simomylodon uccasamamensis*	181	41	0,226519337
MNHN-Bol V 6562	*Simomylodon uccasamamensis*	194,3	47,8	0,246011323
MACN Ma 33.255	*Tamandua* sp.	87,1	9,6	0,11021814
MACN Ma 10.8	*Tamandua* sp.	86,9	9,8	0,112773303
MACN Ma 25911	*Tamandua* sp.	93,3	11,9	0,127545552
UF 201323	*Thinobadistes* cf. *Wetzeli*	248,4	66,7	0,268518519

Raw data of character 367 – Ratio between the maximum proximodistal and anteroposterior length of the astragalus: (0) < 0.80; (1) ≥ 0.80, < 1.00; (2) ≥ 1.00.

CODE	TAXON	Ant-post	Prox-dist	Prox-dist/Ant-post
MCN 170-72V	*Bolivartherium urumaquensis*	81,1	72,3	0,891491985
FMNH P14238	*Catonyx* sp.	123,1	134	1,088545898
MNHN.F.PAM 141 (A.C. 7128)	*Glossotherium robustum*	120,6	108,1	0,896351575
MNHN.F.PAM 141 (A.C. 7114)	*Glossotherium robustum*	120,6	109,2	0,905472637
FMNH P13123	*Hapalops* sp.	29,1	16	0,549828179
MLP SN25	*Lestodon armatus*	180	146,6	0,814444444
MLP 3-824	*Lestodon armatus*	175	143	0,817142857
MLP SN22	*Lestodon armatus*	176	147,6	0,838636364
MLP 50-VII-1-5	*Lestodon armatus*	190	163,5	0,860526316
MLP S.N.	*Lestodon armatus*	156,3	136,3	0,872040947
MLP 3-64	*Lestodon armatus*	180	159	0,883333333
MLP 3-826	*Lestodon armatus*	165	149,1	0,903636364
MLP SN23	*Lestodon armatus*	165	155	0,939393939
FMNH P14228	*Lestodon armatus*	152,2	146,8	0,964520368
AMNH 53855	*Manis gigantea*	32,8	17,4	0,530487805
FMNH P14288	*Mylodon darwinii*	137,4	133,2	0,969432314
FMNH 13363	*Octodontotherium grande*	77,1	48,4	0,627756161
MNHN.F.DES 259	*Orophodon hapaloides*	59,1	39,5	0,668358714
UF 10922	*Paramylodon garbanii*	82,5	68,4	0,829090909
AMNH F:AM 96370	*Paramylodon garbanii*	80,4	80,2	0,997512438
UF 87100	*Paramylodon harlani*	111,5	101,7	0,912107623
UF 64366	*Paramylodon harlani*	114,1	104,8	0,91849255
AMNH 16896-1	*Paramylodon harlani*	133,9	129,5	0,967139656
AMNH 16896-2	*Paramylodon harlani*	135,9	132,1	0,972038263
FMNH P14723	*Paramylodon harlani*	136,4	134,2	0,983870968
MACN 2816(=2953)	*Pleurolestodon acutidens*	110	105,4	0,958181818
MACN Pv 2749	*Scelidotherium* sp.	98,9	99,3	1,004044489
MACN Pv 856	*Scelidotherium* sp.	102,3	108,9	1,064516129
MACN Pv 7023	*Scelidotherium* sp.	96,1	114,5	1,191467222
MACN Pv 9619	*Scelidotherium* sp.	107,3	114,8	1,069897484
MACN Pv 10856	*Scelidotherium* sp.	98,6	110,3	1,118661258
MNHN.F.VIZ 39	*Simomylodon uccasamamensis*	78	64,2	0,823076923

MNHN-Bol V 11779	*Simomylodon uccasamamensis*	80	71,8	0,8975
MNHN.F.AYO 182	*Simomylodon uccasamamensis*	82,6	74,8	0,905569007
MNHN-Bol V 11788	*Simomylodon uccasamamensis*	80,8	73,5	0,909653465
MNHN-Bol V 12518	*Simomylodon uccasamamensis*	78,3	71,8	0,916985951
MNHN.F.POM 64	*Simomylodon uccasamamensis*	78,8	73,8	0,936548223
MNHN-Bol V 12518(2)	*Simomylodon uccasamamensis*	76,9	72,2	0,938881664
UF 312843	*Simomylodon uccasamamensis*	74,4	70,1	0,942204301
UF 201326	*Thinobadistes* sp.	110,5	97,6	0,883257919
UF 93064	*Thinobadistes* sp.	105,9	94,8	0,895184136
AMNH F:AM 102525	*Thinobadistes* sp.	119,8	110,6	0,923205342
UF 201326	*Thinobadistes* sp.	110	101,7	0,924545455
UF 93051	*Thinobadistes* sp.	117,4	108,6	0,925042589

Raw data of character 373 – Calcaneal posterior mediolateral enlargement: (0) absent; (1) present, forming an arched posterior profile; (2) present, forming a broad surface touching the ground (mediolateral width/total length < 0.55); (3) present, forming a very broad surface touching the ground (mediolateral width/total length ≥ 0.55).

CODE	TAXON	MediolatW/TL
FMNH P14238	*Catonyx* sp.	0,47
MACN Pv 91	*Glossotherium robustum*	0,61
MNHN.F.PAM 141 (A.C. 7113)	*Glossotherium robustum*	0,57
MNHN.F.PAM 141 (A.C. 7127)	*Glossotherium robustum*	0,57
MACN Pv 17182	*Lestodon armatus*	0,42
FMNH P14228	*Lestodon armatus*	0,5
MLP 3-65	*Lestodon armatus*	0,49
MPL 3-47	*Lestodon armatus*	0,53
FMNH P14723	*Paramylodon harlani*	0,58
MACN Pv 5742	*Scelidotherium* sp.	0,47
MACN Pv 6149	*Scelidotherium* sp.	0,48
MACN Pv 9376	*Scelidotherium* sp.	0,44
MNHN-Bol V 8541	*Simomylodon uccasamamensis*	0,47
UF 21509	*Thinobadistes segnis*	0,46

Raw data of character 379 – Metatarsal 3 shape (ratio between minimum dorsopalmar depth of shaft and total length): (0) ≤ 0.40; (1) > 0.40, ≤ 0.46; (2) > 0.46, ≤ 0.56; (3) ≥ 0.56.

CODE	TAXON	Length	Dors-palm	Dors-palm/L
MACN Pv 11331	*Glossotherium robustum*	61,1	31,1	0,509001637
MACN Pv 17572	*Glossotherium robustum*	68,4	38,1	0,557017544
MNHN.F.PAM 144	*Glossotherium robustum*	66	39,5	0,598484848
MNHN.F.PAM 141 (A.C.7131)	*Glossotherium robustum*	62	37,5	0,60483871
MNHN.F.PAM 141 (A.C.7118)	*Glossotherium robustum*	60,5	38,5	0,636363636
MACN Pv 10751	*Lestodon armatus*	132,4	58,3	0,440332326
FMNH P14228	*Lestodon armatus*	110,2	50	0,453720508
MACN Pv 10750	*Lestodon armatus*	134,5	61,4	0,456505576
AMNH 53855	*Manis gigantea*	25,7	6,9	0,26848249
MNHN.F.DES 224	*Octodontotherium grande*	56,4	18	0,319148936
MNHN.F.DES 221	*Octodontotherium grande*	61,3	19,6	0,319738989
MNHN.F.DES 220	*Octodontotherium grande*	55,8	18,8	0,336917563
UF 10922	*Paramylodon garbanii*	44,9	22,1	0,4922049
UF 87105	*Paramylodon harlani*	67,9	31,8	0,468335788
AMNH 16896-2	*Paramylodon harlani*	70,4	35,1	0,498579545
FMNH P14723	*Paramylodon harlani*	77,9	40,7	0,522464698
AMNH 16896-1	*Paramylodon harlani*	67,6	38	0,562130178
UF 21509	*Thinobadistes segnis*	64,2	28	0,436137072
UF 93053	*Thinobadistes wetzeli*	77,8	33	0,424164524

Raw data of character 380 – Metatarsal 4 shape (ratio between minimum mediolateral width of shaft and total length): (0) ≤ 0.25; (1) > 0.25, ≤ 0.40; (2) > 0.40.

CODE	TAXON	Length	Mediolat	Mediolat/L
FMNH P14238	*Catonyx* sp.	125,3	55	0,438946528
MNHN.F.PAM 141 (A.C.7132)	*Glossotherium robustum*	98,8	33	0,334008097
MNHN.F.PAM 141 (A.C.7119)	*Glossotherium robustum*	96,1	35,1	0,365244537
MNHN.F.PAM 144	*Glossotherium robustum*	100	37,9	0,379
FMNH P14226	*Lestodon armatus*	165	46,1	0,279393939
FMNH P14228	*Lestodon armatus*	173	48,7	0,28150289
AMNH 53855	*Manis gigantea*	26,6	6,3	0,236842105
FMNH P15072	*Octodontotherim grande*	95,7	17,1	0,178683386
FMNH P15072	*Octodontotherim grande*	87,5	15,7	0,179428571
UF 10922	*Paramylodon garbanii*	83,9	25,1	0,299165673
FMNH P14723	*Paramylodon harlani*	116,3	37,3	0,32072227
AMNH 16896-2	*Paramylodon harlani*	114,5	38,2	0,333624454
AMNH 16896-1	*Paramylodon harlani*	114,3	43,2	0,377952756
UF 21509	*Thinobadistes segnis*	94,7	27,6	0,291446674

Appendix VI. Data S3. Additional bibliographical sources for the codification of individual taxa.

Pholidota:

Gaudin TJ, Emry RJ, Morris J. 2016. *Skeletal Anatomy of the North American Pangolin* Patriomanis Americana *(Mammalia, Pholidota) from the Latest Eocene of Wyoming (USA)*. Washington D.C.: Smithsonian Institution Scholarly Press.

Myrmecophaga:

Gaudin TJ, Branham DG. 1998. The phylogeny of the Myrmecophagidae (Mammalia, Xenarthra, Vermilingua) and the relationship of *Eurotamandua* to the Vermilingua. *Journal of Mammalian Evolution* 5: 237–265.

Sesoko NF, Rahal SC, Bortolini Z, de Souza LP, Vulcano LC, Monteiro FOB, Teixeira CR. 2015. Skeletal morphology of the forelimb of *Myrmecophaga tridactyla*. *Journal of Zoo and Wildlife Medicine* 46: 713–722.

Taylor BK. 1978. The anatomy of the forelimb in the anteater (*Tamandua*) and its functional implications. *Journal of Morphology* 157: 347–368.

Pseudoglyptodon:

Engelmann GF. 1987. A new Deseadan Sloth (Mammalia: Xenarthra) from Salla, Bolivia, and its implications for the primitive condition of the dentition in Edentates. *Journal of Vertebrate Paleontology* 7: 217-223.

McKenna MC, Wyss AR, Flynn JJ. 2006. Paleogene Pseudoglyptodont Xenarthrans from Central Chile and Central Patagonia. *American Museum Novitates*: 1-18.

Pujos F, De Iuliis G. 2007. Late Oligocene Megatherioidea Fauna (Mammalia: Xenarthra) from Salla-Luribay (Bolivia): new data on basal sloth radiation and Cingulata-Phyllophaga split. *Journal of Vertebrate Paleontology* 27: 132-144.

Hapalops and *Nematherium*:

Scott WB. 1903-1904. Mammalia of the Santa Cruz beds: Part 1. Edentata. In: Scott WB, ed. *Reports of the Princeton University Expeditions to Patagonia 1896–1899*. Princeton: Princeton University Press, 1–364.

Toledo N, Bargo MS, Vizcaino SF. 2013. Muscular Reconstruction and Functional Morphology of the Forelimb of Early Miocene Sloths (Xenarthra, Folivora) of Patagonia. *The Anatomical Record* 296: 305–325.

Scelidotherium and *Catonyx*:

Cuenca-Anaya J. 1995. *El aparato locomotor de los escelidotherios (Edentata, Mammalia) y su paleobiología*. Unpublished D. Phil. Thesis, Adjuntament de Valencia.

McDonald HG. 1987. *A systematic review of the Plio-Pleistocene scelidotheriine ground sloths (Mammalia: Xenarthra: Mylodontidae)*. Unpublished D.Phil. Thesis, University of Toronto.

Kiyumylodon lecuonai:

Rinderknecht A, Perea D, McDonald HG. 2007. A new Mylodontinae (Mammalia, Xenarthra) from the Camacho Formation (Late Miocene), Uruguay. *Journal of Vertebrate Paleontology* 27: 744–747.

Lestobradys sprechmanni:

Rinderknecht A, Bostelmann E, Perea D, Lecuona G. 2010. A new genus and species of Mylodontidae (Mammalia: Xenarthra) from the late Miocene of southern Uruguay, with comments on the systematics of the Mylodontinae. *Journal of Vertebrate Paleontology* 30: 899–910.

Mylodon darwinii:

Haro JA, Tauber AA, Krapovickas JM. 2016. The manus of *Mylodon darwinii* Owen (Tardigrada, Mylodontidae) and its phylogenetic implications. *Journal of Vertebrate Paleontology* 36: e1188824.

Haro JA, Tauber AA, Krapovickas JM. 2017. Thoracic member (pectoral girdle and forelimb) bones of *Mylodon darwinii* Owen (Xenarthra, Mylodontidae) from the Late Pleistocene of Central Argentina and their phylogenetic implications. *Paläontologische Zeitschrift* 91: 439–457.

McAfee RK. 2016. Description of new postcranial elements of *Mylodon darwinii* Owen 1839 (Mammalia: Pilosa: Mylodontinae), and functional morphology of the forelimb. *Ameghiniana* 53: 418–443.

Pseudoprepotherium confusum:

Hirschfeld SE. 1985. Ground Sloths form the Friasian La Venta Fauna, with additions to the Pre-Friasian Coyaima Fauna of Colombia, South America. *University of California Publications in Geological Sciences* 128: 1–91.

Pseudoprepotherium venezuelanum:

Collins RL. 1934. Venezuelan Tertiary mammals. *Johns Hopkins University Studies in Geology* 11: 235–244.

Bocquentin J, Guilherme E. 1999. As preguiças mylodontinae (Mammalia, Xenarthra, Mylodontidae) do Neógeno do sítio Niterói, Acre, Brasil. *Acta Geologica Leopoldensia* 22: 57–67.

Negri FR, Bocquentin-Villanueva J, Ferigolo J, Antoine P-O. 2010. A review of Tertiary mammal faunas and birds from western Amazonia. In: Hoorn C, Wesselingh FP, eds. *Amazonia, landscape and species evolution: a look into the past*. Hoboken: Wiley-Blackwell, 245–258.

Appendix VI. Data S4. Complete matrix analyzed in the phylogenetic study of Chapter 8.

	1	**2**	**3**	**4**	**5**	**6**	**7**	**8**	**9**	**10**	**11**	**12**	**13**	**14**	**15**	**16**	**17**	**18**	**19**	**20**	**21**	**22**	**23**	**24**	**25**	**26**	**27**	**28**	**29**
Pholidota	0	-	-	-	-	-	-	-	-	-	-	-	-	-	-	-	-	-	-	-	-	-	-	-	-	-	-	-	-
Euphractus sp.	1	1	1	0	1	0	0	0	1	0	1	1	2	2	1	0	0	0	0	3	0	0	0	0	0	0	0	0	0
Cyclopes sp.	0	-	-	-	-	-	-	-	-	-	-	-	-	-	-	-	-	-	-	-	-	-	-	-	-	-	-	-	-
Tamandua sp.	0	-	-	-	-	-	-	-	-	-	-	-	-	-	-	-	-	-	-	-	-	-	-	-	-	-	-	-	-
Myrmecophaga sp.	0	-	-	-	-	-	-	-	-	-	-	-	-	-	-	-	-	-	-	-	-	-	-	-	-	-	-	-	-
Bradypus sp.	1	2	0	1	1	0	1	0	2	0	2	0	0	2	1	0	0	1	1&2	1	0	0	0	0	0	0&1	0	0	0
Hapalops sp.	1	2	2	0&1	1	2	1	0	2	1	2	0	0	0	1	0	2	1	1	1	1	0	0	0&1	0	1	1	0	0
Nematherium sp.	1	2	0	1	1	0	1	0	2	0	2	0	2	0	1	2	0	1	0	2	1	1	0	0	0	1	0	0	0
Scelidotherium sp.	1	2	0	0	1	0	1	0	2	0	2	0	2	2	1	2	3	1	0	4	2	1	0	0	0	0	0	0	0
Catonyx sp.	1	2	0	0	1	0	1	0	2	0	2	0	2	2	1	2	3	1	0	4	2	1	0	0	0	0	0	0	0
Octodontotherium grande	1	2	0	1	1	0	1	0	?	0	2	?	0	0	1	0	1	1	1	2	1	0	0	0	0	1	0	1	0
Paroctodontotherium calleorum	1	2	0	1	1	0	1	0	2	0	2	0	0	?	?	0	0	?	1	?	1	0	0	0	0	1	0	1	0
Orophodon hapaloides	1	?	0	1	1	0	1	0	2	0	2	?	?	0	1	0	1	1	1	2	?	?	?	0	0	1	0	1	0
Lestobradys sprechmanni	1	2	0	1	1	0	1	0	2	0	2	0	1	1	1	1	?	1	1	?	?	0	0	1	1	1	0	?	1
Thinobadistes sp.	1	2	0	1	1	1&2	1	0	2	0	2	0	1	1	1	1	0	1	1	0	0	0	0	0	1	1	0	1	1
Bolivartherium sp.	1	2	0	1	1	2	1	0	2	0	2	0	1	2	1	1	0	1	1	?	0	0	0	1	0	1	0	1	?
Lestodon armatus	1	2	0	1	1	2	1	0	2	0	3	0	1	1	1	1	0	1	1	0	1	0	0	1	0	1	0	0	1
Sphenotherus zavaletianus	1	?	0	1	1	?	1	0	2	0	3	0	?	1	1	1	?	1	1	?	?	?	?	0	?	?	?	?	?
Simomylodon uccasamamensis	1	2	0	1	1	0	1	0	2	0	2	0	0	0	1	1	0	1	1	2	0	0	0	0	0&1	1	0	1	0
Glossotheridium chapadmalense	1	2	0	1	1	0	1	0	2	0	2	0	0	0	1	1	0	1	1	2	0	0	0	0	0	1	0	1	0
Paramylodon garbanii	1	2	0	1	1	0	1	0	2	0	2	0	0	0	1	1	0	1	1	2	1	0	0	0	0&1	1	0	1	0
Paramylodon harlani	1	2&3	0	1	1	0	1	0	2	0	2	0	0	0	1	1	0	1	1	1&2	1	0	0	0	0&1	1	0	1	0
Glossotherium robustum	1	2	0	1	1	0&1	1	0	2	0	2	0	0&2	0	1	1	0	1	1	1	0	0	0	0	0	1	0	1	0
Glossotherium tarijense	1	2	0	1	1	0&1	1	0	2	0	2	0	0&2	0	1	1	0	1	1	0	0&1	0	0	0	0&1	1	0	1	0
Glossotherium tropicorum	1	2	0	1	1	1	1	0	2	0	2	0	0	0	1	1	0	1	1	1	0	0	0	0	1	1	0	1	0
Glossotherium phoenesis	1	2	0	1	1	1	1	0	2	0	2	0	0	0	1	1	0	1	1	2	0	0	0	0	1	1	0	1	0
Octomylodon sp.	1	4	0	0	1	-	1	0	2	0	2	?	-	-	1	0	1	-	-	-	-	-	-	-	0	-	?	?	-
Brievabradys laventensis	1	2	0	1	1	0	1	0	2	0	2	0	1	1	1	0	0	1	1	2	0	0	0	0	0	1	0	1	1
Baraguatherium takumara	1	2	0	0	1	0	1	0	2	0	2	?	?	0	0	0	0	?	0	?	?	?	?	0	0	?	?	?	?
Glossotheriopsis pascuali	1	?	0	1	1	0	1	0	2	0	2	0	0	?	?	?	0	1	1	2	0	1	0	0	0	1	?	1	0
Octodontobradys puruensis	1	2	0	0	1	0	1	0	2	0	2	0	2	0	2	0	0	1	0	2	?	?	0	0	0	?	0	0	0
Pseudoglyptodon sp.	1	3	1	1	?	0	1	0	1	0	1	0	0	0	1	0	3	1	1	1	?	?	0	0	0	1	0	0	0
Eionaletherium tanycnemius	?	?	?	?	?	?	?	?	?	?	?	?	?	?	?	?	?	?	?	?	?	?	?	?	?	?	?	?	?
Pleurolestodon acutidens	1	2	0	1	1	0	1	0	2	0	2	?	0	0	1	1	0	1	1	2	0	0	0	0	0	1	0	1	0
Mylodon darwinii	1	3	0	1	1	-	1	0	2	0	2	0	-	0	1	1	0	-	0	1	-	-	-	0	0	1	0	0	-
Kiyumylodon lecuonai	1	?	0	1	1	?	1	0	2	0	2	?	?	0	1	1	0	1	1	2	?	?	?	0	?	?	?	?	?
Pseudoprepotherium venezuelanum	1	?	0	1	1	?	1	?	?	?	?	?	0	?	0	1	0	?	?	0	?	?	?	?	0	0	?	?	?	?
Pseudoprepotherium confusum	1	2	0	1	1	0	1	0	2	0	2	0	?	0	1	0	0	1	0	2	2	1	0	0	0	1	0	0	0
Mirandabradys sp.	1	2	0	?	?	0	1	?	?	?	?	?	?	?	?	0	?	?	?	?	?	?	?	0	?	0	?	0	?	?
Urumacotherium sp.	1	2	0	1	1	0	1	0	2	0	2	0	1	1	0	0	0	1	0	?	2	1	0	0	0	0	1	0	2

	30	31	32	33	34	35	36	37	38	39	40	41	42	43	44	45	46	47	48	49	50	51	52	53	54	55	56	57	58
Pholidota	-	-	-	-	-	-	-	0	2	0	-	-	-	0	0	-	-	3	-	-	-	-	0	-	2	1	0	0&2	0
Euphractus sp.	0	1	0	0	0	0	0	0	2	0	2	2	2	0	0	1	1	0	0	0	0	1	1	0	0	0	0	1	0
Cyclopes sp.	-	-	-	-	-	-	-	0	0	0	-	2	0	0	0	0&1	1	0	2	0	1	2	0	-	2	1	1	0	0
Tamandua sp.	-	-	-	-	-	-	-	0	0	0	-	0	-	0	0	-	-	3	0	0	1	0	0	-	2	2	0	0	0
Myrmecophaga sp.	-	-	-	-	-	-	-	0	0	0	-	0	-	0	0	-	-	3	0	0	1	0	0	-	2	1	0	0	0
Bradypus sp.	6	2	0	0	0	2	3	4	1	0	0&1&2	2	2	1	0	1	0&1	0	2	1	1	2	0	0	1&2	2&3	1	3	0&1
Hapalops sp.	0	2	1	1	1	2&4	1	1&2	3	1	0	1&2	1&2	1	0	1	1	0&1	2	1	1	1	0	0	0	2	2	2	0
Nematherium sp.	4	1	0	4	4	7	5	1&3	1	0	0	1	?	0	0	1	0	2	0	1	1	1	1	1	0	2	2	2	0
Scelidotherium sp.	4	3	4	5	5	7	5	2	1	0	0	2	2	0	0	1	0	2	0	1	1	0	1	1	0	1	2	2	?
Catonyx sp.	4	3	4	5	5	7	5	5	1	0	0	2	2	0	0	1	0	2	0	1	1	0	1	1	0	1	2	2	0
Octodontotherium grande	0	1	0	6	6	7	3	2	1	0	1	2	2	0	0	1	0	2	0	1	1	0	1	1	?	?	?	?	?
Paroctodontotherium calleorum	?	5	?	6	?	3	?	?	?	?	?	?	?	?	?	?	?	?	?	?	?	?	?	?	?	?	?	?	?
Orophodon hapaloides	0	1	0	0	0	7	3	?	1	0	0	?	?	0	?	?	?	?	?	?	?	?	?	?	?	?	?	?	?
Lestobradys sprechmanni	1	1	4	4	4	7	4	2	1	0	0	?	?	?	?	?	?	?	?	?	?	1	1	1	0	?	2	1	1
Thinobadistes sp.	1	1	0	4	0	7	4	2	1	0	0	2	2	0	0	?	0	0	1	1	1	1	1	1	0	2	2	1	1
Bolivartherium sp.	6	1	0	4	0	7	4	?	1	0	0	?	?	0	0	?	?	?	?	?	?	?	?	?	?	?	?	?	?
Lestodon armatus	0&1	1	0	4	0	7	4	4	1	0	0	2	1	0	0	1	0	1	1	1	1	1	1	1	0	3	2	1	1
Sphenotherus zavaletianus	1	?	0	?	4	?	4	?	1	0	0	?	?	0	?	?	?	?	?	?	?	?	?	?	?	?	?	?	?
Simomylodon uccasamamensis	0&1	1	3	4	4	7	4	3	1	0	0	2	?	0	1	1	0	1	0	1	1	0	0	1	0	2	2	2	1
Glossotheridium chapadmalense	0	1	3	4	4	7	4	4	1	0	0	2	2	0	1	1	0	?	0	1	1	0	0	1	0	2	2	2	1
Paramylodon garbanii	0	1	3	4	4	7	4	4	1	0	0	2	?	0	1	1	?	?	0	1	1	1	1	1	0	2	2	2	1
Paramylodon harlani	0	1	3	4	4	7	4	3&4	1	0	0&1	2	1&2	0	1	0&1	0	2	0	1	1	0	1	1	0	2	2	2	1
Glossotherium robustum	0	1	3	4	4	7	4	3	1	0	0	2	2	0	1	1	0	2	0	1	1	0	1	1	0	2	2	2	1
Glossotherium tarijense	0	1	3	4	4	7	4	2	1	0	0	?	2	0	1	1	0	?	0	1	1	0	1	1	0	2	2	2	1
Glossotherium tropicorum	0	1	3	4	4	7	4	2	1	0	0	2	2	0	1	0	0	0	0	1	1	1	1	1	0	2	2	2	1
Glossotherium phoenesis	0	1	3	4	4	7	4	3	1	0	0	2	2	0	1	1	0	1	?	1	1	0	1	1	0	2	2	2	1
Octomylodon sp.	-	4	5	6	6	6	3	5	3	1	0	1	2	0	?	1	0	0	2	1	?	2	0	1	0	2	2	2	?
Brievabradys laventensis	1	1	0	0	0	7	3	4	1	0	0	?	?	0	?	?	?	?	?	?	?	?	?	?	?	?	?	?	?
Baraguatherium takumara	0	?	5	6	6	?	3	?	2	?	0	?	?	0	0	?	?	?	?	?	?	?	?	?	?	?	?	?	?
Glossotheriopsis pascuali	0	1	?	?	?	?	?	?	?	?	?	?	?	?	?	?	?	?	?	?	?	?	?	?	?	?	?	?	?
Octodontobradys puruensis	3	4	5	6	6	7	3	2	1	0	0	?	2	0	0	1	0	0	?	1	?	0	0	0	0	2	1	2	0
Pseudoglyptodon sp.	6	6	7	7	8	8	6	3	2	1	1	?	?	0	?	?	?	?	?	?	?	?	?	?	?	?	?	?	?
Eionaletherium tanycnemius	?	?	?	?	?	?	?	?	?	?	?	?	?	?	?	?	?	?	?	?	?	?	?	?	?	?	?	?	?
Pleurolestodon acutidens	1	1	3	4	4	7	4	4	1	0	1	2	?	0	1	0	0	2	0	1	1	0	1	1	0	?	?	2	?
Mylodon darwinii	0	1	0	4	0	7	4	3	1	0	1	2	2	0	?	1	?	2	0	1	?	0	1	1	?	2	2	?	?
Kiyumylodon lecuonai	0	?	0	?	0	?	4	4	1	0	1	2	2	0	1	1	0	2	1	1	1	0	0	1	0	?	2	2	?
Pseudoprepotherium venezuelanum	0	?	0	?	0	?	4	0	1	0	1	?	?	0	?	?	?	?	?	?	?	?	?	1	?	?	2	?	?
Pseudoprepotherium confusum	0	1	0	0	0	7	4	2	1	0	1	2	?	0	?	?	1	?	?	1	?	0	0	1	0	2	2	2	0
Mirandabradys sp.	?	?	?	?	?	?	?	?	?	?	?	?	?	?	?	?	?	?	?	?	?	?	?	?	?	?	?	?	?
Urumacotherium sp.	0	2	1	1	1	4	0	?	1	0	0	?	?	0	0	1	0	?	?	?	?	?	0	1	?	?	?	?	?

	59	60	61	62	63	64	65	66	67	68	69	70	71	72	73	74	75	76	77	78	79	80	81	82	83	84	85	86	87
Pholidota	0	0	1	1	-	0	1	1	0	1	0	1	0	0	0	0	-	-	-	-	-	0	0	3&4	0	0	1	1	0
Euphractus sp.	0	0	0	2	0	0	1	0	0	0	1	1	0	0	0	0	-	0	0	1	0	1	0	4	1	0	0	1	0
Cyclopes sp.	2	0	0	0	-	1	1	0	0	0	0	1	0	1	0	0	-	-	1	0	0	1	0	4	0	0	1	0	0
Tamandua sp.	2	0	0	0	-	1	1	0	0	0	0	1	0	1	0	0	-	-	0	?	?	1	0	1	0	0	0	0	0
Myrmecophaga sp.	2	0	0	0	-	1	1	0	0	0	0	1	0	1	0	0	-	-	1	0	0	1	0	0	0	0	0	0	0
Bradypus sp.	0	0	1	1	0	0	1	0&2	0	0	0	1	0	1	0	1	0&1	0	1	2	1	1	2	4	0	0	4	1	0
Hapalops sp.	0	1	1	2&3	0	0	1&2	2	0	1	0	1	1	0&1	0&1	1	0&1	1&2	?	?	?	?	2	2&3	0	1	2&3	0&1	0
Nematherium sp.	1	0	1	2	1	0	1&2	2	0	1	0	1	1	0	1	1	0	0	1	3	1	?	1	2	0	0	3	0	0
Scelidotherium sp.	0&1	0	1	3	1	0	2	0	0	2	0	0	0	0	0&1	1	0	0	?	?	?	?	0	0	0	0	1	0	1
Catonyx sp.	2	0	1	2	1	0	2	2	0	2	0	0	1	0	1	1	0	0	1	3	1	?	?	0	0	0	1	1	1
Octodontotherium grande	?	?	?	3	0	0	1	?	2	1	0	?	0	?	1	1	0	0	?	?	?	?	?	3	1	0	4	3	1
Paroctodontotherium calleorum	?	?	?	?	?	?	?	?	?	?	?	?	?	?	?	?	?	?	?	?	?	?	?	3	1	?	?	3	1
Orophodon hapaloides	?	?	?	?	0	?	?	?	?	?	?	?	?	?	1	1	0	0	?	?	?	?	?	?	?	?	?	?	?
Lestobradys sprechmanni	0	1	1	2	1	0	1	?	?	1	?	?	0	?	1	1	1	2	?	?	?	?	?	?	?	?	?	?	?
Thinobadistes sp.	0	1	1	2	1	0	0	1	1	1	0	1	0	0	1	1	0	1	1	3	1	?	1	2	0	1	2	3	1
Bolivartherium sp.	?	?	1	2	0	0	0	1	1&2	1	0	1	0	1	1	1	0	1	?	?	?	?	?	?	0	?	?	?	?
Lestodon armatus	0	1	1	1	1	0	0	1	2	1	0	0	0	0	1	1	0	2	?	?	?	?	?	0	0	0	3	2	1
Sphenotherus zavaletianus	?	?	1	?	0	0	0	1	?	?	0	1	0	0	1	1	0	1	?	?	?	?	?	?	?	?	?	?	?
Simomylodon uccasamamensis	0	1	1	1	1	0	0	1	2	1	0	0	0	0	1	1	0	0	?	?	?	?	1	3	0	0	3	2	1
Glossotheridium chapadmalense	0	1	1	1	0	0	0	1	2	1	0	0	0	0	1	1	0	0	?	?	?	?	?	2	0	0	3	2	1
Paramylodon garbanii	0	1	1	?	0	0	?	?	?	?	?	?	?	?	?	1	0	0	?	?	?	?	?	?	?	?	?	?	?
Paramylodon harlani	0	1	1	2	0&1	0	0	1	2	1	0	0	0	0	1	1	0	0	1	3	1	1	1	0	0	0	3	2	1
Glossotherium robustum	0	1	1	2	1	0	0	1	2	1	0	0	0	0	1	1	0	0	1	3	1	?	0&1	2	0	0	3	3	1
Glossotherium tarijense	0	1	1	2	1	0	0	1	?	1	0	0	0	0	1	1	0	0	?	?	?	?	1	2	0	0	3	2	1
Glossotherium tropicorum	0	1	1	2	1	0	0	1	2	1	0	1	0	0	1	1	0	0	?	?	?	?	?	2	0	0	3	2	1
Glossotherium phoenesis	0	1	1	2	1	0	0	1	1	1	0	1	0	0	1	1	0	0	?	?	?	?	0	2	0	0	3	2	?
Octomylodon sp.	1	?	1	3	0	0	2	?	0	2	1	1	1	0	1	1	0	-	?	?	?	?	?	?	0	0	3	1	?
Brievabradys laventensis	?	?	1	2	1	0	1	?	?	?	0	?	0	?	1	1	0	0	?	?	?	?	?	?	0	0	4	?	1
Baraguatherium takumara	?	?	1	?	1	?	?	?	0	?	?	?	?	?	?	1	0	0	?	?	?	?	?	?	?	?	?	?	?
Glossotheriopsis pascuali	?	?	?	?	?	?	?	?	?	?	?	?	?	?	?	?	?	?	?	?	?	?	?	?	?	?	?	?	1
Octodontobradys puruensis	1	0	1	3	1	0	1	0	0	1	0	1	1	1	1	1	0	0	?	?	?	?	?	?	?	?	?	?	?
Pseudoglyptodon sp.	?	?	1	?	1	0	?	?	?	0	0	1	0	?	?	0	-	?	?	?	?	?	?	?	?	?	3	?	?
Eionaletherium tanycnemius	?	?	?	?	?	?	?	?	?	?	?	?	?	?	?	?	?	?	?	?	?	?	?	?	?	?	?	?	?
Pleurolestodon acutidens	0	?	1	2	1	0	0	1	2	1	0	1	0	0	1	1	0	0	?	?	?	?	?	3	0	0	3	2	1
Mylodon darwinii	?	?	?	2	1	0	0	1	2	2	0	0	0	0	1	1	0	0	?	?	?	?	?	0	0	0	3	1	1
Kiyumylodon lecuonai	0	?	?	?	?	0	0	?	?	?	?	0	?	?	?	1	0	0	?	?	?	?	?	?	?	?	?	?	?
Pseudoprepotherium venezuelanum	?	?	1	3	1	0	1	0	1	2	0	1	1	0	1	1	0	0	?	?	?	?	?	?	?	?	?	?	?
Pseudoprepotherium confusum	1	1	1	3	1	0	1	0	1	2	0	1	1	0	1	1	0	0	?	?	?	?	1	0	0	?	3	?	1
Mirandabradys sp.	?	?	?	?	?	?	?	?	?	?	?	?	?	?	?	?	?	?	?	?	?	?	?	?	?	?	?	?	1
Urumacotherium sp.	?	?	?	1	0	0	1	0	1	?	0	1	1	0	1	1	0	0	?	?	?	?	?	1	0	0	3	2	1

	88	89	90	91	92	93	94	95	96	97	98	99	100	101	102	103	104	105	106	107	108	109	110	111	112	113	114	115	116
Pholidota	0	0	2	0	0	0	2	0	-	2	0	0	1	0	0	-	0	-	0	1	0	-	-	1	-	1	1	0	0
Euphractus sp.	0	0	1	0	0	0	0	1	1	0	0	2	0	0&1	1	-	0	0	2	1	1	0	0	-	0	0	0	6	-
Cyclopes sp.	0	0	0	0	1	0	2	0	0	2	0	0	2	1	0	-	0	-	0	1	0	-	0	2	-	1	1	0	0
Tamandua sp.	0	0	0	0	0	0	2	0	0	2	0	0	2	0	0	-	0	-	0	1	0	-	0	2	-	1	1	0	0
Myrmecophaga sp.	0	0	0	0	1	0	2	0	0	2	0	0	2	0	0	-	0	-	0	1	0	-	0	-	-	1	1	0	0
Bradypus sp.	0	1	1	0	0	0	2	0	0	1	0	1	0	1	2	0	0	0	0	1	1	1	1	-	0	1	3	0	?
Hapalops sp.	0	0	1	0	0	0&2	2	0	1	0&1	0	1	0	1	0	0	0	0	1&2	1	1	1	0&1	2	1	1	2	4	0
Nematherium sp.	0	?	1	0	0	0	2	0	?	0	0	1	0	0&1	0	0	0&1	0	0	1	1	1	1	0&1	0	1	3	0	0
Scelidotherium sp.	0	0	1	0	0	1	1	0	0	1	1	1	2	1	0	0	1	1	0	0	1	1	1	0	0	0	2	0	0
Catonyx sp.	0	0	1	0	0	1	1	0	0	0	1	1	2	1	0	0	1	1	0	0	1	0	1	0	1	0	2	0	0
Octodontotherium grande	1	0	1	?	0	1	1	0	0	0	1	1	0	1	0	?	?	?	0	1	1	?	1	2	0	1	?	?	?
Paroctodontotherium calleorum	1	?	1	?	0	1	1	0	0	0	1	1	?	?	?	1	1	0	0	?	1	?	1	2	?	1	?	?	?
Orophodon hapaloides	?	?	?	?	?	?	?	?	?	?	?	?	?	?	?	?	?	?	?	?	?	?	?	?	?	?	?	?	?
Lestobradys sprechmanni	1	?	?	1	?	?	?	?	?	?	1	1	?	?	?	?	?	?	1	?	?	?	?	?	?	1	?	?	?
Thinobadistes sp.	1	?	1	1	1	0	?	1	0	0	1	1	0	1	0	1	1	0	0	1	1	?	?	1	0	1	3	2	-
Bolivartherium sp.	?	?	?	?	1	0	?	?	?	0	1	1	?	?	?	1	1	0	2	1	1	?	1	1	0	1	?	?	?
Lestodon armatus	1	0	1	1	1	1	?	1	?	0	1	1	1	1	0	1	1	0	2	?	?	?	?	1	?	1	3	1	0
Sphenotherus zavaletianus	?	?	?	?	?	?	?	?	?	?	?	?	?	?	?	?	?	?	?	?	?	?	?	?	?	?	?	?	?
Simomylodon uccasamamensis	1	?	1	1	1	0	0	1	0	1	1	1	0&1	1	0	1	1	0	1	1	1	0	1	0	0	1	3	1	0
Glossotheridium chapadmalense	1	?	1	1	1	0	0	1	0	1	1	1	1	1	0	1	1	0	1	1	1	0	1	0	0	1	3	1	0
Paramylodon garbanii	?	?	?	?	?	?	?	1	0	?	?	?	?	?	?	1	?	?	?	?	?	?	?	?	?	1	?	?	?
Paramylodon harlani	1	1	1	1	1	0	0	1	0	1	1	1	1	1	0	1	1	0	1	1	1	0	1	0	0	1	3	1	1
Glossotherium robustum	1	1	1	1	1	0	0	1	0	1	1	1	?	1	0	1	1	0	1	1	1	?	1	0	?	1	3	1	0
Glossotherium tarijense	1	1	1	1	1	0	0	1	0	1	1	1	?	1	0	1	1	0	1	1	1	0	1	0	0	1	?	1	0
Glossotherium tropicorum	1	1	1	1	1	0	1	1	0	1	1	1	?	?	?	1	1	0	1	1	1	0	1	0	0	1	?	1	?
Glossotherium phoenesis	1	1	1	1	1	0	0	?	0	1	1	1	1	1	0	1	1	0	1	1	1	0	1	0	0	1	?	1	0
Octomylodon sp.	?	?	1	1	?	?	?	0	0	?	?	?	?	?	?	?	?	0	0	?	1	?	?	?	?	?	?	?	?
Brievabradys laventensis	0	?	1	1	0	?	?	?	?	?	?	?	?	?	?	?	?	?	1	?	?	?	1	?	0	?	?	?	?
Baraguatherium takumara	?	?	?	?	?	?	?	?	?	?	?	?	?	?	?	?	?	?	?	?	?	?	?	?	?	?	?	?	?
Glossotheriopsis pascuali	1	?	?	?	?	?	?	?	?	?	?	1	?	1	?	?	?	?	1	?	1	?	?	?	?	?	?	?	?
Octodontobradys puruensis	?	?	?	?	?	?	?	?	?	?	?	?	?	?	?	?	?	?	1	?	?	?	1	?	?	?	?	?	?
Pseudoglyptodon sp.	?	?	?	?	?	?	?	?	?	?	?	?	2	1	?	?	?	?	?	?	?	?	?	?	?	?	?	?	?
Eionaletherium tanycnemius	?	?	?	?	?	?	?	?	?	?	?	?	?	?	?	?	?	?	?	?	?	?	?	?	?	?	?	?	?
Pleurolestodon acutidens	1	0	1	1	1	0	0	1	0	1	1	1	1	1	0	1	1	0	0	1	1	0	1	0	0	1	3	1	0
Mylodon darwinii	0	0	1	1	1	0	1	1	0	1	1	1	?	?	?	1	1	0	1	1	1	0	?	0	0	0	3	0	1
Kiyumylodon lecuonai	?	?	?	?	?	?	?	?	?	?	?	?	?	?	?	?	?	?	?	?	?	?	?	?	?	?	?	?	?
Pseudoprepotherium venezuelanum	?	?	?	?	?	?	?	?	?	?	?	?	?	?	?	?	?	?	?	?	?	?	?	?	?	?	?	?	?
Pseudoprepotherium confusum	0	?	1	1	0	0	?	0	0	1	0	1	?	1	0	1	1	0	1	1	1	?	1	2	0	1	?	?	?
Mirandabradys sp.	?	?	?	2	0	0	?	?	?	1	1	?	?	?	?	?	?	?	?	?	?	?	?	?	?	?	?	?	?
Urumacotherium sp.	1	?	1	1	?	0	?	0	0	?	?	1	?	1	0	?	1	?	1	?	?	?	1	2	0	1	?	?	?

	117	118	119	120	121	122	123	124	125	126	127	128	129	130	131	132	133	134	135	136	137	138	139	140	141	142	143	144	145
Pholidota	0	0	0	0	2&4	1	0	0	0	0	1	0	0	0&1	0	0	0	0	1	0	0	0	0	0	0	?	0	0	-
Euphractus sp.	0	1	0	0	0	1	0	0	0	0	1	0	0	0	0	0	0	1	1	0	0	0	1	1	0	0	0	0	1
Cyclopes sp.	0	?	1	0	0	0	0	2	1	0	3	1	0	0	0	0	-	-	0	-	0	0	1	1	0	0	0	1	-
Tamandua sp.	0	1	2	0	0	0	0	-	1	-	3	1	1	0	0	0	-	-	0	-	2	0	1	1	1	1	0	0	0
Myrmecophaga sp.	0	?	1	0	0	0	0	-	1	-	3	1	1	0	0	0	-	-	0	-	2	0	1	1	1	0	0	0	0
Bradypus sp.	?	0	2	1	1	1	1	0	1	0	0	0	0	2	1	0	0	2	2	1	0	0	0	1	0	3	0	1	2
Hapalops sp.	0	?	?	1	3	4	1	0	1	0	0	0	0	1&2	1	0	1	2	2	2	0	0	1	0	0	3	1	1	3
Nematherium sp.	0	?	?	1	4	1	1	1	1	0	0	0	0	1	?	?	1	2	2	2	0	0	1	0	0	2	1	1	3
Scelidotherium sp.	1	?	?	1	5	1	1	1	0	1	0	0	0	1	1	0	1	2	2	2	1	0	1	1	0	2	0	0	3
Catonyx sp.	1	?	2	1	5	1	1	1	1	1	0	0	0	2	1	0	1	2	2	2	?	0	1	0	0	0	0	0	3
Octodontotherium grande	?	?	?	1	4	3	1	?	1	?	0	0	0	2	1	?	1	2	2	2	1	0	1	0	0	0	0	0	3
Paroctodontotherium calleorum	?	?	?	?	4	3	1	?	?	?	?	0	?	?	?	?	?	?	?	?	1	?	?	?	?	?	?	?	?
Orophodon hapaloides	?	?	?	?	?	?	?	?	?	?	?	?	?	?	?	?	?	?	?	?	?	?	?	?	?	?	?	?	?
Lestobradys sprechmanni	?	?	?	?	?	3	?	?	?	?	?	?	?	?	?	?	?	?	?	?	?	?	?	?	?	?	?	?	?
Thinobadistes sp.	0	?	?	1	4	3	1	1	1	1	0	0	0	2	?	?	1	2	2	2	0	0	1	0	0	0	0	1	3
Bolivartherium sp.	?	?	?	?	4	3	1	?	?	?	?	?	?	?	?	?	?	?	?	?	?	?	?	?	?	?	?	?	?
Lestodon armatus	1	?	?	?	4	3	1	1	1	0	0	0	0	2	?	?	1	2	2	2	1	0	?	?	0	0	0	0	3
Sphenotherus zavaletianus	?	?	?	?	?	?	?	?	?	?	?	?	?	?	?	?	?	?	?	?	?	?	?	?	?	?	?	?	?
Simomylodon uccasamamensis	1	?	?	1	4	3	1	1	1	1	0	0	0	2	1	0	1	2	2	2	1	0	1	0	0	0	0	0	3
Glossotheridium chapadmalense	1	?	?	1	4	3	1	1	1	1	0	0	0	2	1	0	1	2	2	2	1	0	1	0	0	0	0	0	3
Paramylodon garbanii	?	?	?	1	4	3	1	?	?	?	?	?	?	?	?	?	?	?	?	?	?	?	?	?	?	?	?	?	?
Paramylodon harlani	1	?	2	1	4	3	1	1	1	1	0	0	0	2	1	0	1	2	2	2	1	0	1	0	0	0&1	0	0	3
Glossotherium robustum	1	?	?	1	4	3	1	1	1	1	0	0	0	2	1	0	1	2	2	2	1	0	?	?	0	1	0	0	3
Glossotherium tarijense	1	?	?	1	4	3	1	1	1	1	0	0	0	2	1	?	1	2	2	2	1	0	1	0	0	0	0	0	?
Glossotherium tropicorum	?	?	?	1	4	3	1	1	1	1	0	0	0	2	1	?	1	2	2	2	1	0	1	0	?	?	?	?	?
Glossotherium phoenesis	1	?	?	1	4	3	1	1	1	1	0	0	0	2	1	?	1	2	2	2	1	0	1	0	0	0	0	0	?
Octomylodon sp.	?	?	?	?	?	?	?	0	?	?	0	0	0	1	?	?	1	2	2	2	0	0	?	?	?	?	0	0	3
Brievabradys laventensis	?	?	?	?	?	3	1	1	?	0	0	0	0	2	?	?	1	?	2	?	?	?	1	?	0	?	?	?	?
Baraguatherium takumara	?	?	?	?	?	?	?	?	?	?	?	?	?	?	?	?	?	?	?	?	?	?	?	?	?	?	?	?	?
Glossotheriopsis pascuali	?	?	?	?	?	?	1	?	?	?	?	?	?	?	?	?	?	?	?	?	?	?	?	?	?	?	?	?	?
Octodontobradys puruensis	?	?	?	?	?	?	1	?	?	?	?	?	?	?	?	?	?	?	?	?	?	?	?	?	?	?	?	?	?
Pseudoglyptodon sp.	?	?	?	?	?	2	?	?	?	?	?	?	?	?	?	?	?	?	?	?	?	?	?	?	?	2	?	?	2
Eionaletherium tanycnemius	?	?	?	?	?	?	?	?	?	?	?	?	?	?	?	?	?	?	?	?	?	?	?	?	?	?	?	?	?
Pleurolestodon acutidens	1	?	?	1	4	3	1	1	1	?	0	0	0	2	?	?	1	2	2	2	1	0	1	0	0	0	0	0	3
Mylodon darwinii	1	?	?	1	4	3	1	1	1	0	0	0	0	2	1	0	1	2	2	2	1	0	1	0	0	?	0	0	3
Kiyumylodon lecuonai	?	?	?	?	?	?	?	?	?	?	?	?	?	?	?	?	?	?	?	?	?	?	?	?	?	?	?	?	?
Pseudoprepotherium venezuelanum	?	?	?	?	?	?	?	?	?	?	?	?	?	?	?	?	?	?	?	?	?	?	?	?	?	?	?	?	?
Pseudoprepotherium confusum	?	?	?	1	4	2	1	1	1	?	0	0	0	?	?	?	1	2	2	2	1	0	1	0	0	2	0	1	?
Mirandabradys sp.	?	?	?	?	?	2	?	?	?	?	?	?	?	?	?	?	?	?	?	?	?	?	?	?	?	?	?	?	?
Urumacotherium sp.	?	?	?	?	?	3	?	1	?	0	?	?	0	2	?	?	?	2	2	2	?	?	1	?	0	?	?	0	?

	146	**147**	**148**	**149**	**150**	**151**	**152**	**153**	**154**	**155**	**156**	**157**	**158**	**159**	**160**	**161**	**162**	**163**	**164**	**165**	**166**	**167**	**168**	**169**	**170**	**171**	**172**	**173**	**174**
Pholidota	-	-	-	-	-	-	-	-	-	-	0	1	0&1	0	0	0	0	1	0	0	1	0	1	0	1	2	2	0	1
Euphractus sp.	2	0	-	-	-	-	0	0	0	0	2	1	0	0	0	0	1	0	2	0	0	0	3	0	0	-	0	0	0
Cyclopes sp.	-	-	-	-	-	-	-	-	-	-	0	0	0	1	0	0	0	1	0	1	1	0	0	1	0	0	0	0	1
Tamandua sp.	0	0	-	-	-	-	-	-	-	1	1	0	0	0&1	0	0	0	0	0	1	1	0	0	0	0	0	0	0	1
Myrmecophaga sp.	0	0	-	-	-	-	-	-	-	1	1	0	0&1	1	0	0	0	0	0	1	1	0	0	0	0	0	0	0	1
Bradypus sp.	2	0	-	1	1	1	2	1	0	1	0	1	2&3	1	1	1	2	0	3	1	0	0&1	2	0	1	0	1	0	2
Hapalops sp.	1&2	1	1	1	1	1	1	1	0	1	0	1	2	1	1	0&1	2	0	1	0&1	0	1	2	1	1	0	1	0	?
Nematherium sp.	?	1	?	?	?	?	1	?	?	1	0	1	2	1	1	0	2	?	?	0&1	0	0	1	1	1	0	1	0	2
Scelidotherium sp.	0	0	0	1	1	0	0	1	1	1	0	1	1&2	0	1	0	2	0	1	0	0	1	1	1	1	0	2	0	3
Catonyx sp.	0	0	0	1	0	0	0	1	1	1	0	1	2	0	1	1	2	0	1	0	0	0	1	1	0	0	2	0	?
Octodontotherium grande	2	0	0	1	0	?	0	?	?	1	0	?	1	?	?	?	?	?	?	?	?	0	2	1	1	0	?	0	?
Paroctodontotherium calleorum	?	?	?	?	?	?	?	?	?	1	0	1	?	?	?	?	?	?	?	?	?	0	2	0	1	0	?	0	?
Orophodon hapaloides	?	?	?	?	?	?	?	?	?	?	?	?	?	?	?	?	?	?	?	?	?	?	?	?	?	?	?	?	?
Lestobradys sprechmanni	?	?	?	?	?	?	?	?	?	?	?	?	?	?	?	?	?	?	?	?	?	?	?	?	?	?	?	?	?
Thinobadistes sp.	1	0	0	0	0	1	0	1	0	1	0	1	?	?	?	?	?	?	?	?	?	0	2	0	1	1	?	1	3
Bolivartherium sp.	?	?	?	?	?	?	?	?	?	1	0	?	?	?	?	?	?	?	?	?	?	?	?	?	?	?	?	1	?
Lestodon armatus	1	0	0	1	0	0	2	1	0	1	2	1	1	0	?	1	?	?	?	?	?	0	2	1	1	1	?	0	3
Sphenotherus zavaletianus	?	?	?	?	?	?	?	?	?	?	?	?	?	?	?	?	?	?	?	?	?	?	?	?	?	?	?	?	?
Simomylodon uccasamamensis	1	0	0	0	0	1	0	1	0&1	1	0	1	2	0	1	1	2	?	?	?	?	0	3	1	1	1	?	1	3
Glossotheridium chapadmalense	1	0	0	0	0	1	0	1	1	1	0	1	2	0	1	1	2	?	?	0	?	0	3	1	1	1	?	1	?
Paramylodon garbanii	?	?	?	?	?	?	?	?	?	?	?	?	?	?	?	?	?	?	?	?	?	0	?	1	?	1	?	?	?
Paramylodon harlani	1	0	0	0	0	0	0	1	1	1	0	1	2	0	1	1	2	0	1	0	0	0	2	1	1	1	2	1	3
Glossotherium robustum	0	0	0	0	0	0	0	1	1	1	0	1	2	0	1	1	?	?	?	?	?	0	2	1	1	1	?	1	3
Glossotherium tarijense	?	0	?	?	?	?	?	?	?	1	0	1	2	?	?	?	?	?	?	?	?	?	2	1	?	?	2	1	3
Glossotherium tropicorum	?	0	?	?	?	?	?	?	?	1	0	1	2	0	1	1	2	?	?	0	0	0	2	1	1	1	2	0	3
Glossotherium phoenesis	?	0	?	?	?	?	?	?	?	1	0	1	2	0	1	1	2	?	?	0	0	0	2	1	1	1	2	1	3
Octomylodon sp.	?	0	?	0	1	?	2	?	0	1	0	1	?	?	?	?	?	?	?	?	?	0	1	1	1	0	?	?	?
Brievabradys laventensis	?	?	?	?	?	?	?	?	?	?	?	?	?	1	1	1	2	?	?	?	?	?	?	?	?	?	?	?	?
Baraguatherium takumara	?	?	?	?	?	?	?	?	?	?	?	?	?	?	?	?	?	?	?	?	?	?	?	?	?	?	?	?	?
Glossotheriopsis pascuali	?	?	?	?	?	?	?	?	?	?	?	?	?	?	?	?	?	?	?	?	?	?	?	?	?	?	?	?	?
Octodontobradys puruensis	?	?	?	?	?	?	?	?	?	?	?	?	?	?	?	?	?	?	?	?	?	?	?	?	?	?	?	?	?
Pseudoglyptodon sp.	?	?	?	?	?	?	?	1	?	?	?	?	?	?	?	?	?	?	?	?	?	?	?	?	?	?	?	?	?
Eionaletherium tanycnemius	?	?	?	?	?	?	?	?	?	?	?	?	?	?	?	?	?	?	?	?	?	?	?	?	?	?	?	?	?
Pleurolestodon acutidens	1	0	0	0	0	0	0	1	1	1	0	1	?	?	?	1	2	?	?	0	?	0	1	1	1	1	2	1	?
Mylodon darwinii	0	0	0	0	0	0	0	1	1	1	0	1	2&3	0	1	1	2	0	1	0	0	0	2	1	0	1	2	1	3
Kiyumylodon lecuonai	?	?	?	?	?	?	?	?	?	?	?	?	?	?	?	?	?	?	?	?	?	?	?	?	?	?	?	?	?
Pseudoprepotherium venezuelanum	?	?	?	?	?	?	?	?	?	?	?	?	?	?	?	?	?	?	?	?	?	?	?	?	?	?	?	?	?
Pseudoprepotherium confusum	?	0	?	?	?	?	?	?	?	1	0	1	2	1	1	0	2	?	1	0	0	0	1	1	1	0	?	1	3
Mirandabradys sp.	?	?	?	?	?	?	?	?	?	?	?	?	?	?	?	?	?	?	?	?	?	?	?	?	?	?	?	?	?
Urumacotherium sp.	?	?	?	?	?	?	?	?	?	?	?	?	?	?	?	?	?	?	?	?	?	?	1	1	1	0	?	?	?

	175	176	177	178	179	180	181	182	183	184	185	186	187	188	189	190	191	192	193	194	195	196	197	198	199	200	201	202	203
Pholidota	0	1	0	-	0	0	0	0	-	-	0	0	1	-	0	-	1&2	1	0&1	1&2	0	0	0	0	0	0	0	0	1
Euphractus sp.	0&1	1	1	0	0	0	1	2	0	1	0	0	1	0	1	1	1	0	0	0	0	1	0	0&1	0	0	0	0	2
Cyclopes sp.	0	1	0	-	1	0	1	1	0	0	0	2	1	-	0	1	2	2	0	1	0	0	0	0	0	0	0	0	0
Tamandua sp.	0	1	0	-	1	0	0	1	0	0	0	1	1	-	0	0	1	1	1	1	1	0	0	0	2	0	0	0	1
Myrmecophaga sp.	0	1	0	-	1	0	0	1	0	0	0	2	0	-	0	0	2	1	1	0	1	0	0	0	2	0	0	1	1
Bradypus sp.	1&2	1	1	0	1	1	0	2	1	0	0	1	2	0	1	0	2	1	1	1	0	1	0	2	0	0	0	0&1	1
Hapalops sp.	1	1	0&1	0	0&1	0&1	0&1	2	1	1	1	0&1	0&1	0	0&1	0	2	1	1	0&1	1	1	0	1	0	0	0	1	1
Nematherium sp.	1	0	0	0	1	0&1	0	2	0	0	0	1	2	0	0	0	2	1	0	1	1	1	0	?	0	0	0	0	1
Scelidotherium sp.	1	0	0	1	0&1	0	0	2	0	0	0	1	0	0	1	0	2	1	0	1	0	0	0	1	1	0	0	0	2
Catonyx sp.	1	0	0	0	0&1	0	1	2	0	0	0	1	1	0	1	0	2	1	0	1	1	1	0	1	1	0	0	0	2
Octodontotherium grande	1	1	?	0	?	0	0	2	0	0	0	1	1	?	0	0	1	0	1	1	0	1	0	1	?	?	?	?	?
Paroctodontotherium calleorum	1	?	0	?	1	0	0	2	0	0	0	1	?	?	0	0	0	1	1	?	0	?	?	?	?	?	?	?	?
Orophodon hapaloides	?	?	?	?	?	?	?	?	?	?	?	?	?	?	?	?	?	?	?	?	?	?	?	?	?	?	?	?	?
Lestobradys sprechmanni	?	?	?	?	?	?	?	?	?	?	?	?	?	?	?	?	?	?	?	?	?	?	?	?	?	?	?	?	?
Thinobadistes sp.	1	0	0	0	?	0	0	2	0	0	0	0	2	0	0	0	0	1	0	1	0	1	0	?	?	?	?	?	?
Bolivartherium sp.	2	0	?	?	?	?	0	2	0	0	0	?	?	?	0	?	0	?	0	?	0	?	?	?	?	?	?	?	?
Lestodon armatus	2	0	0	0	?	0	0	2	0	0	0	1	0	0	0	0	0	1	0	1	0	1	0	?	?	?	?	0	0
Sphenotherus zavaletianus	?	?	?	?	?	?	?	?	?	?	?	?	?	?	?	?	?	?	?	?	?	?	?	?	?	?	?	?	?
Simomylodon uccasamamensis	1	0	0	0	1	0	0	2	0	0	0	0	2	0	0	0	0	1	0	2	0	?	0	?	?	?	?	?	0
Glossotheridium chapadmalense	1	0	0	0	1	0	0	2	0	0	0	0	1	0	0	0	1	1	0	2	0	1	0	?	?	?	?	0	0
Paramylodon garbanii	?	?	?	?	?	?	?	2	?	?	?	?	?	?	?	0	1	1	0	?	0	?	?	?	?	?	?	?	0
Paramylodon harlani	1	0	0	0	1	0	0	2	0	0	0	1	1&2	0	0	0&1	1	1	0	1	0	1	0	2	0	0	0	1	0
Glossotherium robustum	1	?	0	0	?	0	0	2	0	0	0	0	1	0	0	0	1	1	0	1	0	1	0	1	0	0	0	0	0
Glossotherium tarijense	1	?	0	?	1	0	0	2	0	0	0	0	?	0	0	0	1	1	0	1	0	1	0	?	?	?	?	?	?
Glossotherium tropicorum	1	0	0	0	1	0	0	2	0	0	0	0	1	0	0	0	0	1	0	2	0	1	0	1	?	?	?	?	0
Glossotherium phoenesis	1	0	0	0	?	0	0	2	0	0	0	0	1	0	0	0	0	1	0	2	0	1	0	?	?	?	?	?	?
Octomylodon sp.	1	?	0	0	?	0	0	2	?	?	?	1	?	0	?	?	?	?	?	?	?	?	?	?	?	?	?	?	?
Brievabradys laventensis	1	?	?	?	?	?	?	?	?	?	?	?	?	?	?	?	?	?	?	?	?	?	?	?	?	?	?	?	?
Baraguatherium takumara	?	?	?	?	?	?	?	?	?	?	?	?	?	?	?	?	?	?	?	?	?	?	?	?	?	?	?	?	?
Glossotheriopsis pascuali	?	?	?	?	?	?	?	?	?	?	?	?	?	?	?	?	?	?	?	?	?	?	?	?	?	?	?	?	?
Octodontobradys puruensis	?	?	?	?	?	?	?	?	?	?	?	?	?	?	?	?	?	?	?	?	?	?	?	?	?	?	?	?	?
Pseudoglyptodon sp.	?	?	?	?	?	?	?	?	?	?	?	?	?	?	?	?	?	?	?	?	?	?	?	?	?	?	?	?	?
Eionaletherium tanycnemius	?	?	?	?	?	?	?	?	?	?	?	?	?	?	?	?	?	?	?	?	?	?	?	?	?	?	?	?	?
Pleurolestodon acutidens	1	0	0	0	1	0	0	2	0	0	0	0	0	0	0	0	0	1	0	2	0	?	?	?	?	?	?	?	0
Mylodon darwinii	2	0	0	0	1	0	0	2	0	0	0	1	1	0	0	1	0	1	0	1	0	1	0	2	0	0	0	0&1	0
Kiyumylodon lecuonai	?	?	?	?	?	?	?	?	?	?	?	?	?	?	?	?	?	?	?	?	?	?	?	?	?	?	?	?	?
Pseudoprepotherium venezuelanum	?	?	?	?	?	?	?	?	?	?	?	?	?	?	?	?	?	?	?	?	?	?	?	?	?	?	?	?	?
Pseudoprepotherium confusum	1	?	0	2	1	0	0	2	0	0	?	1	0	0	0	0	1	1	1	1	1	1	0	?	?	?	0	?	?
Mirandabradys sp.	?	?	?	?	?	?	0	2	?	?	?	?	?	?	?	?	?	?	1	?	?	?	?	?	?	?	?	?	?
Urumacotherium sp.	?	?	0	?	?	?	0	2	?	?	0	2	?	0	0	?	?	?	1	?	1	?	?	?	?	?	?	?	?

	204	205	206	207	208	209	210	211	212	213	214	215	216	217	218	219	220	221	222	223	224	225	226	227	228	229	230	231	232
Pholidota	0	0	1	2	0&1	1	0	0	0	0	0	0	1	0	0	0	?	?	0	0	2	0	?	?	?	0	0	?	0
Euphractus sp.	1	0	1	0	1	1	0	0	0	1	1	0	1	1	2	1	0	?	1	0	0	0	0	0	1	0	2	?	0
Cyclopes sp.	1	0	1	2	0&1	1	0	1	0	0	0	0	2	0	0	0	?	?	0	0	0	0	?	0	?	0	1	?	1
Tamandua sp.	1	0	1	0	0	1	0	1	0	0	0	0	2	0	0	0	?	?	0	0	?	0	?	?	?	1	0	?	1
Myrmecophaga sp.	1	0	1	0	0&1	1	0	1	0	0	0	1	2	0	0	0	?	?	0	0	?	0	?	?	?	1	0	?	1
Bradypus sp.	1	1	1	0	1	1	0	1	1	0	1	1	1	2	1	1	1	0	0	0	1	1	1	2	1	1	1	1	1
Hapalops sp.	0	1	1	0	1	0	0	0	0	0	0	0	1	2	2	1	1	0	1	1	1	0	1	2	1	1	1	1	1
Nematherium sp.	0	1	0	1	0	0	0	0	0	1	0	?	2	2	2	1	1	0	0	1	1	0	0	2	1	1	2	1	1
Scelidotherium sp.	0	1	0	0	1	0	0	0	0	1	0	0	2	2	2	1	1	0	0	1	1	0	0	2	0	1	2	1	1
Catonyx sp.	0	1	0	0	1	0	0	?	0	1	0	?	0&2	2	2	1	1	0	0	1	1	0	0	2	0	1	2	1	1
Octodontotherium grande	0	1	?	?	?	?	?	?	0	?	?	?	?	?	?	1	1	?	?	?	?	0	0	?	?	1	?	?	1
Paroctodontotherium calleorum	?	?	?	?	?	?	?	?	?	?	?	?	?	?	?	?	?	?	?	?	?	?	?	?	?	?	?	?	?
Orophodon hapaloides	?	?	?	?	?	?	?	?	?	?	?	?	?	?	?	?	?	?	?	?	?	?	?	?	?	?	?	?	?
Lestobradys sprechmanni	?	?	?	?	?	?	?	?	?	?	?	?	?	?	?	?	?	?	?	?	?	?	?	?	?	?	?	?	?
Thinobadistes sp.	?	?	?	?	?	?	?	?	0	?	?	?	?	?	?	1	1	0	?	1	1	0	?	?	?	1	2	?	1
Bolivartherium sp.	?	?	?	?	?	?	?	?	?	?	?	?	?	?	?	?	?	?	?	?	?	?	?	?	?	?	?	?	?
Lestodon armatus	0	1	0	0	0	0	?	?	0	2	0	?	0	1	?	0	1	0	0	1	?	0	?	1	?	1	0	?	1
Sphenotherus zavaletianus	?	?	?	?	?	?	?	?	?	?	?	?	?	?	?	?	?	?	?	?	?	?	?	?	?	?	?	?	?
Simomylodon uccasamamensis	0	1	0	0	0	0	0	1	0	1	0	0	0	2	2	1	?	0	0	0	?	0	?	1	0	1	0	0	1
Glossotheridium chapadmalense	0	1	0	0	0	0	?	1	0	1	0	?	0	1	2	0	1	0	0	0	?	0	?	?	0	1	0	0	1
Paramylodon garbanii	0	1	?	?	?	?	?	?	0	?	?	?	?	2	?	1	?	0	?	?	1	?	0	?	?	?	0	?	?
Paramylodon harlani	0&1	1	0	0	0&1	0	0	1	0	1&2	0	0	0	1&2	1&2	0&1	1	?	?	1	?	0&1	?	1&2	0	1	0	0	1
Glossotherium robustum	0	1	0	0	0	0	0	1	0	2	0	0	0	1&2	2	0&1	1	?	0	0	?	0	?	1	0	1	0	0	1
Glossotherium tarijense	0	1	?	?	?	?	?	?	0	2	0	?	0	1	?	0	?	0	0	?	1	0	0	1	0	1	0	?	1
Glossotherium tropicorum	0	1	?	?	?	?	?	?	0	2	0	0	0	1	?	0	1	0	0	1	1	0	0	1	0	1	0	0	1
Glossotherium phoenesis	0	1	?	?	?	?	?	?	0	2	0	?	0	1&2	?	0&1	1	0	0	0	1	0	0	1	0	1	0	?	1
Octomylodon sp.	?	?	?	?	?	?	?	?	?	?	?	?	?	?	?	?	?	?	?	?	?	?	?	?	?	?	?	?	?
Brievabradys laventensis	?	?	?	?	?	?	?	?	?	?	?	?	?	?	?	?	?	?	?	?	?	?	?	?	?	?	?	?	?
Baraguatherium takumara	?	?	?	?	?	?	?	?	?	?	?	?	?	?	?	?	?	?	?	?	?	?	?	?	?	?	?	?	?
Glossotheriopsis pascuali	?	?	?	?	?	?	?	?	?	?	?	?	?	?	?	?	?	?	?	?	?	?	?	?	?	?	?	?	?
Octodontobradys puruensis	?	?	?	?	?	?	?	?	?	?	?	?	?	?	?	?	?	?	?	?	?	?	?	?	?	?	?	?	?
Pseudoglyptodon sp.	?	?	?	?	?	?	?	?	?	?	?	?	?	?	?	?	?	?	?	?	?	?	?	?	?	?	?	?	?
Eionaletherium tanycnemius	?	?	?	?	?	?	?	?	?	?	?	?	?	?	?	?	?	?	?	?	?	?	?	?	?	?	?	?	?
Pleurolestodon acutidens	?	?	?	0	?	?	?	0	0	?	0	?	?	?	?	?	?	?	?	?	?	?	?	?	?	?	?	?	?
Mylodon darwinii	0	1	0	0	0&1	0	0	0	0	0&1	0	0	0	2	2	1	1	0	0	1	1	0	0	2	0	1	2	1	1
Kiyumylodon lecuonai	?	?	?	?	?	?	?	?	?	?	?	?	?	?	?	?	?	?	?	?	?	?	?	?	?	?	?	?	?
Pseudoprepotherium venezuelanum	?	?	?	?	?	?	?	?	?	?	?	?	?	?	?	?	?	?	?	?	?	?	?	?	?	?	?	?	?
Pseudoprepotherium confusum	0	1	?	?	?	?	?	?	0	?	?	?	2	?	?	1	1	0	1	1	1	0	0	2	0	1	2	1	1
Mirandabradys sp.	?	?	?	?	?	?	?	?	?	?	?	?	?	?	?	?	?	?	?	?	?	?	?	?	?	?	?	?	?
Urumacotherium sp.	?	?	?	?	?	?	?	?	?	?	?	?	?	?	?	?	?	?	?	?	?	?	?	?	?	?	?	?	?

	233	234	235	236	237	238	239	240	241	242	243	244	245	246	247	248	249	250	251	252	253	254	255	256	257	258	259	260	261
Pholidota	0	?	?	0	?	?	0&1	0	0	?	?	1	0&1	1	1	0	0	1	0	0	0	0	?	?	?	0	1	?	0
Euphractus sp.	0	1	?	2	0	0	0	0	0	2	1	1	0	1	1	0	0	0	0	0	0	0&1	0	0	2	1	0	0	0
Cyclopes sp.	0	1	?	0	0	?	1	0	2	0	0	1	0	1	1	0	0	1	1	1	0	0	?	?	?	1	2	?	1
Tamandua sp.	0	1	?	0	0	?	1	0	2	0	1	1	0	1	1	0	0	0	1	1	0	0	?	?	?	1	2	?	1
Myrmecophaga sp.	0	1	?	0	0	?	1	0	2	0	1	1	0	1	1	0	0	0	1	1	0	0	?	?	?	1	2	?	1
Bradypus sp.	1	0	0	1	0	0	0	1	0	0	1	1	0	1	1	0	0	0	1	2	0	0	?	0	2	0	1	1	0
Hapalops sp.	1	0	0	1	1	1	0	1	1	1	1	1	0	1	0	0	0	1	1	2	1	1	0	1	1	1	1	1	0
Nematherium sp.	1	0	0	1	1	1	1	0	1	1	?	0	?	?	?	?	?	?	?	2	1	1	0	1	1	1	2	1&3	0
Scelidotherium sp.	1	1	0	1	0	2	2	0	1	1	1	0	0	0	0	0	1	1	0	2	1	1	1	1	1	1	3	2	0
Catonyx sp.	1	1	0	1	0	2	2	0	1	1	2	0	0	0	0	0	?	?	?	2	1	1	1	1	1	1	3	2	0
Octodontotherium grande	1	?	0	1	0	1	?	0	1	0	?	0	0	0	1	1	?	1	0	2	1	1	1	?	0	2	2	3	0
Paroctodontotherium calleorum	?	?	?	?	?	?	?	?	?	?	?	?	?	?	?	?	?	?	?	?	?	?	?	?	?	?	?	?	?
Orophodon hapaloides	?	?	?	?	?	?	?	?	?	?	?	?	?	?	?	?	?	?	?	?	?	?	?	?	?	?	?	?	?
Lestobradys sprechmanni	?	?	?	?	?	?	?	?	?	?	?	?	?	?	?	?	?	?	?	?	?	?	?	?	?	?	?	?	?
Thinobadistes sp.	1	1	1	1	?	1	2	?	1	?	?	?	?	?	?	?	?	?	?	2	?	1	0	1	1	?	?	?	0
Bolivartherium sp.	?	?	?	?	?	?	?	?	?	?	?	?	?	?	?	?	?	?	?	?	?	?	?	?	?	?	?	?	?
Lestodon armatus	1	1	1	1	0	2	1	0	1	1	0	0	0	0	1	1	1	1	1	2	1	1	0	1	1	2	3	2	0
Sphenotherus zavaletianus	?	?	?	?	?	?	?	?	?	?	?	?	?	?	?	?	?	?	?	?	?	?	?	?	?	?	?	?	?
Simomylodon uccasamamensis	1	1	0	1	0	1	1	0	1	1	0	0	?	0	1	1	1	1	0	2	1	1	0	1	1	1	3	1	0
Glossotheridium chapadmalense	1	1	1	1	0	1	1	0	1	1	?	0	?	?	?	?	?	?	?	2	1	1	0	1	1	2	3	3	0
Paramylodon garbanii	1	1	1	1	0	1	1	?	?	1	?	0	?	0	1	1	1	1	0	2	0	1	0	1	1	2	2	1	0
Paramylodon harlani	1	1	1	1	0	1	1	0	1	1	0	0	1	0	1	1	1	1	0	2	1	1	0	1	1	2	3	1&2	0
Glossotherium robustum	1	1	1	1	0	1	1	?	1	1	?	0	0	?	?	1	1	1	0	2	1	1	0	1	1	2	3	3	0
Glossotherium tarijense	1	1	1	1	0	1	1	0	1	1	?	?	?	0	1	1	1	1	0	2	1	1	0	?	1	2	3	2	0
Glossotherium tropicorum	1	1	1	1	0	1	1	0	1	1	0	0	?	0	1	1	1	1	0	2	1	1	0	1	1	2	3	3	0
Glossotherium phoenesis	1	1	1	1	0	1	1	0	1	1	0	0	0	0	1	1	1	1	0	2	1	1	0	1	1	2	3	2	0
Octomylodon sp.	?	0	?	1	?	?	?	?	?	?	?	?	?	?	?	?	?	?	?	?	?	?	?	?	?	?	?	?	?
Brievabradys laventensis	?	?	?	?	?	?	?	?	?	?	?	?	?	?	?	?	?	?	?	?	?	?	?	?	?	?	?	?	?
Baraguatherium takumara	?	?	?	?	?	?	?	?	?	?	?	?	?	?	?	?	?	?	?	?	?	?	?	?	?	?	?	?	?
Glossotheriopsis pascuali	?	?	?	?	?	?	?	?	?	?	?	?	?	?	?	?	?	?	?	?	?	?	?	?	?	?	?	?	?
Octodontobradys puruensis	?	?	?	?	?	?	?	?	?	?	?	?	?	?	?	?	?	?	?	?	?	?	?	?	?	?	?	?	?
Pseudoglyptodon sp.	?	?	?	?	?	?	?	?	?	?	?	?	?	?	?	?	?	?	?	?	?	?	?	?	?	?	?	?	?
Eionaletherium tanycnemius	?	?	?	?	?	?	?	?	?	?	?	?	?	?	?	?	?	?	?	?	?	?	?	?	?	?	?	?	?
Pleurolestodon acutidens	1	1	1	1	0	?	?	?	?	?	?	?	?	?	?	?	?	?	?	?	?	1	0	1	1	?	?	?	0
Mylodon darwinii	1	1	1	1	0	1	1	0	1	1	1	0	1	0	1	1	1	1	1	2	1	1	0	1	1	2	3	3	0
Kiyumylodon lecuonai	?	?	?	?	?	?	?	?	?	?	?	?	?	?	?	?	?	?	?	?	?	?	?	?	?	?	?	?	?
Pseudoprepotherium venezuelanum	?	?	?	?	?	?	?	?	?	?	?	?	?	?	?	?	?	?	?	?	?	?	?	?	?	?	?	?	?
Pseudoprepotherium confusum	1	1	0	1	0	1	1	0	1	0	1	0	0	0	0	1	1	1	0	2	1	1	0	1	1	1	3	3	0
Mirandabradys sp.	?	?	?	?	?	?	?	?	?	?	?	?	?	?	?	?	?	?	?	?	?	?	?	?	?	?	?	?	?
Urumacotherium sp.	?	?	?	?	?	?	?	?	?	?	?	?	?	?	?	?	?	?	?	?	?	?	?	?	?	?	?	?	?

	262	263	264	265	266	267	268	269	270	271	272	273	274	275	276	277	278	279	280	281	282	283	284	285	286	287	288	289	290
Pholidota	1&2	?	0	1	1	0	1	0	?	0	0&1	?	0&1	1	1	0	2	0	0	0	0	2	0	1	1	1	0	0	0
Euphractus sp.	0	1	0	1	0	0	1	0	2	0	0	0	0	1	0	0	0	0	1	0	0	0	3	1	1	0	0	1	1
Cyclopes sp.	1	0	1	1	1	1	1	0	0	0	0	1	0	1	0	0	1	0	1	0	0	2	0	0	1	?	?	?	?
Tamandua sp.	2	0	1	1	1	0	1	?	0	0	1	1	1	1	0	0	0	0	1	0	0	0	0	0	1	0	0	1	1
Myrmecophaga sp.	2	0	1	1	1	0	1	?	0	0	1	1	1	1	0	0	0	1	1	0	0	0	1	0	1	0	0	1	1
Bradypus sp.	1	1	1	0	1	0	1	1	1	0	1	1	0	1	0	0	2	1	1	0	0	0	2	0	0	1	1	1	0
Hapalops sp.	0	1	1	1	1	0	0&1	1	1	0	?	?	?	?	0	0	2	1	1	0	2	0	3	0	1	1	1	1	0
Nematherium sp.	1	1	1	1	1	1	1	1	1&2	?	1	1	?	?	0	0	2	1	0	0	1	2	1	1	1	?	?	?	?
Scelidotherium sp.	1	2	1	1	1	1	0&1	1	3	?	1	1	0	0	0	0	2	1	1	0	1	2	1	0	1	1	1	1	0
Catonyx sp.	1	2	1	1	1	1	0&1	1	3	?	?	?	?	?	0	0	2	1	1	0	1	2	1	0	1	1	1	1	0
Octodontotherium grande	?	2	?	?	1	1	?	?	3	?	?	?	?	?	0	0	2	1	1	0	1	2	1	0	1	?	?	?	?
Paroctodontotherium calleorum	?	?	?	?	?	?	?	?	?	?	?	?	?	?	?	?	?	?	?	?	?	?	?	?	?	?	?	?	?
Orophodon hapaloides	?	?	?	?	?	?	?	?	?	?	?	?	?	?	?	?	?	?	?	?	?	?	?	?	?	?	?	?	?
Lestobradys sprechmanni	?	?	?	?	?	?	?	?	?	?	?	?	?	?	?	?	?	?	?	?	?	?	?	?	?	?	?	?	?
Thinobadistes sp.	?	2	1	1	1	1	?	?	?	?	?	?	?	?	0	0	2	?	1	1	1	2	?	0	1	1	1	1	0
Bolivartherium sp.	?	?	?	?	?	?	?	?	?	?	?	?	?	?	?	?	?	?	?	?	?	?	?	?	?	?	?	?	?
Lestodon armatus	2	2	1	1	1	1	0	?	3	?	1	1	1	0	0	0	2	1	0	0	1	2	1	0	1	1	1	1	0
Sphenotherus zavaletianus	?	?	?	?	?	?	?	?	?	?	?	?	?	?	?	?	?	?	?	?	?	?	?	?	?	?	?	?	?
Simomylodon uccasamamensis	?	2	1	1	1	1	0	1	2	?	?	?	?	?	0	0	2	1	1	0	1	2	1	0	1	1	1	1	0
Glossotheridium chapadmalense	?	2	1	1	1	1	0	?	3	1	?	?	?	?	0	0	2	1	1	0	1	2	?	0	1	?	?	?	?
Paramylodon garbanii	?	?	?	?	1	1	?	?	1	0	?	?	?	?	0	0	2	1	1	0	1	2	?	?	1	?	?	?	?
Paramylodon harlani	1&2	2	1	1	1	1	0	?	?	0	1	1	1	0	0	0	2	1	1	0	1	2	1	0	1	1	1	1	0
Glossotherium robustum	1	2	1	1	1	1	0	?	3	1	1	1	?	1	0	0	2	1	1	0	1	2	1	0	1	1	1	1	0
Glossotherium tarijense	1	2	1	1	1	1	0	?	2	1	?	?	?	?	0	0	2	1	1	0	1	2	1	0	1	?	?	?	?
Glossotherium tropicorum	1	2	?	?	1	1	0	0	2	1	?	?	?	?	0	0	2	1	1	0	1	2	1	1	1	?	?	?	?
Glossotherium phoenesis	1	2	1	1	1	1	0	?	2	1	?	?	?	?	0	0	2	1	1	0	1	2	1	0	1	?	?	?	?
Octomylodon sp.	?	?	?	?	?	?	?	?	?	?	?	?	?	?	0	0	2	?	?	?	?	2	?	?	1	?	?	?	?
Brievabradys laventensis	?	?	?	?	?	?	?	?	?	?	?	?	?	?	?	?	?	?	?	?	?	?	?	?	?	?	?	?	?
Baraguatherium takumara	?	?	?	?	?	?	?	?	?	?	?	?	?	?	?	?	?	?	?	?	?	?	?	?	?	?	?	?	?
Glossotheriopsis pascuali	?	?	?	?	?	?	?	?	?	?	?	?	?	?	?	?	?	?	?	?	?	?	?	?	?	?	?	?	?
Octodontobradys puruensis	?	?	?	?	?	?	?	?	?	?	?	?	?	?	?	?	?	?	?	?	?	?	?	?	?	?	?	?	?
Pseudoglyptodon sp.	?	?	?	?	?	?	?	?	?	?	?	?	?	?	?	?	?	?	?	?	?	?	?	?	?	?	?	?	?
Eionaletherium tanycnemius	?	?	?	?	?	?	?	?	?	?	?	?	?	?	?	?	?	?	?	?	?	?	?	?	?	?	?	?	?
Pleurolestodon acutidens	?	?	?	?	?	?	?	?	?	?	?	?	?	?	0	0	2	1	1	0	?	2	?	0	1	?	?	?	?
Mylodon darwinii	1	2	1	1	1	1	0	1	3	1	1	1	1	0	0	0	2	1	1	0	1	2	1	0	1	1	1	1	0
Kiyumylodon lecuonai	?	?	?	?	?	?	?	?	?	?	?	?	?	?	?	?	?	?	?	?	?	?	?	?	?	?	?	?	?
Pseudoprepotherium venezuelanum	?	?	?	?	?	?	?	?	?	?	?	?	?	?	?	?	?	?	?	?	?	?	?	?	?	?	?	?	?
Pseudoprepotherium confusum	?	2	1	0	1	1	1	1	2	1	?	?	?	0	0	0	2	1	1	0	1	2	1	0	1	?	?	?	?
Mirandabradys sp.	?	?	?	?	?	?	?	?	?	?	?	?	?	?	?	?	?	?	?	?	?	?	?	?	?	?	?	?	?
Urumacotherium sp.	?	?	?	?	?	?	?	?	?	?	?	?	?	?	?	?	?	?	?	?	?	?	?	?	?	?	?	?	?

	291	292	293	294	295	296	297	298	299	300	301	302	303	304	305	306	307	308	309	310	311	312	313	314	315	316	317	318	319
Pholidota	0	0	0	0	0	0	1	-	0	0	0	0	0	0	0	0	0	0	1	0	0	0	0	1	1	0	0	0	0
Euphractus sp.	1	0	0	1	0	0	0	-	0	1	0	0	1	1	0	0	0	0	0	0	0	0	0	1	0	0	0	0	0
Cyclopes sp.	?	?	?	?	?	?	?	?	?	?	?	?	?	?	?	?	?	?	?	?	?	?	?	?	?	?	?	?	?
Tamandua sp.	1	0	0	1	0	1	0	-	1	0	0	?	2	1	1	0	1	0	1	0	0	0	1	0	1	0	0	0	0
Myrmecophaga sp.	1	0	0	1	0	1	0	-	1	0	0	0	2	1	1	0	1	0	1	0	0	0	1	0	2	0	0	0	0
Bradypus sp.	0	1	1	0	0	1	1	-	1	1	0	-	0	0	1	1	0	0	1	0	0&1	0	1	0	2	1	1	0	1
Hapalops sp.	0	1	1	1	0&1	1	1	-	1	0	0	0	1	0	1	0	0	0	0	0	1	0	1	0	1	1	0	1	1
Nematherium sp.	?	?	?	?	?	?	?	?	1	0	1	1	1	0	1	0	1	0	0	0	1	0	1	1	2	1	0	1	1
Scelidotherium sp.	0	1	1	1	1	1	0	0	1	1	1	1	2	2	1	0	1	0	0	1	0	1	1	1	2	1	0	1	1
Catonyx sp.	0	1	1	1	1	1	0	0	1	1	1	1	2	2	1	0&1	1	0	0	1	0	1	1	1	2	1	0	1	1
Octodontotherium grande	?	?	?	?	?	?	?	?	?	?	?	?	?	?	?	?	?	?	?	?	?	?	?	?	?	?	?	?	?
Paroctodontotherium calleorum	?	?	?	?	?	?	?	?	?	?	?	?	?	?	?	?	?	?	?	?	?	?	?	?	?	?	?	?	?
Orophodon hapaloides	?	?	?	?	?	?	?	?	?	?	?	?	?	?	?	?	?	?	?	?	?	?	?	?	?	?	?	?	?
Lestobradys sprechmanni	?	?	?	?	?	?	?	?	?	?	?	?	?	?	?	?	?	?	?	?	?	?	?	?	?	?	?	?	?
Thinobadistes sp.	0	1	1	1	1	1	0	?	1	1	0	0	1	2	1	1	1	1	0	0	0&1	0&1	1	2	2	0	0	0	1
Bolivartherium sp.	?	?	?	?	?	?	?	?	?	?	?	?	?	?	?	?	?	?	?	?	?	?	?	?	?	?	?	?	?
Lestodon armatus	0	1	1	1	1	1	0	1	1	1	0	0	2	2	1	1	1	2	1	0	0	2	1	1&2	1&2	0	0	0	1
Sphenotherus zavaletianus	?	?	?	?	?	?	?	?	?	?	?	?	?	?	?	?	?	?	?	?	?	?	?	?	?	?	?	?	?
Simomylodon uccasamamensis	0	1	1	1	1	1	0	0	1	1	0	0	1	2	1	1	1	1	0	0	0	1	1	1&2	1	0	0	0	1
Glossotheridium chapadmalense	?	?	?	?	?	?	?	?	1	?	0	0	?	2	1	1	1	?	0	0	0	1	1	?	?	?	?	?	?
Paramylodon garbanii	?	?	?	?	?	?	?	?	?	?	?	?	?	?	?	?	?	?	?	?	?	?	?	?	?	?	?	?	?
Paramylodon harlani	0	1	1	1	1	1	0	0	1	1	0	0	2	2	1	1	1	2	0	0	0	1	1	1	1	0	1	0	1
Glossotherium robustum	0	1	1	1	1	1	0	0	1	1	0	0	2	2	1	1	1	2	1	0	0	1	1	1	1	0	1	0	1
Glossotherium tarijense	?	?	?	?	?	?	?	?	1	1	0	0	2	2	1	1	1	2	1	0	0	1	1	?	?	?	?	?	?
Glossotherium tropicorum	?	?	?	?	?	?	?	?	1	1	0	0	2	2	0	1	1	2	1	0	0	1	1	1	1	0	1	0	1
Glossotherium phoenesis	?	?	?	?	?	?	?	?	1	1	0	0	2	2	1	1	1	2	0	0	0	1	1	1	1	0	1	0	1
Octomylodon sp.	?	?	?	?	?	?	?	?	?	?	?	?	?	?	?	?	?	?	?	?	?	?	?	?	?	?	?	?	?
Brievabradys laventensis	?	?	?	?	?	?	?	?	?	?	?	?	?	?	?	?	?	?	?	?	?	?	?	?	?	?	?	?	?
Baraguatherium takumara	?	?	?	?	?	?	?	?	?	?	?	?	?	?	?	?	?	?	?	?	?	?	?	?	?	?	?	?	?
Glossotheriopsis pascuali	?	?	?	?	?	?	?	?	?	?	?	?	?	?	?	?	?	?	?	?	?	?	?	?	?	?	?	?	?
Octodontobradys puruensis	?	?	?	?	?	?	?	?	?	?	?	?	?	?	?	?	?	?	?	?	?	?	?	?	?	?	?	?	?
Pseudoglyptodon sp.	?	?	?	?	?	?	?	?	?	?	?	?	?	?	?	?	?	?	?	?	?	?	?	?	?	?	?	?	?
Eionaletherium tanycnemius	?	?	?	?	?	?	?	?	?	?	?	?	?	?	?	?	?	?	?	?	?	?	?	?	?	?	?	?	?
Pleurolestodon acutidens	?	?	?	?	?	?	?	?	?	?	?	?	?	?	?	?	?	?	?	?	?	?	?	?	?	?	?	?	?
Mylodon darwinii	0	1	1	1	1	1	0	0	1	1	0	0	2	2	1	1	1	2	1	0	0	1	1	1	1	0	1	0	1
Kiyumylodon lecuonai	?	?	?	?	?	?	?	?	?	?	?	?	?	?	?	?	?	?	?	?	?	?	?	?	?	?	?	?	?
Pseudoprepotherium venezuelanum	?	?	?	?	?	?	?	?	?	?	0	0	1	?	?	0	1	1	?	?	?	?	1	?	?	?	?	?	?
Pseudoprepotherium confusum	?	?	?	?	?	?	0	?	1	1	0	0	1	2	1	0	1	1	0	0	0	0	1	2	1	0	0	0	1
Mirandabradys sp.	?	?	?	?	?	?	?	?	?	?	?	?	?	?	?	?	?	?	?	?	?	?	?	?	?	?	?	?	?
Urumacotherium sp.	?	?	?	?	?	?	?	?	?	1	0	0	1	?	1	0	?	1	?	?	?	?	1	?	?	?	?	?	?

	320	321	322	323	324	325	326	327	328	329	330	331	332	333	334	335	336	337	338	339	340	341	342	343	344	345	346	347	348
Pholidota	-	1	1	0	1	0	0	0	0	0	0	?	-	-	-	-	?	0	0	0	0	0&1	0	0	0	0	0	1	0
Euphractus sp.	0	0	1	0	0	0	1	0	0	1	1	?	?	?	?	?	?	0	0	0	0	?	0	0	0	0	0	1	0
Cyclopes sp.	?	?	?	?	?	?	?	?	?	?	?	?	?	?	?	?	?	?	?	?	?	?	?	?	?	?	?	?	?
Tamandua sp.	0	1	0	0	0	0	0	0	0	1	1	?	1	1	1	0	?	0	0	0	0	1	0	0	0	0	0	0	0
Myrmecophaga sp.	0	1	0	0	0	0	1	0	0	1	1	?	0	?	?	?	?	0	0	0	0	?	0	0	0	0	0	0	0
Bradypus sp.	0	2	0	0	-	?	?	1	0	1	1	0	1	2	0	0	0	-	-	1	0	0	0	1	0	0	0	0	0
Hapalops sp.	0	1	0	0	0	0	0	1	0	1	1	?	?	?	?	?	?	0	1	1	0	?	0	0	1	1	0	1	1
Nematherium sp.	1	1	1	0	0	0	0	1	0	1	?	1	?	0	0	0	0	?	?	?	0	1&2	0	?	?	?	?	?	?
Scelidotherium sp.	0	1	2	1	0	0	0	1	0	1	1	1	0	2	1	0	0	1	0	1	0	2	1	2	2	2	0&1	2	2
Catonyx sp.	0	1	2	1	0	0	0	1	0	1	1	1	0	2	1	0	0	1	0	1	0	2	1	1	2	2	0&1	2	2
Octodontotherium grande	?	?	?	?	?	?	?	?	?	1	1	0	?	?	?	?	0	0	?	0	0	0	0	?	?	?	?	?	?
Paroctodontotherium calleorum	?	?	?	?	?	?	?	?	?	?	?	?	?	?	?	?	?	?	?	?	?	?	?	?	?	?	?	?	?
Orophodon hapaloides	?	?	?	?	?	?	?	?	?	?	?	?	?	?	?	?	?	?	?	0	0	1	?	?	?	?	?	?	?
Lestobradys sprechmanni	?	?	?	?	?	?	?	?	?	?	?	?	?	?	?	?	?	?	?	?	?	?	?	?	?	?	?	?	?
Thinobadistes sp.	1	1	2&3	1	0	0	1	1	1	1	1	0	1	2	1	0&1	0&1	1	1	0	0&1	0&1	0	1	1	1	1	1	1
Bolivartherium sp.	?	1	3	2	1	?	1	1	1	?	?	?	?	?	?	?	?	?	?	?	?	?	?	?	1	1	1	1	1
Lestodon armatus	1	1	2&3	2	2	0	1	1	1	1	1	0	1	?	?	?	0	1	1	0	0&1	1	0	1	1	1	1	1	1
Sphenotherus zavaletianus	?	?	?	?	?	?	?	?	?	?	?	?	?	?	?	?	?	?	?	?	?	?	?	?	?	?	?	?	?
Simomylodon uccasamamensis	0&1	1	3	2	1	0	1	?	?	1	1	0	1	1	1	1	1	1	1	0	0&1	0	0	1	1	1	1	1	1
Glossotheridium chapadmalense	?	?	?	?	?	?	?	?	?	?	?	?	?	?	?	?	?	?	?	?	?	?	?	?	?	?	?	?	?
Paramylodon garbanii	?	1	3	?	1	1	1	1	1	1	1	0	1	1	1	1	?	?	?	0	1	0	0	?	1	1	1	1	1
Paramylodon harlani	1	1	3	2	1	1	1	1	1	1	1	0	1	1	1	0&1	1	0&1	1	0	1	1	0	1	1	1	1	1&2	1
Glossotherium robustum	1	1	3	2	2	1	1	1	1	1	1	0&1	1	1	1	1	1	1	1	0	1	1	0	1	1	1	1	1	1
Glossotherium tarijense	?	?	?	?	?	?	?	?	?	?	?	?	?	?	?	?	?	?	?	?	?	?	?	?	?	?	?	?	?
Glossotherium tropicorum	1	1	3	2	1	1	1	1	1	?	?	?	?	?	?	?	?	?	?	?	?	?	?	?	1	1	1	1	1
Glossotherium phoenesis	1	?	?	2	1	1	1	?	?	1	1	0	1	1	1	1	1	?	?	0	1	1	0	1	1	1	1	1	1
Octomylodon sp.	?	?	?	?	?	?	?	?	?	?	?	?	?	?	?	?	?	?	?	?	?	?	?	?	?	?	?	?	?
Brievabradys laventensis	?	?	?	?	?	?	?	?	?	?	?	?	?	?	?	?	?	?	?	?	?	?	?	?	?	?	?	?	?
Baraguatherium takumara	?	?	?	?	?	?	?	?	?	?	?	?	?	?	?	?	?	?	?	?	?	?	?	?	?	?	1	?	1
Glossotheriopsis pascuali	?	?	?	?	?	?	?	?	?	?	?	?	?	?	?	?	?	?	?	?	?	?	?	?	?	?	?	?	?
Octodontobradys puruensis	?	?	?	?	?	?	?	?	?	?	?	?	?	?	?	?	?	?	?	?	?	?	?	?	?	?	?	?	?
Pseudoglyptodon sp.	?	?	?	?	?	?	?	?	?	?	?	?	?	?	?	?	?	?	?	?	?	?	?	?	?	?	?	?	?
Eionaletherium tanycnemius	?	?	?	?	?	?	?	?	?	?	?	?	?	?	?	?	?	?	?	?	?	?	?	?	1	1	0	1	2
Pleurolestodon acutidens	?	?	?	?	?	?	?	?	?	?	?	?	?	?	?	?	?	?	?	?	?	?	?	?	?	?	?	?	?
Mylodon darwinii	1	1	3	2	2	1	1	1	1	1	1	0	1	1	1	1	1	1	0	0	1	0	0	?	?	?	1	?	1
Kiyumylodon lecuonai	?	?	?	?	?	?	?	?	?	?	?	?	?	?	?	?	?	?	?	?	?	?	?	?	?	?	?	?	?
Pseudoprepotherium venezuelanum	?	?	?	?	?	?	?	?	?	?	?	?	?	?	?	?	?	?	?	?	?	?	?	?	1	0	1	1	1
Pseudoprepotherium confusum	0	1	1	2	0	0	0	1	0	1	1	0	?	?	?	?	0	?	?	0	0	0	?	?	1	0	0&1	1	1
Mirandabradys sp.	?	?	?	?	?	?	?	?	?	?	?	?	?	?	?	?	?	?	?	?	?	?	?	?	1	0&1	1	1	1&2
Urumacotherium sp.	?	?	?	?	?	?	?	?	?	?	?	?	?	?	?	?	?	?	?	?	?	?	?	?	1	0	?	1	?

	349	350	351	352	353	354	355	356	357	358	359	360	361	362	363	364	365	366	367	368	369	370	371	372	373	374	375	376	377
Pholidota	1	2	0	0	0	0	1	0	0	1	0	0	0	0	0	0	0&1	0	0	-	0	0	0	0	0&1	0&1	0	1	0
Euphractus sp.	0	0	1	0	1	?	0	0	0	0	0	0	0	?	1	0	0&1	1	?	-	0	0	0	?	?	0	?	1	0
Cyclopes sp.	?	?	?	?	?	?	?	?	?	?	?	?	?	?	?	?	?	?	?	?	?	?	?	?	?	?	?	?	?
Tamandua sp.	0	2	0	0	2	0	1	0	0	0	0	0	0	0	0	0	0	0	0	-	0	0	0	0	0	0	0	?	0
Myrmecophaga sp.	0	2	0	0	2	0	1	0	0	0	0	0	0	0	0	0	0	0	0	-	0	?	0	0	0	0	0	?	0
Bradypus sp.	1	2	0	0	0	0	0	0	0	1	0	0	0	0	0	0	0	0	?	?	?	0	?	?	1	0	0	-	-
Hapalops sp.	0	1	0	0	1	0	0	0	1	0	0	0&1	1	0	0	0	0	0&1	0	0	0	0	0	0	1	0	0	1	0
Nematherium sp.	?	?	?	?	?	?	?	?	?	?	?	?	?	?	?	?	?	?	?	?	0	0	?	1	1	0	0	?	?
Scelidotherium sp.	1	2	1	1	0	1	1	1	2	1	1&2	1	1	0	1	0	0	1	2	0	0	0	0	1	2	0	0	0	0
Catonyx sp.	1	2	1	1	0	1	1	1	2	1	1	1	1	0	1	0	0	1	2	0	0	0	0	1	2	0	0	0	0
Octodontotherium grande	?	?	?	?	?	?	1	1	1	1	1	1	1	0	0	0	0	?	0	0	0	0	0&1	0	?	?	?	?	?
Paroctodontotherium calleorum	?	?	?	?	?	?	?	?	?	?	?	?	?	?	?	?	?	?	?	?	?	?	?	?	?	?	?	?	?
Orophodon hapaloides	?	?	?	?	?	?	?	?	?	?	?	?	?	?	?	?	?	?	0	0	0	0	0	0	?	?	?	?	?
Lestobradys sprechmanni	?	?	?	?	?	?	?	?	?	?	?	?	?	?	?	?	?	?	1	2	0	0	?	0	?	?	?	?	?
Thinobadistes sp.	1	2	0	0	2	1	1	1&2	2	1&2	1	1	1	1	1	1	1	1	1	2	0	0	1	0	2	1	0	1	1
Bolivartherium sp.	1	2	0	0	1	0	?	?	?	?	?	?	?	?	?	?	?	?	1	2	0	0	1	0	?	?	?	?	?
Lestodon armatus	1	2	0	1	2	1	1	2	2	1&2	1&2	1	1	1	1	1	1	1	1	2	0	0	1	0	2	1	0	1	1
Sphenotherus zavaletianus	?	?	?	?	?	?	?	?	?	?	?	?	?	?	?	?	?	?	?	?	?	?	?	?	?	?	?	?	?
Simomylodon uccasamamensis	1	2	0	1	2	1	1	1	2	1&2	1	1	1	0	1	1	1	1	1	1	1	0	1	0	2	1	0	2	?
Glossotheridium chapadmalense	?	?	?	?	?	?	?	?	?	?	?	?	?	?	?	?	?	?	?	?	?	?	?	?	?	?	?	?	?
Paramylodon garbanii	1	2	0	1	2	1	1	2	2	2	2	1	1	?	1	1	2	1	1	0	1	1	1	0	?	?	1	?	?
Paramylodon harlani	1	2	0	1	2	1	1	2	2	2	2	1	1	1	1	1	2	1	1	1	1	1	1	0	3	1	1	2	0
Glossotherium robustum	1	2	0	1	2	1	1	2	2	2	2	1	1	1	1	1	2	1	1	1	1	1	1	0	3	1	1	2	0
Glossotherium tarijense	?	?	?	?	?	?	1	2	2	1&2	2	1	1	1	1	1	2	?	?	?	?	?	?	?	?	?	?	?	?
Glossotherium tropicorum	1	2	0	1	2	1	?	?	?	?	?	?	?	?	?	?	?	?	?	?	?	?	?	?	?	?	?	?	?
Glossotherium phoenesis	1	2	0	1	2	1	1	2	2	2	2	1	1	1	1	1	2	1	1	1	1	1	1	0	2	1	1	?	?
Octomylodon sp.	?	?	?	?	?	?	?	?	?	?	?	?	?	?	?	?	?	?	?	?	?	?	?	?	?	?	?	?	?
Brievabradys laventensis	?	?	?	?	?	?	?	?	?	?	?	?	?	?	?	?	?	?	?	?	?	?	?	?	?	?	?	?	?
Baraguatherium takumara	0	?	?	?	1	0	?	?	?	?	?	?	?	?	?	?	?	?	?	?	?	?	?	?	?	?	?	?	?
Glossotheriopsis pascuali	?	?	?	?	?	?	?	?	?	?	?	?	?	?	?	?	?	?	?	?	?	?	?	?	?	?	?	?	?
Octodontobradys puruensis	?	?	?	?	?	?	?	?	?	?	?	?	?	?	?	?	?	?	?	?	?	?	?	?	?	?	?	?	?
Pseudoglyptodon sp.	?	?	?	?	?	?	?	?	?	?	?	?	?	?	?	?	?	?	?	?	?	?	?	?	?	?	?	?	?
Eionaletherium tanycnemius	0	2	0	0	1	0	1	0	0	1	0	0	0	0	0	0	?	?	?	?	?	?	?	?	?	?	?	?	?
Pleurolestodon acutidens	?	?	?	?	?	?	?	?	?	?	?	?	?	?	?	?	?	?	1	1	1	0	1	0	?	?	?	?	?
Mylodon darwinii	?	?	0	1	2	?	1	2	2	2	2	1	1	1	1	1	2	?	1	1	1	1	1	0	?	?	?	?	?
Kiyumylodon lecuonai	?	?	?	?	?	?	?	?	?	?	?	?	?	?	?	?	?	?	?	?	?	?	?	?	?	?	?	?	?
Pseudoprepotherium venezuelanum	1	1	0	0	1	0	1	0	0	?	0	?	?	0	?	?	?	?	?	?	?	?	?	?	?	?	?	?	?
Pseudoprepotherium confusum	1	1&2	0	0	1	0	1	0&1	1	1	1	1	1	0	0	0	1	?	0&1	1	1	0	1	0	2	0	0	1	?
Mirandabradys sp.	0	2	0	0	0&1	1	1	1	1	1	1	1	1	0	0	0	?	?	?	?	?	?	?	?	?	?	?	?	?
Urumacotherium sp.	1	2	0	0	1	0	1	1	1	?	1	?	?	?	?	?	?	?	0	1	1	0	?	0	?	?	?	?	?

	378	379	380	381	382	383
Pholidota	1	0	0	0	0	0
Euphractus sp.	0	?	?	0	0	0
Cyclopes sp.	?	?	?	?	?	?
Tamandua sp.	0	0	0	0	0	0
Myrmecophaga sp.	0	0	0	0	0	0
Bradypus sp.	-	-	-	1	-	0
Hapalops sp.	0	?	?	0	0	0
Nematherium sp.	?	?	?	?	?	0
Scelidotherium sp.	0	?	?	1	0	0
Catonyx sp.	0	?	2	1	0	0
Octodontotherium grande	0	0	0	?	0	?
Paroctodontotherium calleorum	?	?	?	?	?	?
Orophodon hapaloides	?	?	?	?	?	?
Lestobradys sprechmanni	?	?	?	?	?	?
Thinobadistes sp.	0	1	1	0	0&1	0
Bolivartherium sp.	?	?	?	?	?	?
Lestodon armatus	0	1	1	0	1	0
Sphenotherus zavaletianus	?	?	?	?	?	?
Simomylodon uccasamamensis	?	?	?	?	?	1
Glossotheridium chapadmalense	?	?	?	?	?	?
Paramylodon garbanii	0	2	1	?	?	1
Paramylodon harlani	1	2	1	0	1	1
Glossotherium robustum	1	2&3	1	0	1	1
Glossotherium tarijense	?	?	?	?	?	?
Glossotherium tropicorum	?	?	?	?	?	?
Glossotherium phoenesis	1	2	1	?	1	1
Octomylodon sp.	?	?	?	?	?	?
Brievabradys laventensis	?	?	?	?	?	?
Baraguatherium takumara	?	?	?	?	?	?
Glossotheriopsis pascuali	?	?	?	?	?	?
Octodontobradys puruensis	?	?	?	?	?	?
Pseudoglyptodon sp.	?	?	?	?	?	?
Eionaletherium tanycnemius	?	?	?	?	?	?
Pleurolestodon acutidens	?	?	?	?	?	1
Mylodon darwinii	?	?	?	?	?	1
Kiyumylodon lecuonai	?	?	?	?	?	?
Pseudoprepotherium venezuelanum	?	?	?	?	?	?
Pseudoprepotherium confusum	0	3	1	?	?	0
Mirandabradys sp.	?	?	?	?	?	?
Urumacotherium sp.	?	?	?	?	?	?

Appendix VI. Data S5. Synapomorphies and autapomorphies common to the 87 trees resulting from the analysis of the total matrix (40 taxa). Nodes refer to Figure 8.9. Character numbers and states shown in bold type are optimized as unambiguous synapomorphies/autapomorphies, those in plain type are ambiguous synapomorphies/autapomorphies.

Euphractus sp.: **52(0→1)**, **54(1&2→0)**, **55(1→0)**, **62(1→2)**, **69(0→1)**, **83(0→1)**, **85(1→0)**, **94(2→0)**, **95(0→1)**, **97(2→0)**, **99(0&1→2)**, **100(1→0)**, **102(0→1)**, **106(0→2)**, **113(1→0)**, **114(1→0)**, **115(0→6)**, **156(0→2)**, **164(0→2)**, **168(1&2→3)** , **174(1→0)**, **177(0→1)**, **181(0→1)**, **189(0→1)**, **192(1→0)**, **194(1→0)**, **203(1→2)**, **213(0→1)**, **214(0→1)**, **218(0&1→2)**, **222(0→1)**, **230(1→2)**, **236(0&1→2)**, **259(1→0)**, **262(1→0)**, **266(1→0)**, **278(1&2→0)**, **300(0→1)**, **309(1→0)**, **315(1→0)**, **321(1→0)**, **326(0→1)**, **350(2→0)**, **351(0→1)**, **355(1→0)**, **363(0→1)**, **366(0→1)**.

Cyclopes sp.: **51(1→2)**, **163(0→1)**, **169(0→1)**, **181 (0→1)**, **192(1→2)**, **203(1→0)**, **207(0→2)**, **243(1→0)**, **267(0→1)**, **283(0→2)**.

Tamandua sp.: **55(1→2)**, **77(1→0)**, **119(1→2)**, **142(0→1)**, **191(2→1)**.

Myrmecophaga sp.: **82(1→0)**, **187(1→0)**, **194(1→0)**, **202(0→1)**, **215(0→1)**, **279(0→1)**, **284(0→1)**, **326(0→1)**, **332(1→0)**.

Bradypus sp.: **37(2&3→4)**, 38(2→1), **51(1→2)**, **57(2→3)**, **85(3→4)**, **89(0→1)**, **102(0→2)**, **130(1→2)**, **139(1→0)**, **152(1→2)**, **161(0→1)**, **177(0→1)**, **180(0→1)**, **187(1→2)**, **212(0→1)**, **214 (0→1)**, **215(0→1)**, **225(0→1)**, **258(1→0)**, **265(1→0)**, **286(1→0)**, **294(1→0)**, **300(0→1)**, **303(1→0)**, **306(0→1)**, **317(0→1)**, **321(1→2)**, **341(1→0)**, **349(0→1)**, **353(1→0)**, **355(1→0)**, **381(0→1)**.

Hapalops sp.: **3(0→2)**, **6(0→2)**, **10(0→1)**, **17(0→2)**, **27(0→1)**, **32(0→1)**, **33(0→1)**, **34(0→1)**, **36(3→1)**, **38(1&2→3)**, **39(0→1)**, **60(0→1)**, **66(0→2)**, **76(0→1&2)**, **84(0→1)**, **96(0→1)**, **106(0→1&2)**, **112(0→1)**, **115(0→4)**, **122(1→4)**, **143(0→1)**, **147(0→1)**, **167(0→1)**, **184(0→1)**, **185(0→1)**, **202(0→1)**, **222(0→1)**, **262(1→0)**, **350(2→1)**, **355(1→0)**, **358(1→0)**.

Nematherium sp.: **16(0→2)**, **33(0→4)**, **34(0→4)**, **66(0→2)**, **86(1→0)**, **143(0→1)**, **147(0→1)**, **187(1→2)**, **193(1→0)**, **207(0→1)**, **280(1→0)**, **285(0→1)**, **320(0→1)**, **333(1&2→0)**.

Scelidotherium sp.: **62(2→3)**, **71(1→0)**, **86(1→0)**, **125(1→0)**, **140(0→1)**, **167(0→1)**, **178(0→1)**, **187(1→0)**, **195(1→0)**, **196(1→0)**, **343(1→2)**.

Catonyx sp.: **37(2→5)**, **59(1→2)**, **66(0→2)**, **112(0→1)**, **142(2→0)**, **161(0→1)**, **170(1→0)**, **181(0→1)**, **243(1→2)**.

Octodontotherium grande: 17(0→1), 34(0→6), 40(0→1), 192(1→0), 341(1→0).

Paroctodontotherium calleorum: **31(1→5)**, **35(7→3)**, **169(1→0)**.

Orophodon hapaloides: 17(0→1), 28(0→1).

Lestobradys sprechmanni: **24(0→1)**, **32(0→4)**, **65(0→1)**, **75(0→1)**, **76(1→2)**.

Thinobadistes sp.: **106(1→0)**.

Bolivartherium sp.: **14(1→2)**, **30(1→6)**, **63(1→0)**, **72(0→1)**, **353(2→1)**, **354(1→0)**.

Lestodon armatus: **11(2→3)**, **21(0→1)**, **28(1→0)**, **62(2→1)**, **70(1→0)**, **76(1→2)**, **93(0→1)**, **156(0→2)**, **173(1→0)**, **324(1→2)**, **352(0→1)**.

Sphenotherus zavaletianus: **11(2→3)**, **63(1→0)**.

Simomylodon uccasamamensis: 37(4→3), 82(2→3), 187(1→2), 235(1→0), 258(2→1), 260(2&3→1), 270(3→2).

Glossotheridium chapadmalense: 63(1→0), 191(0→1), 219(1→0), 260(2&3→3).

Paramylodon garbanii: **51(0→1)**, 63(1→0), **253(1→0)**, **259(3→2)**, 260(2&3→1), 270(3→1), **368(1→0)**.

Paramylodon harlani: 341(0→1).

Glossotherium robustum: 20(2→1), 86(2→3), 142(0→1), 260(2&3→3), 324(1→2).

Glossotherium tarijense: 20(1&2→0), 37(3→2).

Glossotherium tropicorum: 20(2→1), 37(3→2), **45(1→0)**, **47(1→0)**, **51(0→1)**, **94(0→1)**, **173(1→0)**, 260(2→3), **285(0→1)**, **305(1→0)**.

Glossotherium phoenesis: **67(2→1)**, 309(1→0).

Octomylodon sp.: **2(2→4)**, **17(0→1)**, 35(7→6), 37(2→5), **38(2→3)**, 39(0→1), 51(1→2), 63(1→0), 65(1→2), 68(1→2), 69(0→1).

Brievabradys laventensis: no autapomorphies.

Baraguatherium takumara: 15(1→0).

Glossotheriopsis pascuali: 22(0→1).

Octodontobradys puruensis: 15(1→2), 30(0→3), 38(2→1), 51(1→0), 56(2→1), 106(0→1).

Pseudoglyptodon sp.: **2(2→3)**, **17(0→3)**, **32(0→7)**, **33(0→7)**, **34(0→8)**, **39(0→1)**, **63(0→1)**, **122(1→2)**.

Eionaletherium tanycnemius: **348(1→2)**.

Pleurolestodon acutidens: **40(0→1)**, **45(1→0)**, **82(2→3)**, **106(1→0)**, **168(2→1)**, **187(1→0)**.

Mylodon darwinii: **19(1→0)**, **20(1&2→1)**, 28(1→0), 37(3&4→3), 88(1→0).

Kiyumylodon lecuonai: 48(0→1), 52(1→0).

Pseudoprepotherium venezuelanum: **37(2→0)**, **357(1→0)**, **359(1→0)**.

Pseudoprepotherium confusum: no autapomorphies.

Mirandabradys sp.: **91(0→2)**, **122(1→2)**.

Urumacotherium sp.: **14(0→1)**, **15(1→0)**, **26(1→0)**, **27(0→1)**, **29(0→2)**, **31(1→2)**, **32(0→1)**, **33(0→1)**, **34(0→1)**, **35(7→4)**, **62(2→1)**, **63(1→0)**, **186(1→2)**.

Node A (Pilosa): **119(0→1)**, **125(0→1)**, **159(0→1)**, **179(0→1)**, **186(0→1)**, **232(0→1)**, **251(0→1)**, **264(0→1)**, **285(1→0)**, **296(0→1)**, **299(0→1)**, **305(0→1)**, **313(0→1)**, **314(1→0)**, **322(1→0)**.

Node B (Vermilingua): **38(1&2→0)**, **57(1→0)**, **59(0→2)**, **62(1→0)**, **64(0→1)**, **86(1→0)**, **90(1→0)**, **122(1→0)**, **127(1→3)**, **128(0→1)**, **135(1→0)**, **157(1→0)**, **168(1&2→0)**, **216(1→2)**, **239(0→1)**, **241(0&1→2)**, **259(1→2)**, **261(0→1)**, **263(1→0)**.

Node C: **41(2→0)**, **47(0→3)**, **51(1→0)**, **82(4→1)**, **85(1→0)**, **129(0→1)**, **137(0→2)**, **141(0→1)**, **156(0→1)**, **195(0→1)**, **199(0→2)**, **230(1→0)**, **262(1→2)**, **274(0→1)**, **278(1→0)**.

Node D (Folivora): **37(0→2&3)**, **85(1→3)**, **142(0→2)**, **145(1→2)**.

Node E: **3(1→0)**, **9(1→2)**, **11(1→2)**, **74(0→1)**, **100(1&2→0)**.

Node F (Eufolivora): **344(0→1)**, **345(0→1)**, **348(0→1)**.

Node G: **357(0→1)**, **361(0→1)**.

Node H (Mylodontidae): 13(0→2), 19(1→0), **20(1→2)**, **35(2→7)**, 46(1→0), 59(0→1), 63(0→1), 283(0→2), 346(0→1).

Node I: **4(1→0)**, 31(1→4), **32(0→5)**, **33(0→6)**, **34(0→6)**, 62(2→3).

Node J: **52(1→0)**, **345(1→0)**, **354(1→0)**, **369(0→1)**.

Node K: **40(0→1)**, **62(2→3)**.

Node L (Scelidotheriinae): **4(1→0)**, **14(0→2)**, **16(0→2)**, **17(0→3)**, **20(2→4)**, **26(1→0)**, **31(1→3)**, **32(0→4)**, **33(0→5)**, **34(0→5)**, **55(2→1)**, **65(1→2)**, **70(1→0)**, **82(1&2→0)**, **85(3→1)**, **93(0→1)**, **100(0&1→2)**, **105(0→1)**, **107(1→0)**, **111(1&2→0)**, **113(1→0)**, **121(4→5)**, **126(0→1)**, **146(1&2→0)**, **159(1→0)**, **189(0→1)**, **193(1→0)**, **199(0→1)**, **203(1→2)**, **238(1→2)**, **239(1→2)**, **255(0→1)**, **303(1→2)**, **310(0→1)**, **332(1→0)**, **341(1→2)**, **342(0→1)**, **344(1→2)**, **345(1→2)**, **347(1→2)**, **348(1→2)**, **351(0→1)**, **352(0→1)**, **353(1→0)**, **357(1→2)**, **363(0→1)**, **367(0→2)**, **376(1→0)**, **381(0→1)**.

Node M: **21(1→0)**, **30(0→1)**, **37(2→4)**.

Node N (Mylodontini + Lestodontini): **16(0→1)**, **33(0→4)**, **65(1→0)**, **92(0→1)**, **159(1→0)**.

Node O (Lestodontini): **20(2→0)**, **47(2→1)**, **48(0→1)**, **51(0→1)**, **57(2→1)**, **76(0→1)**, **368(1→2)**, **377(0→1)**.

Node P: **25(0→1)**, **37(4→2)**.

Node Q: **34(0→4)**.

Node R: **6(0&1→2)**, **24(0→1)**, **106(1→2)**, **175(1→2)**.

Node S (Mylodontini): **13(1→0)**, **32(0→3)**, **34(0→4)**, **44(0→1)**, **111(1→0)**, **369(0→1)**, **383(0→1)**.

Node T: **30(1→0)**, 70(1→0), 211(0→1).

Node U: 6(0→1), 25(0→1), 47(2→1), 70(0→1), 191(0&1→0), 194(1→2).

Appendix VI. Data S6. Synapomorphies and autapomorphies common to the 2 trees resulting from the analysis of the pruned matrix (38 taxa). Nodes refer to Figure 8.10. Character numbers and states shown in bold type are optimized as unambiguous synapomorphies/autapomorphies, those in plain type are ambiguous synapomorphies/autapomorphies.

Euphractus sp.: **52(0→1)**, **54(1&2→0)**, **55(1→0)**, **62(1→2)**, **69(0→1)**, **83(0→1)**, **85(1→0)**, **94(2→0)**, **95(0→1)**, **97(2→0)**, **99(0&1→2)**, **100(1→0)**, **102(0→1)**, **106(0→2)**, **113(1→0)**, **114(1→0)**, **115(0→6)**, **156(0→2)**, **164(0→2)**, **168(1&2→3)** , **174(1→0)**, **177(0→1)**, **181(0→1)**, **189(0→1)**, **192(1→0)**, **194(1→0)**, **203(1→2)**, **213(0→1)**, **214(0→1)**, **218(0&1→2)**, **222(0→1)**, **230(1→2)**, **236(0&1→2)**, **259(1→0)**, **262(1→0)**, **266(1→0)**, **278(1&2→0)**, **300(0→1)**, **309(1→0)**, **315(1→0)**, **321(1→0)**, **326(0→1)**, **350(2→0)**, **351(0→1)**, **355(1→0)**, **363(0→1)**, **366(0→1)**.

Cyclopes sp.: **51(1→2)**, **163(0→1)**, **169(0→1)**, **181 (0→1)**, **192(1→2)**, **203(1→0)**, **207(0→2)**, **243(1→0)**, **267(0→1)**, **283(0→2)**.

Tamandua sp.: **55(1→2)**, **77(1→0)**, **119(1→2)**, **142(0→1)**, **191(2→1)**.

Myrmecophaga sp.: **82(1→0)**, **187(1→0)**, **194(1→0)**, **202(0→1)**, **215(0→1)**, **279(0→1)**, **284(0→1)**, **326(0→1)**, **332(1→0)**.

Bradypus sp.: **37(2&3→4)**, **51(1→2)**, **57(2→3)**, **85(3→4)**, **89(0→1)**, **102(0→2)**, **130(1→2)**, **139(1→0)**, **152(1→2)**, **161(0→1)**, **177(0→1)**, **180(0→1)**, **187(1→2)**, **212(0→1)**, **214 (0→1)**, **215(0→1)**, **225(0→1)**, **258(1→0)**, **265(1→0)**, **286(1→0)**, **294(1→0)**, **300(0→1)**, **303(1→0)**, **306(0→1)**, **317(0→1)**, **321(1→2)**, **341(1→0)**, **349(0→1)**, **353(1→0)**, **355(1→0)**, **381(0→1)**.

Hapalops sp.: **3(0→2)**, **6(0→2)**, **10(0→1)**, **17(0→2)**, **27(0→1)**, **32(0→1)**, **33(0→1)**, **34(0→1)**, **36(3→1)**, **38(1&2→3)**, **39(0→1)**, **60(0→1)**, **66(0→2)**, **76(0→1&2)**, **84(0→1)**, **96(0→1)**, **106(0→1&2)**, **112(0→1)**, **115(0→4)**, **122(1→4)**, **143(0→1)**, **147(0→1)**, **167(0→1)**, **184(0→1)**, **185(0→1)**, **202(0→1)**, **222(0→1)**, **262(1→0)**, **350(2→1)**, **355(1→0)**, **358(1→0)**.

Nematherium sp.: **16(0→2)**, **33(0→4)**, **34(0→4)**, **66(0→2)**, **86(1→0)**, **97(1→0)**, **143(0→1)**, **147(0→1)**, **187(1→2)**, **193(1→0)**, **207(0→1)**, **280(1→0)**, **285(0→1)**, **320(0→1)**, **333(1&2→0)**.

Scelidotherium sp.: **62(2→3)**, **71(1→0)**, **86(1→0)**, **125(1→0)**, **140(0→1)**, **167(0→1)**, **178(0→1)**, **187(1→0)**, **195(1→0)**, **196(1→0)**, **343(1→2)**.

Catonyx sp.: **37(2→5)**, **59(1→2)**, **66(0→2)**, **97(0→1)**, **112(0→1)**, **142(2→0)**, **161(0→1)**, **170(1→0)**, **181(0→1)**, **243(1→2)**.

Octodontotherium grande: **17(0→1)**, **192(1→0)**.

Paroctodontotherium calleorum: **31(1→5)**, **35(7→3)**, **169(1→0)**.

Lestobradys sprechmanni: **24(0→1)**, **32(0→4)**, **65(0→1)**, **75(0→1)**, **76(1→2)**.

Thinobadistes sp.: **106(1→0)**.

Bolivartherium sp.: **14(1→2)**, **30(1→6)**, **63(1→0)**, **72(0→1)**, **353(2→1)**, **354(1→0)**.

Lestodon armatus: **11(2→3)**, **21(0→1)**, **28(1→0)**, **62(2→1)**, **70(1→0)**, **76(1→2)**, **93(0→1)**, **156(0→2)**, **173(1→0)**, **324(1→2)**, **352(0→1)**.

Sphenotherus zavaletianus: **11(2→3)**, **63(1→0)**.

Simomylodon uccasamamensis: **37(4→3)**, **82(2→3)**, **187(1→2)**, **235(1→0)**, **258(2→1)**, **260(2&3→1)**, **270(3→2)**.

Glossotheridium chapadmalense: **63(1→0)**, 191(0→1), **219(1→0)**.

Paramylodon garbanii: **51(0→1)**, **253(1→0)**, **259(3→2)**, **368(1→0)**.

Paramylodon harlani: **341(0→1)**.

Glossotherium robustum: **86(2→3)**, **142(0→1)**, 324(1→2).

Glossotherium tarijense: 20(1&2→0), 37(3→2).

Glossotherium tropicorum: 37(3→2), **45(1→0)**, **47(1→0)**, **51(0→1)**, **94(0→1)**, **173(1→0)**, **285(0→1)**, **305(1→0)**.

Glossotherium phoenesis: **67(2→1)**, 309(1→0).

Octomylodon sp.: **2(2→4)**, **17(0→1)**, **38(2→3)**, **63(1→0)**.

Brievabradys laventensis: no autapomorphies.

Baraguatherium takumara: **15(1→0)**.

Octodontobradys puruensis: **15(1→2)**, **30(0→3)**, **51(1→0)**, **56(2→1)**, **106(0→1)**.

Pseudoglyptodon sp.: **2(2→3)**, **17(0→3)**, **32(0→7)**, **33(0→7)**, **34(0→8)**, **39(0→1)**, **63(0→1)**, **122(1→2)**.

Eionaletherium tanycnemius: **348(1→2)**.

Pleurolestodon acutidens: **40(0→1)**, **45(1→0)**, **82(2→3)**, **106(1→0)**, **168(2→1)**, **187(1→0)**.

Mylodon darwinii: **19(1→0)**, **20(2→1)**, **37(4→3)**.

Kiyumylodon lecuonai: **48(0→1)**, **52(1→0)**.

Pseudoprepotherium venezuelanum: **37(2→0)**, **357(1→0)**, **359(1→0)**.

Pseudoprepotherium confusum: no autapomorphies.

Mirandabradys sp.: **91(0→2)**, **122(1→2)**.

Urumacotherium sp.: **14(0→1)**, **15(1→0)**, **26(1→0)**, **27(0→1)**, **29(0→2)**, **31(1→2)**, **32(0→1)**, **33(0→1)**, **34(0→1)**, **35(7→4)**, **62(2→1)**, **63(1→0)**, **186(1→2)**.

Node 1 (Pilosa): **119(0→1)**, **125(0→1)**, **159(0→1)**, **179(0→1)**, **186(0→1)**, **232(0→1)**, **251(0→1)**, **264(0→1)**, **285(1→0)**, **296(0→1)**, **299(0→1)**, **305(0→1)**, **313(0→1)**, **314(1→0)**, **322(1→0)**.

Node 2 (Vermilingua): **38(1&2→0)**, **57(1→0)**, **59(0→2)**, **62(1→0)**, **64(0→1)**, **86(1→0)**, **90(1→0)**, **122(1→0)**, **127(1→3)**, **128(0→1)**, **135(1→0)**, **157(1→0)**, **168(1&2→0)**, **216(1→2)**, **239(0→1)**, **241(0&1→2)**, **259(1→2)**, **261(0→1)**, **263(1→0)**.

Node 3: **41(2→0)**, **47(0→3)**, **51(1→0)**, **82(4→1)**, **85(1→0)**, **129(0→1)**, **137(0→2)**, **141(0→1)**, **156(0→1)**, **195(0→1)**, **199(0→2)**, **230(1→0)**, **262(1→2)**, **274(0→1)**, **278(1→0)**.

Node 4 (Folivora): **37(0→2&3)**, **85(1→3)**, **142(0→2)**, **145(1→2)**.

Node 5: **3(1→0)**, **9(1→2)**, **11(1→2)**, **74(0→1)**, **100(1&2→0)**.

Node 6 (Eufolivora): **344(0→1)**, **345(0→1)**, **348(0→1)**.

Node 7: **357(0→1)**, **361(0→1)**.

Node 8 (Mylodontidae): **13(0→2)**, **19(1→0)**, **20(1→2)**, **35(2→7)**, **46(1→0)**, **59(0→1)**, **63(0→1)**, **283(0→2)**, **346(0→1)**.

Node 9: **4(1→0)**, **32(0→5)**, **33(0→6)**, **34(0→6)**, **62(2→3)**.

Node 10: no synapomorphies.

Node 11: **47(0→2)**, **48(2→0)**, **52(0→1)**, **124(0→1)**.

Node 12: **87(0→1)**, **98(0→1)**.

Node 13: **349(0→1)**.

Node 14 (Scelidotheriinae): **4(1→0)**, **14(0→2)**, **16(0→2)**, **17(0→3)**, **20(2→4)**, **26(1→0)**, **31(1→3)**, **32(0→4)**, **33(0→5)**, **34(0→5)**, **55(2→1)**, **65(1→2)**, **70(1→0)**, **82(1&2→0)**, **85(3→1)**, **93(0→1)**, **100(0&1→2)**, **105(0→1)**, **107(1→0)**, **111(1&2→0)**, **113(1→0)**, **121(4→5)**, **126(0→1)**, **146(1&2→0)**, **159(1→0)**, **189(0→1)**, **193(1→0)**, **199(0→1)**, **203(1→2)**, **238(1→2)**, **239(1→2)**, **255(0→1)**, **303(1→2)**, **310(0→1)**, **332(1→0)**, **341(1→2)**, **342(0→1)**, **344(1→2)**, **345(1→2)**, **347(1→2)**, **348(1→2)**, **351(0→1)**, **352(0→1)**, **353(1→0)**, **357(1→2)**, **363(0→1)**, **367(0→2)**, **376(1→0)**, **381(0→1)**.

Node 15 (Mylodontinae): **13(2→1)**, **60(0→1)**, **67(0→1)**, **86(1→2)**, **91(0→1)**, **103(0→1)**, **122(1→3)**, **191(2→1)**, **248(0→1)**, **308(0→1)**, **316(1→0)**, **318(1→0)**, **323(1→2)**, **339(1→0)**, **341(1→0)**, **371(0→1)**.

Node 16: **52(1→0)**, **345(1→0)**, **354(1→0)**, **369(0→1)**.

Node 17 (*Pseudoprepotherium*): **40(0→1)**, **62(2→3)**.

Node 18: **19(0→1)**, **22(1→0)**, **28(0→1)**, **67(1→2)**, **71(1→0)**, **142(2→0)**, **168(1→2)**, **195(1→0)**, **247(0→1)**, **258(1→2)**.

Node 19: **13(1→0)**, **33(0→6)**, **82(2→3)**, **83(0→1)**, **86(2→3)**, **93(0→1)**.

Node 20: **21(1→0)**, **30(0→1)**, **37(2→4)**.

Node 21 (Mylodontini + Lestodontini): **16(0→1)**, **33(0→4)**, **65(1→0)**, **92(0→1)**, **159(1→0)**.

Node 22 (Lestodontini): **20(2→0)**, **47(2→1)**, **48(0→1)**, **51(0→1)**, **57(2→1)**, **76(0→1)**, **368(1→2)**, **377(0→1)**.

Node 23: **6(0&1→2)**, **24(0→1)**, **106(1→2)**, **175(1→2)**.

Node 24: **25(0→1)**, **37(4→2)**.

Node 25: **34(0→4)**.

Node 26 (Mylodontini): **13(1→0)**, **32(0→3)**, **34(0→4)**, **44(0→1)**, **111(1→0)**, **369(0→1)**, **383(0→1)**.
Node 27: **30(1→0)**, **70(1→0)**, **211(0→1)**.
Node 28: **52(1→0)**, **62(2→1)**, **151(0→1)**, **168(2→3)**.
Node 29: **303(1→2)**, **308(1→2)**, **317(0→1)**, **325(0→1)**, **359(1→2)**, **365(1→2)**, **370(0→1)**, **375(0→1)**.
Node 30: **82(2→0)**, **116(0→1)**, **186(0→1)**, **198(1→2)**, **245(0→1)**.
Node 31: **32(3→0)**, **34(4→0)**, **40(0→1)**.
Node 32 (*Paramylodon*): 191(0→1), **271(1→0)**.
Node 33 (*Glossotherium*): **37(4→3)**, **213(1→2)**, 219(1→0), **341(0→1)**.
Node 34: 25(0→1), 47(2→1), **70(0→1)**, 194(1→2).

Appendix VI. Table S7. Tip species and age ranges used to calibrate the phylogeny in Chapter 8. Asterisks indicate taxa that have been *a posteriori* excluded from the phylogenetic analyses, due to lack of data. Symbol "⊥" is applied to indicate absence of accurate stratigraphic data, and consequently the limit (upper or lower) of the SALMA/NALMA is considered.

Taxon	FAD (Ma)	LAD (Ma)	Age and/or South/North American Land Mammal Age	Representative geological and geographical occurrences	Lead References
Euphractus sp.	1.8	0.0	Ensenadan to Present	Argentina, Bolivia, Brazil	McKenna & Bell 1997
Cyclopes sp.	0.012	0.0	Holocene to Present	Brazil, Panama, Peru	fossilworks.org
Myrmecophaga sp.	9.0	0.0	Huayquerian to Present	Central and South America	Gaudin *et al.* 2018
Tamandua sp.	1.8	0.0	Ensenadan to Present	Panama, Brazil, Peru, Venezuela	McKenna & Bell 1997
Bradypus sp.	0.012	0.0	Holocene to Present	Panama, Brazil, Peru	fossilworks.org
Hapalops sp.	19	11.8	Santacrucian to Laventan	Argentina, Bolivia, Brazil, Chile	McDonald & De Iuliis 2008; fossilworks.org
Nematherium sp.	17.5	16.3	Santacrucian	Argentina, Chile	McDonald & De Iuliis 2008; fossilworks.org
Scelidotherium sp.	4.5	0.012	Chapadmalalan to Bonaerian	Argentina	McDonald 1987; McDonald & De Iuliis 2008; fossilworks.org
Catonyx sp.	1.8	0.012	Ensenadan to Bonaerian	Localities throughout southern cone	McDonald 1987; McDonald & De Iuliis 2008; fossilworks.org
Baraguatherium takumara	19.3	17.2	Colhuehuapian-Santacrucian, Early Miocene	Castillo Fm, Cerro la Cruz, northwestern Venezuela	Rincón *et al.* 2014, 2016
Bolivartherium sp.	6.7	4.0	Late Miocene – Early Pliocene	Urumaco and Codore Fms., Falcón, northwestern Venezuela	Cande & Kent 1992; Linares 2004a, b; Carlini *et al.* 2006
Brievabradys laventiensis	13.8	12.8	Laventan	La Victoria Fm, Quebrada La Venta, Colombia	Madden *et al.* 1997; Villarroel 2000
Eionaletherium tanycnemius	~10.0	~7.0	Late Miocene	Urumaco Fm (middle member), Falcón, northwestern Venezuela	Linares 2004b; Rincón *et al.* 2015
Glossotheridium chapadmalense	4.5	3.3	Chapadmalalan	Chapadmalal Fm, Buenos Aires Province, Argentina	Carlini & Scillato-Yané 1999; Vizcaíno *et al.* 2004b; McAfee 2009
**Glossotheriopsis pascuali*	16.3	8	Middle-Late Miocene	Argentina (Rio Negro, Tucumán and Catamarca Provinces) and Colombia	Scillato-Yané 1976; Esteban & Abdala 1993; Esteban *et al.* 2014
Glossotherium phoenesis	0.12	0.012	Late Pleistocene	Intertropical Brazil	Cartelle *et al.* 2019
Glossotherium robustum	~0.7	0.01	Late Ensenadan to Lujanian	Localities throughout southern cone, between latitudes of 20°S and 40°S	Hoffstetter 1963; Carlini & Scillato-Yané 1999; MacFadden *et al.* 2013; Martínez *et al.* 2013; Pitana *et al.* 2013; Varela *et al.* 2016
Glossotherium tarijense	~1.1	0.7	late-Early to early-Middle Pleistocene (late Ensanadan)	Tolomosa Fm., Tarija, Southern Bolivia	MacFadden *et al.* 2013
Glossotherium tropicorum	0.0235	0.0170	late Middle to Late Pleistocene (Lujanian)	Coastal areas of Ecuador and Peru	De Iuliis *et al.* 2017
Kiyumylodon lecuonai	⊥9.0	⊥5.3	Huayquerian, Late Miocene	Camacho Fm, Uruguay	Rinderknecht *et al.* 2007
Lestodon armatus	5.3	0.01	Montehermosan to Lujanian	Localities throughout	Hoffstetter 1963; Carlini & Scillato-Yané

				southern cone, between latitudes of 20°S and 40°S	1999; Deschamps *et al.* 2001; MacFadden *et al.* 2013; Varela *et al.* 2016
Lestobradys sprechmanni	⊥9.0	⊥5.3	Huayquerian, Late Miocene	Camacho Fm, Uruguay	Rinderknecht *et al.* 2010
Mirandabradys sp.	13.7	5.7	Middle – Late Miocene	Socorro, Urumaco and Codore Fms, Falcón, northwestern Venezuela	Cande & Kent 1992; Linares 2004a; Carlini *et al.* 2006
Mylodon darwinii	~0.7	0.01	Late Ensenadan to Lujanian	Localities throughout southern cone between latitudes of 20°S and 40°S	Hoffstetter 1963; Alberdi *et al.* 1987; Borrero *et al.* 1991; Carlini & Scillato-Yané 1999; Brandoni *et al.* 2010; MacFadden *et al.* 2013; Varela *et al.* 2016
Octodontobradys puruensis	⊥9.0	~5.0	Huayquerian-Montehermosan, Late Miocene - Pliocene	Solimões Fm, Acre, Brazil	Santos *et al.* 1993b; Cozzuol 2006
Octodontotherium grande	29.4	24.2	Desedean	Deseado Fm, La Flecha, Santa Cruz; Argentina	MacFadden *et al.* 1985; Pujos & De Iuliis 2007; Shockey & Anaya 2011
Octomylodon sp.	10.0	9.0	Chasicoan – late Miocene	Arroyo Chasicó and Ituzaingó Fms, Argentina	Scillato-Yané 1977; Brandoni 2013
**Orophodon hapaloides*	29.4	24.2	Desedean	Deseado Fm, La Flecha, Santa Cruz; Argentina	Pujos & De Iuliis 2007; Shockey & Anaya 2011
Paramylodon garbanii	4.7	2.5	Early and Late Pliocene (early and early late Blancan)	Central America and southern North America	Robertson, 1976; Morgan 2008; McDonald & Morgan 2011
Paramylodon harlani	2.5	0.01	Pleistocene	North America	Morgan & Hulbert, 1995; Morgan 2008; McDonald *et al.* 2004
Paroctodontotherium calleorum	26.5	25.5	Desedean	Salla Beds, Bolivia	Shockey & Anaya 2011
Pleurolestodon acutidens	6	5	Huayquerian, Late Miocene	"Araucano" Fm, Catamarca, Argentina	Rovereto 1914; Marshall & Patterson 1981; Esteban *et al.* 2014
Pseudoglyptodon sp.	31.5	25.6	Oligocene (Tinguiririan to Deseadan)	Abanico Fm., Central Chile and Salla Beds, Bolivia	McKenna *et al.* 2006; Pujos & De Iuliis 2007
Pseudoprepotherium confusum	13.6	12.2	Laventan, Middle Miocene	La Victoria and Villavieja Fms, Quebrada La Venta, Colombia	Hirschfeld 1985; Madden *et al.* 1997
Pseudoprepotherium venezuelanum	9	6.5	Late Miocene	Yuca Fm., Venezuela; Solimões Fm, Acre, Brazil	Collins 1934; Hirschfeld 1985; Bocquentin & Guilherme 1999; Negri *et al.* 2010
Simomylodon uccasamamensis	5.3	2.58	Pliocene	Bolivian Altiplano, Central South America	Saint-André *et al.* 2010
Sphenotherus zavaletianus	⊥9.0	⊥5.3	Huayquerian, late Miocene	"Araucano" Fm, Catamarca and Ituzaingó Fm, Entre Ríos (Argentina)	Ameghino 1891b; Esteban 1999; Brandoni 2013
Thinobadistes sp.	9.0	5.9	Earliest to Late early Hemphillian	Florida to Texas, southeastern North America	Webb 1989; Morgan 2008
Urumacotherium sp.	⊥13.8	~5.0	Middle Miocene to Early Pliocene	Ipururo Fm, Fitzcarrald, Peru; Solimões Fm, Acre, Brazil; Urumaco Fm, Falcón, northwestern Venezuela	Bocquentin-Villanueva 1984; Bocquentin & Guilherme 1999; Negri & Ferigolo 2004; Negri *et al.* 2010; Tejada-Lara *et al.* 2015

Appendix VI. Table S8. Relevant South and North American Land Mammal Ages, best current estimates. Abbreviations: Ma, millions of years; ka, thousands of years; CE, Current Era. Modified from Slater *et al.* (2016).

SALMA	RANGE		REFERENCES
Platan	8.5 ka	1492 CE	Cione & Tonni 1995; Tonni 2009
Lujanian	128 ka	8.5 ka	Tonni 2009
Bonaerian	400 ka	128 ka	Tonni 2009
Ensenadan	1.8 Ma	0.4 Ma	Tonni 2009
Marplatan	3.3 Ma	1.8 Ma	Reguero *et al.* 2007; Tomassini *et al.* 2013
Chapadmalalan	4.5 Ma	3.3 Ma	Cione *et al.* 2007; Woodburne 2010; Deschamps *et al.* 2013; Tomassini *et al.* 2013
Montehermosan	5.3 Ma	4.5 Ma	Tomassini *et al.* 2013
Huayquerian	9.0 Ma	5.3 Ma	Marshall *et al.*1979; Cione *et al.* 2007; Woodburne 2010; Tomassini *et al.* 2013
Chasicoan	10.0 Ma	9.0 Ma	Flynn & Swisher 1995
Mayoan	11.8 Ma	10 Ma	Flynn & Swisher 1995
Laventan	13.8 Ma	11.8 Ma	Flynn & Swisher 1995
Colloncuran	15.5 Ma	14 Ma	Flynn & Swisher 1995
Friasian	16.3 Ma	15.5 Ma	Flynn & Swisher 1995
Santacrucian	19.0	16 Ma	Vizcaíno *et al.* 2012b; Perkins *et al.* 2012
Colhuehuapian	21.0 Ma	20.1 Ma	Dunn *et al.* 2013
Deseadan	29.4 Ma	24.2 Ma	Dunn *et al.* 2013
Tinguiririca n	33.6 Ma	31.3 Ma	Dunn *et al.* 2013

NALMA	RANGE		REFERENCES
Rancholabrean	~0.24 Ma	0.011 Ma	Sanders *et al.* 2009
Irvingtonian	1.8 Ma	~0.24 Ma	Bell *et al.* 2004
Blancan	4.9 Ma	1.8 Ma	Bell *et al.* 2004
Hemphillian	9.0 Ma	4.9 Ma	Tedford *et al.* 2004

APPENDIX VII

Appendix VII. Table S1. Linear and angular measurements of the bony labyrinth of *Glossotherium robustum* (MACN Pv 13553). Linear measurements are expressed in millimeters and angular measurements in degrees (after Schmelzle *et al.* 2007 and Billet *et al.* 2012, 2013).

BL and vestibule	Measurement
IEH	18.51
VW	9.92
VH	5.58
Semicircular canals	**Measurement**
IEH	18.56
ASCW	7.95
ASCL	9.47
ASCP	26.75
PSCW	8.58
PSCL	10.18
PSCP	29.72
LSCW	6.59
LSCL	5.29
LSCP	18.56
Angle ASC/PSC	78.8°
Angle ASC/LSC	77.5°
Angle PSC/LSC	76.9°
Cochlea	**Measurement**
CocL	29.82
CocW	10.05
CocH	5.36
Ncoils	1.9

Appendix VII. Figure S2. Shape differentiation of the bony labyrinth (a), semicircular canals (b), and cochlea (c) in the present sample of specimens, and associated patterns of morphological transformation on the first two PCres with shape data corrected for allometry (i.e., body mass). Symbols: same as Figures 9.2–9.4.

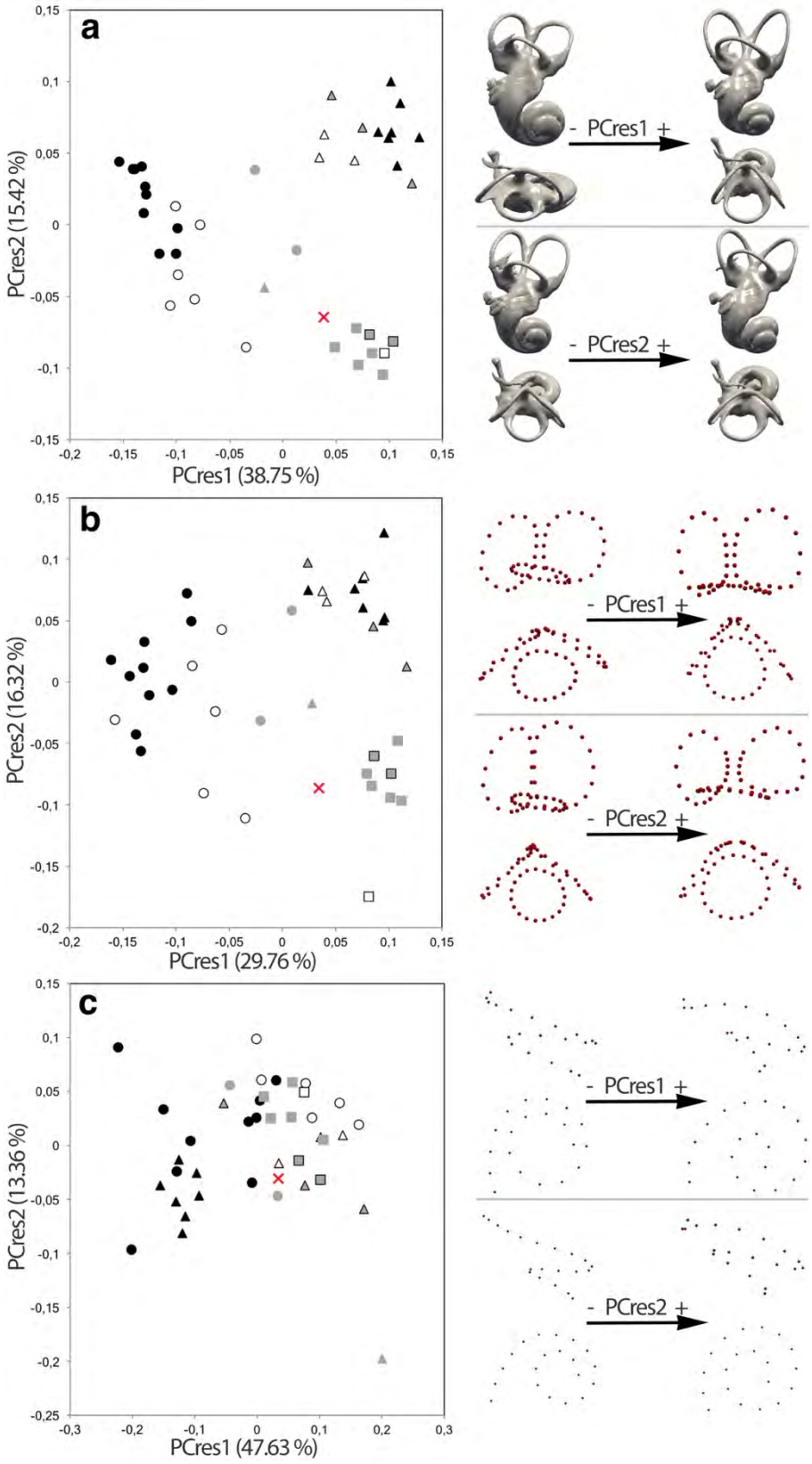

Appendix VII. Figure S3. Shape differentiation of the bony labyrinth (a), semicircular canals (b), and cochlea (c) in the present sample of specimens, and associated patterns of morphological transformation on the first two PCres with shape data corrected for allometry (i.e., centroid size). Symbols: same as Figures 9.2–9.4.

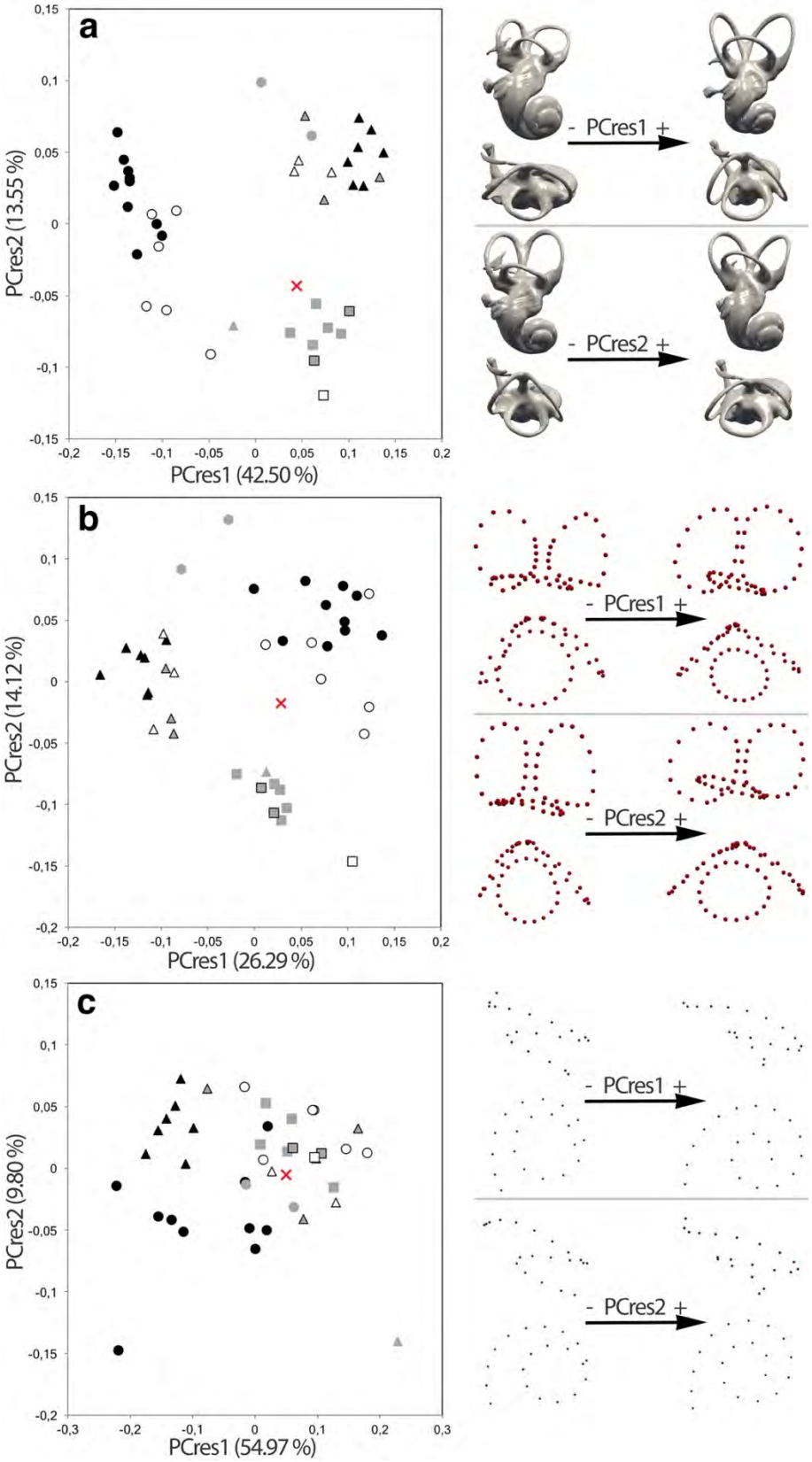

Appendix VII. Figure S4. Shape differentiation of the bony labyrinth (a), semicircular canals (b), and cochlea (c) explained by variation in body mass in the present sample of specimens and corresponding differences in shape between taxa with small (left) and large (right) body masses. ASV = allometric shape vectors. Symbols: same as Figures 9.2–9.4.

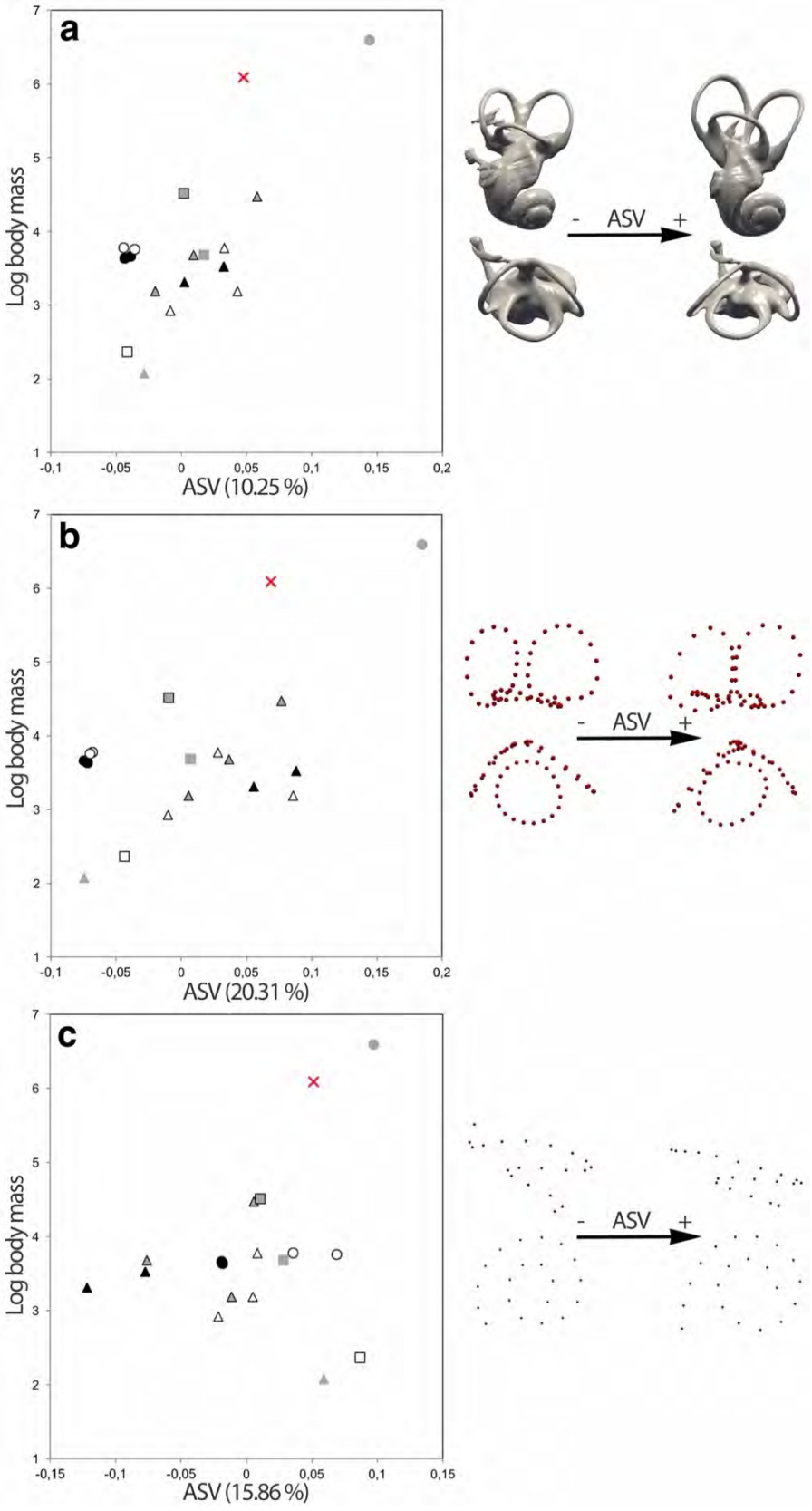

Appendix VII. Figure S5. Shape differentiation of the bony labyrinth (a), semicircular canals (b), and cochlea (c) explained by variation in centroid size in the present sample of specimens, and corresponding differences in shape between taxa with small (left) and large (right) centroid sizes. ASV = allometric shape vectors. Symbols: same as Figures 9.2–9.4.

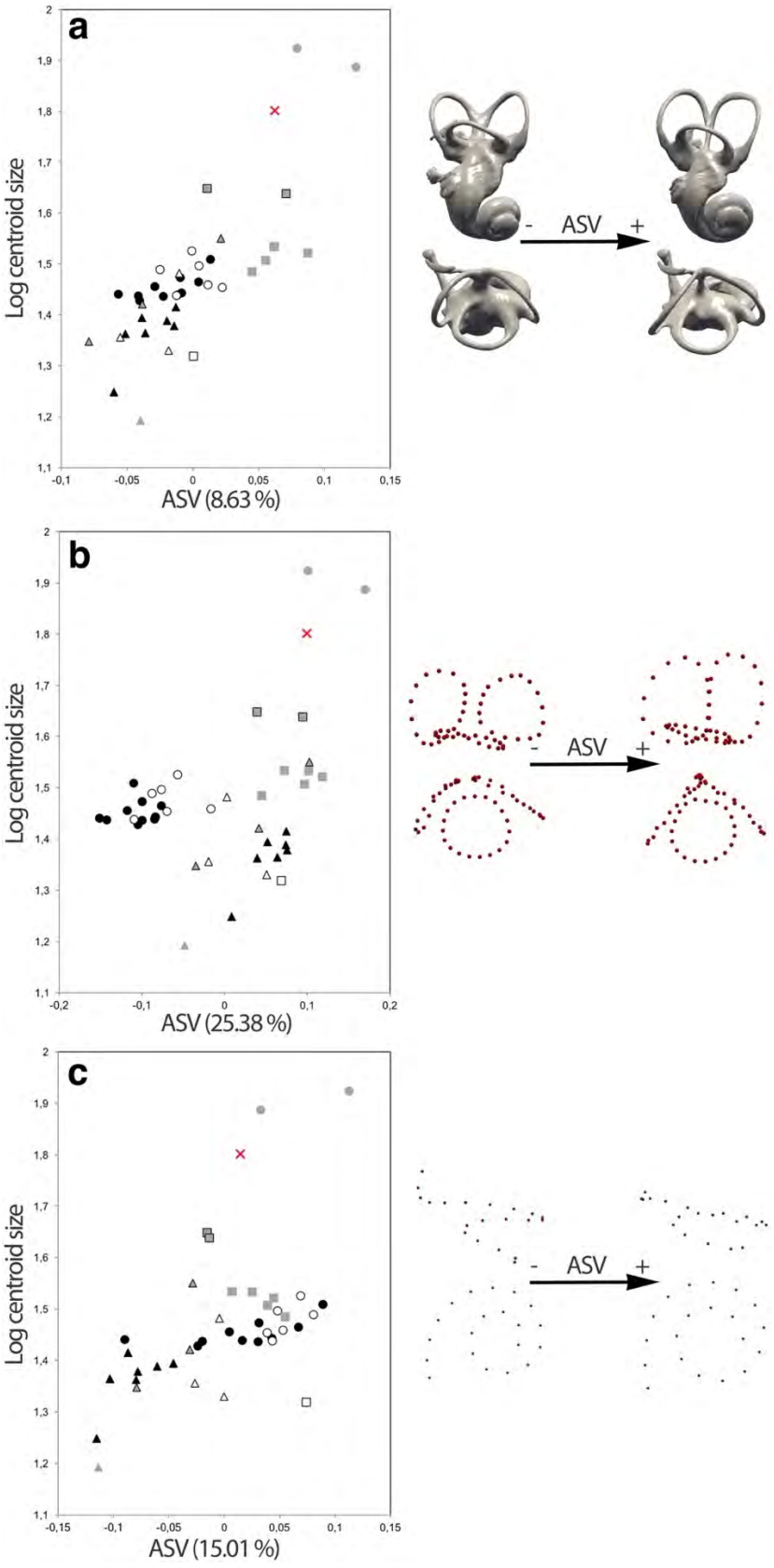

Appendix VII. Figure S6. First (a) and second (b) 2 singular warp (SW) scores for the subsets defined on the cochlea and the semicircular canals. At the bottom: associated covariation patterns found from the analysis of 80 semilandmarks in the whole sample. Symbols: same as Figures 9.2–9.4.

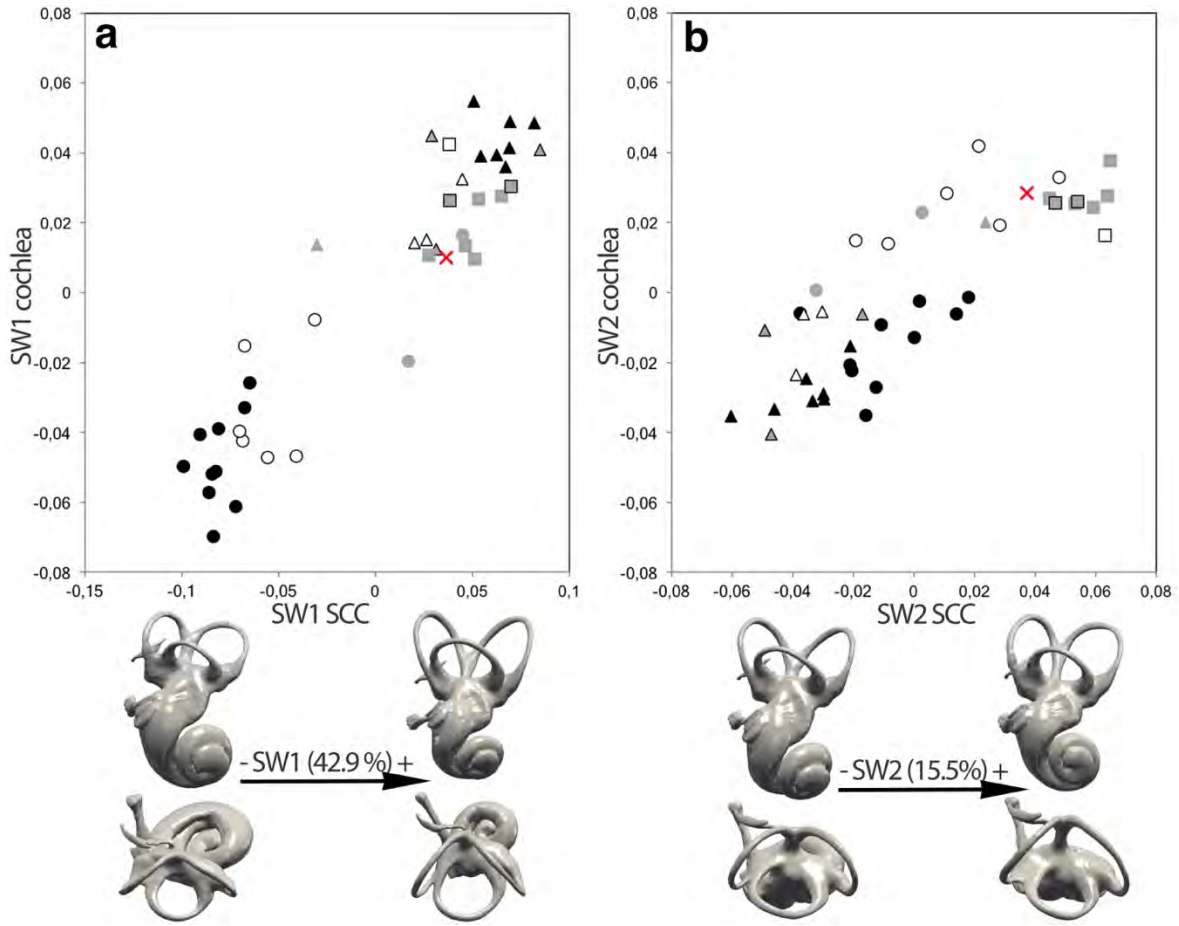

REFERENCES

REFERENCES

Alberdi MT, Menegaz A, Prado JL. 1987. Formas terminales de *Hippidion* (Mammalia, Perissodactyla) de los yacimientos del Pleistoceno tardío-Holoceno de la Patagonia (Argentina y Chile). *Estudios Geológicos* 43: 107–115.

Ameghino F. 1883. Sobre una nueva colección de mamíferos fósiles recogidos por el Profesor Pedro Scalabrini en las barrancas del Paraná. *Boletín de la Academia Nacional de Ciencias de Córdoba* 5: 257–306.

Ameghino F. 1885. Nuevos restos de mamíferos fósiles Oligocenos recogidos por el Profesor Pedro Scalabrini y pertenecientes al Museo Provincial de la ciudad de Paraná. *Boletín de la Academia Nacional de Ciencias de Córdoba* 8: 5–207.

Ameghino F. 1889. Contribución al conocimiento de los mamíferos fósiles de la República Argentina. *Actas de la Academia Nacional de Ciencias de Córdoba* 6: 1–1027

Ameghino F. 1891a. Caracteres diagnósticos de cincuenta especies nuevas de mamíferos fósiles argentinos. *Revista Argentina de Historia Natural* 1: 129–167.

Ameghino F. 1891b. Sobre algunos restos de mamíferos fósiles, recogidos por el señor Manuel B. Zavaleta en la formación miocena de Tucumán y Catamarca. *Revista Argentina de Historia Natural* 1: 88–101.

Ameghino F. 1894. Première contribution à la connaissance de la faune mammalogique des couches à *Pyrotherium*. *Boletín del Instituto Geográfico Argentino* 15: 603–660.

Ameghino F. 1895. Sur les édentés fossiles de l'Argentine (examen critique, révision et correction de l'ouvrage de la M. R. Lydekker). *Revista del Jardín Zoológico de Buenos Aires* 3: 97–192.

Ameghino F. 1897. Mammifères Crétacés de l'Argentine. Deuxième contribution à la connaissance de la faune mammalogique des couches à *Pyrotherium*. *Boletín del Instituto Geográfico Argentino* 18: 406–521.

Ameghino F. 1898. *Première notice sur le Neomylodon listai: un représentant vivant des anciens édentés gravigrades fossiles de l'Argentine*. La Plata: Imprenta La Libertad.

Ameghino F. 1902. Notas sobre algunos mamiferos fosiles, nuevos ó poco conocidos del valle de Tarija. *Anales del Museo de Historia Natural de Buenos Aires* 8: 225–261.

Ameghino F. 1904. Nuevas especies de mamíferos, cretáceos y terciarios de la República Argentina. *Anales de la Sociedad Científica Argentina* 58: 1–142.

Amson E, Argot C, McDonald HG, Muizon C de. 2015a. Osteology and functional morphology of the forelimb of the marine sloth *Thalassocnus* (Mammalia, Tardigrada). *Journal of Mammalian Evolution* 22: 169–242.

Amson E, Argot C, McDonald HG, Muizon C de. 2015b. Osteology and functional morphology of the hind limb of the marine sloth *Thalassocnus* (Mammalia, Tardigrada). *Journal of Mammalian Evolution* 22: 355–419.

Amson E, Muizon C de, Gaudin TJ. 2016. A reappraisal of the phylogeny of the Megatheria (Mammalia: Tardigrada), with an emphasis on the relationships of the Thalassocninae, the marine sloths. *Zoological Journal of the Linnean Society* 179: 217–236.

Amson E, Billet G, Muizon C de. 2018. Evolutionary adaptation to aquatic lifestyle in extinct sloths can lead to systemic alteration of bone structure. *Proceedings of the Royal Society B* 285: 20180270.

Anaya F, MacFadden BJ. 1995. Pliocene mammals from Inchasi, Bolivia: the endemic fauna just before the Great American Interchange. *Bulletin of the Florida Museum of Natural History* 39: 87–140.

Anaya F, Pachero J, Pili LA. 1989. Hallazgo de mesotherinos en la formación Kasira (Terciario) en el Sud Boliviano, Prov. Modesto Omiste – Dpto. Potosí. *Boletín del Servicio Geológico de Bolivia* 4: 41–46.

Anderson MJ. 2001. A new method for non-parametric multivariate analysis of variance. *Austral ecology* 26: 32–46.

Anthony HE. 1919. The indigenous land mammals of Porto Rico, living and extinct. *Memoirs of the American Museum of Natural History* 2: 331–435.

Anthony J. 1953. Morphologie externe du télencéphale dans le genre *Bradypus* L. (Edentata). *Mammalia* 17: 1–149.

Antoine PO, Marivaux L, Croft DA, Billet G, Ganerød M, Jaramillo C, Martin T, Orliac MJ, Tejada J, Altamirano AJ, Duranthon F, Fanjat G, Rousse S, Salas Gismondi R. 2012. Middle Eocene rodents from Peruvian Amazonia reveal the pattern and timing of caviomorph origins and biogeography. *Proceedings of the Royal Society B* 279: 1319–1326.

Antoine PO, Salas-Gismondi R, Pujos F, Ganerød M, Marivaux L. 2017. Western Amazonia as a hotspot of mammalian biodiversity throughout the Cenozoic. *Journal of Mammalian Evolution* 24: 5–17.

Bapst DW. 2012. paleotree: an R package for paleontological and phylogenetic analyses of evolution. *Methods in Ecology and Evolution* 3: 803–807.

Bargo MS, De Iuliis G, Vizcaíno SF. 2006a. Hypsodonty in Pleistocene ground sloths. *Acta Palaeontologica Polonic*a 51: 53–61.

Bargo MS, Toledo N, Vizcaíno SF. 2006b. Muzzle of South American Pleistocene ground sloths (Xenarthra, Tardigrada). *Journal of Morphology* 267: 248–263.

Bargo MS, Vizcaíno SF. 2008. Paleobiology of Pleistocene ground sloths (Xenarthra, Tardigrada): biomechanics, morphogeometry and ecomorphology applied to the masticatory apparatus. *Ameghiniana* 45: 175–196.

Bargo MS, Vizcaíno SF, Archuby FM, Blanco RE. 2000. Limb bone proportions, strength and digging in some Lujanian (Late Pleistocene-Early Holocene) mylodontid ground sloths (Mammalia: Xenarthra). *Journal of Vertebrate Paleontology* 20: 601–610.

Barone R, Bortolami R. 2004. *Anatomie comparée des mammifères domestiques. Tome 6, Neurologie I, Système Nerveux Central*. Paris: Vigot Frères.

Bell CJ, Lundelius EL Jr, Barnosky A, Graham RW, Lindsay, EH, Ruez DR Jr, Semken HA Jr, Webb SD, Zakrzewski RJ. 2004. The Blancan, Irvingtonian, and Rancholabrean mammal ages. In: Woodburne MO, ed. *Late Cretaceous and Cenozoic mammals of North America: biostratgraphy and geochronology*. New York: Columbia University Press, 232–314.

Bell MA, Lloyd GT. 2015. strap: an R package for plotting phylogenies against stratigraphy and assessing their stratigraphic congruence. *Palaeontology* 58: 379–389.

Benoit J, Essid EM, Marzougui W, Ammar HK, Lebrun R, Tabuce R, Marivaux L. 2013. New insights into the ear region anatomy and cranial blood supply of advanced stem Strepsirhini: evidence from three primate petrosals from the Eocene of Chambi, Tunisia. *Journal of Human Evolution* 65: 551–572.

Bergqvist LP, Abrantes EAL, Avilla LDS. 2004. The Xenarthra (Mammalia) of São José de Itaboraí Basin (upper Paleocene, Itaboraian), Rio de Janeiro, Brazil. *Geodiversitas* 26: 323–337.

Berlin JC, Kirk EC, Rowe TB. 2013. Functional implications of ubiquitous semicircular canal non-orthogonality in mammals. *PLoS One* 8: e79585.

Bertrand OC, Amador-Mughal F, Silcox MT. 2017. Virtual endocast of the early Oligocene *Cedromus wilsoni* (Cedromurinae) and brain evolution in squirrels. *Journal of Anatomy* 230: 128–151.

Billet G, Germain D, Ruf I, Muizon C de, Hautier L. 2013. The inner ear of *Megatherium* and the evolution of the vestibular system in sloths. *Journal of Anatomy* 223: 557–567.

Billet G, Hautier L, Asher RJ, Schwarz C, Crumpton N, Martin T, Ruf I. 2012. High morphological variation of vestibular system accompanies slow and infrequent locomotion in three-toed sloths. *Proceedings of the Royal Society B* 279: 3932–3939.

Billet G, Hautier L, de Thoisy B, Delsuc F. 2017. The hidden anatomy of paranasal sinuses reveals biogeographically distinct morphotypes in the nine-banded armadillos (*Dasypus novemcinctus*). *PeerJ* 5: e3593.

Billet G, Hautier L, Lebrun R. 2015a. Morphological diversity of the bony labyrinth (inner ear) in extant xenarthrans and its relation to phylogeny. *Journal of Mammalogy* 96: 658–672.

Billet G, Muizon C de, Schellhorn R, Ruf I, Ladevèze S, Bergqvist L. 2015b. Petrosal and inner ear anatomy and allometry amongst specimens referred to Litopterna (Placentalia). *Zoological Journal of the Linnean Society* 173: 956–987.

Blanco RE, Rinderknecht A. 2008. Estimation of hearing capabilities of Pleistocene ground sloths (Mammalia, Xenarthra) from middle-ear anatomy. *Journal of Vertebrebrate Paleontology* 28: 274–276.

Blanco RE, Rinderknecht A. 2012. Fossil evidence of frequency range of hearing independent of body size in South American Pleistocene ground sloths (Mammalia, Xenarthra). *Comptes Rendus Palevol* 11: 549–554.

Blaney SPA. 1990. Why paranasal sinuses? *Journal of Laryngology and Otology* 104: 690–693.

Blanton PL, Biggs NL. 1969. Eighteen hundred years of controversy: the paranasal sinuses. *American Journal of Anatomy* 124: 135–148.

Bocquentin J. 1979. *Mammifères fossiles du Pléistocène supérieur de Muaco, État de Falcón, Venezuela*. Unpublished D. Phil. Thesis, Université Pierre et Marie Curie.

Bocquentin-Villanueva J. 1984. Un nuevo representante de la subfamilia Prepotheriinae (Mammalia, Edentata) proveniente del Mioceno de Venezuela. *III Congreso Latinoamericano de Paleontología, Oaxtepec, México, Memoria* 3: 516–523.

Bocquentin J, Guilherme E. 1999. As preguiças mylodontinae (Mammalia, Xenarthra, Mylodontidae) do Neógeno do sítio Niterói, Acre, Brasil. *Acta Geologica Leopoldensia* 22: 57–67.

Bond M, Tejedor MF, Campbell KE Jr, Chornogubsky L, Novo N, Goin F. 2015. Eocene primates of South America and the African origins of New World monkeys. *Nature* 520: 538–541.

Borrero LA, Lanata JL, Cárdenas P. 1991. Reestudiando cuevas: nuevas excavaciones en Última Esperanza, Magallanes. *Anales del Instituto de la Patagonia* 20: 101–110.

Boscaini A, Gaudin TJ, Mamani Quispe B, Münch P, Antoine P-O, Pujos F. 2019a. New well-preserved craniodental remains of *Simomylodon uccasamamensis* (Xenarthra: Mylodontidae) from the Pliocene of the Bolivian Altiplano: phylogenetic, chronostratigraphic and palaeobiogeographical implications. *Zoological Journal of the Linnean Society* 185: 459–486.

Boscaini A, Gaudin TJ, Toledo N, Mamani Quispe B, Antoine P-O, Pujos F. 2019b. The earliest well-documented occurrence of sexual dimorphism in extinct sloths: evolutionary and palaeoecological insights. *Zoological Journal of the Linnean Society*. doi:10.1093/zoolinnean/zlz011.

Boscaini A, Iurino DA, Billet G, Hautier L, Sardella R, Tirao G, Gaudin TJ, Pujos F. 2018a. Phylogenetic and functional implications of the ear region anatomy of *Glossotherium robustum* (Xenarthra, Mylodontidae) from the Late Pleistocene of Argentina. *The Science of Nature* 105. doi:10.1007/s00114-018-1548-y.

Boscaini A, Iurino DA, Sardella R, Tirao G, Gaudin TJ, Pujos F. 2018b. Digital cranial endocasts of the extinct sloth *Glossotherium robustum* (Xenarthra, Mylodontidae) from the Late Pleistocene of Argentina: Description and comparison with the extant sloths. *Journal of Mammalian Evolution*. doi:10.1007/s10914-018-9441-1.

Boscaini A, Pujos F, Gaudin TJ. 2019c. A reappraisal of the phylogeny of Mylodontidae (Mammalia, Xenarthra) and the divergence of mylodontine and lestodontine sloths. *Zoologica Scripta*. doi:10.1111/zsc.12376

Boule M, Thévenin A. 1920. *Mammifères fossiles de Tarija*. Paris: Imprimerie nationale.

Brambilla L, Ibarra DA. 2019. *Archaeomylodon sampedrinensis*, gen. et sp. nov., a new mylodontine from the middle Pleistocene of Pampean Region, Argentina. *Journal of Vertebrate Paleontology* 38: e1542308.

Brandoni D. 2013. Los Tardigrada (Mammalia, Xenarthra) del Mioceno tardío de Entre Ríos, Argentina. In: Brandoni D, Noriega JI, eds. *El Neógeno de la Mesopotamia argentina*. Asociación Paleontológica Argentina, Publicación Especial 14: 135–144.

Brandoni D, Ferrero BS, Brunetto A. 2010. *Mylodon darwini* Owen (Xenarthra, Mylodontidae) from the Late Pleistocene of Mesopotamia, Argentina, with remarks on individual variability, paleobiology, paleobiogeography, and paleoenvironment. *Journal of Vertebrate Paleontology* 30: 1547–1558.

Bremer K. 1994. Branch support and tree stability. *Cladistics* 10: 295–304.

Brown B. 1903. A new genus of ground sloth form the Pleistocene of Nebraska. *Bulletin of the American Museum of Natural History* 19: 569–583.

Buckley M, Fariña RA, Lawless C, Tambusso PS, Varela L, Carlini AA, Powell JE, Martinez JG. 2015. Collagen sequence analysis of the extinct giant ground sloths *Lestodon* and *Megatherium*. *PloS One* 10: e0139611.

Bugge J. 1979. Cephalic arterial pattern in New World edentates and Old World pangolins with special reference to their phylogenetic relationships and taxonomy. *Acta Anatomica* 105: 37–46.

Cabrera Á. 1936. Las especies del género "*Glossotherium*". *Notas del Museo de La Plata* 1: 193–206.

Cande SC, Kent DV. 1992. A new geomagnetic polarity time scale for the Late Cretaceous and Cenozoic. *Journal of Geophysical Research: Solid Earth* 97: 13917–13951.

Carlini AA, Brandoni D, Sánchez R, Sánchez-Villagra MR. 2018. A new Megatheriinae skull (Xenarthra, Tardigrada) from the Pliocene of northern Venezuela – implications for a giant sloth dispersal to Central and North America. *Palaeontologia Electronica* 21: 1–12.

Carlini AA, Scillato-Yané GJ. 1999. Evolution of Quaternary Xenarthrans (Mammalia) of Argentina. In: Tonni EP, Cione AL, eds. *Quaternary Vertebrate Palaeontology in South America*. Quaternary of South America and Antarctic Peninsula 12: 149–175.

Carlini AA, Scillato-Yané GJ. 2004. The oldest Megalonychidae (Xenarthra: Tardigrada); phylogenetic relationships and an emended diagnosis of the family. *Neues Jahrbuch für Geologie und Paläontologie, Abhandlungen* 233: 423–443.

Carlini AA, Scillato-Yané GJ, Sánchez R. 2006. New Mylodontoidea (Xenarthra, Phyllophaga) from the Middle Miocene-Pliocene of Venezuela. *Journal of Systematic Palaeontology* 4: 255–267.

Cartelle C. 1991. Um novo Mylodontinae (Edentata, Xenarthra) do Pleistoceno final da região intertropical brasileira. *Anais da Academia Brasileira de Ciências* 63: 161–170.

Cartelle C, Bohórquez GA. 1982. *Eremotherium laurillardi* Lund, 1842. Parte I. Determinação específica e dimorfismo sexual. *Iheringia Séries Geológica* 7: 45–63.

Cartelle C, De Iuliis G. 1995. *Eremotherium laurillardi*: the Panamerican Late Pleistocene megatheriid sloth. *Journal of Vertebrate Paleontology* 15: 830–841.

Cartelle C, De Iuliis G. 2006. *Eremotherium laurillardi* (Lund) (Xenarthra, Megatheriidae), the Panamerican giant ground sloth: taxonomic aspects of the ontogeny of skull and dentition. *Journal of Systematic Palaeontology* 4: 199–209.

Cartelle C, De Iuliis G, Boscaini A, Pujos F. 2019. Anatomy, possible sexual dimorphism, and phylogenetic affinities of a new mylodontine sloth from the Late Pleistocene of intertropical Brazil. *Journal of Systematic Palaeontology*. doi:10.1080/14772019.2019.1574406.

Cartelle C, De Iuliis G, Lopes Ferreira R. 2009. Systematic revision of tropical brazilian scelidotheriine sloths (Xenarthra, Mylodontoidea). *Journal of Vertebrate Paleontology* 29: 555–566.

Cattoi NV. 1966. Edentata. In: Borrello AV, ed. *Paleontografia Bonaerense*. La Plata: Comisión de Investigaciones Científicas de La Provincia de Buenos Aires, 59–99.

Cerdeño E, Vera B, Schmidt GI, Pujos F, Mamani Quispe B. 2012. An almost complete skeleton of a new Mesotheriidae (Notoungulata) from the Late Miocene of Casira, Bolivia. *Journal of Systematic Palaeontology* 10: 341–360.

Chiarello AG. 2008. Sloth ecology. An overview of field studies. In: Vizcaíno SF, Loughry WJ, eds. *The Biology of the Xenarthra*. Gainesville: University Press of Florida, 269–280.

Christiansen P, Fariña RA. 2003. Mass estimation of two fossil ground sloths (Mammalia, Xenarthra, Mylodontidae). *Senckenbergiana Biologica* 83: 95–101.

Cione AL, Tonni EP. 1995. Bioestratigrafía y cronología del Cenozoico Superior de la región Pampeana. In: Alberdi MT, Leone G, Tonni EP, eds. *Evolución biológica y climática de la región pampeana durante los últimos cinco millones de años. Un ensayo de correlación con el Mediterráneo occidental*. Madrid: Monografías del Museo Nacional de Ciencias Naturales 12: 47–74.

Cione AL, Tonni EP. 1996. Reassesment of the Pliocene–Pleistocene continental time scale of Southern South America. Correlation of the type Chapadmalalan with Bolivian sections. *Journal of South American Earth Sciences* 9: 221–236.

Cione A, Tonni E, Bargo S, Bond M, Candela AM, Carlini AA, Deschamps CM, Dozo MT, Esteban GI, Goin FJ, Montalvo CI, Nasif N, Noriega JI, Ortiz Jaureguizar E, Pascual R, Prado JL, Reguero MA, Scillato-Yané GJ, Soibelzon L, Verzi DH, Vieytes EC, Vizcaíno SF, Vucetich MG. 2007. Mamíferos continentales del Mioceno tardío a la actualidad en la Argentina: cincuenta años de estudio. In: Archangelsky S, Sanchez T, Tonni EP, eds. *Ameghiniana*, *Edición Especial 50 Aniversario*. Buenos Aires: Asociación Paleontológica Argentina, Publicación Especial 11: 257–278.

Clack AA, MacPhee RD, Poinar HN. 2012. *Mylodon darwinii* DNA sequences from ancient fecal hair shafts. *Annals of Anatomy* 194: 26–30.

Clemente CD. 1985. *Gray's Anatomy*. Philadelphia: Lea and Febiger.

Clutton-Brock TH, Guinness FE, Albon SD. 1982. *Red deer: behavior and ecology of two sexes*. Chicago: University of Chicago Press.

Collins RL. 1934. Venezuelan Tertiary mammals. *Johns Hopkins University Studies in Geology* 11: 235–244.

Coltorti M, Abbazzi L, Ferretti MP, Iacumin P, Ríos FP, Pellegrini M, Pieruccini P, Rustioni M, Tito G, Rook L. 2007. Last glacial mammals in South America: a new scenario from the Tarija Basin (Bolivia). *Naturwissenschaften* 94: 288–299.

Constantinescu GM, Schaller O. 2012. *Illustrated Veterinary Anatomical Nomenclature*. Stuttgart: Enke.

Cope ED. 1889. The Edentata of North America. *The American Naturalist* 23: 657–664.

Coutier F, Hautier L, Cornette R, Amson E, Billet G. 2017. Orientation of the lateral semicircular canal in Xenarthra and its links with head posture and phylogeny. *Journal of Morphology* 278: 704–717.

Cozzuol MA. 2006. The Acre vertebrate fauna: age, diversity, and geography. *Journal of South American Earth Sciences* 21: 185–203.

Croft DA. 2007. The middle Miocene (Laventan) Quebrada Honda fauna, Southern Bolivia and a description of its notoungulates. *Palaeontology* 50: 277–303.

Cunningham JA, Rahman IA, Lautenschlager S, Rayfield EJ, Donoghue PC. 2014. A virtual world of paleontology. *Trends in ecology & evolution* 29: 347–357.

Cuvier G. 1796. Notice sur le squelette d'une très grande espèce de quadrupède inconnue jusqu'à présent, trouvée au Paraguay, et déposé au cabinet d'histoire naturelle de Madrid. *Magasin Encyclopédique: ou Journal des Sciences, des Lettres et des Arts* 1: 303–310.

Czerwonogora A, Fariña RA. 2013. How many Pleistocene species of *Lestodon* (Mammalia, Xenarthra, Tardigrada)? *Journal of Systematic Palaeontology* 11: 251–263.

Czerwonogora A, Fariña RA, Tonni EP. 2011. Diet and isotopes of late Pleistocene ground sloths: first results for *Lestodon* and *Glossotherium* (Xenarthra, Tardigrada). *Neues Jahrbuch für Geologie und Palaontologie - Abhandlungen* 262: 257–266.

Danilo L, Remy J, Vianey-Liaud M, Mérigeaud S, Lihoreau F. 2015. Intraspecific variation of endocranial structures in extant *Equus*: a prelude to endocranial studies in fossil equoids. Journal of Mammalian Evolution 22: 561–582

Darwin C. 1871. *The descent of man and selection in relation to sex*. London: John Murray.

Darwin C. 1874. *The descent of man and selection in relation to sex*. Second edition. London: John Murray.

David R, Droulez J, Allain R, Berthoz A, Janvier P, Bennequin D. 2010. Motion from the past. A new method to infer vestibular capacities of extinct species. *Comptes Rendus Palevol* 9: 397–410.

David R, Stoessel A, Berthoz A, Spoor F, Bennequin D. 2016. Assessing morphology and function of the semicircular duct system: introducing new *in-situ* visualization and software toolbox. *Scientific Reports* 6: 32772.

De Iuliis G. 2018. Recent progress and future prospects in fossil xenarthran studies, with emphasis on current methodology in sloth taxonomy. *Journal of Mammalian Evolution* 25: 449–458.

De Iuliis G, Cartelle, C. 1999. A new giant megatheriine ground sloth (Mammalia: Xenarthra: Megatheriidae) from the late Blancan to early Irvingtonian of Florida. *Zoological Journal of the Linnean Society* 127: 495–515.

De Iuliis G, Cartelle C, McDonald HG, Pujos F. 2017. The mylodontine ground sloth *Glossotherium tropicorum* from the late Pleistocene of Ecuador and Peru. *Papers in Palaeontology* 3: 613–636.

De Iuliis G, Gaudin TJ, Vicars M. 2011. A new genus and species of nothrotheriid sloth (Xenarthra, Tardigrada, Nothrotheriidae) from the late Miocene (Huayquerian) of Peru. *Palaeontology* 54: 171–205.

De Iuliis G, Pujos F, Toledo N, Bargo MS, Vizcaíno SF. 2014. *Eucholoeops* Ameghino, 1887 (Xenarthra, Tardigrada, Megalonychidae) from the Santa Cruz Formation, Argentine Patagonia: implications for the systematics of Santacrucian sloths. *Geodiversitas* 36: 209–255.

Dechaseaux C. 1958. Encéphales de xénarthres fossiles. In: Piveteau J, ed. *Traité de Paléontologie*. Paris: Masson and Cie, 637–640.

Dechaseaux C. 1962a. Encéfalos de Notongulados y de Desdentados Xenarthros Fósiles. *Ameghiniana* 2: 193–209.

Dechaseaux C. 1962b. Singularités de l'encéphale de *Lestodon*, mammifère édenté géant du Plésitocène d'Amérique du Sud. *Comptes Rendus de l'Académie des Sciences* 254: 1470–1471.

Dechaseaux C. 1971. *Oreomylodon wegneri*, édenté gravigrade du Pléistocène de l'Équateur - Crâne et moulage endocrânien. *Annales de Paleontologie* 57: 243–285.

Delsuc F, Catzeflis FM, Stanhope MJ, Douzery EJP. 2001. The evolution of armadillos, anteaters and sloths depicted by nuclear and mitochondrial phylogenies: implications for the status of the enigmatic fossil *Eurotamandua*. *Proceedings of the Royal Society* B 268: 1605–1615.

Delsuc F, Kuch M, Gibb GC, Hughes J, Szpak P, Southon J, Enk J, Duggan AT, Poinar HN. 2018. Resolving the phylogenetic position of Darwin's extinct ground sloth (*Mylodon darwinii*) using mitogenomic and nuclear exon data. *Proceedings of the Royal Society B* 285: 20180214.

Delsuc F, Kuch M, Gibb GC, Karpinski E, Hackenberger D, Szpak P, Martínez JG, Mead JI, McDonald HG, MacPhee RDE, Billet G, Hautier L, Poinar HN. 2019. Ancient mitogenomes reveal the evolutionary history and biogeography of sloths. *Current Biology* 29: 2031–2042.

Deschamps CM, Esteban GS, Bargo MS. 2001. El registro más antiguo del género *Lestodon* Gervais, 1855 (Xenarthra, Tardigrada, Mylodontidae) (Monhermosense, Plioceno Temprano). *Ameghiniana* 38: 151–157.

Deschamps CM, Vucetich MG, Montalvo CI, Zárate MA. 2013. Capybaras (Rodentia, Hydrochoeridae, Hydrochoerinae) and their bearing in the calibration of the late Miocene-Pliocene sequences of South America. *Journal of South American Earth Sciences* 48: 145–158.

Dozo MT. 1987. The endocranial cast of an early Miocene edentate, *Hapalops indifferens* Ameghino (Mammalia, Edentata, Tardigrada, Megatheriidae). Comparative study with brains of recent sloths. *Journal für Hirnforschung* 28: 397–406.

Dozo MT. 1994. Interpretación del molde endocraneano de *Eucholoeops fronto*, un Megalonychidae (Mammalia, Xenarthra, Tardigrada) del Mioceno temprano de Patagonia (Argentina). *Ameghiniana* 31: 317–329.

Dozo MT, Martínez G. 2016. First digital cranial endocasts of late Oligocene Notohippidae (Notoungulata): implications for endemic South American ungulates brain evolution. *Journal of Mammalian Evolution* 23:1–16.

Dunn RE, Madden RH, Kohn MJ, Schmitz MD, Strömberg CAE, Carlini AA, Ré GH, Crowley J. 2013. A new chronology for middle Eocene-Early Miocene South American Land Mammal Ages. *Bulletin of the Geological Society of America* 125: 539–555.

Edinger T. 1950. Frontal sinus evolution (particularly in the Equidae). *Bulletin of the Museum of Comparative Zoology at Harvard College* 103: 411–496.

Ekdale EG. 2013. Comparative anatomy of the bony labyrinth (inner ear) of placental mammals. *PLoS One* 8: e66624.

Ekdale EG. 2016. Form and function of the mammalian inner ear. *Journal of Anatomy* 228: 324–337.

Ekdale EG, Racicot RA. 2015. Anatomical evidence for low frequency sensitivity in an archaeocete whale: comparison of the inner ear of *Zygorhiza kochii* with that of crown Mysticeti. *Journal of Anatomy* 226: 22–39.

Ekdale EG, Rowe T. 2011. Morphology and variation within the bony labyrinth of zhelestids (Mammalia, Eutheria) and other therian mammals. *Journal of Vertebrate Paleontology* 31: 658–675.

Elliot-Smith GE. 1898. The brain in the Edentata. *Transactions of the Linnean Society of London* 7: 277–394.

Engelmann GF. 1985. The phylogeny of the Xenarthra. In: Montgomery GG, ed. *The Evolution and Ecology of Armadillos, Sloths and Vermilinguas*. Washington: Smithsonian Institution Press, 51–64.

Engelmann GF. 1987. A new Deseadan Sloth (Mammalia: Xenarthra) from Salla, Bolivia, and its implications for the primitive condition of the dentition in Edentates. *Journal of Vertebrate Paleontology* 7: 217–223.

Esteban GI. 1996. *Revisión de los Mylodontinae cuaternarios (Edentata-Tardigrada) de Argentina, Bolivia y Uruguay. Sistemática, filogenia, paleobiología, paleozoogeografía y paleoecología*. Unpublished D.Phil. Thesis, Universidad Nacional de Tucumán.

Esteban GI. 1999. Nuevo registro de *Sphenotherus* (Xenarthra, Mylodontidae) en el Terciario superior del valle de El Cajón (provincia de Catamarca, Argentina). Revisión sistemática del género. *Ameghiniana* 36: 317–321.

Esteban G, Abdala F. 1993. Nuevos restos de *Glossotheriopsis* (Edentata, Tardigrada) de Tiopunco (Provincia de Tucumán). Analisis filogenetico preliminar. X Jornadas Argentinas de Paleontologia de Vertebrados. *Ameghiniana* 30: 328–329.

Esteban G, Nasif N, Georgieff S. 2014. Cronobioestratigrafía del Mioceno tardío–Plioceno temprano, Puerta de Corral Quemado y Villavil, Provincia de Catamarca, Argentina. *Acta Geologica Lilloana* 26: 165–192.

Evans HE. 1993. *Miller's Anatomy of the Dog*. Third edition. Philadelphia: Saunders.

Evernden JF, Kriz SJ, Cherroni C. 1966. Correlaciones de las formaciones terciarias de la cuenca altiplánica a base de edades absolutas, determinadas por el método potasio-argón. *Servicio Geológico de Bolivia, Hoja Informativa* 1: 10–12.

Evernden JF, Kriz SJ, Cherroni C. 1977. Potassium-argon ages of some Bolivian rocks. *Economic Geology* 72: 1042–1061.

Fairbairn DJ, Blanckenhorn WU, Székely T. 2007. *Sex, size and gender roles: evolutionary studies of sexual size dimorphism*. New York: Oxford University Press.

Fariña RA, Vizcaíno SF, Bargo MS. 1998. Body mass estimations in Lujanian (Late Pleistocene–Early Holocene of South America) mammal megafauna. *Mastozoología Neotropical* 5: 87–108.

Fariña RA, Vizcaíno SF. 2003. Slow moving or browsers? A note on nomenclature. *Senckenbergiana Biologica* 83: 3–4.

Farke AA. 2007. Morphology, constraints, and scaling of frontal sinuses in the hartebeest, *Alcelaphus buselaphus* (Mammalia: Artiodactyla, Bovidae). *Journal of Morphology* 268: 243–253.

Farke AA. 2008. *Function and evolution of the cranial sinuses in bovid mammals and ceratopsian dinosaurs*. Unpublished D. Phil. Thesis, Stony Brook University.

Farke AA. 2010. Evolution and functional morphology of the frontal sinuses in Bovidae (Mammalia: Artiodactyla), and implications for the evolution of cranial pneumaticity. *Zoological Journal of the Linnean Society* 159: 988–1014.

Farris JS, Albert VA, Källersjö M, Lipscomb D, Kluge AG. 1996. Parsimony jackknifing outperforms neighbor-joining. *Cladistics* 12: 99–124.

Felsenstein J. 1985. Confidence limits on phylogenies: an approach using the bootstrap. *Evolution* 39: 783–791.

Fernicola JC, Toledo N, Bargo MS, Vizcaíno SF. 2012. A neomorphic ossification of the nasal cartilages and the structure of paranasal sinus system of the glyptodont *Neosclerocalyptus* Paula Couto 1957 (Mammalia, Xenarthra). *Palaeontolgia Electronica* 15: 1–22.

Fernicola, JC, Vizcaíno, SF, De Iuliis G. 2009. The fossil mammals collected by Charles Darwin in South America during his travels on board the HMS Beagle. *Revista de la Asociación Geológica Argentina* 64: 147–159.

Flower W. 1883. On the arrangement of the orders and families of existing Mammalia. *Proceeding of the Zoological Society of London* 1883: 178–186.

Flynn JJ, Swisher III CC. 1995. Cenozoic South American Land Mammal Ages: correlations to global geochronologies. *Geochronology, Time Scales and Global Stratigraphic Correlation, SEPM Special Publication* 54: 317–333.

Forasiepi AM, MacPhee RDE, Hernández del Pino S. 2019. Caudal cranium of *Thylacosmilus atrox* (Mammalia, Metatheria, Sparassodonta), a South American predaceous sabertooth. *Bulletin of the American Museum of Natural History* 433: 1–64.

Frailey CD. 1986. Late Miocene and Holocene mammals, exclusive of the Notongulata, of the Río Acre Region, Western Amazonia. *Contributions in Science* 374: 1–46.

Garzione CN, Hoke GD, Libarkin JC, Withers S, MacFadden B, Eiler J, Ghosh P, Mulch A. 2008. Rise of the Andes. *Science* 320: 1304–1307.

Gaudin TJ. 1995. The ear region of edentates and the phylogeny of the Tardigrada (Mammalia, Xenarthra). *Journal of Vertebrate Paleontology* 15: 672–705.

Gaudin TJ. 2004. Phylogenetic relationships among sloths (Mammalia, Xenarthra, Tardigrada): the craniodental evidence. *Zoological Journal of the Linnean Society* 140: 255–305.

Gaudin TJ. 2011. On the osteology of the auditory region and orbital wall in the extinct West Indian sloth genus *Neocnus* Arredondo, 1961 (Placentalia, Xenarthra, Megalonychidae). *Annals of Carnegie Museum* 80: 5–28.

Gaudin TJ, Biewener AA. 1992. The functional morphology of xenarthrous vertebrae in the armadillo *Dasypus novemcinctus* (Mammalia, Xenarthra). *Journal of Morphology* 214: 63–81.

Gaudin TJ, Branham DG. 1998. The phylogeny of the Myrmecophagidae (Mammalia, Xenarthra, Vermilingua) and relationship of *Eurotamandua* to the Vermilingua. *Journal of Mammalian Evolution* 5: 237–265.

Gaudin TJ, Croft DA. 2015. Paleogene Xenarthra and the evolution of South American mammals. *Journal of Mammalogy* 96: 622–634.

Gaudin TJ, De Iuliis G, Toledo N, Pujos F. 2015. The basicranium and orbital region of the Early Miocene *Eucholoeops ingens* Ameghino, (Xenarthra, Pilosa, Megalonychidae). *Ameghiniana* 52: 226–240.

Gaudin TJ, Hicks P, Di Blanco Y. 2018. *Myrmecophaga tridactyla* (Pilosa: Myrmecophagidae). *Mammalian Species* 50: 1–13.

Gaudin TJ, Wible JR. 2006. The phylogeny of living and extinct armadillos (Mammalia, Xenarthra, Cingulata): a craniodental analysis. In: Carrano MT, Gaudin TJ, Blob RW, Wible JR, eds. *Amniote paleobiology: perspectives on the evolution of mammals, birds and reptiles*. Chicago: University of Chicago Press, 153–198.

Gelfo JN, Goin FJ, Woodburne MO, Muizon C de. 2009a. Biochronological relationships of the earliest South American Paleogene mammalian faunas. *Palaeontology* 52: 251–269.

Gelfo JN, Reguero MA, López GM, Carlini AA, Ciancio MR, Chornogubsky L, Bond M, Goin FJ, Tejedor M. 2009b. Eocene mammals and continental strata from Patagonia and Antarctic Peninsula. *Museum of Northern Arizona Bulletin* 64: 567–592.

Gervais H, Ameghino, F. 1880. *Les Mammifères fossiles de l'Amérique du* Sud. Paris: F. Savy and Buenos Aires: Hermanos Igon.

Gervais P. 1855. *Recherches sur les mammifères fossiles de l'Amérique méridionale*. Paris: P. Bertrand.

Gervais P. 1869. Mémoire sur les formes cérébrales propres aux édentés vivants et fossiles. *Nouvelles Archives du Musée d'Histoire Naturelle de Paris* 5: 1–56.

Gervais P. 1873. Mémoire sur plusieurs espèces de Mammifères fossiles propres à l'Amérique méridionale. *Mémoires de la Société Géologique de France* 9: 1–44.

Gill T. 1872. Arrangement of the families of mammals, with analytical tables. *Smithsonian Miscellaneous Collections* 11: 1–98.

Gingerich PD. 1981. Variation, sexual dimorphism, and social structure in the early Eocene horse *Hyracotherium* (Mammalia, Perissodactyla). *Paleobiology* 7: 443–455.

Goffart M. 1971. *Function and form in the sloth*. Oxford: Pergamon Press.

Goloboff P, Farris J, Nixon K. 2008. TNT, a free program for phylogeny analysis. *Cladistics* 24: 774–786. Available online at http://www.lillo.org.ar/phylogeny/tnt/

Gosselin-Ildari AD. 2006. *Functional morphology of the bony labyrinth in primates*. Unpublished D. Phil. Thesis, The University of Texas at Austin.

Greenwood AD, Castresana J, Feldmaier-Fuchs G, Pääbo S. 2001. A molecular phylogeny of two extinct sloths. *Molecular Phylogenetics and Evolution* 18: 94–103.

Guth C. 1961. *La région temporale des Edentés*. Unpublished D. Phil. Thesis, Université de Paris.

Hammer Ø, Harper DAT, Ryan PD. 2001. PAST: Paleontological Statistics Software Package for education and data analysis. *Palaeontologia Electronica* 4: 1–9.

Haro JA, Tauber AA, Krapovickas JM. 2016. The manus of *Mylodon darwinii* Owen (Tardigrada, Mylodontidae) and its phylogenetic implications. *Journal of Vertebrate Paleontology* 36: e1188824.

Haro JA, Tauber AA, Krapovickas JM. 2017. Thoracic member (pectoral girdle and forelimb) bones of *Mylodon darwinii* Owen (Xenarthra, Mylodontidae) from the Late Pleistocene of Central Argentina and their phylogenetic implications. *Paläontologische Zeitschrift* 91: 439–457.

Hautier L, Billet G, Eastwood B, Lane J. 2014. Patterns of morphological variation of extant sloth skulls and their implication for future conservation efforts. *The Anatomical Record* 297: 979–1008.

Hay OP. 1919. Descriptions of some mammalian and fish remains from Florida of probably Pleistocene age. *Proceedings of the United States National Museum* 56: 103–112.

Hayssen V. 2008. *Bradypus pygmaeus* (Pilosa: Bradypodidae). *Mammalian Species* 812: 1–4

Hayssen V. 2010. *Bradypus variegatus* (Pilosa: Bradypodidae). *Mammalian Species* 42: 19–32

Hayssen V. 2011. *Choloepus hoffmanni* (Pilosa: Megalonychidae). *Mammalian Species* 43: 37–55.

Hirschfeld SE. 1985. Ground sloths form the Friasian La Venta Fauna, with additions to the Pre–Friasian Coyaima Fauna of Colombia, South America. *University of California Publications in Geological Sciences* 128: 1–91.

Hoffstetter R. 1948. Nota preliminar sobre los Edentata Xenarthra del Pleistoceno Ecuatoriano. II: Mylodontidae. *Boletín de Informaciones Científicas Nacionales de Quito* 2: 19–42.

Hoffstetter R. 1949. Nuevas observaciones sobre los Edentata del Pleistoceno superior de la Sierra ecuatoriana. *Boletín de Informaciones Científicas Nacionales de Quito* 3: 67–99.

Hoffstetter R. 1952. Les mammifères pléistocènes de la République de l'Équateur. *Mémoires de la Société Géologique de France* 66: 1–391.

Hoffstetter R. 1956. Contribution à l'étude des Orophodontoidea, Gravigrades cuirassés de la Patagonie. *Annales de Paléontologie* 42: 27–64.

Hoffstetter R. 1961. Description d'un squelette de *Planops* (Gravigrade du Miocène de Patagonie). *Mammalia* 25: 57–96.

Hoffstetter R. 1963. Note préliminaire sur la faune pléistocène de Tarija (Bolivie). *Bulletin du Muséum National d'Histoire Naturelle* 35: 194–203.

Hoffstetter R. 1968. Un gisement de mammifères déséadiens (Oligocène inférieur) en Bolivie. *Comptes Rendus de l'Académie des Sciences* 267: 1095–1097.

Hoffstetter R. 1977. Un gisement de mammifères miocènes à Quebrada Honda (sud bolivien). *Comptes Rendus de l'Académie des Sciences* 285: 1517–1520.

Hoffstetter R. 1986. High Andean mammalian faunas during the Plio–Pleistocene. In: Vuilleumier F, Monasterio M, eds. *High altitude tropical biogeography*. New York: Oxford University Press, 219–245.

Hoffstetter R, Martínez C, Mattauer M, Tomasi P. 1971a. Lacayani, un nouveau gisement bolivien de mammifères déséadiens (Oligocène inférieur). *Comptes Rendus de l'Académie des Sciences* 273: 2215–2218.

Hoffstetter R, Martínez C, Muñoz-Reyes J, Tomasi P. 1971b. Le gisement d'Ayo Ayo (Bolivie), une succession stratigraphique Pliocène–Pléistocène datée par des mammifères. *Comptes Rendus de l'Académie des Sciences* 273: 2472–2475.

Hoffstetter R, Martínez C, Tomasi P. 1972. Nouveaux gisements de mammifères néogènes dans les couches rouges de l'Altiplano bolivien. *Comptes Rendus de l'Académie des Sciences* 275: 739–742.

Hyrtl J. 1854. Beiträge zur vergleichenden Angiologie. V. Das arterielle Gefäss-System der Edentaten. *Akademie der Wissenschaften Wien. Denkschriften der Mathematisch-Naturwissenschaftlichen Klasse* 6: 21–64.

International Commission on Zoological Nomenclature (ICZN). 1999. *International Code of Zoological Nomenclature*. Fourth edition. London: The International Trust for Zoological Nomenclature.

Isaac JL. 2005. Potential causes and life-history consequences of sexual size dimorphism in mammals. *Mammal Review* 35: 101–115.

Janis CM. 1990. Correlation of cranial and dental variables with dietary preferences in mammals: a comparison of macropodoids and ungulates. *Memoirs of the Queensland Museum* 28: 349–366.

Janis CM, Ehrhardt D. 1988. Correlation of relative muzzle width and relative incisor width with dietary preference in ungulates. *Zoological Journal of the Linnean Society* 92: 267–284.

Jerison HJ. 1991. Fossil Brains and the evolution of the neocortex. In: Finlay BL, Innocenti G, Scheich H, eds. *The Neocortex, Ontogeny and Phylogeny*. Boston: Springer, 5–19.

Jolicoeur P. 1963. The multivariate generalization of the allometry equation. *Biometrics* 19: 497–499.

Jones MG, Spells KE. 1963. A theoretical and comparative study of the functional dependence of the semicircular canal upon its physical dimensions. *Proceedings of the Royal Society B* 157: 403–419.

Kielan-Jaworowska Z. 1986. Brain evolution in Mesozoic mammals. In: Flanagan KM, Lillegraven JA, eds. *Vertebrates, Phylogeny, and Philosophy*. Contributions to Geology (University of Wyoming) Special Paper 3: 21–34.

Klingenberg CP. 2016. Size, shape, and form: concepts of allometry in geometric morphometrics. *Development Genes and Evolution* 226: 113–137.

Kraglievich L. 1921a. Estudios sobre los Mylodontinae. Descripción comparativa del genero *Pleurolestodon* Rov. *Anales del Museo Nacional de Historia Natural de Buenos Aires* 31: 95–118.

Kraglievich L. 1921b. Estudios sobre los Mylodontinae. Descripción del cráneo y mandíbula del *Pseudolestodon myloides gallenii* n. sbsp. *Anales del Museo Nacional de Historia Natural de Buenos Aires* 31: 119–134.

Kraglievich L. 1925. Cuatro nuevos Gravigrados de la fauna araucana chapadmalense. *Anales del Museo Nacional de Historia Natural "Bernardino Rivadavia"* 33: 215–235.

Kraglievich L. 1926. Notas sobre Gravígrados de Sud América. I. Indicios de evolución progresiva en dos astrágalos y un calcáneo de *Megatherium*. *Anales del Museo Nacional de Historia Natural de Buenos Aires* 34: 21–29.

Kraglievich L. 1928. *Mylodon darwini* Owen es la especie genotipo de *Mylodon* Owen. Rectificación de la nomenclatura genérica de los Milodontes. *Revista de la Sociedad Argentina de Ciencias Naturales* 9: 169–185.

Kraglievich L. 1934. Contribución al conocimiento de *Mylodon darwini* Owen y especies afines. *Revista del Museo de la Plata* 34: 255–292.

Krishtalka L, Stucky RK, Beard KC. 1990. The earliest fossil evidence for sexual dimorphism in primates. *Proceedings of the National Academy of Sciences* 87: 5223–5226.

Kurtén B. 1955. Sex dimorphism and size trends in the cave bear, *Ursus spelaeus* Rosenmüller and Heinroth. *Acta Zoologica Fennica* 90: 1–48.

Lamb S, Hoke L. 1997. Origin of the high plateau in the central Andes, Bolivia, South America. *Tectonics* 16: 623–649.

Lammers AR, Dziech HA, German RZ. 2001. Ontogeny of sexual dimorphism in *Chinchilla lanigera* (Rodentia: Chinchillidae). *Journal of Mammalogy* 82: 179–189.

Langworthy OR. 1935. A physiological study of the cerebral motor cortex and the control of posture in the sloth. *Journal of Comparative Neurology* 62: 333–348.

Lara-Ruiz P, Chiarello AG. 2005. Life-history traits and sexual dimorphism of the Atlantic forest maned sloth *Bradypus torquatus* (Xenarthra: Bradypodidae). *Journal of Zoology* 267: 63–73.

Latham J, Davies H. 1795. Faunula indica. In: Forster JR, ed. *Faunula Indica id est catalogus animalium Indiae Orientalis*. Second edition. Halle: Gebauer, 1–38.

Lavenu A. 1984. Age pliocène de la formation Remedios, dans l'Altiplano bolivien: caractères de la tectonique pliocène. *Comptes Rendus de l'Académie des Sciences* 299: 1051–1054.

Lavenu A, Bonhomme MG, Vatin-Perignon N, De Pachtere P. 1989. Neogene magmatism in the Bolivian Andes between 16 S and 18 S: Stratigraphy and K/Ar geochronology. *Journal of South American earth sciences* 2: 35–47.

Lebrun R. 2008. *Evolution and development of the strepsirrhine primate skull*. Unpublished D. Phil. Thesis, Université Montpellier II and University of Zürich.

Lebrun R. 2014. ISE-MeshTools software. Available online at http://morphomuseum.com/meshtools

Lebrun R, de León MP, Tafforeau P, Zollikofer C. 2010. Deep evolutionary roots of strepsirrhine primate labyrinthine morphology. *Journal of Anatomy* 216: 368–380.

Linares OJ. 2004a. Nuevos restos del género *Lestodon* Garvais, 1855 (Xenarthra, Tardigrada, Mylodontidae), del Mioceno tardío y Plioceno temprano de Urumaco (Venezuela), con descripción de dos nuevas especies. *Paleobiología Neotropical* 2: 1–14.

Linares OJ. 2004b. Bioestratigrafía de la fauna de mamíferos de las formaciones Socorro, Urumaco y Codore (Mioceno medio-Plioceno temprano) de la región de Urumaco, Falcón, Venezuela. *Paleobiología Neotropical* 1: 1–26.

Linnaeus C. 1758. *Systema naturae per regna tria naturae, secundum classes, ordines, genera, species, cum characteribus, differentiis, synonymis, locis*. Volume 1. Tenth edition. Stockholm: Holmiae.

Lund PW. 1839. Blik paa Brasiliens Dyreverden för Sidste Jordomvaeltning. Anden Afhandling: Patteedyrene. *Danske Videnskabernes Selskabs Naturvidenskabelig og Mathematisk Afhandlinger* 8: 61–144.

Lund PW. 1842. Blik paa Brasiliens Dyreverden för Sidste Jordomvaeltning. Anden Afhandling: Patteedyrene. *Danske Videnskabernes Selskabs Naturvidenskabelig og Mathematisk Afhandlinger* 9: 137–208.

Lydekker R. 1894. The extinct edentates of Argentina. *Anales del Museo de La Plata* 3: 1–118.

MacFadden BJ, Anaya F, Argollo J. 1993. Magnetic polarity stratigraphy of Inchasi: a Pliocene mammal–bearing locality from the Bolivian Andes deposited just before the Great American Biotic Interchange. *Earth and Planetary Science Letters* 114: 229–241.

MacFadden BJ, Campbell KE Jr, Cifelli RL, Siles O, Johnson NM, Naeser CW, Zeitler PK. 1985. Magnetic polarity stratigraphy and mammalian fauna of the Deseadan (Late Oligocene-Early Miocene) Salla Beds of Northern Bolivia. *The Journal of Geology* 93: 223–250.

MacFadden BJ, Siles O, Zeitler P, Johnson NM, Campbell JKE. 1983. Magnetic polarity stratigraphy of the middle Pleistocene (Ensenadan) Tarija Formation of Southern Bolivia. *Quaternary Research* 19: 172–187.

MacFadden BJ, Wang Y, Cerling TE, Anaya F. 1994. South American fossil mammals and carbon istotopes: a 25 million-year sequence from the Bolivian Andes. *Paleogeography Paleoclimatology Paleoecology* 107: 257–268.

MacFadden BJ, Zeitler PK, Anaya F, Cottle JM. 2013. Middle Pleistocene age of the fossiliferous sedimentary sequence from Tarija, Bolivia. *Quaternary Research* 79: 268–273.

MacPhee RDE, Iturralde-Vinent MA. 1994. First Tertiary Land mammal from Greater Antilles: an early Miocene sloth (Xenarthra, Megalonychidae) from Cuba. *American Museum Novitates* 3094: 1–13.

MacPhee RDE, Iturralde-Vinent MA. 1995. Origin of the Greater Antillean land mammal fauna, 1: new Tertiary fossils from Cuba and Puerto Rico. *American Museum Novitates* 3141: 1–31.

Macrini TE, Flynn JJ, Ni X, Croft DA, Wyss AR. 2013. Comparative study of notoungulate (Placentalia, Mammalia) bony labyrinths and new phylogenetically informative inner ear characters. *Journal of Anatomy* 223: 442–461.

Macrini TE, Muizon C de, Cifelli RL, Rowe T. 2007a. Digital cranial endocast of *Pucadelphys andinus*, a Paleocene metatherian. *Journal of Vertebrate Paleontology* 27: 99–107.

Macrini TE, Rougier GW, Rowe T. 2007b. Description of a cranial endocast from the fossil mammal *Vincelestes neuquenianus* (Theriiformes) and its relevance to the evolution of endocranial characters in therians. *Anatomical Record* 290: 875–892.

Madden R, Guerrero J, Kay RF, Flynn JJ, Swisher III CC, Walton AH. 1997. The La Ventan stage and age. In: Kay RF, Madden RH, Cifelli RL, Flynn JJ, eds. *Vertebrate paleontology in the Neotropics. The Miocene fauna of La Venta, Colombia*. Washington and London: Smithsonian Institution Press, 499–519.

Maddison WP, Maddison DR. 2011. Mesquite: a modular system for evolutionary analysis. Version 3.04. Available online at http://mesquiteproject.org/

Main MB, Weckerly FW, Bleich VC. 1996. Sexual segregation in ungulates: new directions for research. *Journal of Mammalogy* 77: 449–461.

Malinzak MD, Kay RF, Hullar TE. 2012. Locomotor head movements and semicircular canal morphology in primates. *Proceedings of the National Academy of Sciences, U.S.A.* 109: 17914–17919.

Manoussaki D, Chadwick RS, Ketten DR, Arruda J, Dimitriadis EK, O'Malley JT. 2008. The influence of cochlear shape on low-frequency hearing. *Proceedings of the National Academy of Sciences, U.S.A.* 105: 6162–6166.

Marshall LG, Hoffstetter R, Pascual R. 1983. Mammals and stratigraphy: geochronology of the continental mammal–bearing Tertiary of South America. *Palaeovertebrata (Mémoire Extraordinaire)*: 1–93.

Marshall LG, Butler RF, Drake RE, Curtis GH, Tedford RH. 1979. Calibration of the Great American Interchange. *Science* 204: 272– 279.

Marshall LG, Patterson B. 1981. Geology and geochronology of the mammal-bearing Tertiary of the Valle de Santa María and Río Corral Quemado, Catamarca Province, Argentina. *Fieldiana Geology* 9: 1–80.

Marshall LG, Sempéré T. 1991. The Eocene to Pleistocene vertebrates of Bolivia and their stratigraphic context: a review. In: Suárez-Sorouco R, ed. *Fósiles y Facies de Bolivia*, *Vertebrados*. Volume 1. Santa Cruz: *Revista Técnica de YPFB* 12: 631–652.

Marshall LG, Swisher CC, Lavenu A, Hoffstetter R, Curtis GH. 1992. Geochronology of the mammal–bearing late Cenozoic on the northern Altiplano, Bolivia. *Journal of South American Earth Sciences* 5: 1–19.

Martínez G, Gutiérrez MA, Tonni EP. 2013. Paleoenvironments and faunal extinctions: analysis of the archaeological assemblages at the Paso Otero locality (Argentina) during the Late Pleistocene–Early Holocene. *Quaternary International* 299: 53–63.

McAfee RK. 2009. Reassessment of the cranial characters of *Glossotherium* and *Paramylodon* (Mammalia: Xenarthra: Mylodontidae). *Zoological Journal of the Linnean Society* 155: 885–903.

McAfee RK. 2016. Description of new postcranial elements of *Mylodon darwinii* Owen 1839 (Mammalia: Pilosa: Mylodontinae), and functional morphology of the forelimb. *Ameghiniana* 53: 418–443.

McDonald HG. 1987. *A systematic review of the Plio-Pleistocene scelidotheriine ground sloths (Mammalia: Xenarthra: Mylodontidae)*. Unpublished D.Phil. Thesis, University of Toronto.

McDonald HG. 1995. Gravigrade xenarthrans from the Early Pleistocene Leisey Shell Pit 1A, Hillsborough County, Florida. *Bulletin of the Florida Museum of Natural History* 37: 345–373.

McDonald HG. 1997. Xenarthrans: Pilosans. In: Kay RF, Madden RH, Cifelli RL, Flynn JJ, eds. *Vertebrate paleontology in the Neotropics. The Miocene fauna of La Venta, Colombia*. Washington and London: Smithsonian Institution Press, 233–245.

McDonald HG. 2003. Xenarthran skeletal anatomy: primitive or derived? (Mammalia, Xenarthra). *Senckenbergiana biologica* 83: 5–18.

McDonald HG. 2006. Sexual dimorphism in the skull of Harlan's ground sloth. *Contributions in Science* 510: 1–9.

McDonald HG. 2018. An overview of the presence of osteoderms in sloths: implications for osteoderms as a plesiomorphic character of the Xenarthra. *Journal of Mammalian Evolution* 25: 485–493.

McDonald HG, Agenbroad LD, Manganaro HC. 2004. Late Pleistocene mylodont sloth *Paramylodon harlani* (Mammalia: Xenarthra) from Arizona. *The Southwestern Naturalist* 49: 229–238.

McDonald HG, De Iuliis G. 2008. Fossil history of sloths. In: Vizcaíno SF, Loughry WJ, eds. *The Biology of the Xenarthra*. Gainesville: University Press of Florida, 39–55.

McDonald HG, Morgan GS. 2011. Ground sloths of New Mexico. *New Mexico Museum of Natural History and Science Bulletin* 53: 652–663.

McDonald HG, Muizon C de. 2002. The cranial anatomy of *Thalassocnus* (Xenarthra, Mammalia), a derived nothrothere from the Neogene of the Pisco Formation (Peru). *Journal of Vertebrate Paleontology* 22: 349–365.

McDonald HG, Pelikan S. 2006. Mammoths and mylodonts: exotic species from two different continents in North American Pleistocene faunas. *Quaternary International* 142–143: 229–241.

McDonald HG, Perea D. 2002. The large scelidothere *Catonyx tarijensis* (Xenarthra, Mylodontidae) from the Pleistocene of Uruguay. *Journal of Vertebrate Paleontology* 22: 677–683.

McDonald HG, Rincón AD, Gaudin TJ. 2013. A new genus of megalonychid sloth (Mammalia, Xenarthra) from the late Pleistocene (Lujanian) of Sierra De Perija, Zulia State, Venezuela. *Journal of Vertebrate Paleontology* 33: 1226–1238.

McKenna MC, Bell SK. 1997. *Classification of Mammals above the Species Level*. New York: Columbia University Press.

McKenna MC, Wyss AR, Flynn JJ. 2006. Paleogene pseudoglyptodont xenarthrans from Central Chile and Central Patagonia. *American Museum Novitates* 3536: 1–18.

McNab BK. 1985. Energetics, population biology, and distribution of xenarthrans, living and extinct. In: Montgomery GG, ed. *The evolution and ecology of armadillos, sloths and vermilinguas*. Washington: Smithsonian Institution Press, 219–232.

Miño-Boilini ÁR. 2012. *Sistemática y evolución de los Scelidotheriinae (Xenarthra, Mylodontidae) cuaternarios de la Argentina. Importancia bioestratigráfica, paleobiogeográfica y paleoambiental*. Unpublished D. Phil. Thesis, Universidad de La Plata.

Miño-Boilini ÁR, Zurita AE. 2015. Dimorphism in Quaternary Scelidotheriinae (Mammalia, Xenarthra, Phyllophaga). *Palaeontologia Electronica* 18: 1–16.

Mones A. 1986a. Palaeovertebrata sudamericana. Catálogo sistemático de los vertebrados fósiles de America del Sur - Parte I. Lista preliminar y bibliografía. *Courier Forschungsinstitut Senckenberg* 82: 1–625.

Mones A. 1986b. El status de *Pseudodiodomus annaratoneii* (Ameghino) (Rodentia: Dinomyidae?) y de *Diodomus copei* Ameghino (Xenarthra: Megalonychidae). *Comunicaciones Paleontológicas del Museo de Historia Natural de Montevideo* 17: 229–236.

Montellano-Ballesteros M, Carranza-Castañeda Ó. 1986. Descripción de un milodóntido del Blancano temprano de La Mesa Central de México. *Universidad Nacional Autónoma de Mexico, Instituto de Geología, Revista* 6: 193–203.

Montellano-Ballesteros M, Román-Carrión JL. 2011. Redescubrimiento de material tipo depositado en la colección del Museo de Historia Natural "Gustavo Orcés V." del Instituto de Ciencias Biológicas, Escuela Politécnica Nacional, Quito, Ecuador. *Boletín de la Sociedad Geológica Mexicana* 63: 379–392.

Montes C, Cardona A, Jaramillo C, Pardo A, Silva JC, Valencia V, Ayala C, Pérez-Angel LC, Rodriguez-Parra LA, Ramirez V, Niño H. 2015. Middle Miocene closure of the Central American seaway. *Science* 348: 226–229.

Moore DM. 1978. Post-glacial vegetation in the South Patagonian territory of the giant ground sloth, *Mylodon*. *Botanical Journal of the Linnean Society* 77: 177–202.

Moore WJ. 1981. *The Mammalian skull*. Cambridge: Cambridge University Press.

Morgan GS. 2005. The Great American Biotic Interchange in Florida. *Bulletin of the Florida Museum of Natural History* 45: 271–311.

Morgan GS. 2008. Vertebrate fauna and geochronology of the Great American Biotic Interchange in North America. In: Lucas SG, Mogan GS, Spielmann JA, Prothero DR, eds. Neogene Mammals. *Bulletin of the New Mexico Museum of Natural History And Science* 44: 93–140.

Morgan GS, Hulbert RC Jr. 1995. Overview of the geology and vertebrate paleontology of the Leisey Shell Pit local fauna, Hillsborough County, Florida. *Bulletin of the Florida Museum of Natural History* 37: 1–92.

Muizon C de. 1991. La fauna de mamíferos de Tiupampa (Paleoceno inferior, Formación Santa Lucia), Bolivia. In: Suárez-Sorouco R, ed. *Fósiles y Facies de Bolivia, Vertebrados*. Volume 1. Santa Cruz: *Revista Técnica de YPFB* 12: 575–624.

Muizon C de. 1999. Marsupial skulls from the Deseadan (late Oligocene) of Bolivia and phylogenetic analysis of the Borhyaenoidea (Marsupialia, Mammalia). *Geobios* 32: 483–509.

Muizon C de, McDonald HG, Salas R, Urbina M. 2003. A new early species of the aquatic sloth *Thalassocnus* (Mammalia, Xenarthra) from the Late Miocene of Peru. *Journal of Vertebrate Paleontology* 23: 886–894.

Muizon C de, McDonald HG, Salas R, Urbina M. 2004. The youngest species of the aquatic sloth *Thalassocnus* and a reassessment of the relationships of the nothrothere sloths (Mammalia: Xenarthra). *Journal of Vertebrate Paleontology* 24: 287–397.

Muller M. 1999. Size limitations in semicircular duct systems. *Journal of Theoretical Biology* 198: 405–437.

Naples VL. 1982. Cranial osteology and function in the tree sloths, *Bradypus* and *Choloepus*. *American Museum Novitates* 2739: 1–41.

Negri FR, Ferigolo J. 2004. Urumacotheriinae, nova subfamília de Mylodontidae (Mammalia, Tardigrada) do Mioceno Superior-Plioceno, América do Sul. *Revista Brasileira de Paleontología* 7: 281–288.

Negri FR, Bocquentin-Villanueva J, Ferigolo J, Antoine P-O. 2010. A review of Tertiary mammal faunas and birds from western Amazonia. In: Hoorn C, Wesselingh FP, eds. *Amazonia, landscape and species evolution: a look into the past*. Hoboken: Wiley-Blackwell, 245–258.

Novacek MJ. 1993. Patterns of diversity in the mammalian skull. In: Hanken J, Hall BK, eds. *The Skull, Patterns of Structural and Systematic Diversity*. Volume 2. Chicago: University of Chicago Press, 438–545.

Nowak RM. 1999. *Walker's Mammals of the World*. Baltimore and London: The John Hopkins University Press.

Nyakatura JA. 2012. The convergent evolution of suspensory posture and locomotion in tree sloths. *Journal of Mammalian Evolution* 19: 225–234.

Oliva C, Brandoni D. 2012. Primer registro de Mylodontinae (Tardigrada, Mylodontidae) en el Huayqueriense (Mioceno tardío) de la provincia de Buenos Aires, Argentina. *Revista del Museo Argentino de Ciencias Naturales* 14: 325–332.

Orliac MJ, Benoit J, O'Leary MA. 2012. The inner ear of *Diacodexis*, the oldest artiodactyl mammal. *Journal of Anatomy* 221: 417–426.

Orliac MJ, O'Leary MA. 2016. The inner ear of *Protungulatum* (pan-Euungulata, Mammalia). *Journal of Mammalian Evolution* 23: 337–352.

Owen R. 1839. Fossil Mammalia. In: Darwin C, ed. *The zoology of the voyage of H.M.S. Beagle, under the command of Captain Fitzroy, during the years 1832 to 1836*. London: Smith, Elder & Co., 41–80.

Owen R. 1842. *Description of the skeleton of an extinct gigantic sloth*, Mylodon robustus, *Owen, with observations on the osteology, natural affinities, and probable habits of the megatheroid quadrupeds in general*. London: R. & J.E. Taylor.

Pascual R. 2006. Evolution and geography: the biogeographic history of South American land mammals. *Annals of the Missouri Botanical Gardens* 93: 209–230.

Patterson B, Segall W, Turnbull WD. 1989. The ear region in xenarthrans (= Edentata: Mammalia). Part I. Cingulates. *Fieldiana Geology* 18: 1–46

Patterson B, Turnbull WD, Segall W, Gaudin TJ. 1992. The ear region in xenarthrans (= Edentata: Mammalia). Part II. Pilosa (sloths, anteaters), palaeanodonts, and a miscellany. *Fieldiana Geology* 24: 1–78

Paula Couto C de. 1967. Pleistocene Edentates of the West Indies. *American Museum Novitates* 2304: 1–55.

Pérez-Barbería FJ, Gordon I. 1998. The influence of sexual dimorphism in body size and mouth morphology on diet selection and sexual segregation in cervids. *Acta Veterinaria Hungarica* 46: 357–367.

Pérez-Barbería FJ, Gordon I. 1999. Body size dimorphism and sexual segregation in polygynous ungulates: an experimental test with Soay sheep. *Oecologia* 120: 258–267.

Perier A, Lebrun R, Marivaux L. 2016. Different level of intraspecific variation of the bony labyrinth morphology in slow- versus fast-moving primates. *Journal of Mammalian Evolution* 23: 353–368.

Perkins ME, Fleagle JG, Heizler MT, Nash B, Bown TM, Tauber AA, Dozo MT. 2012. Tephrochronology of the Miocene Santa Cruz and Pinturas formations, Argentina. In: Vizcaíno SF, Kay RF, Bargo MS, eds. *Early Miocene Paleobiology in Patagonia*. Cambridge: Cambridge University Press, 23–40.

Pitana VG, Esteban GI, Ribeiro AM, Cartelle C. 2013. Cranial and dental studies of *Glossotherium robustum* (Owen, 1842) (Xenarthra: Pilosa: Mylodontidae) from the Pleistocene of southern Brazil. *Alcheringa* 37: 147–162.

Presslee S, Slater GJ, Pujos F, Forasiepi AM, Fischer R, Molloy K, Mackie M, Olsen JV, Kramarz A, Taglioretti M, Scaglia F, Lezcano M, Lanata JL, Southon J, Feranec R, Bloch J, Hajduk A, Martin FM, Salas Gismondi R, Reguero M, Muizon C de, Greenwood A, Chait BT, Penkman K, Collins M, MacPhee RDE. 2019. Palaeoproteomics resolves sloth relationships. *Nature Ecology & Evolution* 3: 1121–1130.

Prothero DR, Raymond KR. 2008. Variation and sexual size dimorphism in Pleistocene ground sloths (Xenarthra). *Bulletin of New Mexico Museum of Natural History & Science* 44: 331–333.

Prothero JW, Sundsten JW. 1984. Folding of the cerebral cortex in mammals. *Brain, Behavior and Evolution* 24: 152–167.

Pujos F. 2002. *Contribution à la connaissance des Tardigrades (Mammalia: Xenarthra) du Pléistocène péruvien: systématique, phylogénie, anatomie fonctionnelle et extinction*. Unpublished D. Phil. Thesis, Muséum national d'Histoire naturelle de Paris.

Pujos F, De Iuliis G. 2007. Late Oligocene Megatherioidea Fauna (Mammalia: Xenarthra) from Salla–Luribay (Bolivia): new data on basal sloth radiation and Cingulata–Phyllophaga split. *Journal of Vertebrate Paleontology* 27: 132–144.

Pujos F, De Iuliis G, Argot C, Werdelin L. 2007. A peculiar climbing Megalonychidae from the Pleistocene of Peru and its implication for sloth history. *Zoological Journal of the Linnean Society* 149: 179–235.

Pujos F, De Iuliis G, Cartelle C. 2017. A paleogeographic overview of tropical fossil sloths: towards an understanding of the origin of extant suspensory sloths? *Journal of Mammalian Evolution* 24: 1–20.

Pujos F, De Iuliis G, Mamani Quispe B. 2011. *Hiskatherium saintandrei*, gen. et sp. nov.: an unusual sloth from he Santacrucian of Quebrada Honda (Bolivia) and an overview of middle Miocene, small megatherioids. *Journal of Vertebrate Paleontology* 31: 1131–1149.

Pujos F, De Iuliis G, Mamani Quispe B, Adnet S, Andrade Flores R, Billet G, Fernández-Monescillo M, Marivaux L, Munch P, Prámparo MB, Antoine P-O. 2016. A new nothrotheriid xenarthran from the early Pliocene of Pomata–Ayte (Bolivia): new insights into the caniniform–molariform transition in sloths. *Zoological Journal of the Linnean Society* 178: 679–712.

Pujos F, Gaudin TJ, De Iuliis G, Cartelle C. 2012. Recent advances on variability, morpho-functional adaptations, dental terminology, and evolution of sloths. *Journal of Mammalian Evolution* 19: 159–169.

R Development Core Team. 2013. *R: A Language and Environment for Statistical Computing*. Vienna: R Foundation for Statistical Computing. Available online at http://www.r-project.org/

Ralls K. 1977. Sexual dimorphism in mammals: avian models and unanswered questions. *The American Naturalist* 111: 917–938.

Reguero MA, Candela AM. 2011. Late Cenozoic mammals from the northwest of Argentina. In: Salfity JA, Marquillas RA, eds. *Cenozoic geology of the Central Andes of Argentina*. Salta: SCS Publisher, 411–426.

Reguero MA, Candela AM, Alonso RN. 2007. Biochronology and biostratigraphy of the Uquía Formation (Pliocene–Early Pleistocene, NW Argentina) and its significance in the Great American Biotic Interchange. *Journal of South American Earth Sciences* 23: 1–16.

Reguero MA, Gelfo JN, López GM, Bond M, Abello A, Santillana SN, Marenssi SA. 2014. Final Gondwana breakup: the Paleogene South American native ungulates and the demise of the South America–Antarctica land connection. *Global and Planetary Change* 123: 400–413.

Reinhard KR, Miller ME, Evans HE. 1962. The craniovertebral veins and sinuses of the dog. *American Journal of Anatomy* 111: 67–87.

Renne PR, Mundil R, Balco G, Min K, Ludwig KR. 2010. Joint determination of ^{40}K decay constants and $^{40}Ar^{*}/^{40}K$ for the Fish Canyon sanidine standard, and improved accuracy for $^{40}Ar/^{39}Ar$ geochronology. *Geochimica et Cosmochimica Acta* 74: 5349–5367.

Richard-Hansen C, Vié J-C, Vidal N, Kéravec J. 1999. Body measurements on 40 species of mammals from French Guiana. *Journal of Zoology* 247: 419–428.

Rincón AD, Solórzano A, Benammi M, Vignaud P, McDonald HG. 2014. Chronology and geology of an Early Miocene mammalian assemblage in North of South America, from Cerro La Cruz (Castillo Formation), Lara State, Venezuela: implications in the 'changing course of Orinoco River' hypothesis. *Andean Geology* 41: 507–528.

Rincón AD, McDonald HG, Solórzano A, Núñez Flores M, Ruiz-Ramoni D. 2015. A new enigmatic Late Miocene mylodontoid sloth from northern South America. *Royal Society Open Science* 2: 140256.

Rincón AD, Solórzano A, McDonald HG, Flores MN. 2016. *Baraguatherium takumara*, gen. et sp. nov., the earliest mylodontoid sloth (Early Miocene) from northern South America. *Journal of Mammalian Evolution* 24: 179–191.

Rinderknecht A, Bostelmann E, Perea D, Lecuona G. 2010. A new genus and species of Mylodontidae (Mammalia: Xenarthra) from the late Miocene of southern Uruguay, with comments on the systematics of the Mylodontinae. *Journal of Vertebrate Paleontology* 30: 899–910.

Rinderknecht A, Perea D, McDonald HG. 2007. A new Mylodontinae (Mammalia, Xenarthra) from the Camacho Formation (Late Miocene), Uruguay. *Journal of Vertebrate Paleontology* 27: 744–747.

Robertson JS. 1976. Latest Pliocene mammals from Haile XV A, Alachua County, Florida. *Bulletin of the Florida Museum of Natural History* 20: 111–186.

Rose KD, Emry RJ. 1993. Relationships of Xenarthra, Pholidota, and fossil "edentates": the morphological evidence. In: Szalay FS, Novacek MJ, McKenna MC, eds. *Mammal Phylogeny: Placentals*. New York: Springer-Verlag, 81–102.

Roth G, Dicke U. 2005. Evolution of the brain and intelligence. *Trends in cognitive sciences* 9: 250–257.

Rougier GW, Wible JR, Hopson JA. 1992. Reconstruction of the cranial vessels in the Early Cretaceous mammal *Vincelestes neuquenianus*: implications for the evolution of the mammalian cranial vascular system. *Journal of Vertebrate Paleontology* 12: 188–216.

Rovereto C. 1914. Los estratos araucanos y sus fósiles. *Anales del Museo Nacional de Buenos Aires* 25: 1–249.

Ruckstuhl K, Neuhaus P. 2005. *Sexual segregation in vertebrates: the ecology of the two sexes*. New York: Cambridge University Press.

Ruf I, Volpato V, Rose KD, Billet G, de Muizon C. 2016. Digital reconstruction of the inner ear of *Leptictidium auderiense* (Leptictida, Mammalia) and North American leptictids reveals new insight into leptictidan locomotor agility. *Paläontologische Zeitschrift* 90: 153–171.

Saint-André P-A. 1993. *Hoffstetterius imperator* n. g., n. sp. du Miocéne supérieur de l'Altiplano bolivien et le statut des Dinotoxodontinés (Mammalia, Notoungulata). *Comptes Rendus de l'Académie des Sciences* 316: 539–545.

Saint-André P-A. 1994. *Contribution à l'étude des grands mammifères du Néogène de l'altiplano bolivien*. Unpublished D. Phil. Thesis, Museum national d'Histoire naturelle de Paris.

Saint-André P-A. 1996. Deux nouveaux Édentés (Mammalia, Xenarthra) *Trachycalyptoides achirense* nov. gen. et nov. sp. (Glyptodontidae, Sclerocalyptinae) et *Xyophorus villarroeli* nov. sp. (Megatheriidae, Nothrotheriinae) du Huayquérien (Miocéne supérieur) de l'Altiplano bolivien. *Bulletin du Muséum National d'Histoire Naturelle* 18: 79–106.

Saint-André P-A, De Iuliis G. 2001. The smallest and most ancient representative of the genus *Megatherium* Cuvier, 1796 (Xenarthra, Tardigrada, Megatheriidae), from the Pliocene of the Bolivian Altiplano. *Geodiversitas* 23: 625–645.

Saint-André P-A, Pujos F, Cartelle C, De Iuliis G, Gaudin TJ, McDonald HG, Mamani Quispe B. 2010. Nouveaux paresseux terrestres (Mammalia, Xenarthra, Mylodontidae) du Néogène de l'Altiplano bolivien. *Geodiversitas* 32: 255–306.

Sakai ST, Arsznov BM, Lundrigan BL, Holekamp KE. 2011. Brain size and social complexity: a computed tomography study in hyaenidae. *Brain, Behavior and Evolution* 77: 91–104.

Sanders AE, Weems RE, Albright LB. 2009. Formalization of the mid-Pleistocene "Ten Mile Hill beds" in South Carolina with evidence for placement of the Irvingtonian–Rancholabrean boundary. *Museum of Northern Arizona Bulletin* 64: 369–375.

Santos JCR, De Iuliis G. 1993. Nova interpretacao sistemática de *Urumacotherium garciai* Bocquentin-Villanueva, 1984, um Edentata-Tardigrada do Huayqueriense da Venezuela. X Jornadas Argentinas de Paleontologia de Vertebrados. *Ameghiniana* 30: 340.

Santos JCR, De Iuliis G, Silva EG 1993a. Novo achados de *Urumacotherium* Bocqentin-Villanueva, 1984 (Edentata - Tardigrada) no Huayqueriense–Montohermosense do estado do Acre, Brasil. X Jornadas Argentinas de Paleontologia de Vertebrados. *Ameghiniana* 30: 340.

Santos JCR, Rancy A, Ferigolo J. 1993b. Octodontobrayinae, uma nova subfamília de Orophodontidae (Edentata, Tardigrada) do Mioceno Superior–Plioceno do Estado do Amazonas, Brasil. *Ameghiniana* 30: 255–264.

Sargis EJ. 2002. Functional morphology of the forelimb of tupaiids (Mammalia, Scandentia) and its phylogenetic implications. *Journal of Morphology* 253: 10–42.

Schinz HR. 1825. Das Thierreich eingetheilt nach dem Bau der Thiere als Grundlage ihrer Naturgeschichte und der vergleichen den Anatomie, Volume 4. Stuttgart and Tubingen: JG Cotta.

Schmelzle T, Sánchez-Villagra MR, Maier W 2007. Vestibular labyrinth diversity in diprotodontian marsupial mammals. *Mammalian Study* 32: 83–97.

Scillato-Yané GJ. 1976. El más antiguo Mylodontinae (Edentata, tardigrada) conocido: *Glossotheriopsis pascuali* n. gen., n. sp., del "Colloncurense" (Mioceno Superior) de la provincia de Río Negro (Argentina). *Ameghiniana* 13: 333–334.

Scillato-Yané GJ. 1977. Octomylodontinae: nueva subfamilia de Mylodontidae (Edentata, Tardigrada). Descripción del cráneo y mandíbula de *Octomylodon robertoscagliai* n. sp., procedentes de la formación Arroyo Chasico (edad Chasiquense, Plioceno temprano) del sur de la provincia de Buenos Aires (Argentina). Algunas consideraciones filogenéticas y sistemáticas sobre los Mylodontoidea. *Publicaciones del Museo Municipal de Ciencias Naturales de Mar del Plata «Lorenzo Scaglia»* 2: 123–140.

Scillato-Yané GJ. 1981. Nuevo Mylodontinae (Edentata, Tardigrada) del "Mesopotamiense" (Mioceno Tardío-Plioceno) de la Provincia de Entre Rios. *Ameghiniana* 18: 29–34.

Scott WB. 1903-1904. Mammalia of the Santa Cruz beds: Part 1. Edentata. In: Scott WB, ed. *Reports of the Princeton University Expeditions to Patagonia 1896–1899*. Princeton: Princeton University Press, 1–364.

Shine R. 1989. Ecological causes for the evolution of sexual dimorphism: a review of the evidence. *The Quarterly Review of Biology* 64: 419–461.

Shockey BJ, Anaya F. 2008. Postcranial osteology of mammals from Salla, Bolivia (late Oligocene): form, function, and phylogenetic implications. In: Sargis EJ, Dagosto M, eds. *Mammalian Evolutionary Morphology: A Tribute to Frederick S. Szalay*. Dordrecht: Springer, 135–157.

Shockey BJ, Anaya F. 2011. Grazing in a new late Oligocene mylodontid sloth and a mylodontid radiation as a component of the Eocene–Oligocene faunal turnover and the early spread of grasslands/savannas in South America. *Journal of Mammalian Evolution* 18: 101–115.

Shockey BJ, Croft DA, Anaya F. 2007. Analysis of function in the absence of extant functional homologues: a case study using mesotheriid notoungulates (Mammalia). *Paleobiology* 33: 227–247.

Silcox MT, Bloch JI, Boyer DM, Godinot M, Ryan TM, Spoor F, Walker A. 2009. Semicircular canal system in early primates. *Journal of Human Evolution* 56: 315–327.

Simpson GG. 1980. *Splendid Isolation. The Curious History of South American Mammals*. New Heaven: Yale University Press.

Simpson GG, Paula Couto C de. 1981. Fossil mammals from the Cenozoic of Acre, Brazil. III - Pleistocene Edentata Pilosa, Proboscidea, Sirenia, Perissodactyla and Artiodactyla. *Iheringia Séries Geológica* 6: 11–73.

Sipla JS, Spoor F. 2008. The physics and physiology of balance. In: Thewissen JGM, Nummela S, eds. *Sensory Evolution on the threshold: adaptations in secondarily aquatic vertebrates*. Berkeley and Los Angeles: University of California Press, 227–232.

Slater GJ, Cui P, Forasiepi AM, Lenz D, Tsangaras K, Voirin B, de Moraes–Barros N, MacPhee RDE, Greenwood AD. 2016. Evolutionary relationships among extinct and extant sloths: the evidence of mitogenomes and retroviruses. *Genome Biology and Evolution* 8: 607–621.

Solounias N, Moelleken SM. 1993. Dietary adaptation of some extinct ruminants determined by premaxillary shape. *Journal of Mammalogy* 74: 1059–1971.

Solounias N, Teaford M, Walker A. 1988. Interpreting the diet of extinct ruminants: the case of a non-browsing giraffid. *Paleobiology* 14: 287–300.

Specht M. 2007. *Spherical surface parameterization and its application to geometric morphometric analysis of the braincase*. Unpublished D. Phil. Thesis, University of Zürich.

Specht M, Lebrun R, Zollikofer CPE. 2007. Visualizing shape transformation between chimpanzee and human braincases. *The Visual Computer* 23: 743–751.

Spillmann F. 1931. *Die Säugetiere Ecuadors im Wandel der Zeit*. Quito: Universidad Central.

Spoor F, Garland T, Krovitz G, Ryan TM, Silcox MT, Walker A. 2007. The primate semicircular canal system and locomotion. *Proceedings of the National Academy of Sciences, U.S.A.* 104: 10808–10812.

Steinmann G. 1929. *Geologie von Peru*. Heidelberg: Carl Winters Universitätsbuchhandlung.

Stock C. 1917. Further observations on the skull structure of mylodont sloths from Rancho La Brea. *Bulletin of the Department of Geology*, *University of California Publications* 10: 165–178.

Stock C. 1925. Cenozoic gravigrade Edentates of Western North America with special reference to the Pleistocene Megalonychinae, and Mylodontidae of Rancho La Brea. *Carnegie Institution of Washington Publications* 331: 1–206.

Storch G, Habersetzer J. 1991. Rückverlagerte Choanen und akzessorische Bulla tympanica bei rezenten Vermilingua und *Eurotamandua* aus dem Eozän von Messel (Mammalia: Xenarthra). *Zeitschrift für Säugetierkunde* 56: 257–271.

Suárez-Soruco R, Díaz-Martínez E. 1996. Léxico estratigráfico de Bolivia. *Revista Técnica de Yacimientos Petroliferos Fiscales Bolivianos* 17: 1–227.

Takai F. 1982. Fossil mammals from the Tarija basin, Bolivia. *The Research Institute of Evolutionary Biology* 3: 1–72.

Takai F, Arózqueta B, Mizuno T, Yoshida A, Kondo H. 1984. On fossil mammals from the Tarija Department, Southern Bolivia. *Contribution from the Research Institute of Evolutionary Biology* 4: 1–63.

Tandler J. 1901. Zur vergleichenden Anatomie der Kopfarterien bei den Mammalia. *Anatomische Hefte* 18: 328–368.

Tedford, RH, Albright III LB, Barnosky, AD, Ferrusquia-Villafranca I, Hunt RM Jr, Storer JE, Swisher III CC, Voorhies RM, Webb SD, Whistler PD. 2004. Mammalian biochronology of the Arikareean through Hemphillian interval (Late Oligocene through Early Pliocene epochs). In: Woodburne MO, ed. *Late Cretaceous and Cenozoic mammals of North America: biostratigraphy and geochronology*. New York: Columbia University Press, 169–231.

Tejada-Lara JV, Salas-Gismondi R, Pujos F, Baby P, Benammi M, Brusset S, De Franceschi D, Espurt N, Urbina M, Antoine P-O. 2015. Life in proto-Amazonia: Middle Miocene mammals from the Fitzcarrald Arch (Peruvian Amazonia). *Palaeontology* 58: 341–378.

Thiery G, Ducrocq S. 2015. Endocasts and brain evolution in Anthracotheriidae (Artiodactyla, Hippopotamoidea). *Journal of Anatomy* 227: 277–285.

Toledo N. 2016. Paleobiological integration of santacrucian sloths (Early Miocene of Patagonia). *Ameghiniana* 53: 100–141

Toledo N, Cassini GH, Vizcaíno SF, Bargo MS. 2014. Mass estimation of Santacrucian sloths from the Early Miocene Santa Cruz Formation of Patagonia, Argentina. *Acta Palaeontologica Polonica* 59: 267–280.

Tomassini RL, Montalvo CI, Deschamps CM, Manera T. 2013. Biostratigraphy and biochronology of the Monte Hermoso Formation (early Pliocene) at its type locality, Buenos Aires Province, Argentina. *Journal of South American Earth Sciences* 48: 31–42.

Tonni E. 2009. Los mamíferos del Cuaternario de la Región Pampeana de Buenos Aires, Argentina. In: Ribeiro AM, Bauermann SG, Cherer CS, eds. *Quaternario Do Rio Grande do Sul: integrando conhecimentos*. Porto Alegre: Monografias da Sociedade Brasileira de Paleontologia, 193–205.

Van der Merwe NJ, Bezuidenhout AJ, Seegers CD. 1995. The skull and mandible of the African elephant (*Loxodonta africana*). *Onderstepoort Journal of Veterinary Research* 62: 245–260.

Varela L, Fariña RA. 2016. Co-occurrence of mylodontid sloths and insights on their potential distributions during the late Pleistocene. *Quaternary Research* 85: 66–74.

Varela L, Tambusso PS, Fariña RA. 2016. Inner and middle ear 3D reconstruction of the extinct giant sloth *Lestodon armatus.* Washington DC: ICVM-11 abstracts.

Varela L, Tambusso PS, McDonald HG, Fariña RA. 2018. Phylogeny, macroevolutionary trends and historical biogeography of sloths: insights from a Bayesian morphological clock analysis. *Systematic Biology* 25: 204–218.

Villarroel CA. 2000. Un Nuevo Mylodontinae (Xenarthra, Tardigrada) en la Fauna de La Venta, Mioceno de Colombia: el estado actual de la familia Orophodontoidae. *Revista de la Academia Colombiana de Ciencias Exactas, Físicas y Naturales* 24: 117–127.

Vinuesa V, Iurino DA, Madurell-Malapeira J, Liu J, Fortuny J, Sardella R, Alba DM. 2016. Inferences of social behavior in bone-cracking hyaenids (Carnivora, Hyaenidae) based

on digital paleoneurological techniques: implications for human–carnivoran interactions in the Pleistocene. *Quaternary International* 413: 7–14.

Vizcaíno SF, Bargo MS, Cassini GH, Toledo N. 2016. *Forma y función en paleontología de vertebrados*. La Plata: Editorial de la Universidad de La Plata.

Vizcaíno SF, Cassini GH, Toledo N, Bargo MS. 2012. On the evolution of large size in mammalian herbivores of Cenozoic faunas of southern South America. In: Patterson BD, Costa LP, eds. *Bones, clones and biomes. The history and geography of recent neotropical mammals*. Chicago: University of Chicago Press, 76–101.

Vizcaíno SF, Kay RF, Bargo MS. 2012b. Background for a paleoecological study of the Santa Cruz Formation (late Early Miocene) on the Atlantic coast of Patagonia. In: Vizcaíno SF, Kay RF, Bargo MS, eds. *Early Miocene Paleobiology in Patagonia*. Cambridge: Cambridge University Press, 1–22.

Vizcaíno SF, Fariña RA, Bargo MS, De Iullis, G. 2004a. Functional and phylogenetic assessment of the masticatory adaptations in Cingulata (Mammalia, Xenarthra). *Ameghiniana* 41: 651–664.

Vizcaíno SF, Fariña RA, Zárate M, Bargo MS, Schultz P. 2004b. Palaeoecological implications of the mid-Pliocene faunal turnover in the Pampean Region (Argentina). *Palaeogeography, Palaeoclimatology, Palaeoecology* 213: 101–113.

Vizcaíno SF, Toledo N, Bargo MS. 2018. Advantages and limitations in the use of extant xenarthrans (Mammalia) as morphological models for paleobiological reconstruction. *Journal of Mammalian Evolution* 25: 495–505.

Vizcaíno SF, Zárate M, Bargo MS, Dondas A. 2001. Pleistocene burrows in the Mar del Plata area (Argentina) and their probable builders. *Acta Palaeontologica Polonica* 46: 289–301.

Webb SD. 1985. The interrelationships of tree sloths and ground sloths. In: Montgomery GG, ed. *The ecology and evolution of armadillos, sloths, and vermilinguas*. Washington, DC: Smithsonian Institution Press, 105–112.

Webb SD. 1989. Osteology and relationships of *Thinobadistes segnis*, the first mylodont sloth in North America. In: Redford KH, Eisenberg JF, eds. *Advances in Neotropical Mammalogy*. Gainesville: Sandhill Crane Press, 469–532.

Weidenreich F. 1924. Über die pneumatischen Nebenräume des Kopfes. Ein Beitrag zur Kenntnis des Bauprinzips der Knochen, des Schädels und des Körpers (Knochenstudien: III. Teil). *Zeitschrift für Anatomie und Entwicklungsgeschichte* 72: 55–93.

Weidenreich F. 1941. The brain and its role in the phylogenetic transformation of the human skull. *Transactions of the American Philosophical Society* 31: 320–442.

Wible JR, Gaudin TJ. 2004. On the cranial osteology of the yellow armadillo *Euphractus sexinctus* (Dasypodidae, Xenarthra, Placentalia). *Annals of the Carnegie Museum of Natural History* 73: 117–196.

Wible JR. 2010. Petrosal anatomy of the nine-banded armadillo, *Dasypus novemcinctus* Linnaeus, 1758 (Mammalia, Xenarthra, Dasypodidae). *Annals of the Carnegie Museum of Natural History* 79: 1–28.

Witmer LM. 1997. The evolution of the antorbital cavity of archosaurs: a study in soft-tissue reconstruction in the fossil record with an analysis of the function of pneumaticity. *Journal of Vertebrate Paleontology* 17: 1–73.

Woodburne MO. 2010. The Great American Biotic Interchange: dispersals, tectonics, climate, sea level and holding pens. *Journal of Mammalian Evolution* 17: 245–264.

Zárate MA, Bargo MS, Vizcaíno SF, Dondas A, Scaglia O. 1998. Estructuras biogénicas en el Cenozoico tardío de Mar del Plata (Argentina) atribuibles a grandes mamíferos. *Revista de la Asociación Argentina de Sedimentología* 5: 95–103.

Zurita AE. Camacho M, Miño-Boilini ÁR, Candela AM, Cuadrelli F, Krmpotic CM, Solís N. 2017. Xenarthra (Mammalia) from a new late Neogene fossiliferous locality in Northwestern Argentina. *Journal of South American Earth Sciences* 80: 229–236.